# Reconstruction of sedimentary environment and climate conditions by multi-geochemical investigations of Late Palaeozoic glacial to postglacial sedimentary sequences from SW-Gondwana.

Dissertation

zur

Erlangung des Doktorgrades (Dr. rer. nat.)

der

Mathematisch-Naturwissenschaftlichen Fakultät

der

Rheinischen Friedrich-Wilhelms-Universität Bonn

Vorgelegt von

Kay Scheffler

aus Wuppertal

Bonn 2004

**Ernst zu nehmende Forschung erkennt man daran,**
**daß plötzlich zwei Probleme existieren,**
**wo es vorher nur eines gegeben hat.**

Thorstein Bunde Veblen (1857-1929)

# *Acknowledgment*

This thesis developed by co-operation between the Mineralogical-Petrological Institute, University of Bonn and the Department of organic Geochemistry, University of Cologne. Many people were incorporated in this project and sincere thanks are given to them all.
Special thanks go to my supervisors Prof. Dr. S. Hoernes (Bonn) and PD Dr. L. Schwark (Cologne) who supported this study with their knowledge and fruit full discussions.
M. Werner (University Würzburg/TH Aachen), B. Millsteed, D. Bühmann (South Africa) and E. Vaz dos Santos (Brazil) are thanked for sample material, sample data and additional field information from sample localities in Namibia, South Africa, Botswana and Brazil.
Furthermore, A. Hilder, S. Appleby (Bonn) are gratefully acknowledged for assistance in sample preparation. B. Stapper and numerous helping hands of the Geological Institute of Cologne are thanked for guiding through the organic geochemical analytic.
My parents are thanked for their interest in my work and their continuous support during the last years.
At last I would like to thank Nicol Ecke who accompanied me thought ups and downs, especially towards the end of this work.

# Contents

# 1. Introduction

The global climate comprises a complex interplay between atmosphere, land and ocean. Any aberration in one of these compartments can result in climate change. For a better understanding of the global interaction of climate forcing factors, it is important to investigate paleoclimate records. Factors controlling global climate and atmospheric $CO_2$ level have been discussed for fossil systems (Hyde et al., 1999; Crowley and Baum, 1992; Berner, 1994; Frakes et al., 1992; Martini, 1997). In the view of today's discussion on change from icehouse to greenhouse conditions (IPCC, 2001), the study of a fossil analogue icehouse-greenhouse transition may prove valuable. The most extensive Phanerozoic glaciation and its termination occurred during the Carboniferous-Permian on the southern hemispherical Gondwana supercontinent (Fig. 1-1a). The glaciation lasted 90 Ma (Crowell, 1978) during an episode of supercontinentality comparable to the Proterozoic continent constellation. Sealevel fluctuations with amplitudes of several decimetres up to hundred metres (Soreghan and Giles, 1999) are recorded in cyclic sedimentation sequences in North America, Europe and Eurasia (Crowell, 1978; Heckel, 1986; Ross and Ross, 1985). Isbelll et al. (2003) indicate that cyclothems and episodes of late Palaeozoic glaciation overlap temporally, but they do not coincide on a finer time scale. In India evidence of Gondwana glaciation is recorded by the Upper Carboniferous Talchir Formation (Banerjee, 1966).

Glacial conditions on the Southern Hemisphere and the contemporaneous extension of marine and terrestrial life in equatorial regions influenced the atmospheric $CO_2$ content ($pCO_2$). The marked drop in $pCO_2$ (Berner, 1994) at the end of the Carboniferous coincides with times of contrasting climate evolution between polar and equatorial regions. Carbon isotopes were used to report these global changes due to isotopic fractionation processes between atmospheric ($CO_2$), organic (biomass and sedimentary organic matter) and inorganic carbon reservoirs (e.g. Kump and Arthur, 1999; Hayes et al., 1999). The influence of the Gondwana glaciation on global climate is documented by variations in $\delta^{13}C$ measured on brachiopods from equatorial regions (Bruckschen et al., 1999; Veizer et al., 1999).

The climate changes during the late Palaeozoic are documented in comparable sedimentary units from South America, South Africa, Namibia, Tanzania, Antarctica, India and Australia (Crowell, 1978; Caputo and Crowell, 1985; Veevers and Powell, 1987) (Fig. 1-1b). Their Upper Carboniferous to Triassic deposits are combined to form the "Karoo sediments" or "Karoo Supergroup" with type localities in the Main Karoo Basin in South Africa, where the complete stratigraphic record is preserved.

**Figure 1-1a**

Continent constellation of the southern hemisphere during the late Palaeozoic (polar view) adapted from Faure & Cole (1999).

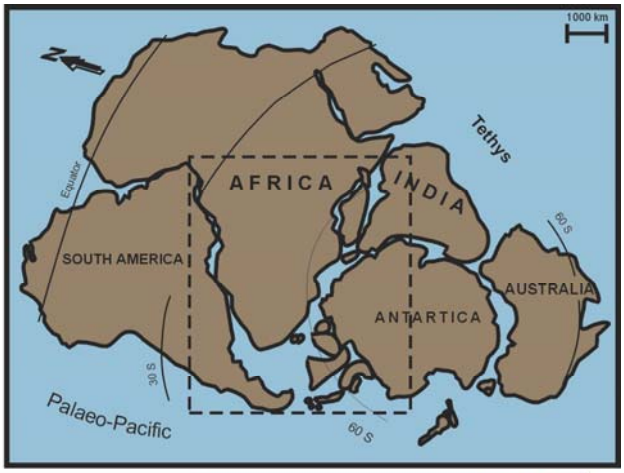


**Figure 1-1b**

Paleogeographic reconstruction of south Gondwana during the late Palaeozoic (after Visser & Praekelt, 1996).
Major ice-flow directions recorded in deglaciation sequences I, II and III (after Visser, 1997) indicate clockwise change in provenance.

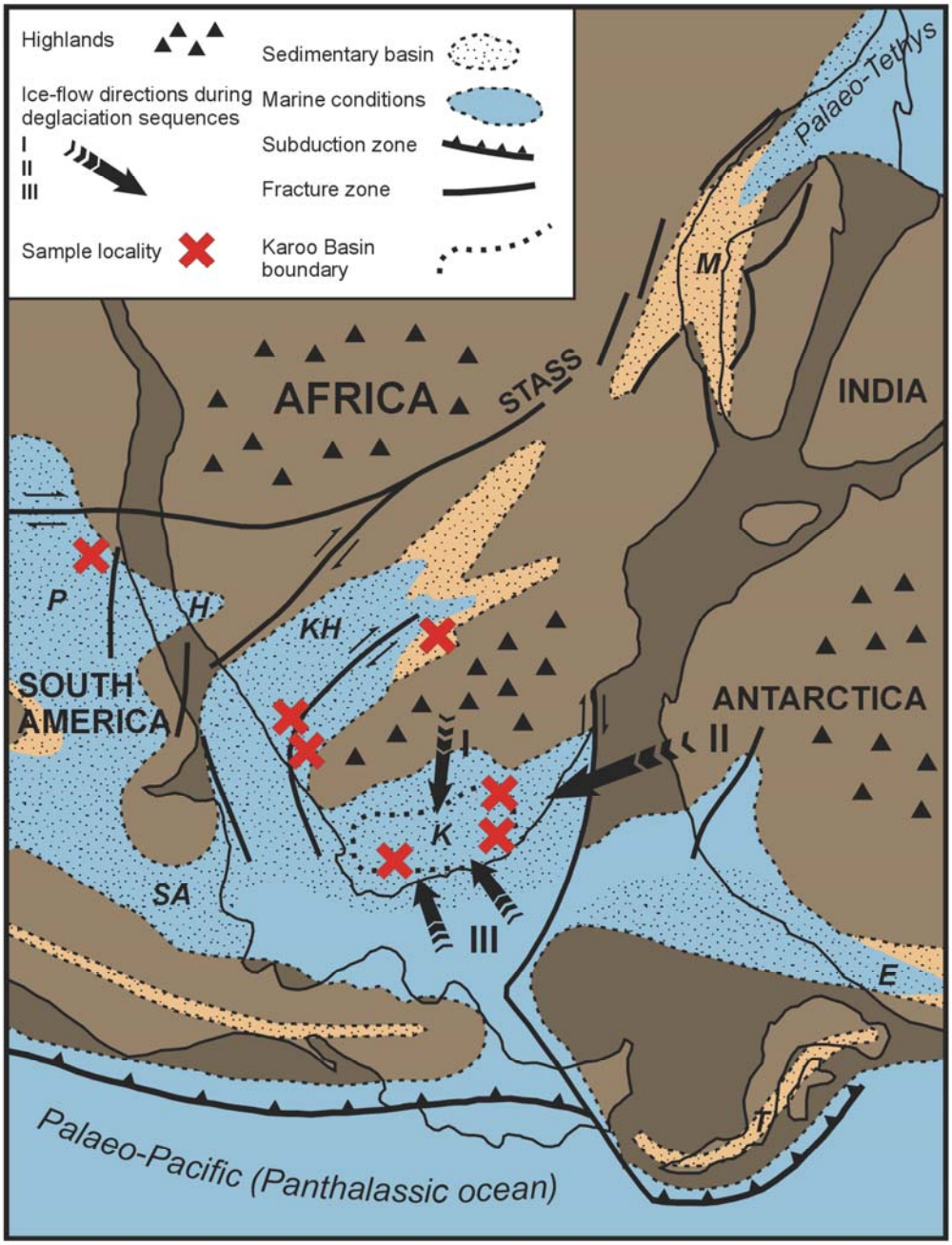


**P** = Paraná Basin; **H** = Huab Basin; **K** = Karoo Basin; **SA** = Siera Australes; **M** = Malagasy Basin; **KH** = Kalahari Basin; **E** = Ellsworth Basin; **T** = Trinity Basin; **STASS** = southern transafrican shear system

By comparing climate proxy signals from polar and equatorial regions, insight into the synchronicity of global climate processes can be obtained. Because geochemical signals can be affected by diagenesis, changes in provenance or weathering processes, reliable information of climatic and sedimentary evolution can only be achieved by combining a variety of geochemical information to obtain parameters, which can be used as proxy signals for provenance, climate and sedimentary environment. Sedimentological and mineralogical investigations (Bühmann and Bühmann 1990) have been carried out for glacial sedimentary sequences of the Karoo Basin, but only preliminary geochemical analyses of the Dwyka Group sedimentary rocks exist.

This thesis aims to provide detailed geochemical analyses of the lower Karoo Supergroup sediments in southwestern Gondwana with focus on the Karoo Basin in South Africa. The geochemical analyses are interpreted in terms of climate changes during the Upper Carboniferous to the late Permian.

The mineralogical composition (XRD analyses by D. Bühmann), major and trace elements are used to describe the sampled sequences in the different localities. Oxygen isotopes of the silicate phases reveal information about sedimentary and diagenetic processes and are used to support the interpretation of mineralogical and geochemical signals. Element geochemical parameters (CIA, Zr/Ti, Rb/K, V/Cr) are used to record changes of the climate conditions and paleoenvironment. Further information can be obtained from carbon isotopes of organic matter. Since the $\delta^{13}C_{org}$ signature can be influenced by variable proportions of marine versus terrestrial derived plants and its state of preservation, organic geochemical investigations (TOC, C/N, lipid biomarker analyses) are used to characterise the organic matter.

By multi proxy geochemical investigations the following questions have to be answered:

- *What happened during, while and after climate changes in the sedimentary environments?*
- *Are changing environmental conditions recorded in the geochemical composition of the sediments?*
- *Did post-sedimentary processes (diagenesis to low-grade metamorphism) significantly modified the primary sediment composition (mineralogical and geochemical)?*
- *Can these processes be distinguished?*
- *Can climate information/trends be extracted from proxy signals?*
- *Are interactions of regional and global climate systems detectable?*

## 1.2 Climatic evolution during deposition of the Karoo Supergroup

The Karoo Basin in South Africa formed part of a major depocentre during the late Palaeozoic (Fig. 1-1b). Several studies describe and characterise climate conditions and evolution of the depositional environments while and after glacial, interglacial and postglacial phases during the late Palaeozoic in southern Gondwana (Frakes et al., 1992; Golonka and Ford, 2000; Visser, 1995, 1997; Cole, 1992).

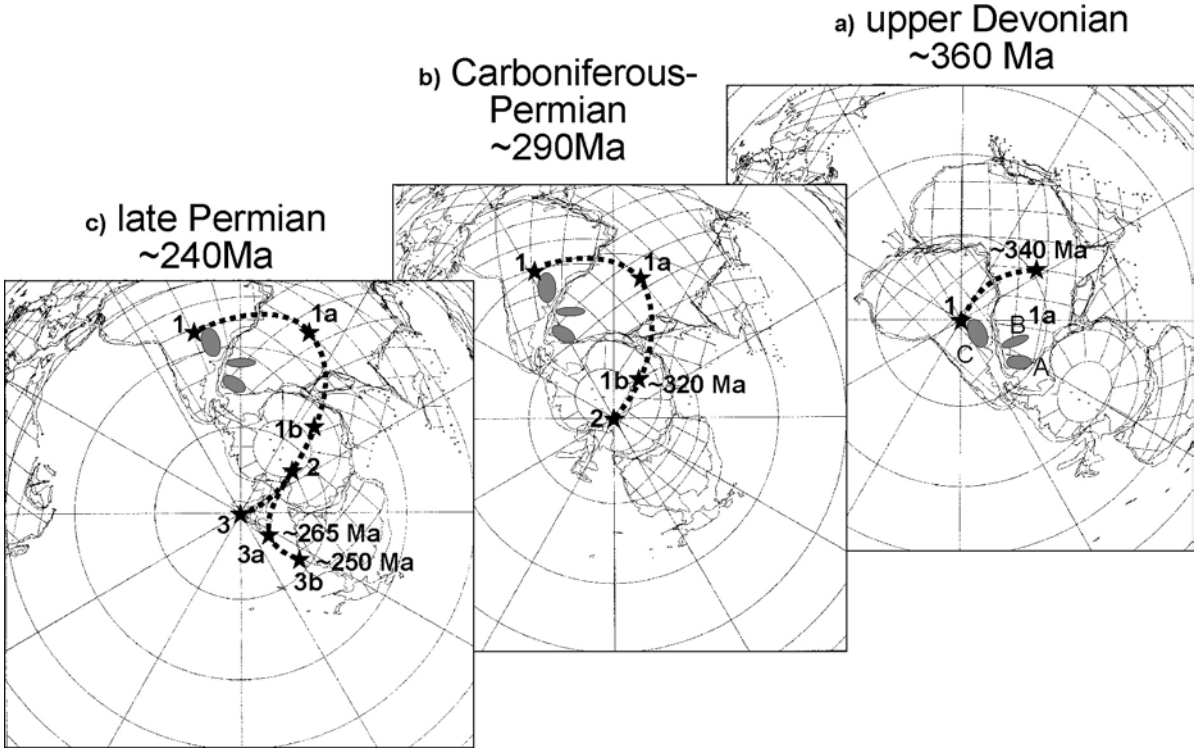


**Figure 1-2a-c**

Configuration and position of south Gondwana during the upper Palaeozoic on the southern hemisphere. Paleomaps adapted from Smith et al. (1981). Pol position and wander path compiled from Powell and Li (1994) (**1a, 1b, 3a & 3b**) and Smith et al. (1981) (**1, 2 & 3**). A= Karoo Basin, B= Kalahari Basin, C= Paraná Basin.

The Gondwana strata contain three distinct and separate units of upper Palaeozoic glacial deposits. Primary glacial conditions are recorded during the Late Devonian to earliest Permian in South America (Lopéz-Gamundí et al., 1993). During the late Palaeozoic south Gondwana underwent a clockwise rotation through Polar Regions (Crowell, 1983) (Fig. 1-2a-c). Different ice spreading centres developed on the southern Gondwana continent during the upper Palaeozoic (Hyde et al., 1999). The complete glacial period lasted from the upper Devonian to the Middle Permian (Veevers and Powell, 1987). Following the apparent polar wander path (Veevers and Powell, 1987), first glacial sediments deposited during the upper Devonian in South America (Fig. 1-2a). In the course of the Visean, tillite and diamictites

accumulated in northwest Africa and South America. Glacial conditions dominated during the Namurian the sedimentation in southern America and central Africa (Veevers and Powell, 1987). The first glacial sediments of the Karoo Supergroup deposited during the Upper Carboniferous to Early Permian in South Africa (Fig. 1-2b). During the Middle to Late Permian, the late Palaeozoic glaciation was terminated as recorded in glacial deposits from Australia (Fig. 1-2c).

Glacial I (late Devonian) and II (Namurian) were characterised by alpine glaciers of limited extent (Isbell et al., 2003). Waning and waxing of these alpine glaciers would have produced sea-level fluctuations, insufficient for generation of cyclothems. Only during Glacial III (upper Carboniferous to Middle Permian), south Gondwana was covered by extended ice sheets. Changes in mass balance of these ice sheets have produced sea-level changes that can be inferred from the cyclothems in the northern hemisphere (Isbell et al., 2003).

During Glacial III climate variations between glacial and interstadial phases are recorded in cyclic phases of deposition in the Karoo Basin of South Africa, in the Paraná Basin, Brasil, and in upper Carboniferous Dwyka sediments of south Namibia. After termination of the late Palaeozoic glaciation phase, new sedimentary environments had established in south Gondwana. Climate conditions changed and triggered by meltdown of the glaciers, the sealevel rose. Following deposition of clastic debris during the glacial period, the deposition of carbonates, phosphates and organic rich mudstones indicates changing sedimentary environments at temperate climate conditions during the post glacial phase.

The Karoo, Kalahari and Paraná Basins formed a contiguous sedimentary environment, connected by more or less continuous seaways. Whether this environment can be described as an “Inlandsea” or if it was connected with the Panthalassa Ocean in the south and full marine conditions could temporarily establish, is still in discussion (Visser and Praekelt, 1996; Smith et al., 1993; Faure and Cole, 1999).

In the upper Karoo Supergroup, terrestrial sediments can be associated with arid climate conditions. In general, a progressive shift from glacial to cool-moist conditions to warm-humid, semi-arid and finally hot arid conditions seems to have taken place in all late Palaeozoic southern Gondwana basins (Johnson et al., 1996).

## 1.3 Absolute ages and stratigraphic correlation

Partly conflicting age determinations of the Karoo sediments were discussed by several authors (e.g. Grill, 1997; Visser, 1990; Cole, 1992). Correlations and age determinations were mainly based on macrofossils, pollen and spores. Marine bivalves (*Eurydesma mytiloides*) (Dickins, 1961) were reported from glacial deposits in South America, Namibia, Botswana and Australia (López-Gamundi et al., 1993; Dickins, 1996; Visser, 1997). The low

fossil content of the Dwyka deglaciation sequences DS I – IV hampered a precise correlation to an absolute time scale. A synchronous and widespread unit in the Karoo Supergroup is the Whitehill Formation. The fossil remains of a reptile fauna (*mesosaurus fauna*) in the Whitehill shales were used by Oelofson (1987) to correlate the South American and south African strata.

Catuneanu et al. (1998) used the coherency between sedimentation phases and tectonic pulses of the Cape Fold Belt for age determination of the sedimentary units in the Karoo Basin. The episodic pulses at 292±5, 278±2, 258±2, 246±2, 239, 230±3, 223 and 215±3 Ma in the fold and thrust belt were dated by K-Ar and Ar-Ar technique on whole rock samples and newly formed micas (open stars in Fig. 1-3) by Hälbich (1983) and Gresse et al. (1992). However, the lack of absolute ages by radiometric determination methods hampered a satisfactory correlation of the Karoo sediments to a global time scale.

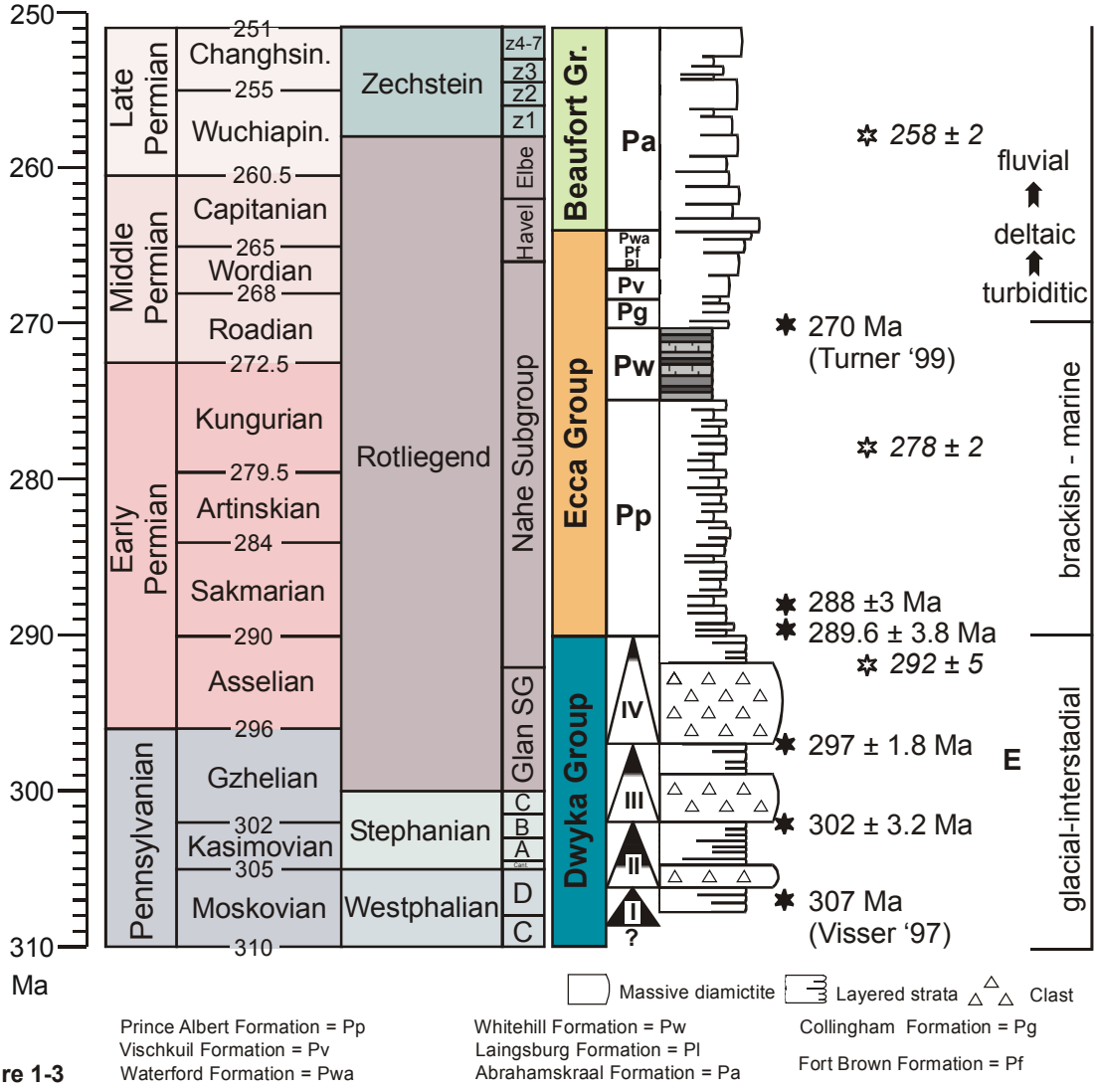


**Figure 1-3**

Stratigraphy and facies evolution of the lower Karoo Supergroup. E = Euredesma transgression; filled stars = sensitive high-resolution microprobe (SHRIMP) ages after Bangert et al., (1999); open stars ages by Hälbich (1983) and Gresse (1992); Timescale after German Strat. Comm. (2002).

Visser (1997) estimates for the base of the Dwyka Group approximately 307 Ma, which corresponds to a mid-Moscovian age according to the time scale used in figure 1-3. $^{206}Pb/^{238}U$ determinations of magmatic zircons by sensitive high-resolution ion microprobe (SHRIMP) analysis by Bangert et al. (1999) yielded reliable ages for the Dwyka glacial/interstadial phases and for the Dwyka/Ecca boundary. In the south Namibian Dwyka Group, zircons in two tuff horizons at the top of DS II yielded radiometric ages of 299.2 ± 3.2 and 302 ± 3.0 Ma (Bangert et al., 1999). In the Karoo Basin of South Africa magmatic zircons from ash fall tuffs at the top of DS III revealed average $^{206}Pb/^{238}U$ ages of 297 ±1.8 Ma (Bangert et al., 1999). Zircons in two tuff layers closely above the Dwyka/Ecca boundary exhibited ages of 288 ±3.0 and 289.6 ±3.8 Ma (Bangert et al., 1999). Bangert et al. (1999), concluded an age of 302 Ma for the top of DS II, 297 Ma for the top of DS III and 290 Ma for the Dwyka-Ecca boundary (filled stars in Fig. 1-3). Thus, the duration of each deglaciation cycle was calculated to approximately 5-7 Ma.

On the time scale of Menning (2002), the top of DS II is of upper Kasimovian to lower Gzhelian age and the top of DS III of upper Gzhelian to lower Asselian age, thus representing the Carboniferous/Permian boundary. The Dwyka/Ecca boundary and in consequence the transition from glacial to postglacial climate conditions can be correlated to the upper Asselian to lower Sakmarian. U/Pb ages of 270 ±1 Ma from zircons in tuffs of the postglacial Collingham Formation determined by Turner (1999) correlate with a lower-mid Permian age (Roadian).

Based on absolute ages the Dwyka deglaciation sequences, the Dwyka/Ecca boundary (Asselian/Sakmarian boundary) and the Whitehill Formation (upper Kungurian to lower Roadian) can be correlated to a global stratigraphy. According to this the Prince Albert shales in the Karoo Basin were deposited during the Early Permian. The Collingham Formation is of lower Middle Permian age (upper Roadian) whereas the exact ages of the Collingham/Vischkuil, Vischkuil/Laingsburg and Laingsburg/Fort Brown boundaries remain uncertain. In general, Middle to Late Permian ages can be assumed, since the overlying Beaufort Group is usually attributed to the Late Permian to Lower Triassic (Johnson et al., 1996; Smith et al., 1993; Visser, 1995).

# 2. Sample localities

## 2.1 Karoo Basin (South Africa)

The Karoo Basin in South Africa formed part of a major depocentre in an assemblage of sedimentary basins during the late Palaeozoic in south Gondwana (Fig. 1-1b). The basin developed at the southern boundary of the rising Cape orogen as a retroarc foreland basin (Cole, 1992). Along the southwestern continental border of Gondwana, plate motions since the Late Devonian resulted in the subduction of the paleo-Pacific plate (De Wit and Ransome, 1992; Smellie, 1981). During the late Palaeozoic, a complex tectonic system established from South American along southern Africa, across Antarctica to eastern Australia (Visser and Praekelt, 1996). Subduction processes led to formation of a magmatic arc, its volcanic activity reported by tuff horizons. Volcanic ashes became most dominant in the sedimentary sequence during deposition of the Permian Collingham Formation (Visser, 1995; Smith et al., 1993). The Karoo Basin contains the complete sedimentary record from the Late Carboniferous Dwyka Group to the Early Jurassic basalts of the Drakensberg Group (Fig. 2-1). Glacial Dwyka Group sediments discordantly rest on early Palaeozoic basement rocks of the Cape Supergroup. A hiatus of approximately 30 Ma, at the southern basin border, thins out towards the north (Visser, 1987).

| Group | Formation |
|---|---|
| Drakensberg | |
| Stormberg | Clarens |
| | Elliot |
| | Molteno |
| Beaufort | Burgersdorp |
| | Katberg |
| | Balfour |
| | Teekloof |
| | Middleton |
| | Abrahamskraal - Koonap |
| Ecca | Waterford |
| | Fort Brown |
| | Laingsburg - Ripon |
| | Vischkuil - Colligham |
| | Whitehill |
| | Prince Albert |
| Dwyka | deglaciation cycles |

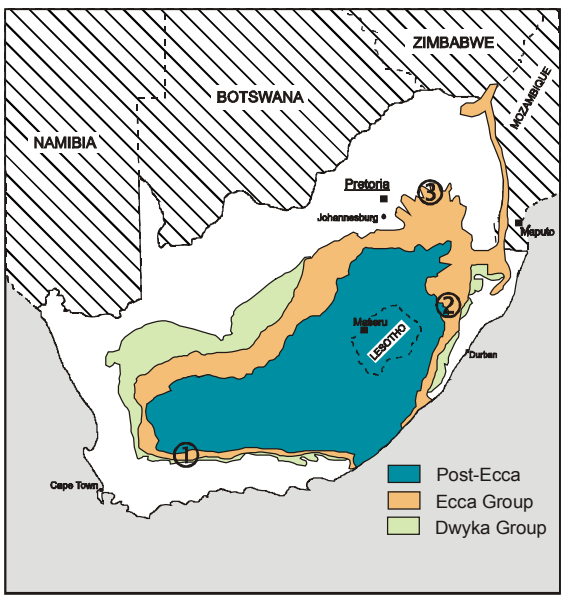


**Figure 2-1**

Stratigraphy of the Karoo supergroup in the southern Karoo Basin of South Africa. Outcrop of lower Karoo Supergroup sediments in South Africa. Sample localities are numbered 1-3. 1 = Sediment sequences from Laingsburg area, 2 = MPU core, 3 = Coal seam sequence from the Witbank Basin.

Comparable with the deposition of the Cape Supergroup, first glacial detritus of the Karoo Supergroup derived from northern provenances (Cargonian Highlands). The clastic debris was deposited on the stable shelf along the southern continental margin of Gondwana. The Late Carboniferous to Early Permian glacial sediments reaches their maximum thickness in the southern parts of the depocentre. Close to the northern basin borders, the sedimentary units thin out. Four deglaciation cycles are recorded in the Karoo Basin of South Africa (Theron and Blignault, 1975; Visser, 1997). Each deglaciation sequence consists of a basal zone with massive diamictites overlain by a terminal zone of softer, stratified and better-sorted sedimentary rocks (Theron and Blignault, 1975). By changing directions of glacier marks variations in ice flow direction over southern Africa during DS I – IV (Fig. 1-1b) are documented (Visser, 1997; Theron and Blignault, 1975). Ice advances during the glacial phases of deglaciation sequences I & II derive from northern and eastern provenances. During DS III and IV ice flow directions from northeast were replaced by glacier advance from south-eastern regions. The northern and eastern provenances (South African/Cargonian Highlands and Eastern Antarctica) consisted of Precambrian cratonic rocks whilst the southern provenances are associated with a magmatic arc along the Palaeo-Pacific margin (Visser, 1989). The Dwyka Group in the northern basin ends with coal-bearing fluviodeltaic sequences (Smith et al., 1993), overlain in places by marine shales of the Pietermaritzburg Formation of the northern Ecca Group (Catuneanu et al., 1998).

Increasing temperatures, rising sealevel and anoxic redox conditions, mark the onset of postglacial conditions. Subsiding troughs in front of the rising Cape orogen formed characteristic sedimentary environments along the southern basin margin. The troughs were filled with flysch-type deposits whereas sedimentation in the central basin was dominated by debris flow deposits of silt and mud (Smith et al., 1993).

The postglacial Ecca Group of the southern Karoo Basin comprises the Prince Albert, Whitehill, Collingham Vischkuil, Laingsburg, Fort Brown and Waterfront Formations (Fig. 1-2). During deposition of the Ecca Group, the east-west trending depocentre of the southern Karoo Basin was sustained by continued downwarping. This tectonic regime allowed the accumulation of almost 2000 m of flysch-type Ecca sediments on top of the Dwyka diamictites along the rising Cape Fold Belt (Smith et al., 1993). Dark-coloured shales of the Prince Albert Formation contain carbonatic and phosphatic lenses. The Whitehill Formation forms a marked white weathering horizon. The unit is predominantly composed of black, carbonaceous, pyrite-bearing shales. By the distinctive Mesosaurus reptile fauna, the Whitehill Formation can be correlated with the Irati shales in the Paraná Basin of Brazil (Oelofsen and Araujo, 1987). In the southern Karoo Basin the Whitehill Formation is conformably overlain by the Collingham Formation (Millsteed, 1999). The alternating siltstones and shale horizons are interpreted as deposits of a distal submarine fan facies,

associated with pelagic sedimentation (Catuneanu et al., 1998). Tuff beds in the Collingham Formation were delivered from an eruptive centre close to the subduction zone along the Palaeo-Pacific margin of South America (Viljonen, 1994). Johnson et al. (1997) have described thin tuffaceous beds also in southern and western outcrops of the Whitehill Formation. The replacement of carbonaceous shales by turbiditic deposits indicates a rapid change in the tectonic regime of south Gondwana. The sedimentation rates increased during the transition from glacial and postglacial open-marine (30 m/Ma), to deltaic (300 m/Ma), up to fluvial (500 m/Ma) sedimentation during the Beaufort Group (Visser, 1995). The changing sedimentary conditions were accompanied by increasing volcanic activity and uplift of the provenances during the Ecca Group (Wickens and DeVilliers, 1992). In the sampled area, a subbasin with a specific facies established during the Collingham Formation (Laingsburg Subbasin). The overlying coarsening upward sequences of the Vischkuil and Laingsburg Formations represent the change from distal to proximal sedimentary environments (Smith et al., 1993). The upper Ecca Group in the southwestern Karoo Basin is composed of deltaic shales and sandstones of the Fort Brown and Waterfront Formation. The sediments were deposited in a regressive, shallow-marine to fluvially dominated deltaic environment (Smith et al., 1993; Catuneanu et al., 1998). Terrestrial dominated sedimentary systems prevail during the Beaufort Group. Deltas advanced from the west, south and northeast into the former marine environment (Rust et al., 1991). Fluvio-lacustrine sediments were laid down on broad subsiding alluvial plains. The upper Karoo sequence renewed uplift in the southern and eastern provenances and progressive aridification led to the accumulation of fluvial and flood-fan, playa and dune complexes (Smith et al., 1993). During the Early Triassic, the sedimentary succession of the Karoo Supergroup is capped by basaltic lavas of the Drakensberg Group. The intensive and widespread extrusion of flood basalts, are interpreted as precursor of the breakup of Gondwana in the late Jurassic (Catuneanu et al., 1998; Turner, 1999).

Samples derived from different localities in the southern Karoo Basin (Fig. 2-1). During field campaigns sedimentary sequences were investigated near Laingsburg (Knütter, 1994; Adelmann, 1995; Fiedler, 1995; Albes, 1996; and Zechner, 2003) (Fig. 2-1, No. 1). The compilation of these profiles yield a nearly complete stratigraphic sequence from the glacial Dwyka Group up to the postglacial Ecca Group.

By the kind cooperation with B.D. Millsteed and D. Bühmann further material was obtained from the south-eastern Karoo Basin. Samples were taken representatively from an approximately 150 m long core (MPU) near Mpushini in the northern KwaZulu-Natal Province (Fig. 2-1, No. 2). The core comprises diamictites from the upper part of the deglaciation sequence IV, the Dwyka/Ecca boundary and shales of the lower Prince Albert Formation.

## 2.2 Witbank coalfield, north-eastern Karoo Basin

On the eastern margin of the Karoo Basin the earliest coal seams formed during the final retreat of the glaciers still under a cold climatic regime on outwash plains along the northern passive basin margin in glacial to subglacial sedimentary environments (Cadle et al., 1993). At approximately 290 Ma full post-glacial climate conditions were finally established. Transgression and regression phases influenced the sedimentation and in combination with continued climate amelioration supported extensive peat and swamp formation. In the northern Karoo Basin the Ecca Group comprises the Pietermaritzburg, Vryheid and Volksrust Formations. During the Vreiheid Formation, several coal seams formed in the northeastern part of the Karoo Basin in the area of the today's Witbank Coalfield. Samples were taken from the Rietspruit coal mine, which is situated 30 km south of Witbank and approximately 116 km east of Johannesburg (Fig. 2-2a).

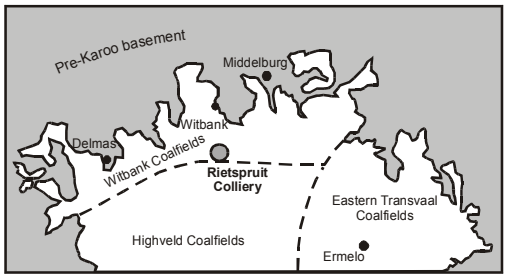


**Figure 2-2a**

The location of the Rietspruit Colliery within the context of the north-eastern sector of the Karoo Basin (after Falcon et al., 1984).

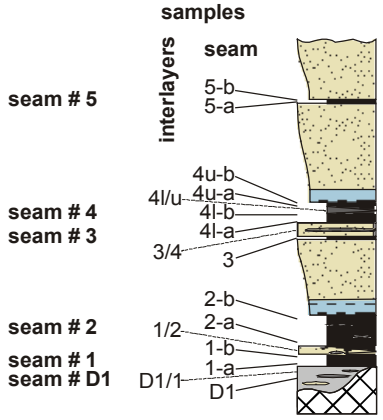


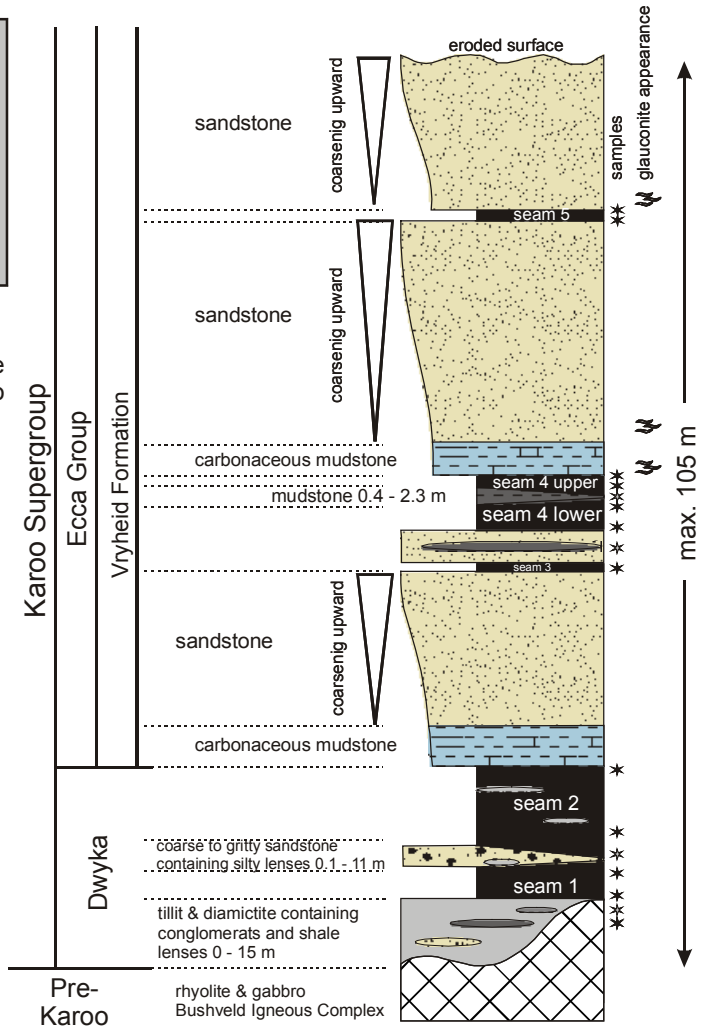


**Figure 2-2b**

Coal seam stratigraphy in the Witbank Basin complied after Cadle et al. (1993); Le Blanc Smith (1980); Falcon et al. (1984).

Five main coal seams are known from the Rietspruit colliery in the Witbank Coalfield (Fig. 2-2a & b). Le Blanc Smith (1980) described a sixth seam at the top of the sequence that occasionally occurs in other pits in the region. Organic matter accumulated in lower and upper delta plain and fluviatile environments. The Pietermaritzburg Formation is not encountered in the Rietspruit coalfield and the Volksrust Formation is absent from the stratigraphic record because of the present level of erosion (Le Blanc Smith, 1980).

The seams are separated by thick clastic sediments (Fig. 2-2b). Coarsening upward sequences are developed between seam No. 2 and 3, between seam No. 4-upper and 5 and in the overlaying strata of seam No. 5. Carbonate bearing mudstones form the top of seam No. 2 and No. 4. Glauconite, indicative for brackish-marine conditions, is reported for the overlying clastic sediments of seam No. 4, 5 and 6 (Le Blanc Smith 1980; Falcon et al., 1984; Cadle et al., 1993). Marker horizons suitable for absolute age information such as tuff layers are missing in the succession. However, microfloral investigations allow for a robust relative age correlation. A significant change in the pollen assemblage is documented by Falcon et al. (1984) in seam 2. Below this boundary, during phase 1, a monosaccate non-striate pollen assemblage is predominant. The corresponding gymnospermous flora is associate with earliest postglacial climate conditions. In consequence, the onset of sedimentation in the Witbank Basin can be correlated with initial glacier retreat. Thus, initial accumulation of organic matter commences already within the Dwyka Group. The prominent change in the microfloral assemblage supposedly coincides with the Dwyka/Ecca boundary. With the onset of the Ecca group sediments (seam 2-b to 5) the pollen-producing flora markedly changed as indicated by the sudden appearance of disaccate and subsequently also striate palynomorphs (Falcon et al., 1984). The increase in number and diversity of the palynomorphs implies a significant extension and diversification of the vegetation, associated with climate amelioration during the early Permian. The floral assemblage of the early Ecca Group was mainly represented by conifers, cordaites, pteridophytes and glossopteris vegetation as typical for the middle Permian of southern Gondwana. The termination of this vegetation phases is associated with progressing temperature rise by the drift into lower latitudes during the Permo-Triassic (Falcon et al., 1984).

Organic and C-isotope geochemical investigations have been carried out on samples of coal seam No. 1 to 5 and on organic rich layers in the clastic sequences between seam No. 4-lower and No. 4-upper, between seam No. 3 and No. 4-lower and between seam No. 1 and 2 (labelled by stars in figure 2-2b). Further organic rich sediments derive from basal units of seam No. 1, which probably are of upper Dwyka age.

## 2.3 Eastern Kalahari Basin (Central Botswana)

During the late Palaeozoic the Kalahari Basin was situated between the Windhoek highland in the north and the Cargonian highlands in the south. It formed an intracratonic basin along the southern extension of the southern transafrica shear system that can be traced from the northeast Africa down to Namibia (Visser, 1995; Visser and Praekelt, 1996) (Fig. 1-1b). Towards the southwest, the basin was probably open to a shallow sea between today's South America and South Africa (Visser, 1997). Comparable to the Karoo Basin of South Africa, marine environments established after the deposition of glacio-marine diamictites. In the eastern Kalahari Basin, the basal Ecca shales rest on fluvioglacial and glaciolacustrine deposits of the Dukwi Formation, the equivalent of the Dwyka Group (Visser, 1995). Postglacial deposits of the Ecca Group comprise lacustrine, deltaic and fluvial deposits of the Tswane, Mea and Tlapana Formation (Johnson et al., 1996). Increasing terrestrial influence in upper stratigraphic positions can be related with the sedimentary remains of prograding deltas from the southern, eastern and northern highlands. Visser (1996) point out that deltaic and paludal sedimentation with coal formation, occurred during sea level high stand in the fault-controlled Kalahari-Zambezi-East Africa basin system upon ice retreat.

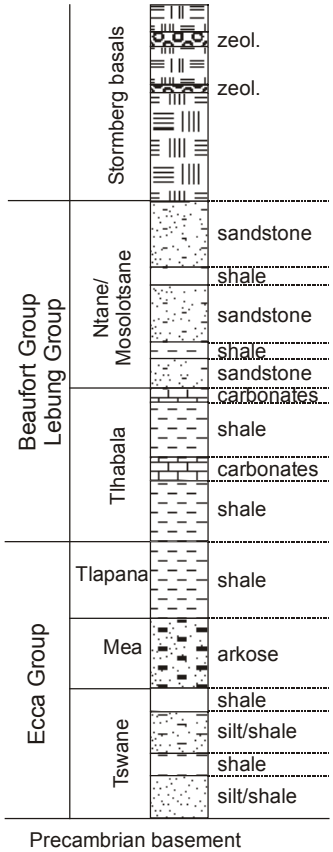


**Figure 2-3**

Stratigraphy of the OGT core, Lithology after XRD analyses by Bühmann & Atanasova (1997).

The Beaufort Group in the eastern Kalahari Basin is represented by the Tlhabala and Ntane/Mosolotsane Formations. The sediments of the Tlhabala Formation (mud-, silt-, sand- and limestones) deposited in lacustrine environments. The age of these deposits is uncertain, but at least parts of the succession can be correlated with the late Permian Beaufort Group of the Karoo Basin (Visser, 1995). The reactivation of pre-existing boundary faults and uplift terminated the sedimentation and contributed to denudation of existing deposits (Visser, 1995). Where the upper layers were not removed by erosion, the Karoo sediments were capped by aeolian sandstones of the Ntane/Mosolotosane Formation (Johnson et al., 1996). The basaltic lava of the Stormberg Group finally covered the sedimentary succession in the eastern Kalahari Basin.

Representative samples were taken from a core (OGT) close to the Orapa kimberlite mine in central Botswana (intrusion age 93 Ma after Jakubec et al., 1996) (Fig. 1-1b). XRD analysis by Bühmann and Atanasova (1997) reveal detailed information on the mineralogical composition of the samples. The Ecca shales and sandstones rest direct on the Precambrian granitic basement (Fig. 2-3). Diamictites of Dwyka age could not be encountered at the base of the cored section (Bühmann and Atanasova, 1997). The Tswane Formation consists of mudstones with approximately 41% kaolinite, covered by arkosic sandstones of the Mea Formation. The following shales of the upper Ecca Group again exhibit high kaolinite contents (Tlapana Formation). Shale and sandstone horizons contain organic carbon contents up to 50%. The mudstones of the Tlhabala Formation in the lower Beaufort/Lebung Group are demarcated from the underlying Ecca shales by illite/smectite interstratifications (Bühmann and Atanasavo, 1997). In the upper part of the Tlhabala Formation carbonates are intercalated in the mudstones. The Mosolotsane Formation rests unconformable on the Tlhabala Formation (Jakubec et al., 1996). Their sandstones are interpreted as aeolian dune deposits. At the top, Stormberg basalts unconformable cover the sedimentary succession in the Orapa core.

The correlation of the samples from the eastern Kalahari Basin to an absolute time scale is difficult due to the lack of reliable marker horizons. Bühmann and Atanasova (1997) supposed that the lower kaolinite bearing mudstones of the Tlhabala Formation are of Ecca and the upper kaolinite free mudstones (Tlhabala Formation) of Beaufort age.

Since it can be assumed that climate changes took place synchronous in the Karoo and Kalahari Basin, significant variations in climate proxies can be used for correlation. Comparable trends are detected from the dated Dwyka/Ecca boundary in the Karoo Basin and from the basal samples in the OGT core (compare Fig. 3-7). Thus it can be assumed that sedimentation restarted in the eastern Kalahari Basin after retreat of the glaciers at approximately 290 Ma. The boundaries of the following Formations are uncertain. If similar sedimentation rates are assumed in the Karoo and Kalahari Basin during deposition of the

Ecca sediments, the lower Beaufort Group can be correlated to the Middle Permian. An upper Middle Permian age (resp. Late Permian after Visser, 1995) is also attributed for the *Tapinocephalus zone* of the lower Beaufort Group in the Karoo Basin.

## 2.4 Namibian localities (Aranos Basin and Warmbad Basin)

Karoo Supergroup sediments are described by several authors from the Huab Basin in the north and from the Aranos-Kalahari Basin and Warmbad Basin in southern Namibia (Ledendecker, 1992; Grill, 1997; Stollhofen, 2000; Bangert et al., 1999; Horsthemke, 1992; Visser, 1983). Samples derive from outcrops in the southern Warmbad Basin (Geiger, 2000) (lower Dwyka Group), from localities near Zwartbas, close to the Namibian/South African border and from the Keetmanshoop (Werner, pers. comm, 2002.).

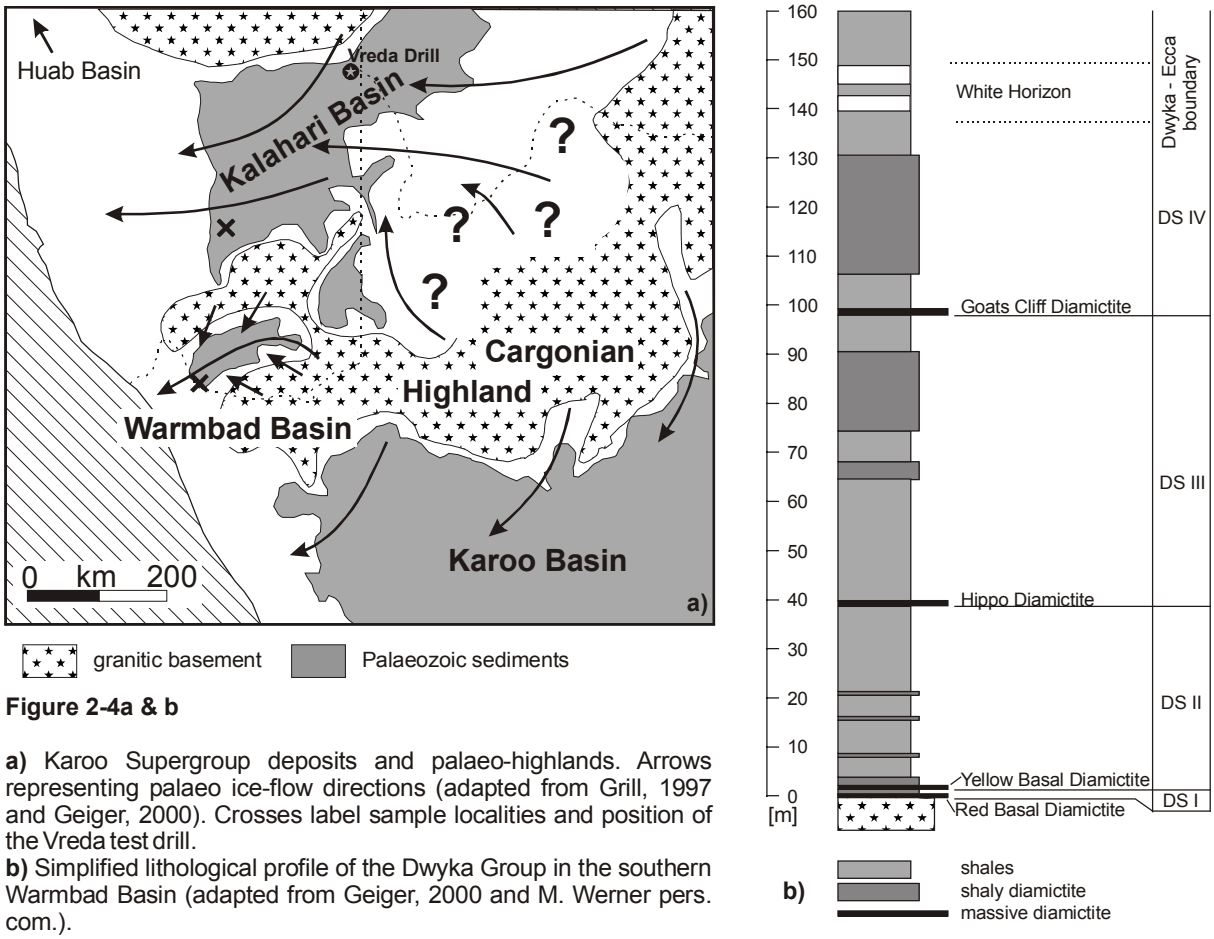


**Figure 2-4a & b**

**a)** Karoo Supergroup deposits and palaeo-highlands. Arrows representing palaeo ice-flow directions (adapted from Grill, 1997 and Geiger, 2000). Crosses label sample localities and position of the Vreda test drill.
**b)** Simplified lithological profile of the Dwyka Group in the southern Warmbad Basin (adapted from Geiger, 2000 and M. Werner pers. com.).

## 2.4.1 Warmbad Basin

The general late Palaeozoic stratigraphic classification into glacial and postglacial deposition phase is similar to the before discussed localities in southern Africa. Glacial Dwyka Group sediments at the base rest unconformably on glacial striated Late Precambrian and Cambrian basement rocks of the Nama Group (Grill, 1997). The glacial history of the Warmbad Basin differs in parts from that of the Kalahari Basin. Different ice flow directions (Fig. 2-4a) indicate that the basin was bounded at least on three sides by mountain ranges. This restriction is different to the rest of the Kalahari Basin and let to an autonomous sedimentary evolution of the Warmbad Basin (Visser, 1987). The glacial debris was deposited into a trough that cuts northward into the Karas Mountains. By rapid disintegration of the glaciers and isostatic rebound, parts of the glacial deposits were removed by erosion processes during interstadial phases. Several bentonite layers, interpreted as ash-fall deposits, are intercalated in glacial and interstadial sediments. The southwestern basin margin, open to marine environments, remained ice-free even during maximum glaciation. Occasionally occurring drafting icebergs brought fine debris into the basin (Visser, 1987).

From field observations and with regard to the deglaciation sequences in the South African Karoo Basin, four deglaciation cycles are described also in the Warmbad Basin (Geiger, 2000). The cycles are demarcated by relative thin but massive diamictites (Fig. 2-4b). Different lithofacies in the glacial strata, point to changing sedimentary environments in the depocentre. The Dwyka/Ecca boundary can not be precisely defined in the transition zone from glacial to postglacial climate conditions. However, white weathered shales form marked horizons (Fig. 2-4b). The Dwyka Group is overlain by postglacial sediments of the Prince Albert, Whitehill, Aussenkjer and Amiberg Formations of the Ecca Group. The siliciclastic debris accumulated in changing sedimentary environments with increasing terrestrial influence.

## 2.4.2 SW Aranos Basin

In the Keetmanshoop area, at the southwestern margin of the Aranos-Kalahari Basin (Fig. 2-4a), the Dwyka Group sediments can be subdivided into glacial and interstadial sequences similar to the Karoo Basin in South Africa.

Dependent on the locality, the Namibian Dwyka sediments contain different number of deglaciation sequences. Grill (1997) subdivided the glacial deposits in south Namibia into a first glacial phase at the base and a second glaciation phase at the top of the Dwyka Group. The glacial deposits are intercalated by interglacial mudstones of the Ganigobis Member. Four deglaciation sequences (DS I-IV) are reported from the Vreda test drill close to the eastern Namibian border (Fig. 2-4a). Between Mariental and Keetmanshoop three

deglaciation sequences in the Dwyka sediments are distinguishable (Bangert et al., 1999). Ice flow directions and glacier advance from northern and eastern provenances were reconstructed by Grill (1997). The depositional setting during each deglaciation sequence changed from fluvioglacial or glaciolacustrine environments to marine conditions during interstadial phases. Ash-fall tuffs in the Dwyka Group sediments were dated by SHRIMP analysis on zircons as discussed in the chapter 1.3 (Bangert et al., 1999). During the postglacial sedimentation phase of the Ecca Group fluvial and wave-dominated delta complexes developed, recorded by the Nossob and Auob Sandstone Members of the Prince Albert Formation (Stollhofen, 2000). The sandstones are separated by mudstones of the Mukorob and Rietmond Shale Members (Fig. 2-5).

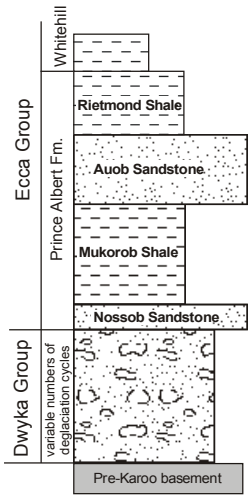


**Figure 2-5**

Simplified sequence of basal Karoo deposits in southern Namibia after Grill (1997).

$C_{org}$ rich deposits of the Whitehill Formation at the top of the Namibian sequences can be correlated by their facies and fossil content with time equivalent strata from the Karoo Basin in South Africa and Paraná Basin, Brazil (Oelofson, 1987; Zalán et al., 1990; Visser, 1995).

## 2.5 Paraná Basin, (Brazil)

After Eyles et al. (1993) three depositional successions (Silurian-Devonian, Late Carboniferous to Jurassic, and Cretaceous) record repeated phases of subsidence in the Paraná Basin. For the Late Carboniferous to Early Permian Itararé Group, the sedimentation started with the deposition of glacial sediments. The oldest Itararé sediments reflect glacio-lacustrine or brackish water settings but an increasing marine influence can be identified stratigraphically upwards through the Itararé Group. Changes between mudstones dominated sequences and diamictites (Zalán et al. 1990) point to comparable glacial/interstadial climate phases while sedimentation as reported from the South African and Namibian Dwyka Group sediments. Subsidence in the Paraná basin was asymmetrical with respect to dextral strike-slip movements along the Guapiara-Curitiba fracture zone, which transected the basin (Eyles and Eyles, 1993). Fully marine conditions are recorded by

the overlaying deltaic sandstones of the Rio Bonito Formation, siltstones of the Palermo Formation and petroliferous shales of the Irati Formation (Eyles et al., 1993).

The Irati Formation can be divided into the Taquaral, Assistencia and Serra Alta Member (Fig. 2-6). Within the latter two distinct levels of bituminous shales, occur southwards of the Curitiba-Guapiara fault zone. Northwards of the fault zone, thin layers of bituminous shales are interbedded with non-bituminous shales and dolomites. Siliceous nodules become increasingly important constituents. Further to the north, the Assistencia Member turns into a monotonous succession of thin layers of siliceous carbonates and shales, a few decimetres thick, some of them still bituminous (Zalán et al., 1990). The type of sedimentary environment is discussed controversially by several authors as it is pointed out by Faure and Cole (1999).

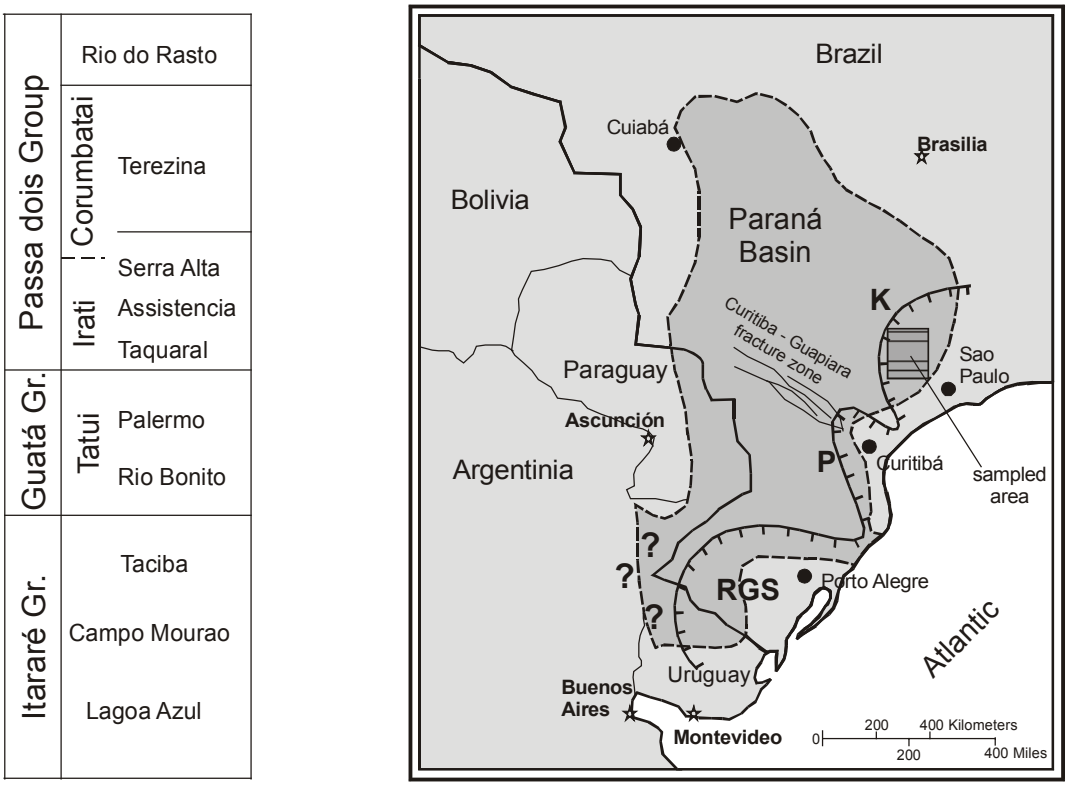


**Figure 2-6**

Location map of southeast Brazil showing the extend of the Paraná Basin with Kaokoveld lobe (K), Paraná lobe (P) and Rio Grande do Sul ice cap (RGS) after dos Santos (1996). Stratigraphical overview after Daemon & Quadros (1969).

After Oelofson (1987) the Irati Formation records the maximum marine extent of the Paraná Basin and contains a distinctive Mesosaurus fauna correlative with the one of the Whitehill Formation of South Africa and Namibia. Visser (1996) assumed movements along the northern part of the Atlantic fracture zone during the early Late Permian, which created a seaway between the Karoo-Kalahari and eastern parts of the Paraná Basin.

With focus on the upper Permian Irati Formation, samples were collected in order to study the glacial/ postglacial transition in the northern Paraná Basin. Most samples were taken in quarries along the highway SP-127 from Rio Claro to Piracicaba and close to Itapetininga in the state of Sao Paulo, Brazil (Fig. 2-6). Samples of the upper Itararé and lower Corumbatai Formation were collected in different quarries between Piracicaba and St. Barbara.
Sample lithologies reach from light coloured fluvial to fluvio-glacial sandstones of the Itararé and Guatá Groups to an interbedded sequence of dark grey shales with varying amounts of carbonate and light grey coloured carbonates in the Irati Formation for which a marine to lacustrine origin was proposed (Zalán et al., 1990). In the lower sections of the Irati Formation millimetre to several centimetres large chert concretions occur. The lower Corumbatai Formation consists of multi-coloured marls and siltstones.

## 2.6 Conclusion

The sample localities rested during the Upper Carboniferous to Early Permian under glacial climate conditions. Due to their position close to the continental boarders, changing sedimentary environments established. Cyclic sedimentary sequences were deposited in consequence of sealevel changes by waning and waxing of continental ice sheets. Dependent on the specific environment of the single sample localities, different sedimentary systems prevailed after the final retreat of the glaciers. Moderate to warm-humid climate conditions and tectonic processes influenced the sedimentation. Arid climate conditions and predominantly terrestrially influenced sedimentary systems characterize the late Permian to early Triassic deposition phase of the Karoo Supergroup.

# 3. Mineralogical composition

Quantitative XRD analyses are presented and compared with selected element concentrations. By means of XRD analyses from samples of the MPU and OGT cores, changes in mineralogical compositions can be detected. Changes between glacial and postglacial phase and during the later postglacial phase are expected. Upon interpretation of the clay mineralogical composition, diagenetic and low-grade metamorphic processes resulting from tectonic or magmatic activity must be taken into account. Results are used to correlate the outcrop sequence from the southern Karoo Basin with the cores sections.

## 3.1 Introduction

Element mobility is controlled by three main factors: (i) by the stability and composition of the minerals in the unaltered rock; (ii) by the stability and composition of the minerals in the alteration product, and (iii) by the composition, temperature and volume of the fluid phase (Rollins, 1995). If and how elements are leached, transported and precipitated from an aqueous solution depends on the ionic potential (charge/radius) of each element (Fig. 3-1).

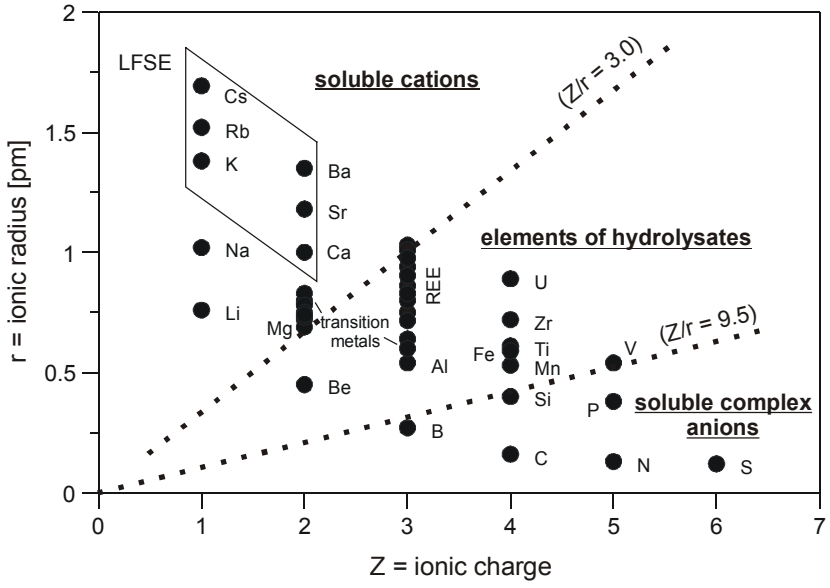


**Figure 3-1**

Geochemical classification of the elements, based on their ionic potential. Radii of ions in octahedral coordination adapted from Shannon (1976).

The ionic potential of an element determines its behaviour during formation of sedimentary rocks and is of essential significance in all mineral-forming processes in aqueous media. Elements with low ionic potential (Z/r < 3.0) such as sodium, calcium and potassium, remain in solution during weathering and transportation. Elements with intermediate ionic potential (3.0 < Z/r > 9.5) are participated by hydrolysis, their ions being associated with hydroxyl groups from aqueous solution. Elements with still higher ionic potential (Z/r > 9.5) form anions containing oxygen, which are usually again soluble (Mason and Moore, 1982). Incompatible elements belonging to the LFS group (Cs, Sr, K, Rb and Ba in Fig. 3-1) are mobile, whereas the HFS elements tend to be immobile. This latter group includes the REE, Sc, Y, Th, Zr, Hf, Ti, Nb, Ta and P. The transition metals Mn, Zn and Cu tend to be mobile, particularly at high temperatures in hydrothermal systems, whilst Co, Ni, V and Cr are immobile (Rollins, 1995).

Sediments are composed of the detrital fraction and new-formed minerals. The compounds contain information about the provenance (allochthonous fraction), and information about environmental/climatic conditions (autochthonous fraction). Therefore, bulk analyses represent a mixture of these factors. The portion of each fraction in the sediment depends largely on the depositional environment. Dependent on the geochemical composition of the provenance (acidic or basic rocks), weathering conditions (chemical or physical processes), transport and sedimentary environment (pH and Eh conditions), different clay minerals can be formed.

Which clay minerals would be newly-formed depended primarily on the element supply and hence on the solubility and mobilisation of the elements. Water as transport medium and the prevailing Eh and pH conditions are the limiting factors of element mobility. The pH of natural waters lies between 4 and 9. Aluminium and silica are immobile under these conditions whereas alkali and alkaline earth elements can be mobilised by normal weathering processes. $Ca^{2+}$ and $Mg^{2+}$ are soluble at pH values < 7.0. At alkaline conditions $Ca^{2+}$ forms amorphous hydroxides, which can also be mobilised, whereas Mg-hydroxides are only slightly soluble. The alkali elements K and Na can be mobilised over the whole pH range and be transported as cations in acidic or alkaline solutions (Mason and Moore, 1985).

Upon weathering, clay minerals are delivered to rivers by erosion where only minor further alteration takes place during transport to the ocean. Chamley (1989) pointed out that transportation by running water causes no identifiable mineralogical changes. Upon encountering seawater, the clay minerals are suddenly placed into a chemical environment different from that during weathering (Berner, 1971). Equilibrium processes take place and the primary formed clay minerals can be transformed into a second clay mineral generation, before reaching their final depositional environment.

During diagenesis and low-grade metamorphic processes, different mineral reactions can proceed (Fig. 3-2). The transition from the early diagenetic zone to the late diagenetic zone is indexed at circa 100°C, and the late diagenetic zone to anchizone transition occurs at circa 200°C (Merriman and Peacor, 1999). Illite tends to be stable during low metamorphic processes. Increasing illite crystallinity is used for temperature estimation during the burial history of sedimentary units (Weaver, 1960). Smectite is exhausted at the expense of illite and chlorite at increasing temperatures. The smectite to illite transition commences at temperatures in the range 70 to 90°C (Freed and Peacor, 1989). During intermediate stages, mixed-layer illite/smectite mineral associations can be formed. In these aggregates the illite content increases with prograding temperatures. The conversion of kaolinite to the iso-chemical mineral phases dicktite or nacrite, is related to processes with interacting hydrothermal solutions. The transformation of kaolinite to dicktite in the matrix of sandstones has been reported with increasing depth beginning at temperatures of approximately 120°C (Ehrenberg et al., 1993). Depending on the element supply during the late stage of deep burial diagenesis, kaolinite breakdown to illite or chlorite. At the beginning of metamorphism (T > 300°C) only sericite and chlorite remain as stable phases (Frey, 1987).

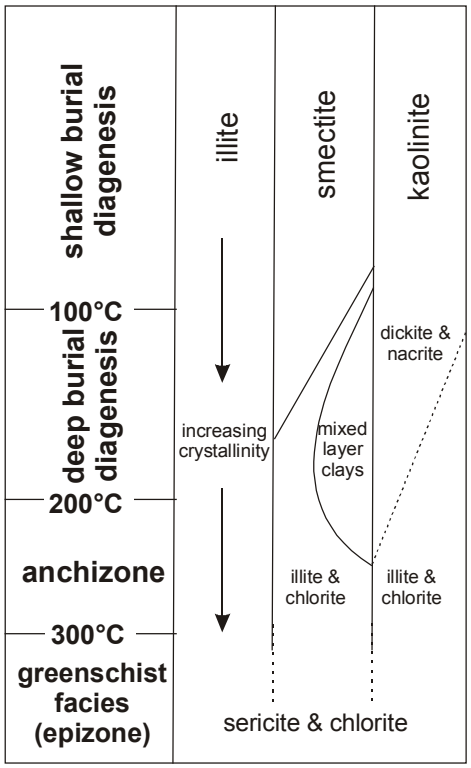


**Figure 3-2**

Stability fields of different clay minerals adapted from Tucker (1992). Temperatures of diagenetic stages from Merriman & Peacor (1999).

## 3.2 Prevalent minerals in sediments

Feldspar as the most abundant mineral in the upper crust behaves sensitive on chemical alteration processes. During cold climate phases, physical weathering has only small effects on the original mineral composition. Under warm and humid climate conditions, increasing precipitation rates favour chemical weathering processes. Kalifeldspar seems to be more resistant against chemical weathering processes than plagioclases or mafic minerals such as olivine or pyroxenes. The stability of plagioclase during surface weathering processes decreases generally with decreasing anorthite content (Füchtbauer, 1988).
The decay of potassium feldspar or muscovite to kaolinite occurs during intense chemical weathering of feldspar and leaching of $K^+$ and $SiO_2$ according to the equation (Berner, 1971):

$$2\ \mathbf{KAlSi_3O_8} + 3\ H_2O \rightarrow \mathbf{Al_2Si_2O_5(OH)_4} + 4\ SiO_2 + 2\ K(OH)$$

Kaolinite formation affords the complete removal of potassium; otherwise, formation of illite and/or montmorillonite will be favoured (Murray, 1988). In general, kaolinite results from subsurface weathering of granites or other acidic crystalline rocks at warm-humid climate conditions. Since the formation of kaolinite demands acidic environments, marine sedimentary systems are excluded from kaolinite formation (Millot, 1970). Sedimentary kaolinite deposits are associated with lacustrine, paludal, deltaic and lagoonal environments (Murray, 1988).
Illite/smectite mixed-layer aggregates are the most abundant clay minerals of sedimentary rocks. They can be formed from different precursors including muscovite, kaolinite and feldspar (Deer et al., 1992). Illite is chiefly formed during weathering in the moderately high pH range in cool to temperate climatic belts and appears to be the most stable clay mineral in marine environments. Most natural illites contain smectite layers, which are regularly or randomly interstratified. Illite/smectite interstratifications are preferentially found in brackish sedimentary environments. During prograding diagenetic processes the frequency of illite layers in illite-smectite aggregates increases (Lindgreen et al., 2000).
Further common constituents of the clay mineral fraction are smectites. The most characteristic features of smectites and montmorillonites are their expandability and the possibility of water adsorption between their structural layers. Depending on the substitution of aluminium by Mg or Fe, montmorillonites are distinguished in saponites (Mg-bearing) or nontronites (Fe-bearing) (Velde, 1992). Montmorillonite seems to be the product of simultaneous weathering of feldspars and ferromagnesian minerals from mafic igneous rocks or pyroclastics, accumulated under moderate pH, but low Eh conditions (Fairbridge, 1967).

During burial diagenesis of mudrocks, increasing depth and temperature facilitate the conversion of di-octahedral smectites (montmorillonite) to illite, and tri-octahedral smectites to chlorite. At stronger acidic conditions, smectites react to convert via smectite/kaolinite to kaolinite (Deer et al., 1993). Montmorillonite can be used to distinguish between different sedimentary environments. The occurrence of smectites is often associated with open marine conditions. The transformation of montmorillonite into chlorite, monitored by increasing marine conditions, has been reported by Millot (1970), and Velde (1995).
Chlorite is a common constituent of altered basic rocks, formed by chemical alteration of primary ferromagnesian minerals such as mica, pyroxene, amphibole, garnet and olivine (Velde, 1995). Some non-detrital chlorites in sediments can be formed during diagenesis by the reaction of dolomite and kaolinite. Griffin and Ingram (1955) pointed out that during progressively increasing salinity, kaolinite is replaced by chlorite. At strong acidic conditions, chlorite can be exhausted to form other clay minerals.

## 3.3 Sample localities

In figures 3-3 and 3-5 the mineral fractions in the sediments of the cores from the eastern Karoo Basin (MPU) and Kalahari Basin (OGT) are displayed (XRD analyses by D. Bühmann). Changes in the element contents of $Al_2O_3$, MgO, CaO, $Na_2O$ and $K_2O$ are compared with changes of the mineralogical composition. The element contents are normalised to 100% and plotted against their position in the sampled sequence. Carbonate bearing samples are excluded from this presentation. From the southern Karoo Basin an equivalent mineralogical data set is not available. Assuming that the investigated sequences can be correlated, the geochemical variations in the sediments from the southern Karoo Basin can be interpreted in consideration of the mineralogical composition of the cores (Fig. 3-7).

### 3.3.1 MPU core

Quantitative XRD analyses by D. Bühmann are displayed in figure 3-3. In accordance with investigations by Paige-Green (1980), Bühmann and Bühmann (1990) and Zechner (2003), quartz, albite, microcline, chlorite and illite are the main mineral phases in the glacial Dwyka sediments. Similar to the relative constant mineralogical composition, the element contents of $Al_2O_3$, MgO, CaO, $Na_2O$ and $K_2O$ show now marked variations in the basal part (basis to 50 m) of the sampled core (Fig. 3-3). Since carbonate bearing samples are unaccounted in the presentation, CaO contents of the Dwyka sediments reflect the anorthite component of the plagioclases. Calcite appears in single layers at the top of the Dwyka Group. MgO can be related to chlorite, whereas sodium is predominantly incorporated in feldspar.

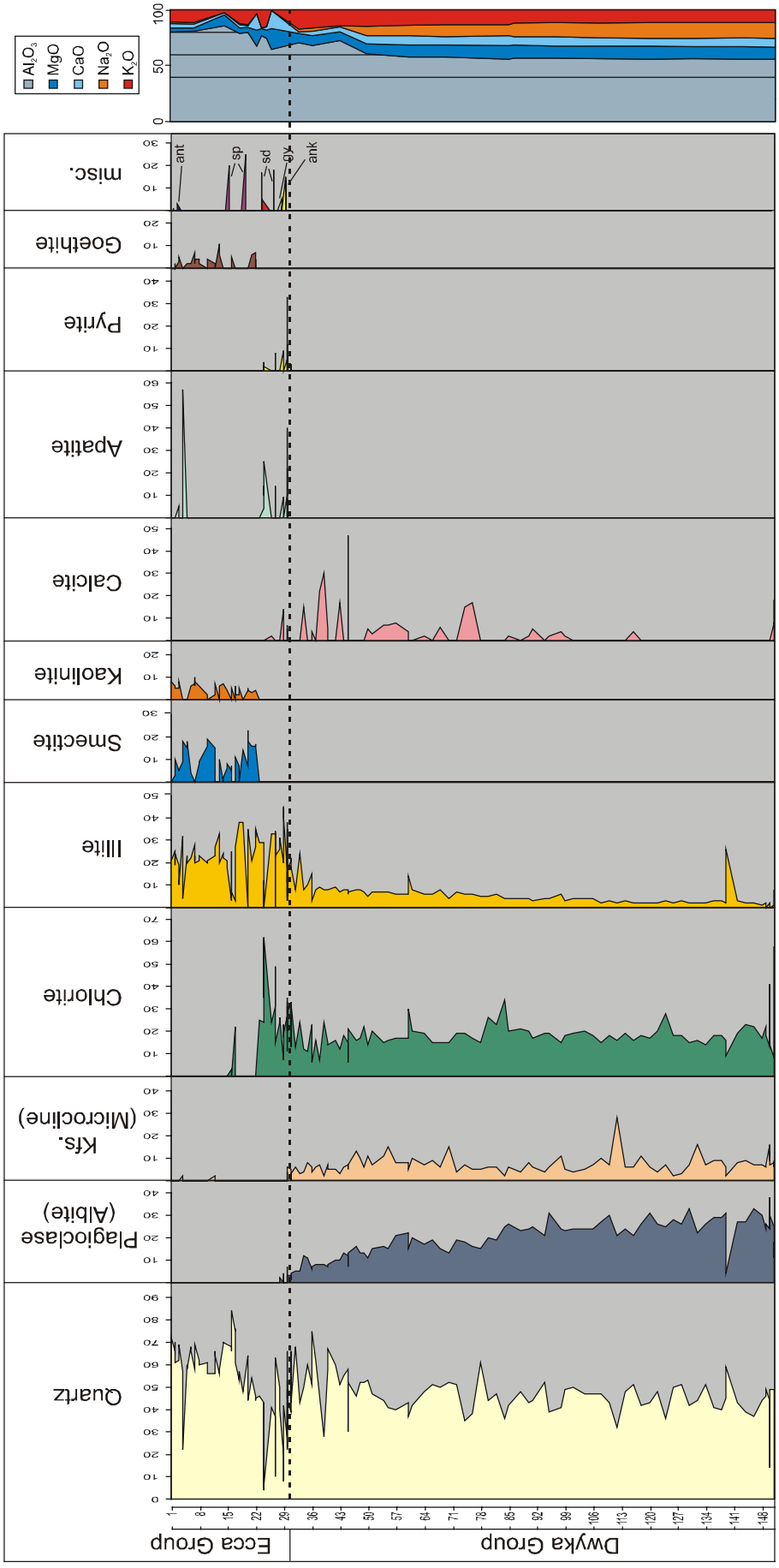


**Figure 3-3**
Vertical distribution of mineral associations in the MPU core from the south western Karoo Basin, determined by D. Bühmann ( by XRD) correlated with selected element oxide contents determined by XRF. ant = anatase, sp = spessartine, sd = siderite, gy = gypsum, ank = ankertie

Increasing illite versus decreasing K-feldspar contents, lead to relative constant $K_2O$ content in the glacial sediments. Despite of variations in the upper Dwyka Group, the proportion between clay minerals vs. feldspar and quartz remain constant. Comparable to the divergent trend between illite vs. microcline and between quartz vs. albite, also the chlorite/illite ratio change towards higher illite contents in the upper Dwyka Group (50 to 29 m).

At the top of the Dwyka Group, $Na_2O$, CaO and MgO contents decrease. In parallel albite and microcline disappear instantaneously. Beside quartz chlorite and illite become the dominant mineral phases. In consequence of higher illite and chlorite proportions the total amount of clay minerals raises form approximately 25% in the Dwyka sediments, up to 55% in the transition zone. In the upper core section the total clay mineral content decrease again to 35%. The disappearance of albite corresponds to decreasing $Na_2O$ and CaO contents. Significant variations in mineralogy and decreasing contents of mobile elements indicate incisive changes in climate and weathering conditions at the transition from the glacial Dwyka to the postglacial Ecca Group.

Additional to changes in the alumosilicate fraction also different minor phases occur at the Dwyka/Ecca boundary. Anoxic conditions in the sedimentary environment are indicated by the formation of apatite and pyrite. The occurrence of ankerite, gypsum and siderite in single layers, confirms the formation of anoxic conditions during deposition of the lower Prince Albert Formation. In the upper core section (22m to top), chlorite is replaced by smectite/montmorillonite as magnesium carrier. Reinforced chemical alteration is indicated by the appearance of kaolinite as additional clay mineral in the Prince Albert shales. Higher portions of clay minerals in the upper quarter of the core are in concert with increasing alumina and decreasing alkali and alkaline earth element contents.

Beside changes in the clay mineral fraction also changes in the Fe-phases occur in the upper core section. Goethite replaced pyrite as main Fe-phase in the upper 22 m of the core. Comparable to the clay minerals, Fe-phases can be used as facies indicators. Goethite and hematite are the most common $Fe^{3+}$ minerals in sediments near the surface (Füchtbauer, 1988). Their occurrence is restricted on aerobic environments, where $Fe^{3+}$ is precipitated as hydroxide or oxide. Under oxic conditions pyrite can be hydrolysed to goethite by the reaction (Berner, 1971)

$$4\ \mathbf{FeS_2} + 10\ H_2O + 15\ O_2 \rightarrow 4\ \mathbf{FeOOH} + 8\ H_2SO_4$$

Since anoxic conditions are presumed during deposition of the Prince Albert shales, secondary alteration processes must be responsible for these changes. The change from pyrite to goethite is accompanied by the change from chlorite/Illite to illite, smectite and kaolinite (Fig. 3-3).

Besides recent alteration processes also diagenetic and low metamorphic processes have altered the primary clay mineral association. As reported in the geological overview, the MPU drill site is situated at the transition between the unfolded Karoo Basin in the north, and the Cape Fold Belt in the south. In consequence, possible effects of the orogenesis on the mineralogical composition can be assumed.

The paragenesis of illite and chlorite is interpreted as progressive diagenetic conversion of a more varied clay composition over long geological times (Berner, 1971; Velde, 1992). At very low temperatures near the surface, the full range of soil clay minerals is stable (Fig. 3-2). Typical for this facies are smectites, mixed-layered alteration products and kaolinite. At increasing temperatures the soil clay mineral assemblage becomes unstable. Smectites are transformed into illite. The mineral paragenesis of illite/smectite mixed-layer minerals, chlorites, kaolinite and mixed-layer chlorite/smectites is typical for this burial stage. The last stage of clay mineral diagenesis is the beginning of metamorphism. The major phases are interlayered illite/smectite, illite, chlorite and kaolinite. The maximum stability of kaolinite is approximately 270°C (Velde, 1992). Therefore, the illite-chlorite- kaolinite-free assemblage marks the end of clay mineralogy and the beginning of metamorphism.

Chlorite formation is not restricted to the burial history of the sediments (Heim, 1990). Chlorite and illite can also be formed during early postsedimentary processes. The transformation of smectite and kaolinite into chlorite is favoured by high salinity (elevated $Mg^{2+}$ concentrations). Dependent on the $Mg^{2+}/K^{+}$ ratio, illite or chlorite appears as secondary clay mineral. Furthermore, Millot (1970) points out that illite and chlorite are the predominant clay minerals in glacial deposits.

To solve the question whether the present clay mineral assemblage represents primary sedimentary conditions or secondary alteration processes, $\delta^{18}O$ values of the silicate phases were determinated (Fig. 3-4a).

The Dwyka sediments exhibit relative constant $\delta^{18}O$ values (mean is +9.08‰) whereas postglacial sediments are markedly depleted in $^{18}O$ (mean is +7.44‰). The first positive and negative excursions of the $\delta^{18}O$ values are restricted on a black shale horizon in the upper Dwyka Group. The pattern repetitive at the Dwyka/Ecca boundary and possibly represents a local, earlier and failed deglaciation. In general the values are outstandingly low for fine-grained clastic sediments, which normally exhibit $\delta^{18}O$ values between +15‰ to +18‰ (Savin and Epstein, 1970). Minerals formed during surface weathering processes are enriched in $^{18}O$ because of high positive fractionation between the new-formed clay mineral and water at low temperatures. In consequence, sub-aerial weathering processes cannot be responsible for the low $\delta^{18}O$ values. It has to be mentioned that low $\delta^{18}O$ values must not necessarily record post-depositional (metamorphic) processes. Primary clay minerals, derived by

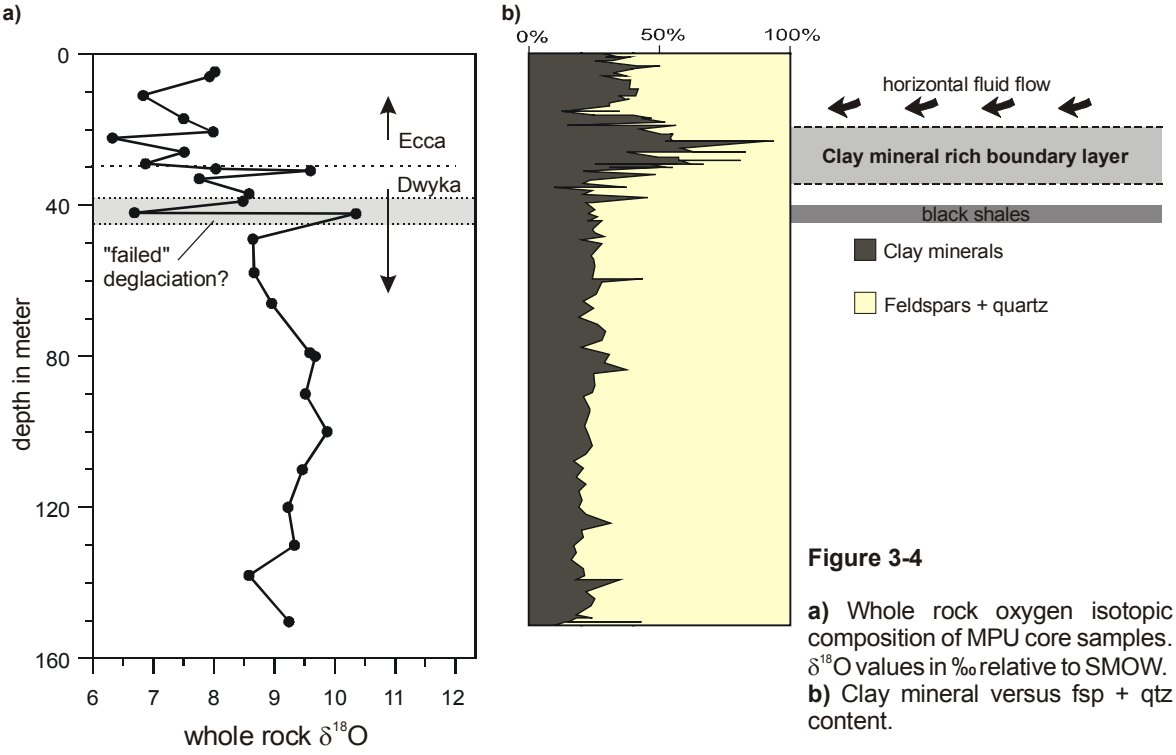


**Figure 3-4**

**a)** Whole rock oxygen isotopic composition of MPU core samples. $\delta^{18}O$ values in ‰ relative to SMOW. **b)** Clay mineral versus fsp + qtz content.

hydrothermal alteration of basalt, contain low $\delta^{18}O$ values in consequence of the elevated temperatures at which they formed (Mühlenbachs, 1987; Sharp, 1999). O'Neil (1987) points out that by isotope exchange reactions with environmental fluids only the isotopes are exchanged and no major-element chemical changes take place. On the other hand Cerling et al. (1985) described the mobilisation of sodium and potassium during hydration processes of siliceous volcanic glass accompanied by isotope exchange reactions.

In contrast to clay minerals, goethite shows only small fractionation to meteoric water (Yapp, 1987). Therefore, goethite formation lowers the $\delta^{18}O$ values of the whole rock oxygen isotopy. However, its appearance in the upper core section cannot be solely responsible for the light $\delta^{18}O$ values. Hence, the original $\delta^{18}O$ values of the clay minerals must be affected by external fluids, which alter the original $\delta^{18}O$ values by fluid/rock interaction during diagenesis or low-grade metamorphism at elevated temperatures.

Duane and Brown (1992) recognised northward migration of fluids during the development of the Cape Fold Belt that caused various low-temperature metamorphic reactions. By investigations of the oxygen isotopic composition of intercalated tuff layers in the Collingham Formation, Knütter (1994) detected very light $\delta^{18}O$ values (around +5‰). In contrast determination of $\delta^{18}O$ values of different tuffs from the Westerwald area (Scheffler, 1999; Hahn, 1999) prove that the volcanic ashes underwent almost immediately low temperature isotope exchange processes, which led to $\delta^{18}O$ values up to +22‰ in last weathering stages. Therefore, the light $\delta^{18}O$ values of the tuff layers in the southern Karoo Basin derive from

post-depositional interaction by meteoric water at hydrothermal conditions. By the means of fluid inclusion studies Egle (1996) estimated temperatures of approx. 200°C for the fluid/rock interaction. Quartz-water oxygen isotope fractionations at this temperature indicate meteoric water as main source for the fluids (Egle, 1996).

Different processes affected the mineralogical, chemical and isotopic composition of the sediments from the MPU core. During the initial phase (sedimentation), the composition of the clastic debris was chiefly controlled by physical weathering processes. Low chemical weathering during the glacial phase, favoured the deposition of quartz, feldspar and clay minerals. The clay mineral fraction was predominantly composed of illite and chlorite as major constituents in glacial sediments (Millot, 1970). Low portions of smectite or illite/smectite interstratifications formed additional constituents of the primary mineralogical composition. During burial diagenesis, the variety of different clay minerals was reduced to the stable phases chlorite and illite. With the onset of postglacial climate conditions, increasing chemical weathering of the parent rocks reduced the amount of feldspar in the siliciclastic debris. Sediments with high clay mineral contents accumulated in anoxic environments as indicated by the occurrence of pyrite in the lower Ecca shales. Due to elevated chemical weathering in the provenance, illite, smectite, kaolinite and in lower abundance chlorite were transported into the basin. This transition zone with high clay mineral content (55%) demarcate the underlying glacial sediments form the postglacial Ecca shales (Fig. 3-4b).

It can be assumed that during prograding diagenesis also the clay mineral fraction of Ecca sediments changed from a more variable composition to the stable clay mineral paragenesis of illite and chlorite. Today's occurrence of smectite and kaolinite in the upper core section can be related to alteration processes in context with fluid migration into the Karoo sediments during the Cape orogenesis. Especially the light $\delta^{18}O$ values of the Ecca shales point to the formation of kaolinite and smectite as consequence of fluid infiltration processes at elevated temperatures (~200°C). The different $\delta^{18}O$ values between Dwyka and Ecca Group can be explained by fluid flow along horizontal pathways (Knütter, 1994). In this context, the clay mineral rich transition zone had possibly acted as boundary layer during fluid flow (Fig. 3-4b). The black shales close to the top of the Dwyka Group might represent a further boundary layer with lower permeability. Because changes in the clay mineral fraction proceed concomitant to the changes of the Fe-phases, the oxidation of pyrite to goethite was also triggered by the infiltrating fluid.

It can be concluded that the total amount of clay minerals represents climate variations whereas the clay composition is at least in parts affected by fluid interaction as well as low metamorphic processes and, therefore display the post-depositional evolution.

## 3.3.2 OGT core

XRD analyses of core samples from Orapa are discussed by Bühmann and Atanasova (1997). The sedimentary record commences in the lower Ecca Group (Tswane Formation) with the supply of siliciclastic material. The clastic fraction is composed of quartz and kaolinite (Fig. 3-5). Microcline and illite occur as minor phases. Comparable to the upper part of the MPU core, sediments in the lower OGT core exhibit elevated $Al_2O_3$ and low alkali and alkaline earth element contents. The occurrence of kaolinite as single clay mineral phase, points to intensive chemical leaching processes in the provenance or in the sedimentary environment. Slightly elevated CaO contents in the Tswane Formation derive from low proportions of siderite and calcite in the sediments.

Beside the occurrence of siderite and barite in single layers, pyrite and high $C_{org}$ contents in the entire Ecca Group indicate anoxic conditions in the sedimentary environment. The occurrence of kaolinite is closely related to the $C_{org}$ rich sediments of the Ecca Group. Acidic solutions from decomposition processes of the organic matter might provide leaching of alkali and alkaline earth elements and lead to the breakdown of a former more variable clay mineral association. Feldspar bearing sandstone horizons represent the Mea Formation. The presence of microcline and plagioclase is indicated by elevated $K_2O$ and $Na_2O$ contents. Increasing albite content from the Mea Formation to the Beaufort Group, point to reduced chemical weathering in the provenance. Shales of the Tlapana Formation represent the top of the Ecca Group. Illite appears as further constituent of the sediment beside kaolinite, quartz, microcline and plagioclase. In accordance with the mineralogical composition, the geochemical analyses yield elevated $K_2O$ contents in the Tlapana Formation. Chemical weathering is reduced in the upper Ecca Group. However, mobilisation of alkali and alkaline earth elements and formation of clay minerals persists. A marked change in the composition of the clay mineral fraction is indicated by smectite and illite/smectite interstratifications in the Tlhabala Formation. Their appearance is used to demarcate the mudstones of the Tlhabana Formation from the underlying Ecca Shales (Bühmann and Atanasova, 1997). Concomitant with decreasing kaolinite versus increasing portions of di-octahedral smectite and illite, the alkali and alkaline earth element contents rise. In contrast to the Ecca Group and the overlying Ntane Formation, microcline is absent in the Tlhabala Formation. Beside quartz, albite, illite, di-octahedral smectite and illite/smectite interstratifications, calcite becomes an additional constituent of the Tlhabala sediments.

Reduced chemical weathering conditions in the Tlhabana and Ntane/Mosolotosane Formations are indicated by elevated alkali and alkaline earth elements contents, representing the change from warm-humid climates during the lower Permian Ecca Group to more arid conditions in the middle Permian Beaufort Group.

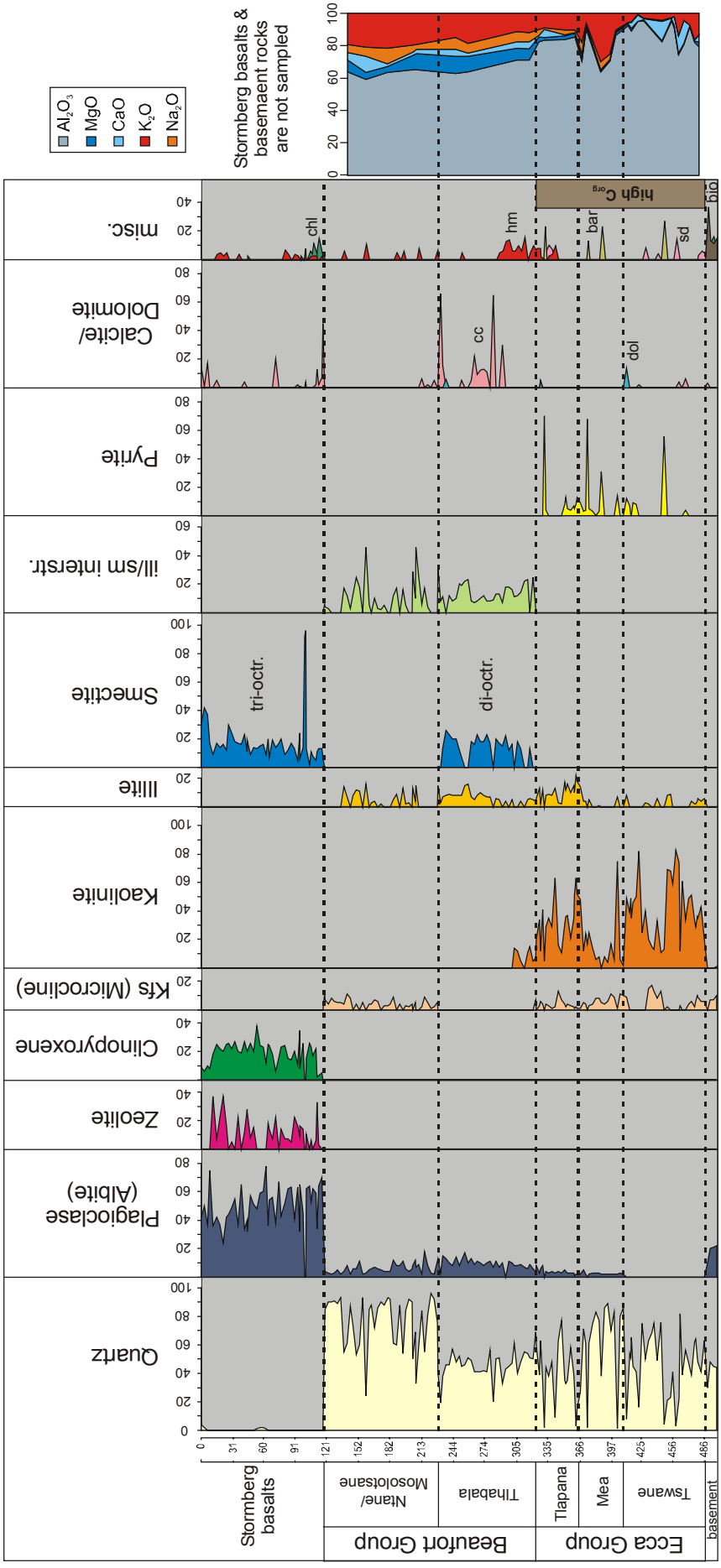


**Figure 3-5**

Vertical distribution of mineral associations in the OGT core determined by D. Bühmann (XRD) correlated with selected element oxide contents determined by XRF.
chl = chlorite, cc = calcite, dol = dolomite, hm = hematite, bar = baryte, sd = siderite, bio = biotite

Microcline and plagioclase bearing sandstones represent the Ntane/Mosolotosane Formation. Illite and illite/smectite interstratifications are constituents of the clay mineral fraction. Pure smectite is absent in the Ntane sandstones. The Stormberg basalts in the upper 120 m of the core produced severe changes in the mineralogical composition (Fig. 3-5). Beside primary magmatic plagioclase and clinopyroxene, tri-octahedral smectite (saponite), corrensite (chlorite/smectite interstratifications), and different zeolites occur as alteration products. Chlorite as further alteration product of mafic rocks is recorded in the bottom layers of the basalts.

Similar to the MPU core, the determination of the whole-rock oxygen isotopic signal can provide further information on the post-sedimentary evolution of the clay minerals in the OGT core. $\delta^{18}O$ values, presented in figure 3-6, reach from +8‰ in the Tswane up to +17.8‰ in the Tlhabala Formation. The kaolinite bearing Ecca sediments exhibit mean $\delta^{18}O$ values of +10.62‰. If kaolinite was formed during weathering, the clay minerals should be markedly enriched in $^{18}O$. Average $\delta^{18}O$ values for normal shales are between +16 to +18‰ (Savin and Epstein, 1970). The low $\delta^{18}O$ values point to hydrothermal processes that re-equilibrate ancient $^{18}O/^{16}O$ ratios. Values close to 18‰ in the Tlhabala Formation (mean is +15.37‰) can be associated with clay mineral formation during weathering processes. Sandstones of the Ntane Formation, exhibit average $\delta^{18}O$ values of +12.03‰. The slightly elevated $\delta^{18}O$ values, in comparison to average $\delta^{18}O$ values of +10‰ for sandstones (Hoefs, 1997), point to clay minerals in the Ntane sandstone matrix.

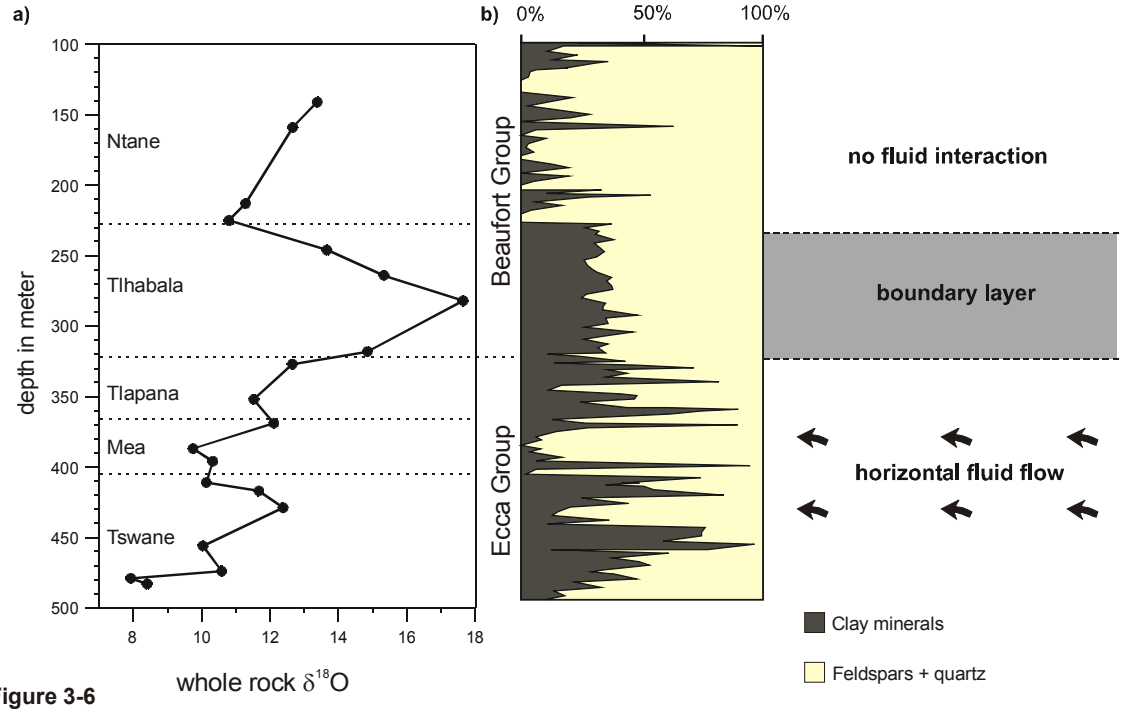


**Figure 3-6**

**a)** Whole rock oxygen isotopic composition of OGT core samples. $\delta^{18}O$ values in ‰ relative to SMOW.
**b)** Clay mineral versus feldspar + quartz content.

In combination with oxygen isotope data and clay mineralogy the following processes can be inferred. During sedimentation of the Ecca Group, clastic debris was deposited under anoxic conditions. This is evidenced by high $C_{org}$ and pyrite contents. The high clay mineral content up to 80%, points to intensive chemical weathering of the precursor rocks at warm-humid climate conditions. A primary, more variable clay mineral association was possibly penetrated by acidic solutions from decomposition of organic matter. Under acidic conditions kaolinite finally remained as single clay mineral.

The relative low $\delta^{18}O$ values in the Ecca shales of approximately +11‰, point to hydrothermal processes, which reduced primary high $\delta^{18}O$ values of around +20‰. Since the shales and mudstones of the overlying Tlhabala Formation exhibit significantly higher $\delta^{18}O$ values, a horizontal fluid flow can be assumed. The heat source for these processes was the emplacement of the kimberlite. The clay rich Tlhabala Formation acted similar to the transition zone at the Dwyka/Ecca boundary in the Karoo Basin, as a boundary layer. Due to the low permeability as a consequence of the high clay mineral content, the original oxygen isotope ratio and mineralogical composition was preserved. The paragenesis illite+smectite+I/S is associated with early to late diagenetic processes at approximately 120°C. The convention of di-octahedral smectites to mixed-layer illite/smectite (I/S) and illite requires minimum temperatures between 70° to 90°C and a maximum temperature of 300°C, when the mixed layer aggregates convert to pure illite or muscovite (Merriman and Peacor, 1999). The clay mineral assemblage of the Ntane sandstones is composed of illite and I/S. Due to the high temperatures from the overlying Stormberg basalts smectite is possibly already exhausted. However, it is questionable if the Tlhabala and Ntane Formations contained the same mineralogical composition since the sedimentation progressively changed to terrestrial conditions during the Beauford Group. The overlying Stormberg basalts contain the mineral paragenesis smectite+corrensite+chlorite. This paragenesis is a common constituent of hydrothermal altered volcanic rocks (Inoue and Utada, 1991). With increasing diagenesis (T > 120°C) smectite is generally replaced by corrensite, which in turn is replaced by chlorite in the late diagenetic zone or low anchizone at approximately 260°C (Frey, 1999).

### 3.3.3 Southern Karoo Basin

The Dwyka Group in the southern Karoo Basin can be characterised as an generally carbonate free member of the Karoo Supergroup (Fig. 3-7a). The clastic sediments contain low CaO contents in relation to the average shale composition of Wedepohl (1967). Similar to the MPU core, these uniform values derive from unaltered plagioclase in the glacial sediments. A first significant change in sedimentation is marked by elevated CaO and $P_2O_5$

contents in the upper Dwyka Group (Fig. 3-7a). Comparable to the MPU core, elevated CaO contents at the Dwyka/Ecca boundary indicate the formation of phosphate minerals. $P_2O_5$ content decreases in the following carbonate rich horizons, which are intercalated in Prince Albert shales. At the top of the Prince Albert Formation high CaO contents again mark significant changes of sedimentary conditions.

Carbonate-bearing black shales of the Whitehill Formation are represented by high CaO values. The occurrence of dolomite in single horizons is indicated by elevated magnesium contents (Fig. 3-7a). In the overlying Collingham Formation carbonates form only minor constituents. Input of clastic material dominates the sedimentation during the Vischkuil, Laingsburg and Fort Brown Formation.

Similar to the MPU and OGT cores, the clastic fraction can be described by the $Al_2O_3$, $Na_2O$, $K_2O$, CaO and MgO contents (Fig. 3-7b). Changing element contents in the Dwyka sediments reflect variable climate conditions. Increasing $Al_2O_3$ and $K_2O$ versus decreasing $Na_2O$, CaO and MgO contents during interstadial phases, mirror increasing illite and/or kaolinite proportions at the expense of albite and chlorite. Chlorite and illite are the major constituents of the clay mineral fraction of the Dwyka Group. Smectite and kaolinite appear only in low proportions (Zechner 2003). By measurements of the illite crystallinity the grade of metamorphism for the postglacial units in the southern Karoo Basin is between the higher diagenetic to lower anchizone. High illite crystallinity in the Dwyka samples derives from magmatic or metamorphic illite/muscovite in the glacial sediments (Zechner, 2003).

The Dwyka/Ecca boundary represents the transition from glacial to postglacial climate conditions. At the top of the Dwyka Group, similar variations in the element contents as during the interstadials can be observed. Decreasing CaO and $Na_2O$ contents can be associated with the lack of plagioclase in the autochthonous mineral fraction. Illite as major clay mineral in the Prince Albert shales is indicated by increasing $K_2O$ contents. Elevated $Al_2O_3$ contents in the lower Prince Albert Formation can be predominantly related to a supply of clay minerals. Higher proportions of clay minerals are favoured by the breakdown of feldspar during chemical weathering processes in the provenance. Highest alumina contents are reached in the middle Prince Albert Formation before the $Al_2O_3$ contents decrease again. Similar variations are recorded in the MPU and OGT cores, where increasing chemical weathering preferred the formation of kaolinite. MgO contents decrease at the Dwyka/Ecca boundary. Sediments of the middle Prince Albert Formation exhibit slightly higher MgO contents, before in the upper Formation and in the following Whitehill Formation the MgO contents decline again. It can be assumed that comparable to the MPU and OGT cores, chlorite is replaced by smectite as Mg container in the postglacial sediments.

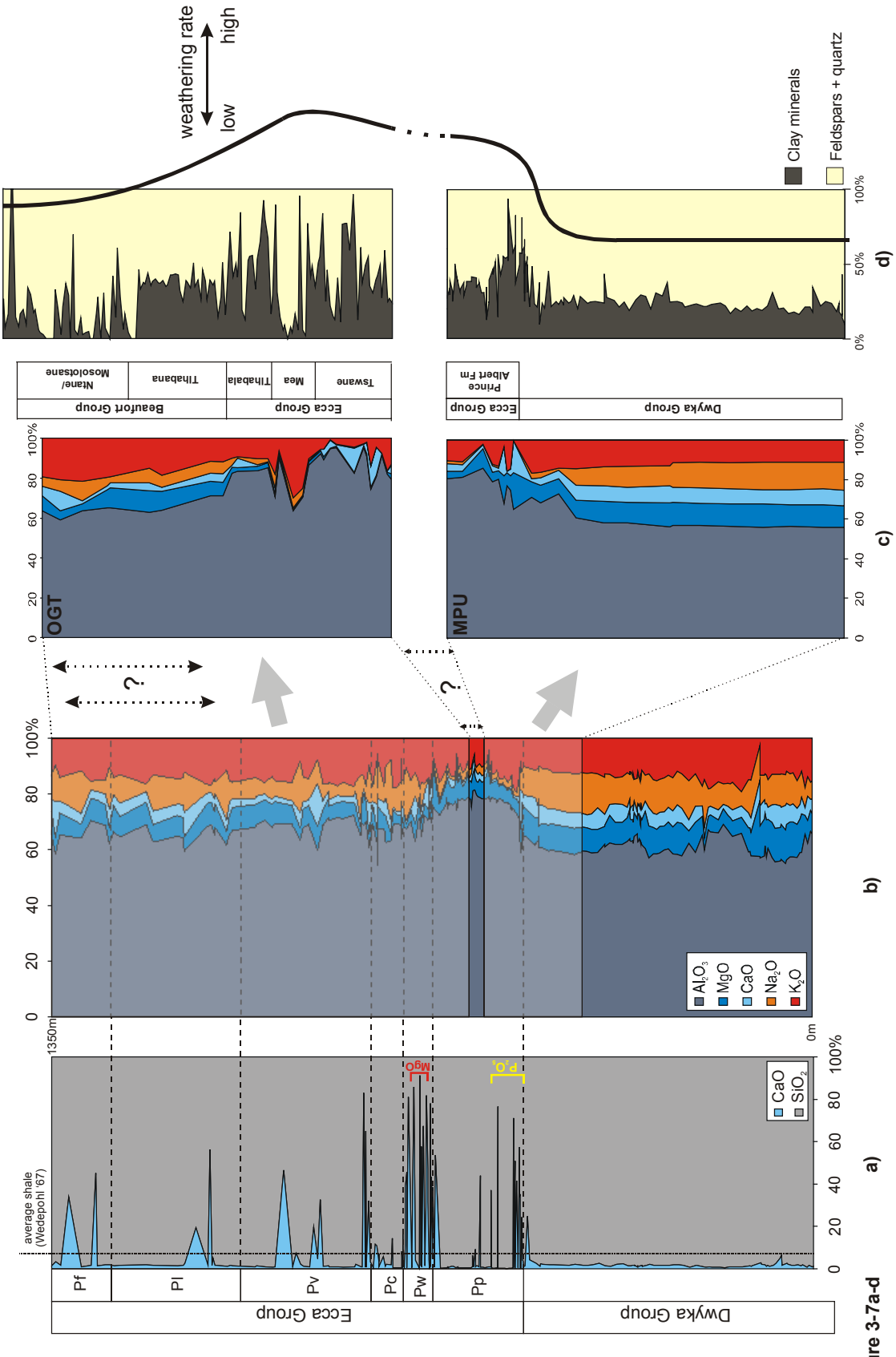


**Figure 3-7a-d**

**a & b)** Vertical distribution of selected element contents from the sample locality in the southern Karoo Basin. Correlated sections are shaded.
**c & d)** Correlated element contents of the MPU and OGT cores and distribution of the clay versus non-clay mineral fraction as index of chemical weathering. Uncertainties in the correlation of the sequences are labeled with ?.

Increasing alkali and alkaline earth element contents in the upper Ecca Group of the OGT core are related to the occurrence of plagioclase resulting from reduced chemical weathering. Comparable to the Kalahari Basin the sedimentary environment of the Karoo Basin shifted during the middle Permian into arid climate belts. Weathering conditions changed and physical weathering and terrestrially influenced sedimentation dominated the middle to upper Permian deposition phase. For the Vischkuil, Laingsburg and Fort Brown Formation the element contents show no further climate controlled changes (Fig. 3-7b). Single peaks in the upper parts of the sequence resulted from regional changes in the sediment supply. Similar to the OGT core, the siliciclastic fraction is dominated by quartz and feldspar. The clay mineral fraction is composed of various clay minerals with illite and chlorite as major constituents.

In figure 3-7c the variations of the element contents of the sample localities discussed before are correlated. Comparable changes in the element contents can be recognised in all three successions. These variations were primarily controlled by climate changes and not by postsedimentary processes such as diagenesis or fluid infiltration. Therefore, despite of differences in sedimentary environments and during the burial history, the cores can be combined to a continuous record of climate variations from the Upper Carboniferous to the Middle/Upper Permian. Climate induced changes of the sedimentary composition are recorded in lower parts of both sequences and can be used for correlation. Uncertainty resides in the estimation of the gap between the MPU and OGT core. Considering the changes in figure 3-7b, the offset between top MPU and basis OGT seems to be rather small. Further uncertainty exists in the correlation of the upper part of the OGT core to the succession of the Karoo Basin, since significant marker horizons are missing.

### 3.3.4. Paraná Basin

The sampled sequence from the Paraná Basin is displayed in figures 3-8a & b. Due to high carbonate contents in the Irati Formation, MgO and CaO contents are excluded from the presentation.

High sodium and potassium contents in the sandstones of the Itararé (Dwyka Group equivalent) and Tatui Formation (Prince Albert Formation equivalent) point to the occurrence of illite and feldspar of the sediments (Fig. 3-8a). The whole-rock oxygen isotopic signal of the silicate phases of the Itararé sandstones is on average +12.07‰ (Fig. 3-8b). Additional clay minerals in the sandstones formed during weathering processes lead to higher $\delta^{18}O$ values than literature data (+10‰, Hoefs, 1997). Decreasing $Na_2O$ contents in the lower Tatui Formation correlate with high $\delta^{18}O$ values of +18.41‰. Since the $Na_2O$ contents remain relative constant, increasing illite versus decreasing feldspar contents are responsible for

these variations. $\delta^{18}O$ values of the siltstones in the upper Tatui Formation range around 14‰. At the transition from the Tatui to Irati Formation, the $\delta^{18}O$ values rise from +14.22 to +17.24‰. The positive excursion can be explained by decreasing feldspar versus increasing clay mineral proportions. This is evidenced by constant $Al_2O_3$ and $K_2O$ versus decreasing $Na_2O$ contents.

Chert concretions in the lower Assistencia Member are indicated by high $SiO_2$ contents (95% $SiO_2$) and high $\delta^{18}O$ values above +25‰. Due to the large oxygen isotope fractionation between $SiO_2$ and water at low temperatures, biogenic silica and cherts have the highest $^{18}O/^{16}O$ ratios observed in rocks (Hoefs, 1997). Especially $\delta^{18}O$ values of biogenic cherts can reach +44‰ whereas silicified ash fall tuffs in general exhibit lower $\delta^{18}O$ values. Therefore, already minor chert contents in clastic sediments can massively influence the oxygen isotope ratio.

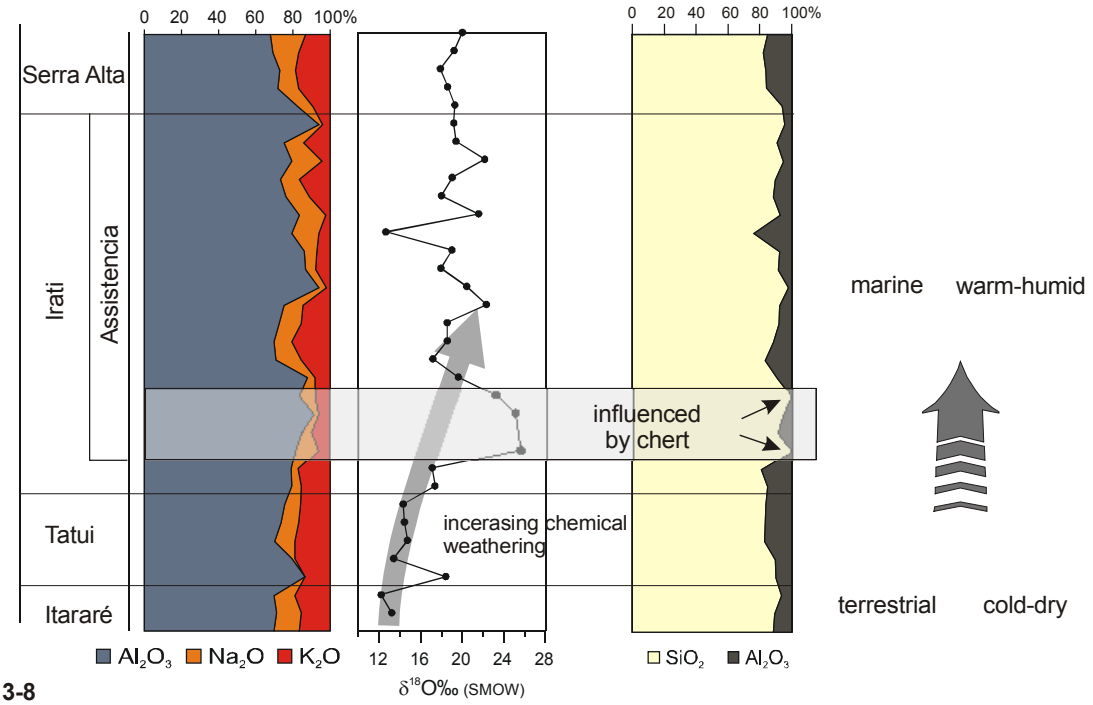


**Figure 3-8**

Variations in selected element contents and the oxygen isotopy of the silicate fraction of samples from the Paraná Basin.

The $\delta^{18}O$ values in the upper Assistencia Member (mean is +19‰) correspond with literature data for average shales (Savin and Epstein, 1970). Clays formed on the continent by interaction of isotopically light ground water acquire lower $\delta^{18}O$ values (detrital smectites: +16 to +18‰; Savin and Epstein, 1970) than authigenic clays, which were formed in the oceans (marine smectites: +26 to +31‰; Savin and Epstein, 1970) in consequences of in $^{18}O$-enriched water. In contrast to the African sample localities the $Na_2O$ contents in the Irati Formation (Whitehill equivalent) do not decrease. Therefore beside illite, authigenicly formed smectite as Na-bearing phase can be assumed as additional clay mineral in the Irati shales.

Since the aluminium content is not markedly elevated in the Assistencia Member increasing clay mineral contents cannot be responsible for the increasing $\delta^{18}O$ values. Assuming that this variation is caused by fractionation processes between newly formed clay minerals and water, than the temperature, salinity or the isotopy of the interacting water must have changed (Scheffler et al., 2001). The high pristine $\delta^{18}O$ values from the northern Paraná Basin indicate that the sediments were not influenced by hydrothermal alteration processes, which would lower the oxygen isotope signal as reported from the Karoo Basin.

## 3.4 Conclusion

The mineralogical and oxygen isotopic composition was influenced by different sedimentary and post-sedimentary processes. Climate conditions and the sedimentary environment are the major controlling factors for the primary clay mineral composition. Postsedimentary processes (diagenesis, hydrothermal alteration) were detected by the combined approach of mineralogical analyses and whole-rock oxygen isotope data. By means of the significant changes in the mineralogical composition the discussed sequences can be combined to provide an overview of the climate evolution during the late Palaeozoic in south Gondwana.

In consequence of glacial climatic conditions, physical alteration processes dominated the weathering during deposition of the Dwyka Group sediments (or equivalents). Indicated by low clay mineral contents, the primary minerals such as feldspars, resided unaltered during transport and deposition (Fig. 3-7d). Increasing chemical weathering at the end of the Dwyka Group sedimentation was triggered by warm and humid climate conditions. Mobile elements were leached from the precursor rocks and newly formed clay minerals replaced the feldspar fraction (Fig. 3-7d). For the upper Ecca to lower Beaufort Group in lower-middle Permian, arid climatic conditions are indicated by re-increasing alkali and alkaline earth element contents and higher feldspar proportions.

In the southern Karoo Basin, the postsedimentary evolution was influenced by fluid migration from the rising Cape Fold Belt into the sedimentary units of the Karoo Basin. By these fluids the $\delta^{18}O$ signal of the clay minerals was altered, whereas the element geochemical composition seems to have been preserved. Also in the Kalahari Basin hydrothermal induced alteration can be detected by low $\delta^{18}O$ values of the clay mineral rich shales in the Ecca Group. These processes can be related with the intrusion of the Kimberlite during the middle Cretaceous. Clay mineral rich shales in the Karoo and Kalahari Basin acted as boundary layers for a horizontal fluid flow. In the northern Paraná Basin the original $\delta^{18}O$ values seems to be conserved. Increasing $^{18}O/^{16}O$ ratios from the Tatui to the Irati Formation indicate changes in the sedimentary environment.

- *The Dwyka sediments are predominantly composed of quartz, plagioclase, microcline, illite and chlorite.*
- *At the Dwyka/Ecca boundary additional mineral phases (pyrite, gips, P-phases such as apatite or dahlite, carbonates) occur in significant concentrations.*
- *During the post-glacial phase the proportion of the clay mineral fraction increased.*
- *New clay minerals beside illite occurred in the lower Ecca Group (kaolinite and smectites).*
- *The Whitehill Formation is characterized by significant concentrations of mineral phases such as pyrite, calcite and dolomite.*
- *During deposition of the post-Whitehill Formations (middle to upper Ecca Group) the feldspar proportion re-increased.*

# 4. Element geochemistry

The element geochemical composition provided information on climatic or environmental conditions. For introduction, $K_2O/Na_2O$ versus $SiO_2/Al_2O_3$ diagrams are used for a geochemical discrimination of the sediments. Variations in major and trace elements, normalised on aluminium, are discussed with regard to climate and/or environmental changes. By means of cluster analysis, characteristic element associations can be defined and their variation during changing climate conditions discussed. Ternary diagrams of the system $Al_2O_3$-$Na_2O$-$K_2O$ are used to report element mobilisation as consequence of chemical alteration processes. At the end of this chapter a preliminary conclusion reviews changing environmental and climate conditions, which influenced the sediment geochemical composition.

## 4.1 Discrimination of the samples by major elements

$SiO_2/Al_2O_3$ ratios are used to differentiate mature and immature sediments (Potter, 1978). Quartz rich sandstones contain high $SiO_2/Al_2O_3$ ratios in consequence of the successive breakdown of aluminosilicates during weathering and transport. Sediments still containing aluminosilicates can be subdivided into two classes due to different $K_2O/Na_2O$ ratios. Low $K_2O/Na_2O$ ratios of graywackes indicate the dominance of albitic plagioclase over potassium feldspars and mica (Pettijohn et al., 1972). By higher K-feldspar contents, chemical analyses of arkoses yield lower $K_2O/Na_2O$ ratios.

It has to be remarked that beside the composition of the clastic detritus, syn- and post-sedimentary processes can alter these element ratios. The type of cementing agent, influenced by diagenetic and low-grade metamorphic processes as well as by the sedimentary environment, may lead to enrichment or depletion of miscellaneous elements. In comparison with the well-established classification of igneous rocks, Pettijohn et al. (1972) point out that a chemical classification of sediments is often not in accordance with the petrographic analysis. Therefore, a geochemical classification can lead to other or contrary nomenclatures as compared to mineralogical or textural rock classifications.

A differentiation between graywackes and arkoses also implicates a discussion about provenance and depositional environment. Arkoses can be defined as feldspar rich sandstones whereas graywackes additionally containing rock fragments and detrital mica beside a plagioclase dominated feldspar fraction (Füchtbauer, 1988). The matrix of both rock types can be different. In arkoses, kaolinite and in graywackes, chlorite can occur as

additional clay mineral of the matrix. The feldspar rich detritus of graywackes and arkoses requires an environment in which erosion, transport and deposition are rapid enough, to preclude chemical weathering of the precursor minerals. In this context the relief is one controlling factor for deposition of arkoses or graywackes. Both rock types can be formed under humid tropical as well as under arid or arctic climate conditions (Pettijohn et al., 1972). Graywackes are in general associated with turbiditic deposits in distal basin positions whereas arkoses are often associated with deltaic environments in rather proximal settings. Whether this classification is applicable to the investigated sedimentary sequences has to be discussed.

However, the used element ratios should contribute to a first overview of the sediments from the different localities in southern Gondwana. The samples are plotted in the $K_2O/Na_2O$ versus $SiO_2/Al_2O_3$ diagrams in figures 4-1a-f with classification after Wimmenauer (1984).

### 4.1.1 $K_2O/Na_2O$ vs. $SiO_2/Al_2O_3$

In figure 4-1a samples from the southern Karoo Basin are labelled by their stratigraphic position. Samples of the Dwyka Group (squares) plot predominantly in to the field of graywackes. A second group comprises samples from the Prince Albert and Whitehill Formations (crosses). In contrast to the Dwyka sediments, the samples of the lower Ecca Group are distributed more dispersedly. By higher $K_2O/Na_2O$ ratios the centre of the scatter plot shifts towards the field of arkoses and shales. Especially in the case of the samples within the field of arkoses, it has to be emphasised that the lower Ecca Group comprises predominantly shales. Therefore, the sample discrimination by geochemical aspects can only indicate “arkosic composition” but cannot be interpreted in view of petrographic or textural aspects. Samples from the middle to upper Ecca Group (Collingham to Fort Brown Formation), are distributed in-between the fields of graywackes and shales (triangles).

The majority of samples (squares) from the lower MPU core by their low $K_2O/Na_2O$ ratios and moderate $SiO_2/Al_2O_3$ ratios are classified as graywackes (Fig. 4-1b). Samples at the transition to the Ecca Group contain higher $K_2O/Na_2O$ ratios and therefore plot within the field of arkoses. The closer the samples are situated to the Dwyka/Ecca boundary the more the $SiO_2/Al_2O_3$ ratios decrease, due to the higher clay content of the samples. Geochemical analyses of postglacial sediments yield in general lower $SiO_2/Al_2O_3$ and higher $K_2O/Na_2O$ ratios and are therefore classified as shales. In comparison to the sediments from localities discussed before, all samples from the OGT core contain $K_2O/Na_2O$ ratios above 1.5 (Fig. 4-1c). The majority of the Ecca Group sediments (crosses) plot into the field of shales. The geochemical classification of the quartz and feldspar rich samples of the Mea Formation confirms their arkosic composition. Samples of the lower Beaufort Group (diamonds) have higher $SiO_2/Al_2O_3$ and lower $K_2O/Na_2O$ ratios than the underlying Ecca Group sediments and

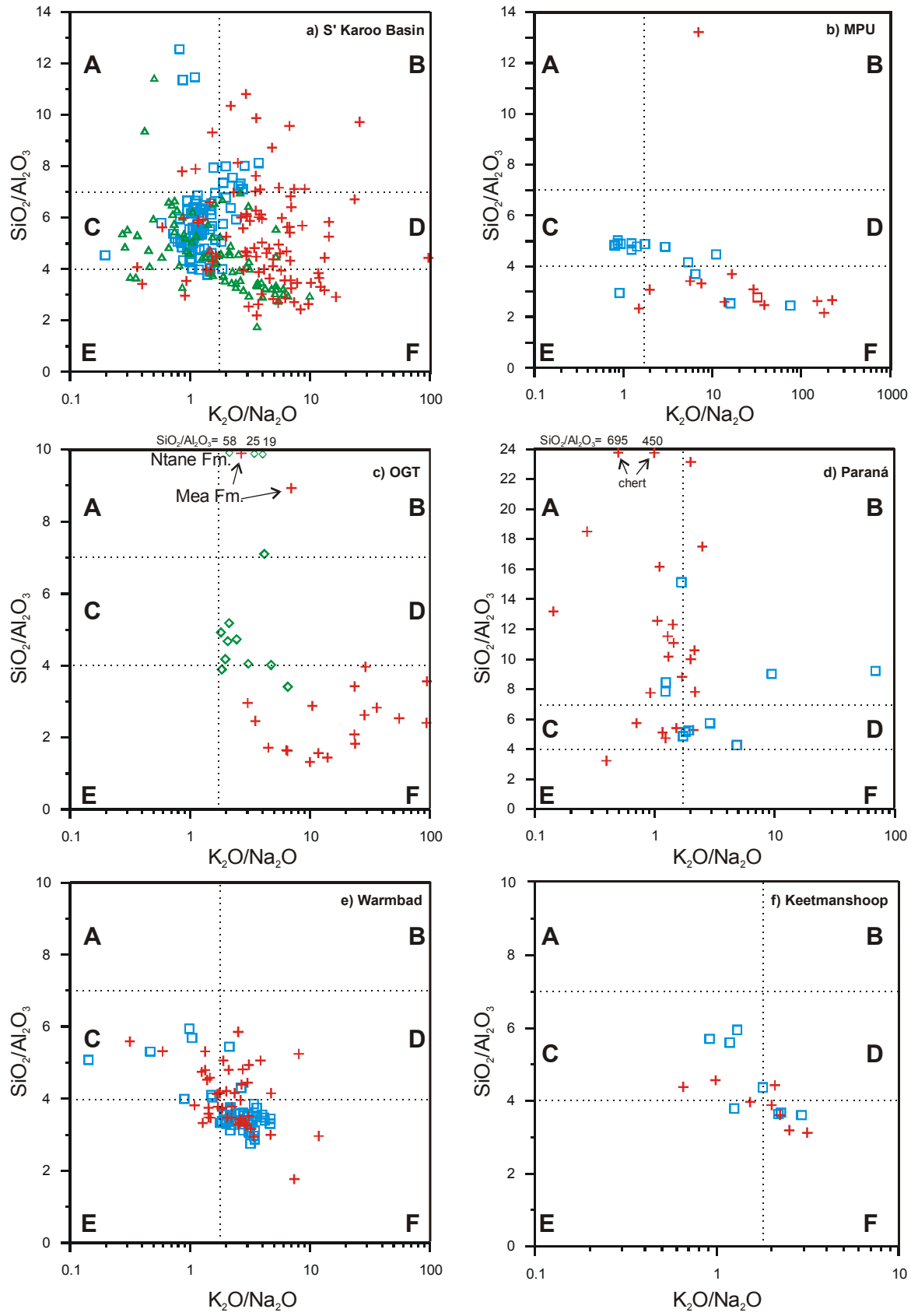


**Figure 4-1 a-f**

$K_2O/Na_2O$ vers. $SiO_2/Al_2O_3$ diagrams. **A**= sandy graywacke, **B**= sandy arkose, **C**= graywacke, **D**= arkose, **E**= clayey graywacke, **F**= shale, squares= glacial sediments, crosses= postglacial sediments (lower Ecca Group or equivalents), triangles= post Whitehill Formations (upper Ecca Group), diamonds= Beaufort Group

plot close to the boundary between arkoses and graywackes. By means of mineralogical composition Bühmann and Atanasova (1997) classified the samples of the Tlhabala Formation as mudstones with quartz, plagioclase and various phyllosilicates. In consideration that field boundaries of geochemical, mineralogical or textural classifications are not identical, only the combination of different methods can lead to reliable results.

Samples from the northern Paraná Basin contain $SiO_2/Al_2O_3$ ratios in the range from 3 to 24, whereas the $K_2O/Na_2O$ ratios plot predominantly in a relative narrow range between graywackes and arkoses (Fig. 4-1d). The high $SiO_2/Al_2O_3$ ratios of several Irati shales (crosses) point to an elevated chert contents in these samples. In general the geochemical classification of the samples form the Irati Formation is inconsistent with the mineralogical/ textural descriptions (Chap. 2.5 & 3.2.4).

The geochemical classification of the samples from the Namibian localities as shales (Fig. 4-1e & f) matches the textural description. Comparable to the Paraná Basin, the glacial sediments of the Dwyka Group (squares) contain lower $SiO_2/Al_2O_3$ ratios than samples from postglacial units (crosses). The samples from both Namibian localities plot in-between the fields of graywackes and shales, similar to the distribution of the samples from the southern Karoo Basin (Fig. 4-1a). Low $K_2O/Na_2O$ ratios are characteristic for both localities.

By plotting the element ratios $K_2O/Na_2O$ versus $SiO_2/Al_2O_3$, differences between glacial and postglacial units and between the different sample localities can be displayed. The higher $SiO_2/Al_2O_3$ and lower $K_2O/Na_2O$ ratios of glacial sediments in the Karoo Basin (Fig. 4-1a & b squares) point to quartz and unweathered feldspars as predominant constituents in the sediments. In the postglacial sediments, the breakdown of feldspar during chemical weathering processes in the provenances, led to decreasing $SiO_2/Al_2O_3$. Increasing $K_2O/Na_2O$ ratios for postglacial deposits of the Prince Albert and Whitehill Formations (Fig. 4-1a & b) can be explained by elevated illite contents. Upper Ecca Group sediments (post-Whitehill) from the southern Karoo Basin, plot in-between the fields of shales and graywackes. Higher quartz contents in the post-Whitehill sediments can be associated with the change from distal to proximal basin settings. Beside changes of the transport energy decreasing $K_2O/Na_2O$ point to higher albite proportions, probably associated with changing weathering conditions from warm-humid to arid climate conditions. The diagonal shift from “immature” to “mature” sediments during the postglacial phase of the upper Ecca Group in figure 4-1a, is also recorded in the samples from the OGT core (Fig. 4-1c). Sediments of the Ecca Group contain lower $SiO_2/Al_2O_3$ and higher $K_2O/Na_2O$ ratios than Beaufort Group sediments.

These differences between Ecca and Beaufort Group samples from the Kalahari and Karoo Basin confirm arid and terrestrially dominated sedimentation during the Middle to Late Permian. The element distribution of samples from the Paraná Basin yields no clear

tendency that can be associated with climate changes (Fig. 4-1d). Distributions of samples from the Warmbad Basin in figure 4-1e indicate a relative constant sedimentary environment during deposition. Changing climate conditions have had only minor effects on the geochemical composition of these sediments.

# 4.2 Element data

## 4.2.1 Introduction

The elements are normalised on their aluminium content, representative for the alumosilicate fraction. The application of element/Al ratios eliminates dilution effects by variable amounts of quartz and carbonates. As a reference the average shale composition given in table 4-1 (Wedepohl, 1969) is plotted as stippled line in figures 4-2, 4-4, 4-6, 4-8, 4-9 and 4-10. The element/Al ratios of the samples are presented versus their position in the sampled sequences, given in meter.

| Si/Al | Ti/Al | Fe/Al | Mn/Al | Mg/Al | Ca/Al | Na/Al | K/Al | P/Al |
|---|---|---|---|---|---|---|---|---|
| 3.11 | 0.05 | 0.55 | 0.01 | 0.18 | 0.18 | 0.13 | 0.34 | 0.01 |

**Table 4-1**

Average shale composition after Wedepohl (1969).

Correlation coefficients can be used to test the quality of the linearity between different elements. The usually applied formula is the Pearson's correlation coefficient (***r***), a numerical measure between 1 and –1. A correlation coefficient of 1 indicates a linear correlation with positive slope, 0 no correlation and –1 a linear correlation with negative slope. To use the Pearson's correlation coefficient the samples must be normally distributed. To measure the deviation from the normal distribution, the Shapiro-Wilk test (1> ***W*** >0) is calculated for each element. Decreasing ***W***-values indicate increasing deviation from the normal probability curve. If the population markedly deviates from the normal distribution, the Pearson's correlation coefficient should not be used. In this case, a better measure of correlation is the Spearman rank order correlation coefficient (ρ). The Spearman rank order coefficient is calculated in a similar way as ***r***. Instead of values, the rank orders are used in the formula of the Pearson's correlation coefficient. The Spearman correlation coefficient is not restricted to a population with normal distribution. Furthermore, it is more robust relating to outliners in the data set. In tables 4-3 to 4-14 both correlation coefficients are displayed due to the inhomogeneous distribution of single element contents.

In the correlation matrix (Tab. 4-3 to 4-14), element pairs of high statistical significance (***p***-level < 0.001) are highlighted. The **p**-level is a measure of the probability that the “0 Hypothesis” ($\mathbf{H_0}$) is valid. In the present case, the “0 Hypothesis” means no correlation between the element pairs. A **p**-level of 0.001 indicates a 0.1% probability that the observed correlation coefficient resulted only by chance. The higher the **p**-level, the less can be assumed that the observed correlation is a reliable indicator of the relation between the respective variables. Therefore, "highly statistical significance" means, that it is very probably true that a linear relation exists between two observed element contents.

It has to be emphasised that the statistical significance is directly influenced by the number of samples. In a data set with high sample number more results will meet by chance the conventional significance level than in datasets with low sample numbers. A reliable **p**-level demands a normal distributed sample population. If this condition is not fulfilled the **p**-level is not representative. However, correlation coefficients below the chosen **p**-level are labelled in tables 4-3 to 4-14. Pearson’s’ correlation coefficient, the Spearman rank order correlation coefficient and ***p***-values were calculated with the software package STATISTICA 4.3 StatSoft, Inc. (1993).

The tool of the cluster analysis is a statistical method to combine relative homogeneous clusters of objects (Backhaus et al., 1996). The purpose is to join together objects (elements) into successively larger clusters (mineral associations). Each object within the cluster will be similar to every other object, and different from objects in other clusters. In other words, the result of cluster analysis is a number of heterogeneous groups with homogeneous contents. The results can be expressed in a dendrogram with a hierarchical structure (StatSoft, Inc. 1993).

At the first step, when each element represents its own cluster, the similarities between the elements (objects) are defined by the chosen distance measure. As distance measure the Spearman rank order correlation coefficient is used. The next step is the linkage of elements with the highest correlation coefficient to one cluster. Now the distances between the new-formed clusters have to be determined. The unweighted pair-group average (UPGA) is used as linkage or amalgamation schedule, respectively. This method tends to join clusters with small variances (Backhaus et al., 1996). The average distance is calculated from the distance between each point in a cluster and all other points in another cluster. The two clusters with the lowest average distance are joined together to form the new cluster (Klemm, 1995). As a result more and more objects are linked together and amalgamate to larger and larger clusters of increasingly dissimilar elements. Finally, in the last step, all objects are joined together. The higher the levels of aggregation, the less similar the members in the respective clusters are Bacher (1994). If a clear "structure" arise from the data the formed clusters and branches of the dendrogram (mineral associations) can be interpreted with

regard to the sedimentary environment. The dendrograms in figures 4-21 to 4-25 were calculated with the program PAST 1.05 from Ø. Hammer and D.A.T. Harper (2003) (http://folk.uio.no/ohammer/past).

Before the element cluster can be correlated with different mineral phases, their characteristic element associations must be defined (Tab. 4-2). Single elements can be bound to different mineral phases. In general these intersections will cause longer distances when elements are linked to clusters (Siehl and Thein, 1978). For the cluster analyses the major elements, transition metal elements as well as rubidium, strontium, zirconium, barium and cerium are used.

| sedimentary fraction | mineral phases | element association |
|---|---|---|
| **silicates** | quartz, feldspar, mica, clay minerals | **Si**, **Al**, **Ti**, Fe, Mg, Ca, **Na**, **K**, **Rb**, Sr, **Zr**, Ba, transition metals, |
| **carbonates** | calcite, dolomite, siderite, etc. | **Ca**, **Mg**, Fe, Mn, Sr, Ba |
| **phosphates** | apatite | **P**, **Ca**, Ce |
| **metal-oxides/ hydroxides/ sulphides** | goethite, hematite, pyrite, etc. | **Fe**, **Mn**, **transition metals**, Zr, Ba |
| **organic matter** | | **transition metals**, Ba |

**Table 4-2**

Element - mineral associations compiled after various authors (Ernst, 1970; Pettijohn et al., 1972; Wedepohl, 1969; Deer et al., 1992; Brumsack, 1989, Shaw et al., 1990; Piper, 1994). Most significant elements are highlighted.

Phyllosilicates, feldspar and quartz can be associated with the branches of Si, Ti, Al, Na, and K. Since Rb can substitute K in feldspar and clay minerals, rubidium is often amalgamated to the element cluster of silicates. Zirconium, a high field strength element, is generally associated with the heavy mineral fraction. Carbonates and phosphates can be related to the element cluster of Ca, Mg and P. Similar to the substitution of K by Rb, Ca can be replaced by Sr in calcium bearing mineral phases such as carbonate or plagioclase. Phosphate minerals often tend to incorporate rare earth elements. Thus, elevated Ce contents point to the formation of phosphates, which requires specific conditions in the sedimentary environment. $Fe^{2+/3+}$ or $Mn^{2+}$ can be replaced in mineral structures by different transition metals. Therefore metal oxides, hydroxides or sulphides are commonly represented by the element cluster of Fe, Mn and transition metals. Depending on the sedimentary environment different Fe/Mn phases can be formed and used as redox proxies. Especially the formation of pyrite indicates anoxic conditions in the sedimentary environment.

## 4.2.2 Major Elements

### 4.2.2.1 Southern Karoo Basin

As pointed out in the chapters before, major climate changes influenced the sedimentation in southern Gondwana during the Upper Carboniferous to lower Permian. The Dwyka Group comprises the lower 520 m in the element/Al plots of figure 4-2a-k. Variations in the element/Al ratios discern interstadial (0 to 31 m, 87.5 to 198.5 m, 306.5 to 371.6 m, 487.4 to 517 m) from glacial climate phases (37 to 85.4 m, 211.3 to 299.7 m, 372.5 to 486.8 m). In interstadial sediments alkali and alkaline earth element contents are lower than in the massive diamictites of the glacial phases (Fig. 4-2a-j). Especially the Na/Al ratios in figure 4-2g point to changing climate conditions during deposition of the Dwyka Group.

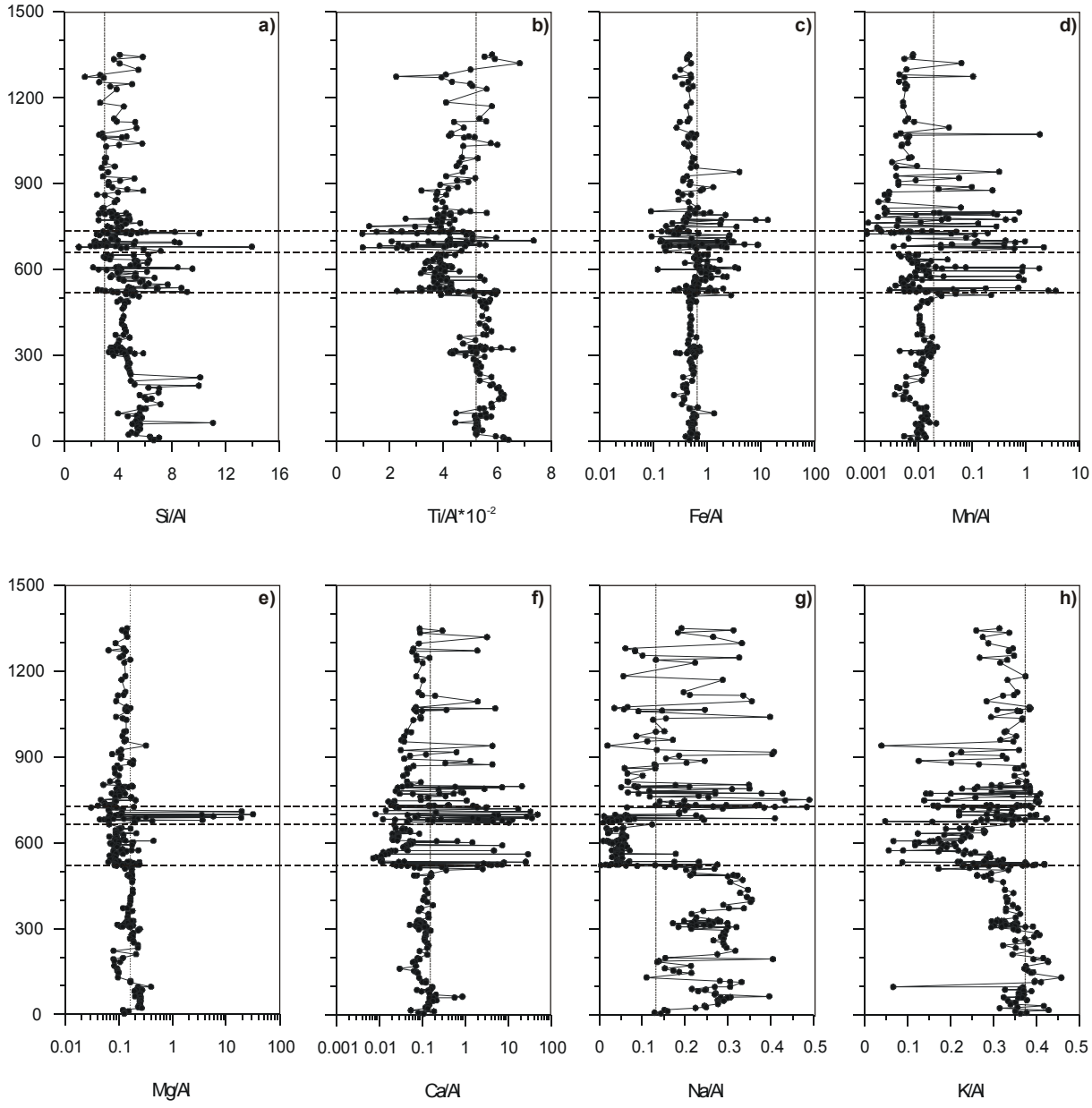

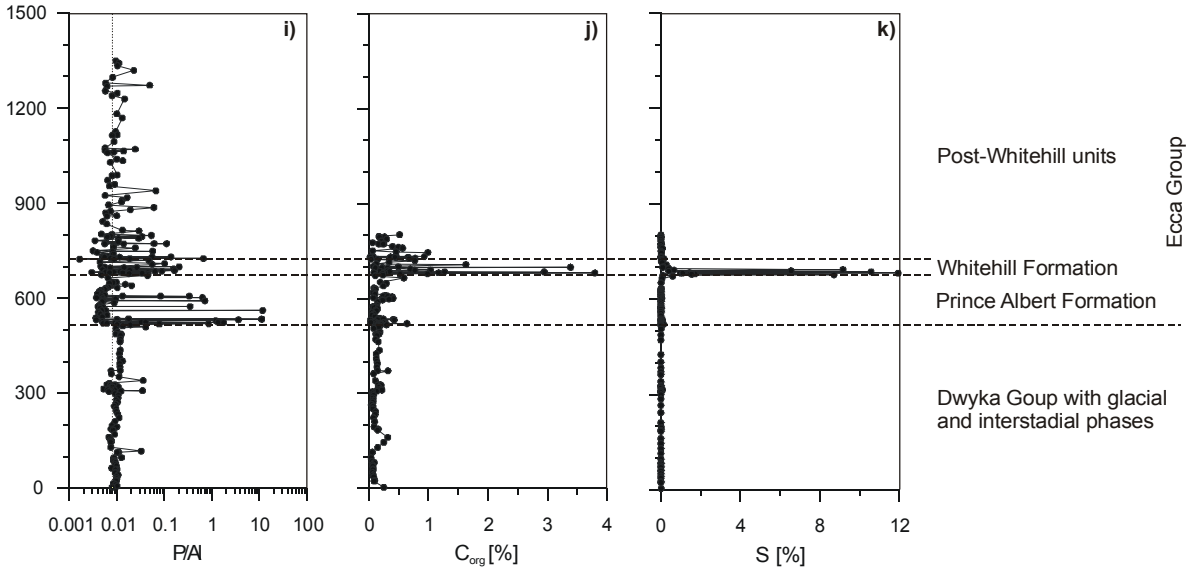


**Figure 4-2 a-k**

Element/Al ratios from samples of the southern Karoo Basin. Dashed lines represent average shale composition after Wedepohl (1969).

In the interstadial units of deglaciation sequence I and II (0 to 21 and 87 to 198 m), element/Al ratios of Si and Ti are elevated (Fig. 4-2a & b). In contrast to the lower interstadial units, the interstadials of the upper deglaciation sequences III and IV (306 to 371 and 372 to 486 m) exhibit lower Ti/Al and Si/Al ratios. Since these immobile elements are not sensitive to climate variations, these trends indicate changes of the provenance. Differences between glacial and interstadial phases can also be recognised in changes of the $C_{org}$ content (Fig. 4-2j). Sediments from interstadial phases contain higher $C_{org}$ contents in comparison to glacial deposits.

In tables 4-3 and 4-4 the correlation coefficients (***r***, ρ) of the major elements and the Shapiro-Wilk tests (**W**) are calculated for the samples from glacial and interstadial units. High positive correlation coefficients are often associated with element substitution in the mineral structure. The substitution of Al by Ti in feldspar or clay minerals is indicated by high positive correlation coefficients in glacial sediments between $TiO_2$ and $Al_2O_3$ (***r*** = 0.96, ρ = 0.93) and diagrammed in figure 4-3a. Dwyka samples show in general lower Al/Ti ratio than samples from post-Dwyka Fromations rather due to changing clay mineral composition than changing provenances. In figure 4-3b two trends can be recognised. Samples with changing carbonate contents plot in the grey shaded area. In consequence of increasing quartz proportions, the $Al_2O_3$ contents decrease, indicated by the negative trend in figure 4-3b. This dilution effect is also reported by the predominantly negative correlation of $SiO_2$ to the other elements (Tab. 4-3 & 4-4).

In the glacial sediments $P_2O_5$ is positively correlated to elements representative for silicate phases ($P_2O_5$-$Al_2O_3$: ρ = 0.91/***r*** = 0.86, $P_2O_5$-$TiO_2$: ρ = 0.89/***r*** = 0.91, $P_2O_5$-$Na_2O$: ρ = 0.91/***r*** =

0.91). Consequently the input of phosphorus during glacial phases is controlled by the siliciclastic supply from the hinterland. In interstadial sediments, low **W**-values for CaO (Tab. 4-4) point to rather bimodal distributed Ca contents. Beside CaO, also MnO and $P_2O_5$ deviate most significantly from the normal distribution (Tab. 4-4). All three elements can be associated with allochthonous mineral phases, generated while and after deposition of the clastic debris. Single positive excursions especially in the P/Al ratios (Fig. 4-2i), point to additional phosphorus minerals or fish scales in single horizons of the interstadial units.

| **W** | **$SiO_2$** | **$TiO_2$** | **$Al_2O_3$** | **$Fe_2O_3$** | **MnO** | **MgO** | **CaO** | **$Na_2O$** | **$K_2O$** | **$P_2O_5$** |
|---|---|---|---|---|---|---|---|---|---|---|
| **$SiO_2$** | 0.804 | **-0.78** | **-0.88** | **-0.90** | **-0.74** | **-0.59** | 0.04 | **-0.63** | **-0.72** | **-0.65** |
| **$TiO_2$** | **-0.69** | 0.83 | **0.96** | **0.79** | 0.50 | 0.30 | -0.46 | **0.79** | **0.69** | **0.91** |
| **$Al_2O_3$** | **-0.76** | **0.93** | 0.83 | **0.88** | **0.55** | 0.43 | -0.43 | **0.76** | **0.78** | **0.86** |
| **$Fe_2O_3$** | **-0.69** | **0.70** | **0.71** | 0.738 | **0.70** | **0.72** | -0.29 | 0.47 | **0.75** | **0.59** |
| **MnO** | -0.52 | 0.43 | 0.40 | 0.53 | 0.931 | 0.49 | 0.25 | 0.31 | 0.33 | 0.42 |
| **MgO** | 0.07 | -0.30 | -0.22 | 0.15 | 0.10 | 0.916 | -0.03 | 0.01 | 0.41 | 0.08 |
| **CaO** | 0.00 | -0.10 | -0.18 | -0.20 | 0.15 | 0.20 | 0.602 | -0.19 | -0.51 | -0.35 |
| **$Na_2O$** | **-0.69** | **0.87** | **0.85** | 0.55 | 0.34 | -0.32 | -0.01 | 0.961 | 0.42 | **0.91** |
| **$K_2O$** | **-0.58** | 0.51 | **0.60** | 0.52 | 0.23 | -0.08 | -0.44 | 0.41 | 0.92 | 0.52 |
| **$P_2O_5$** | **-0.65** | **0.89** | **0.91** | **0.57** | 0.43 | -0.27 | -0.07 | **0.91** | 0.43 | 0.936 |

**Table 4-3**

Major element correlation of 35 samples from glacial units in the Dwyka Group (southern Karoo Basin). Pearson's correlation coefficients (***r***) in the upper right triangle, Spearman rank order correlation coefficients (ρ) in the lower left triangle. Coefficients with **p**-levels <0.001 are highlighted. Results of the Shapiro-Wilk test (**W**-values) are given in the diagonal (grey shaded) array.

| **W** | **$SiO_2$** | **$TiO_2$** | **$Al_2O_3$** | **$Fe_2O_3$** | **MnO** | **MgO** | **CaO** | **$Na_2O$** | **$K_2O$** | **$P_2O_5$** |
|---|---|---|---|---|---|---|---|---|---|---|
| **$SiO_2$** | 0.933 | -0.16 | **-0.49** | **-0.90** | **-0.74** | **-0.53** | **-0.62** | **-0.46** | 0.09 | -0.30 |
| **$TiO_2$** | **-0.50** | 0.955 | **0.78** | 0.00 | -0.18 | 0.30 | -0.44 | 0.39 | **0.56** | -0.06 |
| **$Al_2O_3$** | **-0.82** | **0.72** | 0.958 | 0.28 | -0.03 | **0.56** | -0.29 | **0.66** | **0.58** | 0.13 |
| **$Fe_2O_3$** | **-0.85** | 0.41 | 0.67 | 0.837 | **0.73** | **0.55** | **0.62** | 0.35 | -0.38 | 0.20 |
| **MnO** | **-0.77** | **0.47** | **0.63** | **0.76** | 0.52 | 0.07 | **0.90** | 0.06 | -0.39 | 0.31 |
| **MgO** | **-0.69** | 0.37 | **0.66** | **0.68** | **0.59** | 0.933 | -0.06 | 0.51 | -0.06 | 0.08 |
| **CaO** | **-0.52** | 0.05 | 0.27 | 0.32 | **0.53** | **0.47** | 0.326 | -0.11 | **-0.47** | 0.31 |
| **$Na_2O$** | **-0.63** | 0.35 | 0.68 | 0.54 | 0.42 | **0.47** | 0.24 | 0.968 | 0.17 | 0.12 |
| **$K_2O$** | -0.38 | **0.46** | **0.61** | 0.16 | 0.11 | 0.20 | 0.08 | 0.28 | 0.879 | 0.01 |
| **$P_2O_5$** | **-0.54** | 0.32 | **0.45** | **0.44** | **0.55** | **0.44** | **0.59** | 0.36 | 0.11 | 0.586 |

**Table 4-4**

Major element correlation of 55 samples from interstadial units in the Dwyka Group (southern Karoo Basin). Pearson's correlation coefficients ( ***r***) in the upper right triangle, Spearman rank order correlation coefficients (**ρ)** in the lower left triangle. Coefficients with **p**-levels <0.001 are highlighted. Results of the Shapiro-Wilk test (**W**) are given in the diagonal (grey shaded) array.

Linear relation exists between MnO and $Fe_2O_3$ (Tab. 4-4; $\rho = 0.76$/***r*** = 0.73). Slightly elevated $C_{org}$ contents in the interstadial phases point to dysoxic conditions. Based on this assumption Fe can be associated with the formation of pyrite, whilst Mn bounded to carbonate phases is simultaneously precipitated under anoxic conditions. The high Pearson's correlation coefficient between MnO and CaO (***r*** = 0.90) (Tab. 4-4) pretend an apparent correlation between both elements. Low **W**-values for CaO and MnO (**W** = 0.326) indicate a significant deviation from the normal distribution. Thus, the high correlation coefficient results from outliners with high MnO and CaO contents in the interglacial Dwyka sediments, which can be associated with the occurrence of Mn/Fe-carbonates in single layers. However moderate Spearman rank order correlation coefficients (Tab. 4-4; $\rho = 0.53$ and $\rho = 0.59$) between MnO versus CaO and MgO indicate that Mn is bounded to carbonate phases.

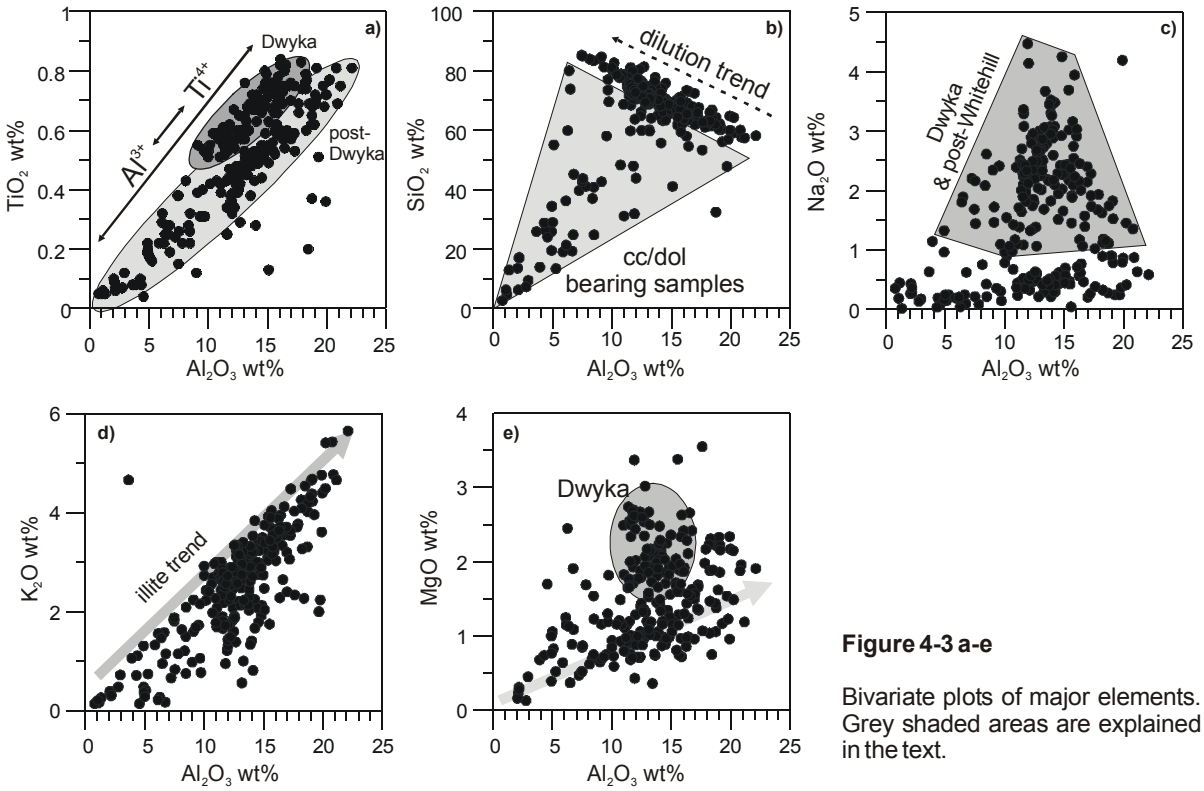


**Figure 4-3 a-e**

Bivariate plots of major elements. Grey shaded areas are explained in the text.

The transition into the post-glacial sedimentation phase (at approx. 520 m) is distinguished by severe changes in most of the element/Al ratios (Fig. 4-2a-k). Frequent changes in the element/Al ratios characterise the sediments of the post-glacial phase mainly due to carbonate occurrence. In comparaison to the average shale composition Ti, Mg, Ca, Na, K and P are depleted in the Prince Albert shales (520 to 675 m) whereas Si and Fe are enriched. Changes in the mineralogical composition are indicated by the sample distribution in figures 4-3c-e. Elevated sodium contents in Dwyka and post-Whitehill sediments can be associated with the occurrence of plagioclase due to low chemical weathering rates (grey

shaded area in Fig. 4-3c). The linear trend in figure 4-3d confirms illite as major potassium bearing mineral phase in all stratigraphic units. Due to additional clay mineral phases, samples of the Prince Albert Formation deviate from this trend. Elevated MgO contents of the Dwyka sediments (Fig. 4-3e) can be associated with the occurrence of chlorite. Lower Mg/Al ratios (Fig. 4-2e & 4-3e) in postglacial sediments indicate the breakdown of chlorite.

| **W** | **$SiO_2$** | **$TiO_2$** | **$Al_2O_3$** | **$Fe_2O_3$** | **MnO** | **MgO** | **CaO** | **$Na_2O$** | **$K_2O$** | **$P_2O_5$** |
|---|---|---|---|---|---|---|---|---|---|---|
| **$SiO_2$** | 0.835 | **0.49** | **0.55** | 0.06 | **-0.54** | 0.10 | **-0.92** | 0.25 | **0.46** | **-0.72** |
| **$TiO_2$** | 0.13 | 0.971 | **0.93** | 0.23 | -0.37 | 0.38 | **-0.69** | 0.26 | **0.76** | **-0.57** |
| **$Al_2O_3$** | 0.12 | **0.90** | 0.954 | 0.30 | **-0.47** | **0.43** | **-0.76** | 0.12 | **0.76** | **-0.60** |
| **$Fe_2O_3$** | -0.21 | 0.25 | 0.35 | 0.954 | 0.02 | **0.68** | -0.33 | -0.19 | -0.22 | -0.28 |
| **MnO** | **-0.80** | -0.36 | -0.35 | 0.33 | 0.396 | -0.05 | **0.43** | -0.04 | -0.31 | 0.04 |
| **MgO** | -0.28 | **0.47** | **0.47** | **0.67** | 0.21 | 0.971 | -0.35 | -0.02 | 0.11 | -0.32 |
| **CaO** | **-0.90** | -0.23 | -0.27 | 0.10 | **0.81** | 0.19 | 0.562 | -0.20 | **-0.53** | **0.83** |
| **$Na_2O$** | **0.43** | 0.28 | 0.20 | -0.11 | -0.39 | -0.08 | -0.38 | 0.79 | 0.15 | -0.17 |
| **$K_2O$** | 0.35 | **0.74** | **0.74** | -0.19 | **-0.66** | 0.11 | **-0.46** | 0.25 | 0.948 | **-0.43** |
| **$P_2O_5$** | **-0.74** | -0.20 | -0.28 | -0.05 | **0.58** | 0.13 | **0.83** | -0.34 | -0.25 | 0.448 |

**Table 4-5**

Major element correlation of 65 samples from the postglacial Prince Albert Formation (southern Karoo Basin). Pearson's correlation coefficients in the upper right triangle (***r***), Spearman rank order correlation coefficients ($\rho$) in the lower left triangle. Coefficients with **p**-levels <0.001 are highlighted. Results of the Shapiro-Wilk test are given in the diagonal (grey shaded) array.

Frequent peaks in the Si/Al, Ca/Al and Mn/Al ratios point to alternating sedimentary conditions. Variable conditions are also expressed by low **W**-values for $SiO_2$, MnO, CaO, and $P_2O_5$ (Tab. 4-5). The bimodally distributed element contents indicate that elevated supply of clastic detritus changed with phases of carbonate formation. Negative correlation coefficients between CaO and $SiO_2$ ($\rho$ = -0.90/***r*** = -0.92) in table 4-5 substantiate that changing environmental conditions dominated the sedimentation during deposition of the Prince Albert Formation. The lower and upper boundary of the Prince Albert Formation is distinguished by high carbonate contents. The sudden increase of Ca/Al and P/Al ratios at the Dwyka/Ecca boundary and correlation coefficients of $\rho$ = 0.83 between CaO and $P_2O_5$, indicate carbonate/phosphate formation. XRD analyses by Albes (1996) identify dahllite [$Ca_5(PO_4,CO_3)_3(OH,F)$] a carbonate-hydroxylapatite as phosphorus bearing phase with abundant $CO_2$ but small content of fluorine. Dahllite can occur as secondary concretions in the sediments or as a primary constituent of bones and teeth (Deer et al., 1992).

At the transition form the Prince Albert to Whitehill Formation, changes in the clay mineral assemblage are represented by increasing element/Al ratios of Ti, Na and K (Figs. 4-2b, g & h). Ti/Al and K/Al ratios reach normal shale composition, whereas Na/Al ratios increase

clearly above the normal shale composition. The Whitehill shales (675 to 725 m) contain high Ca/Al and Mg/Al ratios and high $C_{org}$ and S contents (Figs. 4-2e, f, j & k). The high Mg/Al ratios can be associated with the occurrence of dolomite or Mg-calcite, confirmed by XRD analyses (Adelmann, 1995). Anoxic conditions are assumed in the sedimentary environment during deposition of the Whitehill shales. High sulphur contents in single samples from the Whitehill Formation, point to pyrite formation. However, it is questionable, whether these high sulphur contents (Tab. 4-7) are exclusively bounded to pyrite or organic matter.

| Sample No. | S wt% | $Fe_{calc.}$ wt% | Fe wt% | Fe/S<br>$Fe/S_{pyrite} \approx 0.87$ | $C_{org}$ wt% | CaO wt% | |
|---|---|---|---|---|---|---|---|
| **993499** | 8.7 | 7.58 | 2.8 | 0.32 | 1.3 | 15.06 | 63% excess sulphur |
| **993504** | 11.95 | 10.41 | 1.34 | 0.11 | 0.37 | 25.75 | 87% excess sulphur |
| **993507** | 10.59 | 9.22 | 9.24 | 0.87 | 0.54 | 12.43 | Fe & S bounded to |
| **993509** | 6.55 | 5.7 | 2.57 | 0.39 | 1.35 | 12.99 | 55% excess sulphur |
| **993511** | 9.17 | 7.99 | 0.76 | 0.08 | 1.32 | 26.73 | 90% excess sulphur |

**Table 4-7**

Selected samples from the Whitehill Formation with conspicuously high sulphur contents.

Assuming that all sulphur is bounded to pyrite, the calculated Fe contents ($Fe_{calc}$) in table 4-7 result. In most of the samples significant differences can be recognised between calculated and measured Fe contents. Also the Fe/S ratios of the samples and the stoichiometric Fe/S ratio of pyrite diverge. Due to the low to moderate $C_{org}$ contents, organic sulphur cannot be responsible alone for the high S contents in the discussed samples. Only in sample 993507 high sulphur contents are associated with high pyrite contents. In the other samples, up to ten times higher calculated Fe contents require additional sulphur-bearing phases.

From the southern Karoo Basin near Laingsburg up to 1 cm thick anhydrite layers intercalated with $C_{org}$-rich shales and carbonates are documented (Adelmann, 1996). Furthermore, locally occurring lenticular crystal clasts, which appear to be replacement of gypsum by dolomite (McLachlan and Anderson, 1977) and the cubic shape of the pseudomorphoses, point to primary gypsum/anhydrite formation.

Intercalated $C_{org}$-rich shales-carbonates-gypsum/anhydrite layers indicate specific sedimentary conditions during deposition of the Whitehill shales (Anderson and McLachlan, 1977, 1979). The origin of these laminated deposits point to an environment with a stratified water body (Dean et al., 1975; Degens and Stoffers, 1976). Local trough-like environments and weak bottom water circulation maintained by hypersaline conditions characterize the sedimentary conditions during deposition of the Whitehill Formation in the southern Karoo Basin. However, temporary changes in the sedimentary conditions as indicated by the laminated deposits were caused by flux of organic matter settling though the water column, primary productivity and sediment accumulation rate.

| W | $SiO_2$ | $TiO_2$ | $Al_2O_3$ | $Fe_2O_3$ | MnO | MgO | CaO | $Na_2O$ | $K_2O$ | $P_2O_5$ |
|---|---|---|---|---|---|---|---|---|---|---|
| $SiO_2$ | 0.891 | **0.87** | **0.82** | -0.32 | -0.28 | -0.54 | **-0.93** | **0.62** | **0.76** | -0.01 |
| $TiO_2$ | **0.81** | 0.842 | **0.89** | -0.26 | -0.35 | -0.52 | **-0.88** | 0.48 | **0.82** | 0.06 |
| $Al_2O_3$ | **0.74** | **0.85** | 0.906 | -0.24 | -0.28 | -0.55 | **-0.89** | 0.40 | **0.88** | 0.06 |
| $Fe_2O_3$ | -0.30 | -0.22 | -0.11 | 0.577 | 0.12 | -0.20 | 0.03 | -0.18 | -0.22 | 0.34 |
| MnO | **-0.65** | **-0.63** | -0.56 | 0.48 | 0.425 | -0.05 | 0.22 | -0.27 | -0.34 | -0.03 |
| MgO | -0.29 | -0.26 | -0.18 | -0.15 | 0.40 | 0.637 | **0.66** | -0.30 | -0.41 | -0.10 |
| CaO | **-0.92** | **-0.82** | **-0.80** | 0.22 | 0.74 | 0.40 | 0.806 | -0.54 | **-0.79** | -0.10 |
| $Na_2O$ | **0.68** | **0.64** | 0.54 | -0.30 | -0.50 | -0.21 | **-0.66** | 0.789 | 0.30 | 0.11 |
| $K_2O$ | **0.64** | **0.80** | **0.85** | -0.07 | -0.47 | -0.04 | **-0.65** | 0.53 | 0.899 | 0.01 |
| $P_2O_5$ | -0.32 | -0.19 | -0.10 | 0.49 | 0.43 | 0.28 | 0.34 | -0.24 | -0.08 | 0.645 |

**Table 4-6**

Major element correlation of 27 samples from the Whitehill Formation (southern Karoo Basin). Pearson's correlation coefficients (***r***) in the upper right triangle, Spearman rank order correlation coefficients (ρ) in the lower left triangle. Coefficients with **p**-levels <0.001 are highlighted. Results of the Shapiro-Wilk test (**W**) are given in the diagonal (grey shaded) array.

Changes in the sedimentary environments during deposition of the Whitehill shales are also indicated by the Shapiro-Wilk test and correlation coefficients in table 4-6. Low **W**-values for $Fe_2O_3$, MnO, MgO and $P_2O_5$ indicating changing Eh/pH conditions in the sedimentary environments. Negative correlation coefficients between elements associated with alumosilicates (Si, Al, Ti, Na and K) and elements bounded to carbonates (Ca and Mg) confirm changes between phases of carbonate formation versus accumulation of clastic material.

| W | $SiO_2$ | $TiO_2$ | $Al_2O_3$ | $Fe_2O_3$ | MnO | MgO | CaO | $Na_2O$ | $K_2O$ | $P_2O_5$ |
|---|---|---|---|---|---|---|---|---|---|---|
| $SiO_2$ | 0.844 | **0.37** | **0.39** | **-0.46** | **-0.58** | 0.00 | **-0.78** | 0.36 | 0.35 | -0.05 |
| $TiO_2$ | 0.07 | 0.933 | **0.73** | -0.21 | **-0.35** | **0.68** | **-0.57** | -0.08 | **0.71** | -0.20 |
| $Al_2O_3$ | -0.07 | **0.70** | 0.95 | -0.30 | **-0.40** | **0.60** | **-0.53** | -0.01 | **0.91** | -0.26 |
| $Fe_2O_3$ | **-0.58** | 0.34 | 0.26 | 0.53 | 0.25 | 0.00 | -0.05 | -0.13 | -0.34 | 0.05 |
| MnO | **-0.62** | **-0.40** | **-0.47** | 0.30 | 0.342 | -0.13 | **0.52** | -0.21 | -0.33 | 0.05 |
| MgO | -0.31 | **0.69** | **0.60** | **0.67** | -0.02 | 0.955 | -0.24 | -0.32 | **0.53** | -0.25 |
| CaO | **-0.36** | **-0.53** | **-0.55** | -0.12 | **0.74** | -0.24 | 0.571 | -0.23 | **-0.45** | 0.14 |
| $Na_2O$ | **0.39** | -0.08 | -0.24 | -0.30 | -0.04 | -0.34 | 0.06 | 0.932 | -0.28 | 0.05 |
| $K_2O$ | 0.01 | **0.67** | **0.92** | 0.17 | **-0.55** | **0.54** | **-0.59** | -0.40 | 0.95 | -0.28 |
| $P_2O_5$ | **-0.41** | 0.04 | -0.21 | **0.41** | **0.50** | 0.09 | 0.38 | 0.06 | -0.29 | 0.343 |

**Table 4-8**

Major element correlation of 86 samples from post-Whitehill formations (southern Karoo Basin). Pearson's correlation coefficients (***r***) in the upper right triangle, Spearman rank order correlation coefficients (ρ) in the lower left triangle. Coefficients with **p**-levels <0.001 are highlighted. Results of the Shapiro-Wilk test (**W**) are given in the diagonal (grey shaded) array.

The post-Whitehill sedimentation phase comprises the Collingham, Vischkuil, Laingsburg and lower Fort Brown Formation (725 to 1380 m). Frequently changing element/Al ratios point to changing sedimentary environments during the later post-glacial phase. Variable sedimentary conditions are also indicated by the negative correlation of MnO and CaO versus $SiO_2$, $TiO_2$ and $Al_2O_3$. Anoxic conditions associated with elevated Fe/Al ratios as in the Prince Albert and Whitehill Formations do not seem to persist.

The predominance of illite is indicated by high positive correlation coefficients between $K_2O$, $TiO_2$ and $Al_2O_3$. Due to the positive correlation between MgO versus $TiO_2$, $Al_2O_3$ and $Fe_2O_3$ the occurrence of Mg is not bound to carbonate phases alone. Additional Mg-bearing clay mineral phases such as chlorite or smectites can be assumed in the upper strata of the sampled sequence.

### 4.2.2.2 MPU core (SW Karoo Basin)

Element/Al ratios of the MPU core samples show relative constant values during the Dwyka Group (base to 30.5 m in Fig. 4-4a-k). Comparable element/Al ratios of the Dwyka samples from the southern Karoo Basin (comp. Figs. 4-2a-k) indicate that both sample localities formed a contiguous sedimentary environment. Interstadial sediments of DS III are not encountered in the sampled core. Differing element ratios of Si/Al, Ti/Al and Mg/Al at the base of the core (Figs. 4-4a, b & e) are associated with high chlorite contents in this sample. Thus, the variations do not mark the top of DS III and are therefore not representative for the lower core section.

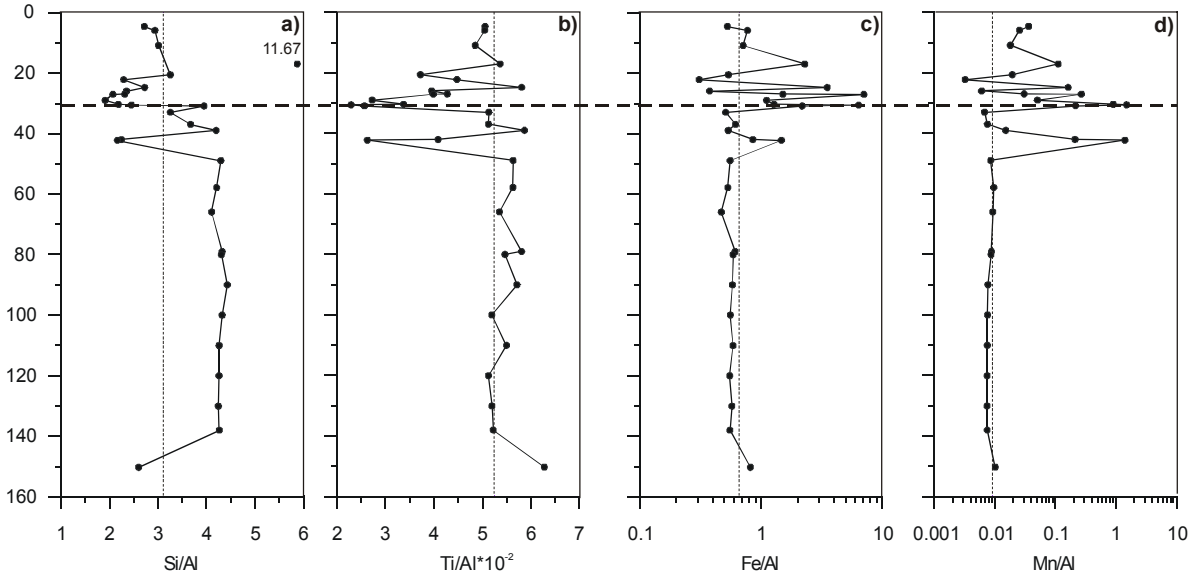

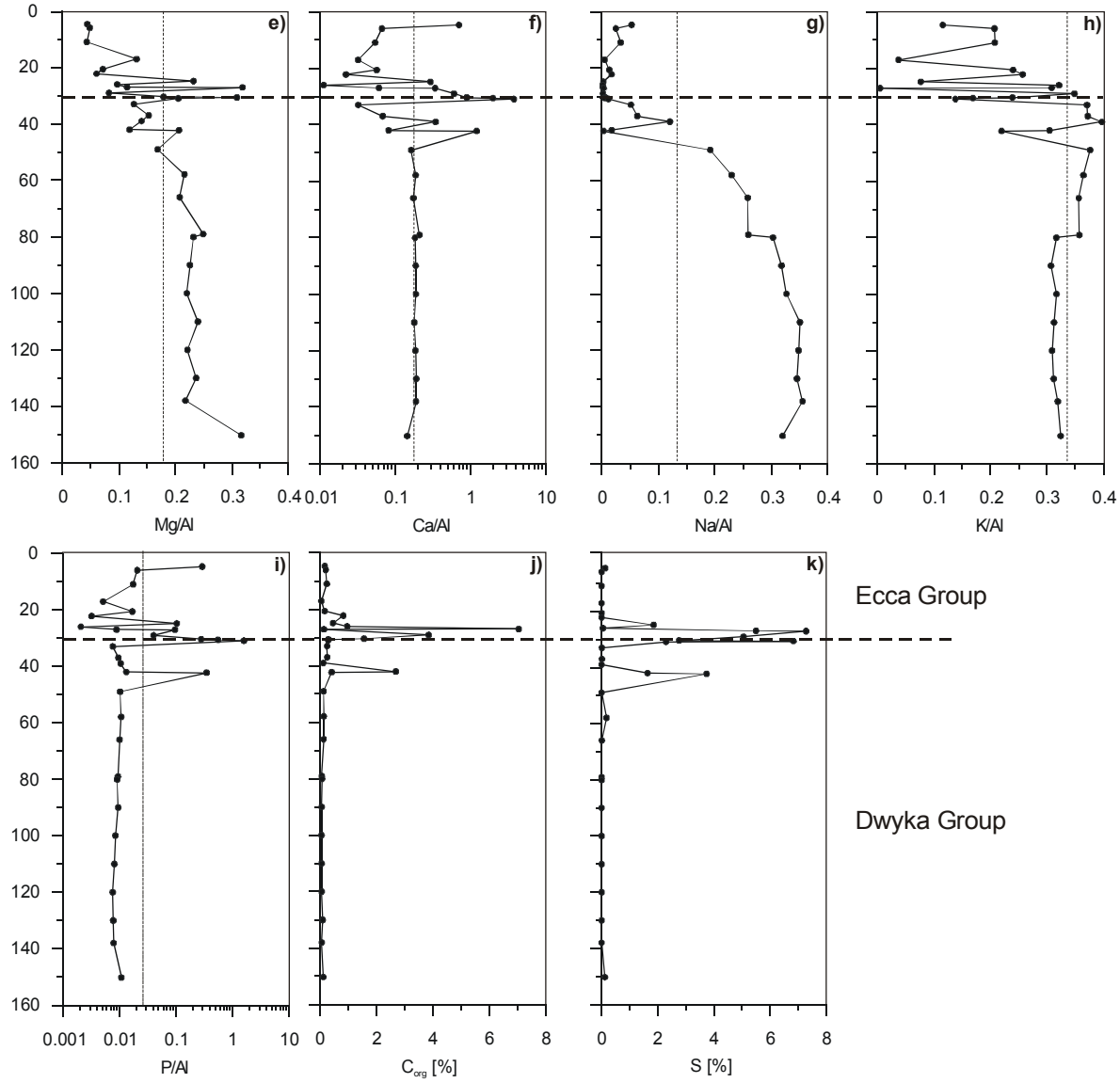


**Figure 4-4 a-k**

Element/Al ratios of samples from the MPU core. Dashed line represent average shale composition after Wedepohl (1969).

Comparable to the southern Karoo Basin, Si and Na (Figs. 4-2a & g) are enriched in the Dwyka sediments in relation to the average shale composition. The other elements show relative good conformity with the reference values. Ti replaced Al in alumosilicates, indicated by positive correlation coefficients in table 4-9 and figure 4-5a. Chemical alteration processes had only negligible effects on the mineral composition during glacial climate conditions. The occurrence of albite caused higher Na/Al and Si/Al ratios. Decreasing albite contents in the upper core section are indicated by declining sodium contents (Fig. 4-5b).

At 42 m, dark coloured carbonate/phosphate-bearing shales are represented by conspicuous peaks in all element/Al ratios, the $C_{org}$ and sulphur contents. As mentioned above, these samples were taken from a several centimetres thick black shale interval overlaid by diamictites in the upper Dwyka Group. The accumulation of the black shales is possibly

associated with an early, failed deglaciation event and the formation of locally anoxic bottom water conditions. At the top of the Dwyka Group, immobile-element/Al ratios (Si/Al, Ti/Al, Fe/Al and Mn/Al; Figs. 4-4a-d) return to similar values as in the lower core section whereas mobile elements such as Mg, Ca and Na are depleted in this section (Figs. 4-4e, f & g). The K/Al ratios differ from the other mobile element/Al ratios (Fig. 4-4h). K/Al ratios of approximately normal shale composition persist up to the Dwyka/Ecca boundary. The decreasing mobile elements contents indicate changes in the alumosilicate fraction. In the glacial Dwyka Group units, quartz, albite, illite and chlorite are the major constituents of the silicate fraction. Lower Ca and Na contents are associated with decreasing albite portions whereas the K/Al ratios were not affected by changing climate conditions. Illite as main clay mineral phase in the complete core is indicated by the linear relation between $Al_2O_3$ versus $K_2O$ in figure 4-5c. Comparable with the southern Karoo Basin the retreat of the glaciers and the transition to postglacial climate conditions can be detected by changing element contents in the interstadial sediments in the top of deglaciation sequence IV.

Carbonates and phosphates formations denote the onset of the Prince Albert Formation (30.5 to top in Fig. 4-4f & i). Anoxic conditions are indicated by elevated sulphur and $C_{org}$ contents (Figs. 4-4j & k). Increasing Fe/Al and Mn/Al ratios in these layers point to pyrite formation (Figs. 4-4c & d). In single samples redox sensitive element/Al ratios reach normal shale composition. Thus anoxic conditions could only temporarily establish during deposition of the Prince Albert shales. In comparison to the glacial sediments, alkali and alkaline earth elements are depleted in sediments of the lower Ecca Group (Figs. 4-4e-h). Especially sodium is nearly completely removed form the sediments of the Prince Albert Formation. These variations at the Dwyka/Ecca boundary were also recorded in the southern sample locality of the Karoo Basin. Hence, a contiguous sedimentary environment for the South African Karoo Basin can be inferred.

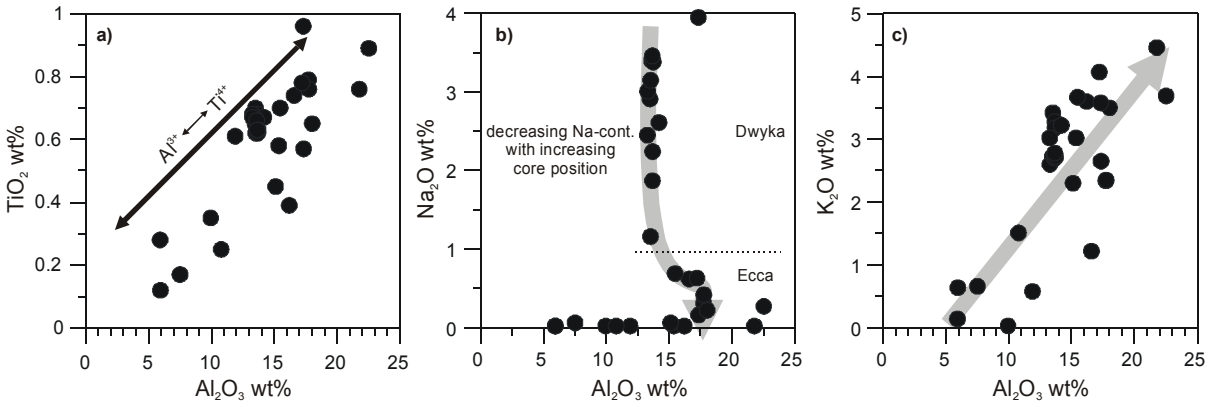

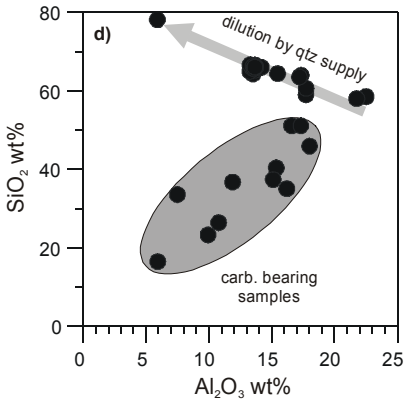


**Figure 4-5 a-d**

Bivariate plots of major elements of samples from the MPU core. Grey shaded areas and arrows are explained in the text.

The correlation matrix in table 4-9 confirms the results of the element/Al ratios in figure 4-4. Oxic and anoxic conditions as well as carbonate/phosphate formation are indicated by low **W**-values for $Fe_2O_3$, MnO, CaO, $P_2O_5$, S and $C_{org}$. Contrasting sedimentary environments are denoted by negative and positive correlation coefficients. Positive correlation exists between elements, associated with alumosilicates or between elements related to carbonates. Both element groups are in general negatively correlated to each other as displayed in figure 4-5d.

| **W** | **$SiO_2$** | **$TiO_2$** | **$Al_2O_3$** | **$Fe_2O_3$** | **MnO** | **MgO** | **CaO** | **$Na_2O$** | **$K_2O$** | **$P_2O_5$** | **S** | **$C_{org}$** |
|---|---|---|---|---|---|---|---|---|---|---|---|---|
| **$SiO_2$** | 0.843 | **0.59** | 0.28 | **-0.74** | **-0.66** | 0.07 | **-0.61** | 0.55 | 0.46 | -0.54 | **-0.83** | -0.36 |
| **$TiO_2$** | 0.26 | 0.898 | **0.79** | -0.48 | **-0.57** | 0.24 | **-0.64** | 0.41 | **0.69** | **-0.57** | **-0.64** | -0.10 |
| **$Al_2O_3$** | -0.08 | **0.63** | 0.938 | -0.40 | -0.30 | -0.07 | -0.44 | -0.01 | **0.75** | -0.40 | -0.41 | 0.21 |
| **$Fe_2O_3$** | **-0.77** | -0.48 | -0.13 | 0.603 | 0.32 | 0.05 | 0.17 | -0.43 | **-0.63** | 0.17 | **0.79** | 0.15 |
| **MnO** | **-0.76** | -0.49 | -0.17 | **0.80** | 0.488 | -0.03 | 0.50 | -0.38 | -0.35 | 0.41 | 0.40 | 0.08 |
| **MgO** | 0.31 | 0.01 | -0.32 | -0.24 | -0.44 | 0.925 | -0.17 | **0.73** | 0.21 | -0.23 | -0.10 | -0.21 |
| **CaO** | -0.39 | -0.47 | -0.52 | 0.24 | 0.39 | 0.21 | 0.646 | -0.28 | -0.46 | **0.96** | 0.31 | 0.01 |
| **Na2O** | **0.69** | 0.44 | 0.06 | **-0.70** | **-0.77** | **0.63** | -0.04 | 0.794 | 0.31 | -0.34 | -0.45 | -0.37 |
| **$K_2O$** | 0.19 | **0.60** | **0.59** | -0.45 | -0.47 | 0.11 | -0.42 | 0.29 | 0.904 | -0.51 | -0.43 | 0.20 |
| **$P_2O_5$** | **-0.73** | -0.28 | -0.07 | **0.64** | **0.78** | -0.32 | **0.58** | -0.45 | -0.43 | 0.493 | 0.21 | -0.04 |
| **S** | **-0.81** | **-0.59** | -0.24 | **0.82** | **0.75** | -0.07 | 0.46 | **-0.61** | -0.29 | **0.61** | 0.567 | 0.42 |
| **$C_{org}$** | **-0.80** | -0.08 | 0.41 | **0.57** | **0.58** | -0.50 | 0.04 | **-0.72** | 0.16 | **0.53** | **0.61** | 0.484 |

**Table 4-9**

Major element correlation of 31 samples from the MPU core (SW Karoo Basin). Pearson's correlation coefficients (***r***) in the upper right triangle, Spearman rank order correlation coefficients (ρ) in the lower left triangle. Coefficients with **p**-levels <0.001 are highlighted. Results of the Shapiro-Wilk test (**W**) are given in the diagonal (grey shaded) array.

### 4.2.2.3 OGT core (eastern Kalahari Basin)

Sediments in the core section between 480 to 325 m contain element/Al ratios of Si, Mg, Ca, Na and K below the average shale composition (Fig. 4-6). Higher Si/Al, Na/Al and K/Al ratios in the arkosic horizons of the Mea (400 to 360 m) and the upper Ntane Formation (225 to top) are associated with the occurrence of quartz, albite and potassium feldspars (Figs. 4-6a, g & h). Low element/Al ratios of Na, K, Mg and Ca (Figs. 4-6e-h) in the Tswane Formation (base to 411 m) point to kaolinite as major clay mineral. Increasing K/Al ratios in the Tlapana shales (363 to 327 m) are associated with the occurrence of illite as additional clay mineral.

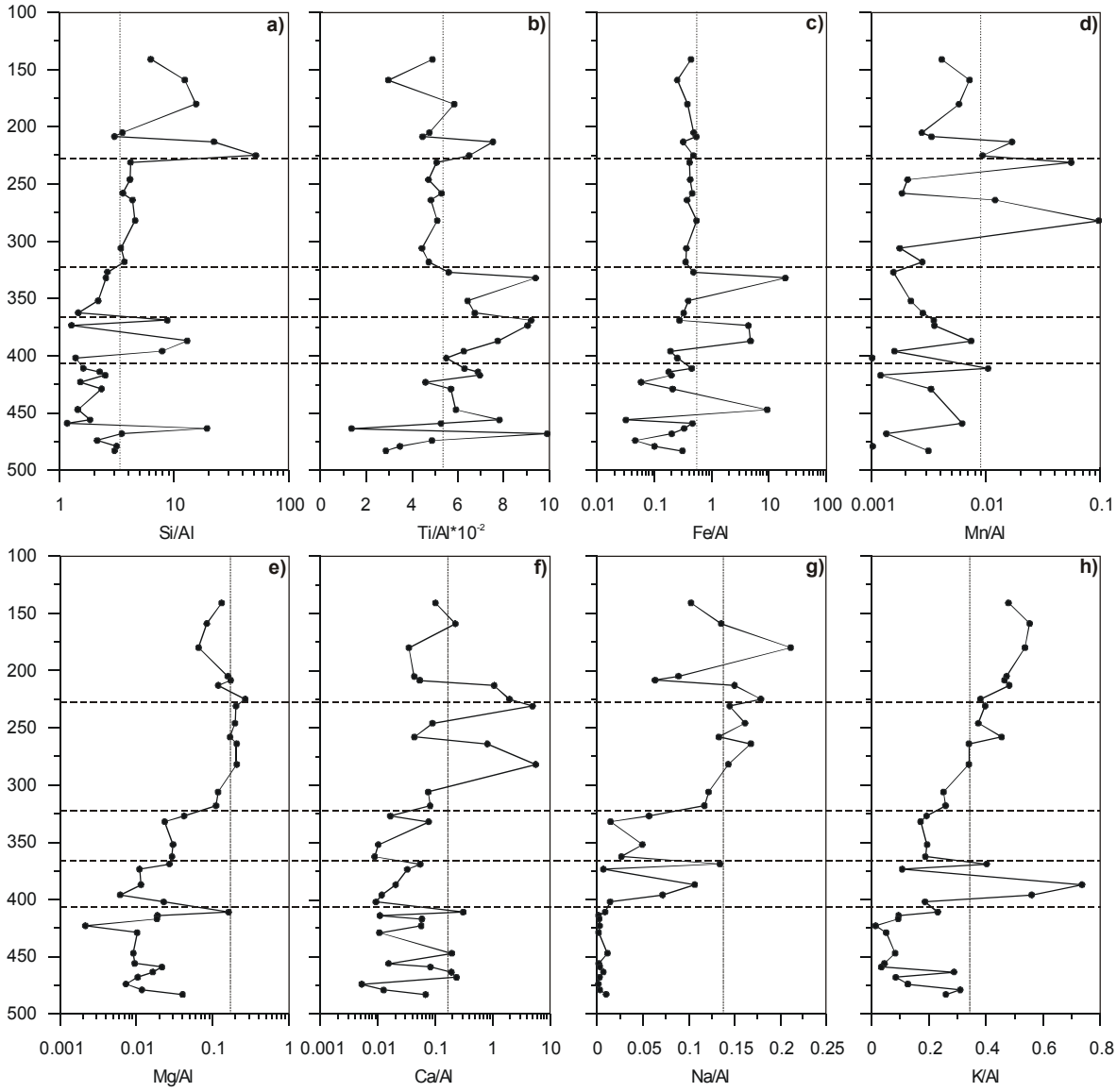

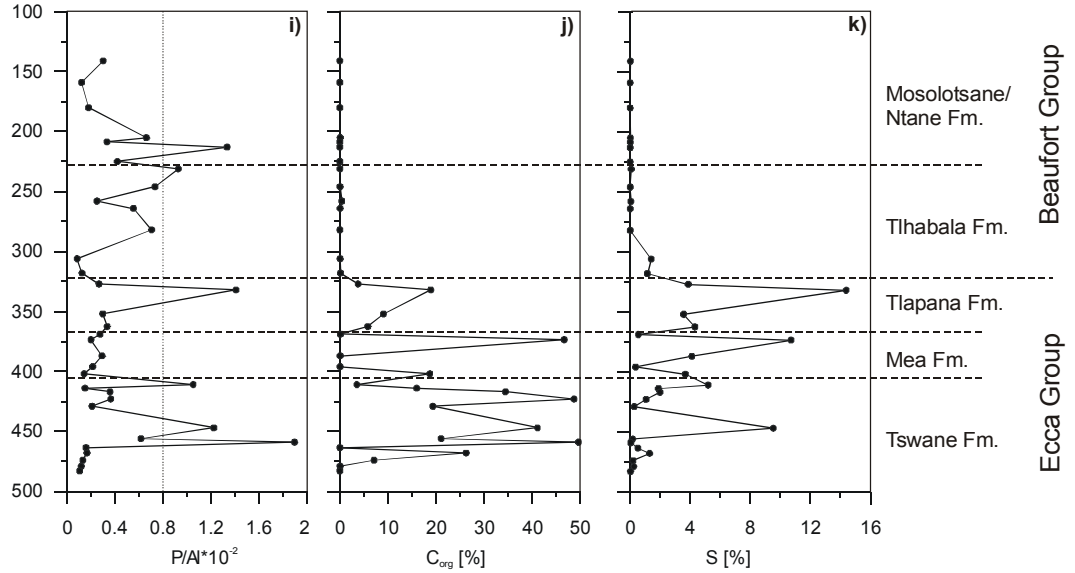


**Figure 4-6 a-k**

Element/Al ratios from the eastern Kalahari Basin, OGT core. Dashed lines represent average shale composition after Wedepohl (1969).

Elevated $C_{org}$ and S contents and high Fe/Al ratios (Figs. 4-6c, j & k) in the lower core section suggested pyrite formation in a reducing environment. However the C/S relationship in the Tswana Fm. refers to sulphur limitation during accumulation of the organic matter. Samples with high Ca contents exhibit elevated Mn/Al ratios whereas Fe/Al ratios are constant in the upper core section (Figs. 4-6c, d & f). Thus, Mn is rather bound to carbonates than to Fe-phases.

Increasing element/Al ratios of Si, Mg, Ca, Na and K at approximately 325 m and sudden decrease of $C_{org}$ and sulphur contents, demarcate the Ecca from the overlying Beaufort Group sediments (Figs. 4-6e, f, g, h & j). Elevated Si/Al, Mg/Al, Na/Al and K/Al ratios in the upper core section, point to feldspar and smectite as additional mineral phases beside quartz, illite and kaolinite. Constantly increasing element/Al ratios indicate a gradual transition from warm-humid to warm-arid climate conditions. However, the severe termination of accumulation or preservation of organic matter requires an additional, not necessarily climate-related process, which influenced the sedimentation in the Kalahari Basin. Possibly, postsedimentary oxidation and decomposition processes led to decay of organic carbon in the sediments. By comparing element/Al ratios from the top of the MPU (25 m) and the lower section of the OGT core (Tswane Fm.), significant similarities can be recognised. In relation to the average shale composition mobile elements are massively depleted in these sections (Figs. 4-4e-h and Figs. 4-6e-h). Since these elements were easily removed by aqueous solutions under warm-humid climate conditions, a comparable climate evolution can be attributed for both localities. High mobile element contents in the Dwyka Group, low contents in the Ecca Group sediments and again high contents in the upper Ecca/lower Beaufort

Group were also detected in the samples of the southern Karoo Basin (Figs. 4-2e-h). Thus, the OGT core can be considered as the continuation of the MPU core. The continuation is certainly not without interruption but the offset between the top of the MPU and the base of the OGT core seems to be rather small.

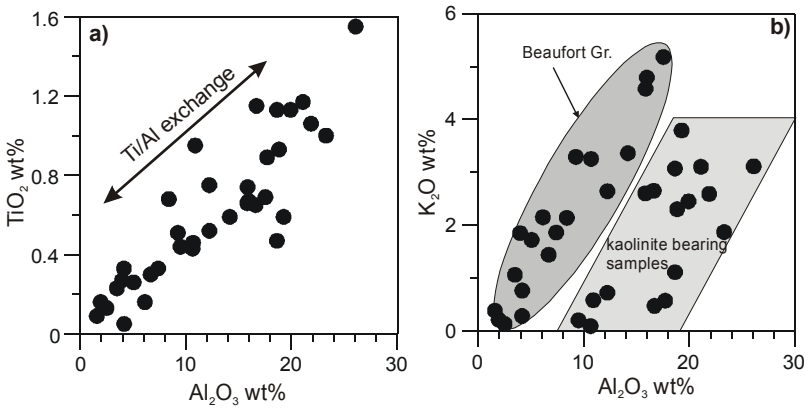


**Figure 4-7 a & b**

Bivariate plots of major elements of samples from the OGT core. Grey shaded areas are explained in the text.

Due to marked differences in geochemistry between lower and upper core section the elements are in general poorly correlated to each other (Tab. 4-10). Due to unimodally distributed $TiO_2$ and $Al_2O_3$ contents (**W** = 0.959 resp. **W** = 0.949) these elements share similar correlation coefficients (***r*** = 0.88, $\rho$ = 0.88). As mentioned above, the high correlation coefficients reveal the substitution of $Al^{3+}$ by $Ti^{4+}$ in alumosilicates (Fig. 4-7a). As a consequence of different kaolinite contents, Ecca and Beaufort Group sediments can be discerned by plotting $Al_2O_3$ versus $K_2O$ (Fig. 4-7b). Due to low **W**-values for CaO and MnO the high positive Pearson's correlation coefficient (***r*** = 0.95) reveals only an apparent linear relation. Thus, the Spearman rank order correlation coefficient yields a more reliable correlation between both elements ($\rho$ = 0.53). A comparable distribution is shown by the element pair $Fe_2O_3$ and S. **W**-values of 0.701 and 0.646, indicate marked deviation from the normal distribution. Therefore, the high Pearson's correlation coefficient (***r*** = 0.89) results from bimodally distributed element contents of Fe and S.

| W | $SiO_2$ | $TiO_2$ | $Al_2O_3$ | $Fe_2O_3$ | MnO | MgO | CaO | $Na_2O$ | $K_2O$ | $P_2O_5$ | S | $C_{org}$ |
|---|---|---|---|---|---|---|---|---|---|---|---|---|
| **$SiO_2$** | 0.947 | -0.16 | -0.04 | **-0.53** | -0.15 | 0.15 | -0.15 | 0.40 | 0.43 | -0.31 | **-0.64** | **-0.79** |
| **$TiO_2$** | -0.24 | 0.959 | **0.88** | -0.19 | -0.11 | 0.18 | -0.21 | 0.00 | 0.28 | 0.38 | -0.06 | 0.02 |
| **$Al_2O_3$** | -0.13 | **0.88** | 0.949 | -0.25 | -0.09 | 0.33 | -0.20 | 0.12 | 0.52 | 0.34 | -0.21 | -0.14 |
| **$Fe_2O_3$** | -0.37 | 0.13 | 0.14 | 0.701 | -0.10 | -0.02 | -0.13 | -0.10 | -0.11 | -0.02 | **0.89** | 0.23 |
| **MnO** | 0.09 | 0.07 | 0.15 | 0.25 | 0.494 | 0.33 | **0.95** | 0.18 | 0.05 | 0.25 | -0.15 | -0.24 |
| **MgO** | 0.28 | 0.30 | 0.42 | 0.28 | **0.67** | 0.790 | 0.24 | **0.71** | **0.71** | 0.48 | -0.22 | -0.46 |
| **CaO** | 0.18 | -0.19 | -0.15 | -0.15 | 0.53 | **0.57** | 0.385 | 0.16 | -0.04 | 0.13 | -0.17 | -0.20 |
| **$Na_2O$** | 0.50 | 0.04 | 0.10 | 0.24 | **0.53** | **0.78** | 0.34 | 0.834 | **0.62** | 0.03 | -0.32 | **-0.56** |
| **$K_2O$** | 0.45 | 0.36 | **0.53** | 0.27 | 0.41 | **0.73** | 0.12 | **0.72** | 0.939 | 0.16 | -0.33 | **-0.65** |
| **$P_2O_5$** | -0.39 | 0.47 | 0.43 | 0.22 | 0.45 | 0.46 | 0.22 | 0.19 | 0.23 | 0.759 | -0.03 | 0.13 |
| **S** | **-0.58** | 0.32 | 0.19 | 0.52 | -0.35 | -0.37 | -0.48 | -0.39 | -0.22 | -0.05 | 0.646 | 0.43 |
| **$C_{org}$** | **-0.77** | 0.41 | 0.23 | 0.20 | -0.42 | -0.48 | -0.45 | **-0.57** | -0.47 | 0.21 | **0.69** | 0.694 |

**Table 4-10**

Major element correlation of 36 samples from the OGT core (Kalahari Basin). Pearson's correlation coefficients (***r***) in the upper right triangle, Spearman rank order correlation coefficients (**ρ**) in the lower left triangle. Coefficients with **p**-levels <0.001 are highlighted. Results of the Shapiro-Wilk test (**W**) are given in the diagonal (grey shaded) array.

### 4.2.2.4 Paraná Basin

The sedimentary sequence of the Paraná Basin was sampled with focus on the post-glacial Irati Formation. The Itararé Group and Tatui Formation were only sampled at lower resolution. Since the samples were taken from different quarries a contiguous sequence as in the before discussed localities cannot be composed. The samples are ordered by their stratigraphic position and listed in equal distance (Figs. 4-8a-k).

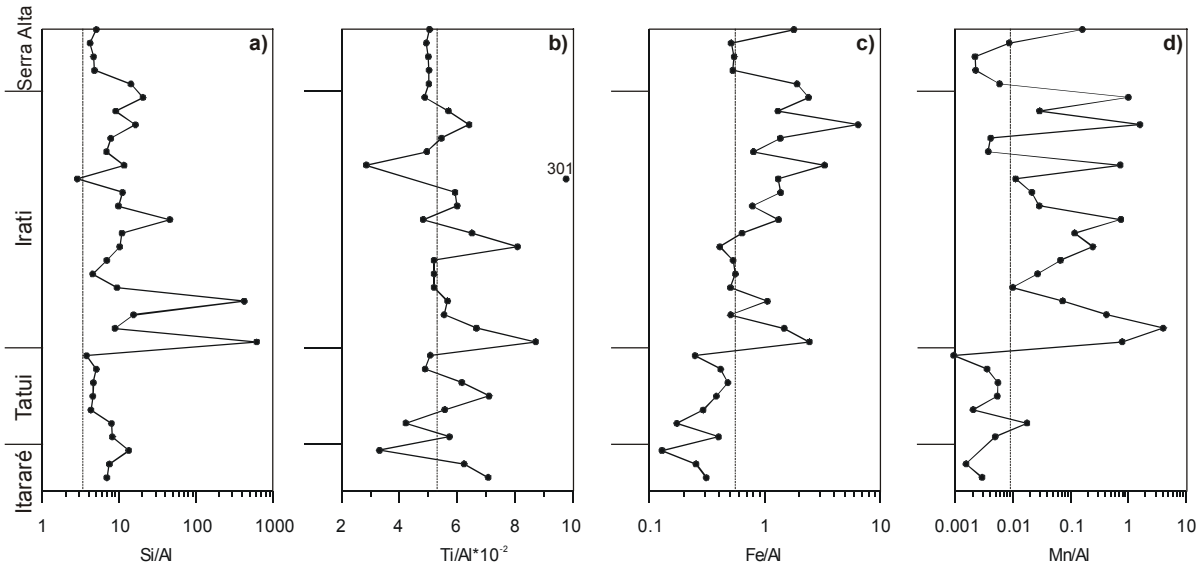

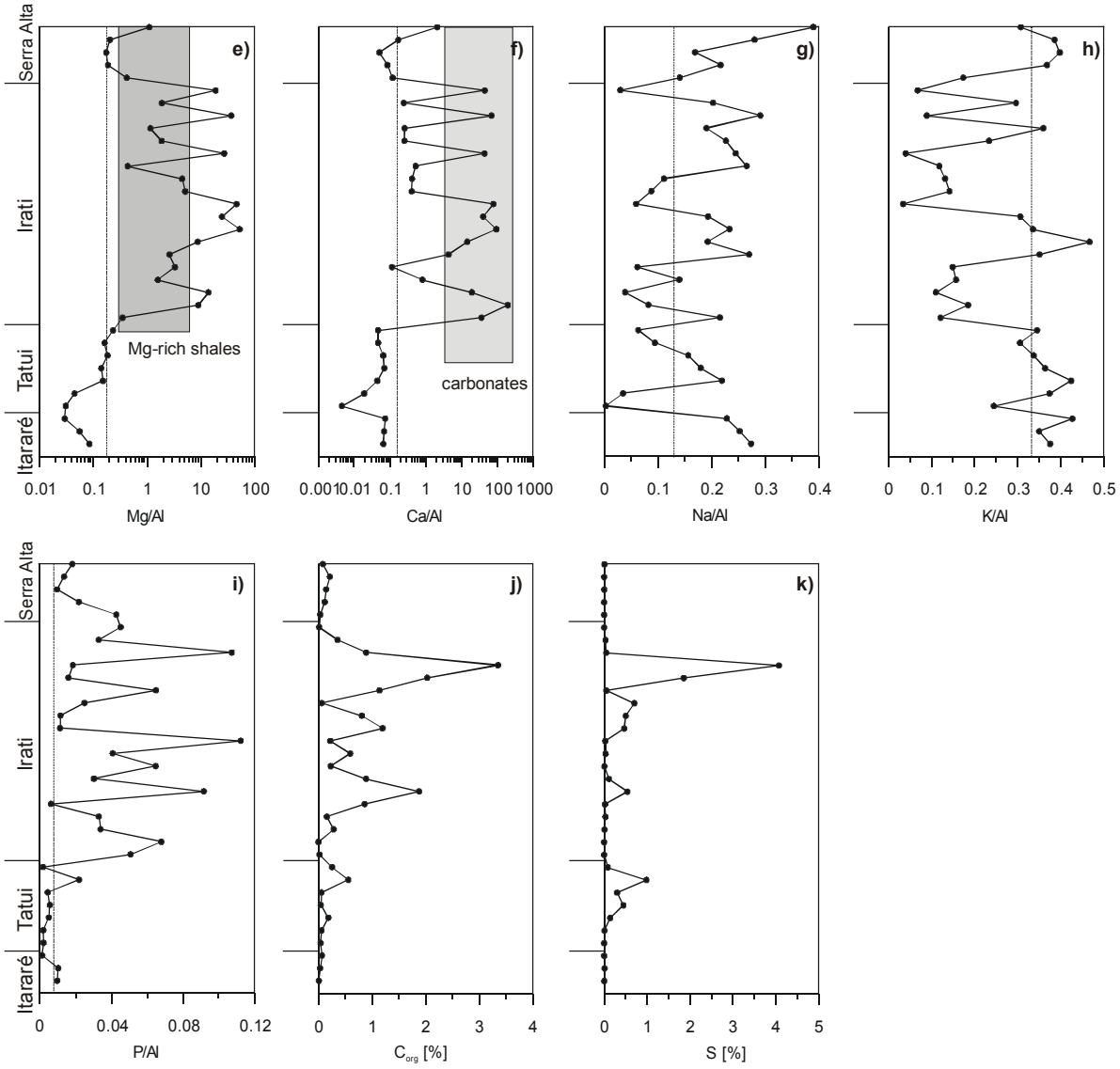


**Figure 4-8 a-k**

Element/Al ratios from the northern Paraná Basin (Brazil). Dashed lines represent average shale composition after Wedepohl (1969).

Samples with exceptionally high Si/Al ratios derive from the lower Irati Formation (Fig. 2-5a). The first peak represents secondary quartz mineralisation and is therefore not representative for the sedimentary sequence. The second peak indicates the occurrence of chert concretions in the sediments of the lower Irati Formation. Intercalated carbonates of the Irati Formation can be differentiated from the shales by peaks in the element/Al ratios of Mn, Mg, Ca and P (Figs. 4-8d, e, f & i). High Mg/Al ratios (around 40) of carbonate bearing samples point to dolomitization processes. Mg/Al ratios ten-times above the average shale composition in non-carbonate bearing samples indicate the occurrence of chlorite or smectite. Their formation is possibly linked with postsedimentary dolomitisation processes. Carbon and oxygen isotopes of the Paraná Basin carbonates reveal that the dolomite was formed during early diagenetic alteration of limestones (De Giovani et al., 1974).

Along the sampled profile, time dependent variations can be recognised. Changes between phases of carbonate formation versus input of clastic material are recorded by high and frequent changes in most of the element/Al ratios (Fig. 4-8). As in the postglacial sediments of the South African sample localities, K/Al and Na/Al ratios decrease in the carbonate free Irati shales below average shale composition (Figs. 4-8g & h). The $C_{org}$ content of the Irati shales ranges between 0.5 and 3.5 wt% and reaches maximum values in the upper Irati Formation (Fig. 4-8j). Sulphur contents are positively correlated with organic carbon (Fig. 4-8j & k). This $C_{org}$/S-coupling is commonly explained by processes of bacterial sulphate reduction (Berner and Raiswell, 1984). Since warm and humid climate conditions are assumed during deposition of the Irati Formation, the alumosilicate fraction is predominantly composed of clay minerals. Low Na/Al and K/Al ratios in the middle Irati Formation point to the occurrence of kaolinite in carbonate free samples. Increasing illite contents towards the top of the Irati Formation are indicated by K/Al ratios of average shale composition. In the glacial and early postglacial phase of the Itararé and Tatui Formations autochthonous potassium feldspar led to elevated K/Al ratios. Comparable to the sample localities in the Karoo and Kalahari Basin, sodium and potassium contents decrease in the postglacial phase, indicating increasing chemical weathering conditions in the provenance.

| W | $SiO_2$ | $TiO_2$ | $Al_2O_3$ | $Fe_2O_3$ | MnO | MgO | CaO | $Na_2O$ | $K_2O$ | $P_2O_5$ | S | $C_{org}$ |
|---|---|---|---|---|---|---|---|---|---|---|---|---|
| **$SiO_2$** | 0.894 | 0.16 | 0.54 | 0.18 | **-0.63** | **-0.72** | **-0.91** | 0.33 | 0.52 | 0.01 | 0.07 | -0.19 |
| **$TiO_2$** | 0.37 | 0.513 | **0.60** | **0.72** | -0.20 | -0.27 | -0.30 | **0.63** | 0.32 | 0.46 | 0.12 | -0.15 |
| **$Al_2O_3$** | 0.39 | **0.98** | 0.896 | **0.54** | -0.45 | **-0.58** | **-0.68** | **0.79** | **0.92** | 0.36 | 0.13 | -0.14 |
| **$Fe_2O_3$** | 0.14 | **0.68** | **0.67** | 0.863 | -0.04 | -0.19 | -0.38 | **0.65** | 0.30 | **0.57** | 0.34 | 0.11 |
| **MnO** | **-0.69** | -0.39 | -0.41 | -0.12 | 0.646 | 0.25 | **0.74** | -0.24 | -0.42 | -0.15 | -0.19 | -0.12 |
| **MgO** | **-0.87** | -0.35 | -0.38 | -0.06 | **0.54** | 0.824 | 0.52 | -0.47 | **-0.63** | -0.11 | 0.03 | 0.40 |
| **CaO** | **-0.90** | -0.50 | -0.52 | -0.24 | **0.75** | **0.74** | 0.712 | -0.47 | **-0.60** | -0.16 | -0.20 | 0.00 |
| **$Na_2O$** | 0.23 | **0.81** | **0.81** | **0.73** | -0.32 | -0.23 | -0.29 | 0.862 | **0.74** | 0.51 | 0.12 | -0.11 |
| **$K_2O$** | 0.45 | **0.90** | **0.92** | **0.56** | -0.50 | -0.46 | **-0.57** | **0.78** | 0.880 | 0.23 | 0.07 | -0.16 |
| **$P_2O_5$** | -0.04 | 0.54 | 0.52 | **0.77** | -0.02 | 0.06 | -0.01 | **0.75** | 0.45 | 0.780 | 0.21 | 0.23 |
| **S** | -0.25 | 0.25 | 0.20 | 0.27 | -0.02 | 0.38 | 0.07 | 0.23 | 0.08 | 0.33 | 0.458 | **0.82** |
| **$C_{org}$** | -0.44 | -0.15 | -0.13 | 0.11 | 0.08 | **0.66** | 0.24 | -0.01 | -0.13 | 0.20 | **0.66** | 0.692 |

**Table 4-11**

Major element correlation of 34 samples from the northern Paraná Basin, Brazil. Pearson's correlation coefficients (***r***) in the upper right triangle, Spearman rank order correlation coefficients (ρ) in the lower left triangle. Coefficients with **p**-levels <0.001 are highlighted. Results of the Shapiro-Wilk test (**W**) are given in the diagonal (grey shaded) array.

Changing sedimentary environments between carbonate formation and deposition of clastic material are also indicated by negative correlation coefficients between MgO, CaO and MnO versus $SiO_2$, $TiO_2$ and $Al_2O_3$ (Tab. 4-11). The changing sedimentary conditions are also expressed by relative low **W**-values for all elements. High positive correlation coefficients ($\rho$) between $K_2O$ and $Na_2O$ versus $TiO_2$ and $Al_2O_3$ point to the occurrence of feldspars or with reference to the fine laminated sediments to illite or smectites. The close relation between $C_{org}$ and S contents is indicated by positive correlation coefficients in table 4-11

### 4.2.2.5 Warmbad Basin

The succession from the Warmbad Basin in southern Namibia comprises sediments from the glacial Dwyka Group to the postglacial Whitehill Formation. Their element/Al ratios are shown in figure 4-9a-k. The sequence commences with glacial deposits of the Dwyka Group, which rest discordantly on Precambrian basement rocks. Steep escarpments in the sampled area inhibit the sampling of a contiguous succession from the Warmbad Basin. The gap in the element/Al ratios of figures 4-9i-k comprise parts of the Prince Albert Formation between 192 to 292 m. Sediments of the Whitehill Formation (383 m to top) terminate the succession.
Si/Al and Na/Al ratios approach average shale composition (Figs. 4-9a & g) whereas in the Karoo Basin, the glacial Dwyka sediments are markedly enriched in Si and Na (Figs. 4-2a & g). Cyclic variations in the element/Al ratios of alkali and alkaline earth elements as in the Karoo Basin are missing (Figs. 4-9e-f). By the means of Na/Al ratios glacial and interstadial climate phases in the southern Karoo Basin can be discerned. In the Warmbad Basin variations in the Na/Al and other weathering sensitive element/Al ratios are too low for a reliable subdivision of the deposits in glacial and interstadial phases. After Visser (1983) erosion processes removed large parts of the glacial deposits during interstadial phases. Therefore, only field observations allow a reliable differentiation between glacial and interstadial phases.
Lower Si/Al ratios of the Dwyka Group sediments of the Warmbad Basin versus higher Si/Al ratios in Dwyka sediments from the Karoo Basin (Fig. 4-9a) indicate a higher clay mineral content due to lower sedimentation rates. In the main Karoo Basin (Fig. 4-2a) the glacial debris accumulated on a stable shelf whereas the depocentre of the Warmbad Basin was surrounded by a mountainous highland.
Samples from the lower Dwyka Group show relative homogenous element/Al ratios without marked outliners. Elevated Mn/Al and Ca/Al ratios (Figs. 4-9e & f) indicate limited carbonate formation in single samples. Temporary changes of the sedimentary conditions during deposition of the upper Dwyka Group are indicated by single peaks in all element/Al ratios (Fig. 4-9). A relatively constant mineralogical composition of the shales in the lower Dwyka shales is confirmed by XRD analyses. Quartz, albite and illite were identified as main mineral

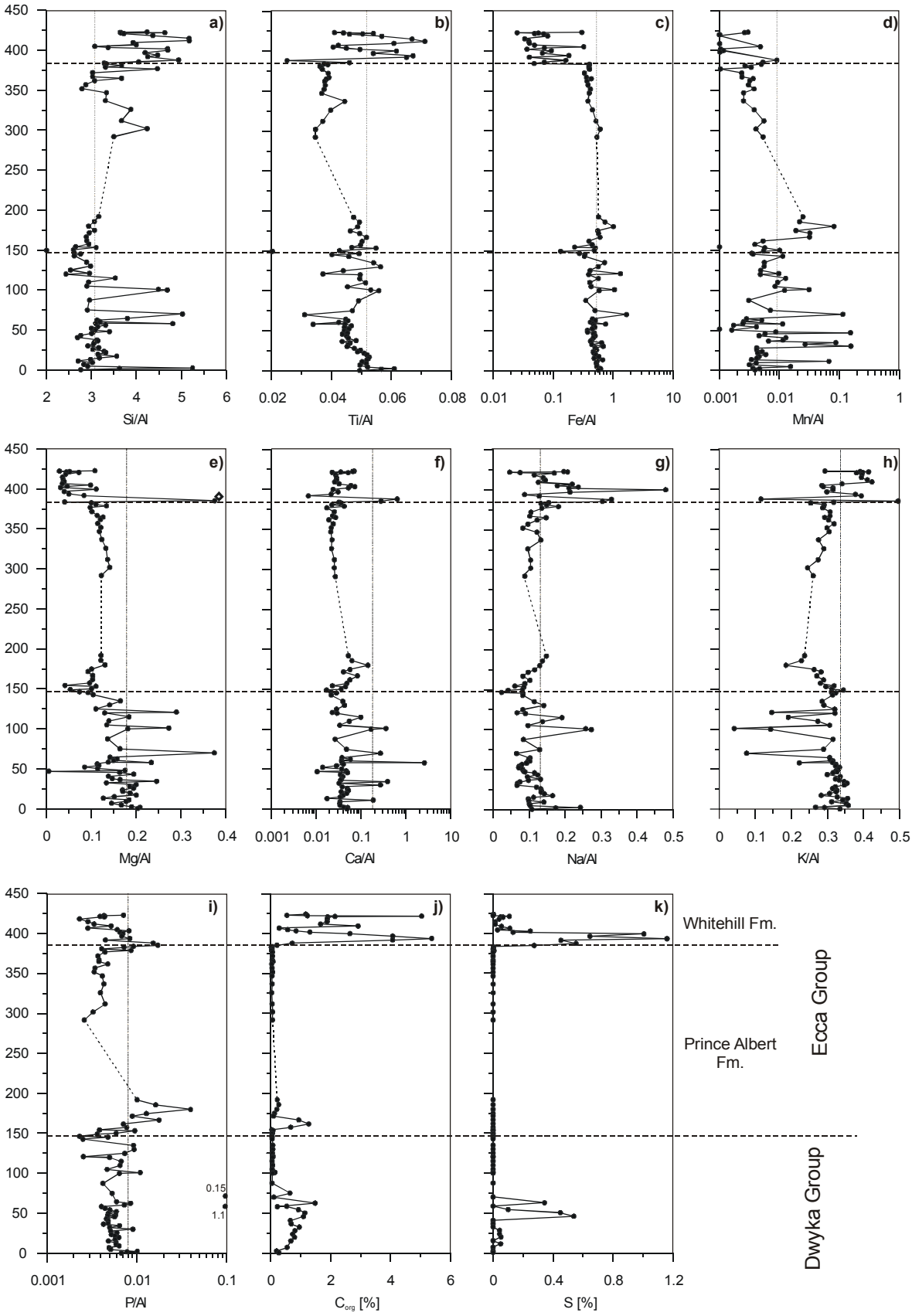


**Figure 4-9 a-k**

Element/Al ratios from the Warmbad Basin in southern Namibia. Dashed lines represent average shale composition after Wedepohl (1969).

phases (Geiger, 2000). Chlorite, kaolinite and calcite/dolomite represent minor constituents. Because of different sample localities element/Al ratios and the $C_{org}$ content change between lower (0 to 60 m) and upper Dwyka Group (60 to 145 m) (Fig. 4-9j). In the upper Dwyka Group conspicuous peaks in the Si/Al ratio point to an elevated input of quartz. Simultaneous decreasing K/Al ratios below the average shale composition (Fig. 4-9h) indicate lower illite contents. Since the other alkali and alkaline earth element/Al ratios are elevated in samples with higher Si/Al ratios (Fig. 4-9e-g), increasing proportions of feldspar seems to be responsible for these variations in the upper Dwyka Group.

| **W** | **$SiO_2$** | **$TiO_2$** | **$Al_2O_3$** | **$Fe_2O_3$** | **MnO** | **MgO** | **CaO** | **$Na_2O$** | **$K_2O$** | **$P_2O_5$** |
|---|---|---|---|---|---|---|---|---|---|---|
| **$SiO_2$** | 0.920 | -0.15 | -0.05 | -0.30 | -0.34 | -0.27 | **-0.54** | **0.54** | -0.15 | -0.45 |
| **$TiO_2$** | -0.26 | 0.852 | **0.81** | -0.30 | -0.23 | -0.14 | **-0.63** | 0.39 | **0.72** | **-0.59** |
| **$Al_2O_3$** | -0.31 | **0.70** | 0.875 | -0.25 | -0.16 | -0.18 | **-0.62** | -0.04 | **0.86** | **-0.55** |
| **$Fe_2O_3$** | **-0.50** | 0.15 | -0.11 | 0.707 | 0.21 | **0.61** | -0.03 | -0.15 | **-0.48** | -0.08 |
| **MnO** | -0.32 | -0.07 | -0.03 | 0.27 | 0.472 | -0.12 | 0.14 | -0.31 | -0.06 | -0.02 |
| **MgO** | -0.27 | 0.01 | -0.25 | **0.64** | 0.34 | 0.956 | 0.01 | 0.10 | -0.32 | -0.10 |
| **CaO** | -0.13 | -0.22 | -0.36 | 0.24 | 0.38 | **0.50** | 0.338 | -0.25 | -0.44 | **0.94** |
| **$Na_2O$** | 0.30 | 0.37 | 0.01 | 0.15 | -0.03 | 0.29 | 0.21 | 0.978 | -0.22 | -0.28 |
| **$K_2O$** | -0.35 | **0.51** | **0.77** | -0.13 | -0.08 | -0.32 | **-0.48** | -0.26 | 0.758 | -0.36 |
| **$P_2O_5$** | -0.25 | 0.04 | -0.17 | 0.33 | 0.09 | 0.23 | 0.44 | 0.16 | -0.30 | 0.178 |

**Table 4-12**

Major element correlation of 49 samples from the Dwyka Group (southern Warmbad Basin, south Namibia). Pearson's correlation coefficients (***r***) in the upper right triangle, Spearman rank order correlation coefficients (**ρ**) in the lower left triangle. Coefficients with **p**-levels <0.001 are highlighted. Results of the Shapiro-Wilk test (**W**) are given in the diagonal (grey shaded) array.

In the localities before discussed, decreasing element/Al ratios at the Dwyka/Ecca boundary were interpreted as climate controlled signals. Comparable distinct signals are not recorded in the element/Al ratios of samples from the Warmbad Basin. However, increasing $C_{org}$ contents and P/Al and Mn/Al ratios (Figs. 4-9d & i) at the Dwyka/Ecca boundary point to anoxic conditions in the sedimentary environment. The composition of the alumosilicate fraction remains relative constant as indicated by only low changes in the element/Al ratios of Ca, Na and K. Ca/Al and Na/Al ratios increase whereas the K/Al ratios decrease (Figs. 4-9f, g & h). Element/Al ratios of Si and Ti show no significant variations at the transition to postglacial climate conditions (Figs. 4-9a & b). The onset of the Whitehill Formation is denoted by increasing Si/Al, Ti/Al, Na/Al, K/Al and P/Al ratios whereas Fe/Al and Mg/Al ratios decrease. Simultaneous increasing $C_{org}$ and sulphur contents point to anoxic conditions in

the sedimentary environment of the Warmbad Basin during deposition of the Whitehill Formation. With exception of two, probably dolomite or Mg-calcite bearing samples with higher Mg/Al and Ca/al ratios, the Whitehill samples contain on average lower Mg/Al and Ca/Al ratios than the Prince Albert shales. Mobilisation of alkali or alkaline earth elements due to increasing chemical weathering processes during the postglacial phase is not documented in the Warmbad Basin sediments.

The negative correlation of $SiO_2$ versus all other elements with exception of $Na_2O$, points to the input of quartz and feldspar (Tab. 4-12). Substitution of $Al^{3+}$ by $Ti^{4+}$ in alumosilicates is indicated by the positive correlation between $TiO_2$ and $Al_2O_3$. Illite as major constituent in the sediments (confirmed by XRD analyses; Geiger, 1999) is denoted by the positive correlation between $Al_2O_3$, $TiO_2$ and $K_2O$. Significant deviations from the normal distribution of MnO, MgO, CaO and $P_2O_5$ (low **W**-values in Tab. 4-12) are related to carbonate or phosphate phases. The low **W**-value for $P_2O_5$ derives from phosphate bearing samples in the lower Dwyka Group (Fig. 4-9i). Therefore, the high Pearson's correlation coefficient (**r** = 0.94) reflects only an apparent correlation between CaO and $P_2O_5$.

During the postglacial phase the dilution of the clay and feldspar fraction by the input of $SiO_2$ rich debris is indicated by negative correlation coefficients (Tab. 4-13). Similar to the glacial phase, only $Na_2O$ correlates positive with $SiO_2$. Carbonate/phosphate formation at the Prince Albert/Whitehill boundary is denoted by bimodal distribution of MnO, MgO, CaO and $P_2O_5$ contents (low **W**-values)

| **W** | **$SiO_2$** | **$TiO_2$** | **$Al_2O_3$** | **$Fe_2O_3$** | **MnO** | **MgO** | **CaO** | **$Na_2O$** | **$K_2O$** | **$P_2O_5$** |
|---|---|---|---|---|---|---|---|---|---|---|
| **$SiO_2$** | 0.979 | -0.03 | **-0.73** | **-0.65** | **-0.52** | **-0.48** | -0.25 | 0.14 | -0.23 | **-0.50** |
| **$TiO_2$** | -0.20 | 0.972 | 0.12 | 0.10 | 0.19 | -0.45 | -0.33 | -0.26 | 0.23 | 0.17 |
| **$Al_2O_3$** | **-0.70** | 0.28 | 0.908 | 0.39 | 0.20 | -0.04 | -0.22 | -0.33 | **0.65** | 0.11 |
| **$Fe_2O_3$** | **-0.72** | 0.05 | **0.52** | 0.904 | **0.71** | 0.31 | 0.01 | -0.30 | -0.27 | **0.57** |
| **MnO** | **-0.82** | -0.01 | **0.51** | **0.83** | 0.514 | 0.19 | 0.26 | -0.07 | -0.24 | **0.89** |
| **MgO** | **-0.66** | -0.29 | 0.30 | **0.71** | **0.68** | 0.744 | **0.79** | 0.21 | -0.33 | 0.30 |
| **CaO** | **-0.47** | 0.12 | 0.32 | 0.26 | **0.54** | 0.20 | 0.490 | 0.37 | -0.38 | 0.44 |
| **$Na_2O$** | 0.16 | -0.27 | -0.24 | -0.23 | -0.08 | 0.04 | 0.38 | 0.914 | -0.29 | 0.13 |
| **$K_2O$** | -0.08 | 0.30 | 0.44 | -0.34 | -0.23 | -0.22 | -0.01 | -0.26 | 0.929 | -0.26 |
| **$P_2O_5$** | **-0.58** | 0.21 | 0.30 | 0.40 | **0.54** | 0.34 | **0.70** | 0.35 | -0.16 | 0.644 |

**Table 4-13**

Major element correlation of 49 samples from postglacial units (southern Warmbad Basin, south Namibia). Pearson's correlation coefficients (***r***) in the upper right triangle, Spearman rank order correlation coefficients (**ρ**) in the lower left triangle. Coefficients with **p**-levels <0.001 are highlighted. Results of the Shapiro-Wilk test (**W**) are given in the diagonal (grey shaded) array.

### 4.2.2.6 Keetmanshoop

The sampled sequence is focused on the transition from glacial to postglacial climate conditions (Fig. 4-10). The Nossob sandstone between 66 to 79 m, was not sampled. Because of the low number of samples correlation coefficients were not calculated.

Significant changes at the transition from glacial to postglacial climate conditions as documented from the Karoo and Kalahari Basin cannot be detected in the element/Al ratios from the Keetmanshoop area (Figs. 4-10a-i). Decreasing Si/Al and Ti/Al ratios point to increasing clay mineral contents in the postglacial sediments in contrast to higher feldspar proportions in the glacial deposits. Alkali and alkaline earth element/Al ratios decrease from glacial to postglacial deposition phase (Figs. 4-10e-h). With exception of the Na/Al ratio, all element/Al ratios rest below average shale composition. The good match of the Na/Al ratio to the average shale composition is associated with the higher feldspar content in the sediments. Decreasing element/Al ratios possiblly indicate the occurrence of kaolinite as additional Al bearing phase in the postglacial sediments.

P/Al ratios are in general low in the sampled sequence from the Keetmanshoop area. However, at the transition from glacial to postglacial climate conditions P/Al ratios increase to average shale composition. Comparable temporarily increasing P/Al ratios at the Dwyka/Ecca boundary were detected in all sample localities in southern Gondwana. Sedimentary phosphorus deposits are often associated with specific environments such as nutrient rich up-welling zones, high bioproductivity, oxygen deficiency and reduced clastic input. In ancient sediments phosphorite is also known to occur in association with stromatolites, which are considered to be deposits of very shallow water with profuse algal growth (Banerjee, 1971).

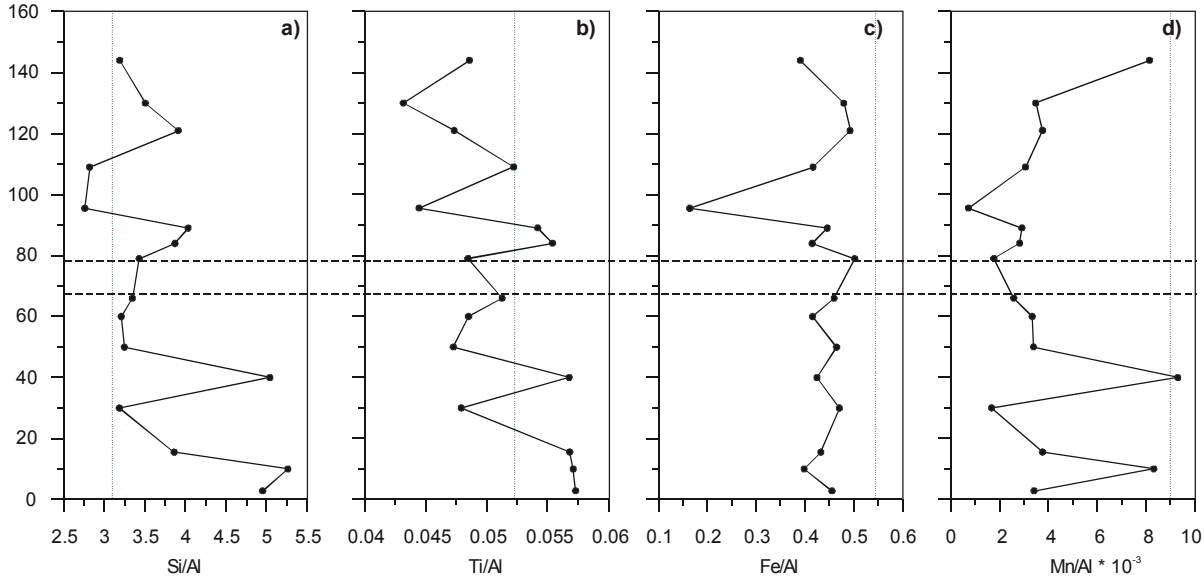

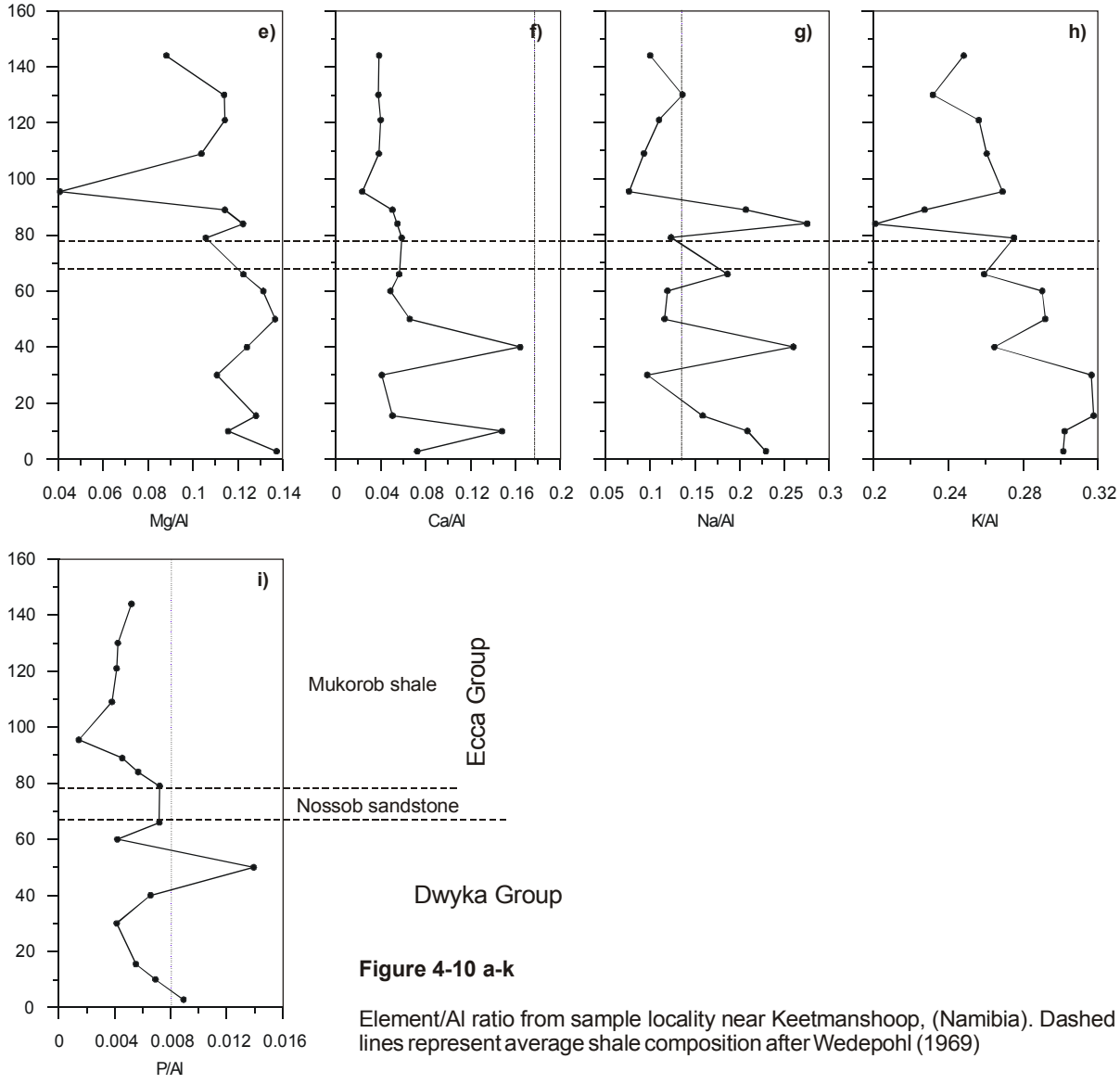


**Figure 4-10 a-k**

Element/Al ratio from sample locality near Keetmanshoop, (Namibia). Dashed lines represent average shale composition after Wedepohl (1969)

The simultaneously increasing phosphorus contents at all sample localities at the Dwyka/Ecca boundary point to an over-regional mechanism for the accumulation of phosphorus. The retreat of continental ice sheets at the Dwyka/Ecca boundary caused a massive meltwater supply into the oceans. Simultaneously, new atmospheric systems established due to warmer continental temperatures carrying coastal surface waters to move ocean wards. Colder and nutrient rich deep water moved up to the ocean surface creating upwelling currents along the coastline. By these currents phosphorus rich matter reached the flooded shelf areas and accumulated at dysoxic to anoxic conditions. Low $C_{org}$ contents versus high phosphorus contents indicate the accumulation of phosphorus under partly oxic conditions (Baturin, 2001). The different phosphorus contents can be related with the sedimentary environment of the single sample localities. In shelf areas with favourable conditions for upwelling currents (southern Karoo Basin) higher phosphorus contents were accumulated whereas in distal positions phosphorus accumulation was less pronounced.

## 4.2.3 Trace elements

### 4.2.3.1 Southern Karoo Basin

Selected trace elements (transition metals, Sr, Zr, and Ba) are presented in addition to the major elements to report changes of the sedimentary environment. To minimise the dilution effect by varying amounts of quartz and/or carbonate, the element are normalised to aluminium.

Some trace elements form mineral species in their own right but most commonly they substitute for major elements in rock forming minerals. Elements of the first transition series vary in valence state and in geochemical behaviour. $Ti^{4+}$ is an incompatible high field strength element whilst $Mn^{2+}$, $Co^{2+}$, $Ni^{2+}$, $Cu^{2+}$, $Zn^{2+}$ as well as $V^{3+}$ and $Cr^{3+}$ are compatible elements (Rollins, 1993). Increasing element contents of V, Cr, Co, Ni, Cu and Zn in sedimentary deposits are often discussed in context with reducing bottom water conditions (Shaw et al., 1990; Piper, 1994; Piper and Perkins, 2004; Alego and Maynard, 2004).

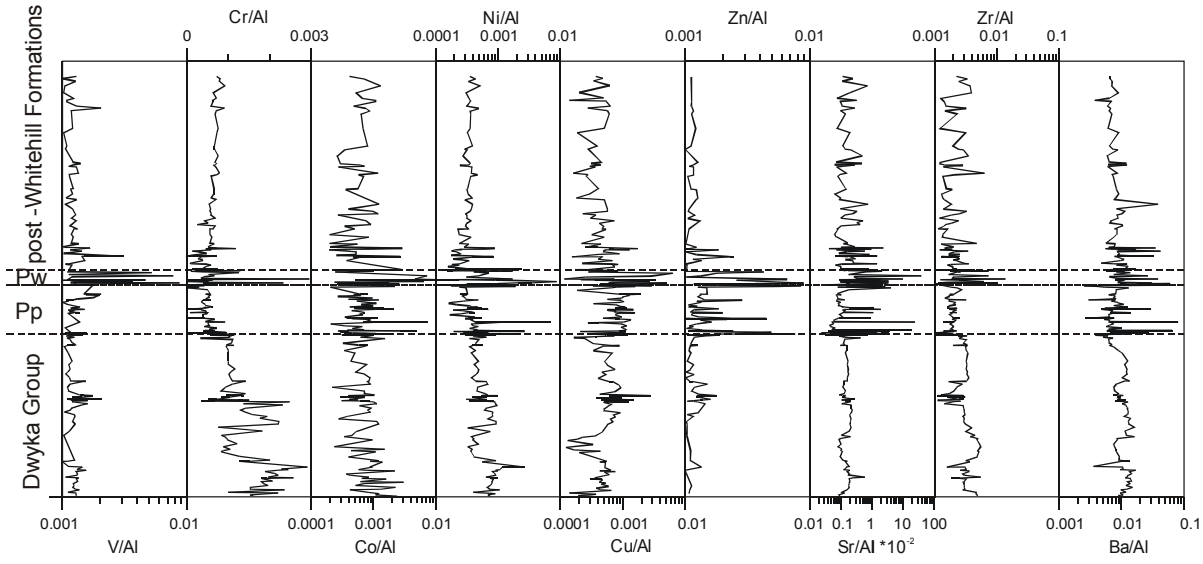


**Figure 4-11**

Selected trace elements from the southern Karoo Basin normalised on their Al content. Pp = Prince Albert Formation, Pw = Whitehill Formation

Small variations of the V/Al ratios in the Dwyka sediments (Fig. 4-11) point to changing clay mineral contents. The carbonate bearing shales of the Whitehill Formation show markedly elevated V contents. The coupling of vanadium to clay minerals is indicated by the linear relation between $Al_2O_3$ and V in figure 4-12a. Elevated vanadium contents in samples from the Prince Albert (Pp) and Whitehill (Pw) Formation of the southern Karoo Basin plot in the grey shaded area. Wedepohl (1978) pointed out that marine sediments and especially bituminous ones show a remarkable increase in vanadium. Shales and recent clays often

contain between 100 and 150 ppm V. Beside vanadium also the element/Al ratios of the transition metals Cr, Co, Ni, Cu, and Zn show high concentrations in the Whitehill Formation (Fig. 4-11). In contrast to V, Cr and Cu, high element/Al ratios of Co and Ni denote also the carbonate bearing samples (CaO > 40 wt%) at the Dwyka/Ecca boundary (Fig. 4-11a). Carbonates and organic carbon acted as reducing agent, favouring the accumulation of transition metal elements in these layers. In oxic environments the occurrence of Ni and Co is closely related to the formation of iron and manganese oxides. In $H_2S$-environments, both elements can replace small amounts of Fe in the mineral structure of pyrite (Berner, 1983) or get incorporated in organic matter.

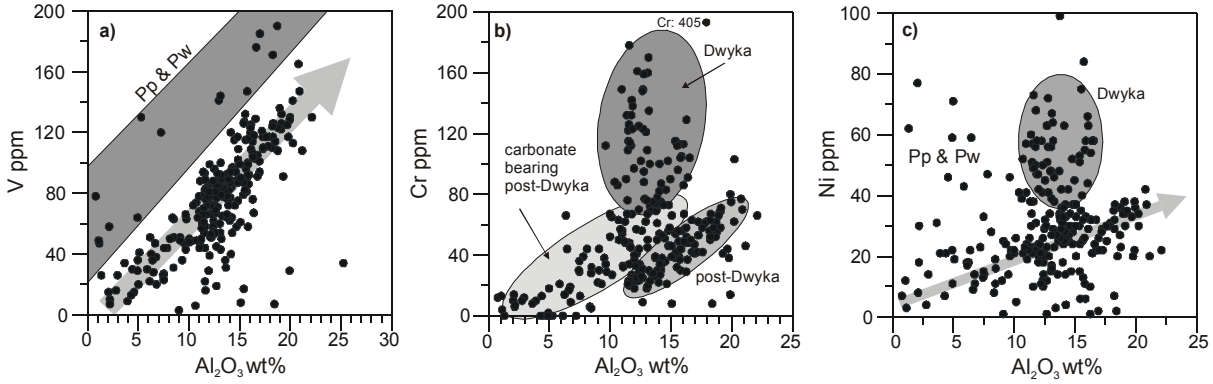


**Figure 4-12 a-c**

Bivariate plots of major and trace elements from the southern Karoo Basin. Signatures are explained in the text.

The occurrence of Cr in sedimentary deposits is associated with the allogenic mineral fraction. Because $Cr^{3+}$ resembles $Al^{3+}$ and $Fe^{3+}$ in its chemical property and ionic size, it behaves similar to these ions during weathering processes, and will be finally get concentrated in clays (Wedepohl, 1978). Average Cr contents for shales can be estimated with 83 ppm and for sandstones with 27 ppm. Sediments deposited under anoxic conditions contain in general higher chromium contents. As displayed in figure 4-12b Cr is positively correlated with the $Al_2O_3$ content. Samples from the Dwyka Group differ from this trend by higher Cr contents (upper dark grey shaded ellipse in Fig. 4-12b). Since these sediments were rather deposited in oxygenated bottom water, mobilisation and precipitation processes cannot explain the elevated Cr contents. As displayed in figure 4-3e, Dwyka sediments can be discerned form the postglacial deposits by elevated Mg contents, due to the occurrence of chlorite. Deer et al. (1993) indicated that $Cr^{3+}$ is present in chlorite in the octahedral interlayer. Thus, high chromium contents may point to the presents of chlorite in the Dwyka sediments. By the breakdown of chlorite, samples from the postglacial units plot into the lower grey shaded ellipse in the $Al_2O_3$ vs. Cr diagram (Fig. 4-12b). Miscellaneous, in general carbonate bearing samples, lie in-between both groups in figure 4-12b.

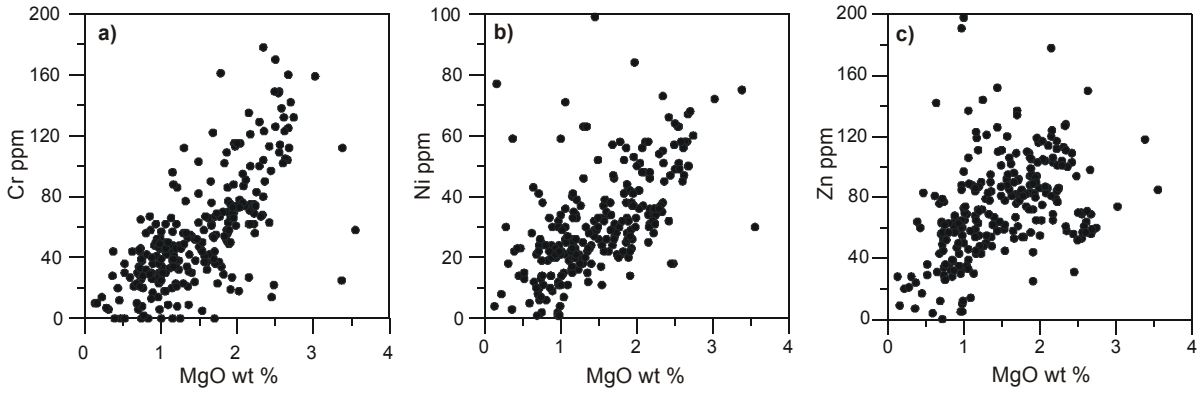


**Figure 4-13 a-c**

Bivariate plots of major and trace elements from the southern Karoo Basin. Signatures are explained in the text.

Since $Ni^{2+}$ or $Zn^{2+}$ can also substitute $Mg^{2+}$ in chlorite, the samples are similarly distributed in the MgO vs. Cr, Ni or Zn diagrams (Figs. 4-13a-c). In consequence, Dwyka samples can be distinguished from the other Formations also by elevated Ni contents (grey ellipse in Fig. 4-12c). In contrast to relatively low Cr contents in samples with low $Al_2O_3$ contents, single samples of the Prince Albert and Whitehill Formation are markedly enriched in Ni (Fig. 4-12c). Cobalt resembles nickel in many of its physical and chemical properties. Due to their intermediate radii between $Mg^{2+}$ and $Fe^{2+}$, $Co^{2+}$ and $Ni^{2+}$ substitute for these cations in several silicates (Shannon and Prewitt, 1969). The replacement of $Mg^{2+}$ in chlorite by $Ni^{2+}$ is displayed by the significant correlation in figure 4-13b ($\rho$ is 0.56) whereas correlation coefficients of $\rho = 0.21$indicate no significant correlation between MgO and Co.

Changing Sr contents are closely related to the carbonate content of the samples (Fig. 4-14a). Conspicuous peaks in the Sr/Al ratio denote carbonate formation at the Dwyka/Ecca boundary and in the Whitehill Formation (Fig. 4-11). Beside Sr, Ca can also be replaced by small amounts of Ba, Co and Zn (Deer et al., 1993).

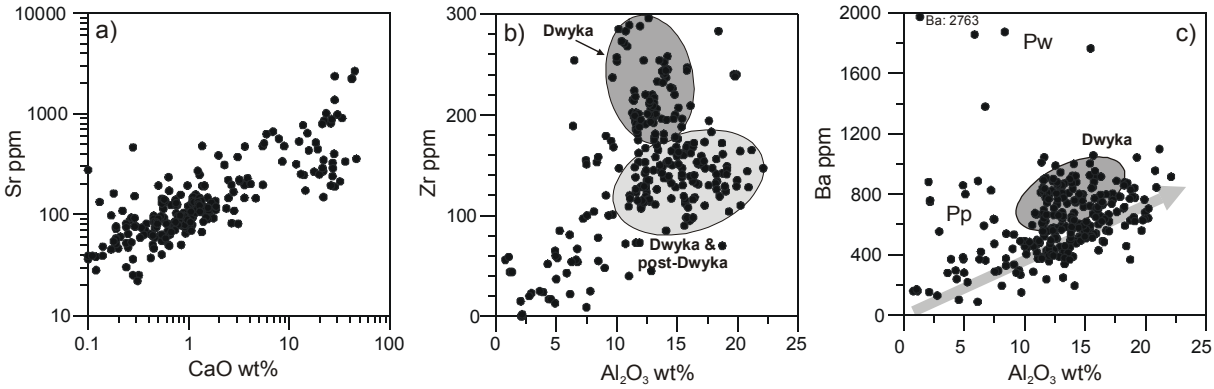


**Figure 4-14 a-c**

Bivariate plots of major and trace elements from the southern Karoo Basin. Signatures are explained in the text.

Zirconium, a classical high field strength element is mainly fixed in zircon. As separate mineral phase zircon formed during late differentiation stages in magmatic processes. In sediments the Zr content is associated with the terrigenous, allochthonous sediment fraction. In the Dwyka Group elevated Zr/Al ratios can denote interstadial phases of DS I and DS II (Fig. 4-11). During interstadial of DS III and at the Dwyka/Ecca boundary Zr/Al ratios decrease whereas in all glacial units the ratios remain relatively constant. Postglacial sediments of the Prince Albert Formation contain lower Zr/Al ratios than the Dwyka sediments. Figure 4-14b indicates that variations in the Zr/Al ratio are controlled by changing zirconium contents and not by variable clay mineral contents. Therefore, material supply from different provenances can be assumed as controlling factor of changing Zr contents during deposition.

Barium a large lithophile element can replace potassium in biotite and K-feldspar. Most Ba in particulate matter resides in barite, the most important Ba mineral. Additionally, Ba can replace Ca in carbonates. Ba is a suitable proxy for paleoproductivity and paleoenvironment (Wehausen et al., 2000). Paytan et al. (1996) pointed out that Ba is also a component of sediment phases not directly related to biogenic productivity, such as windblown silicates and Fe-Mn oxyhydroxides. Therefore, changes in the Ba/Al ratio must not necessary allude to changes in the paleoproductivity. Because of elevated Ba contents, Dwyka samples plot into the ellipse above the labelled $Al_2O_3$/Ba trend indicating the occurrence feldspar (Fig. 4-14c). High Ba/Al ratios during glacial phases versus lower ratios during interstadial phases point to changing weathering conditions. Ba/Al peaks at the Dwyka/Ecca boundary confirm the high carbonate contents of these samples. High Ba contents recorded in the Whitehill Formation (Figs. 4-11 & 4-14c), are possibly associated with elevated deposition of organic matter. In context with phosphate formation at the Dwyka/Ecca boundary and during the Whitehill Formation (Fig. 2-2j) it can be assumed that the nutrient supply temporarily changed.

#### 4.2.3.2 MPU core

Also in the MPU core (Fig. 4-15) conspicuous variations of the trace element contents can be recognised at the Dwyka/Ecca boundary. Increasing element/Al ratios of the transition metals with exception of Cr can be recognised in samples with elevated Sr and $C_{org}$ contents (Figs. 2-3j & 4-15). Elevated transition metal contents are rather associated with the accumulation of organic matter than with carbonate formation as indicated by the correlations shown in figure 4-16. Cr contents decrease constantly throughout the core (Fig. 4-15). In contrast to the other transition metals, Cr is not enriched in strata with elevated $C_{org}$ content. As in the southern Karoo Basin the Cr content seems to be primarily controlled by the chlorite proportions, which decrease in the upper core section (Fig. 3-3).

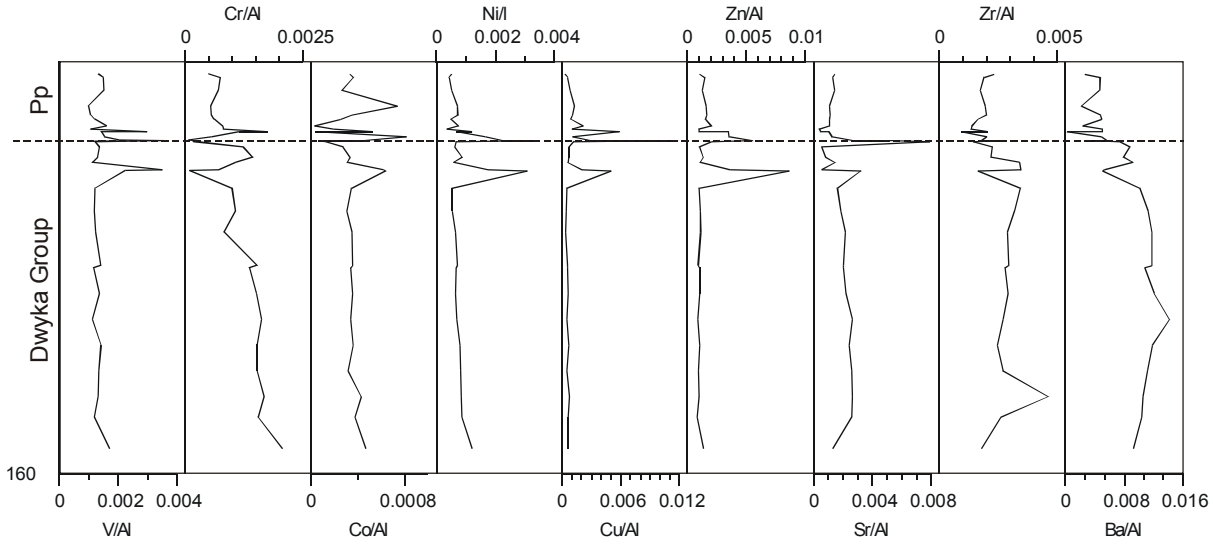


**Figure 4-15**

Selected trace elements from samples of the MPU core normalised to their Al content. Pp = Prince Albert Fm.

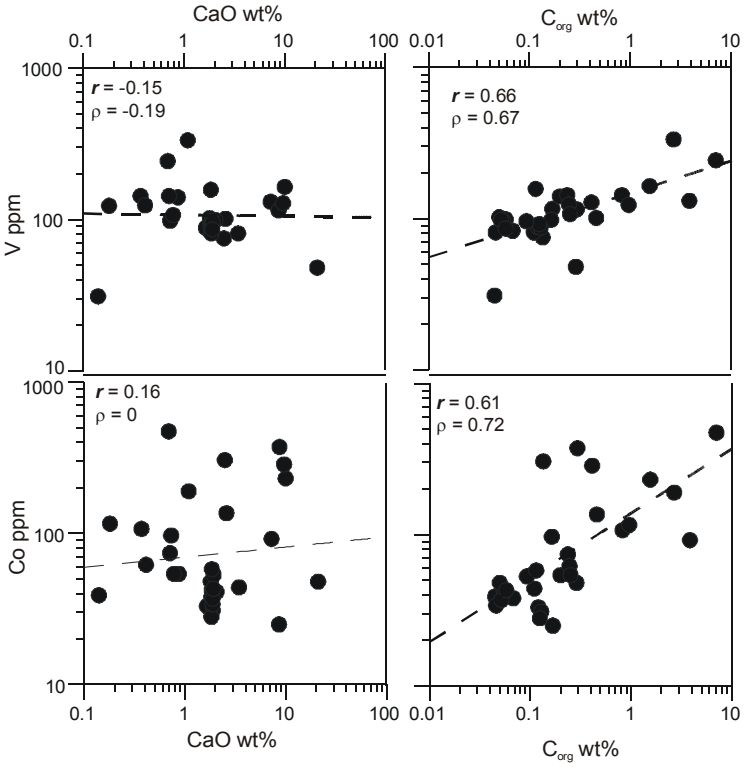


**Figure 4-16**

Correlation of Co and V as representatives of the transition metals versus $C_{org}$ or CaO contents.

Comparable to the Na/Al ratios (Fig. 4-4g), Ba/Al ratios decrease at the Dwyka/Ecca boundary (Fig. 4-15). In contrast to the southern Karoo Basin, Ba is not associated with carbonate phases or organic matter. Because of the linear relation between Ba and $Al_2O_3$ or $Na_2O$, respectively, the barium content is predominantly controlled by the occurrence of albite in the Dwyka Group sediments (Figs. 4-17a & b).

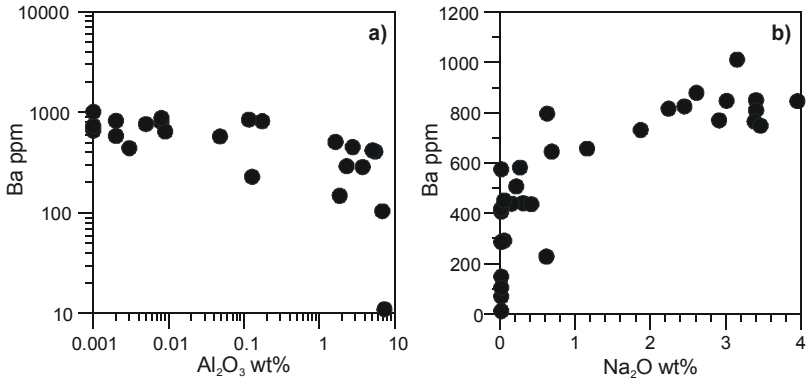


**Figure 4-17a & b**

Bivariate plots of $Al_2O_3$ and $Na_2O$ versus Ba indicate predominantly fixation of Ba to feldspar.

### 4.2.3.3 OGT core

The distribution of the trace elements in the OGT core is shown in figure 4-18. Significantly elevated transition metals contents, as possibly expected due to high amounts of organic matter in the Tswane, Mea and Tlapana Fm. cannot be recognised.

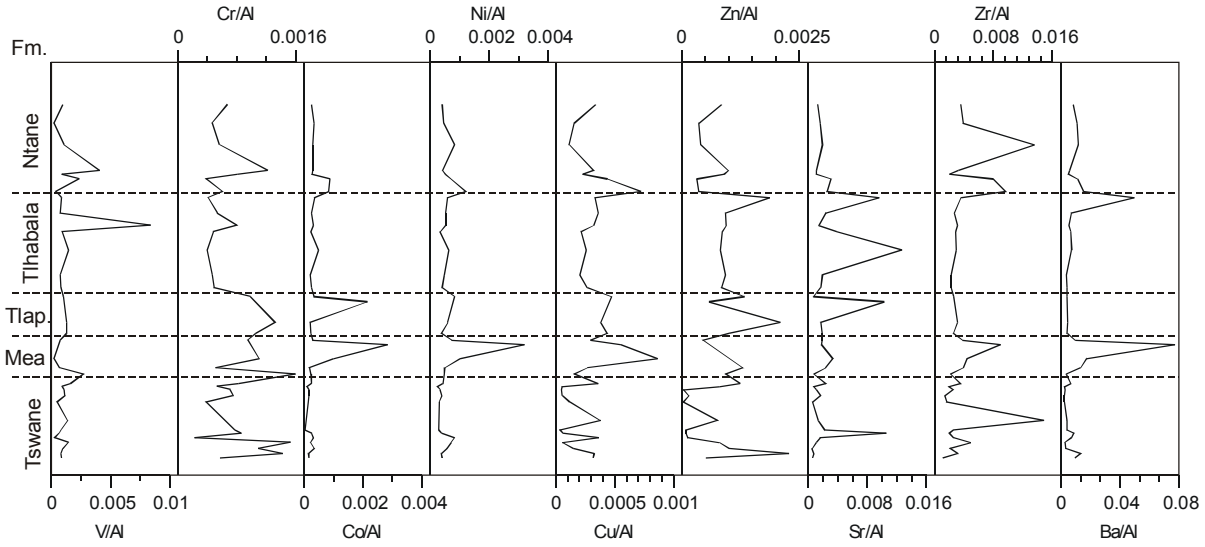


**Figure 4-18**

Selected trace elements from the OGT core of the Kalahari Basin normalised to their Al content.

$C_{org}$ rich samples from the Tswane Formation differ in figures 4-19a & b from the sample series due to lower Cr and Cu contents. In general, samples from the upper Ecca Group contain higher transition metal contents than samples from the lower Ecca Group. As in the localities discussed before, peaks in the Sr/Al ratio denote the occurrence of carbonates (Fig. 4-18). Variations in the Zr/Al ratios cannot be associated with pronounced changes of the provenance during deposition. The single peaks rather pointed to temporary events. In figure 4-19c decreasing zirconium versus increasing $C_{org}$ contents are displayed. Since Zr is associated with the terrigenous heavy mineral fraction it can be assumed that accumulation of organic matter was favoured in low energy sedimentary environments.

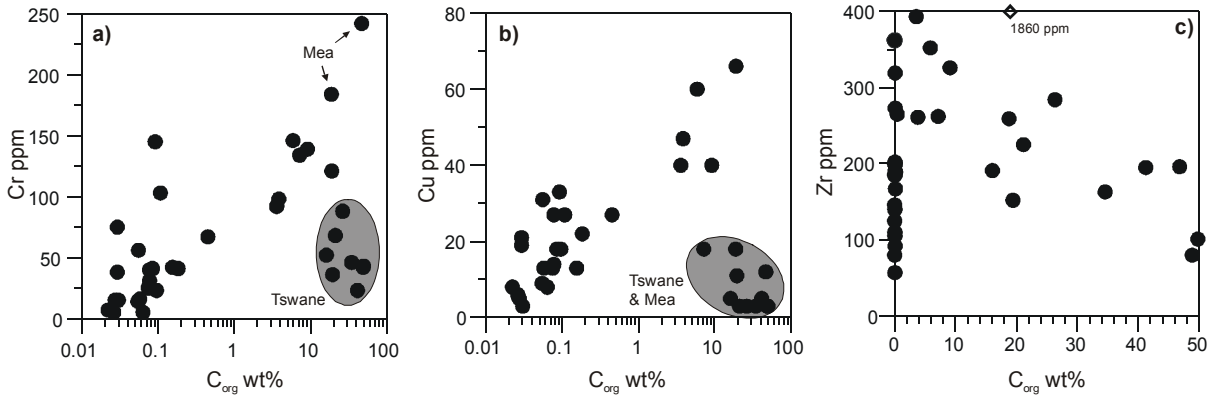


**Figure 4-19a-c**

Bivariate plots of $C_{org}$ versus selected trace elements.

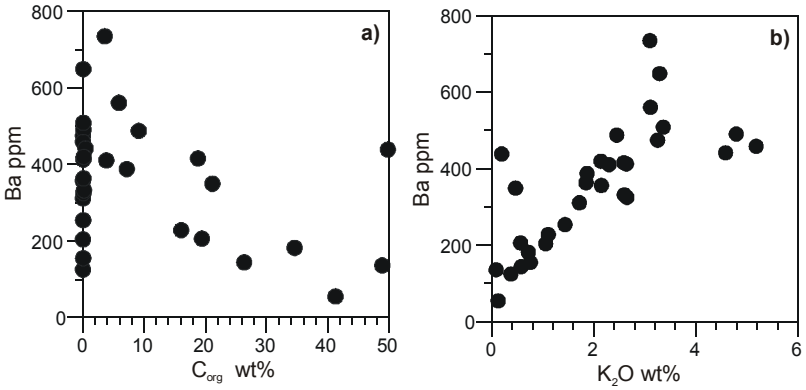


**Figure 4-20a & b**

Bivariate plots of $C_{org}$ versus Ba and $K_2O$ contents.

Similar to the MPU core, Ba cannot be used as proxy of the paleoproductivity. Decreasing Ba versus increasing $C_{org}$ contents and the significant correlation between $K_2O$ and Ba (Figs. 4-20a & b) point to the fixation of Ba to illite or feldspar.

### 4.2.3.4 Warmbad Basin

Trace elements of samples from the Warmbad Basin are displayed in figure 4-21. Differences between lower (0 to 80 m) and upper Dwyka Group (80 to 150 m) derive from a change in sample localities. Higher element/Al ratios of V, Co and Cu, and higher $C_{org}$ contents characterize the lower unit.

At the Dwyka/Ecca boundary (150 m) and in the following Prince Albert Formation (150 to 180 m), significant changes in the trace element contents are not observed. Decreasing element/Al ratios of Co, Ni, Cu, and Zn driven by increasing quartz contents (Figs. 4-22a-c & Fig. 4-21), differentiate the Whitehill from the Prince Albert shales.

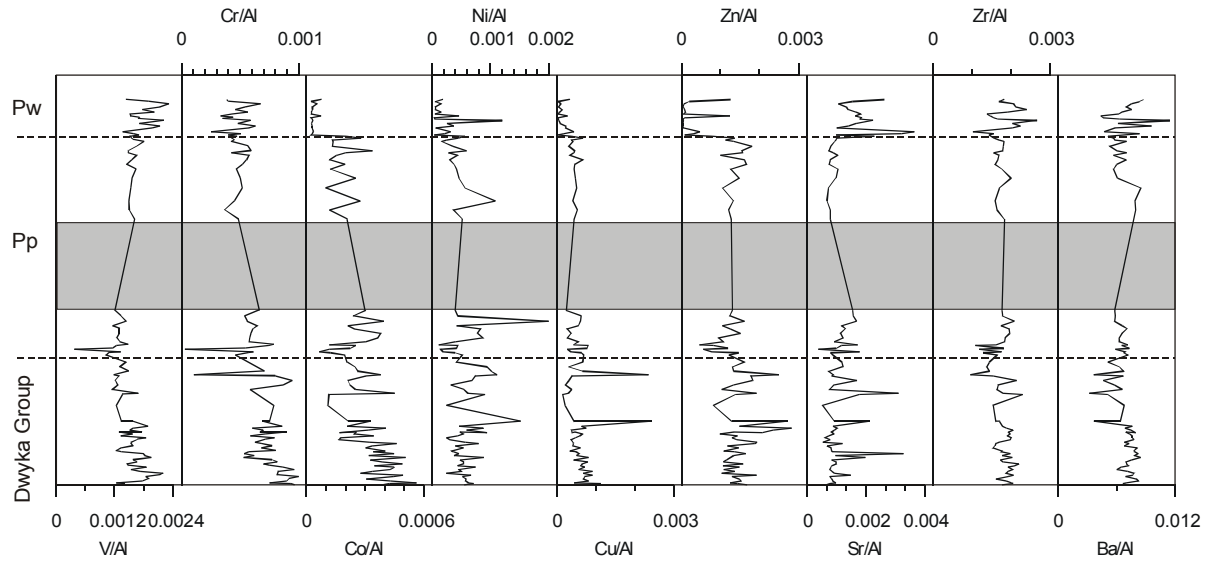


**Figure 4-21**

Selected trace elements from the sampled succession of the Warmbad Basin, normalised to their Al contents.

In contrast to the sample localities of the Karoo Basin, transition metals are not enriched in $C_{org}$ rich sediments of the Whitehill Formation. Only V/Al and Cr/Al ratios rise concomitantly to the $C_{org}$ contents. The carbonate content is in generally low in the sediments from the Warmbad Basin. Slightly increasing Sr/Al ratios (Fig. 4-21) and elevated Si/Al ratios (Fig. 4-22) point to higher feldspar proportions in the Whitehill sediments. Zr/Al ratios range around 0.002. Variations of the Zr/Al ratios, with regard to changing provenance, cannot be detected. Ba is predominantly bounded to feldspar or illite because of predominantly low Ba/Al ratios in most of the samples.

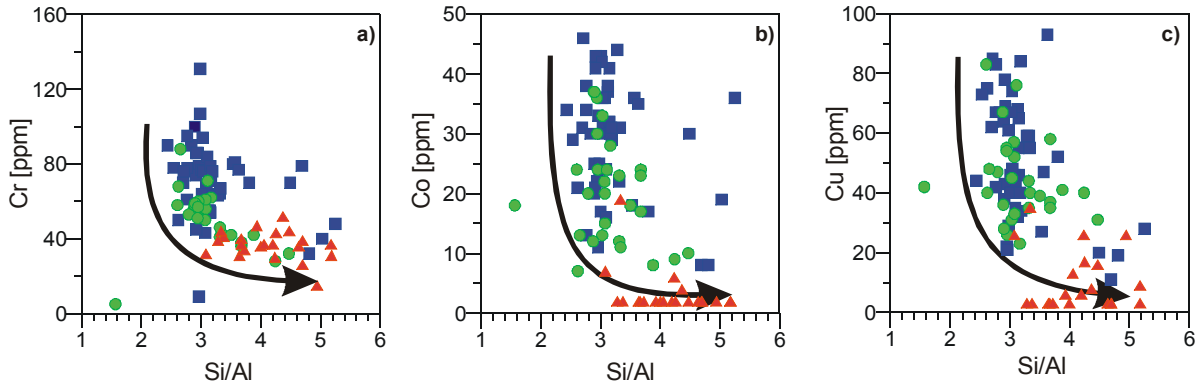


**Figure 4-22a, b & c**

Bivariate plots of Si/Al versus Cr, Co and Cu. Arrows denote dilution trends by the input of quartz. Squares=Dwyka Group, dots=Prince Albert Fm., triangles=Whitehill Fm.

### 4.2.3.5 northern Paraná Basin

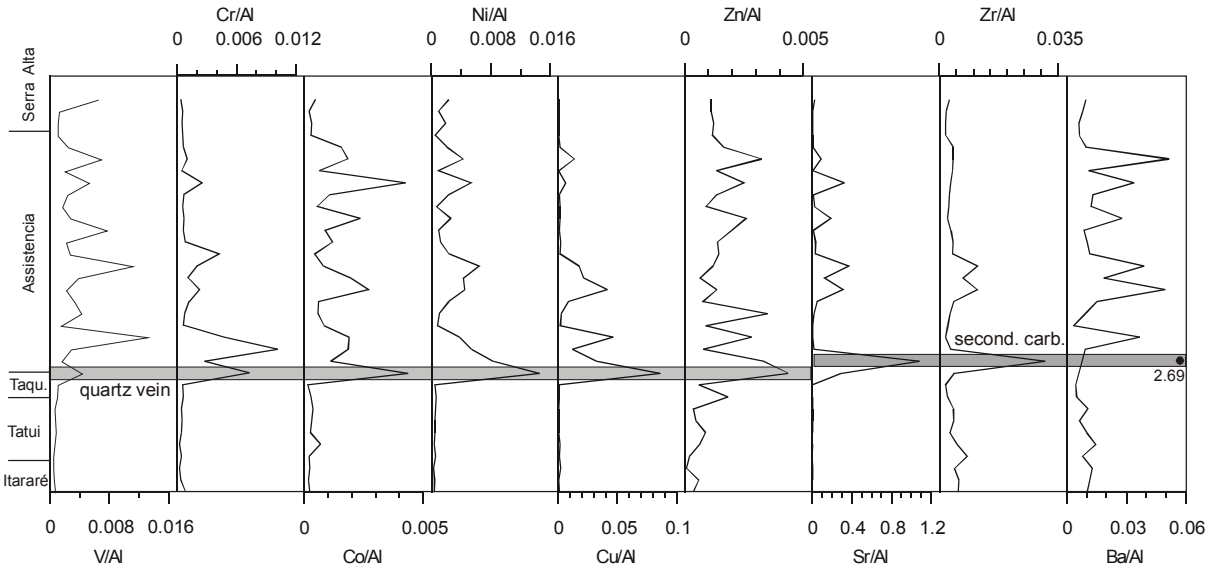


**Figure 4-23**

Selected trace elements from the sampled succession of the Paraná Basin, normalised to their Al contents.

Changes of the trace element contents in samples from the northern Paraná Basin are shown in figure 4-23. Conspicuous changes in the trace element contents occurred at the base of the Assistencia Formation. The first peaks in the element/Al ratios of V, Cr, Co, Ni, Cu and Zn derive from quartz veins in the lower Irati Formation and are therefore not representative for the entire sedimentary succession. High Sr/Al, Zr/Al and Ba/Al (2.69) ratios characterize secondary carbonate concretions in the lower Assistencia Formation.

In carbonate bearing samples the transition metals are enriched in relation to their Al content, whereas the absolute content of these elements is higher in the carbonate free shales. For example, Cr contents are plotted versus $Al_2O_3$ and CaO in figure 4-24a & b.

The better correlation between Cr versus $Al_2O_3$ than versus CaO point to the fixation of Cr in the clastic sediment fraction. Since Cr versus $C_{org}$ also shows no significant correlation (Fig. 4-24c), it can be assumed that transition metals are chiefly bounded to clay minerals. Despite sedimentation under anoxic conditions the absolute transition metal content is rather low in the black shales of the Irati Formation.

Peaks in the Sr/Al ratio indicate the substitution of Ca by Sr and label samples of high carbonate contents (CaO > 30 wt%). High Zr/Al ratios in the middle Assistencia Formation can be associated with high carbonate contents (CaO + MgO are 45%) and therefore with low Al proportions. Comparable with the transition metals, barium is rather bound to the clay mineral fraction than to carbonates or organic matter (Figs. 4-24d-f).

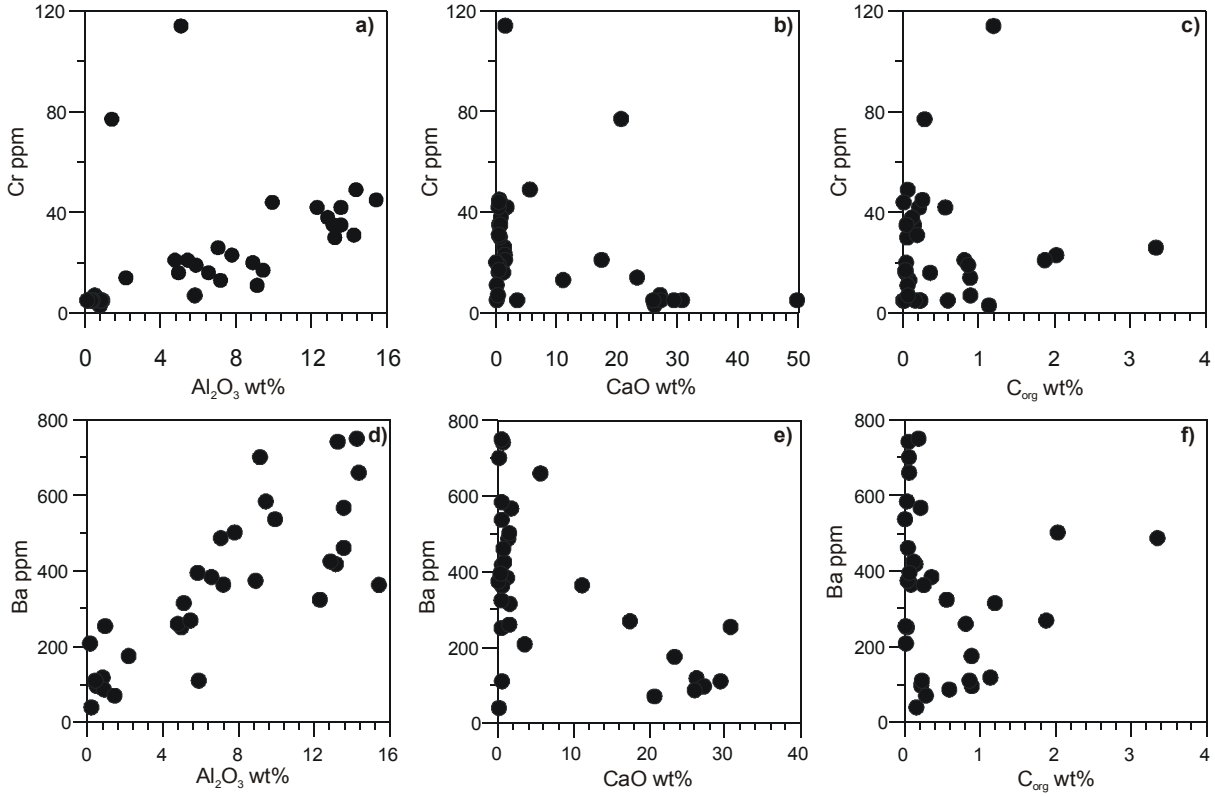


**Figure 4-24a-f**

Bivariate plots of Cr and Ba versus $Al_2O_3$, CaO and $C_{org}$ contents of samples from the Paraná Basin.

## 4.2.4 Cluster analyses

By cluster analysis characteristic element associations can be linked with significant mineral phases. Selected elements were used (major elements, transition metals, Rb, Sr, Zr, Ba and Ce) for the calculation of the following dendrograms (Fig. 4-25 to 4-29).

Element associations, representative for significant mineral phases are displayed in the dendrograms. Low linkage distances (similarity ≈ 1) indicate good correlation between the amalgamated element clusters, high distances impose a lack of correlation (similarity ≈ 0) and distances below zero point to negative correlation between the elements of the linked clusters. As distance matrix the Spearman rank order correlation coefficient and as amalgamation rule/schedule the unweighted pair group average was used.

### 4.2.4.1 Karoo Basin

The cluster analyses of selected elements from the southern Karoo Basin are displayed in figures 4-25 to 4-29. Glacial and interstadial sediments of the Dwyka Group are discussed in separate figures.

### Glacial units

The cluster analysis formed three major branches in the dendrogram of figure 4-25a. The main branch combines the elements Rb, K, Cu, Fe, Zr, Ce, Zn, P, Na, Ti and Al. Low linkage distances (high similarity) indicate good correlation between these elements. However, a well-defined mineral association representative for this cluster cannot be detected. As a first approximation various alumosilicates such as feldspar and clay minerals can be assumed. Marked negative correlation coefficients of $SiO_2$ to the other elements (Tab. 4-3) are shown in the dendrogram by the negative linkage distance between the Si-Ca-branch and the main clusters. The amalgamation of Si and Ca at zero indicates no correlation between both elements. Since the Dwyka sediments are in general carbonate free (Fig. 4-2f), Ca is chiefly bounded to alumosilicate phases such as plagioclase.

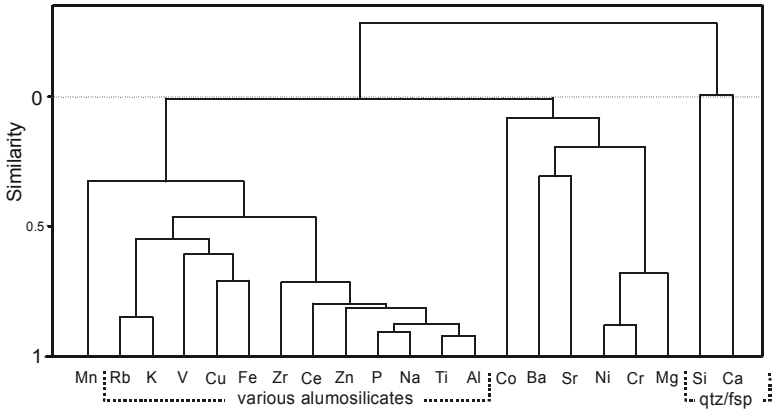


**Figure 4-25**

Cluster analysis of selected elements from glacial Dwyka Group sediments (S' Karoo Basin). 21 variables, 35 cases

Diamictites are in general described as mixture of a wide variety of allogenic and authigenic mineral phases. Thus, a clear designation of single mineral phases cannot be expected. In combination with element/Al ratios in figure 4-2, a mineral association of quartz, feldspar, chlorite, illite, mica and various oxides can be assumed for the glacial Dwyka sediments.

### Interstadial units

In comparison to the cluster analysis of the glacial sediments (Fig. 4-25) the linkage distances in the dendrogram of the interstadial sediments decreased (Fig. 4-26). Si and Zr form a single branch, which is linked to the major branch at high linkage distance (negative correlation). Comparable to the glacial units, the major branch comprises all other elements, which hampered the identification of well-defined mineral paragenesis. The element cluster of Sr-P-Ca seems to indicate low proportions of carbonates or Ca-phosphates in the interstadial sediments. The formation of a separate Si-Zr-cluster, negatively correlated to the other cluster, point to an elevated input of autochthonous mineral phases.

With regard to the comparable element clusters of glacial and interstadial units it can be assumed that despite of climate changes the Dwyka Group sediments contain a relative

constant mineralogical composition. It has to be remarked that assumed changes in provenance could generally mask the obtained signals. However, the formation of carbonates as indicated by the element cluster Sr-P-Ca, points to changing sedimentary conditions during interstadial phases.

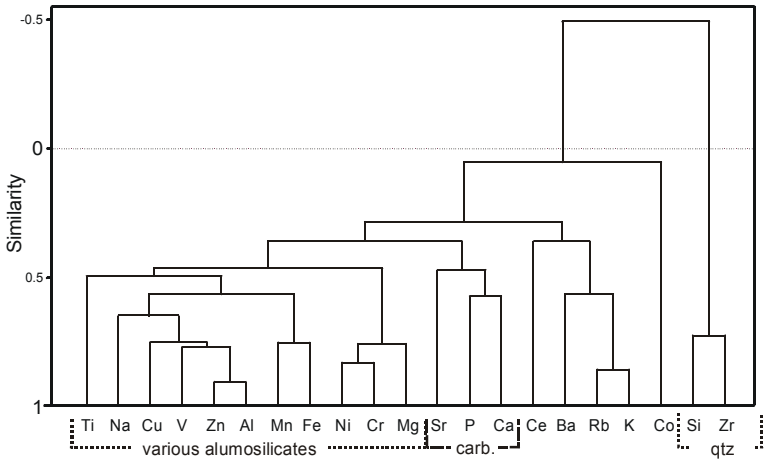


**Figure 4-26**

Cluster analysis of selected elements from interstadial Dwyka Group sediments (S' Karoo Basin).
21 variables, 55 cases

## Prince Albert Formation

In the dendrogram of the Prince Albert Formation (Fig. 4-27) new element clusters are formed. Especially the negative correlated cluster of Si-Zr or Ca is inexistent in the dendrogram of the postglacial sedimentation phase. Instead of this cluster now the elements of Sr, Ca, Mn, P, Ce and Ni are linked with negative distances to the main cluster. Rollins (1995) point out that in carbonat bearing shales, the elements Mn and Sr are chiefly incorporated in the carbonate component. Thus the formation of carbonates in the lower Ecca Group is expressed by amalgamation of Sr, Ca, Mn (Fig. 4-27). In phosphates Ce can replace Ca to a considerable extent (Deer et al., 1994). Thus, the amalgamation of P and in a later step Ce to the carbonate cluster is associated with phosphate formation in distinct horizons of the Prince Albert Formation. If the linkage of Ni to this cluster indicates the fixation of Ni to carbonates or phosphates is questionable.

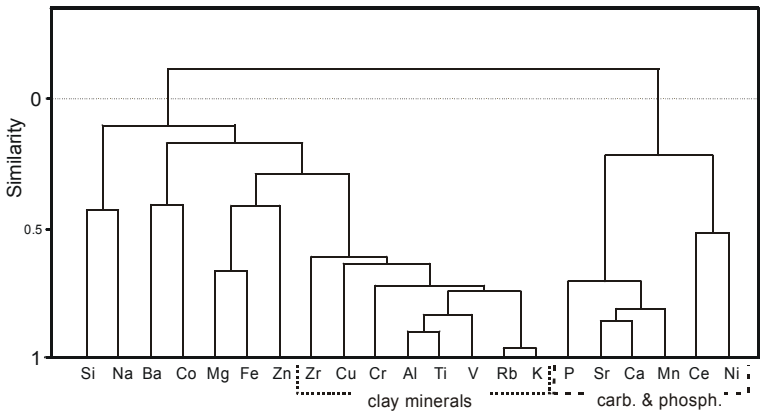


**Figure 4-27**

Cluster analysis of selected elements from sediments of the Prince Albert Fm. (S' Karoo Basin).
21 variables, 65 cases

The alumosilicate fraction is represented by the significant element cluster of Rb, K, Ti, Al and V. The good correlation between K and Rb, in consequence of the substitution of K by Rb in clay minerals, is expressed by short linkage distance. The amalgamation of V, Cr and Cu to this basis cluster can be explained by absorption of theses elements at clay mineral surfaces in reducing environments.

The late fusion (negative distance) of the carbonate/phosphate element cluster and alumosilicate element cluster point to changing sedimentary conditions. Periods of carbonate/phosphate formation alternate with phases of elevated input of siliciclastic material. Therefore, establishing of permanent anoxic conditions during early postglacial times was possibly hampered by frequently changing sedimentary conditions.

**Whitehill Formation**

By cluster analysis the elements of the sediments from the Whitehill Formation are grouped in two clusters (Fig. 4-28). The negative correlation of both element clusters is expressed by high linkage distance (below zero). One branch represents carbonates and Fe/Mn-mineral phases, indicating carbonate formation under anoxic conditions. The amalgamation of Mg to this element cluster points to dolomite formation in the Whitehill sediments. Since anoxic conditions are indicated by high sulphur and $C_{org}$ contents (Figs. 4-2 j & k) during deposition of the Whitehill Formation, the element association of Mn, Fe and transition metals are representative for mineral phases formed under reducing conditions.

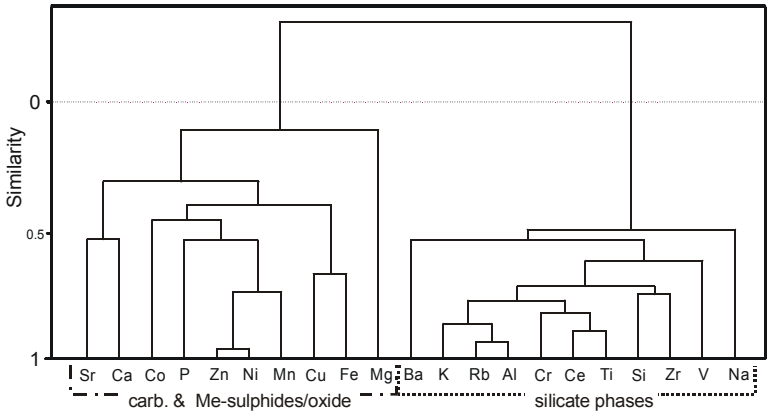


**Figure 4-28**

Cluster analysis of selected elements from sediments of the Whitehill Fm. (S' Karoo Basin). 21 variables, 26 cases

Clay minerals are represented by the element cluster of Rb, Al, K, and Ti. The early amalgamation of Si to this cluster indicates that silica is not chiefly attributed to quartz as in the Dwyka sediments, but rather to alumosilicate phases. V and Cr are linked to the alumosilicate element cluster as consequence of absorption of the cations onto clay mineral surfaces. The high linkage distance between both element clusters point to contrasting sedimentary conditions during deposition of the Whitehill Formation. Phase of elevated siliciclastic input were followed by periods of reduced sedimentation rates whereby carbonates were formed and anoxic conditions could be established.

Beside different carbonate/phosphate minerals, Fe/Mn-oxides and sulphides, kaolinite and illite can be assumed as major mineral phases in the Whitehill Formation.

**post-Whitehill Formations**

The analyses of post Whitehill sediments comprise samples of the Collingham, Vischkuil, Laingsburg and Ford Brown Formations (Fig. 4-29). Sedimentary conditions were dominated by deltaic/turbiditic systems with a predominantly input of siliciclastic debris.

All three main clusters are negatively correlated and amalgamated at high linkage distances. The main branches represent element associations of clay minerals, a more quartz dominated component and the element cluster Ca, Mn, Sr and P representative for carbonates. The latter was also formed in the carbonate bearing Prince Albert Formation. A well-defined element-grouping representative for anoxic conditions as in the Whitehill Formation is missing in the dendrogram of the post-Whitehill sediments.

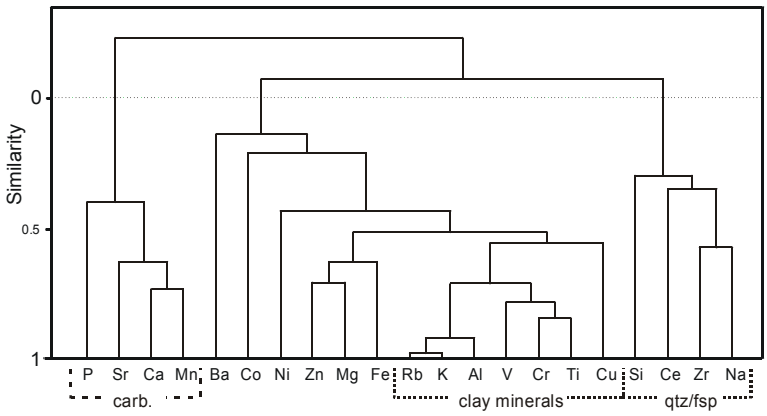


**Figure 4-29**

Cluster analysis of selected elements from post Whitehill sediments.
(S' Karoo Basin). 21 variables, 87 cases

Single peaks in the Ca/Al and Mn/Al ratios (Figs. 4-2a & f) indicate that carbonate formation is restricted exclusively to single layers during deposition of the turbiditic units in the upper Ecca Group. The variable input of siliciclastic material during phases with changing sedimentation rates by turbiditic currents is displayed by separate clusters in figure 4-29. The element cluster of Si, Ce, Zr and Na is associated with the coarser silicate fraction composed of quartz and feldspar. The larger element cluster containing Al and Ti is representative for the clay mineral fraction. The input of changing clastic debris is also reflected by peaks in the Si/Al ratio (Fig. 4-2a). Low Si/Al ratios correspond with the average shale composition whereas high values in the post-Whitehill formations reach arkosic composition.

**Conclusion**

The dendrograms of the cluster analyses in figures 4-25-29 in accordance with the element/Al ratios and correlation coefficients (Tabs. 4-3 to 4-8) represent the sedimentary evolution in the southern Karoo Basin.

Constant element/Al ratios of the clastic Dwyka Group sediments can be associated with deposition in a relatively stable environment. Single peaks in the Si/Al ratios (Fig. 4-2a) point

to short-time variations in the sedimentary environment. The autochthonous debris was predominantly composed of siliciclastic material as indicated by the cluster analyses (Figs. 4-25 & 26). Element clusters representative for carbonates, oxides or sulphides are not formed in the dendrograms of the glacial and interstadial Dwyka Group sediments.

The Prince Albert Formation comprises the initial postglacial sedimentation phase in southern Gondwana. Severe variations in various element/Al ratios indicate significant changes in the sediment supply and in the sedimentary environment. Carbonate formation beside periods of deposition of fine-grained siliciclastic material characterise the sedimentation phase of the Prince Albert Formation.

Dysoxic conditions evolved during the Prince Albert Formation. Anoxic conditions in the Whitehill Formation are indicated by increasing $C_{org}$ and sulphur contents (Figs. 4-2j & k). Consistently, the cluster analysis (Fig. 4-28) determinates element associations, which are associated with mineral phases representative for anoxic conditions.

In consequence of tectonic activity at the southern basin border during the post-Whitehill Formations the sedimentary conditions changed again. The sediment input was now chiefly triggered by the rising Cape Fold Belt. Turbidity currents are recorded by frequent peaks in the element/Al ratios. The formation of element clusters representing quartz/feldspar and clay minerals (Fig. 4-29) points to increasing input of clastic material. Phases of lower sedimentation rates and carbonate formation are recorded by single peaks in the Ca/Al ratio (Fig. 4-2f) as well as by the element cluster P, Sr, Ca and Mn (Fig. 4-29).

### 4.2.4.2 MPU

By cluster analysis significant element associations can be distinguished in the core samples of the southeastern Karoo Basin (Fig. 4-30).

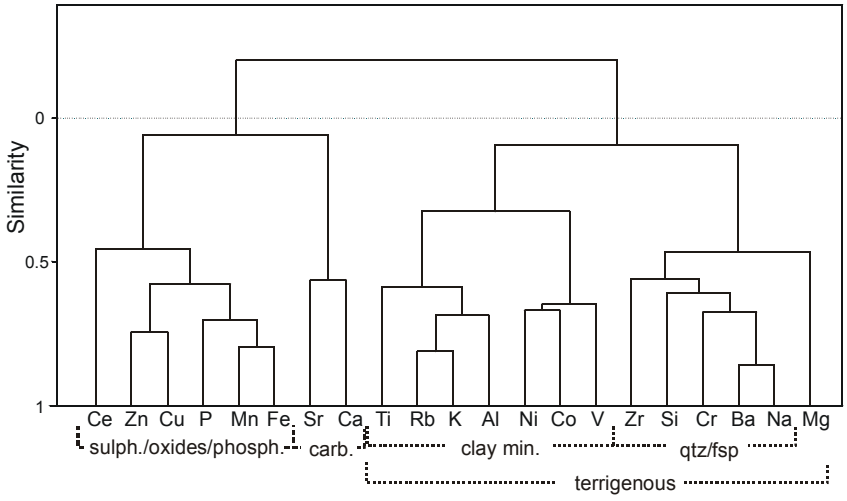


**Figure 4-30**

Cluster analysis of selected elements from MPU drill core samples (SE Karoo Basin). 21 variables, 31 cases
distance matrix: Spearman rank order correlation coefficient; Amalgamation schedule: unweighted pair-group average

The terrigenous mineral fraction is split into two branches. Due to limited chemical weathering during deposition of the Dwyka Group, the Si-Na cluster is associated with the quartz/feldspar fraction. Leaching processes in consequence of humid climate conditions in the Prince Albert Formation favoured the formation of clay minerals, represented by the second cluster with the significant element association Al-Ti-K-Rb. Negatively correlated to these clusters are elements associated with carbonate, phosphate and Fe/Mn-mineral phases. High P/Al ratios at the Dwyka/Ecca boundary accompanied by increasing $C_{org}$ and S contents (Fig. 4-3i, j & k) denote the onset of postglacial climate conditions by phosphate formation at anoxic conditions. Comparable to the dendrograms in figures 4-27 & 4-28, dysoxic/anoxic conditions and phosphate formation is represented by characteristic element clusters. The negative correlation (similarity < 0) between elements associated with silicate phases versus element clusters of carbonates, phosphates and anoxic conditions indicate changing sedimentary conditions during the Dwyka and Ecca Group. In combination with the element/Al ratios, quartz, feldspar and different clay minerals such as illite and chlorite can be assumed as main mineral phases in the sediments of the MPU core.

### 4.2.4.3 OGT

In general shorter linkage distances in comparison to the before discussed dendrograms, are characteristic for the cluster analysis of the OGT core samples (Fig. 4-31). However, well-defined mineral associations by adequate element clusters cannot be discerned.

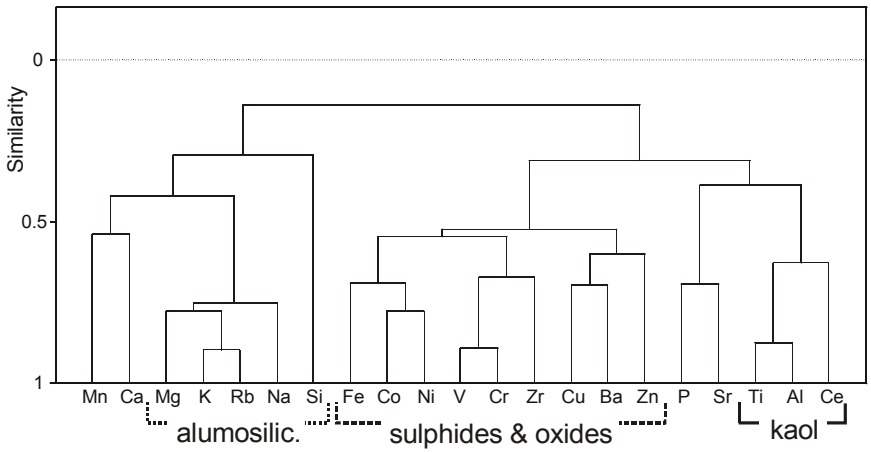


**Figure 4-31**

Cluster analysis of selected elements from OGT drill core samples (Kalahari Basin). 21 variables, 36 cases distance matrix: Sparman rank order correlation coefficient; Amalgamation schedule: unweighted pair-group average

By cluster analysis the elements are divided into two main branches. The similar trends of the element/Al ratios in figures 4-4e, g & h are expressed in the dendrogram by the element cluster K-Rb-Mg-Na. The variations in the element/Al ratios of Si, Mg, Na and K point to changing proportions of quartz, feldspar and clay minerals. The amalgamation of Mg to the K-Rb cluster indicates the occurrence of chlorites and/or smectites. In consequence of slightly increasing Ca/Al ratios due to higher albite proportions in the upper core section (Fig.

4-4f), Ca is amalgamated to the alumosilicate cluster. Since the carbonates in the upper core section contain elevated Mn contents (Fig. 4-4d), also Mn is linked to the alumosilicate cluster. However, both elements are rather representative for the carbonates than for silicate phases. Because kaolinite is the major clay mineral in the lower core (Fig. 3-3), Al and Ti are not linked to the cluster formed by the cations of the alumosilicates. Reducing conditions can be assumed especially for the organic rich sediments in the lower core section. The element cluster Fe, Zr, Ba and transition metal elements, confirm the formation of metal oxides and sulphides.

In combination with the element/Al ratios, the cluster analysis indicates that the siliciclastic mineral fraction is composed of variable proportions of quartz, feldspar and different clay minerals. Further phases are calcite, Fe-oxides and sulphides.

### 4.2.4.4 Paraná Basin

Changing sedimentary conditions, indicated by frequent peaks in various element/Al ratios are also reflected in the dendrogram of figure 4-32. By the cluster analysis of samples from the northern Paraná Basin the elements are grouped in two main clusters representing carbonates and alumosilicate phases.

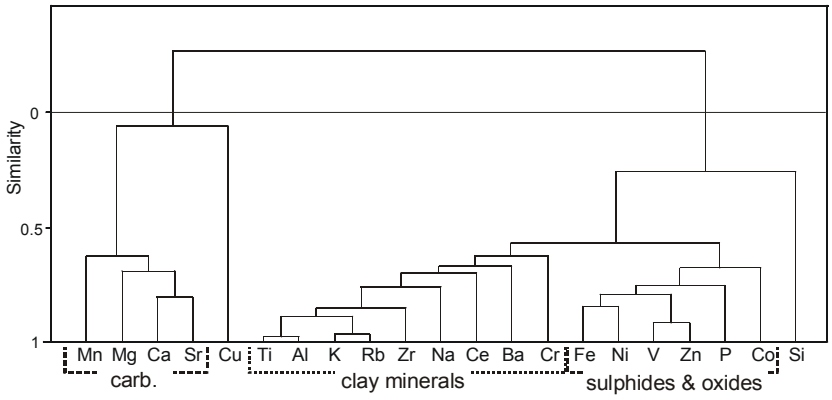


**Figure 4-32**

Cluster analysis of selected elements from northern Parná Basin. 21 variables, 34 cases distance matrix: Spearman rank order correlation coefficient; Amalgamation schedule: unweighted pair-group average

The well-defined element cluster of carbonate phases (Ca-Sr-Mg-Mn) is markedly negatively correlated to the other element clusters. The amalgamation of Mg and Ca point to the formation of dolomite as indicated by the element/Al ratios (Fig. 4-8). Alumosilicates are represented by the element cluster Ti-Al-K-Rb. The catenarian linkage of Zr, Ce, and Cr to this cluster can be explained by absorption of these elements onto clay minerals. The amalgamation of Na and Ba to the alumosilicate cluster refers to the occurrence of feldspar in the coarser sediment fraction of the Itararé and Tatui Formations. In consequence of chert concretions and quartz veins in single samples (Fig. 4-5a) Si formed an individual branch, which is at least linked to the main element cluster. Anoxic conditions in the sedimentary environment during deposition of the Irati Formation are indicated by the accumulation of

organic carbon and elevated sulphur contents (Fig. 4-5j & k). Anoxic conditions and accompanying pyrite formation are denoted by the element cluster of Fe-Ni-V-Zn-P-Co. The grouping of the elements resembles the dendrogram of the Whitehill Formation in figure 4-28. In contrast to figure 4-28, elements representative for anoxic conditions are linked with the element cluster of the alumosilicate phases.

In combination with the element/Al ratios, the samples contain variable proportions of calcite, dolomite, pyrite, illite, chlorite/smectite, quartz and as minor constituent feldspar.

### 4.2.4.5 Warmbad Basin

**Glacial phase**

The cluster analysis of the Dwyka sediments in the Warmbad Basin distinguishes two main branches. Si is linked in the last step to the main clusters in the dendrogram of figure 4-33.

The two main branches discern element associations of allogenic and authigenic mineral phases. Distinct minerals as demonstrated by the cluster analysis of the samples from Paraná Basin cannot be recognised in the Namibian Dwyka sediments. In consideration of the amalgamated elements, it can be assumed that the authigenic mineral fraction is composed of carbonates, phosphates, Fe/Mn-oxides and sulphides.

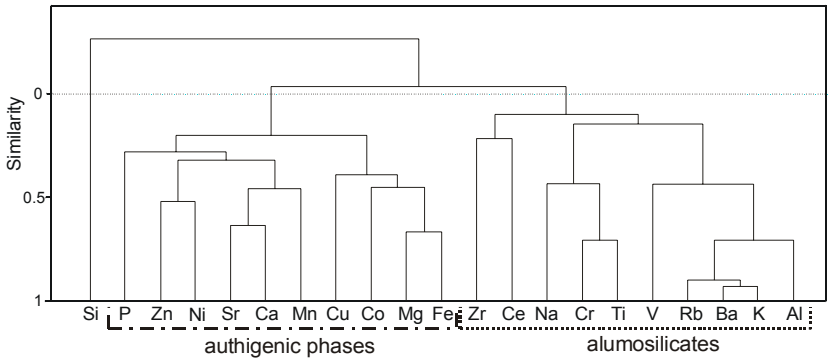


**Figure 4-33**

Cluster analysis of selected elements from Dwyka Group sediments of the Warmbad Basin (southern Namibia). 21 variables, 49 cases distance matrix: Spearman rank order correlation coefficient amalgamation schedule: unweighted pair-group average

Authigenic minerals are represented in the Dwyka sediments only as minor phases, indicated by low correlation coefficients (Tab. 4-12) and high linkage distances in the cluster analysis between the respective elements. These mineral phases are also expressed by peaks in single element/Al ratios (Fig. 4-9). The relative small peaks corroborate the assumption that authigenic phases occur only as minor mineral phases in the glacial sediments. The element association of the second branch can be associated with allogenic mineral phases.

Feldspar and various clay minerals represent the main phases in the Dwyka sediments. Similar to the cluster analyses of the Dwyka sediments from the southern Karoo Basin (Figs. 4-25 & 4-26) Si is linked in a last step to the element cluster.

### Postglacial phase

The samples from the Prince Albert and Whitehill Formations are combined in the dendrogram of the postglacial phase (Fig. 4-34).

Characteristic element clusters can be related to distinct mineral associations. The formation of carbonates/phosphates at the Dwyka/Ecca boundary as assumed by element/Al ratios is indicated in the dendrogram by amalgamation of Ca, P and Sr. A further element cluster can be associated with metal oxides and sulphides. Siliciclastic mineral phases are represented in the dendrogram by two separate clusters. The cluster containing the significant elements Ti and Al is associated with clay minerals. Similar to the dendrograms of figures 4-28 and 4-32, the amalgamation of Zr and Cr as well as Ba and Ce can be explained by absorption of these elements onto clay minerals. The negatively correlated cluster with the element association Si, V, Rb and K can be related to the coarser silicate fraction such as quartz and feldspar.

Comparable to the southern Karoo Basin the Dwyka Group sediments contain a relative constant mineral composition, whereas the postglacial sediments show a more variable composition, indicated by well-defined element clusters.

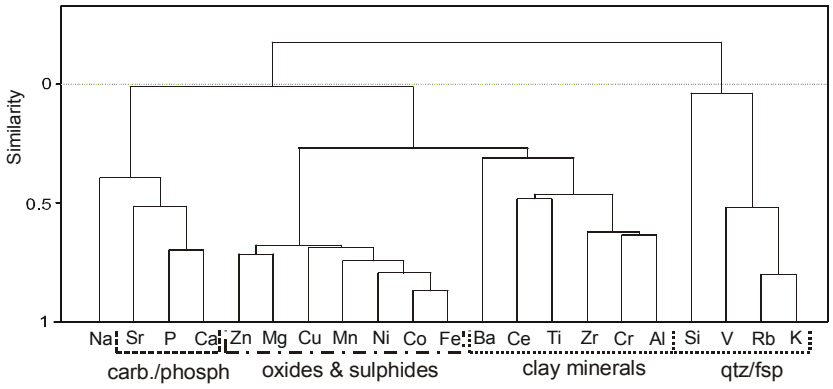


**Figure 4-34**

Cluster analysis of selected elements from postglacial sediments of the Warmbad Basin (southern Namibia).
21 variables, 49 cases
distance matrix: Spearman rank order correlation coefficient amalgamation schedule: unweighted pair-group average

## 4.2.5 $Al_2O_3$–$Na_2O$–$K_2O$ diagrams

Sodium and potassium were mobilised during chemical weathering processes as shown by significant changes in their element/Al ratios. In figures 4-35a-e $Al_2O_3$, $Na_2O$ and $K_2O$ contents are entered in ternary diagrams for each sample locality. Since these variations were controlled by changing weathering conditions, the trends in figures 4-35a-e represent climate changes during deposition. For reference, average compositions of various rock types are additionally displayed.

The samples from the MPU core are shown in figure 4-35a. Unaltered samples plot on the join between diabasic and granitic composition, close to the average upper crust composition (point a, in figure 4-35a). Dwyka samples in the lower MPU core plot close to the join albite - illite. The trend towards Illite points to increasing weathering processes during deposition of the upper Dwyka Group sediments. Furthermore, the diagram illustrates the lower chemical weathering resistance of feldspars with albitic composition in comparison to potassium feldspar. Unweathered samples contain approximately 17 wt% $Na_2O$ and 14 wt% $K_2O$ whereas in weathered samples the residual phases contain only 4 wt% $Na_2O$ but still 18 wt% $K_2O$. The formation of additional clay minerals such as chlorite, kaolinite and smectite is indicated by higher $Al_2O_3$ contents of the samples before illite composition is reached (point b, in figure 4-35a).

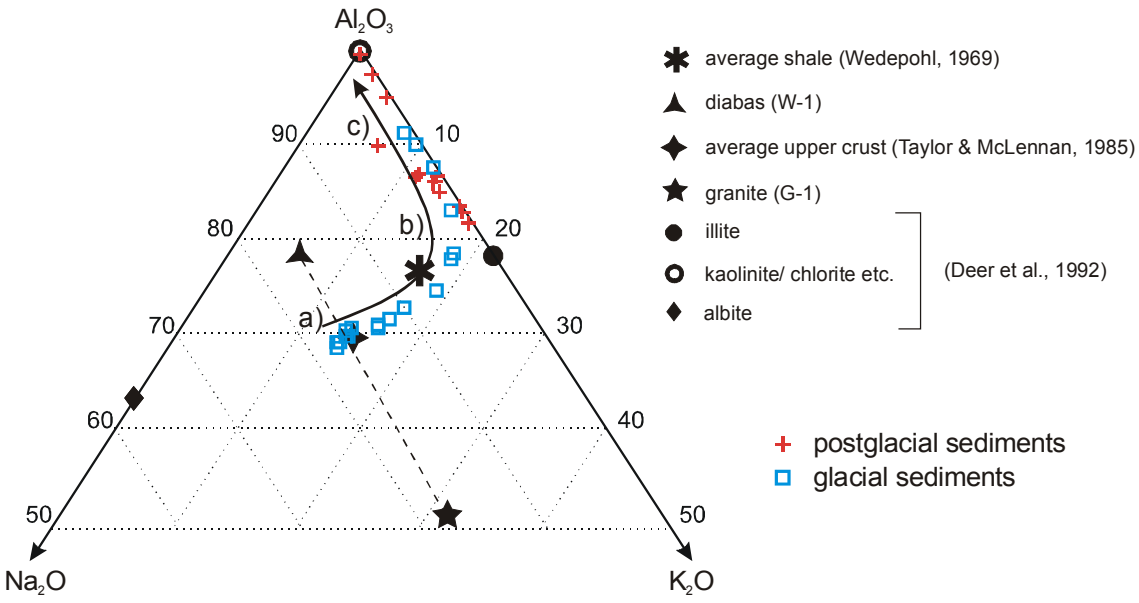


**Figure 4-35a**

MPU core: Changing contents of $Al_2O_3$, $Na_2O$ and $K_2O$ in the ternary diagram indicating changing weathering conditions.

Samples from the transition to postglacial climate conditions and from the Prince Albert Formation plot close to the $Al_2O_3$–$K_2O$ join of the $Al_2O_3$–$Na_2O$–$K_2O$ triangle. In consequence of increasing chemical alteration processes controlled by warm-humid climate conditions, the samples lost their alkali metal contents and plot closer to the Al-corner (point c, in figure 4-26a). The Al-corner of the system $Al_2O_3$–$Na_2O$–$K_2O$ in figures 4-35a-e does not discriminate between chlorite, smectite or kaolinite. Samples close to the top of the triangles represent maximum loss of alkali metal elements during weathering. During intensive chemical weathering also potassium and alkaline earth elements can be mobilised, indicated by kaolinite as sole residual phase of intensely weathered rocks. In consequence, the progression towards higher Al contents is associated with the formation of illite at the expense of potassium feldspar. At advanced stages of chemical weathering, high $Al_2O_3$ contents point to the formation of kaolinite, chlorite or smectite.

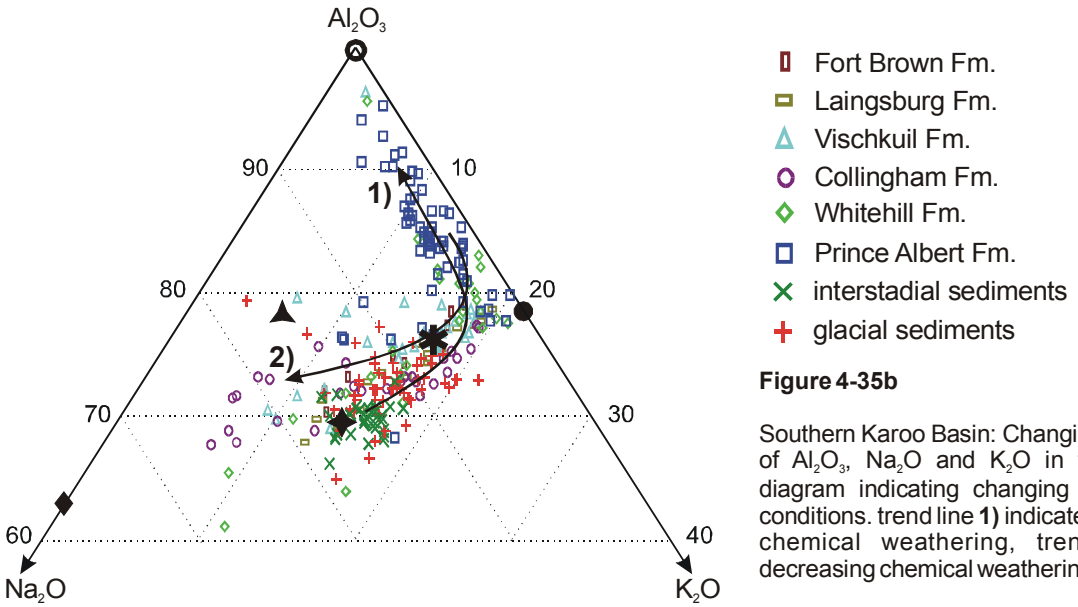


**Figure 4-35b**

Southern Karoo Basin: Changing contents of $Al_2O_3$, $Na_2O$ and $K_2O$ in the ternary diagram indicating changing weathering conditions. trend line **1)** indicate increasing chemical weathering, trend line **2)** decreasing chemical weathering.

Samples from the southern Karoo Basin and the MPU core are distributed similarly in the ternary diagrams (Figs. 4-35a & b). Glacial, interstadial and postglacial sediments of the Dwyka Group and Prince Albert Formation follow arrow 1 in figure 4-35b. Comparable geochemical variations in equivalent units from the southern Karoo Basin and the MPU core point to similar sedimentary conditions in the southern Karoo Basin. Furthermore, unaltered samples from both localities plot at the same positions in the ternary diagram (70% $Al_2O_3$, 15% $Na_2O$, 15% $K_2O$). Consequently it can be assumed, that the clastic debris was delivered from chemical comparable provenances.

Samples from the Whitehill and post-Whitehill formations plot along a reverse trend to higher sodium and potassium contents (arrow 2, in Fig. 4-35b). A similar tendency to increasing alkali metal element contents in higher stratigraphic position is also recorded in the OGT core

samples (Fig. 4-35c). In contrast to the localities from the Karoo Basin discussed before the unweathered OGT samples contain lower $Na_2O$ but higher $K_2O$ contents. Increasing $K_2O$ and $Na_2O$ contents in the OGT core and in the sequence from the southern Karoo Basin are associated with changing climatic phases. Warm-humid climate conditions prevailing during the deposition of the lower Ecca Group sediments favoured chemical alteration processes and thereby the breakdown of feldspars to various clay minerals. Warm-arid conditions prevailed during deposition of the upper Ecca Group sediments. Reduced precipitation hampered any further chemical alteration processes and the breakdown of feldspar in the parent rocks.

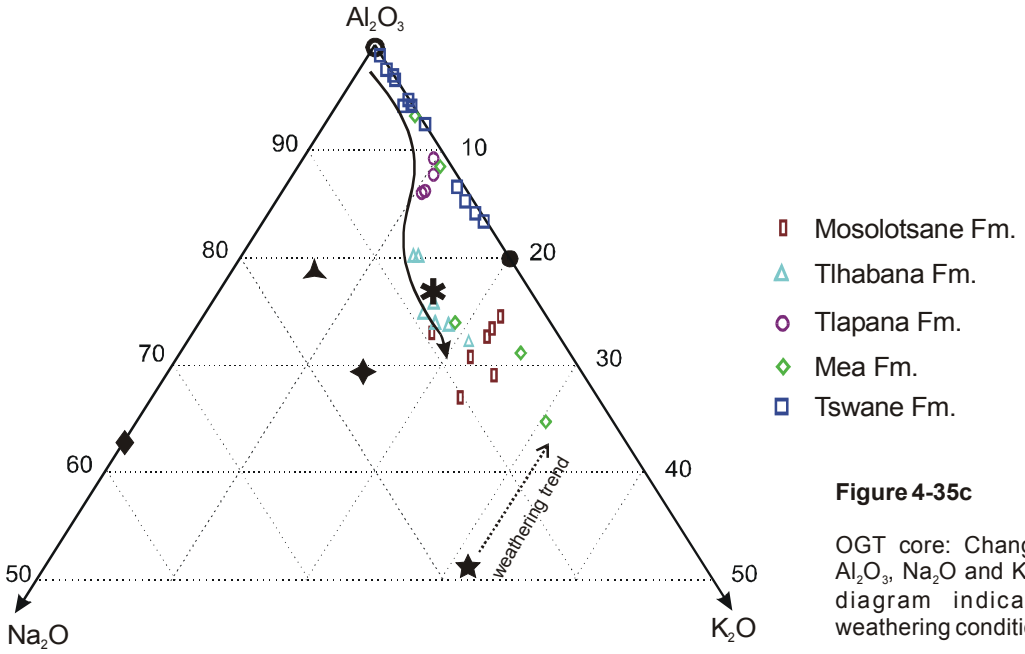


**Figure 4-35c**

OGT core: Changing contents of $Al_2O_3$, $Na_2O$ and $K_2O$ in the ternary diagram indicating changing weathering conditions.

Different geochemical provenances of sediments from the Karoo and Kalahari Basin also influenced the sample distribution in the ternary diagrams. The clastic debris of the unweathered sediments from the Karoo Basin in South Africa points to parent rocks of elevated Al but moderate Na and K contents. In contrast to this, unweathered sediments from the OGT site in the Kalahari Basin contain higher potassium and lower Al contents. In consideration of the sample position in the ternary diagrams it can be concluded that the post-Whitehill deposits in the Karoo Basin derived from reworked sediments of the early Palaeozoic Cape Supergroup. The higher potassium but low Al contents in samples of the upper Ecca Group in the Kalahari Basin point to preserved K-feldspar in the sediments. Therefore, a rather granitic composition of the provenance and/or shorter transport distances can be attributed to the Kalahari Basin sediments. As pointed out in chapter 1, the Cargonian highlands between the southern Kalahari Basin and the northern Karoo Basin border formed a major ice-spreading centre during the glacial phase as well as an important provenance for

the siliciclastic debris. The composition of this highland is unknown but a granitic/arkosic composition can be assumed.

Samples from the northern Paraná Basin (Fig. 4-35d) show no clear weathering trend. Unaltered samples from the glacial Itararé Formation plot close to the average shale composition. Samples from the Tatui Formation contain lower sodium contents indicating increasing chemical weathering as recognized in the equivalent sediments of the Prince Albert Formation in South Africa. The Irati shales do not fit to the observed trend along the $Al_2O_3$–$K_2O$ axis in the ternary diagram. Illite seams to be absent or occur only in low quantity in the Irati Formation. Low $K_2O$ concentrations in most of the Irati shales point to kaolinite, chlorite or smectite as major clay mineral phases since a loss of sodium and potassium and in consequence a relative enrichment of aluminum can be noticed. Similar to the Karoo and Kalahari Basin, reduced chemical alteration processes during deposition of the Serra Alta Formation (post-Whitehill equivalent) are indicated by elevated $K_2O$ and $Na_2O$ contents. These samples plot close to the average shale composition in the ternary diagram of figure 4-35d.

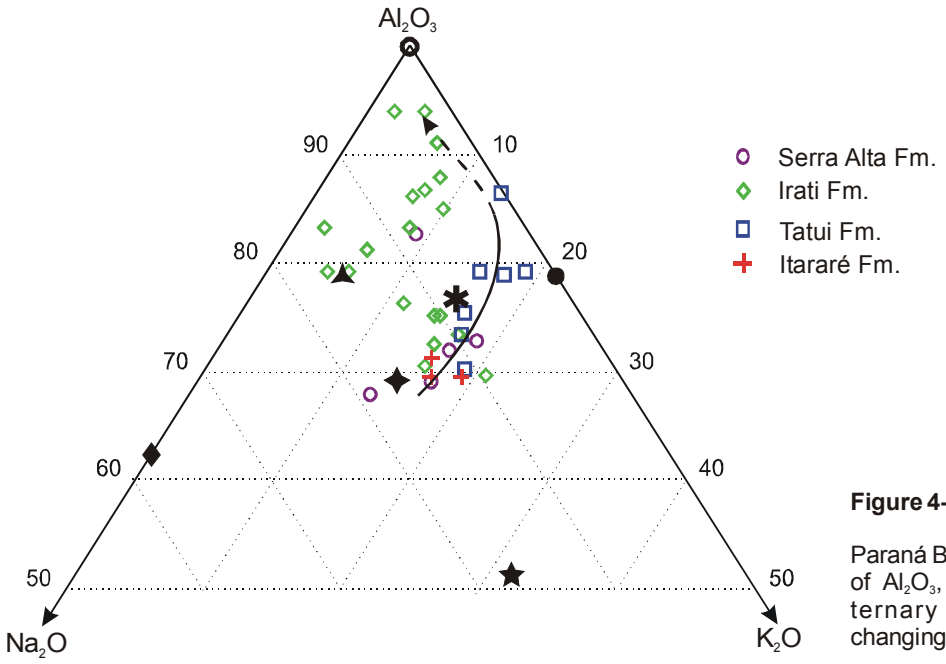


**Figure 4-35d**

Paraná Basin: Changing contents of $Al_2O_3$, $Na_2O$ and $K_2O$ in the ternary diagram indicating changing weathering conditions.

Samples from the Warmbad Basin cluster around the average shale composition in figure 4-35e. Climate variations cannot be recognised in the Warmbad Basin sediments. Also in the $K_2O/Na_2O$ versus $SiO_2/Al_2O_3$ diagram (Fig. 4-1e) only minor variations of the chemical composition of glacial and postglacial samples were noticed. The limited distribution, point to a relative constant sedimentary environment as well as to a constant sediment supply. The majority of $Na_2O$ was already mobilised during initial weathering processes (arrows in Fig. 4-

35e). Furthermore, glacial deposits were eroded during interstadial phases (Visser, 1983). Since warm-humid climate conditions during the postglacial phase also affected the precursor rocks of the Warmbad Basin sediments specific circumstances hampered the $K_2O$ mobilisation.

Beside water and rock type as basic factors for weathering processes, the topography as further controlling factor influenced the chemical composition of the weathering products. In areas with plain topography the water/rock interaction is more intensive than in mountainous regions where weathering products were fast removed from further weathering processes. Sediments formed at these conditions were less affected by alteration processes and weathering stopped at an early stage. As aforementioned the Warmbad Basin was surrounded by mountain ranges. Thus, the siliciclastic debris was eroded and rapidly transported into the basin where further element mobilisation was prevented.

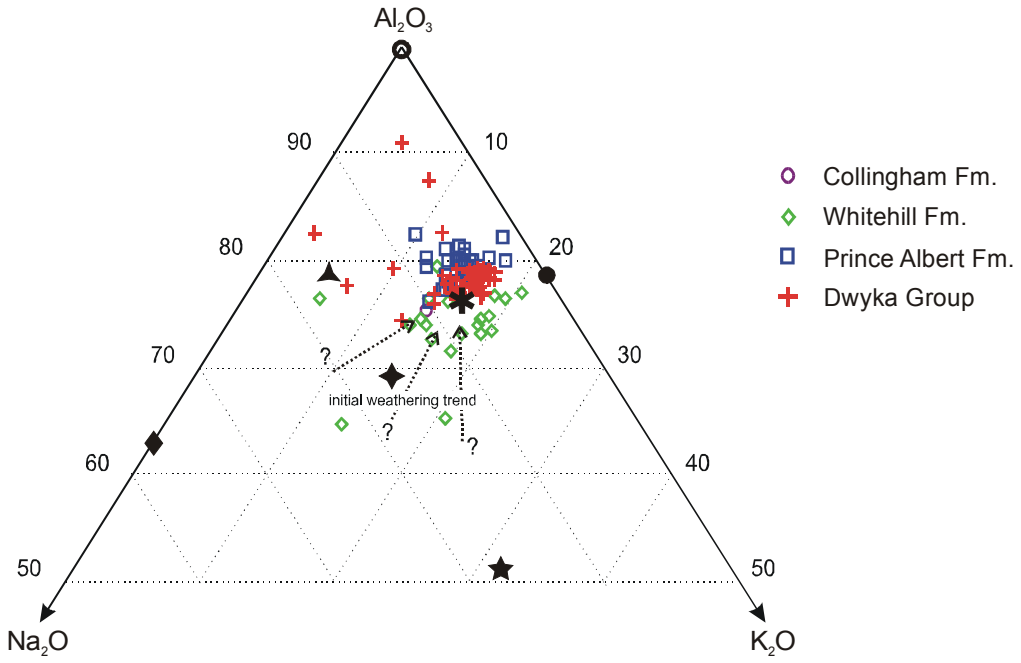


**Figure 4-35e**

Warmbad Basin: Changing contents of $Al_2O_3$, $Na_2O$ and $K_2O$ in the ternary diagram indicating changing weathering conditions.

## 4.3 Conclusion

Time dependent variations in the sedimentary composition of the sampled sequences can be recognised. Single element/Al ratios indicate changes in climate and environmental conditions. The combination of element/Al ratios and dendrograms of cluster analyses provides the possibility to attribute variations of the element geochemistry to changes in the mineralogical composition.

Glacial and interstadial sediments of the Dwyka Group and their time equivalents are in general composed of siliciclastic debris with elevated quartz and feldspar contents. The onset of the postglacial deposition phase is indicated by marked changes in the element/Al ratios. Decreasing alkali and alkaline earth element contents in the sediments point to mobilisation and removal of these elements in the precursor rocks. Newly formed element clusters in the dendrograms of the Prince Albert and Whitehill Formation, confirm the formation of various clay minerals. Carbonates and phosphates were formed at the transition and during the postglacial sedimentation phases. $C_{org}$ contents, representing anoxic conditions, increase in the sediments of the Whitehill Formation. Anoxic conditions are also recorded by elevated S, Fe and transition element contents. In consequence of arid climate conditions during deposition of the post-Whitehill sediments, alkali and alkaline earth element contents increased. Since these variations can be recognised more or less definitive in all sampled sequences, the single profiles can be correlated.

- *Glacial versus interstadial phases can be discerned by changing element/Al ratios of Mg, Ca, Na and K.*
- *Changes in the element/Al ratios of immobile elements (i.e. Ti) are associated with changing provenances.*
- *The Dwyka/Ecca boundary is characterized by increasing element/Al ratios of Ca, K, P, Fe, Mn, Co, Ni, Zn, Sr and Ba as well as by increasing $C_{org}$ and sulphur contents.*
- *Element/Al ratios of Si, Ti, Na, Cr and Zr in general decrease at the Dwyka/Ecca boundary.*
- *The occurrence of carbonates denotes the Dwyka/Ecca boundary.*
- *In relation to the Dwyka Group sediments, those of the Prince Albert Formation contain elevated element/Al ratios of Si, Fe and Cu.*

- *Carbonate-phosphate minerals occur in the Prince Albert Formation.*
- *The Whitehill Formation is characterized by the occurrence dolomite as well as by elevated $C_{org}$ and sulphur contents.*
- *Low element/Al ratios of Ti, Mn, Ca, Na, K, P, V, Cr, Co, Ni, Cu, Zn, Zr and Ba are characteristic for the Prince Albert shales and increase in the Whitehill Formation.*
- *In the post-Whitehill sediments element/Al ratios of Si, Na and P are above the average shale composition whereas element/Al ratios of Ti, Fe, Mn, Mg, Ca and K are below this cut off value.*

# 5. Element geochemical proxies

In the following chapter different element geochemical proxies are presented and discussed concerning their practicability. Zr/Ti ratios are used to discern provenance from climate proxy signals. Climate variations were recorded by elements, which are mobile during chemical alteration processes. Climate driven variations are indicated by mobilisation of alkaline and alkaline earth elements, expressed by the chemical index of alteration (CIA) after Nesbitt and Young (1982). From the multitude of redox proxies, the V/Cr ratio and $C_{org}$ content of the samples were used. Campbell and Williams (1965) established the Rb/K ratio to discern marine and non-marine conditions during sedimentation. Nevertheless, a reliable estimation of the palaeo-conditions can only be obtained by combination and critical discussion of the used proxy signals.

## 5.1 Proxy signals

As pointed out in the previous chapter, single element concentrations show clear time dependent variations. Depending on the redox conditions, salinity and temperature, milieu sensitive elements can be enriched or depleted. By the use of suitable element ratios, it is possible to reconstruct the depositional history and climate evolution.
Since ancient climatic or environmental conditions cannot be directly measured, proxy signals have to be used to obtain information on the ancient sedimentary conditions. Various proxy signals (geochemical, sedimentary and palaeontological) are established to estimate the paleo-composition of seawater and atmosphere (Berner, 2001; Bradley 1985; Hayes et al. 1999; Jones and Manning, 1994; Nesbitt and Young, 1982). These signals can be transferred to obtain information about ancient climatic or environmental conditions. Proxy signal may be altered by secondary processes such as diagenesis. To obtain reliable information it has to be ensured that the material used still contains its original composition, which equilibrated with the surrounding environment.

### 5.1.1 Zr/Ti (provenance proxy)

The geochemistry of sediments depends largely upon the geochemical composition of the precursor rocks from which they derived by weathering processes. Hence, changes of the provenance must be recognised, considered and finally excluded as possible influence on the climate or environmental proxy signals. To obtain information about the geochemical

composition of the provenance rocks, elements have to be used that are immobile during weathering and sedimentation.

The high field strength element zirconium is associated with the heavy mineral fraction of sediments. These minerals are not influenced by changing climate conditions during normal weathering processes and consequently their occurrence in sediments is mainly controlled by the geochemistry of the provenance rocks. It has to be remarked that the Zr content can be influenced by the clay mineral proportion in the sediment. Tobschall (1975) infers from geochemical and mineralogical investigations the absorption of $Zr^{4+}$ at negatively charged clay mineral surfaces. Degenhardt (1957) assumed the replacement of $Al^{3+}$ by $Zr^{4+}$ in kaolinite and montmorillonite. Furthermore, $Ti^{4+}$ can substitute $Al^{3+}$ on the tetrahedral position in sheet silicates. Also impurities of anatase or rutile in clay minerals (Deer et al., 1993) can influence the Zr/Ti ratio. Hence, the Zr as well as the Ti content of the samples can be grain size controlled and must be critically discussed.

However, different provenance rock types can be differentiated by their Zr/Ti ratios. High Zr/Ti ratios point to granitic rocks (G1 granite: Zr/Ti is 0.14) or clastic sediments (average phanerozoic quartz arenite: Zr/Ti is 0.13; Boryta and Condie, 1990). Lower Zr/Ti ratios around 0.067 denote the composition of the average upper crust (Taylor and McLennan, 1985). The „North American shale composite“ (NASC) yields a Zr/Ti ratio of 0.043. Markedly lower Zr/Ti ratios were measured in basic igneous rocks. Andean volcanic rocks yield Zr/Ti ratios between 0.024 for basalts and 0.034 for andesites (Ewart, 1982). Lowest Zr/Ti ratios around 0.01 are representative for primitive magmas of OIB's and MORB's.

If climate or environmental proxy signals correlate with the Zr/Ti ratios, these variations rather indicate changes of the provenance than climate variation. In this case the palaeoenvironmental proxies should not be used as climate indicators.

## 5.1.2 CIA (weathering/climate conditions)

The chemical index of alteration (CIA) provides information about chemical weathering processes, which were controlled by the climate. The chemical index of alteration was defined by Nesbitt and Young (1982) as,

$$CIA = [Al_2O_3/(Al_2O_3+Na_2O+K_2O+CaO^*)]*100$$

using molar proportions. $CaO^*$ represent the amount of calcium incorporated in the silicate fraction. Calcium, sodium and potassium are generally removed from feldspar by aggressive soil pore waters. Consequently the proportion of alumina to alkalis typically increases in the weathering product (Nesbitt and Young, 1982). Changing proportion of feldspar versus clay minerals can be detected by changes of the CIA. High CIA's, due to the removal of alkalis

and alkaline earth elements, are associated with intensive chemical weathering in the provenance. Unaltered rocks such as basalts reveal values between 30 and 45 whereas granites have CIA's of around 50. Illite and montmorillonite range between 75 and 85. Kaolinite and chlorite exhibit the highest values close to 100 as a consequence of the complete removal of K, Na and Ca in kaolinite on the one side and the non-consideration of Mg in chlorite by the CIA on the other side. Average shales typically reach weathering indices ranges from about 70 to 75 (Nesbitt and Young, 1982). It has to be emphasised that the CIA can be influenced by the grain size of the sediments. In general coarse-grained siliciclastic sediments contain higher feldspar/clay mineral ratios than finer ones. In consequence, coarse-grained sediments have generally lower CIA values (Visser and Young, 1990).

Since chemical alteration processes are favoured by warm and humid climate conditions, changes in the CIA provide a direct hint on ancient climate conditions. Low CIA's can be related to cold/arid conditions whereas high CIA's indicate warm/humid climates. For calculating the weathering index only carbonate free samples were chosen, since high CaO concentrations of carbonates would lead to a significant increase of the CIA.

### 5.1.3 Rb/K (palaeosalinity)

Campbell and Williams (1965) used the Rb/K ratio to differentiate sediments formed in fresh water, brackish or marine environments. The use of this element ratio as a salinity proxy is based on the assumption that marine shales contain higher rubidium contents due to higher $Rb^+$ concentration in ocean water than in fresh water environments (0.12 ppm Rb in the oceans in contrast to 0.0013 ppm Rb in rivers; Taylor and McLennan, 1985). If the weathering products enter marine environments, potassium in illite can be replaced by rubidium due to the concentration gradient between the contrasting milieus. Higher Rb concentration in seawater than in freshwater favours higher Rb/K ratios in clay minerals deposited under marine conditions. Accordingly, increasing Rb/K ratios can be related with increasing salinity. Campbell and Williams (1965) attributed Rb/K ratios of $4*10^{-3}$ in shales as indicative of fresh-water to brackish conditions and ratios of approximately $6*10^{-3}$ of marine environments.

Furthermore the Rb/K ratio was used by different authors to record weathering trends. Harriss and Adams (1966) recognised a continuous increase of the Rb/K ratio in the weathering products during chemical alteration processes. Wedepohl (1978) point out that adsorption may play an important role in the concentration of Rb relative to K in late stages of weathering. According to Goldschmidt (1954), higher Rb contents result from the firmer adsorption of $Rb^+$ than $K^+$ at clay mineral surfaces.

Especially in the Karoo Basin the weathering proxy (CIA) and the Rb/K ratio show similar trends (Fig. 4-1 & 4-7) but differences can also detected. In the following chapter the Rb/K ratio is used as proxy to report changes between limnic, brackish or marine conditions. But, it has to be emphasised that no single proxy can be regarded as a definitive indicator of the sedimentary conditions. Only a combination of different independent signals can lead to a reliable reconstruction of the paleoenvironments.

## 5.1.4 V/Cr (palaeo-redox conditions)

Various proxy signals have been established by using transition element contents or ratios to reconstruct palaeoredox conditions (i.e. Krejci-Graf, 1975; Lewan and Maynard, 1982; Shaw et al., 1990; Jones and Manning, 1994; Piper, 1994; Emerson and Huested, 1991; Alego and Maynard, 2004; Piper and Perkins, 2004).

During organic matter and inorganic particles passing different redox boundaries (oxygen respiration, denitrification, sulphate reduction and methane fermentation), while settling through the water column, minor elements can be enriched or depleted (Piper, 1994; Piper and Perkins, 2004; Alego and Maynard, 2004). The decomposition of organic matter commences already in the photic zone and only small fractions of the primary biomass finally accumulate at the water-sediment interface. During sinking through the water column planktonic organic matter can carry minor elements to the sea floor directly, but it also drives redox reactions, which determine the suite of elements that precipitates from bottom water (Piper, 1994). Thus, surface absorption can increase the minor element concentration of sinking organic matter. In consequence, the applicability of the different redox proxies in table 5-1 primarily depends on the distribution of the redox boundaries in the water column, which is in turn controlled by local sedimentary environment.

| | **S-Karoo** | | | **MPU** | | | **OGT** | | | **Paraná** | | |
|---|---|---|---|---|---|---|---|---|---|---|---|---|
| | **W** | **$C_{org}$** | | **W** | **$C_{org}$** | | **W** | **$C_{org}$** | | **W** | **$C_{org}$** | |
| | | **ρ** | ***r*** | | **ρ** | ***r*** | | **ρ** | ***r*** | | **ρ** | ***r*** |
| **$C_{org}$** | 0.48 | 1 | 1 | 0.48 | 1 | 1 | 0.69 | 1 | 1 | 0.69 | 1 | 1 |
| **V/Cr** | 0.74 | **0.54** | 0.13 | 0.47 | **0.73** | 0.08 | 0.59 | -0.13 | -0.18 | 0.64 | 0.25 | -0.02 |
| **Ni/Co** | 0.53 | 0.02 | 0.09 | 0.39 | 0.34 | -0.06 | 0.66 | **0.32** | 0.19 | 0.82 | 0.00 | -0.11 |
| **Ni/V** | 0.61 | -0.45 | -0.13 | 0.85 | -0.16 | 0.07 | 0.39 | -0.33 | 0.22 | 0.69 | -0.05 | -0.1 |
| **U/Th** | 0.64 | 0.17 | 0.22 | 0.66 | 0.21 | 0.28 | 0.58 | -0.15 | -0.18 | 0.69 | **0.34** | 0.51 |

**Table 5-1**

Correlation coefficients between redox-proxies and $C_{org}$ content from different sample localities. **W** = Shapiro Wilk`s test, **ρ**= Spearman rank order correlation coefficient, ***r***= Pearson correlation coefficient.

However, since only under oxygen limited conditions organic matter can be preserved, the different redox proxies can be controlled on their practicability by correlation to the total organic carbon content ($C_{org}$). In table 5-1 different redox-proxies are presented. Since the distribution of the element ratios show in all cases marked divergence from the normal distribution (low **W**-values) the Spearman rank order correlation coefficient is used to test the practicability of the proxy signals.

In both sample localities of the Karoo Basin the V/Cr ratio shows the best correlation with the $C_{org}$ content. In samples of the OGT core from Kalahari Basin only the Ni/Co ratios correlate positively with the $C_{org}$ contents. Remarkable is the negative correlation between the other element ratios to the $C_{org}$ contents. In the Paraná Basin the correlation coefficient between U/Th and $C_{org}$ yields the best correlation. The listed correlation coefficients from the Paraná Basin in table 5-1 in general are low. Therefore, also the V/Cr ratio ($\rho$ is 0.25) can be used as reliable signal for the redox conditions during deposition.

Since the V/Cr ratios show the best accordance to the $C_{org}$ contents its application as redox-proxy is favoured against the other element ratios. Ernst (1970) suggested that the V/Cr ratio can be grain-size dependent and influenced by the carbonate content. If the observed variations in the V/Cr ratio reflect changes of the redox conditions or if it is altered during post sedimentary processes must be discussed for each locality. Especially in the OGT core the V/Cr ratios might lead to misinterpretation of the redox conditions because of the negative correlation coefficient between V/Cr and $C_{org}$.

The redox state in the sedimentary environment is determined via (i) oxygenation of organic carbon by biological respiration ($O_2$ reduction), followed by (ii) denitrification, (iii) sulphate reduction and finally (iv) methane fermentation (Piper, 1994; Berner 1971).

$$\text{(i) } C_6H_{12}O_6 + 6O_2 \rightarrow 6CO_2 + 6H_2O$$

$$\text{(ii) } 5CH_2O + 4NO_3^- + \rightarrow 2N_2 + 4HCO_3^- + CO_2 + 3H_2O$$

$$\text{(iii) } 2CH_2O + SO_4^{2-} + \rightarrow H_2S + 2HCO_3$$

$$\text{(iv) } 2(CH_2O)_n \rightarrow nCH_4 + nCO_2$$

The hierarchy of these reactions is controlled by the reaction yielding the greatest free energy (Froelich et al., 1979). Thus, oxygen respiration proceeds until $O_2$ decreases to a concentration at which denitrification yields equal free energy (Piper, 1994). Normal seawater exhibits approximately 1-8 ml dissolved oxygen per litre. Under an oxic water column, aerobic bacteria and other organisms degrade organic matter settling from the euphotic zone. If sufficient organic matter remains after exhausting all available oxygen, anaerobic

organisms continue to oxidize the organic matter. The boundary between aerobic and anaerobic metabolism can occur in the water column or in the bottom sediment (Raiswell and Berner, 1985; Shaw et al., 1990; Peters and Moldowan, 1993) Dysoxic conditions are established between 0.1 and 1 ml/l whereas oxygen concentrations below 0.1 lead to suboxic conditions in the sedimentary environment. Anoxic conditions (0 ml/l) are reached if oxygen is completely absent from the water. Euxinic conditions are reached in environments where additional free $H_2S$ is present in the water column (Allison et al., 1995; Berner and Raiswell, 1985).

In oxic environment Cr is present as $CrO_4^{2-}$. Under anoxic conditions it is reduced to the less soluble +3 valence state. Also vanadium, present at oxic conditions as $H_2VO_4^-$, is reduced to a less soluble valence state under reducing conditions (Sadiq, 1988). Since the reduction of V occurs at the low-Eh boundary of denitrification, whereas the reduction of Cr occurs at the upper boundary (Piper, 1994), the element ratio of V/Cr can be used as a palaeoproxy for redox conditions. Jones and Manning (1994) indicate that Cr is usually incorporated within the clastic sedimentary fraction where it may substitute for Al within clays, be absorbed, or occur as chromite. Vanadium is bonded to organic matter by incorporation into porhyrins, and is concentrated in sediments deposited under reducing conditions (Jones and Manning, 1994). Glikson et al. (1985) remarked that V is not always correlated with organic matter and may be absorbed by detrital silicate minerals. After Jones and Manning (1994) V/Cr ratios below 2 indicate oxic conditions in the water overlying the sediment, values between 2 and 4.25 dysoxic and values above 4.25 anoxic/aerobic bottom water conditions.

# 5.2 Sample Localities

## 5.2.1 Southern Karoo Basin

The succession from the southern Karoo Basin comprises approximately 1350 m of chiefly siliciclastic sediments. Stratigraphic equivalent units were used as datum (chapter 1.3). Samples between the dated units were interpolated. The sedimentary succession is equivalent to an approximately 40 Ma record of the climatic and sedimentary evolution of south Gondwana. Due to increasing sedimentation rates in the upper Ecca Group a succession of approximately 600 m (Vischkuil, Laingsburg and Fort Brown Formation) is condensed in the upper 3 Ma. Since sample material of the postglacial phase was only available from the Prince Albert, Whitehill, Collingham and lower Vischkuil Formation, the discussion of the postglacial sedimentation phase focuses on the lower Ecca Group. Furthermore, changing sedimentary conditions in the upper Ecca Group hamper the application of the used element-geochemical proxies. The complete succession and the used proxies are presented in figure 5-1. Because of contrasting climatic and sedimentary conditions, glacial and postglacial phase will be separately discussed in figures 5-3 and 5-4.

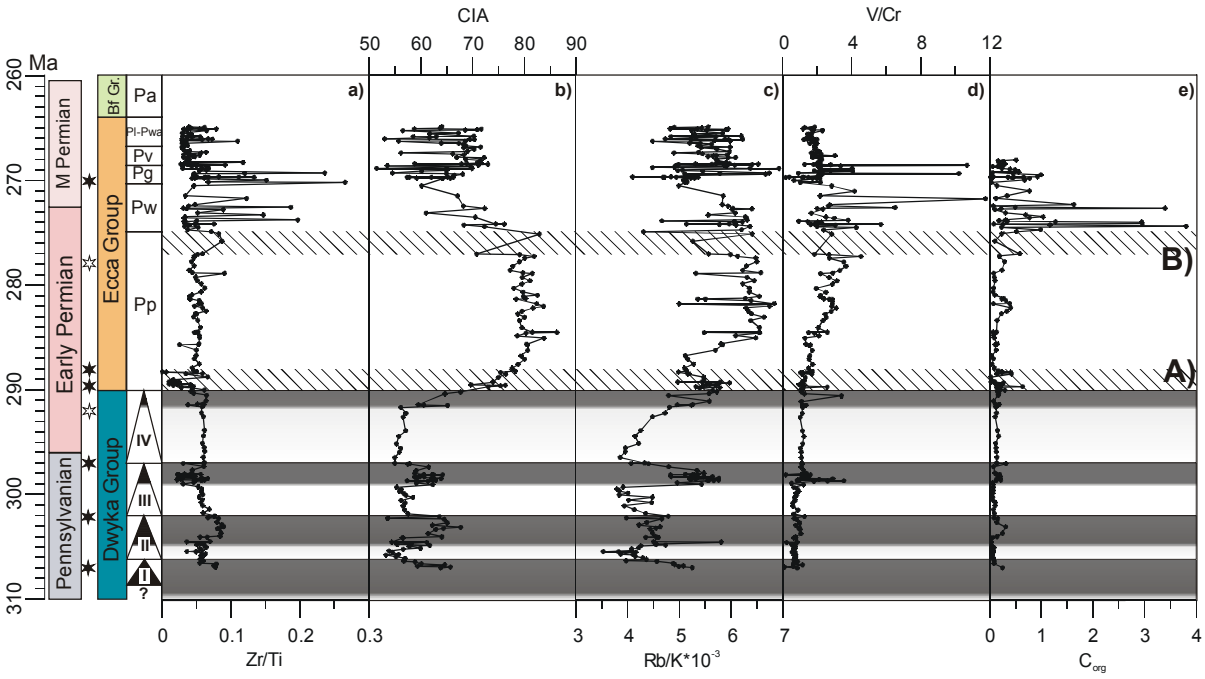


**Figure 5-1 a-e**

Stratigraphy and facies evolution of the lower Karoo Supergroup sedimentary succession; Global stratigraphy (GSC 2002). Filled stars SHRIMP ages after Bangert et al. (1999); open star age by Visser (1997). Gray shaded areas indicating interstadial phases of the Dwyka Group, diagonal hatched fields mark **A)** transition phases between glacial and postglacial phase, **B)** provenance signal, **a)** Zr/Ti (provenance proxy), **b)** CIA (weathering proxy), **c)** Rb/K (salinity proxy), **d)** and **e)** V/Cr and $C_{org}$ (redox proxies). Pp = Prince Albert Fm., Pw = Whitehill Fm., Pg = Collingham Fm., Pv = Vischkuil Fm., Pl - Pwa = Laingsburg to Waterford Fm., Pa = Abrahamskraal Fm. (Beaufort Group).

The Zr/Ti ratio is used as provenance indicator. As aforementioned, the ratio can also be dependent on grain size. Albes (1996) for Dwyka Group and Fiedler (1995) for Collingham to Fort Brown Formation determined grain sizes using thin sections of representative samples. The average grain size of sediments from the Prince Albert and Whitehill Formation were not determined due to the high clay mineral content in these units. However, it can be assumed that in relation to the other units, the Prince Albert and Whitehill shales contain the smallest grain size. Figure 5-2a displays no correlation between grain sizes and Zr/Ti ratios. In contrast to that the correlation between grain size and Si/Al ratio (Fig. 5-2b) reflects dependency between both parameters.

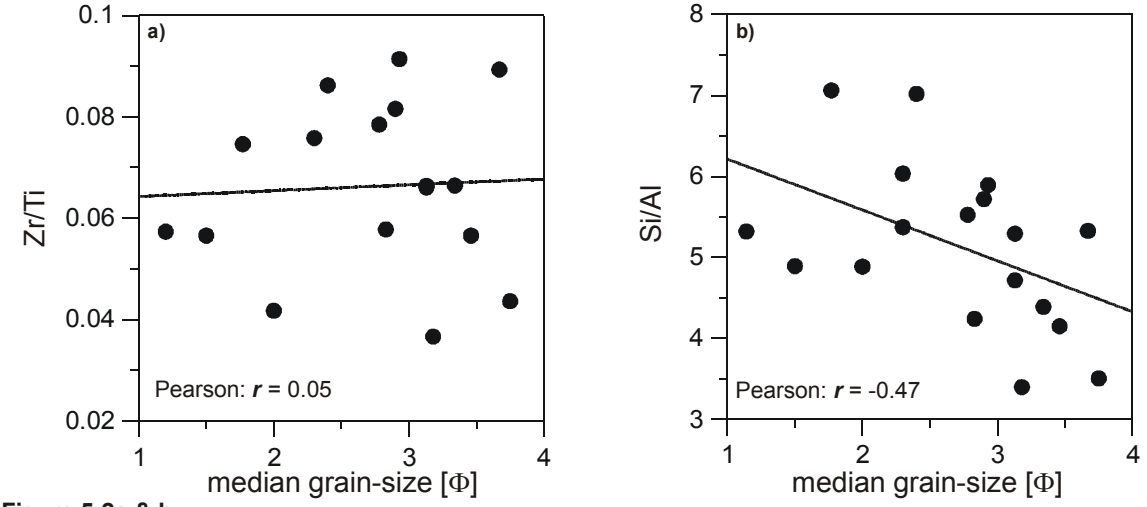


**Figure 5-2a & b**

**a)** Median [Φ] versus Zr/Ti shows no correlation of both parameters; **b)** Median [Φ] versus Si/Al indicates negative correlation between both parameters. Grain sizes adapted from Albes (1996) for the Dwyka Group and Fiedler (1995) for the post-Whitehill Formations. Φ determined after Folk and Ward (1957).

Hence, increasing grain size had only negligible influence on the Zr/Ti ratios. If absorption or exchange processes influenced the Zr/Ti ratio, the fine-grained shales of the Prince Albert and Whitehill Formation would show marked variations in figure 5-1a and 5-4a. Since the most significant changes (interstadial phases, Dwyka/Ecca boundary and Prince Albert/Whitehill Formation) arise from a relative constant baseline value of approximately 0.06, it can be concluded that the Zr/Ti ratio is not dependent on the grain size and can be used as provenance indicator.

**glacial phase**

Multi-geochemical investigations reveal the climate history for southern Gondwana during the deposition of the Upper Carboniferous to Early Permian Dwyka Group (Figs. 5-3a-e).

Zr/Ti ratios indicate provenance change (Fig. 5-3a) for the interstadial phases (DS II median Zr/Ti = 0.076; DS III median Zr/Ti = 0.044), whereas glacial phases exhibit constant Zr/Ti ratios (median 0.058). Higher Zr contents point to a granitic/arkosic rock composition

identifying the northern highlands (Cargonian Highlands) as source region of the debris-flow deposits during the interglacials of DS I & II. Sequences DS III and IV received clastic debris from source regions located near the southern magmatic arc associated with subduction processes and magmatic activity along the paleo-Pacific plate margin (Visser, 1989).

Glacial deposits are intercalated with interstadial periods, which represent temperate climate conditions. Since the glaciers almost exclusively accumulated on land the cyclic climate variations induced sealevel changes. The consequences of these changes are displayed by the chemical index of alteration (CIA after Nesbitt and Young, 1982), the Rb/K (Campbell and Williams, 1965) and V/Cr ratio (Jones and Manning, 1994) and by the organic matter content (Fig. 5-3b-e). Variations in the chemical index of alteration indicate rapid transitions from glacial to interglacial phases (Fig. 5-3b). Cold-arid climate conditions and rare vegetation favour physical weathering during glacial periods. After Visser (1997) the diamictites were deposited as subaqueous aprons and fans, which formed close to the ice-grounding line. Vegetation expansion, soil formation and warm-humid climate conditions during interstadials increased chemical weathering rates as indicated by elevated CIA's.

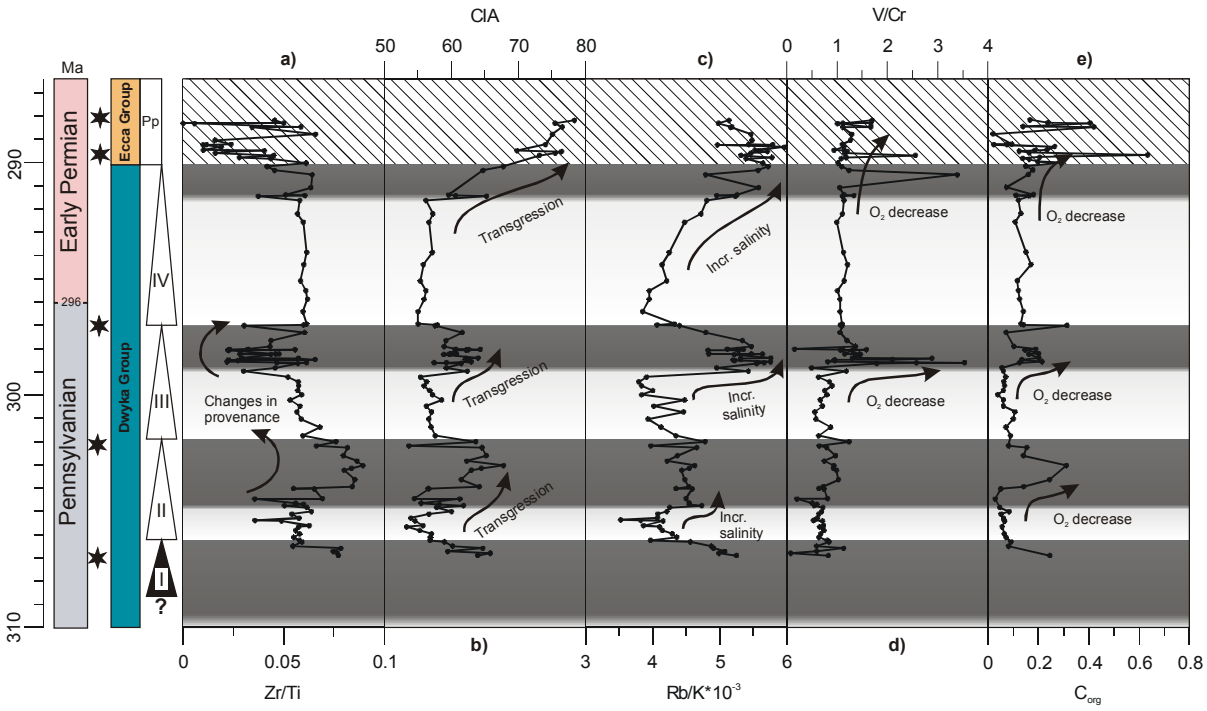


**Figure 5-3 a-e**

Geochemical proxies of glacial and interstadial Dwyka Group sediments from the southern Karoo Basin. Symbols and explanations as in figure 5-1. Gray shaded areas indicating interstadial phases of the Dwyka Group, diagonal hatched field mark transition phases between glacial and postglacial phase.

Differentiation between fully marine phases during the interstadials and limnic or brackish conditions induced by sea level drawdown during glaciation phases is reflected by the Rb/K ratio (Fig. 5-3c). Stadial phases reveal median Rb/K ratios of $4.09*10^{-3}$, interstadials of DS I and II yield Rb/K ratios of $4.78*10^{-3}$, and DS III and IV interstadials exhibit Rb/K ratios of $5.56*10^{-3}$. This agrees with the most pronounced sealevel rise, the *Eurydesma* transgression occurring during the top of DS III. Equivalents of this marked transgressions phases are reported from the Kalahari Basin in Namibia/Botswana (Visser, 1997; Stollhofen et al., 2000), from Argentina (López-Gamundi et al., 1992), India (Wopfner, 1993) and Australia (Dickins, 1996). The transgression event of DS III induced oxygen deficient bottom water conditions associated with sealevel highstands and establishment of water column stratification. This is indicated by higher V/Cr ratios and elevated accumulation and preservation of organic carbon (Fig. 5-3d & e).

Glacial conditions finally retreated between 297 to 292 Ma in the upper Gzhelian for approximately 5 Ma. Initiated by temperature changes and glacier advance, the stratified water column broke down and oxic water conditions established again during the deposition of massive diamictites of the lower DS IV. In the upper DS IV increasing CIA's and Rb/K ratios indicating the recurrence of chemical alteration processes as well as the shift from limnic/brackish to fully marine conditions after glacier retreat. Comparable to the before discussed interstadial phases, the redox-proxy signals (V/Cr and $C_{org}$) point to anoxic bottom water conditions during phases of sealevel rise.

At the transition from glacial to postglacial climate conditions (upper Dwyka to lower Prince Albert Formation) decreasing Zr/Ti ratios report the recurrent influence of the southern magmatic arc on the sedimentary environment (hatched area in Fig. 5-3). The continuously increasing CIA's point to rising temperatures and humid climate conditions which favour element mobilisation during weathering processes. Triggered by the meltdown of extant glaciers and icecaps in the northern mountainous highlands, the progression of marine sedimentary conditions reached a preliminary maximum during the transition phase to moderate climate conditions. This occurred at approximately 291 Ma during the upper Asselian to lower Sakmarian.

**postglacial phase**

With the exception of single peaks, constant Zr/Ti ratios in the Prince Albert Formation following the transition phase indicate sediment supply from consistent provenances (Fig. 5-4a). Continuously increasing CIA's and Rb/K ratios in figure 5-4b & c point to rising temperatures and warm-humid climate conditions. As during interstadial phases the vegetation could expand on land and intensify chemical weathering of precursor rocks by acidic soil solutions. Short-term marine conditions prevailed during the transition to moderate climate conditions in the lower Ecca Group. A freshwater pulse induced by the final meltdown

of extant glaciers in the surrounding mountainous highlands caused a temporary return to brackish water conditions during the lower Prince Albert Formation at 288 Ma (hatched area in figure 5-4). The following, rapidly increasing Rb/K ratios, approaching maximum values during deposition of the Prince Albert Formation (Rb/K is $6.5*10^{-3}$), mark the onset of relatively constant marine conditions in the sedimentary environment accompanied by humid climate conditions in the hinterland. The increasing chemical index of alteration documents intensive chemical weathering conditions in the provenance. At 285 Ma maximum CIA's of around 80 are reached and persist constantly for approximately 10 Ma until the upper Prince Albert Formation (Fig. 5-4b). In contrast to the rapid variations of the V/Cr ratios from glacial to interstadial phases in the Dwyka Group, the increasing V/Cr ratios during the Prince Albert Formation indicate the development of anoxic bottom water conditions in deep water environments.

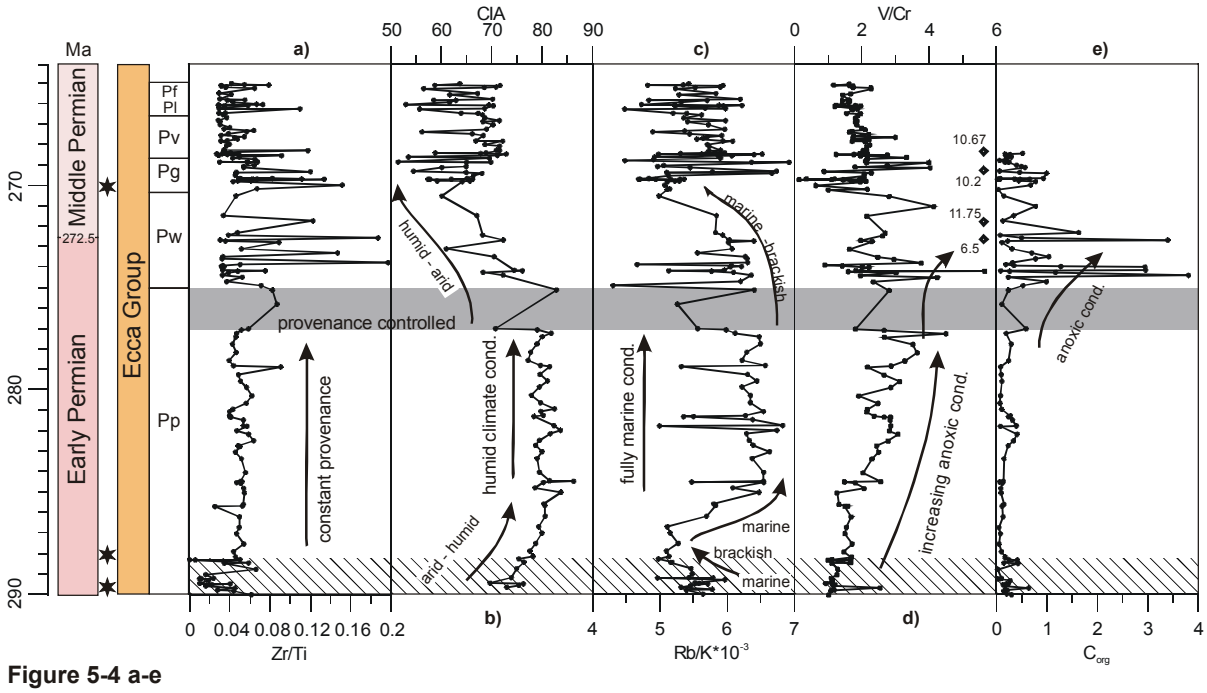


**Figure 5-4 a-e**

Geochemical proxies of postglacial sediments from the southern Karoo Basin. Symbols and explanations as in figure 5-1. Hatched area depicts glacial/postglacial transition.

At the top of the Prince Albert Formation (276 Ma), the Zr/Ti ratios increase to markedly higher values. Phases of tectonic activity of the Cape Fold Belt at approximately 278 Ma, (Hälbich 1983) caused new emerging sedimentary systems at the top of the Prince Albert Formation and coincide with variations in the Zr/Ti ratios (grey shaded area in figure 5-4). Hence, the variations of CIA, Rb/K and V/Cr ratios in this part of the succession are rather provenance controlled. Since the variations in the CIA, Rb/K, and V/Cr ratios at the top of the Prince Albert Formation are source controlled, it can be assumed that intensive chemical

weathering processes continued into the Whitehill Formation. Furthermore, Rb/K and V/Cr ratios indicate that marine conditions and anoxic bottom water persist during the Whitehill Formation until brackish/limnic conditions retreated in the upper Whitehill to lower Collingham Formation (271 Ma). Anoxic marine conditions during deposition of the Whitehill shales are also indicated by distinct elevated organic carbon contents in the sediments (Fig. 5-4e).

The relative constant proxy signals in the Prince Albert Formation disappear with the onset of the Whitehill Formation. As pointed out before, phases of tectonic activity caused development of new sedimentary systems. By the compressional tectonic regime of the Cape Fold Belt, the sedimentary environment shifted from distal/central basin positions during the Prince Albert and Whitehill Formation into more proximal position during deposition of turbiditic sequences of the Collingham and Vischkuil Formations.

Arid conditions revert in the upper Whitehill to lower Collingham Formation. Lower CIA's (80 during Prince Albert Formation to 65 in the Collingham Formation) point to decreasing chemical alteration processes and reduced leaching of mobile elements in the precursor rocks. Additionally shorter sediment transport distances into proximal sedimentary settings also influenced the chemical composition of the siliciclastic detritus and favoured lower CIA's due to higher feldspar contents in coarser grained sediments.

### 5.2.2 MPU core

Similar to the southern Karoo Basin zircon SHRIMP ages from tuff layers in the lower Prince Albert Formation dated by Bangert et al. (1999) were used. 290 Ma is set as datum for the Dwyka/Ecca boundary.

The proxy signals from the eastern Karoo Basin show comparable trends to the succession of the southern Karoo Basin discussed before. Lower Zr/Ti ratios in postglacial sediments point to provenance changes at the Dwyka/Ecca boundary (Fig. 5-5a). Median Zr/Ti ratios decrease from 0.053 during the upper Dwyka Group to 0.037 in the lower Prince Albert Formation. High Zr/Ti ratios in glacial Dwyka sediments indicate sediment supply from northern granitic or arkosic provenances. Similar to the southern Karoo Basin, the shift to lower Zr/Ti ratios occurs at the top of the Dwyka Group. During the transition phase at temperate climate conditions, the glaciers retreated and sedimentary transport processes changed. Siliciclastic debris was supplied over longer distances to the depositional environment. Low Zr/Ti ratios are associated with sediment supply from magmatic provenances along the southern continental margin of Gondwana.

Changes of the climate and sedimentary conditions are detected by variations of the CIA and Rb/K ratios (Figs. 5-5b & c). Fast rising temperatures and the shift from arid to humid climate conditions are recorded by intensive chemical weathering of the precursor rocks in the provenance (CIA: median Dwyka Group is 55, median Ecca Group is 80). Temperate climate

conditions led to the expansion of specific vegetation on the continent, which intensified chemical weathering processes. The melt down of extensive continental ice shields in south Gondwana was induced by warm-humid climate conditions. Starting from the upper Dwyka Group the glacier retreated; the sealevel rose and full marine conditions prevailed in the sedimentary environment during deposition of the lower Prince Albert Formation (Rb/K: median Dwyka Group is $4.5*10^{-3}$, median Ecca Group is $7.1*10^{-3}$).

As indicated by distinct changes of the element/Al ratios and $C_{org}$ contents (Figs. 4-4 a-k & 4-15), also the used proxy signals in figures 5-5 a-e denote an early, temporary deglaciation phase during the upper Dwyka Group. Especially the Rb/K, V/Cr ratios and the $C_{org}$ contents sharply increase, indicating significant changes of the sedimentary conditions. Also the CIA increases at the basis of the black shale interval from average values of 55 to 75. In contrast to the other proxy signals, the CIA did not decrease at the top of the Dwyka Group. It can be assumed that due to regional conditions in the south eastern Karoo Basin (subsidence of the Natal through) specific sedimentary conditions established during the end of the glaciation phase. Evidence for changing sediment supply is indicated by changing Zr/Ti ratios. Thus,, the recorded changes could be associated with eustatic changes (increasing Rb/K ratios during the upper Dwyka Group) coupled with subsidence of the Natal through.

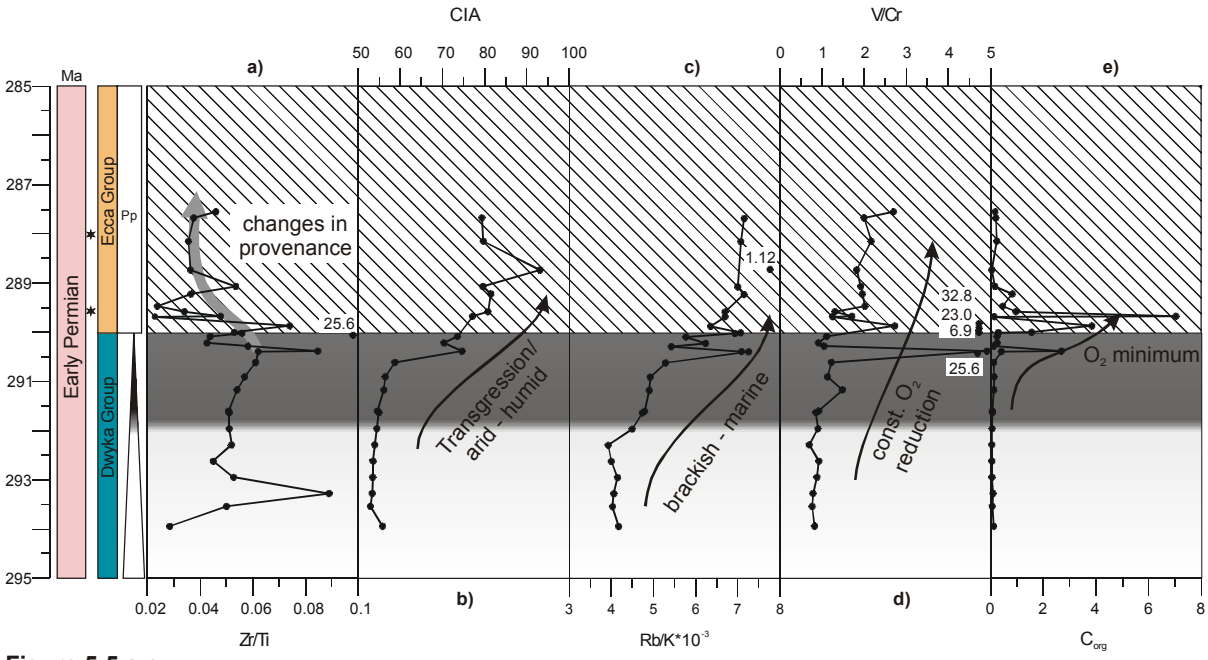


**Figure 5-5 a-e**

Facies evolution at the transition from glacial to postglacial climate conditions in the MPU core is indicated by the used proxies (**a-e**). Gray shaded area indicate interstadial phase of the Dwyka Group, diagonal hatched fields mark transition phases between glacial and postglacial climate conditions. For details see figure 5-1 and text.

Anoxic conditions (Figs. 5-5d & e) constantly developed from oxic conditions during the last glacial maximum (top DS IV) to dysoxic bottom water in the lower Prince Albert Formation. Conspicuous outliners of high V/Cr ratios occur at the Dwyka/Ecca boundary. As assumed by Ernst (1970) the redox proxy is influenced by high carbonate contents in the sediments. Samples with anomalous high V/Cr values (displayed as single points in figure 5-5d) contain also high CaO contents (V/Cr = 25.6 → CaO = 9.6, V/Cr = 6.9 → CaO = 20.9, V/Cr= 23 → CaO = 8.7, V/Cr = 32.8 → CaO = 10.0). As pointed out in chapter 4.2.2.1, elevated CaO contents at the Dwyka/Ecca boundary in the entire Karoo Basin are associated with phosphate formation, which also implies anoxic conditions and high input of organic matter. Beside the phosphate bearing samples, also siliciclastic sediments at the Dwyka/Ecca boundary exhibit elevated V/Cr ratios.

Phosphate formation and high V/Cr ratios in concert with increasing $C_{org}$ contents confirm the development of pronounced anoxic bottom water conditions at the onset of the postglacial sedimentation phase (Fig. 5-5e). After these “anoxic event” of approximately 1 Ma, oxic conditions returned. By the compressional tectonic regime during the early development of the Cape Fold Belt, phases of subsidence led to deepening of the sedimentary environment (Visser, 1992). Comparable to the southern Karoo Basin, increasing V/Cr ratios during the Prince Albert Formation point to continuously decreasing $O_2$ contents in the bottom water. Since deepwater environments and anoxic conditions are postulated for the Whitehill Formation, the increasing V/Cr ratios (Fig. 5-1d & 5-5d) reflect basin subsidence and deepening of the sedimentary environment along the northern boundary of the rising Cape orogen. Similar trends for proxy signals from the southern and south-eastern basin locality confirm the interpretation of the proxies as climate induced signals and postulate a contiguous sedimentary environment at least for the southern basin along the rising Cape Fold Belt.

## 5.2.3 Kalahari Basin (OGT core)

Unconformities in the upper core section, changing sedimentation rates and missing significant lithological units such as the glacial Dwyka Group or the Whitehill Formation, hamper a direct correlation of the OGT core with the Karoo Basin localities. The earliest sedimentary deposits are attributed to the lower Ecca Group (Bühmann and Atanasova, 1997). As pointed out in the chapters before, the OGT core can be considered as continuation of the MPU core. The continuation is certainly not without interruption but the offset between the top of the MPU and basis of the OGT core seems to be rather small. It can be assumed that during glacial periods sedimentary deposits were reworked by erosional processes. At the transition to postglacial climate conditions the sedimentary environment changed, sealevel increased and the sediments were deposited in erosion-

protected positions. Therefore, the basis of the OGT core is set as time equivalent to the Dwyka/Ecca boundary at 290 Ma (Fig. 5-6).

Except for single peaks with Zr/Ti ratios above 0.18, the Ecca and Beaufort Group sediments reveal relatively constant Zr/Ti ratios (median is 0.04). Significant excursions of the Zr/Ti ratio to higher values characterize the Mea Formation (grey shaded area in figure 5-6a). The Mea Formation contains higher quartz and feldspar contents than the Tswane and Tlapana Formations as indicated by variations of the element/Al ratios in figure 4-6. Thus, the CIA and Rb/K ratios (Fig. 5-6b & c) were controlled by changing provenances or transport processes. The high proportions of clay in the sediments of the Tswane, Tlapana and Tlhabala Formation point to low energy environments. Changing sedimentary conditions caused increasing transport energy and led to deposition of the Mea arkoses and sandstones.

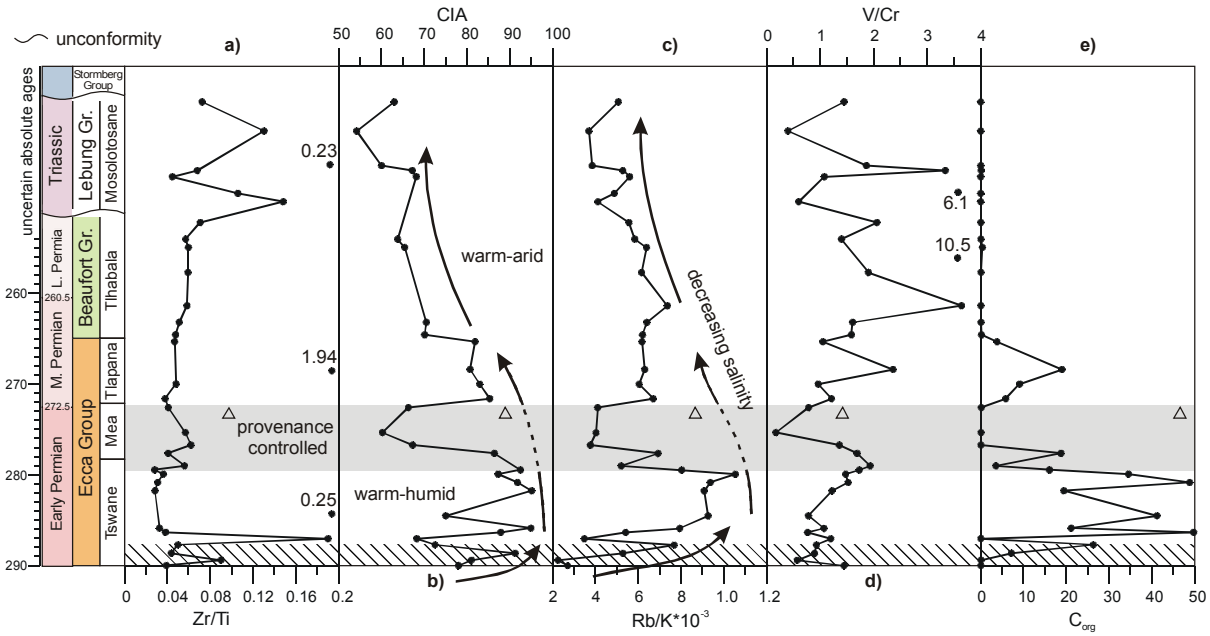


**Figure 5-6 a-e**

Facies evolution during the postglacial sedimentation phases in the Kalahari Basin (OGT core). Hatched area denotes transition from glacial to postglacial conditions. Triangles label single samples which deviates from the general trend in the Mea Formation.

Increasing CIA's (Fig. 5-6b) indicate the transition from glacial to warm-humid climate conditions during sedimentation of the Ecca Group. In consequence of increasing chemical alteration processes and high kaolinite contents in the lower Ecca shales (Tswane Formation), the CIA reaches maximum values of 95. The transition from cold-arid to warm-humid climate conditions was accompanied by sealevel rise, confirmed by high Rb/K ratios in the lower core section (Fig. 5-6c). This CIA change with comparable magnitude is also recorded in the sediments of the Karoo Basin localities. Further correlation in the climate proxy signals from the Karoo and Kalahari Basin can be detected in the upper core and profile sections. Lower CIA's in the upper Ecca and Beaufort Group indicate decreasing

chemical weathering processes (Fig. 5-6b). The restricted leaching of mobile elements from the precursor rocks is associated with the transition from warm-humid to warm-arid climate conditions during the Middle Permian at approximately 265 Ma. Climate changes were not only limited to the Karoo Basin in South Africa but also influenced the sedimentation in the Kalahari Basin. Decreasing Rb/K ratios in the upper Ecca Group (Fig. 5-6c) indicate the retreat of marine/brackish conditions from the eastern Kalahari Basin, which accompanied climate changes in the Middle Permian.

Distinctive differences between the Karoo and Kalahari Basin are revealed by the $C_{org}$ content of sediments in the lower Ecca Group. During the phase of vast marine extension, strata with high $C_{org}$ contents accumulated in the south-eastern Kalahari Basin (Fig. 5-6e). Favourable sedimentary conditions led to approximately 50% $C_{org}$ in single strata of the lower core section. In the central and southern Karoo Basin, significant $C_{org}$ contents are only preserved at the Dwyka/Ecca boundary and in the Whitehill Formation (Fig. 5-1d & e; 5-5d & e). In contrast to the dynamic environment of the southern Karoo Basin, permanent anoxic conditions established in the south-eastern Kalahari Basin after the retreat of the glaciers. During sea level high stand marine conditions transgressed from the south-west far into the Kalahari Basin. It has to be emphasised that despite of high Rb/K ratios in the Ecca Group, fully marine conditions as attributed to the Karoo Basin did not prevail in the south-eastern Kalahari Basin. Draining river systems from the surrounding mountainous highlands (Cargonian highlands) formed prograding deltas into the shallow seaway. Low subsidence rates led to extensive delta plains on which marsh-like paludal environments could establish (Visser, 1996). Since deltaic and paludal environments are postulated for the south-eastern Kalahari Basin, the Rb/K ratio can be rather interpreted as salinity proxy. Due to the marginal basin position of the OGT site, marine conditions entered only temporarily the sedimentary environment.

The comparison of different redox proxies in table 5-1 indicates that the V/Cr ratio provides no reliable information about the redox conditions. In figure 5-6d & e the V/Cr ratios show a divergent trend to the $C_{org}$ contents indicated by the negative Spearman rank order correlation coefficient (Tab. 4-1, $\rho = -0.13$). As pointed out before, reliable information about the depositional environment can only arise by the application of different independent proxies. The (Cu+Mo)/Zn ratio was used by Hallberg (1976, 1982) and Dypvik (1984) as proxy for redox conditions. In sediments deposited under anoxic conditions, the precipitation of Cu is favoured over Zn, due to the solubility products of their sulphides. Mo is added to the numerator because of the observation that it is abundant in sediments deposited under $H_2S$ bearing waters (Jones and Manning, 1994).

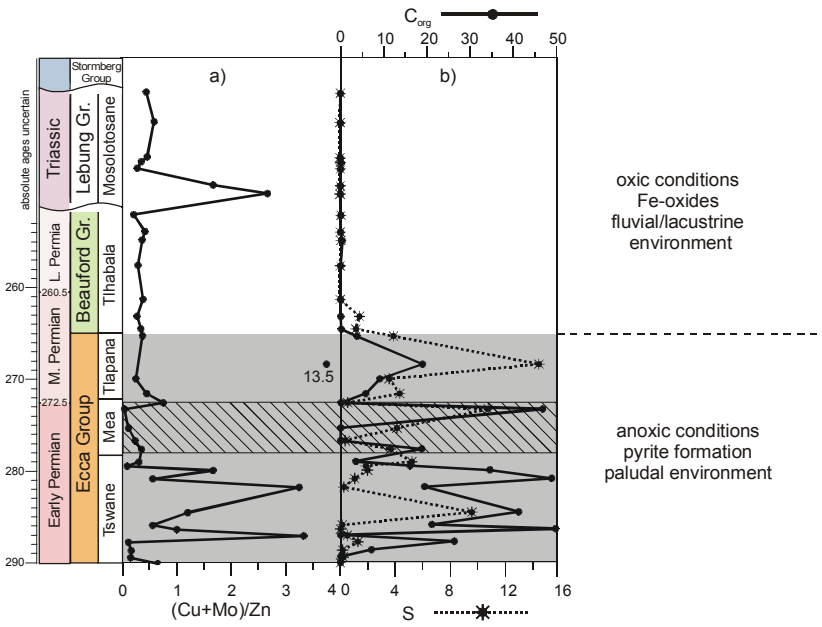


**Figure 5-7 a & b**

Anoxic conditions during deposition of the Ecca Group sediments in the Kalahari Basin indicated by redox proxy signals. Element ratios in the hatched area are provenance controlled.

In figure 5-7a & b elevated (Cu+Mo)/Zn ratios in the lower core section are in concert with high $C_{org}$ contents and confirm anoxic conditions during deposition of the Ecca Group sediments. Comparable to the CIA and the Rb/K ratios, also the (Cu+Mo)/Zn ratios in the Mea Formation were primarily controlled by the provenance (hatched area in figure 5-7). The partial decoupling of $C_{org}$ and sulphur contents is eventually caused by coal formation in sulphate limited, acidic environments.

The climate changes in the Karoo Basin from cold-arid to warm-humid and finally to warm-arid can also be recognised in the Kalahari Basin. The OGT site differs from the Karoo Basin localities by high $C_{org}$ contents in early postglacial sediments. The elevated supply of organic matter can be associated with the marginal position of the sample locality. Since the south-eastern Kalahari Basin was situated in interior continental position in comparison to the Karoo Basin, it can be assumed that temperate climate conditions favoured an earlier expansion of the vegetation. In contrast to the distal situated sample localities of the Karoo Basin, organic matter accumulated in the more proximal basin position in the Kalahari Basin. The sudden disappearance of organic matter in the Beaufort Group denotes a significant change of the sedimentary environment. Possibly the change from paludal and deltaic environments to fluvial and limnic controlled sedimentation can be responsible for the severe decrease of the $C_{org}$ content in the Beaufort Group.

## 5.2.4 Northern Paraná Basin

The proxy signals from the northern Paraná Basin are shown in figure 5-8. High Zr/Ti ratios denote the transition from glacial to postglacial conditions at the Itararé/Tatui boundary. The concomitant rise of the CIA and Rb/K ratios point to provenance controlled signals. Hence, the peaks in the grey shaded area in figure 5-8 were excluded form interpretation. Despite of single excursions to higher and lower values, the Zr/Ti ratios are relatively constant in the postglacial sediments (median is 0.057). Positive excursions are associated with high carbonate contents (> 80% carbonate) whereas negative excursions of the Zr/Ti ratio in the lower Assistencia Formation derive from $SiO_2$ rich samples ($SiO_2$ > 90%). The negative excursion in the upper Assistencia Formation can be explained by the high $Fe_2O_3$ content (> 14%) of the sample. Thus it appears that the provenance did not change significantly during sedimentation of the Irati and lower Corumbatai Formations. Therefore, the variations of the geochemical proxies in the Irati Formation seem to be primarily controlled by climate or environmental changes.

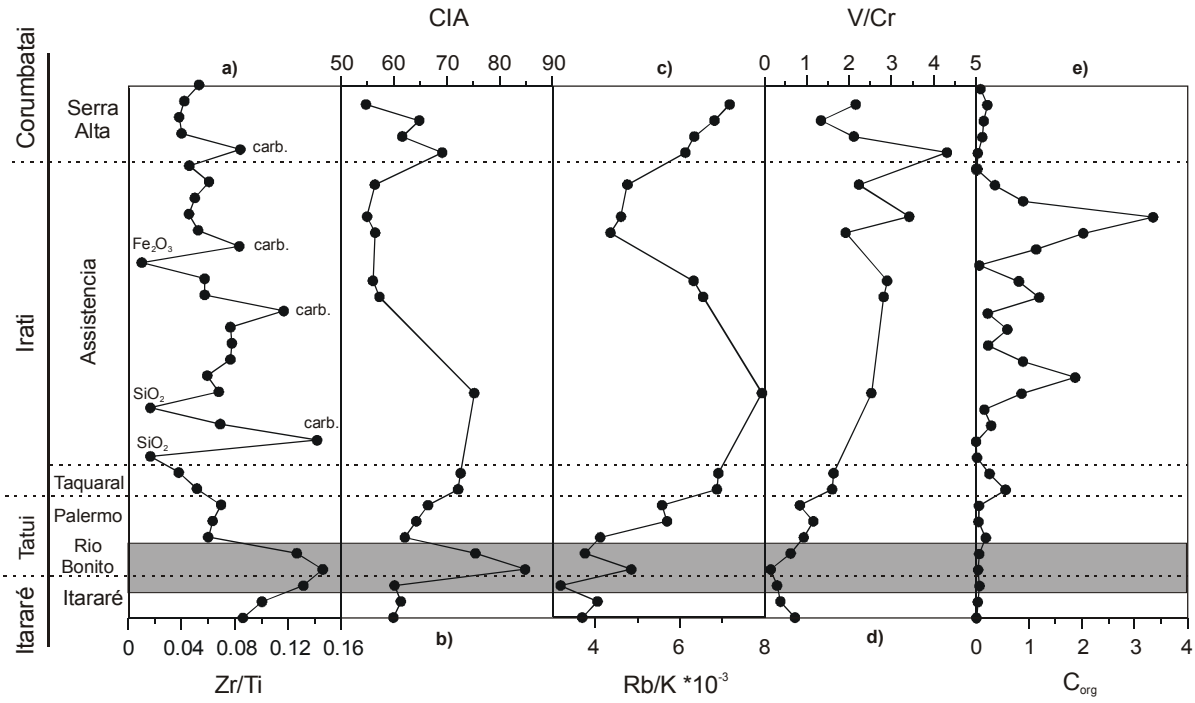


**Figure 5-8 a-e**

Facies evolution during the postglacial sedimentation phases in the Paraná Basin. Samples with more than 1.7 % CaO are not used for calculation the CIA, Rb/K and V/Cr ratios. Provenance controlled signals dominate in the grey shaded area.

As in the localities discussed before the chemical index of alteration reveals information on climate changes. The CIA showed a remarkable, nearly parallel trend to the Rb/K ratio (Figs. 5-8b & c). Supported by the Zr/Ti ratios, the maximum in the CIA and Rb/K ratios at the beginning of the Tatui Formation derived from changes in the provenance. The trend then in principle paralleled the palaeosalinity proxy. After a relative continuous phase in the upper Irati Formation the trend shows more variability within the Serra Alta Member. The variation of Rb/K ratio of carbonate free sediments across the sampled profile is shown in figure 5-8c. Comparable to the CIA, a clear increase of the Rb/K values can be recognised in the middle Irati Formation. Rb/K ratios increase from $4.0*10^{-3}$ in the lower Tatui Formation to $7.9*10^{-3}$ in the lower Assistencis Formation. The upper Assistencia Member revealed lower values before the Rb/K ratio of the sediments of the Serra Alta Member rose again.

The V/Cr ratios show increasing values up to the middle Assistencia Formation. The upper Assistencia and lower Corumbatai Formations represent more varying conditions whereas the anoxic conditions in the lower, in general oxic Corumbatai Formation, are unrealistic and can be explained by diagenetic effects in the silt/sandstones (Scheffler et al., 2001). The organic carbon content in the upper Assistencia Formation increases simultaneous to the V/Cr ratios. The sudden decrease of the $C_{org}$ contents confirms establishing of oxic conditions in the sedimentary environment during deposition of the lower Corumbatai Formation.

Sedimentation evolved from a glacially affected, aerobic environment with dominating clastic input during the Itararé and Tatui Formation to a marine influenced environment with partly euxinic bottom water conditions under humid warm conditions during the lower to middle Irati Formation (Scheffler et al. 2001). Dramatic changes must have had occurred within the middle Assistencia Formation. The relatively constant input of clastic material started to decrease and fully marine conditions changed to dominantly lacustrine conditions. During the same time the CIA indicates a change to cold or arid weathering conditions. Visser and Praekelt (1996) for the early Late Permian describe a change in the tectonic constellation of the northern Paraná Basin. The east west running Curitiba fracture zone (Fig. 2-6) became inactive during this time and sedimentation was controlled by north-trending fracture zones. These new conditions could be reflected in the chemical index of alteration.

Elevated amounts of organic carbon and increasing V/Cr rations within the Taquaral Member document establishment of an oxygen-deficient environment. Changing $C_{org}$ and S contents within the Assistencia Formation and multiple changes between shale and carbonate formation, document frequently changing conditions of the sedimentary environment in the northern Paraná Basin.

## 5.2.5 Warmbad Basin, southern Namibia

Element geochemical proxies fro the Warmbad Basin are shown in figure 5-9. After glacier retreat, erosion of interstadial sediments during rebound phases of the basin floor caused unconformities in the Dwyka succession. Hence, significant changes in the proxy signals as recorded in the Dwyka sediments of the southern Karoo Basin are missing. The differences between lower (303 to 300 Ma) and upper (300 to 290 Ma) Dwyka Group, best expressed by the $C_{org}$ content, derive from different sample localities (Fig. 5-9e). Unpublished SHRIMP ages from Geiger (2000) of tuff layers in DS II and III reveal ages of 302.3 ± 2.1 and 300.3 ± 6.3 Ma, respectively. 290 Ma is used as absolute age for the Dwyka/Ecca boundary and 270 Ma for the top of the Whitehill/lower Collingham Formation.

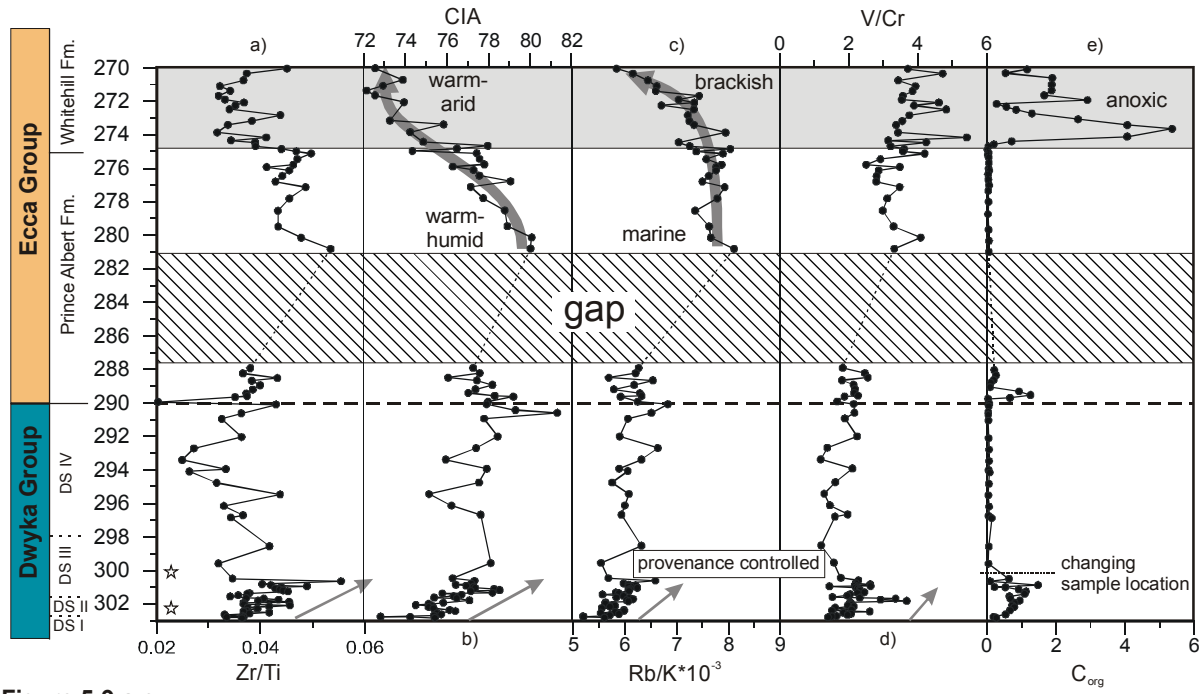


**Figure 5-9 a-e**

Facies evolution of glacial and postglacial sedimentary succession in the Warmbad Basin. Unconfirmities can be expected between DS I and DS II as well as between DSII and DS III. Shading indicates influence by the provenance. Open stars are SHRIMP ages of zircons by Geiger (2000), lower star: 302.3 ± 2.1 Ma; upper star: 300.6 ± 6.3 Ma.

Low correlation coefficients (***r*** = 0.17 and ρ = 0.16) between Si/Al and Zr/Ti ratios indicate that the variations of the Zr/Ti ratio are not grain-size controlled. In general low Zr/Ti ratios of the Dwyka Group sediments in the range from 0.025 to 0.05, around a median of 0.037, point to a rather basic/mafic composition of the provenance (Fig. 5-9a). Significant changes in the Zr/Ti ratio at the Dwyka/Ecca boundary, as in the Karoo Basin, could not be detected in the Warmbad Basin succession. In the Prince Albert Formation the Zr/Ti ratios slightly increased to a median of 0.043 between 0.02 and 0.053, which fits with the average shale composition

(NASC). The highest Zr/Ti ratios were reached in the upper section of the Formation. At the boundary of the Prince Albert/Whitehill Formation, the Zr/Ti ratios suddenly decreased to a median of 0.036 between 0.031 and 0.043 which is comparable to the Zr/Ti ratios of the Dwyka Group (Fig. 5-9a).

The Dwyka Group sediments contain relative high CIA between 73 and 86 in comparison the glacial/interstadial sediments of the southern Karoo Basin (Fig. 5-9b). High CIA's in the Dwyka Group of the Warmbad Basin, point out the high clay mineral content of these sediments. The median CIA of 76 fits with average weathering index of normal shales (Nesbitt and Young, 1982). Provenance influence may have caused the increasing trends in the lower Dwyka Group between 303 and 300 Ma, where the Zr/Ti, CIA, Rb/K and V/Cr ratios rise concomitantly (Figs. 5-9a, b & c).

For the upper Dwyka Group and at the Dwyka/Ecca boundary, climate induced changes cannot be detected using geochemical proxies. Exception is the $C_{org}$ content, which temporarily increased at the Dwyka/Ecca boundary. Comparable changes of the $C_{org}$ content at the Dwyka/Ecca boundary and in the Whitehill Formation were detected in the localities of the Karoo Basin.

Further coincidences in the development of the sedimentary and climate conditions in the Karoo and Warmbad Basins are detectable in the upper Prince Albert and Whitehill Formation by the CIA and Rb/K ratios. The CIA starts to decrease at 280 Ma from 80 to 72 at 270 Ma (Fig. 5-9b). A comparable decrease of chemical alteration processes was observed in the southern Karoo Basin (Fig. 5-4b). There, average CIA's of 80 in the Prince Albert Formation start to decrease between 277 and 275 Ma to a CIA below 70 in the upper Whitehill/lower Collingham Formation. The changes were presumable controlled by emerging arid climate conditions and in consequence reduced chemical weathering.

The variation of the Rb/K ratio in figure 5-9c also shows distinct parallels to the Rb/K ratios of the southern Karoo Basin (Fig. 5-4c). In the Warmbad Basin, Rb/K ratios remain relative constant during the upper Prince Albert Formation (median is $7.7*10^{-3}$) before in the Whitehil Formation the Rb/K ratios start to decrease to Rb/K ratios of around $6.0*10^{-3}$. Comparable changes were reported from the southern Karoo Basin. There, Rb/K ratios decrease during the Whitehill Formation from $6.2*10^{-3}$ to $5.0*10^{-3}$. Thus it appears that also in the Warmbad Basin rather brackish conditions prevailed in the upper Whitehill Formation after predominantly marine conditions during the Prince Albert Formation.

Despite the marginal and autonomous position of the Warmbad Basin, anoxic conditions as well as climate-induced changes can be detected concomitantly for all sample localities. Thus, not only tectonic processes as in the southern Karoo Basin led to changes in the sedimentary environments. Also global processes as for example sealevel changes and new emerging ocean/atmosphere currents must be taken into account to explain the

simultaneous evolution of similar sedimentary conditions at quite different basin positions. The coupling of the sedimentary and climatic evolution in the Karoo and Warmbad Basin is corroborated by the comparable changes of the CIA and Rb/K ratios.

## 5.3 Discussion and conclusion

Element geochemical proxies were used to recognise climate-induced changes in the geochemical composition of the sediments. Despite of the quite different sedimentary settings (central versus marginal basin positions) distinct climate changes were recorded.

Glacial conditions during the Upper Carboniferous indicated by low CIA's point to reduced chemical weathering in the provenances. Phases of temperate climate conditions during the Dwyka Group are proven by increasing CIA's. Concomitant changes in the used proxy signals (Rb/K, V/Cr), indicate interaction between climate, atmosphere and geosphere. The temporary moderate climate conditions during the Dwyka Group led to expanding vegetation on the continents and in the oceans. The bioproductivity influenced the atmospheric $pCO_2$ and favoured chemical weathering of silicates and carbonates whereby the nutrient budget also increased. Simultaneously evolving anoxic conditions in marine environments during interstadials can be related to transgression phases and with formation of a stratified water column with oxygen deficience in the bottom layers. Since altogether four deglaciation sequences are recorded in the South African Karoo Basin with duration of approximately 5 Ma, the prevailing climate and environmental systems were quite stable. In the Warmbad Basin cyclic deposits were not preserved due to recurring erosion of the glacial deposits.

The final retreat of the glaciers is recorded in the southern Karoo Basin and MPU core by a concomitant rise of the CIA and Rb/K ratio. Temporary anoxic conditions established at the Dwyka/Ecca boundary. In the Warmbad Basin a comparable signal in these proxies could not be detected for an equal stratigraphic position. However, the three localities can be correlated due to temporary anoxic conditions, indicated by increasing P/Al and V/Cr ratios as well as by elevated $C_{org}$ contents.

Normal marine conditions returned in the Karoo Basin during deposition of the Prince Albert Formation. In the Kalahari Basin, sedimentation commenced after the final retreat of the glaciers in marsh-like environments. Warm-humid climate conditions established in south Gondwana as indicated by increasing CIA's in all sample localities. In the southern Karoo Basin the subsiding basin floor led successively to anoxic bottom water conditions along the northern margin of the rising Cape Fold Belt. Anoxic conditions during the deposition of the Whitehill and equivalent Formations are detectable in the redox-proxy signals of all samples localities.

During the upper Ecca and lower Beaufort Group, warm-humid climate conditions were replaced by more arid conditions as indicated by decreasing chemical weathering rates. The climate change was accompanied by emerging terrestrial dominated sedimentation at the expense of former marine/turbiditic/deltaic conditions.

- *The proxies applied show simultaneous changes in the entire sedimentary environment, which were interpreted to be primarily climate controlled.*
- *Based on chemofacies signals the sampled successions documents the continuous climate evolution for south Gondwana from the Late Carboniferous (308 Ma) up to the Late Permian (260-255 Ma).*
- *Independent geochemical proxies reflect climate variations during deposition of stadial and interstadial sediments of the glacial Dwyka Group within the central Karoo Basin.*
- *Changing Zr/Ti ratios during deglaciation sequences I–IV point to changing provenances.*
- *The duration of stadial-interstadial cycles have a periodicity of approximately 5 Ma.*
- *Changing Rb/K ratios in the Dwyka Group sediments of the Karoo Basin point to brackish conditions during glacial versus marine conditions during interstadial phases.*
- *Climate changes during the Dwyka Group (glacial/interstadial phases), at the Dwyka/Ecca boundary (glacial to postglacial to warm-humid) and at the Ecca/Beaufort boundary (warm-humid to warm-arid) are denoted by changes in the CIA.*
- *Fully marine conditions prevailed at the Dwyka/Ecca boundary and persisted during the entire Ecca Group and further into the Whitehill Formaton.*
- *Anoxic conditions established in the Karoo Basin of South Africa, Warmbad Basin in south Namibia and Paraná Basin in South America during interstadial phases of the Dwyka Group, at the Dwyka/Ecca boundary and during deposition of the Whitehill/Irati Formation.*

# 6. Organic geochemistry

## 6.1 Introduction

Accumulation and preservation of significant amounts of organic matter in sediments ($C_{org}$ > 1%) requires specific conditions in the sedimentary environment. In consequence, the $C_{org}$ content in sediments can be quite different. The input rate of organic matter by in situ production or allochthonous supply must be higher than the destruction rate, controlled by oxidation processes or bacterial decomposition.

Marine environments with high bio-productivity in surface waters and oxygen deficiency in the bottom waters, favour elevated $C_{org}$ contents in the sediment. In this context, two models are discussed by Pedersen and Calvert (1990). In the stagnant basin model, organic matter sink through a layered water body from the upper aerobic layers into anaerobic bottom waters, where limited degradation of the organic remains occurs. The productivity model is commonly associated with upwelling currents, whereby high nutrient supply triggers the accumulation of organic rich sediments on the continental shelf areas. On the continents, $C_{org}$ rich sediments are known from lacustrine, bog, swamp and marsh like environments. In the latter ones, accumulation of plant material commences under subaerial conditions. Permanently high and stagnant water tables favour anoxic conditions in the water body and hamper, at early stages, any further degradation of organic matter.

For organic facies analyses it has to be verified, if the primary composition of organic matter was preserved, since selective degradation of organic compounds may have had occurred. Therefore, the facies information derived from organic matter must be critically discussed with regard to alteration processes by bacteria and/or thermal maturation. Only by combination of different analytical approaches, reliable information on the sedimentary environment can be obtained. In particular, the interpretation of bulk $\delta^{13}C_{org}$ values result in misleading results, if a detailed characterisation of the organic matter had not been carried out before. Organic matter derived from marine primary photosynthetic production incorporates the $\delta^{13}C$ signature of atmospheric $CO_2$ and thus reveals changes between glacial, interglacial and postglacial $pCO_2$ values (Jasper and Hayes, 1990). Variation in proportions of marine versus terrigenous organic matter sources, stage of degradation, and burial history can alter the carbon isotopes of bulk organic matter (Meyers, 1997).

For characterization of organic matter with respect to biological precursors, environment of deposition and postsedimentary alteration, a variety of approaches were employed. The first

step the $C_{org}$ and S contents were determinated. Samples with sufficient organic matter were then selected for Rock Eval pyrolysis. If the organic matter was suitable for molecular organic geochemical investigations, biomarker analyses were carried out on the aromatic and aliphatic hydrocarbon fraction. A biological marker is any organic compound in the geosphere whose carbon skeleton suggests an unambiguous link with a known natural precursor product (Mackenzie et al. 1982). In addition $\delta^{13}C_{org}$ values were determinated after carefully HCl treatment. Detailed information on the sample preparation are given in chapter 8 (Analytical methods).

By detailed organic geochemical investigations, information about climate, sedimentary environment and post-depositional processes can be obtained. Especially in context with the still unsolved question of the sedimentary conditions during glacial – interstadial phases and during the transition to finally post-glacial climate conditions (Faure and Cole, 1999), combined organic geochemical investigations can provide important continuative information.

## 6.2 $C_{org}$ and S contents

Significant changes in organic carbon and sulphur contents can be recognised in the sediments from all sample localities. The element contents reach from $C_{org}$ and sulphur free sediments in the Dwyka Group, to coaly sediments in the Kalahari Basin with up to 50 wt% $C_{org}$. In the southern Karoo Basin, high sulphur contents point to gypsum as additional sulphur phases, whereas in the sediments of the Kalahari Basin, sulphur is exclusively fixed as pyrite. Maximum and average $C_{org}$ and sulphur contents are given in Table 6-1. The generally lower median $C_{org}$ and sulphur values versus the average element contents indicate the relative irregular distribution of organic matter and sulphur in the sampled sequences.

| | $C_{org}$ [wt.%] | | | S [wt.%] | | |
|---|---|---|---|---|---|---|
| | av. | median | max. | av. | median. | max. |
| southern Karoo Basin | 0.3 | 0.14 | 3.8 | 0.1/(0.4) | 0 | 1.7/(11.95) |
| MPU core | 0.7 | 0.16 | 7.0 | 0.75/(1.2) | 0 | 5.5/(7.3) |
| OGT core | 10.4 | 0.17 | 49.8 | 2.0 | 0.32 | 14.4 |
| Warmbad Basin | 1.1 | 0.28 | 5.4 | 0.1 | 0 | 1.2 |

**Table 6-1**

Average, median and maximum $C_{org}$ and sulphur contents in sediments from different sample localities. Lowest element contents in all localities are close to zero. Numbers in brackets include sulphur contents in gypsum-bearing samples.

In the Karoo Basin glacial and interstadial phases can be discerned due to elevated $C_{org}$ contents in interstadial sediments (Fig. 6-1). In the Warmbad Basin, only sediments from the lower succession contain elevated $C_{org}$ contents. In consequence of erosional processes, the Dwyka Group sediments in the Warmbad Basin are not preserved as a continuous sequence. Therefore, the $C_{org}$ bearing Dwyka sediments of the Warmbad Basin cannot be correlated with the deglaciation cycles in the Karoo Basin.

Short time increases in organic carbon contents can be detected and correlated in time equivalent sediments from the southern Karoo Basin, MPU core and the Namibian Warmbad Basin (Fig. 6-1).

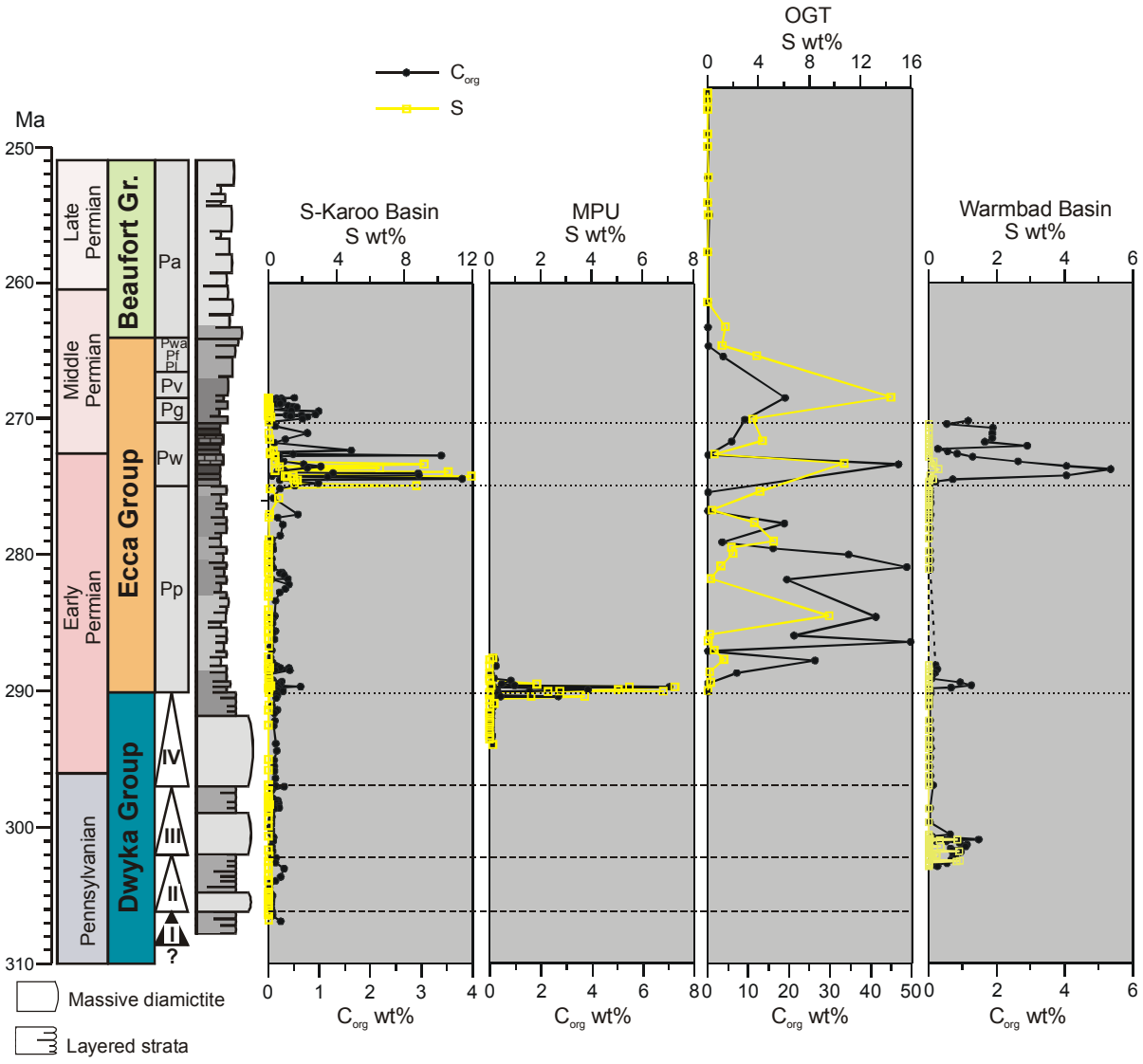


**Figure 6-1**

$C_{org}$ and S contents of the sampled successions in southern Gondwana.

During the transition from glacial to postglacial climate conditions, highest $C_{org}$ contents of 7.03 wt% are measured in the MPU core, before the $C_{org}$ contents decrease again. The change from glacial to postglacial climate conditions during the early Permian, led to a floral expansion on the continents. In marine settings, temperate climate conditions enabled higher bioproductivity. Another factor is that upon rising sea-level, flooding of previously soil and vegetation covered lowlands (marshes) leads to work-up of relative nutrient and organic matter rich sediments. Thus higher marine bioproductivity must not be direct associated with warmer ocean water temperatures.

During short periods of favourable conditions remarkable amounts of organic matter were deposited. In the lower Ecca Group oxic to dysoxic conditions quickly established in the depositional environment of the Main Karoo Basin. Especially during sedimentation of the Whitehill Formation and time equivalent deposits, the recurring of oxygen deficit conditions in the sedimentary environment is indicated by elevated $C_{org}$ and sulphur contents. In the Kalahari Basin a specific sedimentary environment established during the postglacial phase. Variable $C_{org}$ contents of up to 50 wt% in single layers, point to intermittent periods of high input of plant material accompanied by low destruction rates. Core coverage at the OGT site starts at the Dwyka/Ecca boundary. Correlation with other localities, especially in the upper Ecca Group is hampered by lack of absolute age determination and coaly terrestrial environment of deposition.

## 6.3 $C_{org}$ versus S

Weight percent of organic carbon versus weight percent sulphur are plotted in figure 6-2a-d. Berner (1994) proposed that sediments deposited under oxic marine conditions yield C/S ratios of 2.5 (normal marine line = NML). Lower C/S ratios are characteristic for euxinic environments or diagenetic pyrite formation. High C/S ratios are found in non-marine environments where sulphur supply and sulphate reduction is limited. Berner and Raiswell (1984) emphasize that the approach is only valid for finely dispersed organic matter and pyrite. Consequently, any formation of pyrite concretions invalidates the approach as well as non-dispersed, e.g. coaly organic matter accumulation. In the sample localities of the southern Karoo Basin, Warmbad Basin and MPU core the organic matter is finely dispersed. Pyrite concretions were not macroscopically detected. Problematically is the used approach for the samples from the OGT core in which coaly organic matter and pyrite concretions occur.

Single samples from the Kalahari Basin have high $C_{org}$ and S contents. Resulting from high C/S ratios most of these samples plot in the field below the normal marine line, indicating non-marine conditions (Fig. 6-2a). However, temporary marine ingressions into the

northeastern Kalahari Basin can be assumed due the occurrence of pyrite. Samples above the NML belong predominantly to the Tlapana Formation.

Samples from close to the Dwyka/Ecca boundary in the MPU core plot above the NML, indicating euxinic and sulphate-reducing conditions during sedimentation (Fig. 6-2b). Whitehill samples from the southern Karoo Basin are similarly distributed in the C/S plot (Fig. 6-2c). Samples with very high sulphur content (Tab. 4-7) resulting from gypsum/anhydride or other sulphur bearing phases are not presented. Euxinic conditions during sedimentation of the Whitehill Formation are indicated by samples above the normal marine line. Since samples from the Prince Albert and Collingham Formation show higher C/S ratios (Fig. 6-2c), anoxic conditions in marine environments prevailed temporarily. Before and after the deposition of the Whitehill Formation sedimentation was dominated by normal marine conditions with oxygenised bottom waters.

Whether the distribution of the Whitehill samples from the Warmbad Basin (Fig. 6-2d) point to changing conditions is questionable, since it is assumed that anoxic conditions had established in the entire Karoo Basin. The formation of wide spread anoxic conditions in the Whitehill Formation is indicated by the synchronous increase of $C_{org}$ contents in figure 6-1.

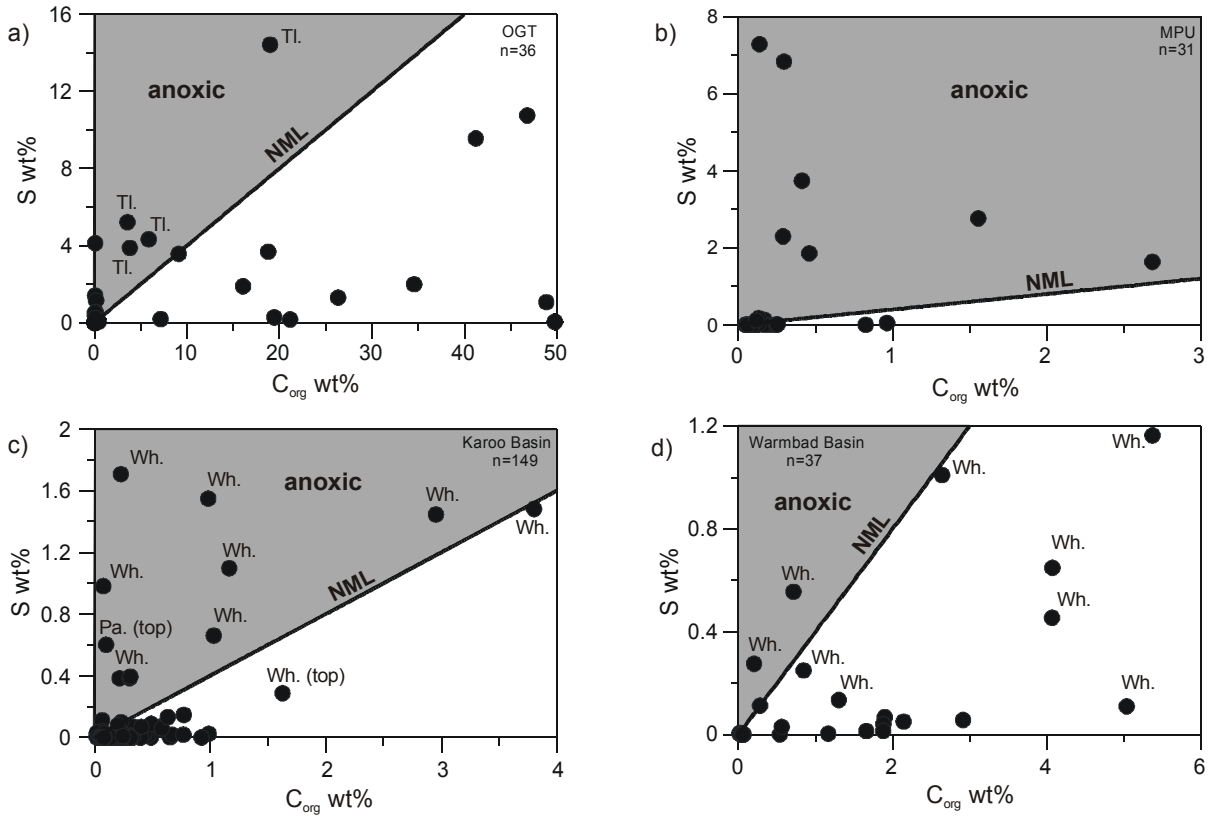


**Figure 6-2 a-d**

$C_{org}$ vs. S diagrams of four successions in southern Gondwana. NML denotes normal marine conditions of bacterial sulphate reduction ($C_{org}$/S= 2.5). n= number of samples. Tl = Tlapana Formation, Wh = Whitehill Formation, Pa = Prince Albert Formation.

## 6.4 Fe–$C_{org}$–S diagrams

Bacterial sulphate reduction takes place only under anoxic conditions. By this process dissolved sulphate and organic matter are exhausted upon $H_2S$ producing reactions (Berner, 1982). If bivalent iron is available, the originated $H_2S$ can react to form pyrite that precipitates from the water column or forms in the sediment. The ternary diagrams after Dean and Arthur (1989) shown in figures 6-3a-d provide a rapid means of recognizing iron, carbon-, and sulphur limitation on pyrite formation. Because ternary diagrams emphasise ratios, the relationship among the three variables are independent of dilution effects caused by changing amounts of siliciclastic or carbonate input.

Iron limitation on pyrite formation is indicated by a concentration of data along a line of constant S/Fe ratio. If all iron is reactive, the constant Fe/S ratio is 1.15, that of stoichiometric pyrite (Dean and Arthur, 1989). When only a portion of the total iron is reactive, the regression line through the data points of constant S/Fe ratios shifts towards the Fe corner. The content of non-reactive iron can be calculated from the axis intercept between regression line and the stoichiometric pyrite composition. Carbon limitation is indicated by a concentration of data along a line of constant $S/C_{org}$ ratio of 0.4. The NML (normal marine line, $S/C_{org}$ = 0.4), representative of marine sediments, is adopted from Berner (1982). Sulphur limitation is suggested by the lack of a systematic Fe-S-$C_{org}$ relationship and residual organic matter that is high in abundance and reactivity (Dean and Arthur, 1989). Samples plotting close to the stoichiometric pyrite line (S = 1.15*Fe) indicate that all sulphur and most of the iron is fixed in pyrite. Samples with only pyritic sulphur cannot have S/Fe ratios below 1.15. Thus, samples below the pyrite line must contain additional forms of sulphur as for instance gypsum, anhydrite, barite or organic sulphur.

### 6.4.1 Karoo Basin

Sediment samples from the glacial and early postglacial phase of the southern Karoo Basin are concentrated in the Fe-corner of the ternary diagram in figure 6-3a. The majority of the Dwyka Group and post-Whitehill sediments show characteristically low sulphur and $C_{org}$ contents. Iron is predominantly bound to silicate phases or Fe-oxides. A few samples from the Prince Albert Formation contain elevated amounts of organic carbon and plot along a line of constant $C_{org}$/S ratios. These sediments were probably deposited in oxygenated environments, in which the amount of organic carbon was insufficient to generate anoxic conditions. Enhanced amounts of sulphur are only reported in one sample from the top of the Prince Albert Formation plotting close to the Fe-S axis.

Samples from the Whitehill Formation are more widely distributed in the ternary diagram. The occurrence of additional sulphur bearing phases is indicated by samples plotting below the

stoichiometric pyrite line (labelled by their sample number in figure 6-3a, comp. Table 4-7). The formation of pyrite and residual non-reactive iron as oxide and silicate phases can be associated with the samples in the centre of the ternary diagram. On the basis of the sample distribution in figure 6-3a, well-defined limiting factors for pyrite formation cannot be recognised. Iron as limiting factor for pyrite formation can be supposed for the samples with constant Fe/S ratio and elevated $C_{org}$ contents (labelled in Fig. 6-3a). According to the interception of the regression line, approximately 48% of unreactive iron can be estimated for these samples.

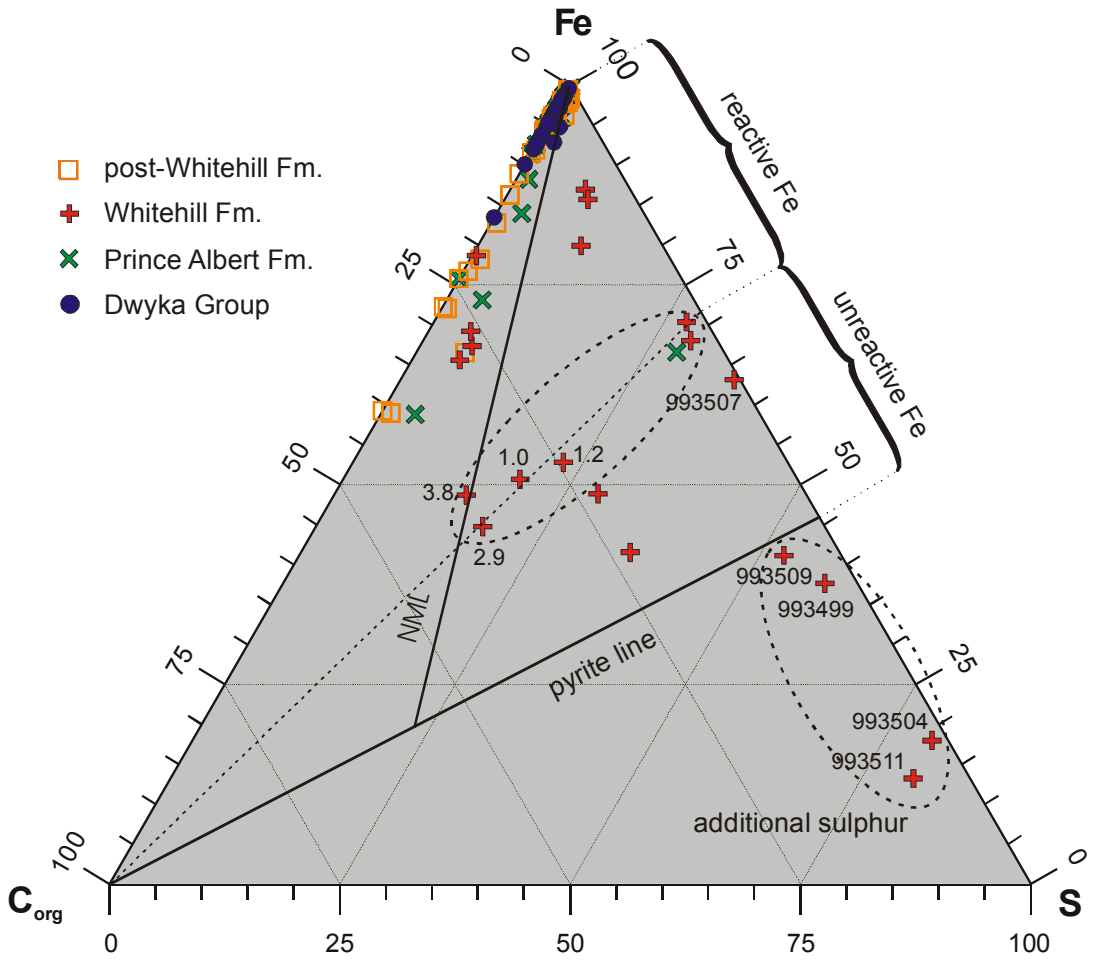


**Figure 6-3a**

Contents of $C_{org}$, S and Fe controlling pyrite formation in sediments from the southern Karoo Basin plotted in a ternary diagram after Dean & Arthur (1989). NML denotes normal marine conditions of bacterial sulphate reduction (S/C = 0.4). Pyrite line represents stoichiometric pyrite composition at variable $C_{org}$ contents.

## 6.4.2 MPU

Similar to the southern Karoo Basin, a clear trend of constant Fe-$C_{org}$-S ratios is missing (Fig. 6-3b). The majority of the Dwyka Group samples plot close to the Fe-corner, indicating that iron was preferentially non-reactive and not available for pyrite formation. Due to elevated oxygen concentrations, iron was precipitated as oxide or hydroxide, which are stable under oxic conditions. Samples with the highest $C_{org}$ contents (labelled in Fig. 6-3b) derive from the Dwyka/Ecca boundary and plot close to the pyrite line.

Comparing samples from the Whitehill Formation of the southern Karoo Basin and from the MPU core reveals that these samples yield similar Fe/S ratios (Figs. 6-3a & b). Comparable contents of non-reactive iron in these samples point to temporarily recurring anoxic conditions in the southern Karoo Basin.

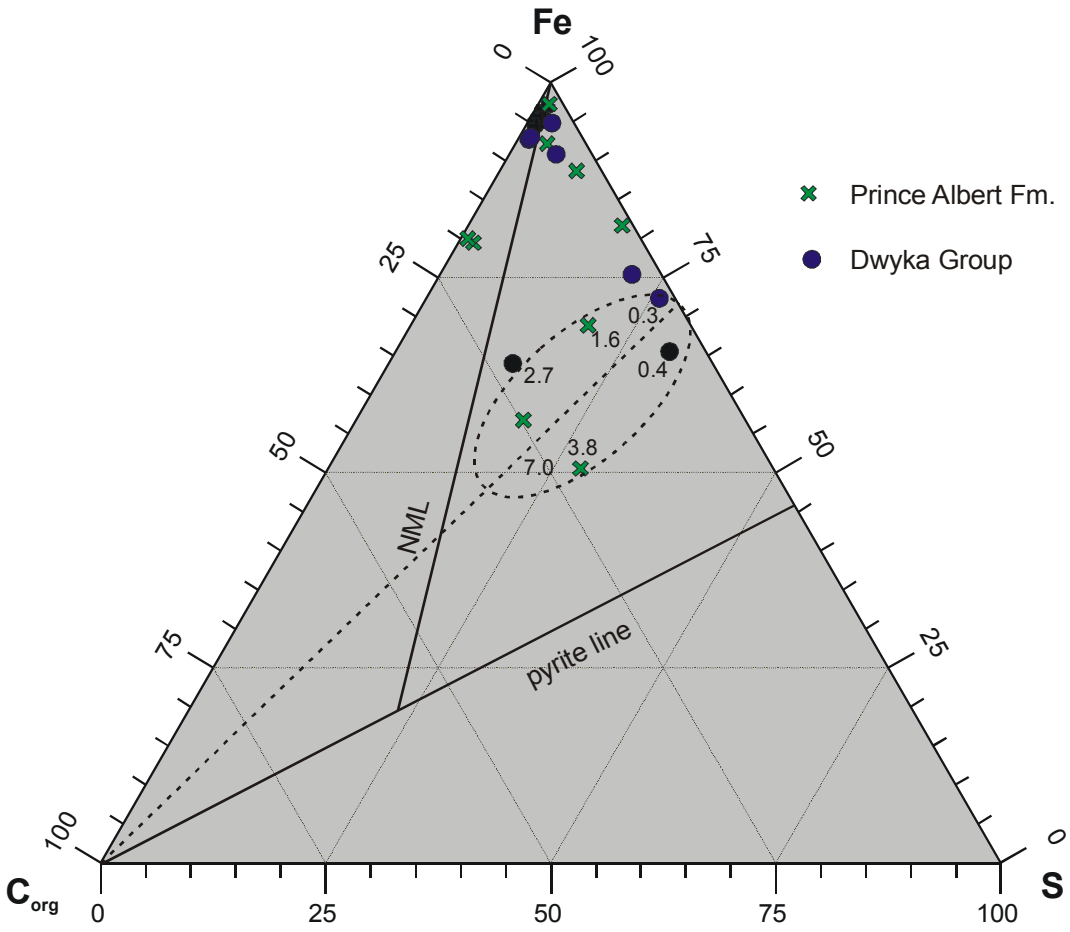


**Figure 6-3b**

Contents of $C_{org}$, S and Fe controlling pyrite formation in sediments from the MPU core plotted in a ternary diagram after Dean & Arthur (1989). NML denotes normal marine conditions of bacterial sulphate reduction (S/C = 0.4). Pyrite line represents stoichiometric pyrite composition at variable $C_{org}$ contents.

## 6.4.3 OGT

The sedimentary environment at the OGT site can be characterised by the sample distribution in the ternary plot of Fe-$C_{org}$-S in figure 6-3c. Due to high $C_{org}$ contents, most of the lower Ecca Group samples (Mea Formation) plot close to the $C_{org}$ corner. In single samples low availability of iron and sulphur hampered pyrite formation. The supply of sulphur and iron temporarily increased during deposition of the organic rich sediments of the Tswane, Mea and Tlapana Formation. Samples with higher proportions of iron and sulphur plot close to the stoichiometric pyrite line. In these samples, all sulphur and most of the iron was reactive and fixed in pyrite. Changes in the sedimentary conditions during deposition of the Ecca Group are indicated by samples with low $C_{org}$ contents plotting close to the Fe-S axis. The formation of anoxic conditions was possibly suppressed by temporarily high sedimentation rates during deposition of the Mea arkoses or by oxygenating conditions, whereby organic matter was decomposed.

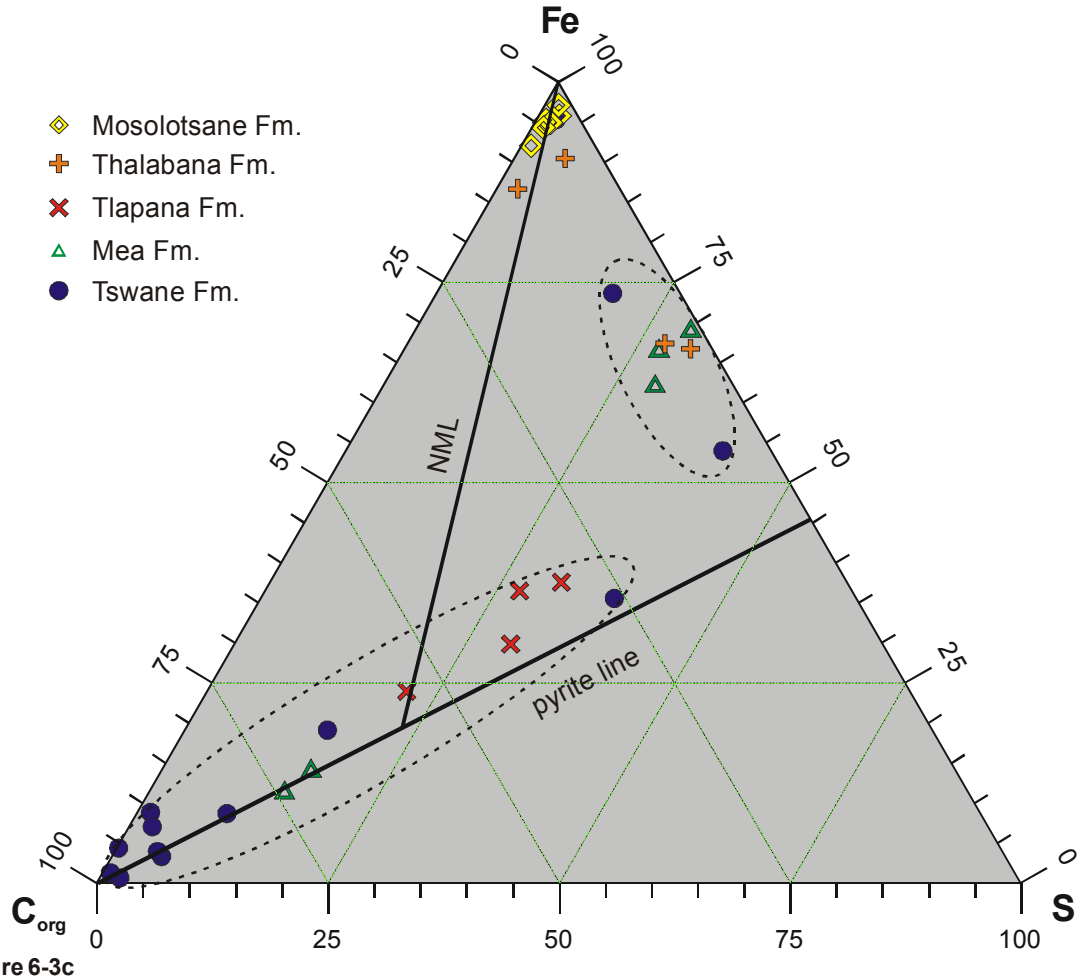


**Figure 6-3c**

Contents of $C_{org}$, S and Fe controlling pyrite formation in sediments from the OGT core plotted in a ternary diagram after Dean & Arthur (1989). NML denotes normal marine conditions of bacterial sulphate reduction (S/C = 0.4). Pyrite line represents stoichiometric pyrite composition at variable $C_{org}$ contents.

Samples of the organic-carbon lean to free Beaufort Group were deposited under oxic conditions. Fluvial/lacustrine and aeolian sedimentary systems established during the deposition of the Thalabana and Mosolotsane Formation (Johnson et al., 1996). Organic matter is absent in these sediments and hematite occurs as main Fe-phase.

### 6.4.4 Paraná

In the ternary diagram of the system Fe-$C_{org}$-S (Fig. 6-3d), the Paraná Basin samples can be divided into three groups, which represent different sedimentary environments. Samples plotting close to the stoichiometric pyrite line (S = 1.15*Fe) indicate that all sulphur and most of the iron is fixed in pyrite. The second group contains lower S/Fe ratios because of less sulphur but higher iron concentrations. Sulphur and iron was fixed in pyrite but excess iron from sedimentary input occurred additionally. The third, iron rich sample group, contains very low amounts of organic carbon and sulphur. In this environment organic carbon was mostly oxidised and pyrite was not precipitated. Iron was fixed in different silicate phases or in oxides. The accumulation of organic matter and the related S contents indicate dysoxic water conditions in the Assistencia Formation. The evolution to a more euxinic sedimentary environment is confirmed by pyrite bearing samples (Fig. 6-3d) from the lower and upper Assistencia Formation (Scheffler et al., 2001).

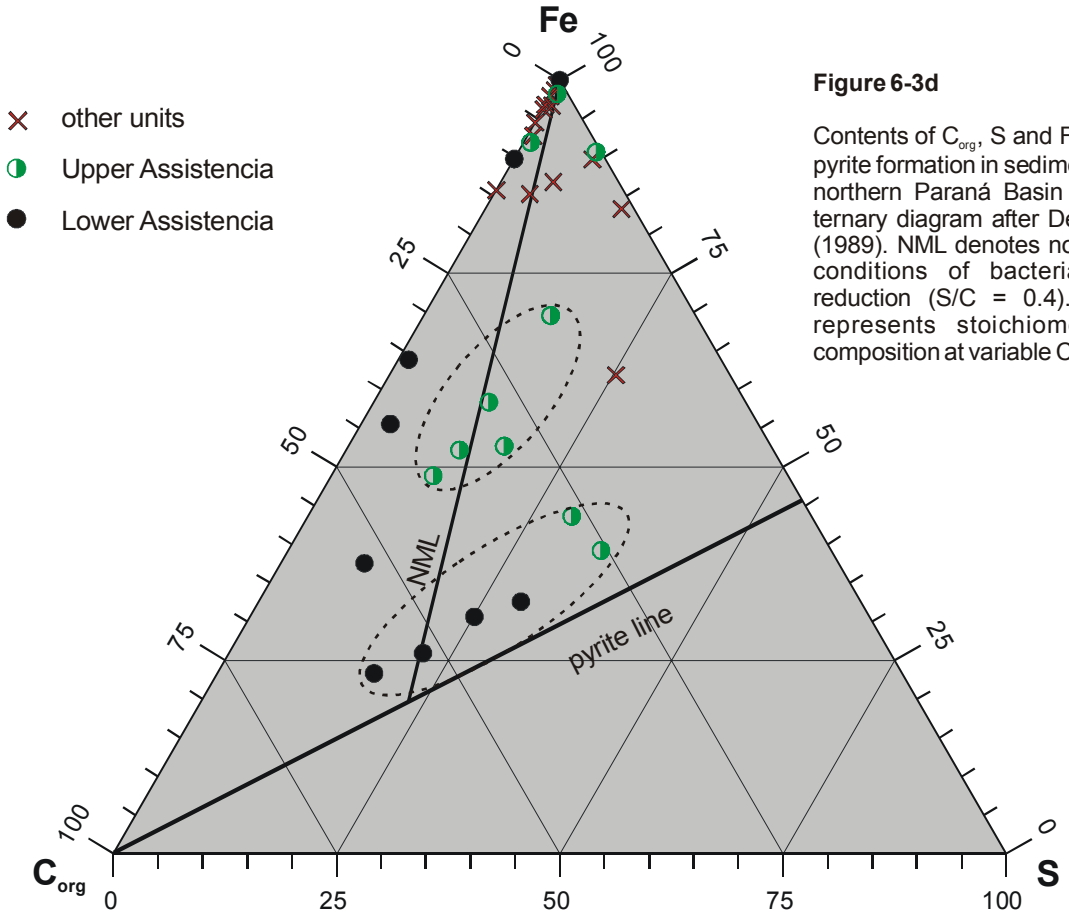


**Figure 6-3d**

Contents of $C_{org}$, S and Fe controlling pyrite formation in sediments from the northern Paraná Basin plotted in a ternary diagram after Dean & Arthur (1989). NML denotes normal marine conditions of bacterial sulphate reduction (S/C = 0.4). Pyrite line represents stoichiometric pyrite composition at variable $C_{org}$ contents.

## 6.5 $\delta^{13}C$, C/N ratios and organic matter composition of Dwyka sediments

As previously noted, independent geochemical proxies reflect climate variations during deposition of stadial and interstadial sediments of the glacial Dwyka Group within the central Karoo-Basin. Elevated $C_{org}$ contents of the interstadial deposits in combination with increasing V/Cr ratios point to anoxic conditions in the sedimentary environment (Fig. 5-3).

The cyclicity of the lower Dwyka Group, as shown by different element ratios and $C_{org}$ contents, can also be seen in the carbon isotopic composition of organic matter (Fig. 6-4a-c). More negative $\delta^{13}C_{org}$ values mark the full glacial environments (for stadials of DS II, median is –25.13‰, and for stadials of DS III, median is –23.95‰), whereas interstadial phases in general are characterized by less negative $\delta^{13}C_{org}$ values (interstadials of DS I have a median of –24.83‰, those of DS II have a median –23.19‰, and those of DS III have a median of –22.86‰). Organic matter derived from marine primary production incorporates the $\delta^{13}C$ signature of atmospheric $CO_2$ and thus reveals the changes between glacial and interglacial $pCO_2$ values (Jasper and Hayes, 1990). Variation in proportions of marine vs. terrigenous organic matter sources, stage of degradation, and burial history can alter the carbon isotopes

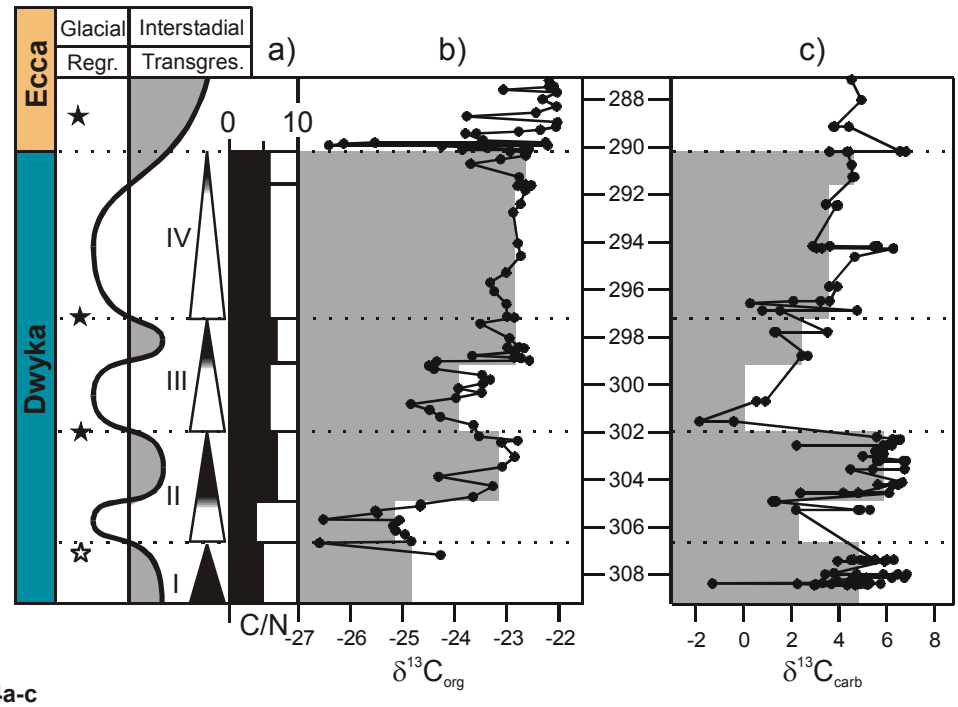


**Figure 6-4a-c**

Carboniferous-Permian climate evolution within the Karoo Basin. Filled stars- SHRIMP ages after Bangert et al. (1999);open star- age by Visser (1997). **a)** Invariable mean C/N ratios for glacial and interstadial phases indicate a constant marine organic-matter source. In **b)** and **c)**, mean $\delta^{13}C$ values for glacial and interstadial phases are shown by gray shading. **b)** $\delta^{13}C_{org}$ for Dwyka sequence. **c)** $\delta^{13}C_{carb}$ for equatorial regions after Veizer et al. (1999); ages corrected by -1m.y. Synchronous evolution of proxies from polar and equatorial regions indicates global control mechanism (Scheffler et al., 2003).

of bulk organic matter (Meyers, 1997). Origin and degree of diagenetic overprint of organic matter were assessed by determination of C/N ratios and biomarker composition. C/N ratios <10 indicate an origin of organic matter from marine algae (Meyers, 1997), whereas terrigenous organic matter yields C/N ratios of >20. Samples from the Dwyka sequence give C/N ratios of <8, indicative of marine-derived organic matter. Glacial and interglacial phases show no significant variation in C/N ratios (Fig. 6-4a).

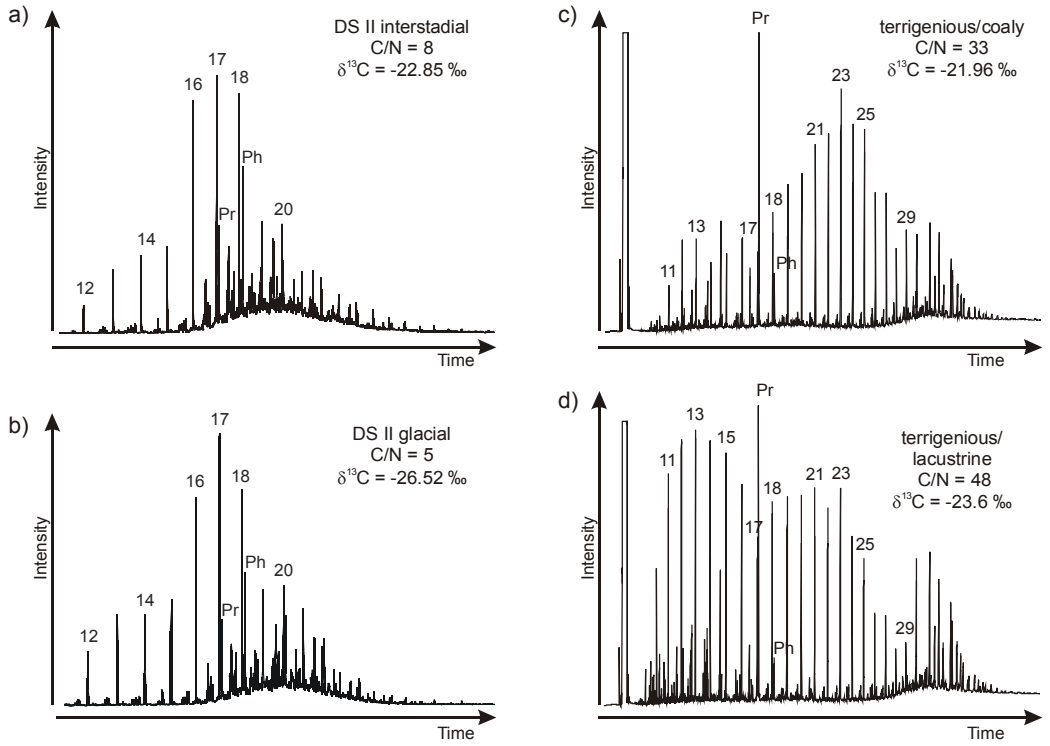


**Figure 6-5a-d**

Dwyka sedimentary lipid distribution; n-alkanes indicated by carbon number, and pristane and phytane denoted as Pr and Ph, respectively. **a)** and **b)** Aliphatic hydrocarbon composition of samples from **a)** interstadial and **b)** glacial phases document fully marine origin of organic matter. **c)** and **d)** Distribution of n-alkanes from basin margins reveals a strong input of land-plant material (Scheffler et al., 2003). Variation of $\delta^{13}C$ values in central basin thus results from changes in $pCO_2$.

GC-MS (gas chromatography–mass spectrometry) analyses of aliphatic hydrocarbon fractions (Figs. 6-5a & b) show a predominance of n-alkanes with carbon numbers in the $C_{16}$ to $C_{18}$ range. These compounds derive from algal biomass and are in strong contrast to land plant–lipids maximizing around *n*-$C_{29}$ in their n-alkane distribution (Meyers, 1997). As for the C/N ratios, no obvious differences can be measured between samples from glacial or interglacial phases. This similarity points towards a consistent marine origin for the organic matter deposited in the basin centre. Deltaic sedimentation systems (Visser, 1997) with strong terrigenous input were established along the northeastern basin margin. High C/N ratios (>30), pristane/phytane ratios greater than 8, and the presence of long-chain aliphatic hydrocarbons indicate a strong terrestrial input into the basin margins (Figs. 6-5c & d). By

comparing the geochemical fingerprints of organic matter from central and marginal basin positions, it can be demonstrated that the distal basin received no significant amounts of terrestrial organic matter during deposition of the entire Dwyka Group. Because the organic carbon was derived exclusively from marine organic matter, variations in its carbon isotopes must originate from $CO_2$ variations between glacial and interglacial phases. Admixture of terrigenous organic matter from vegetation cover of the southern Gondwana continent during ice-free phases can be excluded.

In DS IV carbon isotopic signatures do not reflect the cyclicity shown by the element ratios. The transition from the upper Dwyka Group (mean $\delta^{13}C$ –22.75‰) into postglacial Ecca Group (mean $\delta^{13}C$ –22.25‰) is characterized by a conspicuous excursion to lighter $\delta^{13}C$ values of –26.5‰. This excursion correlates with enhanced tectonic and volcanic activity, which is documented by decreasing $^{87}Sr/^{86}Sr$ ratios at around 290 Ma (Veizer et al., 1999).

## 6.5.1 Discussion

Climate information can be extracted from the $\delta^{13}C$ record of marine bicarbonate. Marine carbonates suitable for carbon isotope determinations were not deposited during sedimentation of the Dwyka Group. Therefore, $\delta^{13}C$ values of the organic carbon in the sedimentary rocks are used to infer climate changes. The isotope variations are driven by the $CO_2$ content in the atmosphere, which affects the organic carbon reservoir. Paired carbonate and organic carbon isotopes have been used to decipher changes in atmospheric $pCO_2$ over the Earth's history (Hayes et al., 1999). Veizer et al. (1999) compiled an extensive set of $\delta^{13}C$, $\delta^{18}O$ and $^{87}Sr/^{86}Sr$ data from paleotropical carbonate fossils. $\delta^{13}C_{org}$ values from south Gondwana and $\delta^{13}C_{carb}$ values from equatorial regions (Fig. 6-4c) show co-evolutionary trends during the Pennsylvanian. Variability lies within the error range of the age determinations. The marked drop at around 303 Ma and the subsequent increase in the $\delta^{13}C_{carb}$ values (Fig. 6-4b) indicates a transition from a warm to a cold climate phase (Bruckschen et al., 1999). The co-variations of $\delta^{13}C_{org}$ from the Karoo Basin in southern Gondwana and the equatorial $\delta^{13}C_{carb}$ of Bruckschen et al. (1999) confirm a global change in the carbon isotope composition during the Pennsylvanian.

The global nature and synchronous onset of regionally observed climate variations are documented by the simultaneous shifts in the $\delta^{13}C$ values of equatorial carbonates and the $\delta^{13}C$ values of organic carbon from the southern-latitude Karoo Basin. The ~5 m.y. periodicity in the duration of stadial-interstadial cycles does not fit any known orbital frequency and requires further investigation.

The clockwise drift of the southern Gondwana continent shifted the Karoo Basin into polar cold-regions and can be regarded as the primary trigger for glaciation processes. This

mechanism is, however, insufficient to explain the cyclic climate variations as well as the terminal and abrupt break down of the ice shields. Warm currents along the eastern coast of Pangea (Kutzbach et al., 1990) transported moist air to polar regions. In combination with high albedo rates and low $pCO_2$, icehouse conditions were established and glaciers started to accumulate in high latitudes. High temperature gradients between equatorial and polar regions favoured the development of a psychrosphere where deep ocean cold-water currents reached equatorial regions. Feedback mechanisms intensified the cooling rates and favored the fixation of water as glaciers on southern continents. This in turn caused a global fall in sea level. During regression phases, $CO_2$ fixing carbonate-complexes were exposed above sea level and carbonate weathering led to increasing $pCO_2$. In concert with phases of enhanced tectonic activity (Stollhofen et al., 2000), elevated atmospheric $CO_2$-release initiated greenhouse conditions. Elevated temperatures established new air/ocean circulation pathways and possibly a retreat of the $CO_2$-fixing psychrosphere. Most importantly, the Pangean closure of the equatorial seaway (Saltzman, 2003) decoupled the evolution of the Panthalassian and Paleotethys Oceans.

As result of reduced equatorial to polar temperature gradients, glaciers retreated and sea level rose. The processes of $CO_2$ release and temperature increase, linked in a positive feedback, caused global warming. The final termination of the Carboniferous–Permian glaciation phase in southern Africa must be viewed to have resulted from the interaction of different climate-controlling factors, including variations in $pCO_2$ values, the continent-ocean configuration, and continental topography, as well as changing atmospheric and oceanic circulation pathways. As the solar system passed through one of the four galactic spiral arms, the cosmic ray flux (CRF) increases, which may have triggered global glaciation (Shaviv, 2002). The poor correlation between CRF-maximum and the timing of the Pennsylvanian glaciation excludes this external forcing mechanism and underlines the need for further investigation.

# 6.6 $\delta^{13}C_{org}$ values of sediments from the Karoo, Paraná and Kalahari Basin.

In figure 6-6 $\delta^{13}C_{org}$ values from different sample localities are displayed in stratigraphic order. Variations of $\delta^{13}C_{org}$ values during sedimentation of the glacial Dwyka Group can be explained with changes in $pCO_2$ during glacial and interstadial phases. Conspicuously low $\delta^{13}C_{org}$ values denote the Dwyka/Ecca boundary. This sudden decrease from median $\delta^{13}C_{org}$ values of –22.9‰ (S' Karoo Basin) and –23.5‰ (MPU) to –26.1‰ and –26.7‰, respectively can also be recognized in the MPU core. Beside the comparable stratigraphic position of the isotope excursion closely above the Dwyka-Ecca boundary, the identical amplitude of 3.2‰ also points to a basin wide process, influencing by the carbon isotope composition of the organic matter.

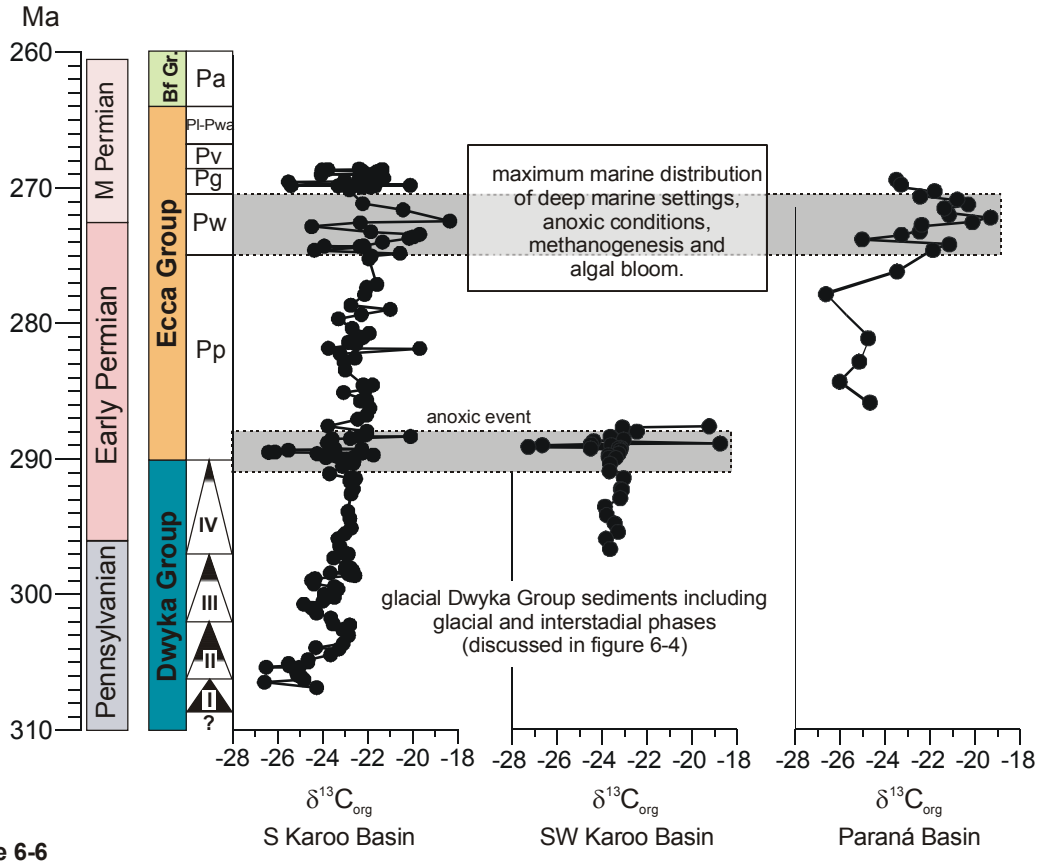


**Figure 6-6**

$\delta^{13}C$ values of the organic matter from the Karoo and Paraná Basin. Simultaneous excursions in different basin positions indicate regional to hemispherical processes.

The major and trace element geochemical composition of these sediments deposited during the transition from glacial to postglacial climate conditions point to a specific sedimentary environment. The negative $\delta^{13}C_{org}$ excursions are accompanied by a reduced siliciclastic input indicated by decreasing Si/Al and Ti/Al ratios (Fig. 4-2a & b and 4-4a & b). The decreasing $\delta^{13}C_{org}$ values are flanked by elevated $C_{org}$ and high manganese and phosphorous contents (Fig. 4-2d & i and 4-4d & i). The enrichment of these elements is associated with the formation of carbonates and/or phosphates under anoxic conditions.

Different processes can influence the carbon isotope composition of the organic matter. Secondary alteration processes in the course of the rising Cape Fold Belt have had little effect on the $\delta^{13}C_{org}$ values (De Wit et al., 2002). Since marine conditions persisted during the transition from glacial to postglacial climate conditions the documented negative carbon isotope spikes can not explained by enhanced supply of terrigenous biomass. Thus, other processes must be responsible for the short-lived negative $\delta^{13}C_{org}$ excursion.

Negative carbon isotope shifts of 2-3‰ can be derived from diagenetic changes and transformation of organic matter to kerogen (Hoefs, 1997; Hayes et al., 1983). Bacterial degradation of biopolymers preferentially eliminates $^{13}C$-enriched carbohydrates and proteins and preserves $^{12}C$-enriched lipids. Decarboxylation reactions remove $^{13}C$-enriched carboxyl groups, leading to $^{13}C$-depletion in the residual (Hoefs, 1997). If these processes are responsible for the sudden $\delta^{13}C_{org}$ decrease of 3‰ at the Dwyka-Ecca boundary is questionable.

The $\delta^{13}C$ value of marine organic matter is dependent on the global carbon flux in a coupled atmosphere-ocean system as discussed by Popp et al. (1998), Hayes et al. (1999), Kump and Arthur (1999) and Boucot and Gray (2001). If source dependent variations in $\delta^{13}C$ of the bulk organic matter can be excluded, the isotopic composition of $C_{org}$ is predominantly controlled by the concentration of dissolved $CO_2$.

Assuming that the observed negative $\delta^{13}C_{org}$ excursion records changes in the carbon isotope composition of the atmosphere, enhanced proportions of light carbon ($^{12}C$) must have entered the atmosphere or the oceanic $CO_2$ reservoir. A possibility for a sudden release of enhanced volumes of isotopic light $CO_2$ is volcanic activity. The $\delta^{13}C$ value of mantle released $CO_2$ is between –8 and –4‰ (Barnes et al., 1978). The excursion to lighter $\delta^{13}C$ values in the Karoo Basin correlates with enhanced tectonic and volcanic activity, which is documented by decreasing $^{87}Sr/^{86}Sr$ ratios at around 290 Ma (Veizer et al., 1999).

A further source of light $CO_2$ is methane with $\delta^{13}C$ values between –110 and -50‰ (Hoefs, 1997). From different sedimentary successions across the Permo-Triassic boundary in southern Gondwana, multiple organic carbon isotope reversals were recorded. De Wit et al. (2002), explained the negative excursions in $\delta^{13}C_{org}$ values by a rapid release of methane

stored as solid $CH_4$-hydrates. Gas hydrates are metastable. Increasing temperature and decreasing pressure can destabilize the solid methane, leading to a sudden liberation of the stored gases (Kvenvolden, 1993). An event like this would produce a global negative shift in $\delta^{13}C$ of carbonates and biomass. In carbon isotope curves obtained from brachiopods from the nothern hemisphere (Veizer et al., 1999; Saltzman, 2003) a negative $\delta^{13}C$ excursion around 290 Ma is missing. Thus, the release of methane into the atmosphere from gas hydrates can be excluded as trigger for the negative $\delta^{13}C_{org}$ excursion at the Dwyka-Ecca boundary. If a smaller release of methane would produces a more regional isotope shift is very questionable due to intensive and rapid atmospheric mixing of released $CH_4$ and its conversion product $CO_2$. In fact it is problematic to solve the question, which process or interaction was responsible for the regional negative $\delta^{13}C_{org}$ excursion.

The most likely explanation for the $\delta^{13}C_{org}$ excursion is a change in the bioproductivity, which occurred during regression – transgression phases at the end of the glaciation phase. However, the formation of anoxic conditions at the Dwyka–Ecca boundary and the possibly basinwide negative $\delta^{13}C_{org}$ spike can be used as marker horizon.

In the siliciclastic sediments of the Prince Albert Formation the $\delta^{13}C_{org}$ values range around a median of –22.3‰. Element geochemical proxies point to marine conditions (Fig. 5-3). Comparable to the Irati Formation of the northern Paraná Basin, the $\delta^{13}C_{org}$ values of the Whitehill sediments show predominantly positive (-18.3‰) excursions from the median. The connection of both sedimentary environments is indicated by a distinctive *Mesosaurus* reptile fauna described by Oelofson (1987). Faure and Cole (1999) detected in time equivalent deposits of Whitehill/Irati age from different localities significant similar positive $\delta^{13}C_{org}$ excursions of approximately 3‰. They attributed the comparable composition of the organic matter (elevated HI-indices) and enrichment of $^{13}C$ in the Whitehill and Irati Formations to a basinwide algae bloom.

In the samples from the Kalahari Basin the $\delta^{13}C_{org}$ values range from –27.62‰ to –21.19‰ around a median of –23.2‰. In the Tswane Formation the $\delta^{13}C_{org}$ values increase from approximately –24 to -22‰ (Fig. 6-7a). This contiguous enrichment of $^{13}C$ in the upper Tswane Formation is possibly associated with an elevated supply of terrigenous organic matter. In palaeozoic sediments $\delta^{13}C_{org}$ of organic matter is different from today's pattern. Heavy $\delta^{13}C_{org}$ values (~ -20 to -24‰) indicate terrigenous organic matter where as lighter $\delta^{13}C_{org}$ values (~ -25 to -30‰) point to marine algae and/or bacterial organic matter (Maynard, 1981, Arthur, 1981).

In the $C_{org}$ vs. $S_2$ diagram (Fig. 6-7b), the samples plot in the field of kerogen type III. The linear regression of most of the samples indicates that the organic matter was supplied from a constant, predominantly terrigenous source. Average $T_{max}$ temperatures of 425°C between

419 and 431°C (Fig. 6-7b) confirm the input of predominantly vascular plant material. Elementgeochemical proxies refer to a marsh-like paludal sedimentary environment, which was only marginally influenced by marine conditions.

The carbon isotope composition of the organic matter in the Ntne/Mosolotsane Formation of –27.62‰ points to a predominantly supply of marine algae or bacterial derived organic matter. Since $C_{org}$ contents of the sediments of the Beaufort and Lebung Groups are below 0.5% Rock Eval data is not available for this core section. Decreasing $\delta^{13}C_{org}$ values can be associated with the change from paludal and deltaic environments during sedimentation of the Ecca Group to fluvial-limnic-aeolian sedimentation in the Beauford and Lebung Groups. In general the Ecca Group sediments contain terrigenous organic matter deposited in permanently aquatic environments. During deposition of the Beaufort and Lebung sediments only temporary aquatic sedimentary environments could establish.

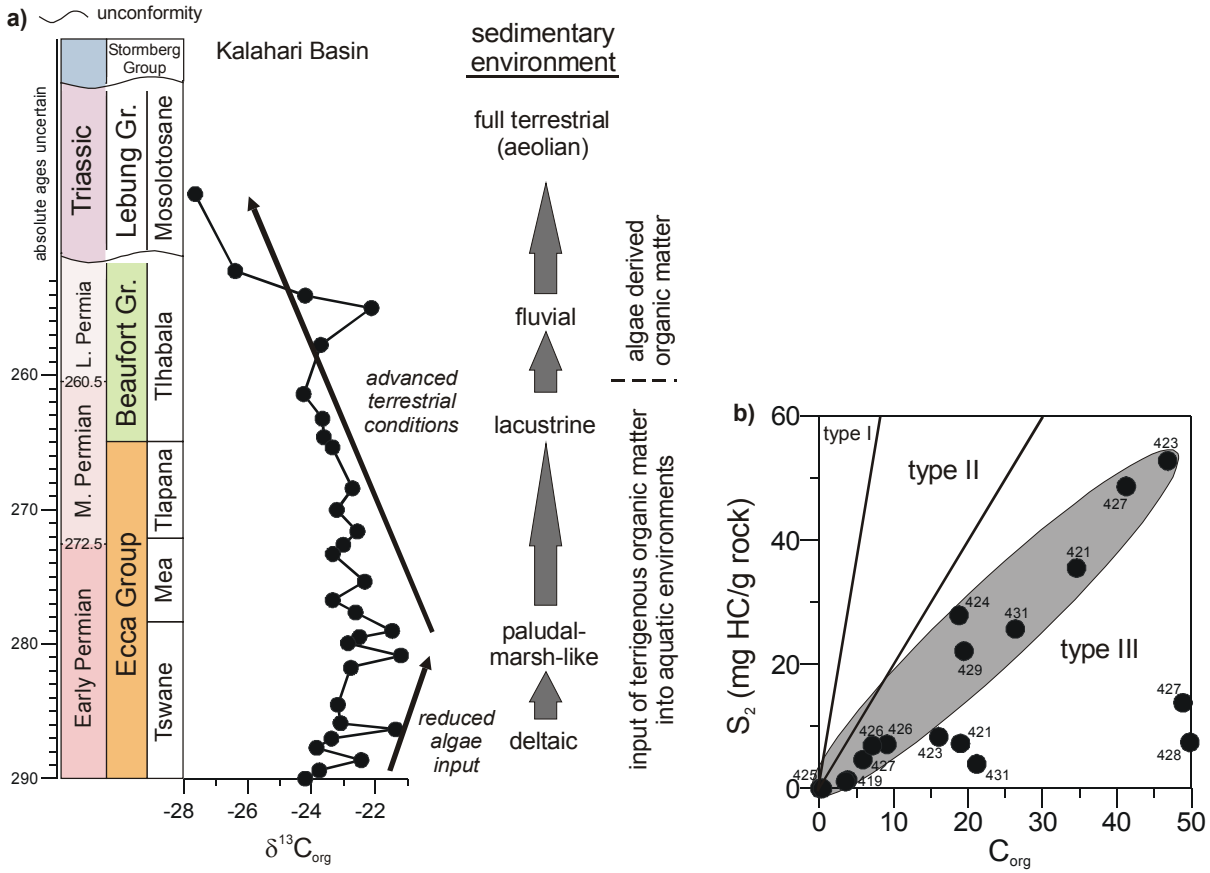


**Figure 6-7a & b**

**a)** Variations in the $\delta^{13}C_{org}$ values can be related with changing sedimentary environments. Deltaic sedimentary environments established in the lower succession after the final retreat of glaciers. Terrestral conditions prevailed finally in the Beauford Group. **b)** $C_{org}$ vs. $S_2$ diagram after Langford & Blanc-Valleron (1990) classified the organic matter of the OGT core as type III kerogen. Samples plotting along a similar slope (grey area) contain organic matter from equivalent sources; numbers at samples denote $T_{max}$ temperatures.

# 6.7 Detailed investigations of the organic matter from the Witbank Basin

## 6.7.1 Introduction

The Upper Carboniferous and Permian sedimentary sequence of the Karoo Basin in South Africa contains a unique record of the climatic and biological evolution after one of the most extensive and intensive glaciation phases in Earth history. The well exposed and documented sedimentary records of this spectacular climate change in the Karoo Basin comprise glacial phases, the deglaciation transitional phase with temperate climate and the postglacial phase with warm-humid climate conditions (Visser, 1995, 1997). The cyclic development of the glaciation/deglaciation sequences was described and discussed by Visser (1997), Stollhofen et al. (2000), Scheffler et al. (2003) and Isbell, (2003a; 2003b). The global effect of the glaciation in terms of atmospheric $CO_2$ content is discussed by several authors and documented by variations in $\delta^{13}C$ measured on brachiopods from equatorial regions (Berner, 1994; Veizer et al., 1999; Bruckschen et al., 1999) and bulk organic matter carbon isotopes (Scheffler et al., 2003).

From the end of the Carboniferous to the early Permian significant climate changes in southern Gondwana are recorded in the rearrangement of the sedimentary systems. Glacial dominated sedimentary systems were replaced by fluvial-deltaic sequences (Visser, 1995; 1997; Stollhofen et al., 2000).

Coal petrographic investigations in numerous coal basins contribute to the knowledge about ancient climatic and environmental conditions (Stach et al., 1982; Teichmüller, 1989; Diessel, 1992; Taylor et al., 1998). The applicability of molecular organic geochemistry in the discussion about climate, depositional environment and type of organic matter has been demonstrated in several studies (Didyk et al., 1978; Mackenzie et al., 1982; Radke et al., 1982; Tissot and Welte, 1984; ten Haven et al., 1988; Alexander et al., 1992; Meyers, 1997; Fabiańska and Kruszewska 2003). This work focuses on the interpretation of organic matter composition of coals and sediments from the Witbank coalfield in the north-eastern Karoo Basin (Figs. 2-2a & b), in which cyclic successions of conglomerates, sandstones, shales and coals are exposed. The observed cyclicity is attributed to persisting climate changes, which triggered eustatic sealevel changes until the Late Permian (Le Blanc Smith, 1980; Falcon et al., 1984; Cadle et al., 1993; Millsteed, 1994).

In a multiproxy approach bulk geochemical, including carbon isotope, and molecular geochemical data are presented. Elemental ($C_{org}$, S and N) and carbon isotopic compositions as well as Rock Eval pyrolyses data were used as screening parameters for bulk organic

matter typing. Biomarker analyses were carried out on the aromatic and aliphatic hydrocarbons to verify and extend the obtained information about sedimentary environment and organic matter type, which is closely related with the climate evolution.

## 6.7.2 Bulk composition of the organic matter

### 6.7.2.1 C, S, N contents and $\delta^{13}C$ values

Organic carbon ($C_{org}$) and sulphur contents of shales and coals from the Witbank Basin are given in table 6-2. $C_{org}$ contents reaches from 0.63 to a maximum of 73.53 wt.%. By their $C_{org}$ contents the samples can be subdivided into three groups. $C_{org}$ contents of maximal 10 wt.% (D1/1, seam 1/2, seam 4u/l), indicate clastic sediment layers between the coal seams. $C_{org}$ contents from 35 to 50 wt.% were measured in seam 2-a, 3, 3/4, 4l-b and in seam 4u-b. Samples with $C_{org}$ contents higher than 60 wt.% represent pure coals (D 1, 1-a & b, 2-b, 4l-a, 4u-a, 5-a & b) and are combined in the third group. The classification into different groups due to their $C_{org}$ contents indicates changing sedimentary conditions during accumulation of the organic matter.

| Seam | $C_{org}$ wt.% | S wt.% | N wt.% | C/S | C/N | $\delta^{13}C_{org}$ | $T_{max}$ | HI | OI | PI | SOM yield (mg/g $C_{org}$) | Saturated HC (%) | Aromatic HC (%) | NSO (%) |
|---|---|---|---|---|---|---|---|---|---|---|---|---|---|---|
| **5-b** | 67,4 | 0,32 | 1,55 | 213 | 44 | -22,05 | 433 | 167 | 6 | 0,029 | 8,34 | 2,0 | 52 | 46 |
| **5-a** | 71,1 | 0,41 | 1,76 | 175 | 40 | -25,07 | 429 | 131 | 3 | 0,016 | 7,05 | 2,0 | 57 | 41 |
| **4u-b** | 35,6 | 0,31 | 0,78 | 115 | 46 | -23,52 | 438 | 47 | 5 | 0,052 | 2,95 | 2,0 | 58 | 40 |
| **4u-a** | 60,8 | 0,34 | 1,23 | 181 | 49 | -23,89 | 431 | 92 | 4 | 0,036 | 4,51 | 2,0 | 61 | 37 |
| **4l/u** | 10,0 | 0,10 | 0,28 | 102 | 36 | -23,16 | 440 | 92 | 6 | 0,057 | 5,90 | 2,1 | 55 | 42 |
| **4l-b** | 37,0 | 0,26 | 0,95 | 143 | 39 | -23,66 | 432 | 172 | 4 | 0,017 | 5,23 | 2,0 | 63 | 35 |
| **4l-a** | 65,4 | 0,28 | 1,54 | 238 | 42 | -22,66 | 434 | 48 | 5 | 0,049 | 3,27 | 2,0 | 62 | 36 |
| **3/4** | 48,3 | 0,40 | 1,2 | 120 | 40 | -24,90 | 430 | 203 | 7 | 0,026 | 10,17 | 2,0 | 56 | 42 |
| **3** | 47,5 | 0,51 | 1,28 | 93 | 37 | -24,09 | 432 | 189 | 8 | 0,022 | 6,27 | 2,0 | 57 | 41 |
| **2-b** | 73,5 | 0,36 | 2,14 | 203 | 34 | -22,70 | 431 | 200 | 7 | 0,021 | 7,07 | 2,0 | 56 | 42 |
| **2-a** | 39,4 | 0,13 | 0,81 | 300 | 49 | -22,82 | 493 | 13 | 4 | 0,134 | 1,80 | 2,0 | 55 | 43 |
| **1/2** | 9,5 | 0,11 | 0,21 | 89 | 45 | -23,23 | 443 | 119 | 6 | 0,065 | 6,51 | 2,0 | 56 | 42 |
| **1-b** | 69,6 | 0,35 | 1,78 | 201 | 39 | -23,58 | 431 | 250 | 6 | 0,029 | 14,73 | 2,0 | 53 | 45 |
| **1-a** | 63,8 | 0,70 | 1,35 | 91 | 47 | -24,08 | 432 | 203 | 6 | 0,024 | 12,72 | 2,0 | 54 | 44 |
| **D1/1** | 0,6 | 0,40 | 0,03 | 1,6 | 21 | -23,47 | 413 | 25 | 35 | 0,543 | 55,96 | 10,0 | 61 | 29 |
| **D1** | 66,9 | 0,32 | 1,48 | 206 | 45 | -23,93 | 425 | 141 | 3 | 0,031 | 10,67 | 2,0 | 54 | 44 |

**Table 6-2**

Stratigraphic position (m), datum is the lowermost seam D1; organic carbon ($C_{org}$), sulphur (S) and nitrogen (N) content in weight %; carbon isotope composition of the organic matter ($\delta^{13}C_{org}$); Rock Eval pyrolysis: $T_{max}$, hydrogen index (HI=mgHC/g$C_{org}$), oxygen index (OI=mg$CO_2$/g$C_{org}$), production index (PI = $S_1/(S_1+S_2)$); soluble organic matter (SOM) yield and relative proportions of saturated hydrocarbons (HC), aromatic HC and NSO compounds.

Low sulphur contents, characteristic for Gondwana coals (Cadle et al., 1993), were detected in the whole succession of the Rietspruit colliery. The values range around a mean of 0.3 wt.% with a maximum value of approximately 0.7 wt.% occurring in the lower part of seam No.1. Samples cannot be subdivided into groups as according to carbon contents.

C/S ratios are used to estimate changes in the sulphate and $O_2$ concentration in sedimentary

environments (Berner and Raiswell, 1983; 1984; Dean and Arthur, 1989). Elevated sulphur content in $C_{org}$ rich sediments is generally associated with the formation of pyrite. Sedimentary pyrite can be formed by the reaction of $H_2S$ produced by bacterial reduction of seawater sulphate in anoxic environments with reactive iron derived from detrital minerals. In consequence, sediments deposited under oxic marine conditions contain C/S ratios of approximately 2.5 whereas lower C/S ratios are characteristic for euxinic environments. High C/S ratios (>> 2.5) are found in non-marine environments where sulphur supply and sulphate reduction is limited (Berner, 1984). With exception of sample D1/1 all samples yield very high C/S ratios (Tab. 6-2) with a median value of 159 indicating that the organic matter accumulated in a predominantly non-marine environment, where suitable conditions for preservation of organic matter prevailed.

C/N ratios can provide additional information about the type of organic matter. Organic matter derived from marine or lacustrine algae yield C/N ratios < 10 whereas C/N ratios > 20 indicate terrigenous organic matter. This distinction arises mainly from the protein richness of algal organic matter (Meyers, 1997). In samples with low $C_{org}$ but high clay mineral contents adsorption of inorganic nitrogen on surfaces and within the interlattice space of clay minerals can lead to misleading interpretations of the C/N ratios (Sampai and Matsumoto, 2001). The C/N ratios of the coals from the Rietspruit colliery range from 34 to 49 with a median of 41 (Tab. 6-2). Thus, the high C/N ratios corroborate the assumption that the coals are preferentially composed of land plant derived organic matter. Influence by inorganic nitrogen can be excluded because of the high $C_{org}$ contents.

Furthermore, carbon isotopes of organic matter can be used to distinguish different sources of the organic matter. For Palaeozoic sediments, lighter $\delta^{13}C$ values (-24 to –30 ‰) are commonly associated with marine organic matter whereas heavier $\delta^{13}C$ values (-20 to –25 ‰) refer to the input of vascular plants (Maynard, 1981; Meyers, 1997; Tyson, 1995). Variability in plant $\delta^{13}C$ is caused by isotopically different carbon sources utilized upon photosynthesis. Beside variation in proportion of marine versus terrigenous organic matter sources also the stage of degradation, i.e. selective preservation of constituents with heavy or light carbon isotopes can alter the $\delta^{13}C$ composition of bulk organic matter.

In the samples from the Rietspruit colliery the $\delta^{13}C$ values of the bulk organic matter range from –25.06 to –22.04 ‰ with a median of –23.55 ‰ (Tab. 6-2). In consequence, the $\delta^{13}C$ values obtained point to preferentially terrestrial sources although $\delta^{13}C$ values alone do not provide clear information about the type of organic matter. An improved characterisation of the organic matter can be achieved by combination of C/N ratios and $\delta^{13}C$ data. High C/N ratios in combination with heavy $\delta^{13}C$ values refer to a predominantly terrigenous source of the organic matter.

### 6.7.2.2 Rock Eval pyrolysis

Rock Eval pyrolysis provides information on the type and thermal maturity of organic matter. In general three different types of organic matter can be discerned. After Tissot and Welte (1984) immature type I kerogen is dominated by aliphatic structures suggesting major contributions from lipids during diagenesis. It appears to be derived from extensive bacterial reworking of lipid-rich algal debris in lacustrine and marine settings and gives exceptionally high hydrogen indices (HI>600) at low OI indices (OI<50). Type II kerogen originates from mixed phytoplankton, zooplankton and bacterial debris usually deposited in marine sediments. For immature samples HI-indices are 400-600 and associated OI-indices range between 50 and 100. Type III kerogen yields low hydrogen indices (HI<300) accompanied by higher OI-indices (OI>100). This type of organic matter is usually derived from woody parts of terrestrial plants.

$T_{max}$ and the production index [PI = $S_1/(S_1+S_2)$] given in table 6-2 reveal information on the maturity of the organic matter since both parameters rise with increasing maturity (Espitalié et al., 1988). If samples of equal maturity are compared, $T_{max}$ can also be influenced by the type of organic matter. This occurs as a consequence of different bond strengths in organic molecules and in general increases from type III to type I kerogen (Peters, 1986).

Rock Eval pyrolysis of samples from the Rietspruit colliery yield median $T_{max}$ of 432°C. PI values below 0.1 (median is 0.03) indicate low thermal maturity of most of the organic matter in the samples. The high PI value in the lower succession derives from the $C_{org}$ lean sample D1/1 ($C_{org}$ = 0.63wt.%) and indicates impregnation by migrating hydrocarbons. The simultaneously decreasing $T_{max}$ (413°C) is also attributed to impregnation and contamination by migrated hydrocarbons (Peters, 1986). Only sample 2-a deviates from the relative homogeneous values in the succession by its exceptionally high $T_{max}$ and simultaneous elevated PI values (493°C, 0.13) that cannot be explained by simple burial diagenesis.

Kerogen types can be determinated by plotting HI versus $T_{max}$ (Espitalé et al., 1988). Since $T_{max}$ is influenced by thermal stress this classification gives an assessment about the type and maturity organic matter. In figure 6-8a the samples plot in the fields of type II and III kerogen. This possibly indicates a mixture of predominantly type III land plant organic matter with temporary supply of type I or II algal derived organic matter. Samples from the shale intercalations 1/2 and 4l/u as well as from the bottom and top of seam 4 (4l-a and 4u-b) yield higher $T_{max}$ values caused by a different type of organic matter. The thermal maturity of the organic matter corresponds to app. 0.5 % of vitrinite reflectivity. Median values of the vitrinite reflectance of the coals in the northern Karoo Basin are given as $R_r$ = 0.68% (Fabiańska and Kruszewska 2003). This corresponds to the beginning of the oil window and will release kerogen-bound lipids as biomarkers into the bitumen fraction.

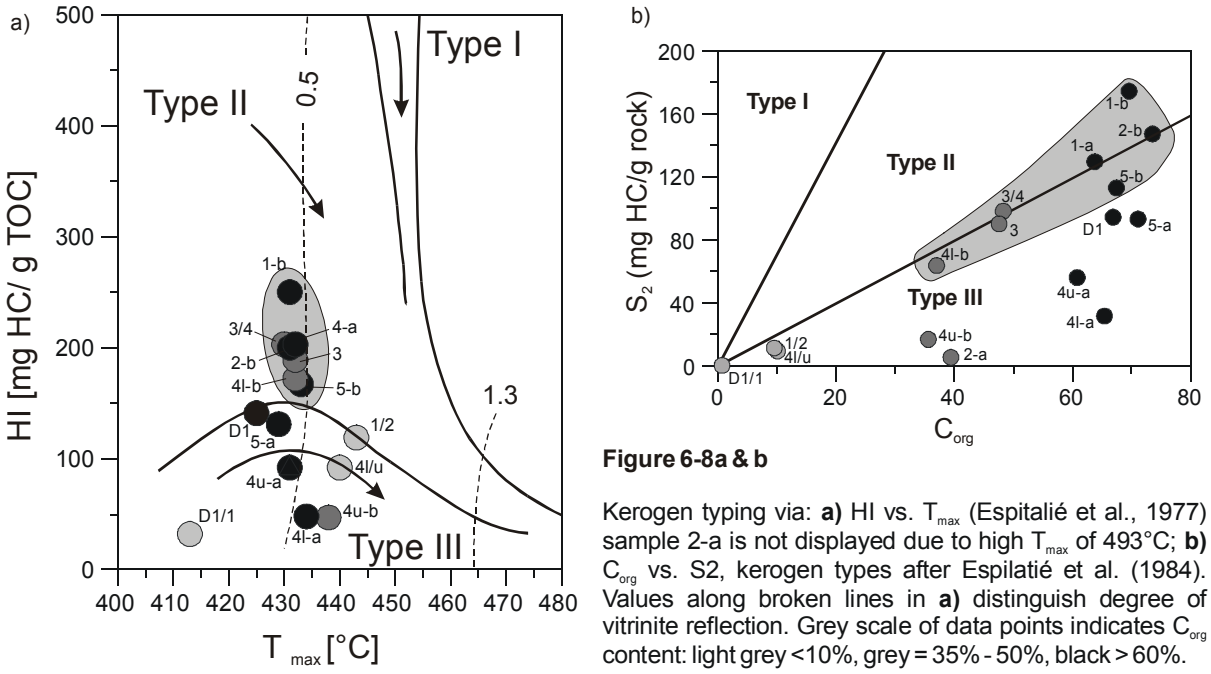


**Figure 6-8a & b**

Kerogen typing via: **a)** HI vs. $T_{max}$ (Espitalié et al., 1977) sample 2-a is not displayed due to high $T_{max}$ of 493°C; **b)** $C_{org}$ vs. S2, kerogen types after Espitalié et al. (1984). Values along broken lines in **a)** distinguish degree of vitrinite reflection. Grey scale of data points indicates $C_{org}$ content: light grey <10%, grey = 35% - 50%, black > 60%.

The $C_{org}$ vs. $S_2$ plot after Langford and Blanc-Valleron (1990) as shown in figure 6-8b allows to identify kerogen types and the magnitude of the mineral matrix effect. The effect of absorption of hydrocarbons by the mineral matrix is significant in samples with $C_{org}$ < 0.5% (Peters, 1986). In contrast to figure 6-8a the samples plot predominantly in the type III field of kerogen as it is characteristic for land plant material. Possibly influence by algae derived organic matter is indicated by samples that plot along the boundary of type II and III kerogen. Thus, samples from seam 1-a, 1-b, 2-b, 3, 3/4, 4l-b and 5b seams to contain organic matter of mixed origin. The same samples can also discerned in figure 6-8a by classification of the organic matter as type II kerogen.

It can be concluded that the coals and sediments contain relatively immature organic matter of predominantly land plant origin with minor algal admixture. Maximum burial temperatures of approximately 100°C during diagenesis can be estimated (beginning of oil window). Sample 2a must have been affected by a secondary alteration effect due to its exceptionally low S2-yield compared to its high $C_{org}$-value.

### 6.7.2.3 Soluble organic matter yield

The amount of soluble organic matter (SOM) is given in table 6-2. Extraction yields vary between 1.8 and 56.0 mg/g $C_{org}$ with a median value of 6.8. Highest extraction yields are reached in seam D1 and 1-a & b with approximately 13.7 mg/g $C_{org}$. Clastic layer D1/1 yields the highest bitumen content of 56 mg/g $C_{org}$, which indicates contamination by migrated hydrocarbons. Bitumen contents above 50 mg/g $C_{org}$ are often associated with mature source rocks or reservoirs containing migrated hydrocarbons (Tissot and Welte, 1984).

The soluble organic matter is predominantly composed of NSO compounds (41%) and aromatic hydrocarbons (57%). Aliphatic hydrocarbons are present in low quantities (2%) only (Tab. 6-2). This is in agreement with a predominantly terrigenous source of organic matter at a low stage of thermal maturation (Tissot and Welte, 1984). An exception is bitumen from clastic layer D1/1, which contains approximately 10% aliphatic hydrocarbons. This again indicates impregnation with migrating bitumens, which upon expulsion from the source rock get enriched in aliphatics (Tissot and Welte, 1984). The ratio of aliphatic to aromatic hydrocarbons remains relative constant throughout the profile around a median of 28 (Fig. 6-9a). Minor deviations towards elevated aliphatic contents occur in the lower part of the succession belonging to the Dwyka Group.

## 6.7.3 Saturated fraction

### 6.7.3.1 n-Alkanes

A suite of n-alkanes from $C_{10}$ to $C_{31}$ as well as isoprenoids can be identified in the gas chromatograms of the saturated hydrocarbons. Furthermore, the pseudohomologues series of the $C_{29}$-$C_{35}$ hopanes as well as Tm$\alpha$ and Tm$\beta$ ($C_{27}$ pentacyclic triterpanes with hopanoidal skeleton) can be detected in concentrations equivalent or higher than neighbouring n-alkanes. For three representative samples gas chromatograms (GCs) of aliphatic hydrocarbons with indication of the most abundant compounds are shown in figures 6-10a-c.

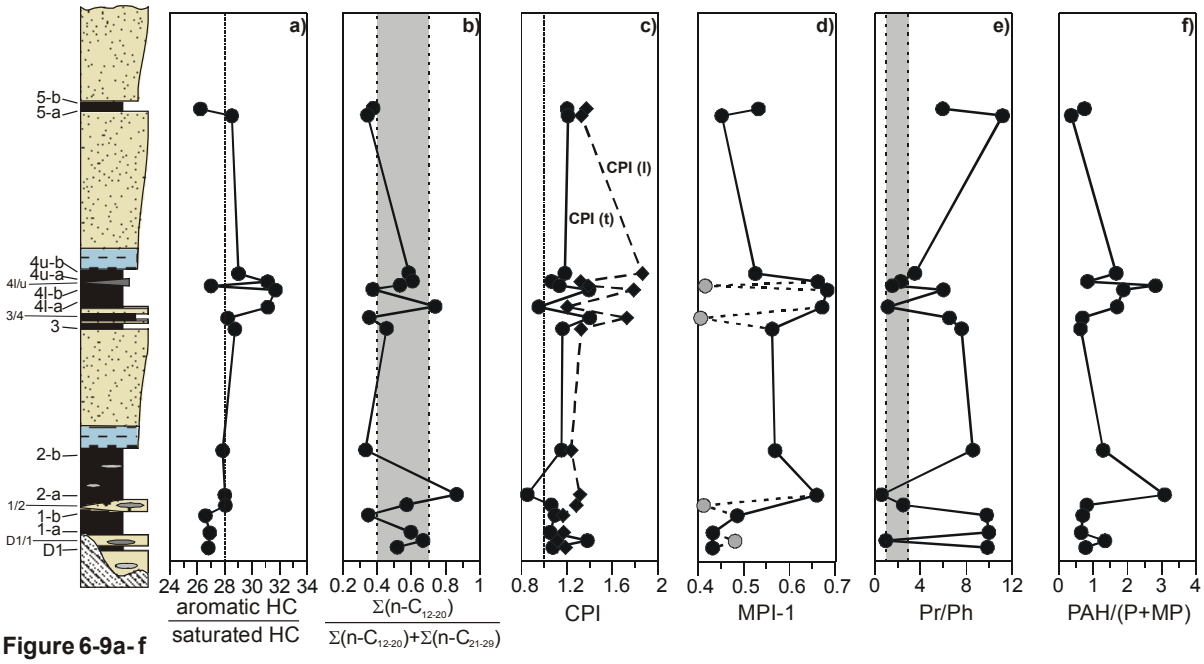


**Figure 6-9a- f**

Biomarker ratios for characterisation of sedimentary environment and organic matter sources. **a)** aromatic versus saturated hydrocarbons (HC); **b)** SLR: ratio of short- ($C_{12-20}$) versus long- (n-$C_{21}$-$_{29}$) chain n-alkanes; **c)** CPI(t): carbon preference index (CPI) from n-$C_{11}$ to n-$C_{29}$, CPI(l) carbon preference index from n-$C_{21}$ to n-$C_{29}$, CPI after Bray and Evans (1961); **d)** MPI-1: methylphenanthrene index after Radke et al., (1982); **e)** Pr/Ph: pristane/phytane ratio; **f)** (PAH)/(P+MP): sum of polyaromatic hydrocarbons (PAH) to the sum of phenanthrene (P) plus methylphenanthrenes (MP). Grey data points in e) denote siliciclastic enriched layers between main coal seams.

To assess the differences in n-alkane distributions the relative proportions of the short versus long chain n-alkanes (short/long ratio = SLR) were determined as sum of n-$C_{12-20}$ versus n-$C_{21-29}$ [$C_{12-20}/(C_{12-20}+C_{21-29})$] in figure 6-9b. Samples containing an unimodal distribution (see Fig. 6-10b) with dominance of short-chain n-alkanes (seam 2-a and 4l-a) give high values above 0.7. Samples with predominantly long-chain n-alkanes (see Fig. 6-10a) yield values below 0.4. Samples containing a bimodal n-alkane distribution such as seam 1/2 (Fig. 6-10c) tend to plot in the grey shaded area between 0.4 and 0.7 (Fig. 6-10b).

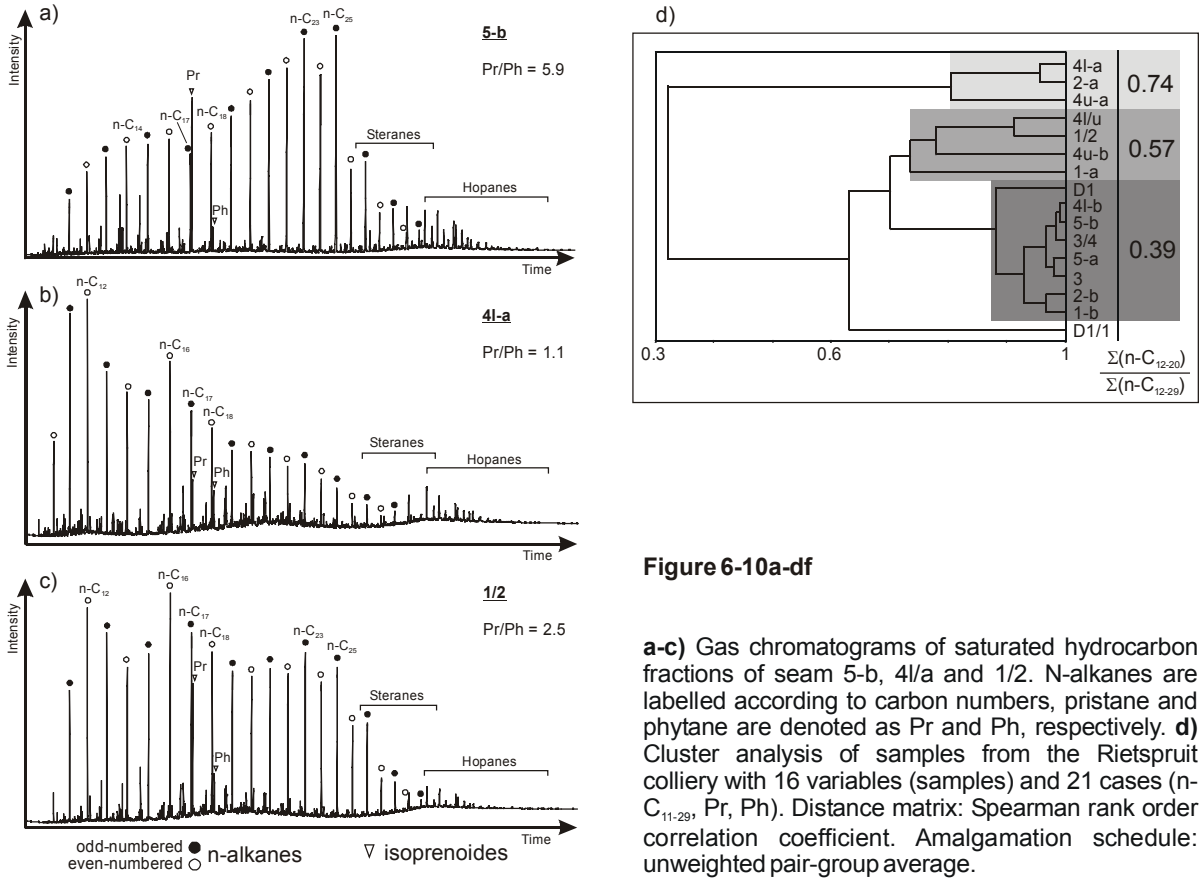


**Figure 6-10a-df**

**a-c)** Gas chromatograms of saturated hydrocarbon fractions of seam 5-b, 4l/a and 1/2. N-alkanes are labelled according to carbon numbers, pristane and phytane are denoted as Pr and Ph, respectively. **d)** Cluster analysis of samples from the Rietspruit colliery with 16 variables (samples) and 21 cases (n-$C_{11-29}$, Pr, Ph). Distance matrix: Spearman rank order correlation coefficient. Amalgamation schedule: unweighted pair-group average.

Short-chain n-alkanes (<n-$C_{20}$) are associated with organic matter derived from algae (Meyers, 1997). Especially the occurrence of n-$C_{15}$, n-$C_{17}$ and n-$C_{19}$ provide evidence for algal biomass (Peters and Moldowan, 1993). However, $C_{15}$-$C_{20}$ n-alkanes with no carbon-number preference may be generated by all types of kerogen during catagenesis (Tissot and Welte, 1984). The n-$C_{15}$ alkane is ubiquitous in the biosphere; it can be found in land plants, in algae, in bacteria and other microbes (Meyers and Ishiwatari, 1993). The major source of long-chain n-alkanes with odd-carbon number preference is associated with organic matter from vascular plants (Eglinton and Hamilton, 1967; Tissot and Welte, 1984). In recent plants long-chain n-alkanes are recorded from leave waxes of terrestrial plants (Eglinton and Hamilton, 1967). The n-alkane distribution of organic matter with high proportion of vascular

| Seam | $(n\text{-}C_{23+25})/(n\text{-}C_{23+25+29+31})$ | $Pr/n\text{-}C_{17}$ | $Ph/n\text{-}C_{18}$ | $(Pr+n\text{-}C_{17})/(Ph+n\text{-}C_{18})$ | $Tm\alpha/(Tm\alpha+Tm\beta)$ | $[C_{32}]22S/(22S+22R)$ | hop./(hop.+ster.) | $2*C_{31}/(C_{30}+C_{32})$ | $C_{29}$-dia/$C_{29}$-reg | $2*C_{29}$-dia/$(C_{28}\text{-dia}+C_{27}\text{-dia})$ | $MA\text{-}C_{27}/MA\text{-}C_{29}$ | 2-MA/2-MP |
|---|---|---|---|---|---|---|---|---|---|---|---|---|
| **5-b** | 0,91 | 1,61 | 0,25 | 1,92 | 0,897 | 0,54 | 0,93 | 1,67 | 0,73 | 1,91 | 3,79 | 0,85 |
| **5-a** | 0,90 | 5,59 | 0,42 | 3,87 | 0,906 | 0,53 | 0,92 | 1,73 | 0,56 | 2,36 | 3,59 | 1,27 |
| **4u-b** | 0,94 | 1,13 | 0,34 | 1,68 | 0,902 | 0,54 | 0,93 | 1,69 | 0,73 | 0,81 | n.d. | 0,95 |
| **4u-a** | 0,86 | 0,71 | 0,34 | 1,39 | 0,915 | 0,58 | 1,00 | 1,52 | n.d | n.d | n.d. | 0,94 |
| **4l/u** | 0,85 | 0,54 | 0,37 | 1,16 | 0,898 | 0,56 | 0,93 | 1,58 | 1,22 | 0,60 | n.d. | 0,15 |
| **4l-b** | 0,93 | 1,19 | 0,17 | 1,62 | 0,934 | 0,57 | 0,95 | 1,82 | 0,88 | 1,94 | 4,26 | 0,56 |
| **4l-a** | 0,84 | 0,49 | 0,53 | 1,19 | 0,912 | 0,57 | 0,96 | 1,28 | 0,94 | 0,94 | n.d. | 1,11 |
| **3/4** | 0,91 | 1,42 | 0,19 | 1,81 | 0,938 | 0,58 | 0,98 | 1,88 | 0,90 | 1,49 | 3,59 | 0,31 |
| **3** | 0,86 | 1,93 | 0,24 | 2,24 | 0,917 | 0,56 | 0,93 | 1,65 | 1,03 | 2,18 | 3,75 | 0,39 |
| **2-b** | 0,82 | 5,79 | 0,56 | 3,62 | 0,931 | 0,57 | 0,94 | 1,53 | 1,05 | 3,09 | 3,11 | 1,07 |
| **2-a** | 0,81 | 0,27 | 0,66 | 1,11 | 0,851 | 0,50 | 0,89 | 1,35 | 1,23 | 0,32 | n.d. | 0,96 |
| **1/2** | 0,90 | 0,75 | 0,37 | 1,56 | 0,927 | 0,60 | 0,93 | 1,67 | 1,40 | 0,95 | n.d. | 0,13 |
| **1-b** | 0,79 | 3,85 | 0,33 | 3,04 | 0,935 | 0,59 | 0,90 | 1,46 | 1,04 | 3,34 | 3,20 | 1,14 |
| **1-a** | 0,84 | 2,17 | 0,22 | 2,59 | 0,924 | 0,58 | 0,92 | 1,72 | 1,12 | 3,28 | 3,38 | 0,93 |
| **D1/1** | 0,68 | 0,85 | 0,92 | 1,00 | 0,922 | 0,60 | 0,88 | 1,41 | 1,18 | 0,47 | n.d. | 0,16 |
| **D1** | 0,82 | 3,54 | 0,32 | 3,09 | 0,930 | 0,57 | 0,92 | 1,72 | 1,07 | 3,32 | 3,42 | 1,00 |

**Table 6-3**

Mid-chain odd n-alkane ratio $(n\text{-}C_{23+25})/(n\text{-}C_{23+25+29+31})$; $Pr/n\text{-}C_{17}$= pristane/heptadecane; $Ph/n\text{-}C_{18}$=phytane/octadecane; $(Pr+n\text{-}C_{17})/(Ph+n\text{-}C_{18})$; $Tm\alpha$=17α(H)-22,29,30-trisnorhopane, $Tm\beta$=17β(H)-22,29,30-trisnorhopane: $Tm\alpha/(Tm\alpha+Tm\beta)$; 17α(H),21β(H)-bishomohopane isomerization at C22: $C_{32}$-22S/(22S+22R); αβ+βα-hopanes ($C_{29}$-$C_{34}$) versus regular αββ+ααα-steranes ($C_{27}$-$C_{29}$): hop./(hop.+ster.); 17α(H),21β(H)-homohopane ratio: $2*C_{31}/(C_{30}+C_{32})$; βα–$C_{29}$-diasteranes vs. αα-$C_{29}$ regular steranes: $C_{29}$-dia/$C_{29}$-reg; $C_{29}$βα(S+R)-diasteranes versus sum of $C_{28}$βα(S+R)- and $C_{27}$βα(S+R)-diasteranes: $2*C_{29}$-dia/($C_{28}$-dia+$C_{27}$-dia); $C_{27}$-monoaromatic steroids versus $C_{29}$-monoaromatic steroids: $MA\text{-}C_{27}/MA\text{-}C_{29}$; 2-methylanthracene versus 2-methylphenanthrene: 2-MA/2-MP.

plants maximise around n-$C_{27}$, n-$C_{29}$, n-$C_{31}$ or n-$C_{33}$ (de Leeuw et al., 1995; Schwark et al., 2002). From peats with high proportions of *Sphagnum* mosses Corrigan et al. (1973); Lehtonen and Ketola (1993) and Nott et al. (2000) recorded an elevated relative abundance of the $C_{23}$ and $C_{25}$ homologue (Tab. 6-3). Especially *Sphagnum recurvum* maximises around n-$C_{23}$ and n-$C_{25}$ where as other *Sphagnum* species contain a second maximum at n-$C_{31}$. With increasing humification, the major homologue changed through n-$C_{25}$ and n-$C_{27}$ to n-$C_{31}$ (Lehtonen and Ketola, 1993).

Another source of preferential enrichment of $C_{23}$ and $C_{25}$ n-alkanes was reported to be aquatic macrophytes (Cranwell et al., 1987; Ficken et al., 2000). Especially reed grasses in temperate environments seem to produce high amounts of n-$C_{23}$ and n-$C_{25}$. In the marine realm more frequently elevated abundances of the n-$C_{21}$ and n-$C_{23}$ have been found and related to a specific algal input (van Kaam-Peters et al., 1997).

The dendrogram shown in figure 6-10d using n-alkanes, pristane and phytane allows to discern the different sample cluster. The branch containing samples 2a, 4l-a & 4u-a represents samples with predominantly short-chain n-alkanes [$C_{12\text{-}20}/(C_{12\text{-}20}+C_{21\text{-}29})$ = 0.74]. Samples containing higher contents of vascular plants (D1, 1-b, 2-b, 3, 3/4, 4l-b, 5-a & 5-b) are combined in the cluster with a lower SLR [$C_{12\text{-}20}/(C_{12\text{-}20}+C_{21\text{-}29})$ = 0.39]. Samples with a bimodal n-alkane distribution (1-a, 1/2, 4l/u & 4u-b) are grouped in a separate cluster indicating mixed sources of the organic matter. The corresponding sedimentary conditions can be associated with an intermediate stage between terrigenous aquatic environments.

Since these samples are linked to the cluster with predominantly long-chain n-alkanes the sedimentary supply was more influenced by the input of terrigenous organic matter than by algal derived biomass.

Postsedimentary processes can alter the primary n-alkane distribution. Especially, bacterial degradation can cause changes in the distribution of odd and even numbered n-alkanes. The carbon preference index (CPI) was originally used by Bray and Evans (1961) as a maturity parameter based on the progressive degradation of odd numbered n-alkanes during coalification. In recent sediments a predominance of odd numbered long-chain n-alkanes reflects the contribution of higher plants. Thermal degradation of kerogen during catagenesis subsequently generates new alkanes without odd/even predominance. Thus the preference for odd numbered molecules progressively disappears (Tissot and Welte, 1984).

In figure 6-9c the modified CPI of the $C_{11}$-$C_{29}$ n-alkane interval labelled as CPI (t) is shown. Furthermore, the CPI (l) of long-chain n-alkanes ($C_{21}$-$C_{29}$) is calculated to detect differences in the odd over even predominance of both intervals. The CPI (t) varies between 0.85 and 1.4. The most significant predominance in even-chain n-alkanes can be recognised in samples of seam 2-a and 4l-a by CPI (t) values below 1. The CPI (l) of long-chain n-alkanes records values above 1 (1.17-1.86), i.e. a significant predominance of odd numbered

n-alkanes. In this interval the CPI (l) of seam 3/4, 4l-b and 4u-b reach the highest values of approximately 1.8 indicating a pronounced input of terrigenous organic matter.

Changing environmental conditions caused the predominant supply of terrigenous organic matter seems to be temporary interrupted by marine/lacustrine conditions. The changes occurred during deposition of individual coal seam as indicated by table 6-4. The ratios of short to long-chain n-alkanes of samples from basal positions within seams (samples 1-a, 2-a, 4l-a and 4u-a) show distinctively higher values than samples from the top of the same seam. An exception in this intra-seam variability is observed in seam 5, in which both samples contain predominantly long-chain n-alkanes as indicated by ratios of 0.34 and 0.36, respectively.

| **Seam** | **1** | | **2** | | **4l** | | **4u** | | **5** | |
|---|---|---|---|---|---|---|---|---|---|---|
| **sample position** | **base** | **top** | **base** | **top** | **base** | **top** | **base** | **top** | **base** | **top** |
| **sample** | **1-a** | **1-b** | **2-a** | **2-b** | **4u-a** | **4u-b** | **4l-a** | **4l-b** | **5-a** | **5-b** |
| **SLR** | 0,6 | 0,35 | 0,87 | 0,33 | 0,61 | 0,58 | 0,74 | 0,38 | 0,34 | 0,36 |
| **Pr/Ph** | 10 | 9,8 | 0,6 | 8,6 | 2,3 | 3,5 | 1,1 | 6 | 11,2 | 5,9 |
| **Pr/n-$C_{17}$** | 2,2 | 3,9 | 0,3 | 5,8 | 0,7 | 1,1 | 0,5 | 1,2 | 5,6 | 1,6 |

**Table 6-4**

Comparison of samples from the base versus top of different seams based on aliphatic biomarker ratios. SLR: relative proportion of short ($C_{12-20}$) versus long chain ($C_{21-29}$) n-alkanes; Pr/Ph and Pr/n-$C_{17}$ see Table 6-3.

### 6.7.3.2 Isoprenoids

The isoprenoids i-$C_{19}$ (pristane) and i-$C_{20}$ (phytane) (in Fig. 6-10a-c labelled Pr and Ph) are assumed to be diagenetic products of the phytylic side chain of chlorophyll (Dydik et al., 1978). Alternative sources of precursors are known to occur (ten Haven et al., 1987). These include bisphytane lipids from methanogens or halophilic bacteria as sources for phytane and zooplankton or tocopherol (vitamin E) as sources for pristane (Goossens et al., 1984; Frimmel et al., 2004). The ratio is usually used to distinguish between oxic (>1) or anoxic (<1) conditions in fossil depositional environments. Ten Haven et al. (1987) pointed out that the ratio also serves as palaeosalinity indicator in hypersaline depositional environments. Hughes et al. (1995) showed that Pr/Ph-ratios <1 indicate marine conditions whereas ratios >3 characterise terrestrial input. Ratios between 1-3 represent lacustrine/marine environments.

The pristane/phytane ratios in the coals from the Rietspruit colliery vary between 0.59 and 11.19 (Fig. 6-9e). Samples from the base of seam 2, 4l and 4u reveal significantly lower

Pr/Ph ratios than corresponding samples from the top of those seams (Tab. 6-3). Similar changes are detected by the ratio of short- versus long-chain n-alkanes. Compared with n-alkane distributions, Pr/Ph ratios in seam 1 indicate no difference between basal and top position whereas in seam 5 significant higher Ph/Ph can be detected in the lower part of the seam.

Increasing Pr/Ph ratios correlate with lower SLR indicating an elevated input of terrigenous organic matter (Fig. 6-11a). The high variability of these two parameters throughout the section implies that the seams were formed in a dynamic environment, which underwent frequent changes between terrestrial and lacustrine/marine conditions. The isoprenoid distribution is also influenced by maturity and biodegradation as indicated by the preservation of pristane over phytane during thermal diagenesis (Tissot and Welte, 1984; Peters and Moldowan, 1993). Elevated Pr/Ph ratios correlate with lower $T_{max}$ values (Fig. 6-11b), which given the lack in thermal maturity differences indicates changes in kerogen type. Thereby, lower $T_{max}$ values correspond to terrigenous and higher to limnic kerogens due to differences in their respective activation energies.

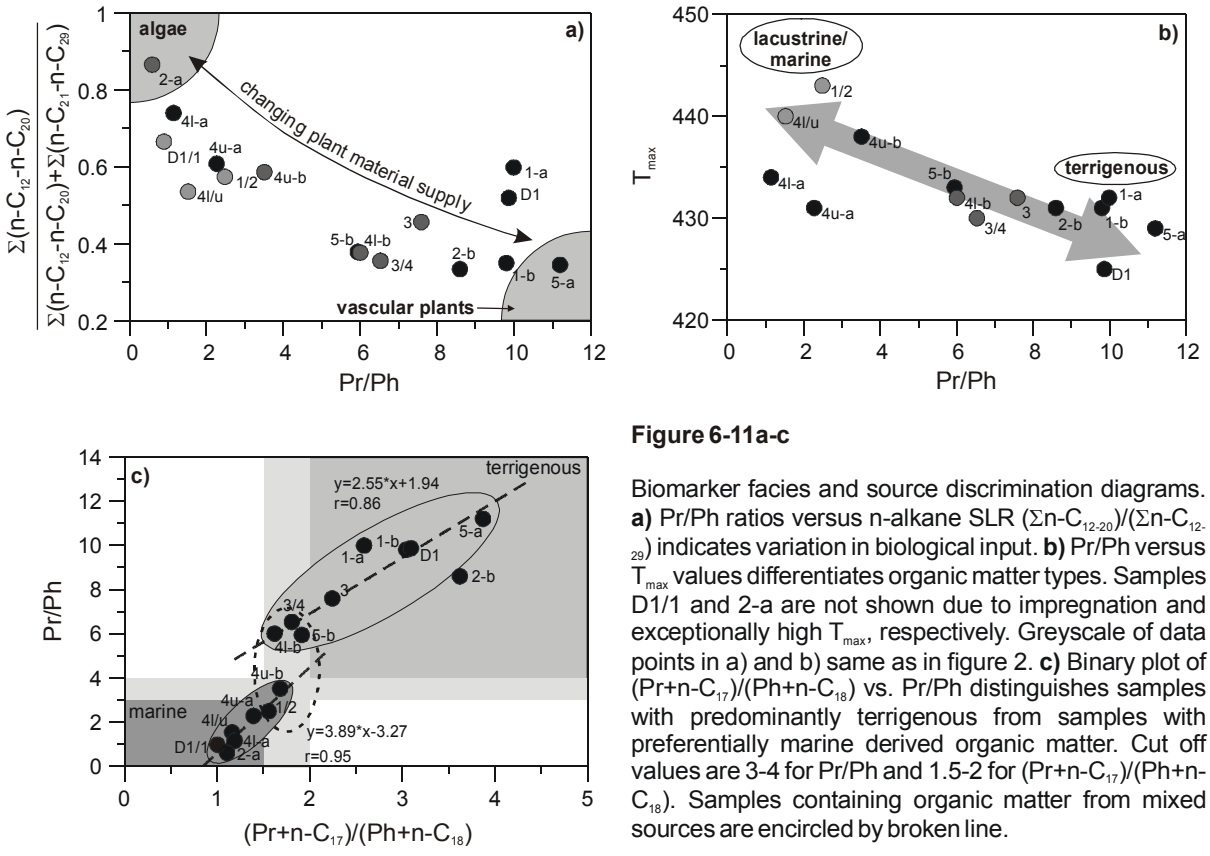


**Figure 6-11a-c**

Biomarker facies and source discrimination diagrams. **a)** Pr/Ph ratios versus n-alkane SLR ($\Sigma$n-$C_{12\text{-}20}$)/($\Sigma$n-$C_{12\text{-}29}$) indicates variation in biological input. **b)** Pr/Ph versus $T_{max}$ values differentiates organic matter types. Samples D1/1 and 2-a are not shown due to impregnation and exceptionally high $T_{max}$, respectively. Greyscale of data points in a) and b) same as in figure 2. **c)** Binary plot of (Pr+n-$C_{17}$)/(Ph+n-$C_{18}$) vs. Pr/Ph distinguishes samples with predominantly terrigenous from samples with preferentially marine derived organic matter. Cut off values are 3-4 for Pr/Ph and 1.5-2 for (Pr+n-$C_{17}$)/(Ph+n-$C_{18}$). Samples containing organic matter from mixed sources are encircled by broken line.

Pr/n-$C_{17}$ ratios vary between 0.27 and 5.79 with a median of 1.3. Ph/n-$C_{18}$ ratios vary between 0.17 and 0.92 with a median of 0.34 (Tab. 6-3). These ratios have been used as maturity and facies indicators (Bailey et al., 1973; Lijimbach, 1975; Volkman et al., 1983; Alexander et al., 1981). For samples of similar maturity, as assumed here, the Pr/n-$C_{17}$ ratio is primarily a facies indicator. As the easily degradable straight chain n-alkanes $C_{17}$ and $C_{18}$ are lost, the more resistant isoprenoids pristane and phytane are conserved (Peters and Moldowan, 1993; Ten Haven et al., 1987). Organic matter in sediments deposited under open water conditions yield ratios less than 0.5 whereas those from inland peat-swamp environments give ratios above 1. Intermediate ratios of 0.5-1 were suggested to indicate deposition in environments with alternating swamp and open-water conditions (Volkman and Maxwell, 1986). In table 6-4 the Pr/n-$C_{17}$ ratios from basal and top positions of the individual seams are compared. Lower Pr/n-$C_{17}$ ratios at the base of seam 1, 2, 4l and 4u are in agreement with lower SLR and result from higher proportions of algal derived organic matter in these seam positions. In seam 5 the trend changes to higher Pr/n-$C_{17}$ ratios at the basis and lower Pr/n-$C_{17}$ ratios at the top of the seam.

To minimize the maturity influence on this parameter Alexander et al. (1981) used the (pristane+n-$C_{17}$)/(phytane+n-$C_{18}$) ratio to characterise the organic facies. In the humic coals studied here the (pristane+n-$C_{17}$)/(phytane+n-$C_{18}$) ratios vary between 1 and 3.87 with a median of 1.74 (Tab. 6-3). The linear relation in figure 6-11c between (pristane+n-$C_{17}$)/(phytane+n-$C_{18}$) and Pr/Ph corroborates the supposed changes between lacustrine/marine and terrestrial depositional phases. Two sample groups can be discriminated in Figure 6-11c. Samples plotting in the field shaded light grey are assumed to be transitional between marine and terrigenous conditions.

## 6.7.4 Cyclic alkanes

### 6.7.4.1 Hopanes

17$\alpha$(H), 21$\beta$(H)-type hopanes from $C_{27}$ to $C_{34}$ excluding $C_{28}$-hopanoids, can be identified in all samples. $C_{35}$ hopanes can be found in most of the samples but concentrations are close to detection limit. 17$\beta$(H),21$\alpha$(H)-hopanes (moretanes) in the $C_{29}$ to $C_{34}$ range are present in lower abundance (Fig. 6-12a). Potential hopane precursors with less than 31 carbon atoms have been identified in ferns and lichens (Chaffee et al., 1986). Extended hopanes (>30 carbon atoms) derive from hopanepolyol precursors, which occur as membrane constituents of prokaryotes (Ourisson et al., 1979). Diagenetic alteration of long chain hopanoids yields hopanes with less than 30 C atoms (Peters and Moldowan, 1993).

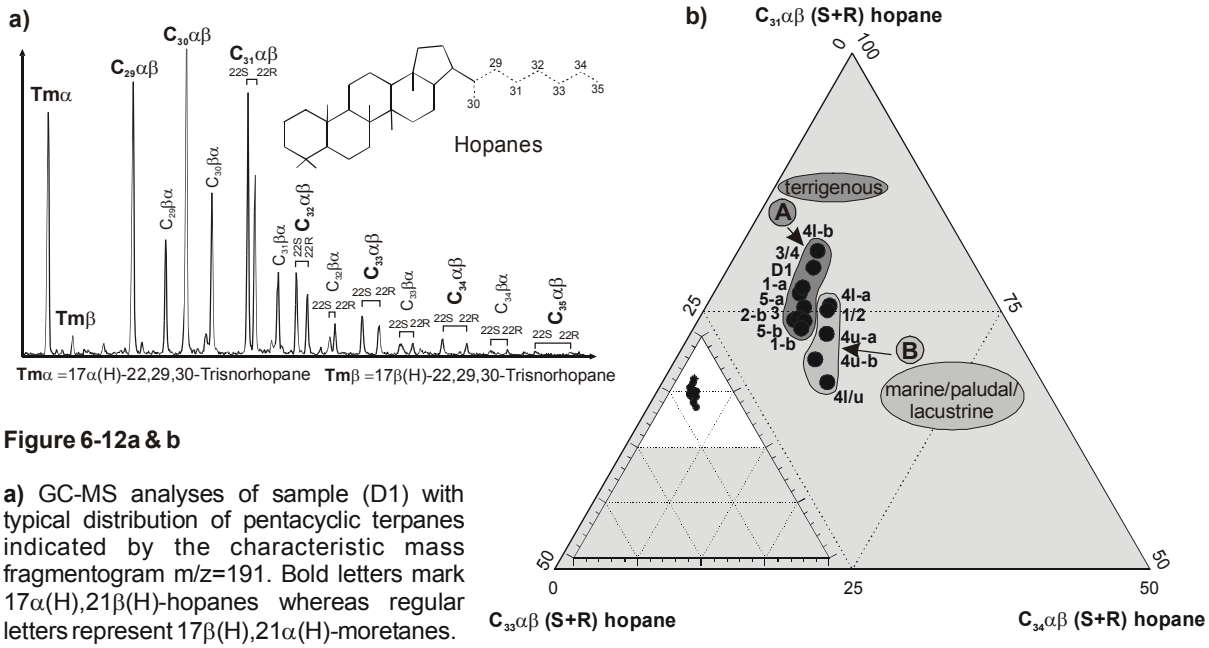


**Figure 6-12a & b**

**a)** GC-MS analyses of sample (D1) with typical distribution of pentacyclic terpanes indicated by the characteristic mass fragmentogram m/z=191. Bold letters mark 17α(H),21β(H)-hopanes whereas regular letters represent 17β(H),21α(H)-moretanes.

**b)** Ternary diagram of $C_{31}$-, $C_{33}$ - and $C_{34}$-hopanes differentiates samples by extended hopane distribution. Elevated $C_{31}$- plus $C_{33}$- vs. $C_{34}$-hopane contents indicate terrigenous and oxic sedimentary environments.

The relative distributions of $C_{31}$ to $C_{35}$ 17α(H),21β(H), 22S and 22R homohopanes have been used as proxy for the redox potential prevailing in the depositional environment (Peters and Moldowan, 1993). In a ternary diagram two sample groups can be discerned mainly by differences in the relative $C_{33}$ and $C_{34}$ hopane contents (Fig. 6-12b). These differences can be associated with changing Eh conditions during deposition of the organic matter in consequence of variable sedimentary environments. Samples of group **A** yield higher Pr/Ph ratios and contain predominantly long-chain n-alkanes thus being of preferential terrigenous origin. Group **B** combines samples with lower Pr/Ph and (Pr+n-$C_{17}$)/(Ph+n-$C_{18}$) ratios related to a higher supply of algal derived organic matter upon deposition.

Trisnorhopanes occurred as Tmα (17α(H)-22,29,30-trisnorhopane) and Tmβ (17β(H)-22,29,30-trisnorhopane) with Tmα dominating in all samples. The presence of Tmβ gives evidence to a generally low thermal maturity of the organic matter since the concentration of 17β(H)-trisnorhopane approaches zero at the beginning of the oil window (Seifert and Moldowan, 1986). Comparable with the Ts/(Ts+Tm) ratio used by Seifert and Moldowan (1978) the Tmα/(Tmα+Tmβ) ratio increases with advanced maturity. The ratio may vary with organic facies depending on lithology (Rullkötter et al., 1985), salinity (Rullkötter and Marzi, 1988), and Eh/pH conditions (Moldowan el al., 1986). Therefore, the Tmα/(Tmα+Tmβ) ratio, if applied as maturity parameter should be used with caution. In samples from the Rietspruit colliery the Tmα/(Tmα+Tmβ) ratios vary from 0.85 to 0.94 with a median of 0.92 corresponding to the beginning of the oil window (Tab. 6-3). The low correlation coefficient between Tmα/(Tmα+Tmβ) and MPI-1 (***r*** = -0,31) implies that both parameters are influenced

by facies changes. However, both parameters indicate a thermal maturity of the coals from the Witbank Basin corresponding to the beginning of the oil window.

Upon maturation biohopanoids bearing the 17β(H),21β(H) configuration are isomerised to the thermodynamically more stable 17α(H),21β(H) and to a lesser extent, 17β(H),21α(H) configurations. A comparable isomerisation process affects the chiral carbon at C-22, leading to a mixture of 22S and 22R epimers in homologues with more than 30 carbon atoms (Ensminger et al., 1977; Ries-Kautt and Albrecht, 1989). Seifert and Moldowan (1986) point out that the 22R epimers of extended 17α(H),21β(H)-homohopanes are more susceptible to biodegradation than their 22S counterparts. The 22S/(22S+22R) ratios of extended hopanes are frequently used as maturity parameters in the low maturity regime. From immature to low mature the 22S/(22S+22R) ratios increase from 0 to an equilibrium value of 0.6, which corresponds to a vitrinite reflectivity of $R_0$% < 0.6 (Seifert and Moldowan, 1986). In the samples from the Witbank Basin the ratios of the (22S/22S+22R)-isomers of the $C_{32}$ hopane vary from 0.50 to 0.6 with a median of 0.57 indicating near equilibrium conditions (Tab. 6-3) Both hopane based maturity parameters show a good linear relation (***r*** = 0.84) as displayed in figure 6-9a. As mentioned above varying activation energies for different types of organic matter may also influence these ratios. Low pH-conditions may lead to elevated contents of 17α(H),21β(H) $C_{31}$ hopanes in immature samples as detected Ries-Kautt and Albrecht (1989) in *Sphagnum* peats. In figure 6-13b the positive correlation (***r*** = 0.68) between the relative abundance of the 17α(H),21β(H)-$C_{31}$ hopane calculated as $2*C_{31}/(C_{30}+C_{32})$) and the predominance of n-$C_{23}$ and n-$C_{25}$ (calculated as $(C_{23}+C_{25}/(C_{23}+C_{25}+C_{29}+C_{31})$, Tab. 6-3) is shown. Higher values of both parameters would be in agreement with an increased supply of *Sphagnum* mosses (Ries-Kautt and Albrecht, 1989; Lehtonen and Ketola, 1993). However, an origin of n-$C_{23}$ and n-$C_{25}$ from aquatic macrophytes cannot be fully ruled out.

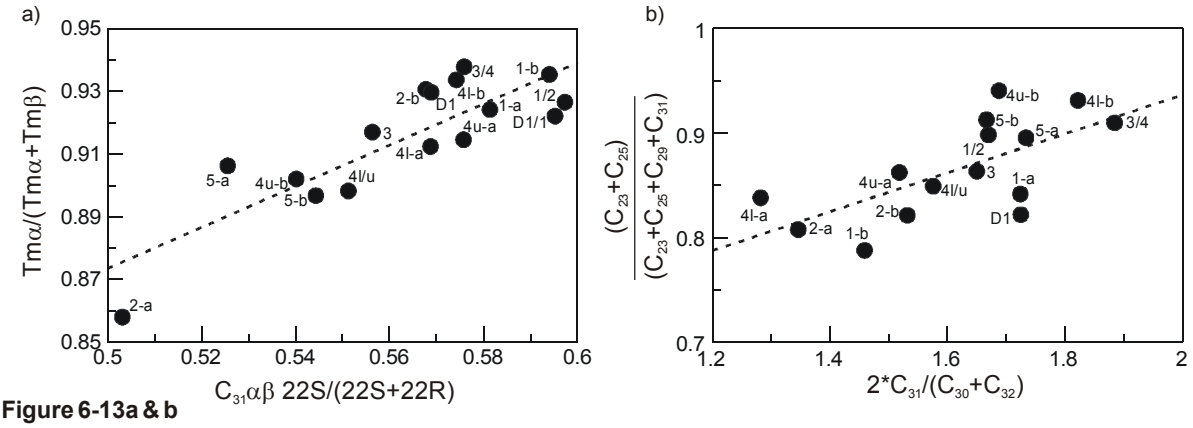


**Figure 6-13a & b**

**a)** Positive linear correlation of $C_{31}$-22S/(22S+22R) ratio versus Tmα/(Tmα+Tmβ); **b)** Elevated contents of $C_{31}$- vs. $C_{30}$- plus $C_{32}$- hopanes ($2*C_{31}/(C_{30}+C_{32})$ correlate with n-alkane distribution maxima at n-$C_{23}$ and n-$C_{25}$. This may be related to specific plant input of *Sphagnum* mosses or aquatic macrophytes.

### 6.7.4.2 Steranes

In the samples from the Witbank Basin the distribution of triterpanes is dominated by hopanes as indicated by hopane/sterane ratios from 0.88 to 1 with a median of 0.93 (Tab. 6-3). This agrees with preferentially terrigenous derived and/or microbially reworked organic matter (Tissot and Welte, 1984; Peters and Moldowan, 1993).

The regular steranes present consist of $C_{27}$ (cholestane), $C_{28}$ (ergostane) and $C_{29}$ (stigmastane) components in ααα (20S+20R) and αββ (20S+20R) configurations. Steranes found in the geosphere are derived from sterols produced in the biosphere (Mackenzie et al., 1982). It is generally assumed that steroids derive from algae, plankton, zooplankton and higher plants (Seifert and Moldowan, 1986). The conversions from sterols to steranes proceed without loss of a carbon atom. Thus, the distribution of $C_{27}$, $C_{28}$ and $C_{29}$ steranes can be used to distinguish different sources of the organic matter since sedimentary biomarker and biological precursor have identical carbon numbers (Mackenzie et al., 1982). High proportions of $C_{29}$ steranes compared to $C_{27}$ and $C_{28}$ steranes indicate a predominant vascular plant input (Huang and Meinschein, 1979; Czochanska et al., 1988; Peters and Moldowan, 1993).

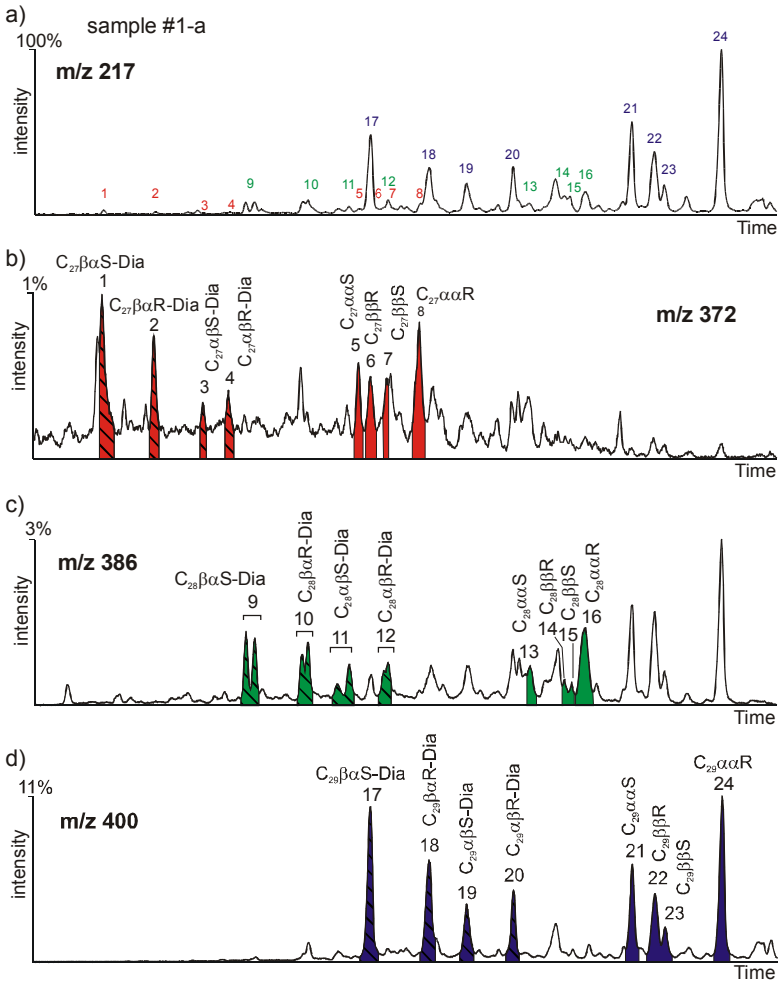


**Figure 6-14a-d**

$C_{27}$, $C_{28}$ and $C_{29}$ regular and diasteranes analyses by SIM-GC/MS showing characteristic mass fragmentograms of m/z 217, 372, 386 and 400 using for compound identification. With exception of sample 4u-a, in all samples sufficient contents of steranes and diasteranes for peak integration could be detected. Predominance of $C_{29}$ steranes and diasteranes versus $C_{28}$ and $C_{27}$ compounds in the saturated fraction of sample 1-a indicates predominantly supply of vascular plants. **a)** m/z 217 total steranes and diasteranes **b)** m/z 372 $C_{27}$ steranes and diasteranes **c)** m/z 386 $C_{28}$ steranes and diasteranes **d)** m/z 400 $C_{29}$ steranes and diasteranes. Note increasing intensity from **b)** to **d)**.

Beside the regular steranes, rearranged steranes also called diasteranes may occur. These differ from the regular steranes by rearrangement of methyl groups from C-10 and C-18 to positions C-5 and C-14 in diasteranes. The conversion of sterols to diasteranes during diagenesis may be catalysed by clay minerals (Sieskind et al., 1979). High diasterane/sterane ratios have been reported from sediments deposited in acidic and oxic environments (Moldowan et al., 1992). Furthermore the diasterane/sterane ratio is influenced by thermal maturity since diasteranes are more stable during diagenesis than steranes. For samples of similar thermal maturity the specificity of $C_{27}$, $C_{28}$ and $C_{29}$-diasterane distribution is comparable to that of the steranes (Peters and Moldowan, 1993).

In the samples from the Witbank Basin $C_{29}$ steranes and diasteranes are by far the most abundant steroidal biomarkers (Fig. 6-14). Two sample groups can be distinguished based on sterane compositions, e.g. when plotting Pr/Ph versus $C_{29}$ diasterane/sterane ratios (Fig. 6-15a). The first group comprising the non-coaly samples D1/1, 1/2 and 4l/u is characterized by high diasterane/sterane and low Pr/Ph ratios caused by specific clay mineral diagenesis. The second group of samples deposited as humic coals and coaly mudstones in a terrigenous environment reveals a positive correlation of Pr/Ph and $C_{29}$ diasterane/sterane ratios. The higher diasterane/sterane ratios are thought to be controlled by more acidic and oxidic conditions (Fig. 6-15a). The sedimentary environment of samples 2-a and 4l-a is characterized by low Pr/Ph ratios and a predominance of short-chain n-alkanes combined with moderate diasterane/sterane ratios. These samples have been influenced by secondary alteration as recognized by aromatic hydrocarbon composition (see below). Sample 5-a deviates from both sample groups due to high pristane and high $C_{29}\alpha\alpha R$ contents.

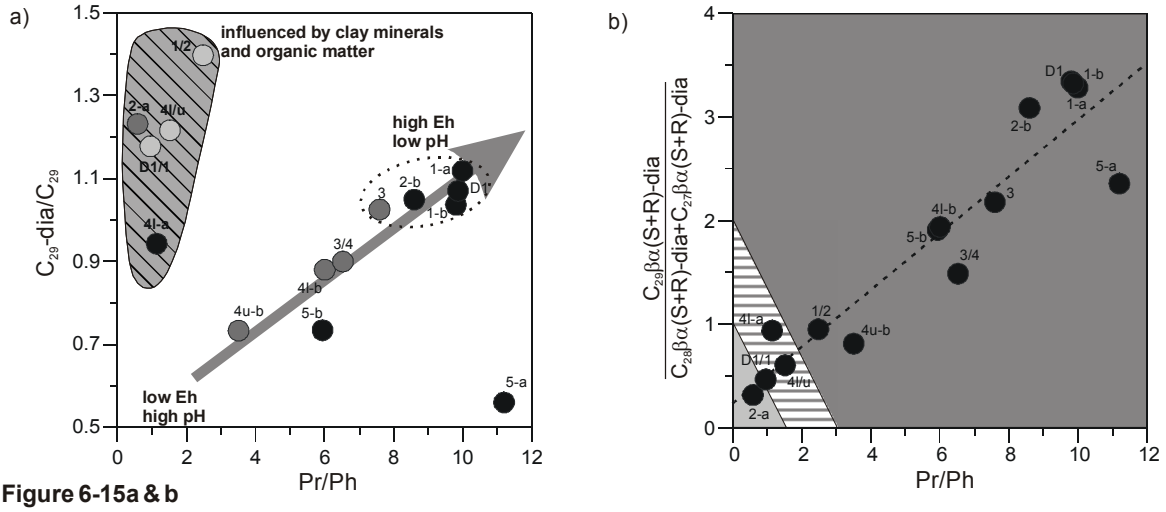


**Figure 6-15a & b**

**a)** The Pr/Ph vs. $C_{29}$-dia/$C_{29}$reg. sterane diagram groups samples according to organic facies. One group shows marine signatures (2-a & 4l-a), low $C_{org}$ and elevated clay mineral contents (D1/1, 1/2 and 4l/u). The remaining samples reveal high $C_{org}$ contents combined with high proportions of terrigenous plant material (D1, 1-a & b, 3/4, 4l-b, 4u-b and 5-b). High Pr/Ph and $C_{29}$-dia/$C_{29}$reg. sterane ratios in the latter group point to high Eh and low pH conditions. **b)** Increasing Pr/Ph vs. predominance of $C_{29}$-components amongst diasteranes point to continuous shift from marine (light grey area in the lower left corner) to transitional environments with estuarine/paludal conditions (hatched area) to terrestrially dominated sedimentary conditions.

A positive correlation (***r*** = 0.93) of Pr/Ph ratios with the relative abundance of $C_{29}$ versus $C_{27}$ and $C_{28}$ diasteranes [2*$C_{29}\beta\alpha$(S+R)-diasterane/($C_{28}\beta\alpha$(S+R)-dia+$C_{27}\beta\alpha$(S+R)-dia)] was observed (Fig. 6-15b). In concert with the high hopane/sterane and diasterane/regular sterane ratios this confirms the significant input of vascular plant material. Samples yielding Pr/Ph ratios <1.5 and diasterane compositions with $C_{29}$<($C_{28}$+$C_{27}$) contain elevated proportions of algal derived organic matter. Transitional conditions between aquatic and terrestrial environments are associated with Pr/Ph ratios varying between 1.5 to 3.0 and diasterane distributions with $C_{29}$ ≤($C_{28}$+$C_{27}$). Most of the samples contain high pristane/phytane ratios (Pr/Ph>3) and $C_{29}$>($C_{28}$+$C_{27}$) diasteranes, resulting from a predominant supply of vascular plant debris.

The relative proportions of $C_{27}$ $C_{28}$ and $C_{29}\beta\alpha$(S+R) diasteranes are displayed in a ternary diagram after Huang and Meinschein (1979) to discern organic matter from marine, lacustrine and terrestrial dominated environments (Fig. 6-15c). A mixing trend between an algal and a terrigenous plant end-member is observed. Terrestrially dominated environments prevailed during deposition of seam D1, 1a & b, 2-b, 3, 4l-b and 5a & b as indicated by the predominance of $C_{29}\beta\alpha$(S+R)-diasteranes. Increasing $C_{28}\beta\alpha$(S+R) and $C_{27}\beta\alpha$(S+R)-diasteranes contents in samples from seam 3/4, 4la, 4u-b and from $C_{org}$ lean interlayers 1/2 and 4l/u point to highly variable conditions in lacustrine/estuarine/paludal sedimentary environments. The predominantly algal origin of sample 2-a based on sterane composition and Pr/Ph ratios is not fully supported by bulk organic matter properties (see above). Secondary alteration processes have to be invoked for this samples as discussed below.

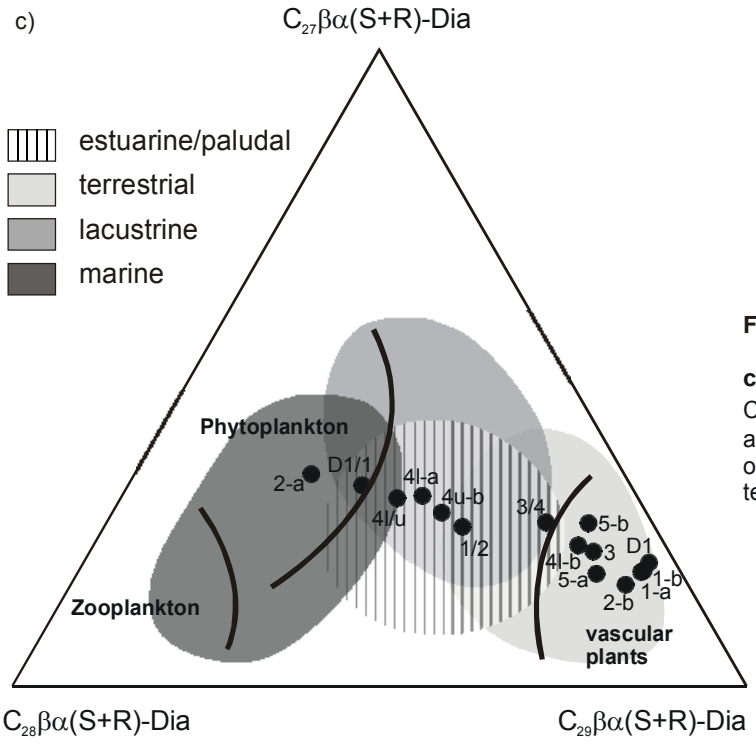


**Figure 6-15c**

**c)** Ternary diagram of $C_{27}$, $C_{28}$ and $C_{29}\beta\alpha$(S+R)-diasteranes modified Huang and Meinschein (1979) distinguishes organic matter of marine, lacustrine and terrestrial sedimentary environments.

During early diagenesis steranes can be aromatised to monoaromatic steroid hydrocarbons (MA), which in an advanced stage of diagenesis can be transferred to triaromatic steroids (TA) by aromatisation and loss of a methyl group (Mackenzie et al., 1982). The formation of MA-steroids has been a subject of controversial discussions (Mackenzie et al., 1982; de Leuw and Baas, 1986; Brassell et al., 1984). From $\Delta^5$-stenol as precursor of all other steroids Mackenzie et al. (1982) described the diagenetic pathway of steroidal hydrocarbons leading to the formation of polyaromatic hydrocarbons during late stage of diagenesis. The formation of monoaromatic steroids commences during early diagenesis with the reduction of $\Delta^5$-stenols to diunsaturated hydrocarbons, the steradienes (Mackenzie et al., 1982). In a further step steradienes can convert to monoaromatic steroids mediated by microbial hydroxylation and subsequent dehydration processes. Finally the formation of A-, B- or C-ring monoaromatic steroids largely depends on the position of the unsaturation in the stenols. The major monoaromatic steroids are C-ring MA-steroids, which are assumed to derive from precursor stenols with a double bound in the side chain on the D-ring. However the precise precursors of A-,B or C-ring MA-steroids and the mechanism of their formation are still under discussion (Carlson et al., 1992). As reported by Seifert and Moldowan (1986) the sterane carbon number distribution do not match necessarily with the MA-steroid carbon number distribution, which in turn do not match TA-steroid carbon number distributions due to preferential aromatisation of functionalised sterenes and steradienes.

Monoaromatic steroid hydrocarbons in the range from $C_{27}$ to $C_{29}$ were identified by their mass fragmentogram m/z = 253 (Fig. 6-16a). Triaromatic steroids from carbon number $C_{26}$ to $C_{28}$ were detected by m/z = 231 fragmentograms (Fig. 6-16b). Since the $C_{26}$20R isomer coelutes with the $C_{27}$20S isomer the distribution of TA-steroids is not further discussed. The distribution of steranes versus mono- and tri-aromatic steranes in the coals from the Witbank Basin differs significantly (Fig. 6-14, 6-16a & b). Steranes are dominated by stigmastanes ($C_{29}$) indicative for vascular plants whereas the MA and TA steroid hydrocarbons contain predominantly $C_{27}$ and $C_{26}$ steroids (Fig. 6-16a & b), which are assumed to derive from algal organic matter or zooplankton. Due to specific condition in the sedimentary environment (acidic and oxic) precursors of MA-$C_{27}$ and TA-$C_{26}$ steranes were possibly preferentially aromatised. MA and TA-steroids were only detected in samples with Pr/n-$C_{17}$ > 1 and Pr/Ph > 6 indicating a predominantly supply of the organic matter from terrestrial provenances as well as oxic conditions in the sedimentary environment. In samples D1/1, 1/2, 2-a, 4l-a, 4l/u and 4u-a & b aromatic steroidal hydrocarbons are close to detection limit. Correlation between Pr/n-$C_{17}$ versus MA-$C_{27}$/MA-$C_{29}$ seems to indicate changing proportions of vascular plants versus algae derived organic matter (Fig. 6-16c). Since only samples with high Pr/Ph ratios contain mono- and triaromatic steroids the supply of aquatic plants was probably rather low. N-alkane distribution with significant preference of n-$C_{23}$ and n-$C_{25}$ was associated with the

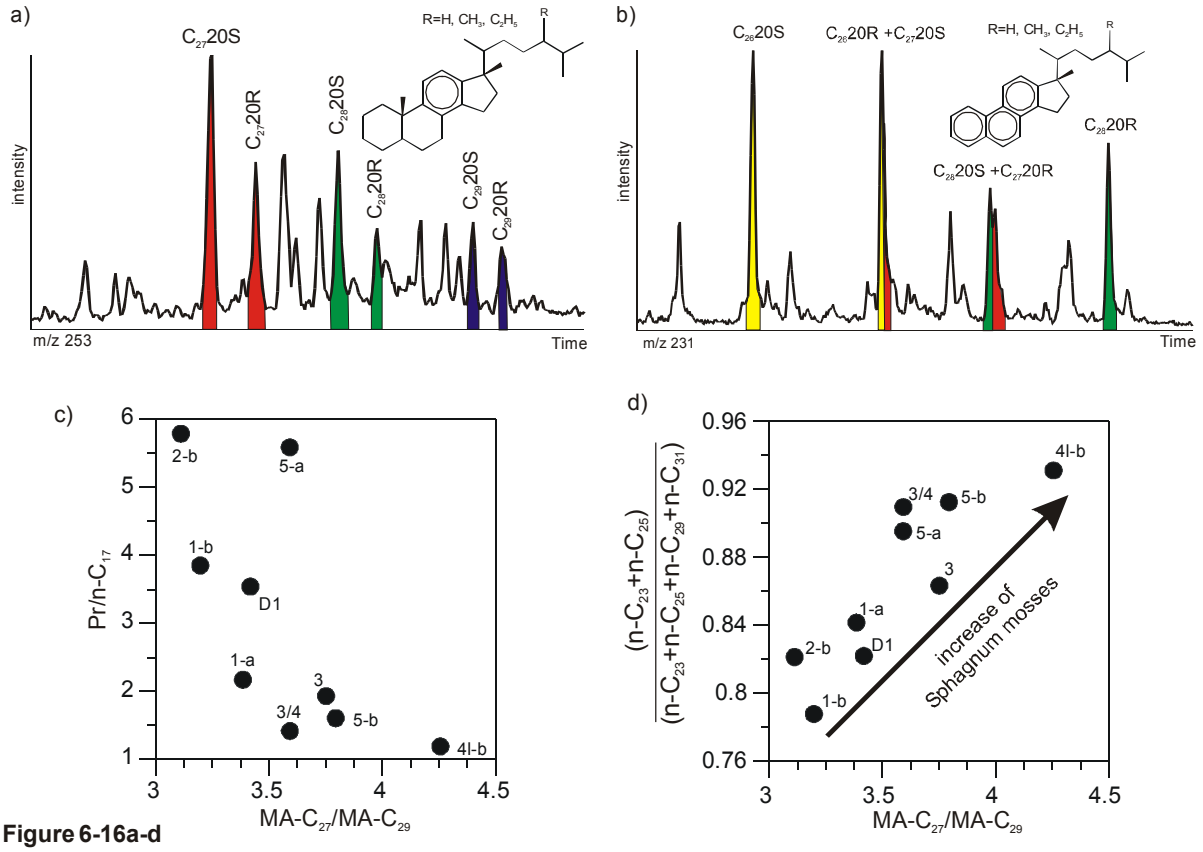


**Figure 6-16a-d**

**a)** Monoaromatic sterane (MA) distribution (m/z 253) shows a predominance of the $C_{27}$-steroids; **b)** Triaromatic steranes (TA) yield predominantly TA-$C_{26}$ (m/z 231); **c)** Correlation of MA-$C_{27}$/MA-$C_{29}$ vs. Pr/n-$C_{17}$ point to changes in plant input; **d)** MA-$C_{27}$/MA-$C_{29}$ vs. predominance of $C_{23}$+$C_{25}$ n-alkanes may indicate input of *Sphagnum* mosses or specific aquatic macrophytes.

input of *Sphagnum* mosses. Beside the positive correlation between (n-$C_{23}$+n-$C_{25}$)/(n-$C_{23}$+n-$C_{25}$+n-$C_{29}$+n-$C_{31}$) versus hopanoid biomarkers in figure 6-12d also a significant correlation of n-alkanes and monoaromatic steroids can be detected. High contents of $C_{28}$-5-en-3β-ol, $C_{29}$-5,22-dien-3β-ol and $C_{29}$-5-en-3β-ol are recorded from recent *Sphagnum* peats by Lethonen and Ketola (1993). Mackenzie et al. (1982) point out that preservation of intact steroid side chains may vary with conditions of sedimentation. Degradation of $C_{28}$ and $C_{29}$ stenols to $C_{27}$ stenols, forming MA-$C_{27}$-steroids upon diagenesis may explain the positive correlation (***r*** = 0.85) between MA-$C_{27}$/MA-$C_{29}$ versus (n-$C_{23}$+n-$C_{25}$)/(n-$C_{23}$+n-$C_{25}$+n-$C_{29}$+n-$C_{31}$) in figure 6-12d and thus indicate the presence of *Sphagnum* related mosses in these samples. Since Lethonen and Ketola (1993) only examined recent *Sphagnum* mosses, it is also possible that the supposed Permian *Sphagnum*–type moss may have synthesised $C_{27}$ sterols, which directly converted to $C_{27}$-MA steroids.

## 6.7.5 Aromatic fraction

With respect to the equal burial depth of the single samples a comparable maturity of the organic matter can be assumed. Vitrinite reflectance values of the coals from the northern Karoo Basin, ranges between 0.63% $R_r$ and 0.78% $R_r$ (Pinheiro et al., 1998; Fabiańska and Kruszewska, 2003). A well-established maturity proxy used for type III kerogen is the methylphenanthrene index (MPI-1 = 1.5*[((2-MP)+(3-MP))/((P)+(1-MP)+(9-MP))]) (Radke et al., 1982). For organic matter of low thermal maturity ($R_0$ < 1.35) the equation $R_c$ = 0.6*MPI-1 + 0.40 allows calculation of equivalent vitrinite reflectance.

In the samples from the Witbank Basin the MPI-1 values range between 0.41 and 0.68 (Fig. 6-9d). The average calculated vitrinite reflectance of $R_c$= 0.70 indicates maximum burial temperatures of 100°C, which corresponds with the beginning of the oil window and is in agreement with the vitrinite reflectivity determined by Pinheiro et al. (1998) and Fabiańska and Kruszewska (2003). Samples from siliciclastic rich layers (1/2, 3/4 and 4l/u) yield low MPI-1 values. Exclusion of these samples raises the MPI-1 from 0.43 in the lower seams (D1 to 1-b) to 0.57, before in seam 4l-a, 4l-b and 4u-a the highest values around 0.67 are reached. In the upper succession the MPI-1 decreases again to an average value of 0.5. As pointed out by Radke et al. (1983) the index is defined for terrigenous organic matter. Since changing sedimentary environments prevailed during deposition of the single seams, the variations in the MPI-1 values rather represent changing plant material input than differences in the burial diagenesis.

Terpenoid and steroidal natural products derived from plants undergo transformations during diagenesis and maturation to produce saturated and aromatic hydrocarbons which are structurally related to their natural product precursors (Alexander et al., 1992). In depositional environments, which favour coal formation, aromatisation of the plant-derived terpenoids is favoured relative to reduction and preservation of saturated biomarkers (Strachan et al., 1988).

Aromatic hydrocarbons of the Rietspruit samples are dominated by naphthalene, phenanthrene, and their alkylated analogues. PAHs (polycyclic aromatic hydrocarbons) and benzohopanes occur in variable proportions (Fig. 6-17). Discussion of the complex composition of alkylated naphthalenes and phenanthrenes is discussed in chapter 6.8.

In recent sediments combustion products of fossil fuels represent the main source of PAHs (Laflamme and Hites, 1978). However, PAHs are also observed in ancient sediments. Their origin can be attributed to three main sources. As in recent sediments their natural occurrence in ancient sediments may result from wildfires mostly initiated by lightning strikes (Killops and Killops, 1993). Furthermore, microbially mediated diagenetic processes may lead to early aromatisation of steroids and triterpenoids (Alexander et al., 1992). Finally some

compounds may derive from polyaromatic precursors synthesized by living organism as for instance fungi (Tissot and Welte, 1984). During coalification of organic matter aromatisation processes dominate the diagenetic reactions.

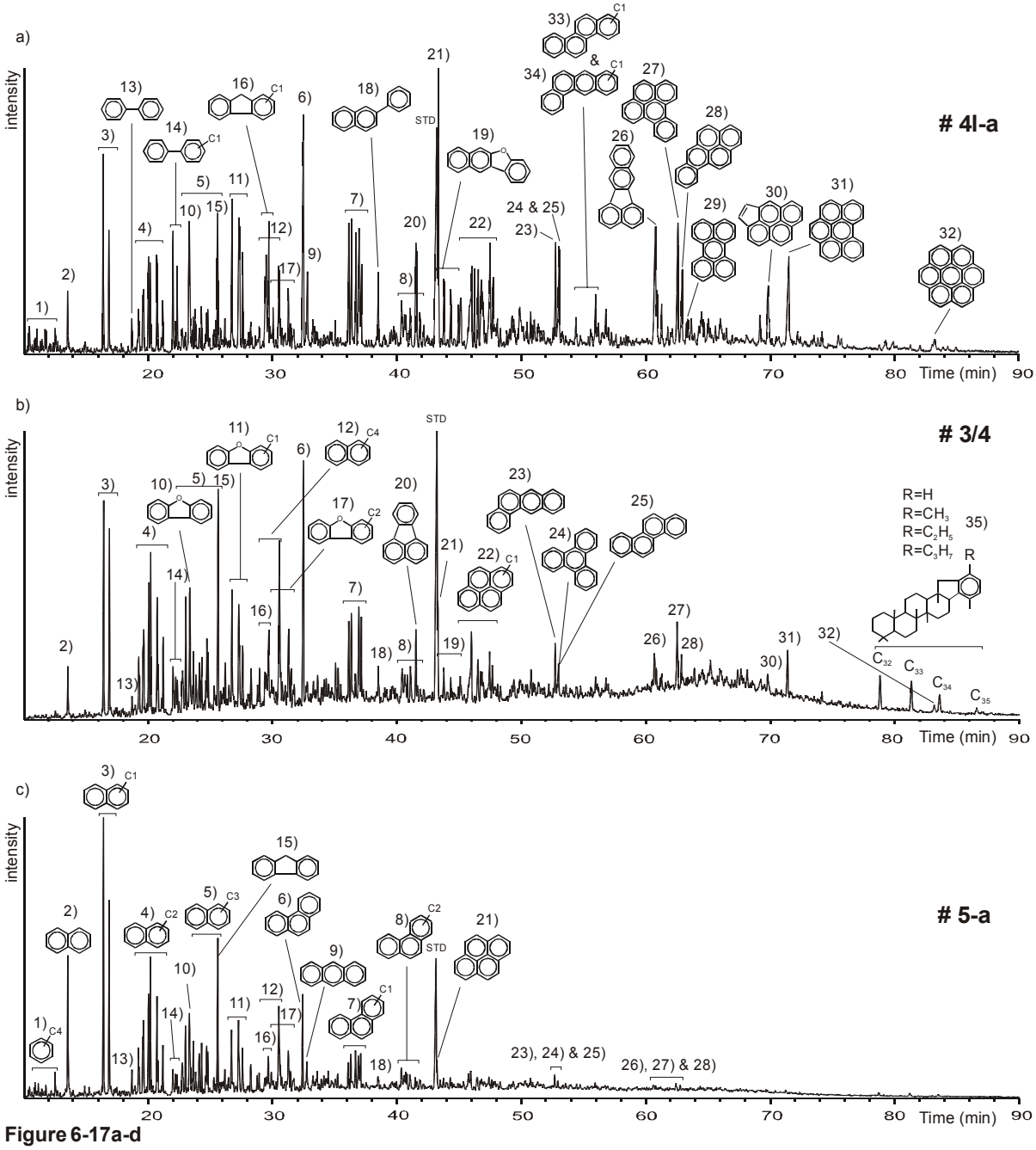


**Figure 6-17a-d**

Total ion chromatograms of the aromatic fraction of representative samples with variable proportions of polycyclic aromatic hydrocarbons. Identified compounds are tetramethylbenzene (1), naphthalene (2) and its methyl- (3), di- (4), tri- (5) and tetramethyl (12) derivatives, phenanthrene (6), methyl- and dimethylphenanthrene (7 & 8), anthracene (9), dibenzofuran and methyl dibenzofurans (10 & 11), biphenyl and methylbiphenyls (13 & 14), fluorene, methyl- and dimethylfluorene (15-17), phenylnaphthalene (18), benzo[*b*]naphthofuran (19) and the polycyclic aromatic hydrocarbons fluoranthene (20), pyrene, methylpyrenes (21 & 22), benz[*a*]anthracene (23), triphenylene (24), chrysene (25), benzo[*k*]fluoranthene (26), benzo[*e*]pyrene (27), benzo[*a*]pyrene (28), perylene (29), indeno[*cd*]pyrene (30), benzo[*ghi*]perylene (31) and coronene (32). In samples with high PAH contents also methylchrysene (33) and methylbenz[*a*]anthracene (34) were detected. The homologous series of the benzohopanes (35) are denoted from $C_{32}$ to $C_{35}$.

Variation in the relative abundance of PAH with 4-6 versus PAH with 3 rings, expressed as PAHs-($\Sigma_{\text{fluoranthene to coronene}}$) versus P+MP-($\Sigma_{\text{phenanthrene + methylphenanthrenes}}$) is presented in figure 6-9f. Samples plot around a median of 0.83 with the highest values of 3.1 and 2.8 reached in sample 2-a and 4l/u, respectively. Samples from seam 4 yield exceptionally high MPI-1, PAH/(P+MP) and aromatic to saturated hydrocarbons ratios (Fig. 6-9a & c). The highest relative abundance of low-molecular weight aromatic hydrocarbons is observed in sample 5-a (Fig. 6-17c). In most of the samples the complete series of polycondensed aromatic hydrocarbons ranging from fluoranthene to coronene can be identified (Fig. 6-17a & b). High bacterial activity can be attributed to the presence of elevated amounts of benzohopanes ($C_{32}$ to $C_{35}$) in samples D1, 1-a & b, 2-b, 3, 3/4 and 4l-b (Fig. 6-17b).

The highest proportions of parent PAHs occur in sample 2a and 4l-a (Fig. 6-17a) and are associated with high abundance of oxygenated PAH components including alkylated dibenzofurans and naphthobenzofurans. These components are attributed to an origin from charcoal and black carbon, deposited in a marine environment. This explains the very high content of natural combustion PAH in combination with a marine algal isoprenoid and steroid composition. It also explains the exceptionally low pyrolysis yield and high $T_{max}$-values upon Rock Eval Analysis despite the high $C_{org}$-content of these two samples. The mixing of the two organic matter sources, i.e. marine algal versus combusted land plant material explains the unusual behaviour of samples 2a and 4l-a in the discrimination diagrams discussed above.

In figure 6-18 the ratio of Pr/n-$C_{17}$ is plotted against the ratio of 2-methylanthracene/2-methly-phenanthrene (2-MA/2-MP). Covariance between the two parameters identifies a mixture between algal and terrestrial sources, whereby elevated Pr/n-$C_{17}$ and 2-MA/2-MP ratios indicate increasingly terrestrial plant input. Whereas phenanthrene and its methylated analogues derive from a variety of non-specific precursor compounds such as steroids and

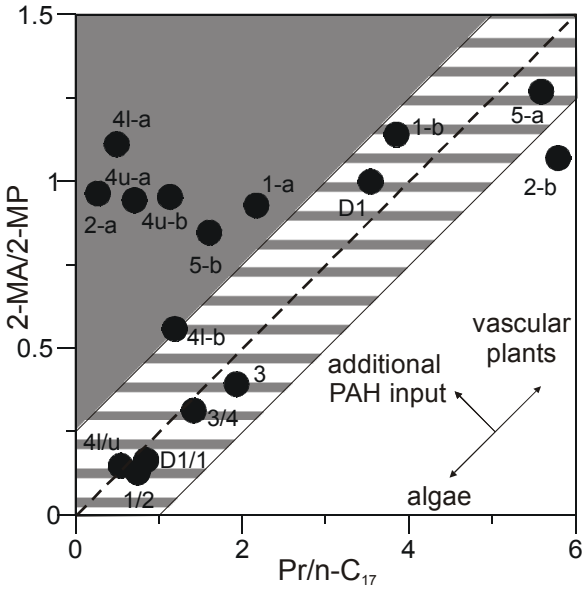


**Figure 6-18**

Cross correlation of Pr/n-$C_{17}$ versus 2-MA/2-MP. Samples in the hatched area reveal mixing of different organic matter types. Samples in the grey shaded field refer to an additional PAH supply by combustion processes or organic matter of advanced oxic- or photo-degradation.

triterpenoids, anthracene and its methyl derivatives are regarded as land plant combustion products (Tissot and Welte, 1984). Thus, a concomitant increase of Pr/n-$C_{17}$ ratios can be attributed to predominantly terrestrial biomass input. A deviation from this trend towards higher 2-MA/2-MP ratios (Fig. 6-18) indicates additional combustion sources. Indication of elevated thermal maturity ($R_c$ = 0.8) in these samples are thus alteration artefacts due to the higher proportions of combusted plant material. The additional input of PAHs is attributed to recurring forest or swamp fires favoured by periods of arid climate conditions.

## 6.7.6 Discussion

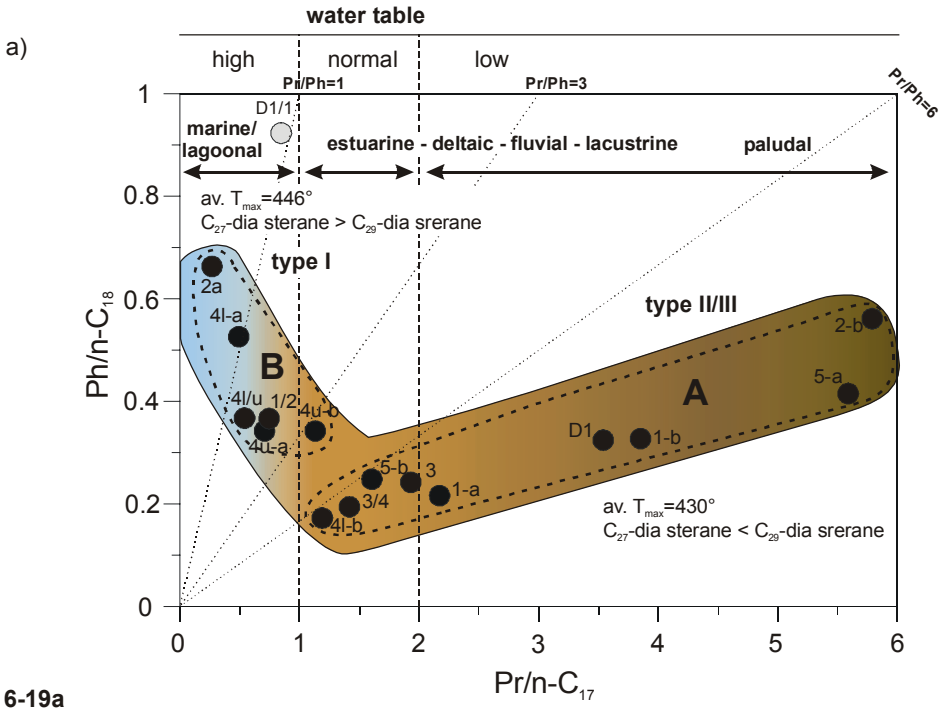


**Figure 6-19a**

**a)** The Pr/n-$C_{17}$ vs. Ph/n-$C_{18}$ diagram depicts variations in sedimentary environments with concomitant changes in biomass input.

Effects of source, depositional environment and maturity on the organic matter composition are best discriminated by the Pr/n-$C_{17}$ and Ph/n-$C_{18}$ diagram (Fig. 6-19a). Two sample groups can be discerned. Group **A** represents terrigenous organic matter and is characterized by high Pr/n-$C_{17}$ ratios and average $T_{max}$ values of 430°C (type II/III kerogen). Pr/Ph ratios above 6 point to oxic conditions in the sedimentary environment. For group **B** samples (Fig. 6-19a) increasing proportions of algal derived organic matter are indicated by lower Pr/n-$C_{17}$ ratios, accompanied by Pr/Ph < 3 and average $T_{max}$ values of 446 °C (type I/II kerogen). The siliciclastic layers 1/2, 4l/u and the upper seam 4 (4u-a & b) accumulated during transitional paralic conditions. The organic matter composition of sample D1/1 (PI > 0.5, $T_{max}$ = 413°C, Pr/n-$C_{18}$ > 0.9) indicates impregnation with migrated hydrocarbons. This

sample is therefore excluded from further discussion. A pronounced input of algal derived organic matter into the sedimentary environment during deposition of seam 2-a and 4l-a is recorded by low Pr/n-$C_{17}$ ratios, low Pr/Ph ratios (< 0.5) and preference of short-chain n-alkanes (Figs. 18a, 9b & e). In context with variation in sedimentary conditions changes in the microbial activity can be detected. Higher proportions of $C_{34}\alpha\beta$ hopanes (Fig. 6-12b, group **B**) can be associated with dysoxic conditions in the sedimentary environment. This is supported by the highest $C_{27}$-diasterane contents in sample 2-a (Fig. 6-15) pointing to a significant algal input. Increasing proportions of $C_{29}$-dia steranes versus $C_{27}$- and $C_{28}$-dia steranes point to conditions continuously changing from aquatic to terrestrial dominated sedimentary environments.

Isoprenoid vs. n-alkane ratios may be affected by burial diagenesis or biodegradation. However, the thickness of the sampled sequence is only 80 m and due to the lack of additional thermal effects or a pronounced unresolved complex mixture the variations in Ph/n-$C_{18}$ ratios are closely related to changes in the depositional environment. The two end members in figure 6-19a represent a predominance of algae (sample 2-a & 4l-a) or vascular plants (2-b & 5-a). Variable proportions of algae or land plant between the two end members allow reconstruction of the water table curve shown in figure 6-19b.

Along the northern margin of the Karoo Basin low subsidence rates promoted the formation of well-drained swamps after the final glacier retreat. The lowermost coal seams cover glaciogenic sedimentary sequences of the Dwyka Group (Cadle et al., 1993). Oxic conditions in the sedimentary environment and high rates of microbial activity is documented in figure 6-9e by Pr/Ph > 8 and by high hopane/n-alkane ratios (Tab. 6-3) in samples from the lower part of the succession (D1, 1-a, 1-b, 2-b and 3/4).

Indications for changing sedimentary conditions arise from the simultaneous predominance of short-chain n-alkanes ($\Sigma C_{12\text{-}20}/[\Sigma C_{12\text{-}20} + \Sigma C_{21\text{-}29}] = 0.85$]), low Pr/Ph ratios (Pr/Ph < 1) and decreasing hopane/n-alkane ratios in samples of seams 1/2 and 2-a (Tab. 6-3). Especially the organic matter of the interlayered sediments between seam 1 and 2 represent a mixture of algal and vascular plant material (Fig. 6-15c). Low Pr/Ph and hopane/n-alkane ratios mark an increasing water table (Fig. 6-19b). Marine ingression during deposition of seam 2-a led to dysoxic conditions in the sedimentary environment where predominantly algae derived organic matter accumulated. With respect to the local setting of the Witbank Basin at the basin margin it is questionable, if marine condition were ever fully established. The high contents of polycondensed aromatic hydrocarbons in seam 2-a point to a nearby terrestrial source for the combusted land plant material. Lagoons, estuaries or protected bays behind barrier islands provided sedimentary environments in which rafted remains of combusted terrestrial pants accumulated together with predominantly algal derived organic matter.

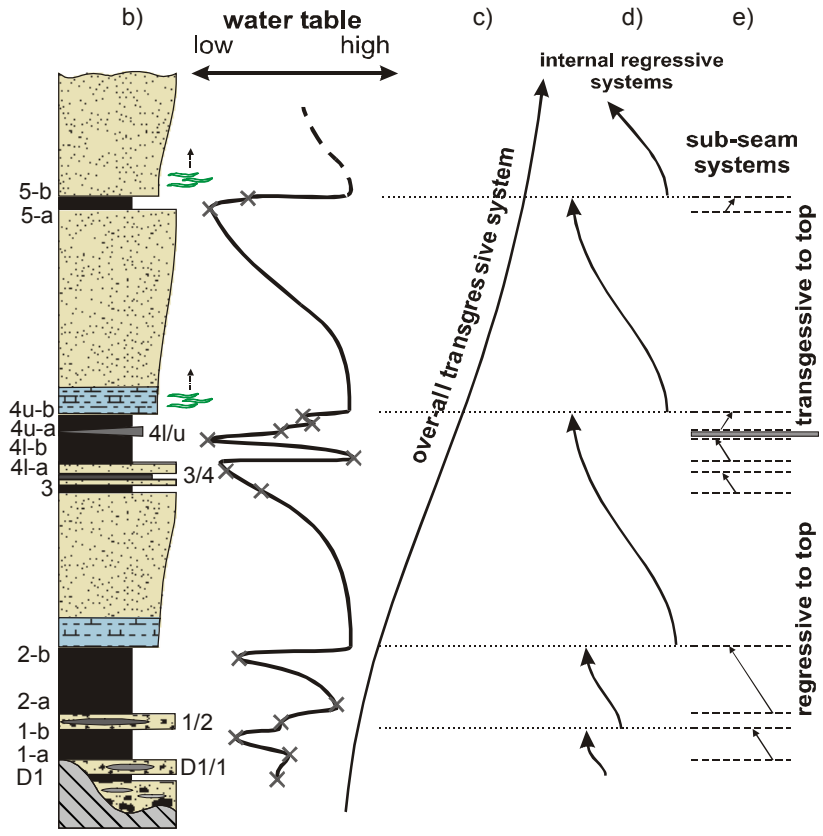


**Figure 6-19b-e**

**b)** Water table curve constructed from organic biomarker data and sedimentological observations reported in the literature. Cyclic sedimentation phases are composed of transgressive systems at the base followed by upward coarsening sequences and terminated by coals with variable organic matter composition. **c-e)** The sedimentary sequence in the Witbank coal field is composed of an overall transgressive system. This main system is based on several internal regressive sequences bearing sub-seam cyclicity. These change from regressive towards top in the lower to transgressive towards top systems in the upper seams.

The recurrence of terrestrial dominated sedimentation during deposition of seam 2-b (Fig. 6-19b) is documented by high Pr/n-$C_{17}$ and high Pr/Ph ratios, by the predominance of long-chain n-alkanes as well as by high $C_{29}$-diasterane proportions. Furthermore, elevated bacterial activity is indicated by a high hopane/n-alkane ratio (Figs. 6-18a, 6-9b, e & 6-15c; Tab. 6-3). The recurrence of terrestrial dominated sedimentation was only short-lived (Fig. 19b) because a basin-wide transgression drowned the terrestrial ecosystem and terminated any further peat accumulation in seam 2 (Cadle et al., 1993). Carbonaceous mudstones followed by coarsening-upward sequences of siltstones, fine-grained sandstones and medium- to coarse-grained arkosic sandstone form the roof of seam 2 (Cadle et al., 1993). The sequence is interpreted as clastic wedge of a shallow delta complex prograding basinward from the north and preparing the stratum upon which the following seams accumulated.

The upward coarsening sequence is capped by the deposits of seam 3. High Pr/Ph ratios (Pr/Ph = 7.6), the predominance long-chain n-alkanes, and elevated $C_{29}$-diasterane proportions indicate input of vascular plant material (Figs. 6-9b, e & 6-15c). $C_{org}$ contents

reduced to 47 wt.% indicate elevated siliciclastic supply during accumulation of the organic matter. The siliciclastic debris, transported by fluvial systems from the northern provenances to the basin margin, is supposed to have accumulated in deltaic settings. The delta plain facies with bay fill sequences and crevasse splay deposits is overlain by coarse grained channel facies, formed by the basinward migration of the fluvial plain over the underlying deltaic platform (Cadle et al., 1993). The terrigenous organic matter from this section (sample 3/4) bears characteristically high Pr/Ph ratios, predominance of long-chain n-alkanes, a pronounced odd over even predominance in the range of n-$C_{23}$ to n-$C_{27}$ as well as recurring bacterial activity by elevated hopane/n-alkane ratios (Figs. 6-9b, d & e; Tab. 6-3).

During deposition of seam 4l-a terrestrial sedimentary conditions were temporarily interrupted (Fig. 6-15b). Low Pr/Ph ratios as well as the predominance of short-chained n-alkanes point to a major input of algal derived organic matter contributing to the lower part of seam 4. Microbial activity was reduced as indicated by low hopane/n-alkane ratios (Tab. 6-3). Comparable to seam 2-a high PAH contents can be associated with elevated supply of rafted, combusted plant remains (Figs. 6-9f & 6-19). High proportions of algal biomass syndeposited with charred land plant debris again require specific sedimentary conditions of lagoons or protected embayments. At the top of seam 4l terrestrial conditions and swamp formation recurred as indicated by Pr/Ph ratios of 6 and n-alkane distribution patterns with characteristic odd over even predominance (Figs. 6-9b & e).

Siliciclastic rich sediments ($C_{org}$ = 10.04 wt.%) intercalated into seam 4 are interpreted as braided river deposits (Cadle et al., 1993). Low Pr/Ph ratios, bimodally distributed n-alkanes and elevated $C_{27}$- and $C_{28}$-diasterane contents refer to a partial supply of algal derived organic matter. In the upper part of seam 4 short-chain components dominate the n-alkane distribution whereas Pr/Ph ratios around 3 point to the influence of vascular plants (Fig. 6-9b & e). Cadle et al. (1993) proposed that the swamps reached maximum basinward position during the accumulation of seam 4. Low water tables favored accumulation of terrestrial derived organic matter while during periods of high water table the peat swamp vegetation drowned. Episodic influence of lacustrine, lagoonal or marine conditions can be observed by the variable composition of the organic matter (Fig. 6-19b).

High PAH contents in the samples from seam 4l-a, 4l-b, 4l/u and 4u-b can be explained with recurring swamp fires (Figs. 6-9f & 6-18). These events are assumed to have occurred during warm seasons favored by low precipitation rates and low water tables in paludal environments. Pronounced seasonality with warm-dry versus temperate-humid conditions seems to have influenced vegetation development in the Witbank Basin during the middle Permian. Comparable to seam 2 the deposition of seam 4 was terminated by a marine transgression as indicated by glauconitic layers in the siliciclastic sediments above seam 4 (Falcon et al., 1984).

The composition of the organic matter in seam 5 indicates a pronounced input of vascular plants. Transgression of the peat swamp by basinal waters during accumulation of seam 5, recorded from other basin positions, caused shallow embayments and lakes to form. Warm climate conditions during the upper Permian lead to massive algal blooms of *Reinschia,* a supposed analogue of today's *Botryococcus braunii*, commonly associated with fresh to brackish water conditions (Cadle et al., 1993). Brackish-marine conditions are also indicated by the presence of glauconite in the sedimentary deposits following seam 5 (Falcon et al., 1984). Increasing basin subsidence after deposition of seam 5 postulated by Cadle et al. (1993) led to landward migration of the depocentre. The low thickness of seam 5 (~1 m) implies that peat accumulation was only short-lived and ceased upon upcoming tectonic activity. Finally, multiple transgression phases during deposition of the Volksrust Formation (Cairncross and Cadle, 1988) terminated the deposition of organic rich sediments along the northern basin border.

The sedimentary sequence in the Witbank Basin comprises various cyclically recurring depositional phases, which differ in duration and intensity (Fig. 6-19c-e). The complete deposition phase represents an overall transgressive system indicated by declining thickness of the coal seams throughout the sequence and by the finally transgressive sediments of the Volksrust Formation (Fig. 6-19c). This major transgressive system is composed of at last four smaller, short-lived cyclic sequences comprising upward-coarsening sediments and coals topped by carbonaceous/glauconitic mudstones, which represent the beginning of a new cycle (Fig. 6-19d). As indicated by changing compositon of the organic matter the sedimentary system changed during deposition of each single seam (Tab. 6-4). Seams 1, 2, 3, 3/4 and 4l are regressive towards the top as indicated by a systematic change from algal to terrigenous derived organic matter (Fig. 6-19e). The overlying glauconite bearing sediments represent transgressive phases, which finally terminated further accumulation of terrigenous organic matter. During deposition of the siliciclastic interlayer 4l/u the general pattern of regressive towards the top changed. In seams 4u and 5 the base was dominated by terrigenous organic matter whereas samples from the roof show an elevated supply of algal material. Beginning with bed 4l/u the depositional system changed from regressive towards the top to transgressive towards the top in the upper part of the succession (Fig. 6-19e).

The setting in which the organic as well as the siliciclastic debris of the investigated succession accumulated was situated close to the shoreline during the whole deposition phase. Dependent on water table, subsidence rate and clastic supply from the hinterland competing sedimentary systems established. Low water tables and low subsiding rates favored maximum peat swamp accumulation in terrestrial environments. During transgressions the swamp vegetation drowned and increasing subsidence led to elevated

supply of clastic material terminating any further peat accumulation. Between these contrasting environments lagoonal, limnic, fluvial and deltaic sedimentary systems with their appropriate vegetation established thoughout the Permian in the Witbank Basin.

Different sedimentary environments developed in the Witbank Basin after the final retreat of the glaciers during the Upper Carboniferous to Early Permian. Since the region was not longer directly affected by polar climate conditions early vegetation started to flourish on the continents. Eustatic sea level changes of the Ecca Sea are supposed to be the main factor for the cyclicity detected in the sedimentary sequence. Falcon et al. (1984) proposed that these regression and transgression phases are predominantly driven by recurring ice ages originating from different ice centres. From this it follows that coal-bearing strata accumulated during glacial phases in times of sea level lowstand when seawater was fixed in glaciers. During interstadial phases coastal swamps drowned during transgressions. Peat accumulation was stopped and siliciclastic detritus was deposited in changing sedimentary environments. The complete coal bearing sequence of the Witbank Basin is assumed to be of Permian age. Since first sediments deposited immediately after the final retreat of the glaciers and the uppermost seam No. 6 is partly eroded, the investigated sedimentary succession in the Witbank Basin comprises approximately 30 Ma of deposition. A reliable estimation about the duration of each cycle is difficult due to the lack of absolute marker horizons in the succession. Furthermore, the duration of each regressive cycle must not be comparable. Glacial induced sealevel changes are often used to explain various late Palaeozoic deposits all over the world, which bear cyclic sedimentary strata (e.g. Heckel, 1986; Ross and Ross, 1985; Veevers and Powell, 1987; Wanless and Sheppard, 1936). However, data from Antarctica indicates that extended areas of central Antarctica were ice free during the Carboniferous, whereas during the Permian, deposition occurred in ice-marginal, periglacial, glaciomarine, glaciolacustrine, and glacially influenced marine or lacustrine settings (Isbell et al., 2003). It is questionable whether ice volumes during the Carboniferous were sufficient to produce the observed sealevel changes with supposed amplitudes up to 200 m. Effects on the global climate system triggered by the Late Palaeozoic glaciation in southern Gondwana are discussed e. g. by Hyde et al. (1999); Raymond et al. (1989); Barnes (1999); Crowley and Baum (1992) and Isbell et al. (2003). During the late phase of the Palaeozoic glaciation the eastward trending pole left single, separate highland icecaps. Waxing and waning of the inland ice might have led to transgression and regression phases on the low lying northern margin of the Karoo Basin. The initiation for the entire glaciation phase with its supposed complex stadial and interstadial phases must be discussed by the combination of different climate-relevant factors such as plate motions, topography, orbital cycles, ocean/atmosphere circulations and continent/ocean distribution which can all directly or indirectly influenced the global climate.

## 6.7.7 Conclusion

Characterization of bulk and molecular composition of a sequence of Permian coals and organic rich sediments from the Rietspruit collier led to the following conclusions.

- *Differences between Dwyka vs. Ecca Group sediments are recognizable by MPI-values and saturate/aromatic hydrocarbon ratios. The transition is located between seams 1 and 2 of the Rietspruit section.*
- *Changing environmental conditions during coal deposition are better expressed in molecular biomarker compositions than in bulk parameters. The ratios of selected isoprenoids vs. n-alkanes differentiate phases of low water table with predominantly terrestrial and bacterial biomass accumulation from transgressive phases with higher algal input.*
- *Steroid biomarker distributions are in agreement with the acyclic hydrocarbon patterns and extended hopanoid distributions support the discrimination of two contrasting depositional regimes with oxic conditions and input of terrestrial organic matter versus anoxic conditions during which predominantly algae derived organic matter accumulated.*
- *Significant distribution of n-alkanes (predominance of $C_{23}$ and $C_{25}$) and MA-steroids may indicate input of Sphagnum mosses and/or specific aquatic macrophytes such as reed grass during phases of low water table.*
- *During periods of low water table extensive wildfires lead to massive input of combustion derived polycyclic aromatic hydrocarbons into aquatic depositional systems. High abundance of wildfire products indicates a pronounced seasonality.*
- *Cyclic development of organic matter composition is linked to glacioeustatic sea level variation triggered by glacial/interglacial phases linked to east-westward movement of ice-centres on the Gondwana mainland.*

# 6.8 Characterisation of vascular plants by specific biomarkers

## 6.8.1 Introduction

Contrasting sedimentary environments established in the Witbank Basin during the Permian (Fig. 2-2b). Regression and transgression phases of the Ecca Sea are regarded as the main factor for the cyclic composition of the sedimentary succession. Falcon et al. (1984) proposed that these fluctuations in sealevel were predominantly driven by recurring stadials with ice centres moving with the pole. Coals and $C_{org}$-rich shales accumulate during glacial phases in times of low sea level, when seawater was bounding in glaciers. During interstadial phases coastal swamps drowned by transgressions. Peat accumulation was stopped and siliciclastic detritus was deposited in changing sedimentary environments.

Beside environmental changes, influencing source and type of organic matter also significant changes in the pollen-producing flora were detected by Falcon et al. (1984). The typical Gondwana *Glossopteris* and *Gangamopteris* flora flourished on the continents of south Gondwana during the Upper Carboniferous to middle Permian (Stewart, 1983). This new plant group marks the transition between the Paleophytic and the Mesophytic era of plant evolution. Extended forest vegetation formed by *Glossopteris* and related species is reported from different late Palaeozoic basins of south Gondwana (Retallack, 1980; López-Gamundi, 1993; Rayner, 1995). The floral assemblage is commonly associated with cool to temperate climate conditions, which established after the final glacier retreat. Beside the characteristic *Glossopteris* Gondwana flora, lycopods, ferns, cordiatales and early gymnosperms are constituents of the postglacial vegetation (Falcon, 1986).

In the Rietspruit area the most significant change in the microfloral assemblage proceeded during deposition of seam 2. Monosaccate, non-striate pollens were replaced by disaccate ones. In elevated positions, disaccate pollens bear corpus striations. This change in the microfloral assemblage is assumed to coincidence with the Dwyka/Ecca boundary. The corresponding monosaccate pollen-producing gymnospermous flora in the lower succession (D1 to seam 2-a) is associated with earliest postglacial climate conditions. The primary plant communities, which locally established directly on glacial tillites, are described as tundra/arctic type vegetation (Le Blanc Smith, 1980; Tankard et al., 1982). During deposition of seam 2-b to 5 the pollen-producing flora markedly changed. The increase in number and diversity of the palynomorphs implies a significant extension of the vegetation, associated with climate amelioration during the early Permian. The floral assemblage of this phase was supposably composed of conifers, cordaites, pteridophytes and glossopteris as it was typical for the middle Permian of southern Gondwana (Stewart, 1983).

## 6.8.2 Excursion into Palaeobotany

During the late Palaeozoic significant changes in the evolution of vascular plants was documented by Stewart (1983), Archangelsky (1990) and Traverse (1988). The evolution of different coniferophytes is assumed to arise from *Progymnospermopsida* in the upper Devonian. Especially *Archaeopteris* exhibits characteristics found in *Cordaitales*, *Voltziales*, *Coniferales* and *Taxales* (Stewart, 1983). *Cordaitales* and *Voltziales* represented the major groups of coniferophytes during the Upper Carboniferous to Middle Permian. *Cordaitales*, become extinct in the Middle to Late Permian. From the *Voltziales* today's *Coniferales* evolved since the Late Permian to Early Triassic (Fig. 6-20). The pollen grains from the different species can vary in size, habit (mono-/ disaccate) and surface structure of the corpus.

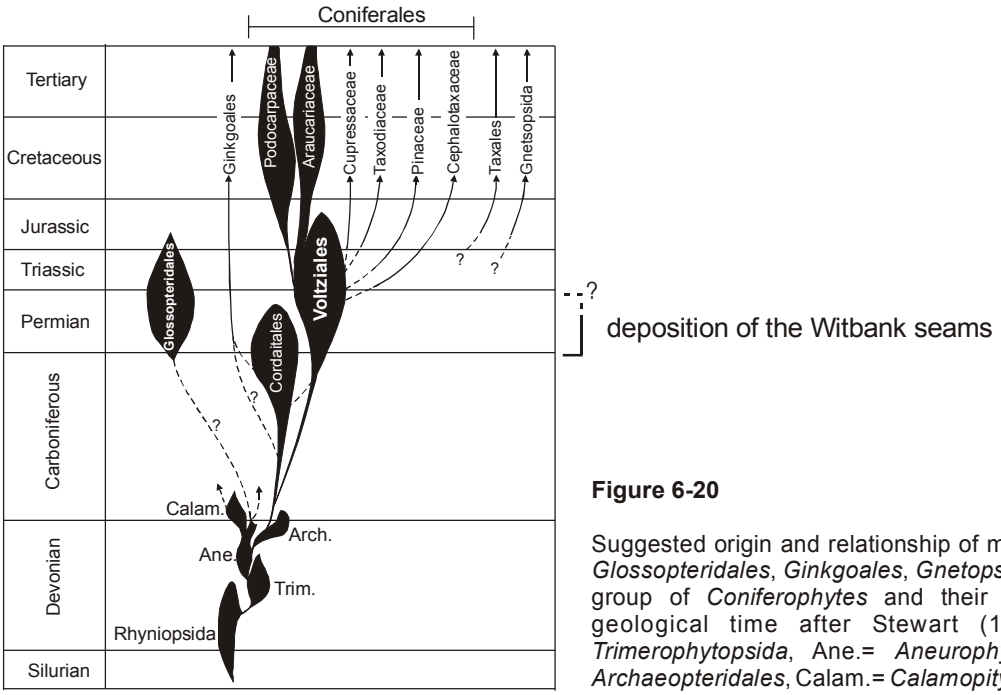


**Figure 6-20**

Suggested origin and relationship of major groups of *Glossopteridales*, *Ginkgoales*, *Gnetopsida*, and major group of *Coniferophytes* and their distribution in geological time after Stewart (1983). Trim.= *Trimerophytopsida*, Ane.= *Aneurophytales*, Arch.= *Archaeopteridales*, Calam.= *Calamopityaceae*

The *Araucariaceae* (trees of the Kauri pine group) provide the oldest coniferous family, occurring since the latest Permian onward (Agashe, 1995). Stewart (1983) pointed out that from wood or leaf fossils it is impossible to determine exactly, when in geological time the *Araucariaceae* made their first appearance. Nevertheless, the radiation of the *Araucariaceae* started in the Early to Middle Jurassic (Stewart, 1983; Miller 1982). A further important member of the *Coniferales* is the *Podocarpaceae* family. First fossil plant remains of this family are recorded from the Upper Triassic in south Gondwana deposits (Africa and Australia) by fossils of *Rissikia* (Stewart, 1983). The bisaccate palynomorphs of *Rissikia* show striations. *Rissikia* joins the rank of "transition-conifers" that seem to bridge the gap between Palaeozoic and Mesozoic conifers (Stewart, 1983).

Beside the coniferophytes, which established on the northern and southern hemisphere, the south Gondwana floral assemblage during the Permian was dominated by *Glossopteris* (Fig. 6-20). *Glossopteris* is known to have originated soon after glaciation in the early Permian as an autonomous plant group, reaching its zenith of development and diversity by the Late Permian. It then began to decline and after the Triassic became extinct (Agashe, 1995). These gymnospermous plants are described as large, forest forming deciduous trees with substantial trunk of Araucarioxylon-type wood providing the biomass for today's Late Palaeozoic coal deposits on the southern hemisphere (Retallack, 1980; Rayner, 1995; Stewart, 1983). Macrofossils such as leafs, roots, stems and fructifications were found in Permian sediments from South Africa, India, Australia, Antarctia and South America. Bisaccate pollen grains with traverse striation on the corpus are characteristically for the *Glossopteris* flora (Stewart, 1983). The tongue shaped leafs can vary in size and internal structure depending on the species from which they derived (i.e. *Glossopteris* and *Gangamopteris*).

## 6.8.3 Specific plant derived biomarkers

Palynological investigations on the coal seams of the Witbank Basin (Falcon et al., 1984; Millsteed, 1994 and 1999) reveal that a significant change in the floral assemblage had occurred during deposition of seam 2. The predominance of a monosaccate pollen-producing flora was replaced by a preference of bisaccate one. By the means of specific organic geochemical biomarker molecules more information about the proposed floral change should be obtained. To eliminate influences by changing type of organic matter, samples with pronounced contents of algal derived material (2-a, 4l-a and D1/1) are excluded from the discussion (grey data points in figure 6-21a-e). As pointed out by Strachnan et al. (1988) and Alexander et al. (1987) aromatisation of plant-derived terpenoids is favoured during coalification relative to reduction and preservation of saturated biomarkers. Thus the following discussion is focused on the aromatic hydrocarbon fraction. In the lower seams from the Witbank Basin the distribution of trimethylnaphthalenes (m/z=170; [TMN]), methylphenanthrenes (m/z=192; [MP]) and dimethylphenanthrenes (m/z=206; [DMP]) are dominated by the isomers of 1,2,5-TMN, 1-MP and 1,7-DMP (Fig. 6-22a). High retene contents are also characteristic for the lower seam unit of seam D1 to 1-a (Fig 6-21a & 6-22a). The formation of retene, agathalene (1,2,5-trimethylnaphthalene [1,2,5-TMN]) and pimanthrene (1,7-dimethylphenanthrene [1,7-DMP]) by aromatisation of bicyclic and tricyclic components of resins was already documented by Ruczika and Hosking (1930). Retene is believed to be derived from abietic acid, a common constituent of conifer resin (Simoneit et al., 1986) as well as from phyllocladane (Alexander et al., 1987) and is used as a general marker for higher plant material (Mackenzie et al., 1982; Chaffee et al., 1986).

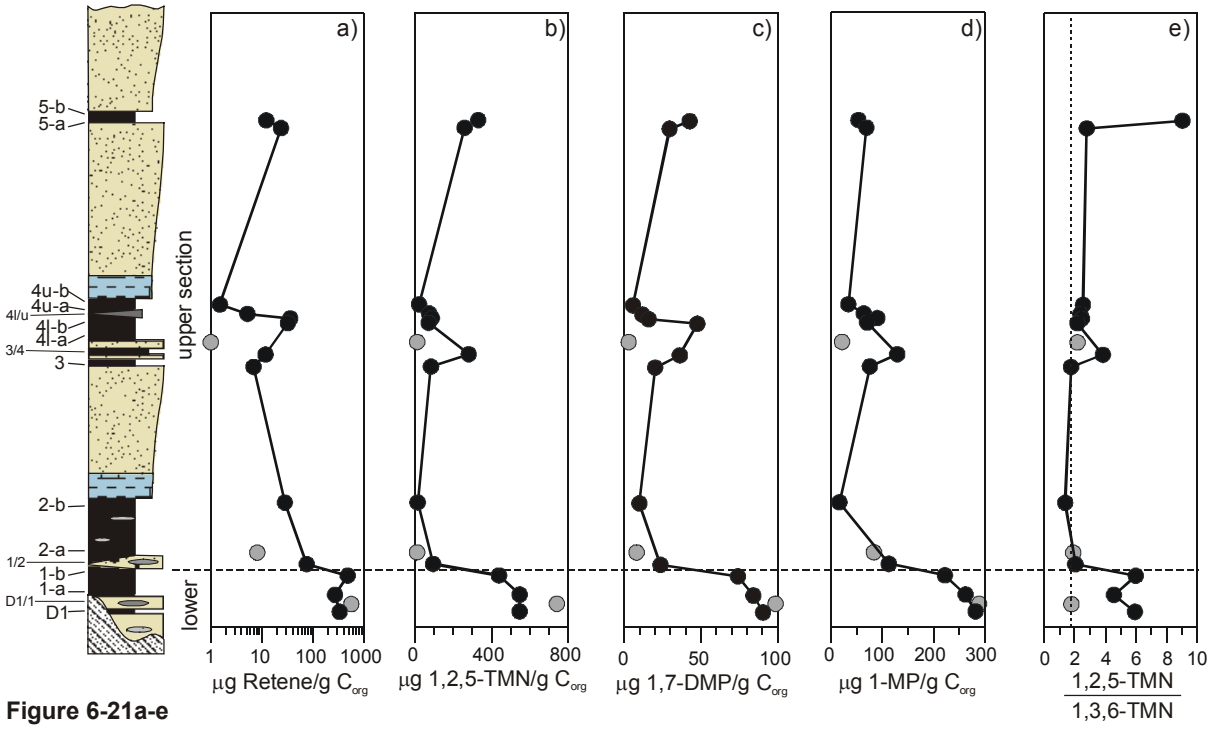


**Figure 6-21a-e**

**a-d)** Significant aromatic hydrocarbon contents displayed as µg/g $C_{org}$ point to changing plant communities during accumulation of the lower and upper seams. **e)** The 1,2,5-TMN /1,3,6-TMN ratio, used as maturity parameter, indicate a general low thermal maturation as well as an elevated input of 1,2,5-TMN in the lower seams.

In figure 6-21a-c the compounds are displayed as µg/g $C_{org}$. The lower succession (seam D1, 1-a and 1-b) contains distinctively higher contents of the aforementioned biomarkers than the upper seams (1/2 to top). Retene contents decrease from 357µg/g $C_{org}$ to 23µg/g $C_{org}$, 1,2,5-TMN contents from 511µg/g $C_{org}$ to 133µg/g $C_{org}$, and 1,7-DMP contents from 82µg/g $C_{org}$ to 21µg/g $C_{org}$ in the upper succession. Furthermore, the 1-MP contents are displayed in figure 6-16d, which can be also regarded as a decomposition product of resinous source material. Average 1-MP contents of 256µg/g $C_{org}$ can be detected in the lower seams whereas in the upper succession an average of 71µg/g $C_{org}$ is reached.

Suitable precursor compounds for 1-MP are abietic as well as podocarpic acid from which 1-MP could generate during maturation processes (Alexander et al., 1992; Campbell and Todd, 1942). The high proportions of 1-MP in seam D1 to 1-b are responsible for the lower MPI-1 values in figure 6-9d. Thus the observed changes between the lower and upper succession in the Witbank Basin can be rather explained by the input of different plant material than by differences in the maturity of the organic matter. The presence of only one of the *Araucariaceae*-diagnostic compounds in figure 6-21a-d would not lead to a reliable characterisation of the organic matter since also other precursor substances than *Araucariaceae* resin may have to be considered. However, the collective presence of these aromatics in the lower succession gives strong evidence for the presence of early conifers.

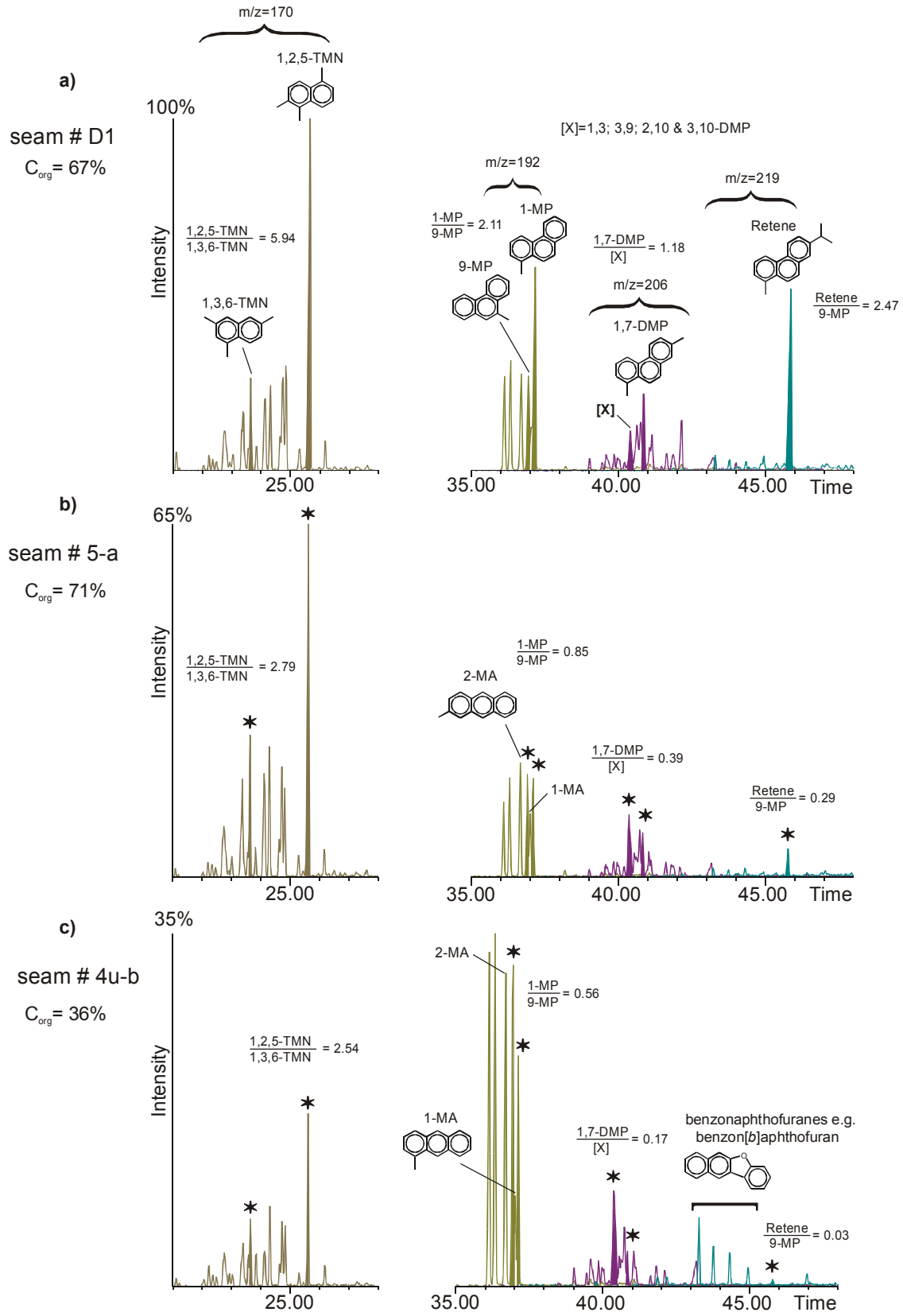


**Figure 6-22a-c**

**a)** Aromatic hydrocarbon distribution of trimethylnaphthalenes (TMN) [m/z = 170], methylphenanthrenes (MP) [m/z = 192], dimethylphenanthrenes (DMP) [m/z = 206] and retene [m/z = 219] shows a predominance of the 1,2,5-TMN, 1-MP and 1,7-DMP isomers. **b and c)** Decreasing isomer ratios and retene contents point to declining input of coniferous plant material. 2-MA denotes 2-methylanthracene. The occurrence of benzonaphthofuranes relates natural combustion processes.

Besides a decrease in total amounts of the compounds displayed in figure 6-22a-c also the proportion of the single isomers change dramatically from the lower to the upper unit. Especially the ratios of 1,2,5-TMN/1,3,6-TMN, 1-MP/9-MP and 1,7-DMP/[X] decrease significantly (Fig. 6-21e & 6-22a-c). Changing contents of the compounds in figure 6-21a-d were also detected by Alexander et al. (1992) in the aromatic fractions of sedimentary deposits of the Cooper (Permian to Triassic) and Eromanga (Early Jurassic to Cretaceous) Basins in Australia. Alexander et al. (1992) related these compounds preferentially to *Araucariaceae* remains in Early Jurassic to Cretaceous sediments of the Eromanga Basin. Bi- and tricyclic diterpenoids have been reported by Thomas (1969) to be present in the resins of fossil Araucariaceae whereas resins from other Coniferales contain higher proportions of tetracyclic diterpenoids. Since fossil remains of *Araucariaceae* are stratigraphically restricted to the strata of the Eromanga Basin, Alexander et al. (1992) were able to discern Permian from Triassic deposits. Oils generated in the two basins can be reliably be discerned by the presence or absence of the specific araucarian biomarker molecules.

The stage of maturation can be determined by the trimethylnaphthalene ratio of 1,2,5-TMN/1,3,6-TMN (Fig. 6-21e). 1,2,5-TMN is initially formed during aromatisation of the natural precursors, and its isomer subsequently reacts to give 1,3,6-TMN and other isomeric trimethylnaphthalenes (Strachan et al., 1988). In consequence, the 1,2,5-TMN/1,3,6-TMN ratio (TNR) decreases with increasing maturity. A TNR of 1.8 is used as cut-off value for samples, which did not receive an enhanced input of 1,2,5-TMN or reached advanced maturity (broken line in Fig. 6-21e). 1,2,5-TMN/1,3,6-TMN ratios in figure 6-21e above this cut-off value denote organic matter with low thermal maturity and/or point to elevated input of 1,2,5-TMN by specific plant material. Especially samples from the lower seams (D1, 1-a & b) as well as the sample of seam 5-b show distinctively high 1,2,5-TMN/1,3,6-TMN ratios of 5.5 and 9.

By using a log [1,2,5-TMN/1,3,6-TMN] vs. log [1-MP/9-MP] plot, Alexander at al. (1992) discerned Permian from Jurassic *Araucariaceae*-bearing sediments of the Australian Cooper and Eromanga Basins. The 1-MP/9-MP ratio is used to express the source related abundance of 1-MP because of the similar stability of both isomers (Radke et al., 1982). Alexandes et al. (1992) concluded that high 1,2,5-TMN in combination with high 1-MP contents are representative biomarkers for the araucarian flora.

In figure 6-23a the Rietspruit samples are displayed in the according log-log plot developed by Alexander et al. (1992). Samples form seam D1, 1-a & b bear high contents of both biomarkers and plot in the upper right corner comparable to the Jurassic sediments of the Eromanga Basin. Most of the samples plot in the lower right quadrant, which can be attributed to sources other than araucarian flora (Alexander et al., 1992). Samples of

Permian age without fossil araucariaceae remains from the Cooper Basin yield similar distributions.

Two other aromatic biomarker ratios were used by Alexander et al. (1992) to discriminate *Araucariaceae*-bearing sediments from sediments with non-specific plant remains (Fig. 6-23b). For discrimination the ratio of 1,7-DMP to the co-eluting 1,3-, 3,9-, 2,10- and 3,10-DMP (expressed as [X]) and the retene/9-MP ratio is calculated. As cut-off values 0.3 and 0.8 are used, respectively. In figure 6-23b the Rietspruit coals are displayed in the double-logarithmic plot of both biomarker ratios. Due to lower 1,7-DMP/[X] ratios, the Carboniferous-Permian sediments from the Rietspruit colliery are shifted in parallel to the position of the samples from of the Eromanga and Cooper Basins. However, samples from the lower succession (D1, 1-a & b and 2-b) plot into the upper right sector, indicating high contents of araucarian biomarker molecules.

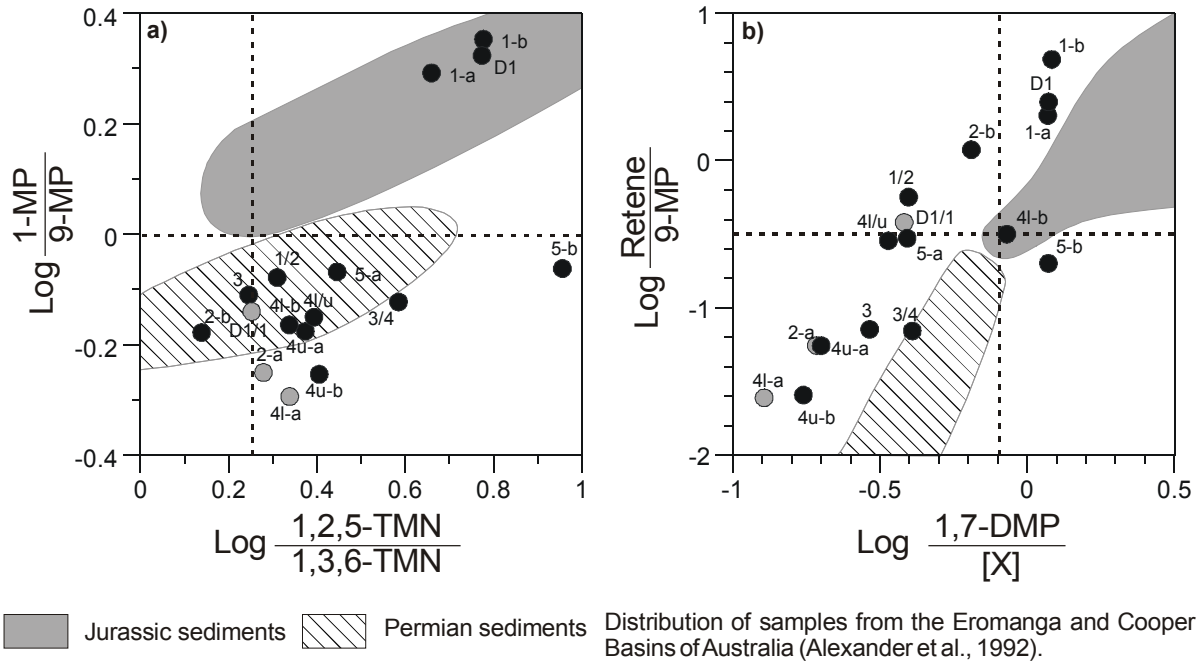


**Figure 6-23a & b**

**a)** Basal seams of lower Permian age from the Witbank Basin show similar alkylphenanthrene ratios to Jurassic *Araucariaceae* bearing sediments from the Eromanga Basin (Australia). **b)** Due to lower 1,7-DMP/[X] ratios samples from the Witbank Basin are shifted from the sample distribution of the Australian samples. However, samples from the lower seams plot into the upper right quadrant close to the distribution of the Jurassic sediments of the Eromanga Basin.

Tetracyclic diterpenoid hydrocarbons can be detected in samples from the lower seams D1, 1-a & b. Diterpanes based on ent-kaurene and phyllocladane skeletons were identified by their massfragmentogram m/z = 274 according to Noble et al. (1985) as shown in figure 6-24a & b. Diagenetic reduction of ent-kaurene and phyllocladane is expected to produce mainly ent-16$\alpha$(H)-kaurane and 16$\alpha$(H)-phyllocladane, respectively. Its a consequence of the

higher thermodynamic stability of 16β(H)-phyllocladane against 16α(H)-phyllocladane, advanced maturation influences the distribution of ent-kaurene and phyllocladane. 16β(H)-phyllocladane/16α(H)-phyllocladane ratio increases with maturity and reach equilibrium of 0.75 - 0.80 for 16β(H)-phyllocladane/(16β(H)-phyllocladan + 16β(H)-phyllocladane) in the early oil window (Alexander et al., 1987). Thus, high 16β(H)-phyllocladane contents in samples D1, 1-a & b indicate that the maturation of the organic matter reached the beginning of the oil window.

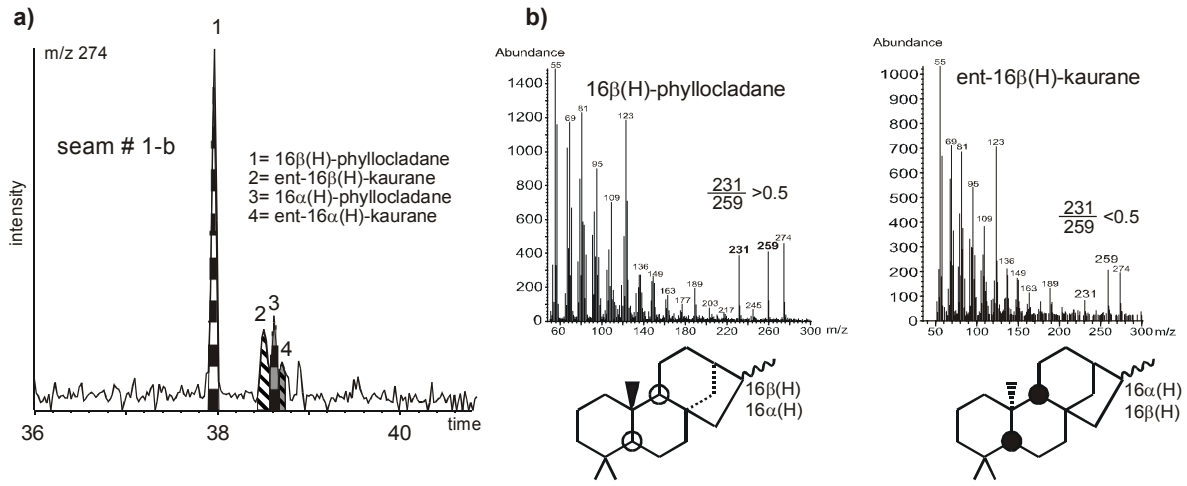


**Figure 6-24a & b**

**a)** Distribution of tetracyclic diterpanes (m/z = 274) in the basal coal seams of the Rietspruit colliery shows predominance of 16β(H)-phyllocladane. **b)** Differentiation between phyllocladane and kaurane according to Noble et al. (1985) by the ratio of the fragment ions [m/z = 231] vs. [m/z = 259].

The parent hydrocarbons of the kaurane and phyllocladane classes occur as mono-unsaturated alkanes, and are particularly abundant in leaf resins of conifers belonging to the *Podocarpaceae*, *Araucariaceae* and *Cupressaceae* families (Hanson, 1969; Noble et al., 1985 Otto and Wilde 2001). Phyllocladane is identified in resins from species of *Podocarpaceae*, while kaurane was detected in *Agathis*, a species of *Araucariaceae* (Noble et al., 1985). It has to be mentioned that especially the occurrence of tetracyclic diterpenoids is not restricted to resinous precursor compounds but also reported from a wide variety of vascular plants.

## 6.8.4 Discussion

By palynological investigations two distinctive and successive floral/vegetational regimes can be discerned in the succession of the Rietspruit colliery in the Witbank Basin. The older one (D1 to 2-a) is characterised by monosaccate microflora assemblage whereas in the following seams (2-b to 5) disaccate pollen are predominant (Falcon et al., 1984). The documented

changes of the microfloral assemblage proceeded during deposition of seam 2. In the aromatic hydrocarbon biomarker distribution significant changes can be recognised even earlier. As displayed in figure 6-21a-e, the most pronounced change in the biomarker distribution took place already after deposition of seam 1 and seems to be completed with onset of seam 2. Thus, the aromatic hydrocarbon biomarker distribution separated the succession earlier than the changes documented in the microfloral assemblage. By biomarker distribution the succession separates between seam 1 and 2 in a lower (seam D1 to 1-b) and upper (seam 1/2 to top) unit. In the lower unit (D1 to 1-b) high proportions of resin derived biomarker molecules point to the presence of early *Coniferales* as main source of the organic matter. During deposition of seam 2 the accumulation of organic matter with high contents of coniferous or related plant remains was terminated and followed by the input of organic matter with low resinous components. In combination with the appearance of bisaccate pollen, the spread of the typical Permian Gondwana vegetation with *Glossopteris* during moderate climate conditions seems to be responsible for this change. The offset between the changes in the biomarker distribution (top of seam 1) versus microfloral association (top of seam 2-a) can be explained by local changes, recorded by the biomarker analyses and with regional changes recorded by the pollen distribution. However, after deposition of seam 1 the region passed through a transitional stage during which the regional climate conditions significantly changed.

The characterization of the organic matter of seam D1, 1-a & b by figures 6-23a & b reveals some problems. As mentioned before the phase of deposition for the seam succession in the Witbank Basin spans the upper Carboniferous to Late Permian. Alexander et al. (1992) point out that the collective presence of 1,2,5-TMN, 1,7-DMP, Retene and 1-MP, which were detected in the lower seams of the Rietspruit colliery, provides strong evidence for the range of natural products which are characteristic of resins from *Araucariaceae*. But, the first appearance of plants of the *Araucariaceae* family is not documented before the Late Permian to early Triassic. Thus, either specific genus of Voltziales or Cordiatales were able to biosynthesise the discussed characteristic aromatic biomarkers or *Araucariaceae* evolved significantly earlier in earth history than previously assumed.

Beside the general application of phyllocladane as marker for vascular plants, the association of kaurane and phyllocladane with *Araucariaceae* or *Podocarpaceae* is also quite problematic since these conifers did not significantly evolved and spread before the Early Triassic. However, the occurrence of phyllocladane or kaurane is also documented from different pre-Permian coals of Germany (Schulze and Michaelis, 1990), Oklahoma (ten Haven et al., 1992), Poland (Fabianska et al., 2003), Scotland (Raymond et al., 1989) and from Permian coals in Australia (Noble et al., 1985). The authors conclude that these compounds might be derived from early conifers such as *Voltziales*, which were assumed to

be able to biosynthesise these diterpanes. Therefore phyllocladane and related tetracyclic diterpenoids can only applied as proxies for vascular plants and should not be used as biomarkers for specific species. However, if actually *Araucariaceae* or related species/genus were responsible for the high retene, 1-MP, 1,2,5-TMN and 1,7-DMP contents in the lower seams, than at least higher kaurane than phyllocladane contents should have been detected. Since this is not the case, other precursors plants than *Araucariaceae* were also able to biosynthesise precursors for these aromatic compounds.

It can be assumed that the observed vegetation change was primary triggered by newly emerging climate conditions after the main retreat of the glaciers. The climate during accumulation of the lower succession was characterized by the cold-polar, periglacial phase, which passed into temperate, postglacial climate conditions during deposition of the upper seams. During earliest phase after glacier retreat, tundra-type vegetation established on the outwash plains. Sub-polar climate conditions are associated with cold-arid conditions during short summers with maximum temperatures closely above 0°C and long winters. Mean annual temperatures during the latest stage of glaciation to earliest post-glacial phase ranged around -7°C (Golonka et al., 1994; Golonka and Ford, 2000). Typical plant communities, associated with these climate conditions, are mosses, shrubs and bushes. The presence of of early *Coniferales* is evidenced by biomarker analysis in seams D1 to 1-b. This vegetation demands further climate amelioration, since sub-polar climate conditions with low temperatures during long winter seasons would have hampered the growth of a coal forming vegetation. Hence, during the Upper Carboniferous average temperatures might have raised and vegetation extended to enable the production of sufficient biomass to form today's coals. Tundra vegetation with coniferous forests at boreal climate conditions point to mean annual temperatures of around 0°C. Thus, a temperature rise led to favourable conditions, which initialised the spread of the postglacial coniferous vegetation as documented by the seams in the Witbank Basin, which in many places rest directly on glacial sediments.

The first phase with coniferous-type vegetation proceeded up to seam 1-b. Before and during accumulation of seam 2-a, major changes in the climate conditions led to expansion of the typical Permian *Glossopteris* flora. The demarcation between the different vegetation phases coincidence with the organic rich shales of the interlayer 1/2, between seam 1-b and 2-a.

The distinctive retreat of resinous precursor derived aromatic hydrocarbons (Fig. 6-21a-d) indicates a major change in the floral composition. Low coniferous biomarker contents but a high accumulation/preservation rate of organic matter point to the evolution and spread of deciduous trees. Thus, in the following vegetation phase (seam 2-a/b to top) the expansion of *Glossopteris* predominantly contributes to the formation of the coal seams.

Perceptions about the Permian climate conditions and annual temperatures in south Gondwana reach from cold-temperate conditions and seasonal extremes with 15° to 20°C

during summer and –20° to -25°C during winter seasons (Plumstead, 1957, Kutzbach and Gallimore 1989 and Crowley et al., 1989) to temperate climate conditions with warm-humid summers with approximately 30°C and frost free winters (Yemane 1993, Rayner, 1995). In consideration of the simultaneous evolving reptile fauna (*Mesosaurus*) in the Karoo Basin and in adjacent basins of today's Namibia (Warmbad Basin) and Brazil (Paraná Basin) during the Permian (Oelofsen, 1987), predominantly frost-free seasons can be assumed. During deposition of the lower seams extant glaciers persisted in the surrounding highlands, whereas in the following deposition phase the ice caps vanished completely. Thus, the final termination of the Late Palaeozoic glaciation phase in south Gondwana, which coincided with the Dwyka-Ecca boundary, occurred presumably after accumulation of seam 1-b.

The sudden floral change during accumulation of the interlayer 1/2 is closely related to a pronounced climate change from boreal climate conditions to temperate conditions, which allowed the expansion of *Glossopteris* as well as the development of a reptile fauna during the middle Permian. The documented climate change in south Gondwana cannot be explained by the drift of the southern continents to lower latitudes alone. Fast climate shifts are often associated with changes in ocean/air circulation pathways, which amongst other factors can be also influenced by the continent distribution.

## 6.8.5 Conclusion

The changes in the distribution of specific aromatic biomarkers in the coals and organic rich sediments from the Rietspruit collier lead to the following conclusions.

- *Specific aromatic biomarkers, previously used to identify presence of Araucariaceae occur in the Rietspruit samples.*
- *Araucarian biomarker predate the fossil evidence for these conifers and thus are attributed to early Voltziales.*
- *Changes in the aromatic hydrocarbon composition preceded palynological changes.*
- *Early Voltziales/Coniferales were able to biosynthesises hydrocarbons, which can be found in fossil and recent resins of the Araucariaceae.*
- *First postglacial vegetation was dominated by an early Coniferales flora.*
- *Glossopteris flora replaced the primary Coniferales flora after the final glacier retreat during the early Permian.*
- *Temperature estimations during the early postglacial vegetation phase range around mean annual temperatures of 0°C. During the late early Permian the temperatures must have rose up to annual means of approximately 15°C.*

# 6.9 Organic matter of the northern Paraná Basin

Samples from the northern Paraná Basin were collected from different quarries NE of Sao Paolo (Scheffler et al., 2001). Single samples were taken from the top of the glacial Itararé Group and from the following Tatui Formation, to record the transition phase from glacial to postglacial climate conditions. The sampling was focused on postglacial sediments of the Irati Formation (including Taquaral, Assistencia and Serra Alta Member) with interbedded strata of carbonates and mudstone horizons (compare fig. 2-6).

## 6.9.1 $C_{org}$, S, $\delta^{13}C_{org}$, carbonate content, $\delta^{13}C_{(cc)}$ and $\delta^{13}C_{(dol)}$

$C_{org}$ contents in table 6-5 reach from close to zero in the lower part of the succession to 3.35 wt% $C_{org}$ in black carbonaceous mudstones of the Assistencia Member. Comparable to the $C_{org}$ contents, sulphur contents range from zero up to 4.55 wt% in the pyrite bearing shales of the Assistencia Member. A positive correlation between $C_{org}$ and S content of ***r*** = 0.89 is commonly explained by processes of bacterial sulphate reduction (Berner and Raisewell, 1984). As discussed for the samples of the Witbank Basin, C/S ratios can be used to verify changes in the $O_2$ concentration in the sedimentary environment (Berner and Raiswell, 1983, 1984; Dean and Arthur, 1989).

Sediments deposited under marine conditions with oxic bottom waters yield C/S ratios of 2.5, whereas lower C/S ratios are characteristic for euxinic environments. High C/S ratios (> 2.5) are found in non-marine environments, where sulphur supply and sulphate reduction is limited (Berner and Raiswell, 1984). Samples in figure 6-25 above the normal marine line (NML) indicate anoxic sedimentary conditions in the bottom water. C/S ratios in table 6-5 range between 0.1 and 41 with a median of 2.4. High C/S ratios derive from samples with carbon and sulphur contents close to detection limit and can therefore not used as redox proxy.

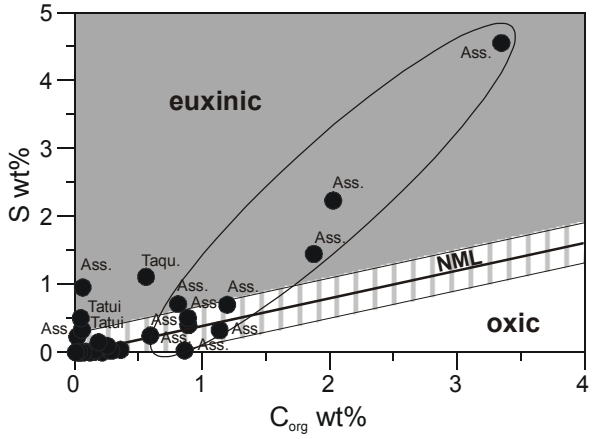


**Figure 6-25**

Facies discrimination by bivariate $C_{org}$ vs. S plot after Berner & Raiswell (1984). NML= denotes normal marine conditions with C/S ratios of 2.5. Normal marine and partially euxinic conditions prevailed during deposition of the Assistencia Formation, as evidenced by high C/S ratios in most of the samples.

The bituminous carbonates and shales of the Irati Formation were deposited during a basin wide transgression phase in the middle Permian after termination of the Carboniferous-Permian Gondwana glaciation. The organic-poor shales of the upper Irati Formation, the Serra Alta Member, were deposited during regressive phases in consequence of the gradual drying out of the epicontinental sea (Zalán et al., 1990).

Carbonate contents were measured by weight loss after HCL treatment and range between 2.4 to 95% (Tab. 6-5). By XRD analyses, changing proportions of coexisting calcite and dolomite were detected. Samples 991914, -29, -31, -32, and -35 contain dolomite; samples 991919, -28, and –36 calcite and samples 991921, -24, and -30 different proportions of both phases. The carbon isotope composition of the organic matter was determined for most of the samples. $\delta^{13}C$ values range from –26.63‰ to –19.41‰ with a median of –22.52‰ (Tab. 6-5). From an average $\delta^{13}C$ value of –25.4‰ in samples from the Itararé and Tatui Formation, $\delta^{13}C$ values increase to approximately –20‰ in the Assistencia Member.

| Fm./Mbr. | Sample | $C_{org}$ [wt%] | S [wt%] | C/S | $\delta^{13}$Corg [‰ PDB] | Carb. [%] | $\delta^{13}$C(cc) [‰ PDB] | $\delta^{13}$C(dol) [‰ PDB] | PI | $T_{max}$ | SOM yield [mg/g $C_{org}$] | $\Sigma$n-$C_{12-20}$/ $\Sigma$n-$C_{12-29}$ | CPI (n-$C_{12-20}$) |
|---|---|---|---|---|---|---|---|---|---|---|---|---|---|
| **S. Alta** | **991914** | 0,08 | 0,01 | 11 | -23,46 | 48 | | -3,28 | | | | | |
| **S. Alta** | **991915** | 0,21 | 0 | | -23,38 | 12 | | | | | 78 | 0,27 | 1,10 |
| **S. Alta** | **991916** | 0,15 | 0,00 | 41 | -21,86 | 9 | | | | | | | |
| **S. Alta** | **991917** | 0,12 | 0 | | -22,46 | 9 | | | | | | | |
| **S. Alta** | **991918** | 0,03 | 0 | | | 13 | | | | | | | |
| **Ass.** | **991919** | 0,01 | 0,01 | 1,9 | | 73 | 0,23 | | | | | | |
| **Ass.** | **991920** | 0,36 | 0,04 | 10 | | 20 | | | 0,93 | 380 | 34 | 0,71 | 1,15 |
| **Ass.** | **991921** | 0,89 | 0,40 | 2 | -20,76 | 88 | 10,29 | 12,34 | 0,31 | 419 | 360 | 0,56 | 1,30 |
| **Ass.** | **991922** | 3,35 | 4,55 | 0,7 | -20,31 | 11 | | | 0,49 | 392 | | | |
| **Ass.** | **991923** | 2,03 | 2,23 | 0,9 | -21,3 | 17 | | | 0,90 | 401 | 58 | 0,74 | 1,29 |
| **Ass.** | **991924** | 1,14 | 0,33 | 3 | -21,12 | 85 | 11,32 | 13,15 | 0,32 | 418 | 435 | 0,60 | 1,46 |
| **Ass.** | **991925** | 0,06 | 0,95 | 0,1 | | 26 | | | | | 149 | 0,64 | 1,23 |
| **Ass.** | **991926** | 0,81 | 0,71 | 1,1 | -19,41 | 29 | | | 0,95 | 391 | 29 | 0,95 | 1,31 |
| **Ass.** | **991927** | 1,20 | 0,70 | 1,7 | -20,13 | 33 | | | 0,84 | 357 | 21 | 0,91 | 1,20 |
| **Ass.** | **991928** | 0,22 | 0,08 | 2,8 | n.d. | 70 | 7,60 | | 0,96 | 318 | | | |
| **Ass.** | **991929** | 0,59 | 0,25 | 2 | -22,41 | 87 | | 1,48 | 0,40 | 406 | 298 | 0,49 | 1,23 |
| **Ass.** | **991930** | 0,23 | 0,07 | 3 | -22,52 | 93 | 1,21 | 1,17 | 0,41 | 421 | 225 | 0,33 | 1,11 |
| **Ass.** | **991931** | 0,89 | 0,50 | 1,8 | -23,3 | 78 | n.d. | -3,31 | 0,58 | 399 | 417 | 0,46 | 0,90 |
| **Ass.** | **991932** | 1,88 | 1,45 | 1,3 | -25,01 | 63 | n.d. | -3,31 | 0,52 | 397 | | | |
| **Ass.** | **991933** | 0,86 | 0,03 | 31 | -21,09 | 29 | | | 0,16 | 419 | 81 | 0,73 | 2,27 |
| **Ass.** | **991934** | 0,16 | 0,03 | 5,7 | | 2 | | | | | | | |
| **Ass.** | **991935** | 0,29 | 0,02 | 13 | -21,84 | 73 | | -11,34 | 0,16 | 423 | | | |
| **Ass.** | **991936** | 0 | 0 | | | 95 | -8,45 | | | | | | |
| **Ass.** | **991937** | 0,02 | 0,23 | | | 10 | | | | | | | |
| **Taqu.** | **991938** | 0,26 | 0,10 | 2,7 | -23,45 | 11 | | | | | 41 | 0,25 | 1,00 |
| **Taqu.** | **991939** | 0,56 | 1,11 | 0,5 | -26,63 | 11 | | | 0,16 | 409 | 60 | 0,51 | 1,04 |
| **Tatui** | **991940** | 0,06 | 0,33 | 0,2 | -25,72 | 9 | | | | | | | |
| **Tatui** | **991941** | 0,05 | 0,50 | 0,1 | -24,69 | 11 | | | | | | | |
| **Tatui** | **991942** | 0,06 | 0,01 | 10 | -26,03 | 6 | | | | | | | |
| **Tatui** | **991943** | 0,04 | 0 | | | 6 | | | | | | | |
| **Itararé** | **991944** | 0,07 | 0 | | -24,67 | 3 | | | | | | | |
| **Itararé** | **991945** | 0,03 | 0,01 | 3,2 | | 4 | | | | | | | |
| **Itararé** | **991946** | 0,01 | 0 | | | 6 | | | | | | | |

**Table 6-5**

S. Alta = Serra Alta Mbr., Ass. = Assistencia Mbr., Taqu. = Taquaral Mbr.; Sample number; Organic carbon ($C_{org}$), sulphur (S) content in weight %; C/S ratios; Carbon isotope composition of calcites and dolomites denoted as $\delta^{13}C_{carb.}$ and $\delta^{13}C_{dol.}$; Rock Eval pyrolysis: production index (PI = $S_1/(S_1+S_2)$ and $T_{max}$; Soluble organic matter (SOM) yield; short to long chain n-alkane ratio of the interval $C_{12}$ to $C_{20}$ versus $C_{12}$ to $C_{29}$; carbon preference index (CPI) in the range of n-$C_{12}$ to n-$C_{20}$.

In figure 6-26 $\delta^{13}C_{org}$ values are displayed together with $\delta^{13}C$ values of calcites and dolomites from the interspersed carbonate layers. All three trends simultaneously shift to higher $\delta^{13}C$ values during the lower to middle Assistencia Member. Maximum values are reached in the upper-middle Assistencia Member. In the upper sequence $\delta^{13}C$ values decrease to –2‰ in the carbonates and to –23.5‰ in the organic matter. The parallel shift of the carbon isotopic composition of the carbonates and organic matter can certainly not explained by changes in $pCO_2$ because of the high amplitude of more than 20‰ in the carbon isotopic composition of the carbonates. Beside changes in type of organic matter also post sedimentary processes can alter the $\delta^{13}C$ of the organic matter. Thus, diagenetic processes have possibly caused changes of the $\delta^{13}C$ values in the organic matter as well as in the carbonates.

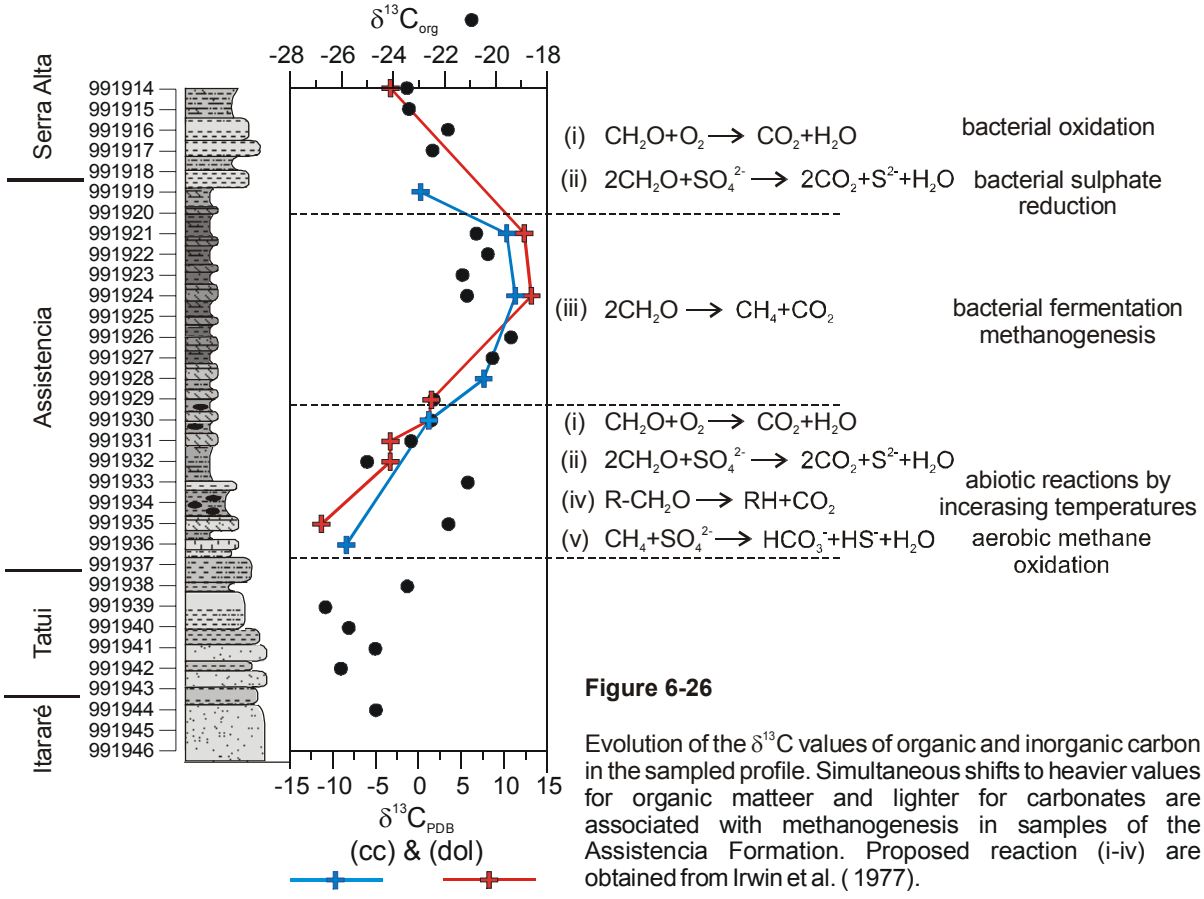


**Figure 6-26**

Evolution of the $\delta^{13}C$ values of organic and inorganic carbon in the sampled profile. Simultaneous shifts to heavier values for organic matteer and lighter for carbonates are associated with methanogenesis in samples of the Assistencia Formation. Proposed reaction (i-iv) are obtained from Irwin et al. ( 1977).

Irwin et al. (1977) described different alteration processes of organic matter, which can be preserved in $\delta^{13}C$ values of diagenetic carbonates. Changing carbon isotope composition of carbonates is explained by generation of $CO_2$ from (i) bacterial oxidation processes of organic matter, (ii) bacterial sulphate reduction, (iii) bacterial fermentation, (iv) thermally-induced decarboxylation and (v) aerobic methane oxidation (reactions are shown in figure 6-26). Especially bacterial fermentation of organic matter produces very heavy $CO_2$ since

bacterial generated methane yields typically very low $\delta^{13}C$ value between -110 and -50‰ (Hoefs, 1997). Irwin et al. (1977) estimated the $\delta^{13}C$ value of the bacterial generated $CO_2$ to be approximately +15‰. By isotope exchange reactions between the original carbonates ($\delta^{13}C \approx 0$‰) and the heavy $CO_2$, the $\delta^{13}C$ values of the carbonates dramatically increase as documented in the $C_{org}$ rich upper-middle Assistencia Member (Fig. 6-26). Light $\delta^{13}C$ values of the carbonates in the upper section possibly derived from bacterial induced sulphate reduction and/or oxidation processes of organic carbon. The enrichment of $^{12}C$ in the carbonates of the lower section can also be explained by reduction or oxidation processes or by $CO_2$ generation from decarboxylation reaction. The rate of this abiotic reaction presumably increases with rising temperatures (Irwin et al., 1977).
De Giovani et al. (1974) documented from the Paraná Basin comparable isotope shifts to light and heavy $\delta^{13}C$ values. They concluded that all investigated samples were altered in their isotopic composition and chemistry.

## 6.9.2 Rock Eval pyrolysis and soluble organic matter yield

The Rock Eval pyrolysis provides general information on the type of organic matter. Detailed description of the method is given by Peters (1986). Hydrogen- (HI) and oxygen-index (OI) are used as parameters to identify different organic facies. The data can be plotted in a modified van Krevelen diagram to determine the type of organic matter. Due to absorption of organic matter at clay minerals, mixtures of minerals with organic carbon produces much lower HI-values, different OI-values and higher $T_{max}$-values than pure organic matter (Espitalie, 1980; Langford and Blanc-Valleron, 1990 and Littke, 1993). The effect of absorption of hydrocarbons by the mineral matrix is significant in samples with $C_{org} < 0.5\%$ (Peters, 1986). The most pronounced effect by the clay mineral matrix for retaining hydrocarbons was observed in illite rich samples. Espitalié et al. (1984) pointed out that the level of absorption cannot simply be related to the major mineralogical type. Some minor constituents, such as metal hydroxid/oxide coatings, may also affect the absorption capacity of the mineral matrix. $T_{max}$ and the production index [$PI = S_1/(S_1+S_2)$] reveal information on the maturity of the organic matter, since both parameters rise with increasing maturity (Espitalié et al., 1988). If samples of equal maturity are compared, $T_{max}$ can also be influenced by the type of organic matter in consequence of different bond strengths in particulate organic matter and increases from type III to type I kerogen (Peters, 1986). Migrated oil affects the $S_2$ and $T_{max}$ of the kerogen (Clementz et al., 1979). Low $T_{max}$ temperatures (less than 435°C) versus high PI values (above 0.3) point to impregnation and contamination by migrated hydrocarbons (Peters, 1986).
In contrast to the relative immature and $C_{org}$ rich samples from the Witbank Basin low $C_{org}$

contents, changing lithology (clay minerals vs. carbonates), advanced thermal maturation and migration of hydrocarbons influenced the Rock Eval analyses of the samples from the Paraná Basin.

The modified van Krevelen diagram in figure 6-27a is used for typifying the kerogen. The kerogen of most of the samples can be classified as type I and II, pointing to marine/sapropelic organic matter. Organic matter in samples from the lower Assistencia Member, between kerogen type II and III, possibly indicate elevated input of terrigenous material. In general, the results obtained from the Rock Eval pyrolysis fit with literature data. Immature organic matter of the upper Assistencia Member in the eastern Paraná Basin is identified by Zalan et al (1990) as kerogen type I, where as the Taquaral and Serra Alta Members contain kerogen type III. Anomalous high PI values from 0.16 to 0.96 with a median of 0.49 point to advanced maturation of the organic matter and/or to migrated hydrocarbons (Tab. 6-5). $T_{max}$ temperatures range between 318 to 423°C (median is 401°C). The negative correlation of $T_{max}$ versus high production indices (Fig. 6-27b) indicates impregnation and contamination by migrated hydrocarbons.

The amount of soluble organic matter (SOM) is given in table 6-5. Extraction yields vary between 21 and 455 mg/g $C_{org}$ with a median value of 80 mg/g $C_{org}$. Bitumen contents above 65 mg/g $C_{org}$ are associated with mature source rocks or reservoirs containing migrated hydrocarbons (Tissot and Welte, 1984). Highest extraction yields are reached in the dolomitised carbonates of the Assistencia Member with a median value of 330 mg/g $C_{org}$. In

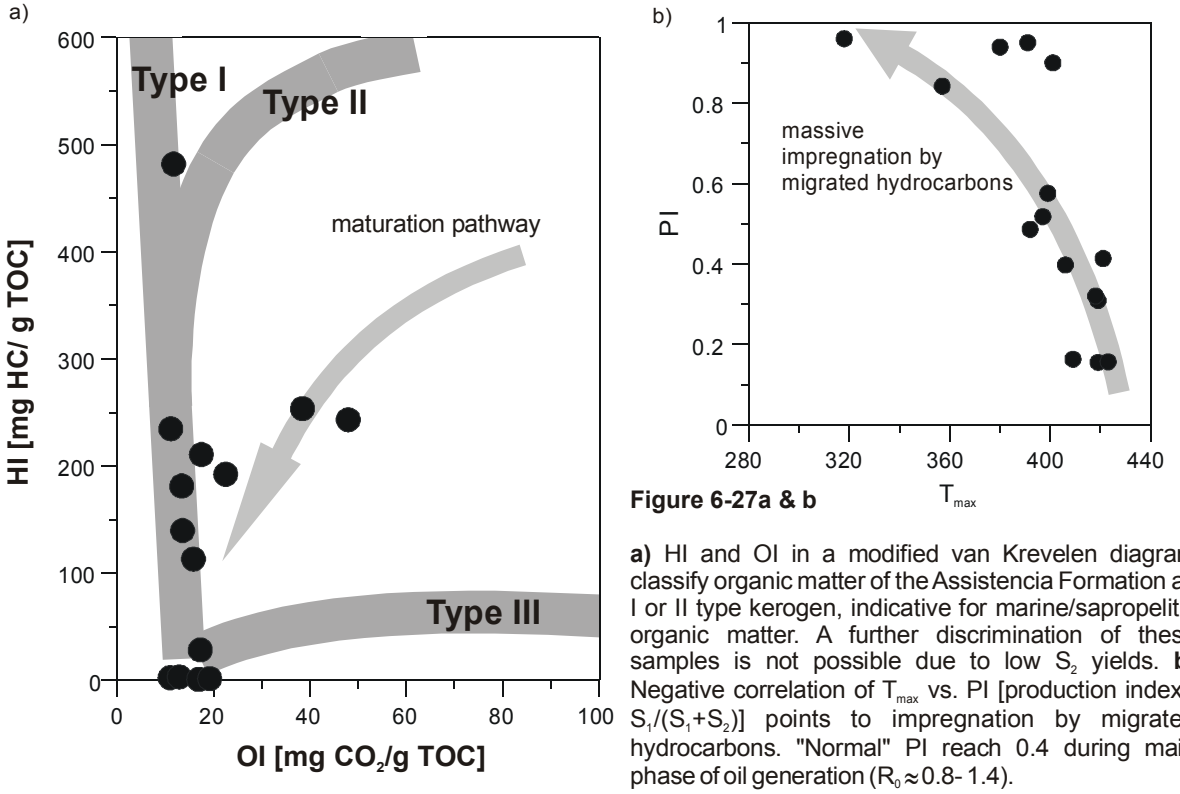


**Figure 6-27a & b**

**a)** HI and OI in a modified van Krevelen diagram classify organic matter of the Assistencia Formation as I or II type kerogen, indicative for marine/sapropelitic organic matter. A further discrimination of these samples is not possible due to low $S_2$ yields. **b)** Negative correlation of $T_{max}$ vs. PI [production index= $S_1/(S_1+S_2)$] points to impregnation by migrated hydrocarbons. "Normal" PI reach 0.4 during main phase of oil generation ($R_0 \approx 0.8$- 1.4).

the other samples extraction yields reach approximately 54 mg extract/g $C_{org}$. The high extraction yields in the dolomites of the Assistencia Member corroborate the assumption that massive migration processes took place during burial diagenesis and altered the primary signals of the organic matter.

However, by the results obtained so far from elemental and carbon isotope analyses, Rock Eval pyrolysis and extraction yield, the following assumptions can be made. The primary composition of the organic matter was altered during post sedimentary processes by bacterial degradation and elevated temperatures during burial diagenesis. Generated hydrocarbons were mobilised and migrated into the carbonates. Despite of partly massive alteration of the primary composition of the organic matter, the kerogen of the organic matter of the Assistencia Member can be classified as type I or II. Presumably unaltered $\delta^{13}C$ values of the organic matter in the samples from the Itararé Group and Tatui Formation point to elevated supply of terrigenous organic matter.

## 6.9.3 Saturated fraction

From gas chromatograms of aliphatic hydrocarbon fraction further information about type of organic matter as well as insights to maturation and migration processes can be obtained. The n-alkane distribution of long versus short-chain n-alkanes is expressed as $\Sigma$n-$C_{12-20}$/$\Sigma$n-$C_{12-29}$ (Fig. 6-28a and table 6-5).

The high variability of 0.67 in this ratio points to changing sedimentary conditions or to postsedimentary alteration processes. Highest values of 0.95 and 0.91, respectively, are reached in the black marls of the Assistencia Member (samples 991926 and 991927). Most samples plot around a median of 0.67, indicating the predominance of short-chain n-alkanes. A predominance of long-chain n-alkanes is indicated by ratios below 0.5 in sample 991938 (0.25) from the base and in sample 991915 (0.27) from the top of the sequence. In general, the preference of short-chain n-alkanes increases from a median value of 0.48 in the Taquaral and lower Assitencia Member, to 0.64 in the middle to upper Assistencia Member. It is questionable if the positive correlation of $\Sigma$n-$C_{12-20}$/$\Sigma$n-$C_{12-29}$ vs. $\delta^{13}C_{org}$ indicates changing supply of different organic matter (Fig. 6-29) or again is controlled by impregnation.

In general, high $\delta^{13}C$ values and predominantly short-chain n-alkanes point to algal derived organic matter, whereas organic matter with lower $\delta^{13}C$ values and long-chain n-alkanes refer to terrigenous sources. The original $\delta^{13}C$ values of the organic matter seems to be altered in consequence of bacterial activity as discussed in figure 6-26. Thus, the observed correlation between both parameters must not necessarily indicate changes of the organic matter but may also reflect postsedimentary alteration.

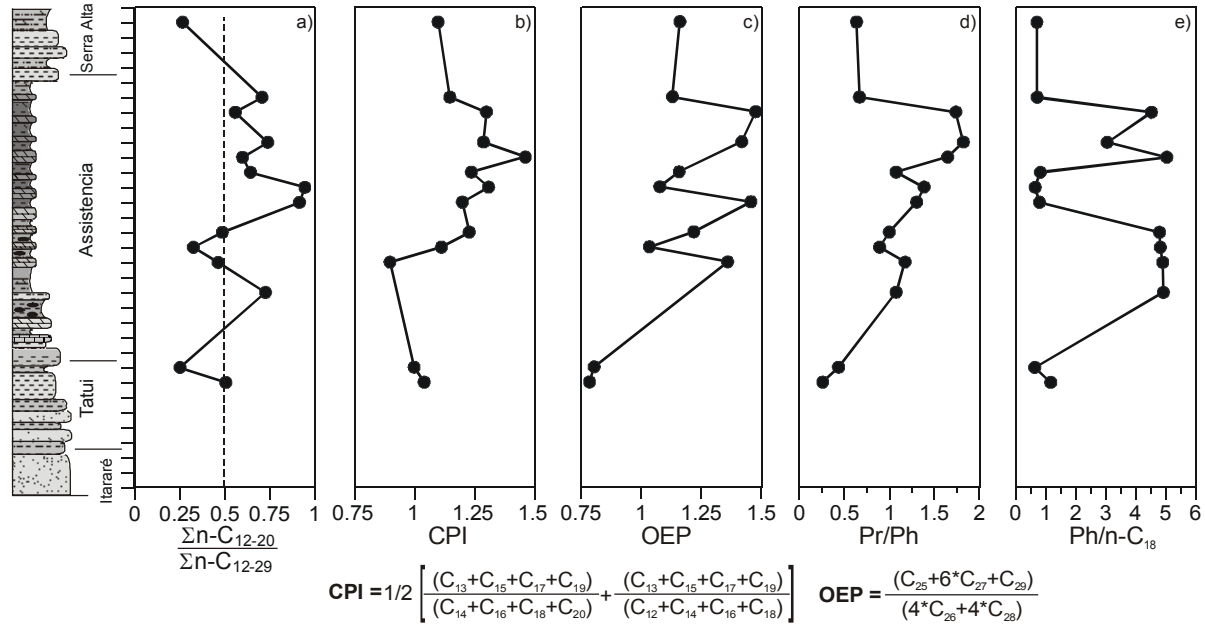


**Figure 6-28a-e**

Facies evolution of late glacial and postglacial sediments in the northern Paraná Basin. Grey scale in the simplified lithology indicates increasing to the $C_{org}$ contents. **a)** Ratio of short to long-chain n-alkanes from carbon number $C_{12}$ to $C_{29}$. **b)** modified carbon preference index after Bray and Evans (1961); **c)** odd over even preference in the interval n-$C_{25}$ to n-$C_{29}$ after Scalan and Smith (1970); **d)** pristane vs. phytane ratio denoted as Pr/Ph is possibly influenced by bacterial activity; **e)** low phytane/n-$C_{18}$ ratios in the middle Assistencia Mbr. label samples which are influence by migrated hydrocarbons.


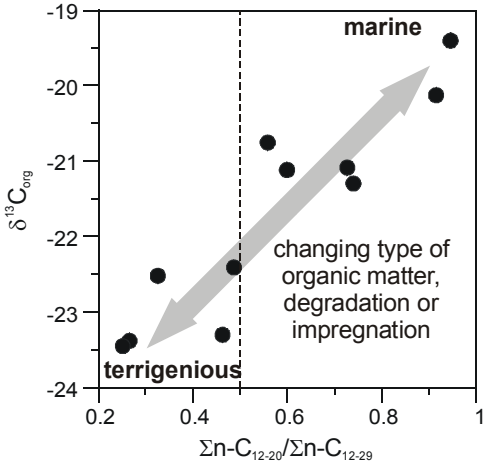


**Figure 6-29**

Relationship between n-alkane distribution and carbon isotopic composition of $C_{org}$ possibly indicates supply of organic matter from different sources (marine vs. terrigenous).

Since the most samples contain predominantly short-chain n-alkanes, the carbon preference index (CPI) after Bray and Evans (1961) of the interval n-$C_{12}$ to n-$C_{20}$ was calculated (Tab. 6-5). The CPI increases from approximately 0.95 up to 1.4 in the upper-middle Assistencia Member (Fig. 6-28b). At the top of Assistencia Member and in the Serra Alta Member the CPI decreases again. In the interval of carbon numbers $C_{25}$ to $C_{29}$ the odd over even predominance is calculated After Scalan and Smith (1970) (Fig. 6-28c). In samples from the Taquaral Member, values below 1 point to the predominance of even numbered n-alkanes. In the upper part of the section the OEP increases. The saw-toothed pattern with OEP values

between 1.01 and 1.5 possibly indicates changing type of organic matter or advanced biodegradation in samples with OEP close to one. From correlation studies of oil and source rocks, Tissot and Welte (1984) concluded that oils from carbonates predominantly exhibit even-chain n-alkanes in the range of n-$C_{22}$ to n-$C_{30}$. Oils generated in shales contain predominantly odd numbered n-alkanes in the same interval. In the samples of the Paraná Basin, no relationship between rock type and OEP can be detected. Due to the predominance of odd numbered n-alkanes, the shales can be assumed as source rocks of the soluble organic matter. Thus, local migration of hydrocarbons from the shales into the carbonates during diagenesis may have occurred.

The isoprenoids i-$C_{19}$ (pristane) and i-$C_{20}$ (phytane) are assumed to be mainly diagenetic products of the phytylic side chain of chlorophyll, although alternative sources of precursors are known to occur (ten Haven et al., 1987). The ratio is usually used to distinguish between oxic (> 1) or anoxic (< 1) depositional environment conditions. Ten Haven et al. (1987) pointed out that the ratio might preferentially serve as palaeosalinity indicator in hypersaline depositional environments. Hughes et al. (1995) show that Pr/Ph-ratios < 1 indicate marine conditions, whereas ratios >3 characterise terrestrial input. Ratios between 1-3 represent marine or lacustrine environments. In figure 6-28d the Pr/Ph-ratio shows a relative constant rise from 0.25 up to 1.8 in the upper Assistencia Member. Low Pr/Ph values of around 0.6 characterize the Serra Alta Member.

Assuming that the Pr/Ph ratios are not altered during diagenesis the increasing ratios would point to elevated input of vascular plants and/or to an oxic environment during deposition of the upper Assistencia Member. Since deposition of the organic carbon and sulphur rich shales and carbonates of the Assistencia Member required anoxic conditions, the Pr/Ph ratio cannot be used as redox proxy.

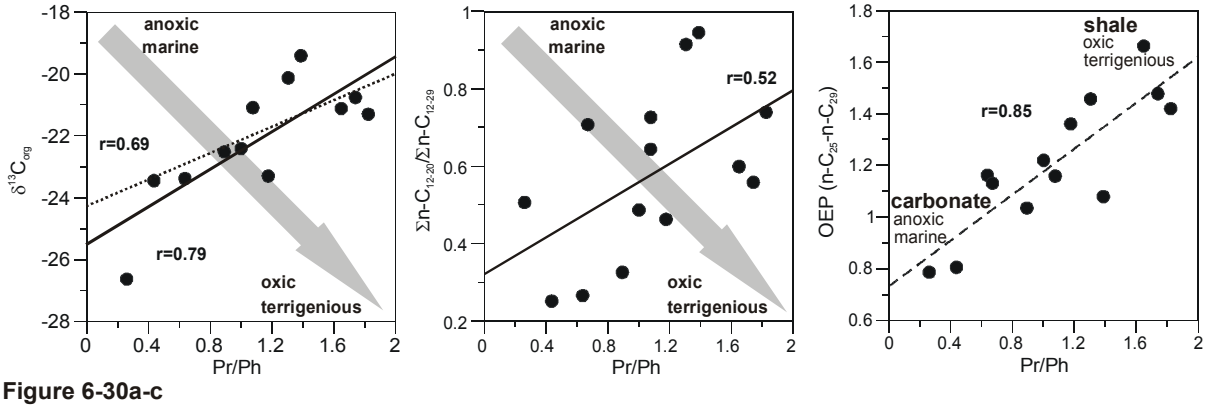


**Figure 6-30a-c**

Bivariate plots of Pr/Ph ratios versus **a)** $\delta^{13}C_{org}$ values **b)** n-alkane distribution indicate that diagenetic alterations of the organic matter mask the primary source signal (marine or vascular plants). **c)** Significant correlation of Pr/Ph vs. OEP can be rather attributed to changing lithology than to changing sedimentary environments.

In figure 6-30a & b the grey arrows mark the expected general trend, if the used parameters were solely influenced by changing supply of marine or vascular plants. In fact, the correlation between Pr/Ph versus $\delta^{13}C$ values of the organic matter (***r*** = 0.69 and 0.79, respectively), and versus $\Sigma$n-$C_{12-20}$/$\Sigma$n-$C_{12-29}$ (***r*** = 0.52) point to additional processes, which altered the primary composition of the organic matter. The correlation between Pr/Ph ratios and the OEP in the range from n-$C_{25}$ to n-$C_{29}$ (***r*** = 0.85) seems to indicate changing type of organic matter (Fig. 6-30c). Besides changing kerogen type and/or Eh/pH conditions, Pr/Ph ratio can also be influenced by the lithology. Moldowan et al. (1985) indicate that Pr/Ph ratios < 1 point to carbonate source rocks whereas ratios > 1 are associated with hydrocarbons derived from shales. Thus, the correlation in figure 6-30c indicate, that the saturated hydrocarbon composition in samples from the Assistencia Member is rather influenced by the lithology than by changing kerogen type.

A noticeable trend can be observed in the Phytane/n-$C_{18}$ ratio. The depth curve reveals a minimum of values in the middle Assistencia Member. The same samples have very low hydrogen indices (HI) around 5 [mg HC/g $C_{org}$], which points towards impregnation by migrated hydrocarbons. This is also evident from $S_1$-yields between 0.15-0.25 mg HC/g rock and production indices of above 0.8.

As shown in figure 6-26, the organic matter of the Assistencia Member was altered by bacterial degradation processes. Furthermore, high production indices, high extraction yields and low Pr/n-$C_{18}$ ratios in single samples refer to impregnation processes, which altered also the primary hydrocarbon composition/distribution. Thus, estimations about different types of organic matter (algae vs. vascular plants) and simultaneous changes in the sedimentary environment (marine vs. lacustrine/deltaic) are quite difficult, especially for samples of the Assistencia Member. In fact, the composition of the saturated hydrocarbon fraction is related with the lithology as indicated by cluster analyses in the dendrogram of figure 6-31. For cluster analyses the n-alkanes in range n-$C_{10}$ to n-$C_{38}$, pristane and phytane were used. Depending on their n-alkane and isoprenoid distribution the samples are combined in single clusters. In the dendrogram three main branches can be discerned. Carbonate free samples (Mg+Ca/Si+Al < 0.1) from the Taquaral (991939 & -39) and Serra Alta Member are combined due to the predominance of long-chain or bimodally distributed n-alkanes (sample 991915 and 991939 in Fig. 6-32a & b). The n-alkane distribution in range from n-$C_{10}$ to n-$C_{30}$ and n-$C_{13}$ to n-$C_{30}$, indicate a partially strong input of terrigenous organic matter.

The branch of samples 991926 and –27 comprises dolomitic shales (Mg+Ca/Si+Al < 1) with predominantly short-chain n-alkanes ($\Sigma C_{12-20}/\Sigma C_{12-29}$ in figure 6-28a is above 0.9). Beside n-alkanes, which maximise in the range of n-$C_{11}$ to n-$C_{15}$, the samples contain elevated proportions of short-chain isoprenoids from i-$C_{14}$ to i-$C_{20}$ (sample 991927 in figure 6-32c). Eglinton (1972) indicate that i-$C_{14}$ to i-$C_{20}$ isoprenoid hydrocarbons can be generated from

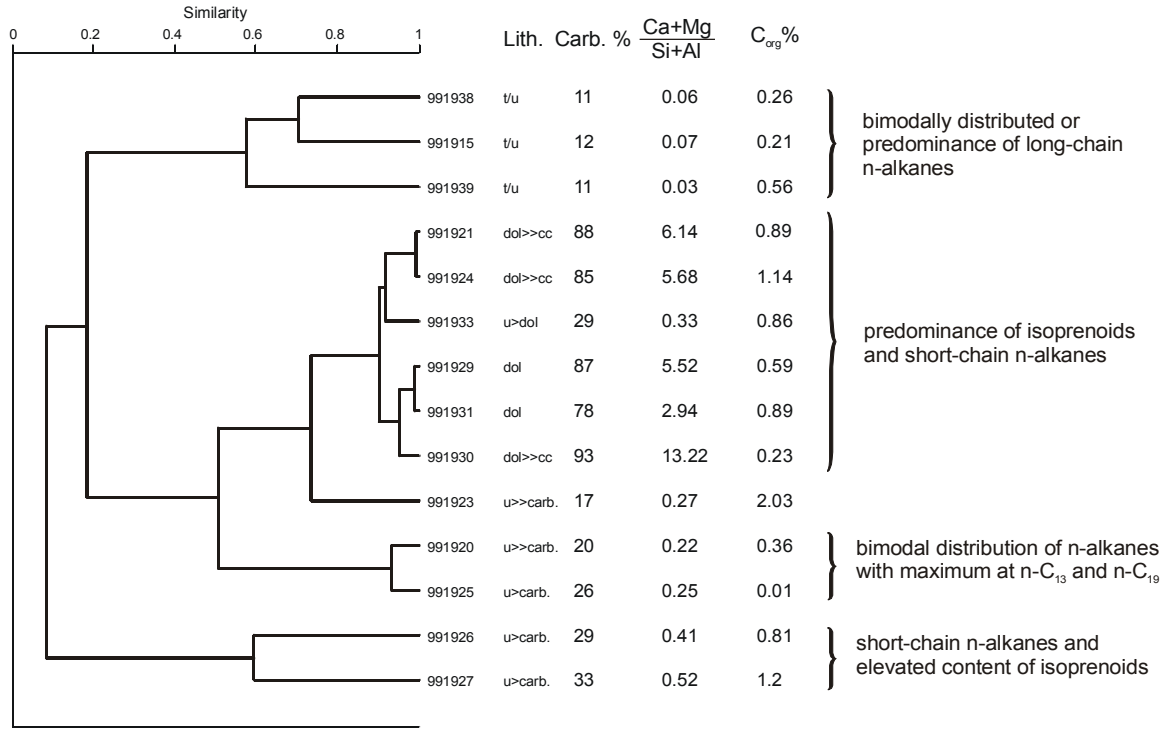


**Figure 6-31**

Cluster analyses of selected samples from the northern Paraná Basin discriminate the samples with regard to lithology and n-akane distribution. 14 variables, 31 cases, distance matrix: correlation coefficient, amalgamation schedule: unweighted pair-group average.

phytol by heating it in the presence of clays. The absence of the $C_{17}$ homologue can be explained by the fact that its formation would require the cleavage of two C-C bonds near the functionalised end in the $C_{20}$ skeleton (Chaffee et al., 1986). Degradation of phytol by marine bacteria is a further source of short-chain isoprenoids (Gillian et al., 1983). Some species of Archaea, including halophiles and methanogens, contain saturated and unsaturated acyclic isoprenoid hydrocarbons in chain-length from $C_{14}$ to $C_{30}$ (Volkman and Maxwell, 1986). Since the changes in the carbon isotope composition of the carbonates and organic matter are triggered by intensive bacterial activity and methanogenesis (Fig. 6-26), the elevated contents of isoprenoids indicate the presence of methanophile Archaea.

The third cluster is composed of two smaller branches. The major cluster combines the samples 991921, -24, -33, -29, -31 and –30. The carbonate contents exceeding 78wt% and (Mg+Ca)/(Si+Al) ratios are above 2. Exception is a carbonatic shale (sample 991933) with carbonate contents of approximately 30wt% and a (Mg+Ca)/(Si+Al) ratio below 0.5. From XRD analyses, dolomite is the main carbonate mineral phase in these samples. The gas chromatograms of these samples are dominated by short-chain isoprenoids and by high pristane and phytane concentrations (Fig. 6-27d & e). A similar distribution of the saturated fraction as in sample 991929, was recovered in oils from the Rio Bonito Formation in the southern part of the Paraná Basin (Zalán et al., 1990). By oil-to-source correlation, Zalán et al. (1990) suggested that the Irati shales were the source rocks of these oils. Comparable to

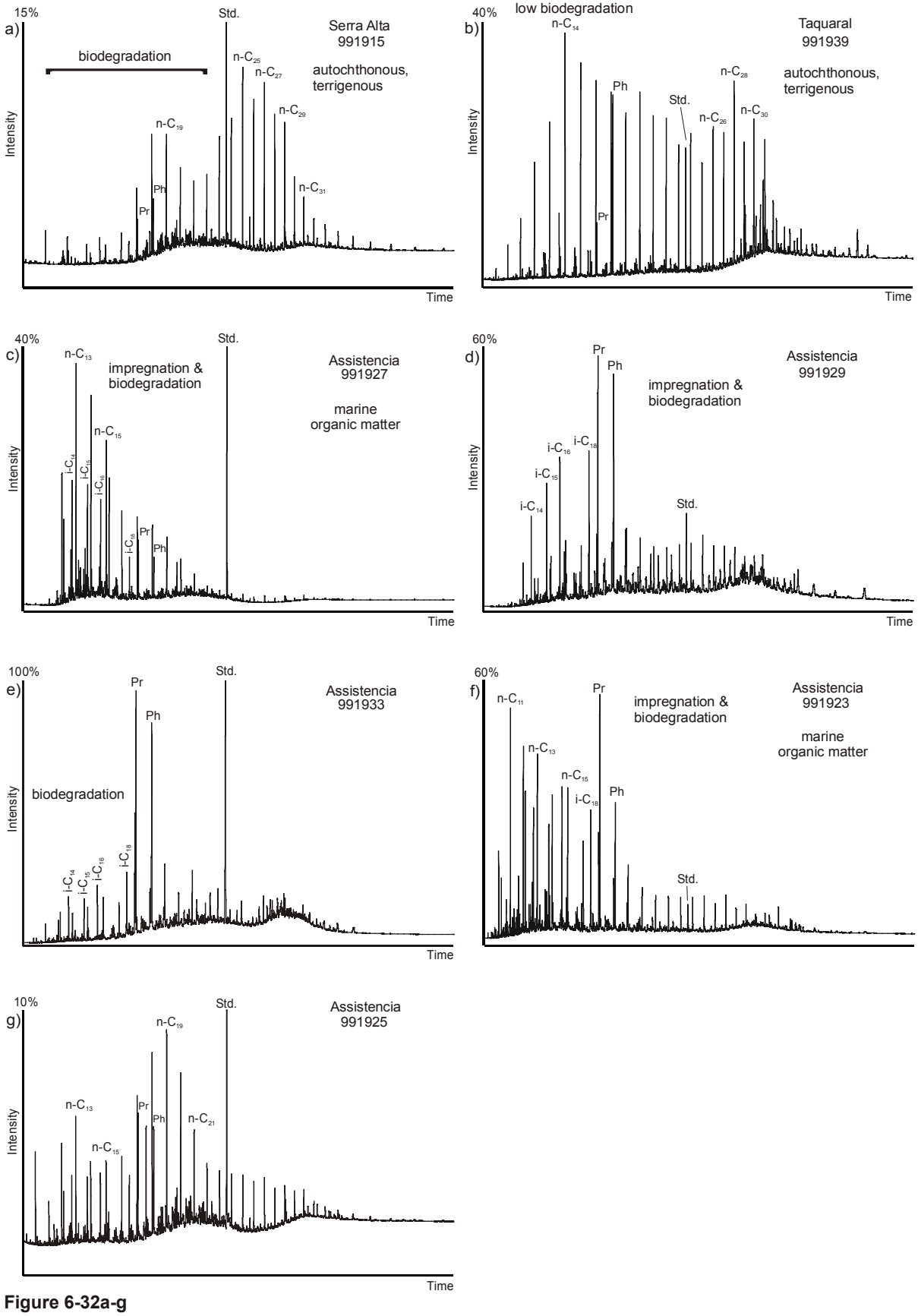


**Figure 6-32a-g**

Lipid distribution in carbonates, marls and carbonate bearing shales of the Irati Formation of the northern Paraná Basin. N-alkanes indicated by carbon number as n-$C_x$, isoprenoids as i-$C_x$ and pristane and phytane as Pr and Ph, respectively.

the gas chromatogram of sample 991933 (Fig. 6-32e), the saturated fraction of the Irati shales is dominated by high pristane and high phytane contents.

Sample 991923, a carbonatic shale (Mg+Ca/Si+Al < 0.5), is amalgamated next to the latter cluster (Fig. 6-31). The n-alkane distribution is dominated by short-chain n-alkanes, similar to the samples 991927 and –26. High pristane and phytane concentrations point to a closer affinity to the dolomitic samples of the major cluster (Fig. 6-32f). In the carbonatic shales of samples 991920 and -25 normal alkanes from n-$C_{11}$ to n-$C_{31}$ can be identified. The distribution maximises around carbon numbers $C_{13}$ and $C_{19}$. Short-chain isoprenoids are high but do not dominate the n-alkanes.

## 6.9.4 Discussion and conclusion

Results from element analyses, carbon isotopy, Rock Eval pyrolysis and lipid biomarker investigations reveal different information about depositional environment and postsedimentary alteration of the organic matter. Especially the organic matter composition in samples of the Assistencia Member was massively influenced by diagenesis. Thus, the interpretation of the data with regard to changes of the depositional environment is problematic.

Changes in vegetation, demonstrated by micro and megafloral remains in the Itararé Formation, are associated with the transition from cold to temperate conditions (Martini and Rocha-Campos, 1991). After the final retreat of glaciers, the predominantly continental deposits of the lower Itararé Formation became marine towards the top (Santos et al., 1996). The postglacial deposits of the Tatui Formation, including the Rio Bonito and Palermo Members, are interpreted as deltaic sandstones. The molecular information obtained from this part of the succession is relative sparse due to very low $C_{org}$ contents of around 0.05wt%.

The carbon isotope composition of the organic matter in samples from the lower (Itararé & Tatui Formation) succession varies around -25‰. High $\delta^{13}C$ values (-20 to –25‰) are commonly associated with marine organic matter, whereas lower values (-22 to –30‰) indicate the supply of vascular plants (Meyers, 1997). Thus, an identification of the organic matter in the Itararé & Tatui Formation based exclusively on carbon isotope composition is not certain. Bimodally distributed or predominantly long-chain n-alkanes ($\Sigma C_{12\text{-}20}/\Sigma C_{12\text{-}29}$ is 0.51 and 0.25, Tab. 6-3) point to a partly terrigenous sources of the organic matter (Fig. 6-32b). This assumption is in accordance with the alluvial-deltaic-coastal sedimentary environments, which are assumed for the upper Itararé and lower Tatui Formation (Martini and Rocha-Campos, 1991).

The further evolution of the depositional environment was characterized by a continuously rising sea level, evidenced by the shelf-related sediments of the upper Tatui Formation (Zalán et al., 1990). Maximum marine conditions were reached during deposition of the Irati

Formation. Fine laminated, bituminous, pyrite-bearing shales and carbonates point to anoxic and $H_2S$ bearing bottom waters. The formation of anoxic conditions was possibly favoured by a stratified and stagnant water column in a marine or through like sedimentary environment of the northern Paraná Basin. Environmental proxies from the organic matter of the Assistencia Member were massively influenced by microbial decomposition and hydrocarbon migration. The relative high $\delta^{13}C_{org}$ values of approximately –20.5‰ point to the supply of marine biomass. Whether methanogenesis and methane oxidation also altered the isotope composition of the organic matter, is questionable. However, the predominance of short-chain n-alkanes in the shales and carbonates is significant and indicates the predominant input of algal derived organic matter.

In the upper Irati Formation a regressive phase followed, associated with the gradual drying out of the Carboniferous-Permian epicontinental sea (Zalán et al., 1990). If the continuous increase of the Pr/Ph ratios point to elevated salinity in the upper Assistencia Member is questionable, since methanogenesis can also alter the isoprenoid content (De Leeuw et al., 1995).

$C_{org}$ contents in the Serra Alta Member decrease again. Thus, information about type of organic matter is rare. The recurring influence of terrigenous–deltaic sedimentary environments is possibly evidenced by decreasing $\delta^{13}C$ values of the organic matter to -23‰ (Fig. 6-21) and by the predominance of long-chain n-alkanes (Fig. 6-32a). Zalán et al. (1990) point out that marine conditions did not return in the following Palaeozoic time and Mesozoic sequences are strictly continental in nature.

The correlation of the Irati Formation (Paraná Basin) with the Whitehill Formation (Karoo Basin) was established by Oelofson and Araujo (1987). Beside palaeontological evidences by the distinct *mesosaurus* reptile fauna indicate the comparable lithology to a similar and time equivalent evolution of both units. Organic rich sales and carbonates represent the major lithology of both units. Furthermore occurring chert lenses in single horizons.

From Rock Eval data and elevated $\delta^{13}C_{org}$ values of samples from the Whitehill, Irati and Huab Formations (Namibia) Faure and Cole (1999) suggested that a temporary microbial bloom covered vast areas of the ancient sedimentary environment. In the overlying Formations, conditions rapidly became unfavourable as indicated by a change from oil shales containing type I kerogen to organic poor shales with kerogen type III.

# 7. Final summary and conclusion

The composition of sediments deposited under glacial and postglacial climate conditions in southern Gondwana basins was investigated to reconstruct climate and environmental conditions. Multiple geochemical investigations (element-geochemical, organic-geochemical and isotope data) were supported by mineralogical data. By this multi proxy approach, information about sedimentary environment and postsedimentary processes can be obtained (Figs. 7-1a-d).

Dependent on the sample locality, different processes modified the geochemical and mineralogical composition of the sediments. At the sample localities in the southern Karoo Basin, Carboniferous-Permian deposits were altered by migrated fluids from the rising Cape orogen. In the Kalahari Basin magmatic intrusions caused geochemical and mineralogical alteration in the postglacial sedimentary succession. Postsedimentary impregnation processes by saline fluids lead to dolomitization of the carbonates in the northern Paraná Basin.

However, climate changes and variation in the sedimentary environment are still detectable by combining suitable geochemical proxies. The element ratios of Zr/Ti, Rb/K, V/Cr as well as the CIA, $C_{org}$ content and $\delta^{13}C_{org}$ values provide a detailed view of the climatic and sedimentary evolution of the glacial-interstadial and postglacial phase in south Gondwana during the late Palaeozoic (Figs. 7-1a, b & d). Paired carbonate and organic carbon isotopes point to global changes in $pCO_2$ during glacial-interstadial phases during the Upper Carboniferous to lower Permian in southern Gondwana (Scheffler et al., 2003).

Beside changes in the element geochemical and mineralogical composition, postsedimentary processes also altered the hydrocarbon composition. Samples suitable for detailed biomarker analyses to reconstruct sedimentary environments and climate conditions were only available from the Witbank Basin. Variable proportions of marine versus terrestrial organic matter indicate recurring sealevel changes, which induced cyclicity of the climate conditions during the postglacial phase (Fig. 7-1c).

The general evolution of the Karoo Basin and adjacent areas from the Upper Carboniferous to late Permian can be described as follows:

Independent geochemical proxies reflect climate variations during deposition of stadial and interstadial phases of the Dwyka Group within the central Karoo Basin. During stadial phases, sea level lowstand caused sediment deposition under non-marine conditions, as indicated by sedimentological and palecological evidence (Visser, 1997) as well as by element geochemical proxies (Fig. 7-1a). Organic matter, however, deposited in distal

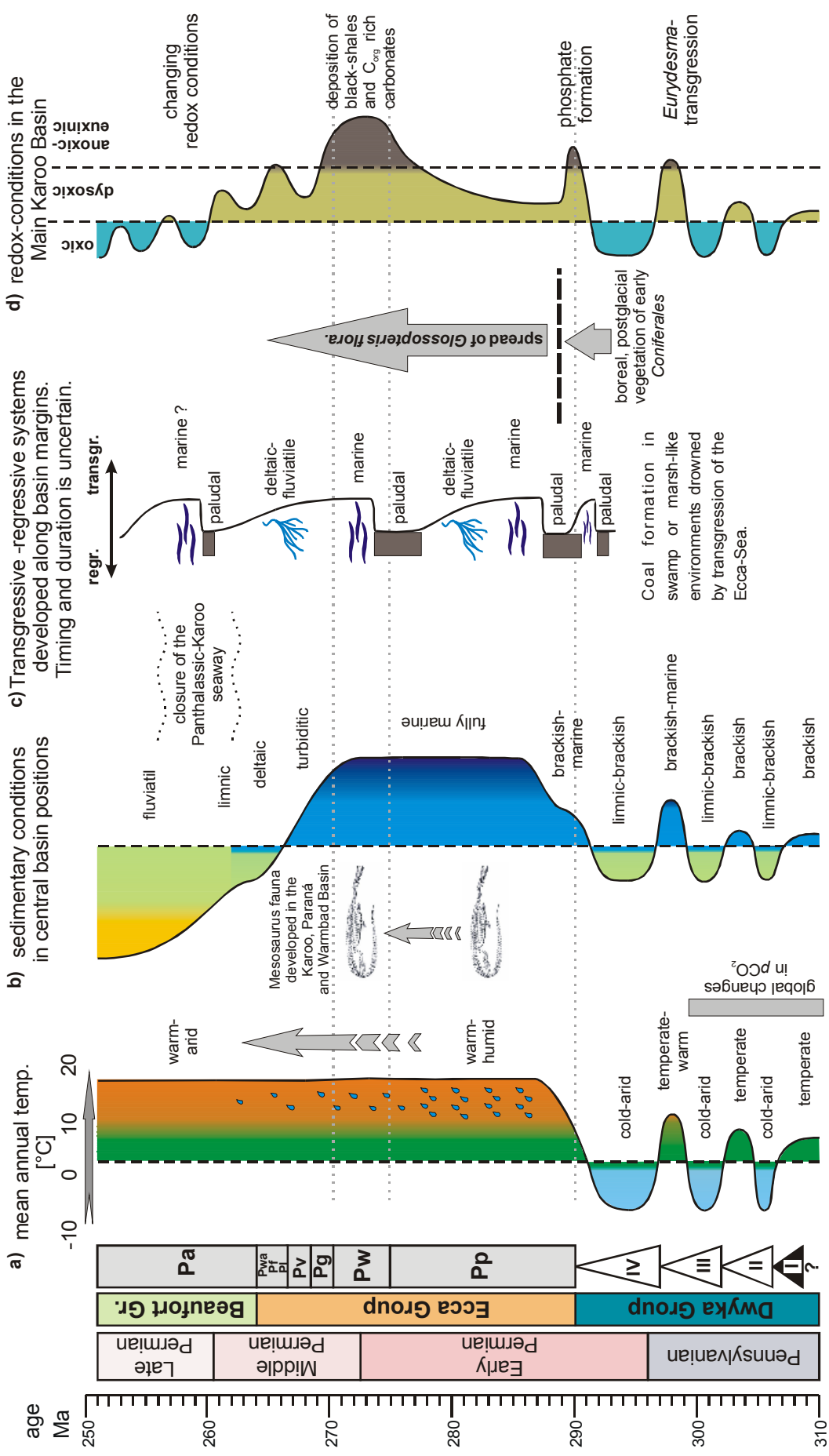


**Figure 7-1a-d**

Generalized evolution of sedimentary environments in the Main Karoo Basin during glacial and postglacial climate phases. Differences depend on specific conditions prevailing in local environments (i.e. distal vs. proximal settings). Pp=Prince Albert Fm., Pw=Whitehill Fm., Pg= Collingham Fm., Pv=Vischkuil Fm., Pl=Laingsburg Fm., Pf =Fort Brown Fm., Pwa= Waterford Fm. & Pa= Abrahamskraal Fm.

regions reveals no terrestrial influence as indicated by comparable aliphatic hydrocarbon distribution of organic matter from glacial versus interstadial sediments. During interstadial phases, sea level rose and marine conditions prevailed. Simultaneously, temperate climate conditions lead to increasing chemical alteration, elevated nutrient supply and thus to increasing bioproductivity. Elevated $C_{org}$ contents and V/Cr ratios in interstadial sediments refer to anoxic conditions in the local depositional environment of the southern Karoo Basin (Figs. 7-1a, b & d).

The global nature of regionally observed climate variations is documented by the simultaneous shifts in the $\delta^{13}C$ values of equatorial carbonates and the $\delta^{13}C$ values of organic carbon from the southern-latitude Karoo Basin. The ~5 m.y. periodicity in the duration of stadial-interstadial cycles does not fit any known orbital frequency. Furthermore, the periodicity is also not in tune with the duration of northern hemispheric cyclothems. The complete melting of an ice sheet covering an area of between 13.4 and 20.3 $*10^6$ $km^2$ would have correspond to a change in sea-level of between 60 and 100 m (Isbell et al., 2003). Different authors assume that waning and waxing of the glaciers during the late Palaeozoic caused sea-level fluctuations with amplitudes up to 200 meters (Wanless & Shepard, 1936; Crowell, 1978; Veevers & Powell, 1987; Ross & Ross, 1987). Cyclothems in North America and Europe (Ramsbottom, 1979; Heckel, 1986) are supposed to be associated with these glacioeustatic cycles. However, the relationship between cyclothems and fluctuations of glacial ice volume in South Gondwana is not evidenced. The absence of Gondwana cyclothems with comparable periodicity to the northern hemisphere cyclothems, and the general missing synchroneity between cyclothems and glaciation phases (Isbell et al., 2003), indicate that waning and waxing of Gondwana ice sheets were not exclusively responsible for the cyclic deposition phases in the northern hemisphere.

Glacial depocenters are inferred to have shifted across Gondwana as the continents drifted across the South Pole (Crowell, 1983; Caputo & Crowell, 1985; Isbell, 2003). The clockwise drift of the southern Gondwana continent can be regarded as the primary trigger for glaciation processes. This mechanism is, however, insufficient to explain the cyclic climate variations as well as the terminal and abrupt break down of the glaciation. Emergence and collapse of ocean-air circulation pathways, variable continent constellations, changing albedo rates and $pCO_2$ caused feedback mechanisms leading to a fragile climate system during the Upper Carboniferous alternating between glacial and interstadial phases. The final termination of the Carboniferous–Permian glaciation phase in southern Gondwana must be considered to have resulted from the interaction of different climate-controlling factors, including the continent-ocean configuration, and continental topography.

The onset of the postglacial phase is characterized by significant changes in sedimentary environments (Figs. 7-1a-d). Predominantly fully marine conditions prevailed and the

formation of anoxic conditions is indicated by the occurrence of $C_{org}$ rich sediments containing mineral phases such as apatite and pyrite (Fig. 7-1d). Comparable proxy signals are obtained from localities within the Karoo Basin and from the Warmbad Basin in Namibia. Especially the accumulation of phosphatic sediments points to high bioproductivity due to elevated nutrient supply. The elevated nutrient budget is associated with progressively increasing chemical weathering, whereby the leached elements acted as fertilizers.

At the basin borders, in terrestrially dominated sedimentary environments, the onset of postglacial climate conditions was recorded by significant changes in the organic matter composition (Fig. 7-1c). During the earliest phase after glacier retreat, tundra-type vegetation covered the glacial debris. The sub-polar climate was related to cold-arid conditions during short summers and long winters, with annual average temperatures of approximately -7°C. During the Upper Carboniferous, average temperatures must have raised to enable the production of sufficient biomass, which formed today's coal deposits. Boreal tundra type vegetation indicates mean annual temperatures of around 0°C. The Dwyka/Ecca boundary coincides with a progressional temperature rise (Fig. 7-1a). Favourable climate conditions led to the spread of the *Glossopteris* flora (Fig. 7-1c). High chemical weathering rates, assumedly fast growing vegetation and the documented reptile fauna (*Mesosaurus*) (Fig. 7-1b), indicate warm-humid climate conditions during the Early to Middle Permian in south Gondwana. Mean annual temperatures of approximately 15 to 20°C, with temperate winters and elevated precipitation can be estimated.

During the Middle to Late Permian the continuous retreat of former marine sedimentary environments commences. Turbiditic deposits were replaced by deltaic basin fills, which were in tune covered by fluvial and lacustrine sediments (Figs. 7-1a & b). The retreat of marine conditions in the Karoo Basin was closely related to the rising Cape Fold Belt, whereby the connection to the Panthalassic Ocean was finally terminated. Arid climate conditions during the Late Permian and Lower Triassic are indicated by redbeds and aeolian deposits of the upper Beaufort and Stormberg/Lebung Groups.

## 7.1 Proposal for further investigations

It was show by Visser (1997), Stollhofen et al. (2001) and this study that the Gondwana glaciation during the late Palaeozoic phased out by alternating stadial and interstadial climate phases. It could be shown that the changes in the sedimentary environment were much more complex than can be explained exclusively by waxing and waning of glaciers. For a detailed view of the sedimentary conditions especially in central basin parts, organic geochemical investigations would provide further information. Applicable sample material should derive from drill sites, which are situated in sufficient distance to the metamorphic influence of the rising Cape Fold Belt in the south and are not affected by intrusion of Mesozoic dykes, which

were injected in the northern parts of the Karoo Basin. Furthermore, detailed investigation of the organic matter of the Vreda test drill at the border of Namibia/Botswana (Fig. 4-2) would decipher the duration of maximum extension of the Ecca-sea into the interior of south Gondwana.

Further detailed investigations of dated sections along the Palaeozoic Gondwana coast are needed to contribute to a better understanding whether the recorded sealevel changes on the northern hemisphere were directly triggered by waning and waxing of the Gondwana glaciation.

# 8 Analytical methods

## 8.1 Sample preparation

All samples were crushed, milled and homogenised. Aliquots of the sample powder were prepared for inorganic-geochemistry, isotope geochemistry and organic geochemical investigations.

For organic geochemical investigations the samples were carefully dried at 40°C. For XRF-analysis aliquots of the sample powder were dried at 110°C for 24 h. To dissolve carbonate minerals up to 2g powdered sample was treated with 30% HCl and heated up to 60°C until the reaction was completed. Afterwards the powder was washed with distilled water to pH 7 and dried for 24 hours at 60°C.

For oxygen isotope measurements of the silicates, the decarbonated material was treated with 10% $H_2O_2$ until complete oxidation of the organic carbon. Oxygen isotopic composition was then determined on washed and dried material (110°C for 24 h).

## 8.2 Element Geochemistry

The powdered and dried samples were mixed 1:6 with lithium-tetra-borate and approximately 1g $NH_3NO_4$. Glass disc were prepared by stepwise heating for 6 minutes at 400, 500, 600, 1000 and 1100°C. The samples were automatically measured using a Philips PW 1480 X-ray fluorescence spectrometer. Intensities were corrected for matrix effects and line overlap by use of the program OXIQUANT (Vogel and Kuipers, 1987). Analysed elements, detection limits and settings are given on the website of the Department of Mineralogy in Bonn (http://www.min.uni-bonn.de).

The lost on ignition was determinated after heating the sample in a ceramic crucible for 20 Minutes at 1000°C.

## 8.3 Bulk parameters of the organic matter

Total carbon and sulphur contents were determined by direct combustion of the untreated sample powder. $C_{org}$ contents were measured after treated the sample powder in a ceramic crucible with concentrated HCl to remove carbonates. The residue were dried, and combusted with pure oxygen in a LECO CS-225 elemental analyser. Total nitrogen contents were measured using a Heraeus Elemental analyser.

Rock Eval pyrolysis was performed using a VINCI Rock Eval-II instrument applying

standards procedures as described in Espitalié et al., (1977; 1980) and Bordenave et al. (1993). About 0.1 gram of the sample was heated to moderate temperatures (200-250°C) in an inert atmosphere, during which hydrocarbons already generated in the source rock were volatilised. Those were measured by a flame ionisation detector as $S_1$. The sample was then stepwise heated up to 550°C whereby the breakdown of kerogen occurs. The temperature of maximum pyrolysis was measured and given as $T_{max}$. Generated volatile products were split in two streams. The resulting hydrocarbons (HC) were measured by the flame ionisation detector ($S_2$). The $CO_2$ content was determined by a thermal conductivity detector ($S_3$). From the $S_2$ and $S_3$ values in combination with the $C_{org}$ content the hydrogen index (HI) and oxygen index (OI) can be determined as HI [mg HC/g $C_{org}$] = $S_2/C_{org}$*100 and OI [mg $CO_2$/g $C_{org}$] = $S_3/C_{org}$ *100.

## 8.4 Biomarker analyses

Pulverized samples were extracted twice with dichloromethane applying accelerated solvent extraction (DIONEX ASE-200) at 75°C and 50 bars pressure as described in Schwark et al. (1998). Both extracts were combined and dichloromethane was carefully evaporated to dryness under reduced pressure (Zymark Turbovap). Asphaltenes were precipitated in a 60-fold excess of hexane to obtain the maltene fraction. The latter was separated into aliphatic hydrocarbons, aromatic hydrocarbons and resins by MPLC (Radke et al., 1980). For compound identification and calculation of biomarker ratios aliphatic and aromatic hydrocarbons were analysed by gas chromatography (GC-FID) and gas chromatography coupled to mass spectrometry (GC/MS) as described in Schwark et al. (1998).

## 8.5 Oxygen isotopy

The oxygen isotopic composition of the silicate fraction was determined by reaction with fluorine gas using a modified Taylor and Epstein-type fluorine line (Taylor and Epstein, 1962). After fluorination and conversion to $CO_2$ a triple collector MS of VG Isogas was used as previously described in Hoernes and van Reenen, (1992).

## 8.6 Carbon isotopy

$\delta^{13}$Corg isotope values were measured after HCl treatment. The sample powder was loaded into tin capsules and dropped into a furnace at 1000°C while in an atmosphere of oxygen. Helium was used as carrier gas. The tin ignites and burns exothermally, and the temperature rises to about 1800°C, oxidising the sample. Complete oxidation is ensured by reaction with $Cr_3O_3$. Silver wool removed sulphur from the gas stream. In a second furnace at 600°C

copper was oxidised by excess oxygen. Water was removed in a trap containing anhydrous magnesium perchlorate.
Carbon isotopes were measured from the gas stream after passing a gas chromatograph by a Europa Scientific 20/20 isotope mass spectrometer.

## 8.7 Statistic analyses

Statistical analysis and clustering was performed using the PAST software package version 1.05 from O. Hammer and D.A.T Harper (2003) available at http://folk.uio.no/ohammer/past.

# 9. References


Adelmann, D., (1995): Geologische Untersuchungen im Übergangsbereich Cape Fold Belt/ Karoo-Becken bei Laingsburg (südwestliche Kap-Provinz / Südafrika): Sedimentpetrographische und geochemische Untersuchungen der Ecca und Beaufort Groups (Teil II). Diplomarbeit, 206 pp., Universität Bonn.

Agashe S.N., (1995): Paleobotany. Plants of the past; their evolution, palaeoenvironment and application in exploration of fossil fuels. 359 p., Oxford.

Albes, D., (1996): Sedimentpetrographische und geochemische Untersuchungen der Dwyka Group und Prince Albert Formation (Permokarbon der Karoo Supergroup, Karoo Becken, Rep. Südafrika). Diplomarbeit, 135 pp., Universität Bonn.

Alego, T.J. and Maynard, J.B., (2004): Trace-element behaviour and redox facies in core shales of Upper Pennsylvanian Kansas-type cyclothems. Chem. Geol., 206: 289-318.

Alexander, R., Kagi, R.I. & Woodhouse, G.W., (1981): Geochemical correlation of Windalia oil and extracts of Winning Group (Cretacous) potential source rocks, Barrow subbasin, Western Australia. AAPG Bull., 65: 2235-250.

Alexander, R.M., Kagi, R.I., Sheppard, P.N., (1983): Relative abundance of dimethylnaphthalene isomers in crude oils. J. Chromatogr., 267: 367– 372.

Alexander, G., Hazai, I., Grimalt, J., Albaiges, J., (1987): Occurrence and transformation of phyllocladanes in brown coals from Nograd Basin, Hungary. Geochim. Cosmochim. Acta, 51: 2065–2073.

Alexander, R., Larcher, A.V., Kagi, R.I. & Price, P.L., (1992): An oil-source correlation study using age specific plant-derived aromatic biomarkers. In: Biological Markers in Sediments and Petroleum. Moldowan, J.M., Albrecht, P. & Philip, R.P. (Eds): Prentice Hall, Englewood Cliffs, N.J. pp. 201-221.

Allison, P.A., Wignall, P.B. & Brett, C.E., (1995): Palaeo-oxygenation: effects and recognition. In: Bosence, D. W. J. & Allison, P. A. (eds.), Marine Palaeonenvironmental Analysis from Fossils, Geol. Soc. Spec. Pub., 83: 97-112.

Anderson, A.M. and McLachlan, I.R., (1979): The oil-shale potential of the Early Permian White Band Formation in southern Africa. Geokongress 77: Geol. Soc. S. Afr. Spec. Pub., 6: 83-89.

Archangelsky, S., (1990): Plant distribution in Gondwana during the late Paleozoic. In: Taylor & Taylor (Eds.), Antarctic paleobiology; it role in the reconstruction of Gondwana. 102-117 pp., Springer-Verlag.

Arthur, M.A., (1981): Knowledge of carbon cycle and stable carbon isotopes contributes to source-rock studies. U.S. Geol. Surv. Prof. Pap., 1981, pp. 40.

Bacher., J., (1994): Clusteranalyse: anwendungsorientierte Einführung. 424 p., Oldenburg.

Backhaus, K., Erichson, B., Plinke, W. & Weiber, R. (1996): Multivariate Analysenmethoden: eine anwendungsorientierte Einführung. 8., verb. Aufl. pp. 591. Springer Verlag, Berlin.

Bailey, N.J.L., Krouse, H.R., Evans, C.R., Rogers, M.A., (1973): Alteration of crude oil by waters and bacteria-evidence from geochemical and isotopic studies. AAPG, 57: 1276-1290.

Banerjee, I., (1966): Turbidites in a glacial sequence; a study from the Talchir Formation, Raniganj coalfield, India. J. Geol., 1966, 74: 593-606.

Bangert, B., Stollhofen, H., Lorenz, V. & Armstrong, R., (1999): The geochronology and significance of ash-fall tuffs in the glaciogenic Carboniferous-Permian Dwyka Group of Namibia and South Africa. J. Afr. Earth Sci., 29: 33-49.

Barnes, C.R., (1999): Paleoceanographic and paleoclimatology: an Earth system perspective. Chem. Geol., 161: 17-35.

Barnes, I., Irwin, W.P. & White, D.E., (1978): Global distribution of carbon dioxide discharges and major zones of seismicity. US Geol. Surv., Water-Res. Inv. 78-39, open file report.

Baturin, G.N., (2001): Phosphorous in the ocean and the earth climate. Oceanology, 41: 133-141.

Bechtel, A., Gruber, W., Sachsenhofer, R.F., Gratzer, R. & Püttmann, W., (2001): Organic geochemical and stable carbon isotopic investigation of coals formed in low-lying and raised mires within the Eastern Alps (Austria). Org. Geochem., 32: 1289-1310.

Berner, R.A., (1971): Principles of chemical sedimentology. 240 p.

Berner, R.A., (1982): Burial of organic carbon and pyrite sulfur in the modern ocean; its geochemical and environmental significance. Science, 282: 451-473.

Berner, R.A., (1994): Geocarb II: A revised model of atmospheric $CO_2$ over Phanerozoic time. Am. J. Sci., 294: 56-91.

Berner, R.A., (2001): Geocarb III: A revised model of atmospheric $CO_2$ over Phanerozoic time. Am. J. Sci., 301: 182-204.

Berner, R.A. and Raiswell, R., (1983): Burial of organic carbon and pyrite sulphur in sediments over Phanerozoic time: a new theory. Geochim. Cosmochim. Acta, 47: 885-862.

Berner, R.A. and Raiswell, R., (1984): C/S method for distinguishing freshwater from marine sedimentary rocks. Geology, 12: 365-368.

Björlykke, K., (1974): Geochemical and mineralogical influence of Ordovician Island Arcs on epicontinental clastic sedimentation. A study of Lower Palaeozoic sedimentation. A study of Lower Palaeozoic sedimentation in the Oslo Region, Norway. Sedimentology, 21: 251-272.

Borchert, H. and Krjeci-Graf, K., (1959): Spurenmetalle in Sedimenten und ihren Derivaten. Bergbauwiss.,6: 205-215.

Boryta, M. and Condie, K.C., (1990): Geochemistry and origin of the Archaean Beit Bridge Complex, Limpopo Belt, South Africa. J. Geol. Soc. Lond., 147: 229-239.

Bosch, K., (1998): Statistik für Nichtstatistiker: Zufall oder Wahrscheinlichkeit. 3. Aufl., 236p.

Boucot, A.J. and Gray, J., (2001): A critique of Phanerozoic climatic models involving changes in the $CO_2$ content of the atmosphere. Earth-Sci. Rev., 56: 1-159.

Bradley, R.S., (1985): Quaternary Palaeoclimatology: Methods of Palaeoclimatic Reconstruction. Unwin Hyman, London, 472 p.

Brasier, M.D., (1995): Fossil indicators of nutrient levels. 1: Eutrophication and climate change. In: Bosence, D.W.J. & Allison, P.A. (Ed.), Marine Palaeonenvironmental Analysis from Fossils, Geol. Soc. Spec. Pub., 83: 113-132.

Brassell, S.C., Mc Evoy, J., Hoffmann, C.F., Lamb, N.A., Peakman, T.M. & Maxwell, J.R., (1984): Isomerisation, rearrangement and aromatisation of steroids in distinguishing early stages of diagenesis. Org. Geochem., 6: 11-23.

Bray, E.E. and Evans, E.D., (1961): Distribution of n-paraffins as a clue to recognition of source beds. Geochim. Cosmochim. Acta, 22: 2-15.

Bruckschen, P., Oesmann, S., and Veizer, J., (1999): Isotope stratigraphy of the European Carboniferous: Proxy signatures for ocean chemistry, climate and tectonics. Chem. Geol., 161: 127–163.

Brumsack, H-J., (1989): Geochemistry of recent TOC-rich sediments from the Gulf of California and the black Sea. Geol. Rundsch., 78/3: 851-882.

Brumsack, H-J., Heydemann, A., Kühn, V., Rachold, V. & Usdowski, E., (1995): Geochemistry and mineralogy of Middle Aptian sediments from the Lower Saxony Basin, NW Germany. N. Jb. Geol. Paläont. Abh., 196: 235-255.

Bühmann, C. and Bühmann, D., (1990): Clay minerals as palaeoenvironment indicators exemplified on a Karoo sequence from the Bothaville area, South Africa. S. Afr. J. Geol., 93: 505-513.

Bühmann, D. and Lepper, J., (1990a): Mineralogy of the Matura Hill bore hole core, Wnkie Concessions, Zimbabwe, with specific reference to its clay mineral content, Geol. Jb., D96: 55-66.

Bühmann, D. and Lepper, J., (1990b): Significant mineral variations in the Lower Karoo deposits of the Mid-Zambezi Basin, Zimbabwe, and their palaeoenvironmental implications. S. Afr. J. Geol., 93: 744-753.

Bühmann, D. and Atanasova, M.T., (1997): Karoo core samples from Orapa and Letlhakane, Botswana: A mineralogical report. 12 p.

Cadle, A.B., Cairncross, B., Christie, A.D.M. & Roberts, D.L., (1993): The Karoo Basin of South Africa: type basin for the coal-bearing deposits of southern Africa. Int. J. Coal Geol., 23: 117-157.

Carincross, B., (1989): Palaeodepositional environments and tectonosedimentary controls of post-glacial Permian coals, Karoo basin, South Africa. Int. J. Coal Geol., 12: 365– 380.

Carincross, B. and Cadle, A.B., (1988): Depositional environment of the Permian Vryheid Formation in the east Witbank Coalfield, Scouth Africa. Int. J. Coal Geol. 91: 1-17.

Campbell, W.P. and Todd, D., (1942): The structure and configuration of resin acids. Podocarpic acid and ferruginol. J. Am. Chem. Soc., 64: 928-935.

Campbell, F.A. and Williams, G.D., (1965): Chemical composition of shales of Mannville Group (Lower Cretaceous) of Central Alberta, Canada. AAPG Bull., 49/1: 81-87.

Caputo, M.V. and Crowell, J.C., (1985): Migration of glacial centers across Gondwana during Palaeozoic area. Geol. Soc. Am. Bull., 96:1020-1036.

Carlson, R.M.K., Croasmun, W.R., Chamberlain, D.E., Moldowan, J.M., (1992): NMR structural studies of $C_{21}$ and $C_{27}$ monoaromatic steroid hydrocarbon biological markers. In: Moldowan, J.M., Albrecht, P. and Philip, R.P. (Eds.), Biological Markers in Sediments and Petroleum.: Prentice Hall: Englewood Cliffs, NJ, pp. 75-105.

Catuneanu, O., Hancox, P.J. & Rubidge, B.S., (1998): Reciprocal flexural behaviour and contrasting stratigraphies: a new basin development model for the Karoo retroarc foreland system, South Africa. Basin Res., 10: 417-439.

Cerling, T.E., Brown, F.H. and Bowman, J.R., (1985): Low temperature alteration of volcanic glass: hydration, Na, K, 18O and Ar mobility. Chem. Geol., 52: 281-293.

Chaffee, A.L., Hoover, D.S., Johns, R.B. & Schweighardt, F.K., (1986): Biological markers extractable from coal. In: Methodes in geochemistry and geophysics. Johns, R.B. (Ed.): Biological markers in the sedimentary record. 311-345.

Clementz, D.M., (1979): Effect of oil and bitumen saturation on source-rock pyrolysis. AAPG Bull., 60: 608-626.

Cody, R.D., (1971): Adsorption and the reliability of trace elements as environmental indicators for shales. J. Sed. Petrology, 41: 461-471.

Connan, J. and Cassou, A.M., (1980): Properties of gas and liquids derived from terrestrial kerogen at various maturation levels. Geochim. Cosmochim. Acta, 44: 1-23.

Connan, J., (1981): Biological markers in crude oils. In: Mason, J.F. (Ed.) Petroleum Geology in China. Penwell, Tusla, pp. 48-70.

Connan, J., (1984): Biodegradation of crude oils in reservoirs. In: Brooks, J. & Welte, D. (Ed.) Advances in Petrolium Geochemistry, vol. 1. pp. 299-335. Academic Press, New York.

Cole, D.I., (1991): Depositional environment of the Dwyka Gruop in the Boshof-Hertzogville region, Orange Free State. S. Afr. J. Geol., 94: 272-287.

Cole, D.I., (1992): Evolution and development of the Karoo Basin. In: De Wit, M.J., Ransome, I.G.D. (Ed.). Inversion tectonics of the Cape Fold Belt, Karoo and Cretaceous basins of southern Africa. 87-99.

Cole, D. I. and Basson, W. A., (1991): Whitehill Formation. In: Johnson, M. R. (Ed.), Catalogue of South African Lithostratigraphic Units. pp. 3-51.

Corfield, R.M., (1995): An introduction to the techniques, limitations and landmarks of carbonate oxygen isotope palaeothermometry. In: Bosence, D.W.J., Allison, P.A. (Eds.), Marine Palaeonenvironmental Analysis from Fossils, Geol. Soc. Spec. Pub., 83: 27-42.

Corrigan, D., Kloos, C., O'Connor, C.S. and Timoney, R.F., (1973): Alkanes from the types of *Sphagnum* moss. Phytochem., 12: 213-214.

Coxhell, S. and Fehlberg, B., (2000): Julia Creek Vanadium and oil shale deposit. AIG Journal. 2000-11: 1-14.

Cranwell, P.A., Eglinton, G., Robinson, N., (1987): Lipids of aquatic organisms as potential contributors to lacustrine sediments. Org. Geochem. 11: 513-527.

Crowell, J.C., (1978): Gondwana glaciation, cyclothems, continental positioning and climate change. Am. J Sci., 278: 1345-1372.

Crowell, J.C., (1983): Ice ages recorded on Gondwana continents. Geol. Soc. of S. Afr. Trans., 86:238-261.

Crowell, J.C. and Frakes, L.A., (1972): Late Paleozoic glaciation: Part V, Karoo Basin, South Africa. Geol. Soc. Am. Bull., 83: 2887-2912.

Crowley, T.J., Hyde, W.T. & Short, D.A., (1989): Seasonal cycle variations on the supercontinent of Pangaea. Geology, 17: 457-460.

Crowley, T.J. and Baum, S.K., (1992): Modelling late Palaeozoic glaciation. Geology, 20: 507-510.

Czochanska, Z, (1988): Geochemical application of sterane and triterpane biomarkers to a description of oils from the Taranaki Basin in New Zealand. Org. Geochem. 12: 123-135.

Dean, W.E., Davis, G.R. & Anderson, R.Y., (1975): Sedimentological significance of nodular and laminated anhydrite, Geology, 3: 367-372.

Dean, W.E. and Arthur, M.A., (1989): Iron-sulfur-carbon relationships in organic-carbon-rich sequences I: Cretaceous western interior seaway. Science, 289: 708-743.

Deer, F.R.S., Howie, R.A. & Zussman, J., (1992): An introduction to the rock-forming minerals. Longman Group Limited, London.

Degenhardt, H., (1957): Untersuchungen zur geochemischen Verteilung des Zirkoniums in der Lithosphaere. Geochim. Cosmochim. Acta, 11: 279-309.

Degens, E.T. and Stoffers, P., (1976): Stratified water as a key to the past. Nature, 263: 22-26.

Dickins, J.M., (1962): *Eurydesma* and Peruvispira from the Dwyka beds of South Africa. Palaeontology, 4: 138-148.

Dickins, J.M., (1996): Problems of a late Palaeozoic glaciation in Australia and subsequent climate in the Permian. Palaeogeogr., Palaeoclimatol., Palaeoecol., 125: 185-197.

Didyk, B.M., Simoneit, B.R.T., Brassell, S.C. & Eglinton, G., (1978): Organic geochemical indicators of palaeoenvironmental conditions of sedimentation. Nature, 272: 216-222.Diessel, C.F.K., (1992): Coal bearing depositional systems. Springer, Berlin, 721 pp.

Duane, D. and Brown, R. (1992): Geochemical open-system behaviour related to fluid-flow and metamorphism in the Karoo Basin. In: Inversion tectonics of the cape fold belt, Karoo and Cretaceous basins of southern Africa. De Wit, M.J., Ransome, I.G.D. (Ed.)., pp. 127-141.

Dypvik, H. (1984): Geochemical composition and depositional conditions of Upper Jurassic and lower Cretaceous Yorkshire clays, England. Geol Mag., 121: 489-504.

De Leuw, J.W. and Baas, M., (1986): Early-stage diagenesis of steroids. In: Johns, R.B. (Ed.), Biological markers in the sedimentary record. Methods in geochemistry and geophysics, 24. Elsevier, Amsterdam, pp. 101-123.

De Leeuw, J. W., Frewin, N.L., van Bergen, P.F., Sinninghe Damsté, J.S. & Collinson, M.E., (1995): Organic carbon as a palaeoenvironmental indicator in the marine realm. In: Bosence, D.W.J. & Allison, P.A. (Eds.), Marine Palaeoenvironmental Analysis from Fossils, Geol. Soc. Spec. Pub., 83: 43-71.

De Villiers and Wickens, H., (1992): Submarine fans of the Permian Ecca Group in the SW Karoo Basin: Their origin and reflection on the tectonic evolution of the basin and its source areas. In: Inversion tectonics of the cape fold belt, Karoo and Cretaceous basins of southern Africa. De Wit, M.J., Ransome, I.G.D. (Ed.)., pp. 117-125.

De Wit, M.J. and Ransome, I.G.D., (1992): Regional inversion tectonics along the southern margin of Gondwana. In: De Wit, M.J., Ransome, I.G.D. (Ed.), Inversion tectonics of the Cape Fold Belt, Karoo and Cretaceous basins of southern Africa. pp. 15-23.

De Wit, M.J., Ghosh, J.G., de Villiers, S., Rakotosolofo, N., Alexander, J., Tripathi, A. & Looy, C., (2002): Multiple organic carbon isotope reversals across the Permo-Triassic boundary of terrestrial Gondwana sequences: Clues to extinction patterns and delayed ecosystem recovery. J. Geol., 110: 227-240.

Egle, S., (1996): Paleo-Hydrology of the Cape Fold Belt and the Karoo Basin South Africa. Diss. Wien.

Eglinton, G. and Hamilton, R.J., (1967): Leaf epicuticular waxes. Science, 156: 1322-1335.

Eglinton, G., (1972): Laboratory simulation of organic geochemical processes. In: Advances in organic geochemistry 1971, H.R. Gaertner & H. Wehner (Eds.) pp. 1-24. Pergamon, Oxford.

Ehrenberg, S.N.; Aagaard, P., Wilson, M.J., Fraser, A.R. & Duthie, D.M.L., (1993): Depth-dependent transformation of kaolinite to dickite in sandstones of the Norwegian continental shelf. Clay Min., 28: 325-352.

Emerson, S.R. and Huested, S.S., (1991): Ocean anoxia and the concentrations of molybdenum and vanadium in seawater. Mar. Chem., 34:177-196.

Ensminger, A., Albrecht, P., Ourisson, G. & Tissot, B., (1977): Evolution of polycyclic alkanes under the effect of burial (Early Toarcian shales, Paris Basin). In: Adv. Org. Geochem. (Campos, R. & Goni, J. Eds) pp. 45-52.

Ernst, W., (1970): Geochemical facies analysis, Methodes in geochemistry and geophysics. pp 152, Amsterdam.

Espitalie, J., (1980): Role of mineral matrix in kerogen pyrolysie; influence on petroleum gerneration and migration. AAPG Bull. 64: 59-66.

Espitalié, J., Maxwell, J.R., Chenet, Y & Barsony, I., (1988): Aspects of hydrocarbon migration in the Mesozoic in the Paris basin as deduced from an organic geochemical survey. In: Advances in organic geochemistry 1987. Mattavelllini, L. & Novelli, L. (Eds)., pp. 467-482. Pergamon, Oxford.

Ewart, A., (1982): The mineralogy and petrology of Tertiary – Recent orogenic volcanic rocks: with special reference to the andesitic – basaltic compositional range. In: Andesites: orogenic andesites and related rocks, Thorpe, R.S., (Ed.), pp. 26-87, Chichester, Wiley.

Eyles, N. and Eyles, C.H., (1993): Glacial geologic confirmation of an intraplate boundary in the Paraná basin of Brazil. Geology, 21: 459-462.

Eyles, C.H., Eyles, N. & Franca, A.B., (1993): Glaciation and tectonics in an active intracratonic basin: the Late Palaeozoic Itararé Group, Paraná Basin, Brazil. Sedimentology, 40: 1-25.

Fabiańska, M.J., Bzowska, G., Matuszewska, M.R. & Skret, U., (2003): Gas chromatography-mass spectrometry in geochemical investigation of organic matter of the Grodziec beds (Upper Carboniferous), Upper Silesian coal basins, Poland. Chem. Erde, 63: 63-91.

Fabiańska, M.J. and Kurszewska, K.J.K., (2003): Relationship between petrographic and geochemical characterisation of selected South African coals. Int. J. coal Geol., 54: 95-114.

Fairbridge, R.W., (1967): Phases of diagenesis and authigenesis. Dev. Sed., 8: 19-89.

Falcon, R.M.S., (1986): A brief review of the origin, formation and distribution of coal in South Africa. In: Mineral deposits of southern Africa. C.R., Anhaeusser & S. Maske (Ed.), Geol. Soc. S. Afr., 2:1979-1898.

Falcon, R.M.S., Pinheiro, H.J. & Shepherd, P., (1984): The palynobiostratigraphy of the major coal seems in the Witbank Basin with lithostratigraphic, chronostratigraphic and palaeocliamtic implications. Commun. Serv. Geol. Portugal, 70: 215-243.

Faure, G., When, K.S., Montello, J.M., Hagen, E.H., Strobel, M. L. & Johnson, K.S., (1993): Isotope composition of the ice and sub-glacial geology near the Allan Hills, Victoria Land, Antarctica. Int.l Gond. Sym., 8: 485-495.

Faure, K., Armstrong, R.A., Harris, C. & Willis, J.P., (1995): Provenance of mudstones in the Karoo Supergroup of the Ellisras basin, South Africa: geochemical evidence. J. Afr. Earth Sci., 23: 189-204.

Faure, K. and Cole, D., (1999): Geochemical evidence for lacustrine microbial blooms in the vast Permian Main Karoo, Paraná, Falkland Islands and Huab basins of southwestern Gondwana. Palaeogeogr., Palaeoclimatol., Palaeoecol., 152: 189-213.

Ferraresi de Giovani, W., Salati, E., Marini, O.J. & Friedman, I., (1974): Unusual isotopic composition of carbonates from Irati Formation, Brazil. Geol. Soc. Am. Bull., 85: 41-44.

Ficken, K.J., Li, B., Swain, D.L., (2000): An n-alkane proxy for the sedimentary input of submerge/floating freschwater aquatic macrophytes. Org. Geochem. 31: 745-749.

Fiedler, K., (1995): Sedimentologie der Oberen Ecca und Unteren Beaufort Groups im Laingsburg-Teilbecken. Diplomarbeit, 169 pp., Universität Bonn.

Frakes, L.A., Francis, J.E., and Syktus, J.I., (1992): Climate modes for the Phanerozoic: Cambridge, Cambridge University Press, 274 p.

Franca, A.B. and Potter, P.E., (1991): Stratigraphy and reservoir potential of glacial deposits of the Itararé Group (Carboniferous-Permian), Paraná Basin, Brazil. AAPG Bull., 75: 62-85.

Freed, R.L. and Peacor, D.R., (1989): Variability in temperature of the smectite/illite reaction in Gulf Coast sediments. Clay Min., 24: 171-180.

Frey, M., (1987): Very low-grade metamorphism of clastic sedimentary rocks. In: M. Frey (Ed.) Low temperature Metamorphism. pp. 9-59 Blackie & son Ltd..

Frey, M., (1999): Low grade metamorphism. pp. 313, Blackwell Science.

Friedman, I. and O'Neil, J.R., (1977): Compilation of stable isotope fractionation factors of geochemical interest. In: Data of Geochemistry, 6th edition., Fleischer, M. (Ed.), U.S. Geol. Surv. Prof. Paper, 440-KK: pp. 12.

Frimmel, A., W. Oschmann & Schwark, L., (2004): Chemostratigraphy of the Posidonia Black Shale, SW-Germany: I – Influence of Sea Level Variation on Organic Facies Evolution, Chem. Geol., 206: 177-198.

Froelich, P.N., Klinkhammer, G.P., Bender, M.L., Luedke, N.A., Heath, G.R., Cullen, D. & Dauphin, P., (1979): Early oxidation of organic matter in pelagic sediments of eastern equatorial Atlantic, suboxic diagenesis. Geochim., Cosmochim. Acta, 43: 1075-1090.

Füchtbauer, H., (1988): Sedimente und Sedimentgesteine. 4th ed. Pp. 1141. Stuttgart.

Gardner, L.R., (1983): Mechanics and kinetics of incongruent feldspar dissolution. Geology, 11: 418-421.

Garlick, G.D. and Dymond, J.R., (1970): Oxygen isotope exchange between volcanic materials and ocean water. Geol. Soc. Am. Bull., 81: 2137-2142.

Geiger, M., (2000): The geology of the southern Warmbad Basin margin – Tephrostratigraphy, age, fossil record and sedimentary environment of Carboniferous-Permian glacigenic deposits of the Dwyka Group, Zwartbas, southern Namibia. Diplomarbeit, 79 pp., Julius-Maximilians-Universität, Würzburg.

German Stratigraphic Commission (Ed.) (2002): Stratigraphic Table of Germany 2002.

Ghore, K.A.R., (2000): High-quality oil-prone source rocks within carbonates of the Silurian Dirk Hartog Group, Gascoyne Platform, western Australia., West. Austr. Geol. Surv., An. Rev. 2000-01: 58-62.

Gillian, F.T., Nichols, P.D, Johns, R.B & Bavor, H.J., (1983): Phytol degradation by marine bacteria. Appl. Environ. Microbiol., 45: 1423-1428.

Giovani, W.F. de, Salati, E., Marini, O.J. & Friedman, I., (1974): Unusual isotopic composition of carbonates from the Irati Formation, Brazil. Geol. Soc. Am. Bull., 85:41-44.

Glikson, M., (1985): Trace elements in oil shales, their source and organic association with particular reference to Australian deposits. Chem. Geol., 53: 155-174.

Goldschmidt, V.M., (1954): Geochemistry. 730 p., Oxford, Clarendon Press.

Golonka, J., Ross, M.I. & Scotese, C.R., (1994): Phanerozoic paleogeographic and paleoclimatic modeling maps. In: Embry, A. F., Beauchamp, B. & Glass, D. J., (Eds.), Pangea; global environments and resources. Vol. 17, pp. 1-47.

Golonka, J. and Ford, D., (2000): Pangaean (Late Carboniferous-Middle Jurassic) paleoenvironment and lithofacies. Palaeogeogr., Palaeoclimatol., Palaeoecol., 161: 1-34.

Goosens, H., de Leeuw, J.W., van de Graaf, B. & Schenk, P.A., (1984): Tocophenols as likely precursors of pristane in ancient sediments and crude oils. Nature, 312: 440-442.

Gresse, P.G., Theron, J.N., Fitch, F.J. & Miller, J.A., (1992): Tectonic inversion and radiometric resetting of the basement in the Cape Fold Belt. In: Inversion tectonics of the cape fold belt, Karoo and Cretaceous basins of southern Africa. De Wit, M.J., Ransome, I.G.D. (Ed.). 217-228.

Griffin G.M. and Ingram, R.L., (1955): Clay minerals of the Neuse River Estuary [North Carolina]. J. Sed. Petr., 25: 194-200.

Grill, H., (1997): The Permo-Carboniferous glacial to marine Karoo record in southern Namibia: sedimentary facies and sequence stratigraphy. Beringeria, 19: pp. 98.

Hälbich, H., (1983): A tectogenesis of the Cape Fold Belt (CFB). Spec. Publ. Geol. Soc. S. Afr., 12: 165-175.

Hahn, C., (1999): Geologische Kartierung im SW Westerwald und geochemische Untersuchungen an tertiären Tuffen der Forschungsbohrung Enspel/Westerwald. Diplomarbeit, Universität Bonn.

Hallberg, R.O., (1976): A geochemical method for inestigation of palaeoredox conditions in sediments. Ambio, Spec. Rep., 4: 139-147.

Hallberg, R.O., (1982): Diagenetic and environmental effects on heavy-metal distribution in sediments: A hypothesis with an illustration of the Baltic sea. In: K.A. Fanning & F.T. Manheim (Ed.), The dynamic environment of the Ocean floor. Lexington Books, Lexington, Mass., pp. 305-316.

Harriss, R.C. and Adams J.A.S., (1966): Geochemical and mineralogical studies on the weathering of granitic rocks. Am. J. Sci., 264: 146-173.

Hayes, J.M., Strauss, H. & Kaufman, A.J., (1999): The abundance of $^{13}C$ in marine organic matter and isotopic fractionation in the global biogeochemical cycle of carbon during the past 800 Ma. Chem. Geol., 161: 103-125.

Hayes, J.M., Kaplan, I.R. & Wedeking, K.W., (1983): Precambrian organic geochemistry, preservation of the record. In: (Schopf, J.W., Ed.) Earth's earliest biosphere: its origin and evolution. pp. 93-132.

Heckel, P.H., (1986): Sea-level curve for Pennsylvanian eustatic marine transgressive-regressive depositional cycles along midcontinent outcrop belt, North America. Geology, 14: 330-334.

Heim, D., (1990): Tone und Tonminerale. Grundlagen der Sedimentologie und Mineralogie. - 157 S., Enke Verlag, Stuttgart.

Hesselbo, S.P., Gröcke, D.R., Jenkyns, H.C., Bjerrum, C.J., Farrimond, P., Morgans Bell, H.S. & Green, O.R., (2000): Massive dissociations of gas hydrate during a Jurassic oceanic anoxic event. Nature, 406: 392-395.

Hoefs, J., (1997): Stable isotope geochemistry. 4$^{th}$ ed. pp. 201. Springer, Berlin.

Hoernes, S. and van Reenen, D.D., (1992): The oxygen-isotopic composition of granulites and retrogressed granulites from the Limpopo Belt as monitor of fluid-rock interaction. – Precambrian Research, 55:353-364.

Hoernes, S., Scheffler, K., Hahn, C. & Knütter, R., (2000): Vulkanoklastische Serien und ihre Bedeutung für die Rekonstruktion des Systemverhaltens metamorpher Serien. Terra Nostra 2000/2: 41-43.

Hofmann, P., Ricken, W., Schwark, L. & Leythaeuser, D., (2000): Carbon-sulfur-iron relationships and $\delta^{13}C$ of organic matter for late Albian sedimentary rocks from the North Atlantic Ocean: Paleoceanographic implications. Palaeogeogr., Palaeoclimatol., Palaeoecol., 163: 97-113.

Holland, M.; Cadle, A.B., Pinheiro, R. & Falcon, R.M.S., (1989): Depositional environments and coal petrography of the Permian Karoo sequence: Witbank Coalfield, South Africa. Int. J. Coal Geol. 11: 143-169.

Holz, M., (1999): Early Permian sequence stratigraphy and the palaeophysiographic evolution of the Parana Basin in southernmost Brazil. J. Afr. Earth Sci. 29: 51-61.

Horsthemke, E., (1992): Fazies der Karoosedimente in der Huabregion, Damaraland, NW.Namibia. Göttinger Arb. Geol. Paläont., 55: pp. 109, Göttingen.

Huang, W.Y. and Meinschein, W.G., (1979): Sterols as ecological indicators. Geochem. Cosmochem. Acta. 43: 739-745.

Hughes, W.B., Holba, A.G. & Dzou, L.I.P., (1995): The ratios of dibenzothiophene to phenanthrene and pristine to phytane as indicators of depositional environment and lithology of petroleum source rocks. Geochim. Cosmochim. Acta, 59: 3581-3598.

Hussler, G., Connan, J. & Albrecht, P., (1984): Novel families of tetra- and hexacyclic aromatic hopanoids predominant in carbonate rocks and crude oils. Org. Geochem., 6: 39-49.

Hyam, D.M., Marshall, J.E.A., Bull, J. M. & Sanderson, D.J., (2000): The structural boundary between East and West Falkland: new evidence for movement history and lateral extent. Mar. Petrol. Geol., 17: 13-26.

Hyde, W.T., Crowley, T.J, Tarasov, L. and Peletier, W.R., (1999): The Pangean ice age; studies with a coupled climate-ice sheet model. Climate. Dyn., 15: 619-629.

Inoue, A. and Utada, M., (1991): Pumpellyite and related minerals from hydrothermally altered rocks at the Kamikita area, northern Honshu, Japan. Can. Min., 29: 255-270.

IPCC, (2001): Third Assessment Report: Climate Change 2001: http://www.ipcc.ch (Februar 2003)

Irwin, H., Curtis, C. & Coleman, M., (1977): Isotopic evidence for source of diagenetic carbonates formed during burial of organic-rich sediments. Nature, 269: 209-213.

Isbell, J.L., Miller, M.F., Wolfe, K.L. & Lenaker, P.A., (2003a): Timing of late Palaeozoic glaciation in Gondwana: was glaciation responsible for the development of northern hemisphere cyclothems? Geo. Soc. Am. Spec. P., 370-01: 1-20.

Isbell, J.L, Lenaker, P.A., Askin, R.A., Miller, M.F. & Babcock, L.E., (2003b): Reevaluation of the timing and extent of late Paleozoic glaciation in Gondwana: Role of the Transantarctic Mountains. Geology, 31: 977-980.

Jakubec, J., Terbrugge, P.J. & Guest, A.R., (1996): Pit slope design at Orapa Mine. Surface Mining, 123-135.

Jasper, J.P., & Hayes, J.M., (1990): A carbon isotope record of $CO_2$ levels during the late Quaternary: Nature, 347: 462–464.

Jobson, A.M., Cook, F.D. & Westlake, D.W.S. (1972): Microbial utilisation of crude oil. App. Microb. 23: 1082-1089.

Johnson, M.R., van Vuuren, C.J., Hegenberger, W.F., Key, R. & Shoko, U., (1996): Stratigraphy of the Karoo Supergroup in southern Africa: an overview. J. Afr. Earth Sci., 23: 3-15.

Johnson , M.R., van Vuuren, C.J., Visser, J.N.J., Cole, D.I., Wickens, de V., Christie, A.D.M. & Roberts, D.L., (1997): The foreland Karoo Basin, South Africa. In: Selley, R.C. (Ed.), Sedimentary Basins of the world, African basins, 269-317.

Jones, R. W., (1987): Organic facies. In: Brooks, J. & Welte, D (Ed.), Adv. Petrol. Geochem., Vol 2., 1-90.

Jones, B. and Manning, D.A.C., (1994): Comparison of geochemical indices used for the interpretation of palaeoredox conditions in ancient mudstones. Chem. Geol., 111: 111-129.

Kemper, E., (1995): The causes of the carbonate and colour changes in the Aptian of NW Germany. N. Jb. Geol. Paläont. Abh., 196: 275-289.

Killlops, S.D. and Killops, V.J., (1993): An introduction to organic geochemistry. pp. 265, Longman Group, England.

Klemm, E., (1995): Das Problem der Distanzbildung in der hierarchischen Clusteranalyse. 229 p. Europäische Hochschulschriften: Reihe 22, Soziologie; Bd. 271.

Knütter, R.K.C., (1994): Geologische Kartierung in der Umgebung von Laingburg (Westliche Kap-Provinz/Südafrika) sowie geochemische Untersuchungen an vulkanischen Gesteinen der Prince Albert-, Whitehill-, Vischkuil und Laingsburg Fms. sowie der Abrahamskral Fm. (Beauford Group). Diplomarbeit, 93 pp, Universität Bonn.

Krejci-Graf, K., (1975): Geochemische Faziesdiagnostik. Freib. Forsch. C224: 80pp.

Kump, L.R. and Arthur, M.A., (1999): Interpreting carbon-isotope excursions: carbonates and organic matter. Chem. Geol., 161: 181-198.

Kutzbach, J.E. and Gallimore, R.G., (1989): Pangean climates: megamonsoons of the megacontinent. J. Geophys. Res., 94: 3341-3357.

Kutzbach, J.E., Guetter, P.J., and Washington, W.M., (1990): Simulated circulation of an idealized ocean for Pangean time: Paleoceanography, 5: 299–317.

Kvenvolden, K.A., (1993): Gas hydrates: geologic perspective and global change. Rev. Geophys., 31: 173-187.

Laflamme, R.E. and Hites, R.A., (1978): The global distribution of polycyclic aromatic hydrocarbons in recent sediments. Geochim. Cosmochim. Acta, 42: 289-303.

Langford, F.F. and Blanc-Valleron, M.-M., (1990): Interpreting Rock-Eval pyrolysis data using graphs of pyrolizable hydrocarbons vs. total organic matter. AAPG Bull., 74: 799-804.

Lawrence, J.R. and Taylor, H.P. Jr., (1971): Deuterium and oxygen-18 correlation: Clay minerals and hydroxides in Quaternary soils compared to meteoric waters. Geochim. Cosmochim. Acta, 35: 993-1003.

Lawrence, J.R. and Taylor, H.P. Jr., (1972): Hydrogen and oxygen isotope systematics in weathering profiles. Geochim. Cosmochim. Acta, 36: 1377-1393.

Le Blanc Smith, G., (1980): Genetic stratigraphy for the Witbank coalfield. Trans. Geol. Soc. S. Afr., 83: 313-326.

Ledendecker, S., (1992): Stratigraphie der Karoosedimente der Huabregion (NW-Namibia) und deren Korrelation mit zeitequivalenten Sedimenten des Paranábeckens (Südamerika) und des Großen Karoobeckens (Südafrika) unter besonderer Berücksichtigung geodynamischer und klimatischern Entwicklung Westgondwanas. Göttinger Arbeiten zur Geologie und Paläontologie, Nr. 54, 87 pp., 29 Fig., 4 Tab.

Lehn, J., Müller-Gronbach, T. & Rettig, S., (2000): Einführung in die Deskriptive Statistik. 135 p.

Lethonen, K. & Ketola, M. (1993): Solvent-extractable lipids of *Sphagnum, Carex, Bryales* and *Carex-Bryales* peats: content and compositional features vs peat humification. Org. Geochem., 20:363-380.

Lewan, M.D. and Maynard, J.B., (1982): Factors controlling enrichment of vanadium and nickel in the bitumen of organic sedimentary rocks. Geochim. Cosmochim. Acta, 46: 2547-2560.

Lewan, M.D., (1983): Effects of thermal maturation on stable isotopes as determined by hydrous pyrolysis of Woodford shale. Geochim. Cosmochim. Acta, 47: 1471-1480.

Lijimbach, G.W.M., (1975): On the origin of petroleum. Proc. 9th World Petrol. Congr. Vol. 2, applied Science Publisher, London, pp. 357-369.

Lindgreen, H., Drits, V.A., Sakharov, B.A., Salyn, A.L., Wrang, P. & Dainyak, L.G., (2000): Illite-smectite structural changes during metamorphism in black Cambrian alum shales from the Baltic area. Am. Mineral., 85: 1223-1238.

Littke, R., (1993): Deposition, diagenesis and weathering of organic matter-rich sediments. Lecture notes in earth sciences, 47: 216 pp.

Littke, R., Klussmann, U., Krooss, B. & Leythauser, D., (1991): Quantification of loss of calcite, pyrite, and organic matter due to weathering of Toracian black shales and effects on kerogen and bitumen characteristics. Geochim. Cosmochim. Acta., 55: 3369-3378.

Longstaffe, F.J., (1987): Stable isotope studies of diaginetic processes. In: Short course in stable isotope geochemistry of low temperature Fluids., Kyser, T.K. (ed), Min. Ass. Canada., 13:187-257.

López-Gamundí, O.R., Cesari, S.N. & Limarino, C.O., (1993): Paleoclimatic significance and age constraints of the Carboniferous coals of Paganzo Basin, western Argentina. In: Banks & Veevers (Eds.) Int. Gondw. Sym., 8: 291-298.

López Gamundí, O.R. & Rossello, E.A., (1998): Basin fill evolution and paleotectonic patterns along the Samfrau geosyncline: the Sauce Grande basin-Ventana foldbelt (Argentina) and Karoo basin-Cape foldbelt (South Africa) revisited. Geol. Rundsch., 86: 819-834.

Mackenzie, S.C., Brassell, S.C., Eglington, G. & Maxwell, J.R., (1982): Chemical fossils: The geological fate of steroids. Science, 217: 491-504.

Marshall, J.D., Brenchley, P.J., Mason, P., Wolff, G.A., Astini, R.A., Hints, L. & Meidla, T., (1997): Global carbon isotopic events associated with mass extinction and glaciation in the late Ordovician. Palaeogeogr., Palaeoclimatol., Palaeoecol., 132: 195-210.

Martini, I.P., (1997): Late glacial and postglacial environmental changes, Quaternary, Carboniferous–Permian and Paleozoic: Oxford, Oxford University Press, 343p.

Martini, I.P. and Rocha-Campos, A.C., (1991): Interglacial and early post-glacial, lower Gondwana coal sequences in the Paraná Basin, Brazil. In: H.P. Ulbrich & A.C. Rocha-Campos (Eds.) Gondwana Seven Proceedings, pp. 317-336.

Mason, B. and Moore, C.B., (1985): Grundzüge der Geochemie. - 340 pp., Enke-Verlag, Stuttgart.

Maynard, J.B., (1981): Carbon isotopes as indicators of dispersal patterns in Devonian-Mississippian shales of the Appalachian Basin. Geology, 9: 262-265.

McLachlan, I.R. and Anderson, A.M., (1977): Carbonates, " Stromatolites" and tuffs in the lower Permian White band Formation. S. Afr. J. Sci., 73: 92-94.

Menning, M. and German Stratigraphic Commission (2002): A geologic time scale 2002. In: German Stratigraphic Commission (ed.), Stratigraphic Tabe of Germany 2002.

Merriman, D. and Peacor, R.J., (1999): Very low-grade metapelites: mineralogy, microfibrics and measuring reaction progress. In: M. Frey & D. Robinson (Eds.) Low-grade Metamorphism. pp. 10-58. Blackwell Sci. Ltd.

Meyers, P.A., (1997): Organic geochemical proxies of palaeoceanografic, paleolimnologic, and paleoclimatic processes. Org. Geochem., 27: 213-250.

Meyers, P.A. and Ishiwatari, R., (1993): Lacustrine organic geochemistry-an overview of indicators of organic matter sources and diagenesis in lake sediments. Org. Geochem., 20:867-900.

Milani, E.J., (1992): Intraplate tectonics and the evolution of the Paraná Basin, SE Brazil. In: Inversion tectonics of the cape fold belt, Karoo and Cretaceous basins of southern Africa. De Wit, M.J., Ransome, I.G.D. (Ed.). pp. 101-108.

Miller, C.N. Jr., (1982): Current status of Paleozic and Mesozoic conifers. In: Taylor, T.N., and Delevoryas, T., (Eds.), Gymnosperms; Paleozoic and Mesozoic., Rev. Palaeobot., Palynol., 37: 99-114.

Millot, G., (1970): Geology of clays; weathering, sedimentology, geochemistry. 429 pp., New York.

Millsteed, B.D., (1999): Palynology of the early Permian coal-bearing deposits near Vereeniging, Free State, South Africa, Bull. Geo. Suv. S. Afr., 81 pp.

Moldowan, J.M., Seifert, W.K., Gallegous, E.J., (1985): Relationship between petroleum composition and depositional environment of petrolium source rocks. AAPG Bull., 69:1255-1268.

Moldowan, J.M., Sundararaman, P. and Schoell, M., (1986): Sensitivity of biomarker properties to depositional environment and/or source input in the lower Toarcian of SW Germany. Org. Geochem. 10: 915-926.

Moldowan, M.J., Lee, C.Y., Sundrararaman, P., Salvatori,T., Alajbeg, A., Gjukic, B., Demaison, G.J., Slougui, N-E. & Watt, D.S., (1992): Sources correlation and maturity assessment of selected oils and rocks from the central Adriatic basin (Italy and Yugoslavia). In: Moldowan, M.J., Albrecht, P. & Philip, P.R. (ed.) Biological markers in sediments and petroleum. 411 pp., Prentice-Hall, London.

Muehlenbachs, K., (1987): Oxygen isotope exchange during weathering and low temperature alteration. In: Stable isotope geochemistry of low temperature processes. T.K. Kyser (Ed.). 187-257, Min. Soc. of Can.

Murray, H. H., (1988): Kaolin minerals; their genesis and occurrences. Rev. in Min. 19: 67-89.

Nesbitt, W.H., Markovics, G. & Price, R.C., (1980): Chemical processes affecting alkalis and alkaline earths during continental weathering. Geochim. Cosmochim. Acta, 44: 1659-1666.

Nesbitt, H.W. and Young, G.M., (1982): Early Proterozoic climates and plate motions inferred from major element chemistry of lutites. Nature, 299: 715-717.

Noble, R.A., Alexander, R., Kagi, R.I. & Knox, J., (1985): Tetracyclic diterpenoid hydrocarbons in some Australian coals, sediments and crude oils. Geochim. Cosmochim. Acta, 44: 2141-2147.

Noble, R.A., Alexander, R., Kagi, R.I. & Knox, J., (1986): Identification of some diterpenoid hydrocarbons in petroleum. Org. Geochem., 10: 825-829.

Nott, C.J., Shucheng,X, Avsej, L.A., Maddy, D., Chambers, F.M. & Evershed, R.P., (2000): n-Alkane distribution in ombrotrophic mires as indicators of vegetation change related to climatic variation. Org. Geochem., 31: 231-235.

Oelofsen, B. and Araújo, D.C., (1983): Palaeoecological implications of the distribution of mesosaurid reptiles in the Permian Irati Sea (Paraná Basin), South America. Rev. Bras. Geoc., 13: 1-6.

Oelofsen, B.W., (1987): The biostratigraphy and fossils of the Whitehill and Irati Shale Formation of the Karoo and Paraná Basins. In: McKenzie, G.D.(Ed.), Int. Gondw. Sym., 6: 131-138.

O'Neil, D.J:, (1987): Preservation of H, C, and O isotopic ratios in the low temperature environment. In Kyser, T.K. (Ed.), Short course in stable isotope geochemistry of low temperature fluids. Min. Ass. Can., 13: 85-121.

Ourisson, G., Albrecht, P., Rohmer, M., (1979): The hopanoids. Palaeochemistry and biochemistry of a group of natural products. Pure Appl. Chem. 51, 709-729.

Otto, A., Simoneit, B.R.T., Wilde, V., Kunzmann, L. and Püttmann, W., (2001): Terpenoid composition of three fossil resins from Cretaceous and Tertiary conifers. Rev. Palaeobot. Palynol., 120: 203-215.

Paige-Green, P., (1980): The clay mineralogy of Dwyka tillite in southern Africa and its effect on the geotechincal properties. Trans. Geol S. Afr., 83: 291-296.

Paytan, A., Kastner, M., Chavez, F.P., (1996): Glacial to interglacial fluctuations in productivity in the equatorial Pacific as indicated by marine barite. Science, 274: 1355-1357.

Perdersen, T.F. and Calvert, S.E., (1990): Anoxia vs productivity: what controls the formation of organic carbon-rich sediments and sedimentary rocks? AAPG Bull., 74: 454-466.

Peters, K.E., (1986): Guidelines for evaluating petroleum source rock using programmed pyrolysis. AAPG Bull., 70: 318-329.

Peters, K.E. and Moldowan, J.M., (1993): The biomarker guide. Interpreting Molecular fossils in petroleum and ancient sediments. 363 pp. Prentice Hall.

Pettijohn, F.J., Potter, P.E. & Siever, R., (1972): Sand and sandstone. 618 pp.; Springer, New York, Heidelberg, Berlin.

Pigg, K.B. and Taylor, T.N., (1993): Anatomically preserved Glossopteris stems with attached leaves from the Central Transarctic Mountains, Antarctica. Amer. J. Bot., 80: 500-516.

Pinheiro, H.J., Pretorius, C.C., Boshoff, H. & du Cann, V., (1998): Analysis of product samples of producing South African colleries., Bull. Mat. Sci. Tech., 112: 1-43.

Piper, D.Z., (1994): Seawater as the source of minor elements in black shales, phosphorites and other sedimentary rocks. Chem. Geol., 117: 95-114.

Piper, D.Z. and Perkins, R.B., (2004): A modern vs. Permian black shale - the hydrography, primary productivity, and water column chemistry of deposition. Chem. Geol., 206: 177-197.

Plumstead, E.P., (1957): Coal in Southern Africa. Univ. Witwatersrand Press, Johannesburg.

Plumstead, E.P., (1969): Three thousand million years of plant life in Africa., Geol. Soc. S. Afr. Trans., 72 (Annex.).

Popp, B.N., Parekh, P., Tilbrook, B., Bidigare, R.R. & Laws, E.A., (1997): Organic carbon $\delta^{13}C$ variations in sedimentary rocks as chemostratigraphic and paleoenvironmental tools. Palaeogeogr., Palaeoclimatol., Palaeoecol., 132: 119-132.

Popp, B.N., Lwas, E.A., Bidigare, R.R., Dore, J.E., Hanson, K.L, Wkeham, S.G., (1998): Effect of phytoplankton cell geometry on carbon isotope fractionation. Geochim. Cosmochim. Acta, 62: 69-77.

Powell, C. M., and Li, Z.X., (1994): Reconstruction of the Panthalassic margin of Gondwanaland. In: Permian-Triassic Pangea basins and foldbelts along the Panthalassan margin of Gondwana. Veevers, J.J. & Powell, C.M. (Eds.). Geol. Soc. Am. Mem., 184: 5-9.

Pysklywec, R.N. and Mitrovica, J.X., (1999): The role of subduction-induces subsidence in the evolution of the Karoo Basin. J. Geol., 107: 155-164.

Radke, M., Willsch, H. & Welte, D.H., (1980): Preparative hydrocarbon group type determination by automated medium pressure liquid chromatography. Anal. Chem., 52: 406-411.

Radke, M., Willsch, H., Leythaeuser, D. & Teichmüller, M., (1982): Aromatic components of coal: relation of distribution pattern to rank. Geochim. Cosmochim. Acta, 46: 1831-1848.

Radke, M., Welte, D.H. & Willsch, H., (1982): Geochemical study on a well in the Western Canada Basin: relation of the aromatic distribution pattern to maturity of organic matter. Geochim. Cosmochim. Acta, 46: 1-10.

Ramsbottom, W.H.C, (1979): Rates of transgression and regression in the Carboniferous of NW Europe. J. Geol. Soc., 136:147-153.

Raymond, A.C., Kelly, P.H., and Lutken, C.B., (1989): Polar glaciers and life at the equator; the history of Dinantian and Namurian (Carboniferous) climate. Geology. 17, 408-411.

Rayner, R.J., (1995): The palaeoclimate of the Karoo: evidence from plant fossils. Palaeogeogr., Palaeoclimatol., Palaeoecol., 119: 385-394.

Retallack, G.J., (1980): Late Carboniferous to Middle Triassic megaflorals from the Sydney Basin. In: Herbert, C. aand Helby, R. (Ed.), A guide to the Sydney Basin. New South Wales Geol. Surv., 26: 384-430.

Ries-Kautt, M. and Albrecht, P., (1989): Hopane-derived triterpenoids in soils. Chem. Geol. 76: 143-151.

Rohmer, M., Bisseret, P. & Neulist, S., (1992): The hopanoides, Prokaryotic Triterpenoids and precursors of ubiquitous molecular fossils. In: Biological markers in sediments. Moldowan, J.M., Albrecht, P. & Philip, R.P (Ed.)., 1-17, Prentice Hall; New Jersey.

Rollins, H., (1995): Using geochemical data: Evaluation, presentation, interpretation. pp. 352 Longman Group, England.

Ross, C.A., and Ross, J.R.P., (1987): Late Paleozoic depositional sequences are synchronous and worldwide. Geology, 13: 194-197.

Routh, J., McDonald, T.J. & Grossman E.L., (1999): Sedimentary organic matter sources and depositional environment in the Yegua formation (Brazos County, Texas). Org. Geochem., 30: 1437-1453.

Rowsell, D.M. and Connan, J. (1979): Oil generation, migration and preservation in the Middle Ecca Sequence near Dannhauser and Wakkerstrom. Geokongress 77: Geol. Soc. S. Afr. Spec. Publ., 6: 131-150.

Ruczika, L. and Hosking, J.R., (1930): Highe terpenoid compounds XLII: dehydrogeneration and isomeration of agathic acid. Helv. Chim. Acta., 13: 1402-1423.

Rullkötter, J., Spiro, B. & Nissenbaum, A., (1985): Biological marker characteristics of oils and asphalts from carbonate source rocks in a rapidly subsiding graben, Dead Sea, Israel. Geochim. Cosmochim. Acta, 49:1357-1370.

Rullkötter, J. and Marzi, R., (1988): Natural and artificial maturation of biological markers in a Toracian shale from northern Germany. Org. Geochem. 13, 639-645.

Rullkötter, J., Littke, R., Jendrzejewski, H.N., Radke, M. & Schaefer, R.G., (1995): Organic matter in dark and light coloured late Middle Aptian marine sediments from the Lower Saxony Basin, NW Germany (Hoheneggelsen KB 3 borehole)). N. Jb. Geol. Paläont. Abh., 196: 257-273.

Sadiq, M., (1988): Thermodynamic solubility relationships of inorganic vanadium in the marine environment. Mar. Chem., 23: 87-96.

Saltzman, M.R., (2003): Late Paleozoic ice age: Oceanic gateway or $pCO_2$? Geology, 31: 151–154.

Sampei, Y. and Matsumoto, E., (2001): C/N ratios in a sediment core from Nakaumi Lagoon, Southwest Japan; usefulness as an organic source indicator. Geochem. J., 35: 189-205.

Santos, P.R. dos, Rocha-Campos, A.C. & Canuto, J.R., (1996): Patterns of late Palaeozoic deglaciation in the Paraná Basin, Brazil. Palaeogeogr., Palaeoclimatol., Palaeoecol., 125: 165-184.

Savin, S.M. and Epstein, S., (1970): The oxygen and hydrogen isotope geochemistry of ocean sediments and shales. Geochim. Cosmochim. Acta, 34: 43-63.

Scalan, R.S. and Smith, J.E., (1970): An improved measure of the odd-even predominance in the normal alkanes of sediment extracts and petroleum. Geochim. Cosmochim. Acta, 34: 611-620.

Scheffler, K., (1999): Geochemische Untersuchungen zu Verwitterung von Tuffen im SW' Westerwald (Teil II). Diplomarbeit, pp. 111, Universität Bonn.

Scheffler, K., Hoerness, S. & Schwark, L., (2001): Changes in the sedimentary environment recorded in late Palaeozoic sediments of the Paraná Basin. Zbl. Geol. Paläont. Teil 1, 2000: 155-166.

Scheffler, K., Hoernes, S. & Schwark. L., (2003): Global changes during Carboniferous–Permian glaciation of Gondwana: Linking polar and equatorial climate evolution by geochemical proxies. Geology, 31: 605-608.

Scheffler, K. & Schwark, L., (2004): Climate-induced cyclic changes in organic matter composition during the final Gondwana deglaciation. Palaeogeogr., Palaeoclimatol., Palaeoecol. (submitted).

Schultze, T. and Michealis, W., (1990): Structure and origin of terpenoid hydrocarbons in some German coals. Org. Geochem., 13: 639-645.

Schulze, P. M., (1994): Beschreibende Statistik. 2. Aufl., 355 p.

Schwark, L., Vliex, M. & Schäffer, P., (1998): Geochemical characterization of Malm Zeta laminated carbonates from the Franconian Alb, SW-Germany; II. In: Grimalt, J. O., Maxwell, J. R & Sinninghe Damste, J. S. (Eds.), Geochemistry of sulphur-rich organic matter in carbohydrate/evaporite depositional environments. Org. Geochem. 29: 1921-1952.

Schwark, L. Zink, K., Lechterbeck J., (2002): Reconstruction of Postglacial to Early Holocene vegetation history in terrestrial Mid-Europe via cuticular lipid biomarkers and pollen records from lake sediments, Geology, 30: 463-466.

Seibolt, E., Müller, G. & Fesser, H., (1958): Chemische Untersuchungen eines Sapropels aus der mittleren Adria. Erdöl und Kohle, 11: pp 296.

Seifert, W.K. and Moldowan, J.M., (1978): Applications of steranes, terpanes, and monoaromatics to the maturation, migration and source of crude oils. Geochim. Cosmochim Acta. 42: 77-95.

Seifert, W. and Moldowan, J.M., (1986): Use of biological markers in petroleum exploration. In: Methodes in Geochemistry and Geophysics (Johns, R.B Ed.) Vol. 24: 261-290.

Shannon, R.D., (1976): Revisted effective ionic radii and systematic studies of interatomic distances in halides and chalcogenides. Acta Cryst. A32: 751-767.

Sharp, Z.D., (1999): Application of stable isotope geochemistry to low.grade metamorphic rocks. In: M. Frey & D. Robinson (ed.) Low-grade metamorphism., pp. 227-260.

Shaviv, N.J., (2002): Cosmic Ray Diffusion from Galactic Spiral Arms, Iron Meteorites, and a possible Climatic Connection. Phys. Rev. Lett., 89: 051102.

Shaw, T.J., Gieskes, J.M. & Jahnke, R.A., (1990): Early diagenesis in differing depositional environments: the response of transition metals in pore water. Geochim. Cosmochim. Acta, 54: 1233-1246.

Sieskind, O., Joly, G. & Albrecht, P., (1979): Simulation of the geochemical transformations of sterols; superacid effect of clay minerals Geochim. Cosmochim. Acta, 43: 1675-1680.

Siehl, A. and Thein, J., (1978): Geochemische Trends in der Minette (Jure, Luxemburg/Lotringen). Geol. Rundsch., 67/3: 1052-1077.

Simoneit, B.R.T., Grimalt, J.O., Wang, T.G., Cox, R.E., Hatcher, P.G. & Nissen-Baum, A., (1986): Cyclic terpenoids of contemporary resinous plant detritus and of fossil woods, ambers and coals. Org. Geochem. 10: 877-889.

Smith, A.G., Hurley, A.M. & Briden, J.C., (1981): Phanerozoic palaeocontinental world maps. pp. 102, Cambr. Univ. Press.

Smith, R.M.H., Eriksson, P.G. & Botha, W.J., (1993): A review of the stratigraphy and sedimentary environments of the Karoo-aged basins of Southern Africa. J Afr. Earth. Sci., 16: 143-169.

Smith, R.M.H. and Ward, P.D., (2001): Pattern of vertebrate extinctions aross an event bed at the Permian-Triassic boundary in the Karoo basin of South Africa. Geology, 29: 1147-1150.

Soreghan, G.S. and Giles, K.A., (1999): Amplitudes of Late Pennsylvanian glacioeustasy. Geology, 27: 255-258.

Sousa, J.J.F., Vugman, N.V. & Mangrich, A.S., (1987): An ESR study on the Irati oil shale kerogen. Chem. Geol., 63: 17-20.

Spotts, J.H. and Silverman, S.R., (1966): Organic dolomite from Point Fermin, California. Amer. Min., 51:1144-1155.

Stach, E., Mackowsky, M-Th., Teichmüller, M., Taylor, G.H., Chandra, D. & Teichmüller, R., (1982): Stach's Textbook of coal Petrology. Bornträger, Berlin.

StatSoft, Inc., (1993): Software package STATISTICA 4.3.

Stewart, W.N., (1983): Palaeobotany and the evolution of plants. Cambridge University Press, Cambridge, pp. 348.

Stollhofen, H., Gerschütz, S., Stanistreet, I.G. & Lorenz V., (1998): Tectonic and volcanic controls on Early Jurassic rift-valley lake deposition during emplacement of Karoo flood basalts, southern Namibia. Palaeogeogr., Palaeoclimatol., Palaeoecol., 140: 185-215.

Stollhofen, H., Stanistreet, I.G., Bangert, B. & Grill, H., (2000): Tuffs, tectonism and glacially related sea-level changes, Carboniferous-Permian, southern Namibia. Palaeogeogr., Palaeoclimatol., Palaeoecol., 161: 127-150.

Strachnan, M.G., Alexander, R. & Kagi, R.I., (1988): Trimethylnaphthalenes in crude oils and sediments: effects on source and maturity. Geochim. Cosmochim. Acta, 52: 1255-1264.

Suess, E., (1980): Particulate organic carbon flux in the oceans-surface productivity and oxygen utilisation. Nature, 288: 260-263.

Tankard, A.J., Erikson, K.A., Hunter, D.R., Jackson, M.P.A., Hobay, D.K. & Minter, W.E.L., (1982): Crustal evolution of Southern Africa; 3.8 billion years of earth history. Springer Verlag, NY, United States, 523 p.

Taylor, H.P. Jr., and Epstein, S., (1962): Relationship between $O^{18}/O^{16}$ ratios in coexisting minerals of igneous and metamorphic rocks; Part 2, Application to petrologic problems. Geol. Soc. Am., 73: 675-693.

Taylor, S.R. and McLennan, S.M., (1985): The continental crust: Its composition and evolution. 312 pp., Blackwell Sci.

Taylor, G.H., Teichmüller, M., Davis, A., Diessel, C.F.K., Littke, R. & Robert, P., (1998): Organic petrology. 704 pp., 70 tab.; Berlin (Borntraeger).

Teichmüller, M., (1989): The genesis of coal from the viewpoint of coal petrology. Int. J. Coal Geol., 12: 1-87.

ten Haven, H.L., de Leeuw, J.W., Rullkötter, J. & Sinninghe Damsté, J.S., (1987): Restricted utility of the pristane/phytane ratio as a palaeoenvironmental indicator. Nature, 330: 641-643.

ten Haven, H.L., De Leeuw, J.W., Sinninghe Damste, J.S., Schenck, P.A., Palmer, S.E., Zumberge, J.E., (1988): Application of biological markers in the recognition of palaeohypersaline environments. In: Lacustrine Petroleum Source Rocks. Fleet, A.J., Kelts, K., Talbot, M.R. (Eds.)., Geol. Soc. Sp. Pub., 40: 123–130.

ten Haven, H.L., Littke, R., Rullkotter, J., (1992): Hydrocarbon biological markers in Carboniferous coals of different maturities. In: Biological Markers in Sediments and Petroleum. Moldowan, J.M., Albrecht, P., Philp, R.P. (Eds.)., Prentice Hall, New Jersey, pp. 142– 155.

Theron J.N. and Blignault H.J., (1975): A model for the sedimentation of the Dwyka Glacials in the southwestern Cape. Int. Gondw. Sym., 3: 347-356.

Thomas, B.R., (1969): Kauri resins – modern and fossil. In: Organic Geochemistry-Methods and Results (Eglington, G. & Murphy, M.T.J., Eds.), Springer, Berlin, pp. 599-618.

Thome, K.N., (1997): Einführung in das Quartär: Das Zeitalter der Gletscher. 287 pp., Springer, Berlin.

Tissot, B., Califet-Debyser, Y., Deroo, G. & Oudin, J.L. (1971): Origin and evolution of hydrocarbons in early Toracian shales, Paris Basin, France. AAPG Bull., 55: 2177-2193.

Tissot, B.T. and Welte, D.H., (1984): Petroleum formation and occurrence. 699 pp., Springer, Berlin.

Traverse, A. (1988): Paleopalynology. 600 pp., Unwin Hyman Ltd., Boston.

Tucker, B.R., (1992): Sedimentary Petrology – An introduction to the orgin of sedimentary rocks. 2ed. 260 pp., Berlin: Blackwell scientific publications.

Turner, B.R., (1986): Tectonic and climatic controls on continental depositional facies in the Karoo Basin of northern Natal, South Africa. Sediment. Geol., 46: 231-257.

Turner, B.R., (1999): Tectonostratigraphical development of the Upper Karoo foreland basin: orogenic unloading versus thermally-induced Gondwana rifting. J. Afr. Earth Sci., 28: 215-238.

Tyson, V.R., (1995): Sedimentary organic matter; organic facies and palynofacies. 615 p., Chapman and Hall.

Van Kaam-Peters, H.M.E., Schouten, S., De Leeuw, J.W. and Damste, J.S.S., (1997): A molecular and carbon isotope biogeochemical study of biomarkers and kerogen pyrolysates of the Kimmeridge Clay Facies: palaeoenvironmental implications. Org. Geochem. 27: 399-422.

Veevers, J.J., (1993): Gondwana facies of the Pangean supersequence: A review. Int. Gondw. Sym. Findlay, Unrug, Banks & Veevers (Eds.)., 8: 513-520.

Veevers, J.J. and Powell, C., (1987) Late Paleozoic glacial episodes in Gondwanaland reflected in transgressive-regressive depositional sequences in Euramerica. Geol. Soc. Am. Bull., 98: 475-487.

Veizer, J., Ala, D., Azmy, K., Bruckschen, P., Buhl, D.; Bruhn, F.; Carden, G.A.F. & Diener, A., (1999) $^{87}Sr/^{86}Sr$, $\delta^{13}C$ and $\delta^{18}O$ evolution of Phanerozoic seawater. Chem. Geol. 161: 59-88.

Veizer, J., Godderis, Y. & François, L.M., (2000): Evidence for decoupling of atmospheric $CO_2$ and global climate during the Phanerozoic eon. Nature, 408: 698-701.

Velde .B., (1992): Introduction to clay minerals. 198pp. Chapman & Hall, London.

Velde, B., (1995): Origin and mineralogy of clays. Clays and the environment. 334 pp., Springer, Berlin.

Vidotti, R. M., Ebinger, C. J. & Fairhead, J. D., (1998): Gravity signature of the western Paraná basin, Brazil. Earth Planet. Sci. Lett., 159: 117-132.

Viljoen, J.H.A., (1994): Sedimentology of the Collingham Formation, Karoo Supergroup. S. Afr. J. Geol., 97(2): 167-183.

Visser, J.N.J., (1987): The palaeogeography of part of southwestern Gondwana during the Permo-Carboniferous glaciation. Palaeogeogr., Palaeoclimatol., Palaeoecol., 61: 205-219.

Visser, J. N. J., (1989): The Permo-Carboniferous Dwyka Formation of southern Africa: deposition by a predominantly subpolar marine ice sheet. Palaeogeogr., Palaeoclimatol., Palaeoecol., 70: 377-391.

Visser, J.N.J., (1990): Glacial bedforms at the base of the Permo-Carboniferous Dwyka Formation along the western margin of the Karoo Basin, South Africa. Sedimentology, 37: 231-245.

Visser, J.N.J., (1992): Basin tectonics in southwestern Gondwana during the Carboniferous and Permian. In: Inversion tectonics of the cape fold belt, Karoo and Cretaceous basins of southern Africa. De Wit, M.J., Ransome, I.G.D. (Ed.), pp. 109-115.

Visser, J.N.J., (1993): A reconstruction of the late Palaeozoic ice sheet on southwestern Gondwana. Int. Gondw. Sym., Findlay, Unrug, Banks & Veevers (Eds.)., 8: 449-458.

Visser, J.N.J., (1995): Post-glacial Permian stratigraphy and geography of southern and central Africa: boundary conditions for climatic modelling. Palaeogeogr., Palaeoclimatol., Palaeoecol., 118: 213-243.

Visser, J.N.J., (1996): Controls on Early Permian shelf deglaciation in the Karoo Basin of South Africa. Palaeogeogr., Palaeoclimatol., Palaeoecol., 125: 129-139.

Visser, J.N.J., (1997): Deglaciation sequences in the Permo-Carboniferous Karoo and Kalahari basins of southern Africa: a tool in the analysis of cyclic glaciomarine basin fills. Sedimentology, 44: 507-521.

Visser, J.N.J. and Loock, J.C., (1978): Water depth in the main Karoo Basin, South Africa, during Ecca (Permian) sedimentation. Trans. Geol. Soc. S. Afr., 81: 185-191.

Visser, J.N.J. and Van den Berg, H.J., (1981): Late Carboniferous glacial and fluvioglacial deposits in the Tshipise Basin, South Africa. Int. Gondw. Sym., Cresswell (Ed.), 5: 111-115.

Visser, J.N.J. and Young, G.M., (1990): Major element geochemistry and paleoclimatology of the Permo-Carboniferous glacigene Dwyka Formation and post-glacial mudrocks in southern Africa. Palaeogeogr., Palaeoclimatol., Palaeoecol., 81: 49-57.

Visser, J.N.J. and Praekelt, H.E., (1996): Subduction, mega-shear systems and Late Palaeozoic basin development in the African segment of Gondwana. Geol. Rundsch., 85: 632-646.

Vliex, M., Schwark, L. & Leythaeuser, D., (1997): Organisch-geochemische und organisch-petrologische Indikatoren für Meeresspiegel-Variationen im permischen Staßfurt-Karbonat in NE-Deutschland. Zbl. Geol. Paläont. Teil 1, 10-12: 1447-1467.

Vogel, W. and Kuipers, G., (1987): A pre-calibrated program for geological applications. – Philips, New Developments, X-Ray Spectrometry TA 11: 2-8.

Volkman, J.K., Alexander, R., Kagi, R.I., Rullkötter, J., (1983): GC-MS characterisation of C27 and C28 triterpanes in sediments and petrolium. Geochim. Cosmochim. Acta. 47: 1033-1040.

Volkman, J.K. and Maxwell, J.R., (1986): Acyclic isoprenoids as biological markers. In: Biological markers in the sedimentary record. Methods in geochemistry and geophysics; 24. Johns, R.B. (Ed.), 364 pp., 82 fig., 28 tab., Elsevier.

Von Brunn, V., (1983): A model for late Dwyka glaciomarine sedimentation in the eastern Karoo Basin. Trans. Geol. Soc South Afr., 86: 199-209.

Wanless, H.R. and Sheppard, F.P., (1936): Sea level and climate changes related to late Palaeozoic cycles. Geol. Soc. Am. Bull., 47: 1177-1206.

Weaver, C.E., (1960): Possible uses of clay minerals in search for oil. AAPG. 44: 1505-1518.

Weaver, C.E., (1989): Developments in Sedimentology 44: Clays, Muds, and Shales. 819 S., Elsevier Sci. Publ., Amsterdam.

Weaver, C.E. and Polland, L.D., (1973): Developments in sedimentology 15: The chemistry of clay minerals. 213 pp., Elsevier Sci. Publ., Amsterdam.

Weber, K., (1972): Notes on the determination of illite crystallinity. Neues Jb. Mineral. Mh. 1972: 267-276.

Wedepohl, K.H, (1969): Composition and abundance of common sedimentary rocks, Chapter 8 in handbook of geochemistry, v. 1. Geol. Surv. Prof. Pap., 1969: 250-271.

Wedepohl, K.H., (Editor) (1978): Handbook of Geochemistry, Vols. I-IV. Springer, Berlin.

Wehausen, R. and Brumsack, H.-J., (2000): Chemical cycles in Pliocene sapropel-bearing and sapropel-barren eastern Mediterranean sediments. Palaeogeogr., Palaeoclimatol., Palaeoecol., 158: 325-352.

Wenger, L.M. and Baker, D.R., (1985): Variations in organic geochemistry of anoxic-oxic black shale-carbonate sequences in the Pennsylvanian of the Midcontinent, U.S.A.. Org. Geochem., 10: 85-92.

Wickens, H. and De Villiers, (1992): Submarine fans of the Permian Ecca Group in the SW Karoo Basin: Their origin and reflection on the tectonic evolution of the basin and its source areas. In: Inversion tectonics of the cape fold belt, Karoo and Cretaceous basins of southern Africa. De Wit, M.J., Ransome, I.G.D. (Ed.), 117-125.

Wilde, P., Quinby-Hunt, M.S. & Erdtmann, B.-D., (1996): The whole rock cerium anomaly: A potential indicator of eustatic sea level changes in shales of the anoxic facies. Sed. Geol., 101: 45-53.

Wimmenauer, W., (1984): Das prävariskische Kristallin im Schwarzwald. Fortschr. Miner., 62: 69-86.

Wopfner, H., (1993): Structural development of Tanzanian Karoo Basins and the break-up of Gondwana. Int. Gondw. Sym., Findlay, Unrug, Banks & Veevers (Eds.), 8: 531-539.

Wright, J., Schrader, H. & Holser, W.T., (1987): Paleoredox variations in ancient oceans recorded by rare earth elements in fossil apatite. Geochim. Cosmochim. Acta, 51: 631-644.

Yapp, C.J., (1987): Oxygen and Hydrogen isotope variations among goethite ($\alpha$–FeOOH) and the determination of paleotemperatures. Geochim. Cosmochim. Acta., 51: 355-364.

Yemane, K., (1993): Contribution of the Late Permian palaeography in maintaining a temperate climate in Gondwana. Nature, 3651: 51-54.

Zalán, P.V., Wolff, S., Conceicao, J.C.J., Marques, A., Astolfi, M.A.M., Vieira, I.S., Appi, V.T. & Zarotto, O.A., (1990): The Paraná Basin, Brazil. In: Interior Cratonic Basins. M. W. Leighton, D. R. Kolata & D. F. Oltz (Ed.), AAPG, 51: 681-708.

Zawada, P.K., (1988): Trace elements as possible palaeosalinity indicators for the Ecca and Beaufort Group mudrocks in the southwestern Orange Free State. S.-Afr. Tydskr. Geol., 91(1): 18-26.

Zechner, J.P., (2003): Stratigraphie und Tektonik am Nordrand des Cape Fold Belt in der Umgebung von Laingsburg (südwestliche Kap-Provinz/Südafrika). Teil 2: Röntgendiffraktometrische Untersuchungen an Peliten der oberen Bokkeveld bis unteren Beaufort Group (mittlers Devon bis oberes Perm). Diplomarbeit, Universität Bonn.

# 10. Appendix

## Geochemical data

**A: southern Karoo Basin**

**B: MPU core**

**C: OGT core**

**D: Paraná Basin**

**E: Warmbad Basin**

**F: Keetmanshoop**

## Mineralogical data

**G: XRD-MPU**

**H: XRD-OGT**

## Organic geochemical data

**I: Paraná Basin**

**J: Witbank Basin**

| Sample | Lab. Nr. | Fm. | rel. Position [m] | Ma | (CaCO3 %) | TC | S | TOC | $\delta^{13}$Corg |
|---|---|---|---|---|---|---|---|---|---|
| A155 | | Pf | 1350 | 264,9 | | | | | |
| A154 | | Pf | 1343 | 265,0 | | | | | |
| A153 | | Pf | 1335 | 265,0 | | | | | |
| A152 | | Pf | 1320 | 265,1 | | | | | |
| F42 | | Pf | 1298 | 265,1 | | | | | |
| A150 | | Pf | 1280 | 265,1 | | | | | |
| A149 | | Pf | 1273 | 265,2 | | | | | |
| A148 | | Pf | 1270 | 265,2 | | | | | |
| A147 | | Pf | 1255 | 265,2 | | | | | |
| A146 | | Pl | 1248 | 265,3 | | | | | |
| A145 | | Pl | 1240 | 265,5 | | | | | |
| A144 | | Pl | 1230 | 265,6 | | | | | |
| A143 | | Pl | 1183 | 265,8 | | | | | |
| A142 | | Pl | 1170 | 265,8 | | | | | |
| A141 | | Pl | 1127 | 265,9 | | | | | |
| A140 | | Pl | 1117 | 266,0 | XRF-analyses: | | | | |
| A139 | | Pl | 1115 | 266,1 | D. Adelman (1995), | | | | |
| A138 | | Pl | 1095 | 266,1 | D. Albes (1996), | | | | |
| A137 | | Pl | 1075 | 266,1 | R.K. Knütter (1994) | | | | |
| A136 | | Pl | 1071 | 266,1 | | | | | |
| A135 | | Pl | 1067 | 266,1 | | | | | |
| A134 | | Pl | 1065 | 266,1 | | | | | |
| A133 | | Pl | 1062 | 266,2 | | | | | |
| A132 | | Pl | 1060 | 266,3 | | | | | |
| A131 | | Pl | 1040 | 266,3 | | | | | |
| A130 | | Pl | 1035 | 266,5 | | | | | |
| A129 | | Pl | 1030 | 266,5 | | | | | |
| A128 | | Pl | 990 | 266,6 | | | | | |
| A127 | | Pv | 988 | 266,7 | | | | | |
| A122 | | Pv | 973 | 266,8 | | | | | |
| A121 | | Pv | 960 | 266,9 | | | | | |
| A120 | | Pv | 955 | 267,0 | | | | | |
| A119 | | Pv | 940 | 267,2 | | | | | |
| A118 | | Pv | 925 | 267,3 | | | | | |
| F28 | | Pv | 918 | 267,3 | | | | | |
| A116 | | Pv | 910 | 267,4 | | | | | |
| A115 | | Pv | 905 | 267,5 | | | | | |
| A114 | | Pv | 895 | 267,6 | | | | | |
| F27 | | Pv | 887 | 267,6 | | | | | |
| A113 | | Pv | 880 | 267,7 | | | | | |
| A112 | | Pv | 875 | 267,7 | | | | | |
| A111 | | Pv | 870 | 267,8 | | | | | |
| A110 | | Pv | 861 | 267,8 | | | | | |
| A109 | | Pv | 860 | 268,0 | | | | | |
| A108 | | Pv | 843 | 268,1 | | | | | |
| A107 | | Pv | 835 | 268,3 | | | | | |
| A106 | | Pv | 815 | 268,3 | | | | | |
| A105 | | Pv | 813 | 268,4 | | | | | |
| A104 | | Pv | 803 | 268,4 | | | | | |
| A103 | 993549 | Pv | 802 | 268,5 | 8,9 | 0,56 | 0,00 | 0,51 | -22,375 |
| A102 | | Pv | 799 | 268,5 | | | | | |
| A101 | | Pv | 797 | 268,5 | | | | | |
| A31 | | Pv | 796,5 | 268,5 | | | | | |
| A30 | 993547 | Pv | 795 | 268,5 | 65,9 | 7,98 | 0,01 | 0,26 | -23,77 |
| A29 | 993546 | Pv | 794 | 268,5 | 9,3 | 0,20 | 0,00 | 0,17 | -24,03 |
| A28 | 993545 | Pv | 790 | 268,6 | | | | | |
| A27 | 993544 | Pv | 788,5 | 268,6 | 11,6 | 0,75 | 0,00 | 0,29 | -22,26 |
| A26 | 993543 | Pg | 782,1 | 268,7 | 5,1 | 0,23 | 0,00 | 0,20 | -21,61 |
| A25 | | Pg | 779 | 268,7 | | | | | |
| K70 | 993542 | Pg | 776,5 | 268,8 | 19,7 | 1,93 | 0,01 | 0,05 | |
| K68 | 993541 | Pg | 772,9 | 268,9 | 7,6 | 0,41 | 0,00 | 0,17 | -14,85 |
| A24 | 993540 | Pg | 772,7 | 268,9 | 9,4 | 0,53 | 0,01 | 0,16 | -13,57 |
| A23 | 993539 | Pg | 772,5 | 268,9 | 7,0 | 0,27 | 0,00 | 0,24 | -23,93 |
| A22 | 993538 | Pg | 772,1 | 268,9 | 8,0 | 0,33 | 0,00 | 0,23 | -21,615 |
| A21 | 993537 | Pg | 764,7 | 269,0 | 13,3 | 1,48 | 0,00 | 0,39 | -22,21 |
| K66 | 993536 | Pg | 761,9 | 269,1 | 4,4 | 0,80 | 0,00 | 0,49 | -21,685 |
| A20 | 993535 | Pg | 759,3 | 269,1 | 8,1 | 0,99 | 0,07 | 0,56 | -21,285 |
| A19 | 993534 | Pg | 750,7 | 269,3 | 5,2 | 0,43 | 0,01 | 0,06 | -23,04 |
| A18 | 993533 | Pg | 749 | 269,3 | | | | | |
| A17 | 993532 | Pg | 747,5 | 269,4 | 6,0 | 0,59 | 0,01 | 0,45 | -22,43 |
| A16 | 993531 | Pg | 745,3 | 269,4 | 4,2 | 1,28 | 0,02 | 0,99 | -25,525 |
| A15 | | Pg | 740 | 269,5 | | | | | |
| K15 | 993530 | Pg | 732,7 | 269,7 | 2,6 | 1,20 | 0,00 | 0,93 | -22,255 |
| K14 | 993529 | Pg | 732,6 | 269,7 | 11,8 | 1,09 | 0,03 | 0,07 | -20,11 |
| K13 | 993528 | Pg | 732,5 | 269,7 | 12,3 | 1,58 | 0,00 | 0,05 | -25,54 |
| K12 | 993527 | Pg | 731,3 | 269,7 | 4,1 | 0,47 | 0,01 | 0,35 | -21,89 |
| K11 | 993526 | Pg | 731,1 | 269,7 | 5,2 | 0,34 | 0,00 | 0,06 | -22,99 |
| K10 | 993525 | Pg | 731 | 269,7 | 7,2 | 0,24 | 0,02 | 0,02 | |
| K9 | 993524 | Pg | 730,9 | 269,7 | 8,4 | 0,85 | 0,00 | 0,65 | -21,67 |
| K8 | 993523 | Pg | 730,8 | 269,7 | 27,0 | 2,78 | 0,01 | 0,46 | -22,28 |
| K7 | 993522 | Pg | 730,7 | 269,8 | 5,9 | 0,71 | 0,02 | 0,43 | -21,895 |
| A14 | | Pg | 727,5 | 269,8 | | | | | |
| A13 | 993521 | Pg | 727,3 | 269,8 | 4,6 | 0,85 | 0,15 | 0,77 | -22,27 |
| K5/2 | 993520 | Pg | 726,1 | 270,0 | 12,1 | 1,30 | 0,02 | 0,67 | -22,815 |
| K5/1 | | Pg | 725,6 | 270,2 | | | | | |
| K3 | 993519 | Pg | 723,7 | 270,2 | 45,8 | 5,96 | 0,02 | 0,03 | |
| A68 | | Pw | 723,3 | 270,5 | | | | 0,14 | |
| A70 | 993518 | Pw | 720 | 271,0 | 6,9 | 0,85 | 0,02 | 0,77 | -22,22 |
| A67 | 993517 | Pw | 714,8 | 271,5 | 2,8 | 0,39 | 0,07 | 0,34 | -20,2 |
| A66 | | Pw | 710 | 271,8 | | | | 0,12 | |

| | | | | | | | | | |
|---|---|---|---|---|---|---|---|---|---|
| **A65** | **993516** | Pw | 707,3 | 272,3 | 15,5 | 1,79 | 0,29 | 1,63 | -18,34 |
| **A64** | **993515** | Pw | 701,3 | 272,4 | 3,6 | 0,09 | 0,11 | 0,07 | -22,42 |
| **A63** | **993514** | Pw | 700 | 272,6 | | 12,99 | 0,09 | 0,49 | |
| **A62** | | Pw | 698,6 | 272,7 | | | | 3,39 | |
| **A61** | **993513** | Pw | 697,5 | 272,7 | 67,1 | 8,21 | 0,38 | 0,22 | -24,35 |
| **A60** | | Pw | 697 | 272,8 | | | | 0,10 | |
| **A59** | **993512** | Pw | 696,3 | 273,1 | 1,8 | 0,35 | 0,38 | 0,30 | -21,86 |
| **A58** | **993511** | Pw | 693 | 273,3 | 47,5 | 5,57 | 9,17 | 0,69 | -19,685 |
| **A57** | **993510** | Pw | 690,9 | 273,5 | 7,8 | 1,16 | 0,66 | 1,03 | -19,97 |
| **A56** | **993509** | Pw | 689 | 273,6 | 43,0 | 2,29 | 6,55 | 0,77 | -20,16 |
| **A55** | **993508** | Pw | 688 | 273,8 | 45,7 | 12,40 | 0,39 | 0,31 | |
| **A54** | **993507** | Pw | 686 | 273,9 | 67,2 | 0,23 | 10,59 | 0,18 | -21,34 |
| **A53** | | Pw | 685 | 273,9 | | | | 0,34 | |
| **A52** | | Pw | 684,5 | 274,0 | | | | 1,27 | |
| **A51** | | Pw | 684 | 274,0 | | | | 2,94 | |
| **A50** | **993506** | Pw | 683,8 | 274,2 | 13,3 | 3,20 | 1,45 | 2,95 | -22,19 |
| **A49** | **993505** | Pw | 682,1 | 274,2 | 9,5 | 0,10 | 0,98 | 0,08 | -23,9 |
| **A48** | **993504** | Pw | 681,8 | 274,2 | 31,1 | 0,14 | 11,95 | 0,26 | -22,34 |
| **A47** | **993503** | Pw | 681,6 | 274,3 | 11,7 | 1,18 | 1,10 | 1,17 | -22,15 |
| **A46** | **993502** | Pw | 681 | 274,4 | | 4,12 | 1,48 | 3,80 | |
| **A44** | **993501** | Pw | 679,6 | 274,5 | 67,8 | 7,56 | 1,71 | 0,23 | -24,37 |
| **A45** | **993500** | Pw | 678,6 | 274,7 | 13,2 | 1,10 | 1,55 | 0,98 | -20,56 |
| **A43** | **993499** | Pw | 676,3 | 274,9 | 60,1 | 2,70 | 8,71 | 0,52 | -21,84 |
| **A42** | **993498** | Pp | 674,3 | 275,1 | 25,0 | 0,29 | 0,10 | 0,23 | -21,945 |
| **A41** | **993497** | Pp | 672 | 275,8 | 66,5 | 7,46 | 0,60 | 0,10 | |
| **D176** | **993496** | Pp | 664,8 | 277,0 | 2,7 | 0,64 | 0,06 | 0,58 | -21,59 |
| **D175** | | Pp | 652,2 | 277,1 | | | | | |
| **D174** | **993495** | Pp | 651,6 | 277,2 | 19,4 | 0,26 | 0,01 | 0,18 | -22,045 |
| **D173** | | Pp | 649,9 | 277,4 | | | | | |
| **D172** | **994219** | Pp | 648,1 | 277,8 | | | | | -22,135 |
| **D171** | | Pp | 644,4 | 278,2 | | | | | |
| **D170** | **994218** | Pp | 640,2 | 278,6 | | | | | -22,73 |
| **D169** | | Pp | 636 | 278,8 | | | | | |
| **D168** | **993494** | Pp | 633,4 | 278,9 | 21,8 | 0,21 | 0,03 | 0,08 | -20,94 |
| **D167** | **993493** | Pp | 632,8 | 279,3 | 14,4 | 0,12 | 0,00 | 0,09 | -22,31 |
| **D166** | **993492** | Pp | 628,8 | 279,6 | 17,6 | 0,12 | 0,00 | 0,10 | -23,8 |
| **D165** | **993491** | Pp | 625,5 | 279,9 | | 0,11 | 0,00 | | |
| **D164** | **993490** | Pp | 622,4 | 280,3 | 8,1 | 0,09 | 0,00 | 0,07 | -22,13 |
| **D163** | **993489** | Pp | 618,1 | 280,6 | 12,6 | 0,10 | 0,00 | 0,06 | -21,93 |
| **D162** | **993488** | Pp | 614,3 | 280,9 | 18,1 | 0,13 | 0,00 | 0,10 | -22,04 |
| **D161** | **994217** | Pp | 611,2 | 281,1 | | | | | -22,585 |
| **D160** | **993487** | Pp | 609,9 | 281,3 | 15,0 | 0,31 | 0,00 | 0,27 | -22,61 |
| **D159** | **993486** | Pp | 607,8 | 281,3 | 13,2 | 0,30 | 0,00 | 0,23 | -22,855 |
| **D157** | | Pp | 607,3 | 281,3 | | | | | |
| **D156** | **993485** | Pp | 607,2 | 281,5 | 11,9 | 0,34 | 0,01 | 0,31 | -22,52 |
| **D155** | **994216** | Pp | 605,7 | 281,8 | | | | | -23,75 |
| **D154** | **993484** | Pp | 602,7 | 281,8 | 36,0 | 0,26 | 0,04 | 0,07 | -19,685 |
| **D153** | | Pp | 602,5 | 282,0 | | | | | |
| **D152** | **993483** | Pp | 600,2 | 282,2 | 21,8 | 0,46 | 0,00 | 0,40 | -23,225 |
| **D151** | **994215** | Pp | 598,5 | 282,5 | | | | | -22,565 |
| **D150** | **993482** | Pp | 595,1 | 282,7 | 16,7 | 0,34 | 0,00 | 0,22 | -23,055 |
| **D149** | | Pp | 592,5 | 282,8 | | | | | |
| **D148** | **993481** | Pp | 592,2 | 283,0 | | | 0,00 | | |
| **D147** | **994214** | Pp | 589,3 | 283,4 | | | | | -22,85 |
| **D146** | **993480** | Pp | 585,9 | 284,0 | | | 0,00 | | |
| **D145** | **993479** | Pp | 578,8 | 284,5 | 7,1 | 0,16 | 0,00 | 0,13 | -22,195 |
| **D144** | **993478** | Pp | 574,4 | 284,5 | 6,4 | 0,08 | 0,00 | 0,06 | -21,68 |
| **D143** | | Pp | 574,2 | 284,5 | | | | | |
| **D142** | **993477** | Pp | 573,8 | 284,5 | 5,9 | 0,13 | 0,00 | 0,11 | -22,195 |
| **D141** | **993476** | Pp | 573,6 | 284,8 | 5,5 | 0,11 | 0,00 | 0,08 | |
| **D140** | **993475** | Pp | 570,8 | 285,0 | 15,6 | 0,12 | 0,00 | 0,08 | |
| **D139** | **993474** | Pp | 568,5 | 285,6 | 12,8 | 0,17 | 0,00 | 0,14 | -22,22 |
| **D138** | **993473** | Pp | 562,6 | 285,7 | 15,1 | 0,13 | 0,00 | 0,10 | -22,32 |
| **D137** | | Pp | 561,8 | 285,7 | | | | | |
| **D136 b** | **993472** | Pp | 561,6 | 286,2 | 18,2 | 0,15 | 0,00 | 0,12 | -21,905 |
| **D136** | **993471** | Pp | 556,3 | 286,7 | 11,8 | 0,07 | 0,00 | 0,04 | |
| **D135** | **994213** | Pp | 550,9 | 287,0 | | | | | |
| **D134** | **993470** | Pp | 547,7 | 287,5 | 8,8 | 0,07 | 0,00 | 0,05 | -23,77 |
| **D133** | **994212** | Pp | 542,5 | 287,9 | | | | | |
| **D132** | **993469** | Pp | 538,5 | 288,2 | 11,2 | 0,19 | 0,00 | 0,17 | -22,06 |
| **D131** | **994211** | Pp | 535,8 | 288,3 | | | | | -22,36 |
| **D130 o** | | Pp | 534,5 | 288,3 | | | | | |
| **D130 u** | **993468** | Pp | 534,4 | 288,3 | 47,6 | 0,83 | 0,07 | 0,41 | -20,09 |
| **D129** | **993467** | Pp | 534,3 | 288,4 | 9,8 | 0,18 | 0,00 | 0,14 | -22,775 |
| **D128** | **994210** | Pp | 532,8 | 288,5 | | | | | -23,585 |
| **D127** | **993466** | Pp | 532,6 | 288,8 | 4,1 | 0,04 | 0,00 | 0,02 | |
| **D126** | **993465** | Pp | 529,5 | 289,0 | | 0,34 | 0,02 | | |
| **D125** | **993464** | Pp | 526,8 | 289,2 | 4,9 | 0,13 | 0,00 | 0,09 | -23,46 |
| **D124** | **994209** | Pp | 524,9 | 289,2 | | | | | |
| **D123** | **993463** | Pp | 524,8 | 289,2 | 78,0 | 6,37 | 0,03 | 0,02 | |
| **D122** | **994208** | Pp | 524,7 | 289,3 | | | | | |
| **D121** | **993462** | Pp | 523,8 | 289,4 | 34,5 | 0,57 | 0,03 | 0,23 | -26,125 |
| **D120** | **994207** | Pp | 522,3 | 289,5 | | | | | -26,41 |
| **D119** | **993461** | Pp | 522,1 | 289,5 | 7,3 | 0,18 | 0,00 | 0,12 | -22,22 |
| **D118** | **994206** | Pp | 521,7 | 289,6 | | | | | -24,245 |
| **D117** | **993460** | Pp | 521 | 289,7 | | 0,69 | 0,13 | 0,63 | -21,75 |
| **D116** | **994205** | Pp | 520 | 289,8 | | | | | -23,38 |
| **D115** | **993459** | Pp | 519 | 289,8 | 14,1 | 0,44 | 0,00 | 0,14 | -22,575 |
| **D68** | **994204** | D7 | 517 | 290,0 | | | | | -22,94 |
| **D67** | **993456** | D7 | 516,4 | 290,1 | 11,8 | 0,18 | 0,01 | 0,15 | -22,62 |
| **D66** | **994203** | D7 | 513,4 | 290,3 | | | | | -22,64 |
| **D65** | **994202** | D7 | 510 | 290,5 | | | | | -23,705 |
| **D64** | **993455** | D7 | 506 | 291,1 | 13,1 | 0,74 | 0,01 | 0,07 | -23,695 |
| **D63** | **994201** | D7 | 494,5 | 291,4 | | | | | -22,765 |

| | | | | | | | | | |
|---|---|---|---|---|---|---|---|---|---|
| **D62** | **994200** | D7 | 488 | 291,4 | | | | | -22,655 |
| **D61** | **993454** | D7 | 487,4 | 291,4 | 14,3 | 0,19 | 0,00 | 0,16 | -22,53 |
| **D60** | **994199** | D6 | 486,8 | 291,6 | | | | | -22,795 |
| **D59** | **994198** | D6 | 483 | 292,2 | | | | | -22,7 |
| **D58** | **993453** | D6 | 471 | 292,5 | 11,3 | 0,22 | 0,00 | 0,11 | -22,74 |
| **D57** | **994197** | D6 | 463,5 | 293,8 | | | | | -22,88 |
| **D56** | **994196** | D6 | 436,5 | 294,4 | | | | | -23,08 |
| **D55** | **993452** | D6 | 425,5 | 295,1 | 11,4 | 0,27 | 0,00 | 0,12 | -22,735 |
| **D54** | **994195** | D6 | 411 | 295,5 | | | | | -23,015 |
| **D53** | **993451** | D6 | 402,2 | 295,9 | 10,9 | 0,19 | 0,00 | 0,13 | -23,32 |
| **D52** | **994194** | D6 | 394,6 | 296,4 | | | | | -23,245 |
| **D51** | **993450** | D6 | 383,5 | 296,9 | 10,3 | 0,26 | 0,00 | 0,13 | -23,01 |
| **D50** | **994193** | D6 | 372,5 | 297,0 | | | | | -23 |
| **D49** | **993449** | D5 | 371,6 | 297,0 | 10,7 | 0,37 | 0,00 | 0,31 | -22,855 |
| **D46** | **993448** | D5 | 362,7 | 297,3 | 11,2 | 0,11 | 0,00 | 0,07 | -23,51 |
| **D44** | | D5 | 352,5 | 297,6 | | | | | |
| **D43** | **993447** | D5 | 340,5 | 297,9 | 8,8 | 0,13 | 0,00 | 0,10 | -22,95 |
| **D42** | | D5 | 331,5 | 298,0 | | | | | |
| **D41** | **993446** | D5 | 327,7 | 298,0 | 16,5 | 0,22 | 0,00 | 0,19 | -22,775 |
| **D40** | | D5 | 327,3 | 298,0 | | | | | |
| **D39** | **993444** | D5 | 327 | 298,1 | 9,1 | 0,24 | 0,00 | 0,15 | -22,99 |
| **D38** | | D5 | 326,2 | 298,1 | | | | | |
| **D37** | **993445** | D5 | 325,9 | 298,2 | 14,7 | 0,17 | 0,00 | 0,20 | -22,67 |
| **D36** | | D5 | 320,7 | 298,2 | | | | | |
| **D35** | | D5 | 320,5 | 298,2 | | | | | |
| **D34** | **993443** | D5 | 320,2 | 298,2 | 9,7 | 0,19 | 0,00 | 0,16 | -22,84 |
| **D33** | | D5 | 319,8 | 298,4 | | | | | |
| **D32** | **993442** | D5 | 314,5 | 298,4 | 8,1 | 0,28 | 0,08 | 0,20 | -23,665 |
| **D31** | | D5 | 314,1 | 298,5 | | | | | |
| **D30** | **993441** | D5 | 312,1 | 298,5 | 12,7 | 0,16 | 0,00 | 0,13 | -22,865 |
| **D29** | | D5 | 311,7 | 298,5 | | | | | |
| **D28** | **993440** | D5 | 310,8 | 298,6 | 12,0 | 0,24 | 0,00 | 0,21 | -22,73 |
| **D27** | | D5 | 308,8 | 298,6 | | | | | |
| **D26** | **993439** | D5 | 307,6 | 298,6 | 6,6 | 0,32 | 0,00 | 0,13 | -22,57 |
| **D 25** | | D5 | 307,3 | 298,6 | | | | | |
| **D 24** | **993438** | D5 | 306,2 | 298,8 | 10,1 | 0,09 | 0,00 | 0,05 | -24,345 |
| **D 114** | **993437** | D4 | 299,7 | 299,0 | 7,0 | 0,15 | 0,00 | 0,06 | -24,495 |
| **D 113** | | D4 | 294,8 | 299,2 | | | | 0,07 | |
| **D 112** | **993436** | D4 | 286 | 299,4 | 10,3 | 0,10 | 0,00 | 0,06 | -23,475 |
| **D 111** | | D4 | 279 | 299,6 | | | | 0,07 | |
| **D 110** | | D4 | 273 | 299,8 | | | | 0,06 | |
| **D 109** | **993435** | D4 | 265,8 | 300,0 | 9,9 | 0,06 | 0,00 | 0,04 | |
| **D 108** | | D4 | 259,7 | 300,2 | | | | 0,06 | |
| **D 107** | | D4 | 251,8 | 300,5 | | | | 0,06 | |
| **D 106** | **993434** | D4 | 242,7 | 300,7 | 10,3 | 0,18 | 0,00 | 0,11 | -24,84 |
| **D 105** | | D4 | 234 | 301,0 | | | | 0,10 | |
| **D 104** | | D4 | 223,5 | 301,4 | | | | 0,07 | |
| **D 103** | **993433** | D4 | 211,3 | 301,7 | 9,1 | 0,18 | 0,00 | 0,09 | -23,64 |
| **D 102** | | D3 | 198,5 | 302,0 | | | | | |
| **D 101** | **993432** | D3 | 194,5 | 302,2 | 3,7 | 0,11 | 0,03 | 0,08 | -23,535 |
| **D 100** | **993431** | D3 | 187,5 | 302,3 | 3,9 | 0,19 | 0,00 | 0,15 | -22,795 |
| **D 99** | **993430** | D3 | 184,5 | 302,6 | | 0,15 | 0,00 | 0,14 | -23,11 |
| **D 98** | | D3 | 170,7 | 302,8 | | | | | |
| **D 97** | **993429** | D3 | 161,5 | 303,0 | 2,8 | 0,35 | 0,00 | 0,31 | -22,85 |
| **D 96** | | D3 | 153,8 | 303,1 | | | | | |
| **D 95** | | D3 | 149,3 | 303,2 | | | | | |
| **D 94** | **993428** | D3 | 145,8 | 303,6 | 5,0 | 0,28 | 0,00 | 0,24 | -23,09 |
| **D93** | **993427** | D3 | 129,8 | 303,9 | | 0,15 | 0,00 | 0,14 | -24,31 |
| **D92** | | D3 | 117,7 | 304,0 | | | | | |
| **D91** | **993426** | D3 | 114,5 | 304,0 | 7,4 | 0,08 | 0,00 | 0,05 | -23,27 |
| **D90** | | D3 | 113,8 | 304,4 | | | | | |
| **D88** | **993425** | D3 | 97,3 | 304,5 | 10,0 | 0,34 | 0,00 | 0,03 | |
| **D 89** | | D3 | 96,7 | 304,6 | | | | | |
| **D 87** | | D3 | 89,5 | 304,7 | | | | | |
| **Z 20** | | D3 | 87,5 | 304,7 | | | | | |
| **Z 19** | **993424** | D2 | 85,4 | 304,8 | 11,6 | 0,18 | 0,00 | 0,05 | -24,65 |
| **Z 18** | **993423** | D2 | 82,2 | 305,0 | 8,6 | 0,11 | 0,00 | 0,08 | -24,66 |
| **Z 17** | **993422** | D2 | 75 | 305,1 | 11,4 | 0,19 | 0,00 | 0,05 | -25,52 |
| **Z 16** | **993421** | D2 | 70,8 | 305,3 | 12,1 | 0,31 | 0,00 | 0,06 | -25,48 |
| **Z 15** | | D2 | 64 | 305,4 | | | | | |
| **Z 14** | **993420** | D2 | 61 | 305,4 | 15,7 | 0,92 | 0,00 | 0,06 | -26,515 |
| **Z 13** | **993419** | D2 | 60 | 305,4 | 10,4 | 0,25 | 0,00 | 0,07 | -25,06 |
| **Z 12** | | D2 | 59 | 305,6 | | | | | |
| **Z 11** | **993418** | D2 | 51 | 305,7 | 2,9 | 0,33 | 0,00 | 0,06 | -25,18 |
| **Z 10** | | D2 | 49 | 305,8 | | | | | |
| **Z 9** | **993417** | D2 | 43 | 306,0 | 10,9 | 0,22 | 0,00 | 0,06 | -25,13 |
| **Z 8** | **993416** | D2 | 37 | 306,1 | 11,3 | 0,25 | 0,00 | 0,07 | -24,95 |
| **Z 7** | | D1 | 31 | 306,2 | | | | | |
| **Z 6** | **993415** | D1 | 26 | 306,3 | 4,2 | 0,26 | 0,00 | 0,09 | -24,83 |
| **Z 5** | **993414** | D1 | 23,3 | 306,5 | 11,3 | 0,36 | 0,00 | 0,08 | -26,59 |
| **Z 4** | | D1 | 16 | 306,6 | | | | | |
| **Z 3** | | D1 | 12,2 | 306,7 | | | | | |
| **Z 2** | | D1 | 7 | 306,8 | | | | | |
| **Z 1** | **993413** | D1 | 4 | 306,9 | 6,4 | 0,36 | 0,01 | 0,25 | -24,27 |

| Lab.-Nr. | 992610 | 992611 | 992612 | 992613 | 992614 | 992615 | 992616 | 992617 | 992618 | 992619 | 992620 | 992621 | 992622 | 992623 | 992624 | 992625 | 992626 |
|---|---|---|---|---|---|---|---|---|---|---|---|---|---|---|---|---|---|
| Drill Nr. | 8 | 11 | 20 | 32 | 39 | 43 | 46 | 47 | 48 | 49 | 54 | 58 | 62 | 70 | 78 | 81 | 85 |
| Depth | 4,66-4,70 | 5,97-6,00 | 10,95-10,97 | 17,08-17,10 | 20,6-20,62 | 22,21-22,25 | 24,75-24,90 | 25,98-26,00 | 26,98-27,00 | 27,05-27,08 | 29,05-29,055 | 30,39-30,41 | 30,59-30,62 | 30,90-30,93 | 33,00-33,02 | 36,98-36,00 | 38,98-39,00 |
| Group | Ecca | Ecca | Ecca | Ecca | Ecca | Ecca | Ecca | Ecca | Ecca | Ecca | Ecca | Ecca | Dwyka | Dwyka | Dwyka | Dwyka | Dwyka |
| Formation | Pp | Pp | Pp | Pp | Pp | Pp | Pp | Pp | Pp | Pp | Pp | Pp | Dwyka | Dwyka | Dwyka | Dwyka | Dwyka |
| $SiO_2$ | 51,07 | 58,97 | 60,6 | 78,09 | 63,95 | 58,51 | 36,72 | 58,01 | 40,31 | 23,3 | 35,05 | 37,36 | 16,49 | 33,56 | 63,51 | 64,37 | 64,25 |
| $TiO_2$ | 0,74 | 0,79 | 0,76 | 0,28 | 0,57 | 0,89 | 0,61 | 0,76 | 0,58 | 0,35 | 0,39 | 0,45 | 0,12 | 0,17 | 0,78 | 0,7 | 0,7 |
| $Al_2O_3$ | 16,58 | 17,73 | 17,75 | 5,91 | 17,34 | 22,52 | 11,89 | 21,77 | 15,36 | 9,94 | 16,2 | 15,11 | 5,94 | 7,5 | 17,21 | 15,47 | 13,51 |
| $Fe_2O_3$ | 6,62 | 10,37 | 9,54 | 10,25 | 7,05 | 5,25 | 31,64 | 6,19 | 17,59 | 53,14 | 13,6 | 14,58 | 28,71 | 12,38 | 6,64 | 7,2 | 5,48 |
| MnO | 0,41 | 0,31 | 0,22 | 0,45 | 0,23 | 0,05 | 1,32 | 0,09 | 0,32 | 1,83 | 0,56 | 9,36 | 6,13 | 1,11 | 0,08 | 0,08 | 0,14 |
| MgO | 0,64 | 0,75 | 0,67 | 0,68 | 1,09 | 1,19 | 2,42 | 1,85 | 1,54 | 2,78 | 1,17 | 2,37 | 1,61 | 1,35 | 1,91 | 2,07 | 1,66 |
| CaO | 8,58 | 0,87 | 0,71 | 0,14 | 0,73 | 0,37 | 2,58 | 0,18 | 0,69 | 2,49 | 7,24 | 9,98 | 8,68 | 20,95 | 0,41 | 0,78 | 3,44 |
| $Na_2O$ | 0,62 | 0,31 | 0,42 | 0,02 | 0,16 | 0,27 | 0,02 | 0,02 | 0,02 | 0,02 | 0,02 | 0,06 | 0,02 | 0,06 | 0,63 | 0,69 | 1,16 |
| $K_2O$ | 1,22 | 2,34 | 2,35 | 0,14 | 2,65 | 3,69 | 0,58 | 4,46 | 3,02 | 0,03 | 3,6 | 2,3 | 0,64 | 0,66 | 4,07 | 3,67 | 3,42 |
| $P_2O_5$ | 5,896 | 0,446 | 0,378 | 0,037 | 0,357 | 0,088 | 1,5 | 0,055 | 0,166 | 1,166 | 0,79 | 5,148 | 4,02 | 14,566 | 0,16 | 0,181 | 0,172 |
| $SO_3$ | 0,012 | 0,012 | 0,012 | 0,012 | 0,012 | 0,012 | 2,106 | 0,012 | 4,372 | 6,836 | 5,264 | 1,124 | 9,061 | 1,461 | 0,012 | 0,012 | 0,012 |
| LOI | 7,38 | 6,25 | 6,02 | 3,94 | 5,21 | 5,94 | 8,53 | 5,27 | 14,76 | +1,21 | 11,36 | 0,58 | 17,35 | 5,41 | 3,79 | 3,78 | 5,79 |
| Sum | 99,77 | 99,15 | 99,43 | 99,95 | 99,35 | 98,78 | 99,92 | 98,67 | 98,73 | 101,88 | 95,24 | 98,42 | 98,77 | 99,18 | 99,20 | 99,00 | 99,73 |
| Sc | 15 | 16 | 16 | 7 | 17 | 21 | 9 | 22 | 15 | 4 | 7 | 17 | 4 | 2 | 24 | 13 | 13 |
| V | 116 | 140 | 143 | 31 | 98 | 143 | 101 | 123 | 243 | 75 | 131 | 164 | 115 | 48 | 124 | 107 | 81 |
| Cr | 43 | 70 | 66 | 17 | 51 | 73 | 50 | 94 | 142 | 60 | 48 | 5 | 5 | 7 | 112 | 117 | 77 |
| Co | 29 | 34 | 25 | 23 | 32 | 30 | 2 | 22 | 43 | 2 | 70 | 36 | 2 | 5 | 25 | 27 | 22 |
| Ni | 45 | 39 | 48 | 22 | 66 | 58 | 46 | 39 | 98 | 36 | 142 | 179 | 109 | 26 | 56 | 71 | 41 |
| Cu | 25 | 54 | 74 | 39 | 97 | 107 | 136 | 116 | 472 | 305 | 92 | 231 | 373 | 48 | 62 | 54 | 44 |
| Zn | 94 | 141 | 121 | 51 | 152 | 187 | 129 | 115 | 83 | 186 | 307 | 440 | 174 | 83 | 96 | 112 | 79 |
| Ga | 17 | 20 | 26 | 10 | 23 | 32 | 16 | 33 | 21 | 10 | 18 | 24 | 11 | 8 | 31 | 21 | 20 |
| As | 30 | 18 | 22 | 4 | 93 | 52 | 13 | 14 | 299 | 177 | 42 | 53 | 234 | 5 | 4 | 4 | 5 |
| Rb | 83 | 139 | 138 | 12 | 154 | 219 | 54 | 248 | 168 | 8 | 190 | 135 | 52 | 38 | 195 | 190 | 154 |
| Sr | 127 | 121 | 134 | 33 | 102 | 126 | 68 | 46 | 37 | 55 | 108 | 213 | 163 | 314 | 52 | 67 | 103 |
| Y | 107 | 47 | 44 | 15 | 56 | 55 | 47 | 44 | 31 | 32 | 117 | 252 | 199 | 332 | 25 | 34 | 35 |
| Zr | 204 | 178 | 162 | 61 | 183 | 195 | 87 | 155 | 166 | 48 | 173 | 143 | 89 | 57 | 205 | 179 | 244 |
| Nb | 10 | 15 | 15 | 2 | 9 | 16 | 7 | 12 | 6 | 4 | 2 | 8 | 2 | 2 | 11 | 8 | 6 |
| Mo | 2 | 4 | 6 | 2 | 5 | 6 | 8 | 2 | 96 | 2 | 20 | 6 | 4 | 2 | 2 | 2 | 2 |
| Sn | 7 | 7 | 7 | 7 | 7 | 20 | 7 | 8 | 7 | 9 | 7 | 33 | 7 | 7 | 17 | 38 | 7 |
| Ba | 228 | 440 | 436 | 69 | 438 | 582 | 148 | 575 | 406 | 11 | 419 | 451 | 104 | 291 | 796 | 645 | 657 |
| La | 39 | 64 | 89 | 43 | 46 | 47 | 78 | 53 | 101 | 43 | 35 | 77 | 40 | 210 | 38 | 101 | 25 |
| Ce | 108 | 78 | 92 | 33 | 77 | 89 | 85 | 114 | 153 | 126 | 60 | 198 | 211 | 351 | 43 | 101 | 78 |
| Pr | 8 | 6 | 11 | 3 | 8 | 12 | 8 | 10 | 13 | 5 | 11 | 19 | 13 | 30 | 7 | 9 | 8 |
| Nd | 53 | 35 | 45 | 26 | 40 | 39 | 32 | 66 | 74 | 64 | 51 | 161 | 138 | 185 | 27 | 53 | 31 |
| Sm | 7 | 7 | 6 | 4 | 6 | 6 | 7 | 5 | 8 | 12 | 4 | 12 | 13 | 17 | 5 | 5 | 4 |
| Hf | 4 | 3 | 4 | 2 | 4 | 5 | 2 | 4 | 2 | 2 | 4 | 2 | 2 | 2 | 6 | 4 | 6 |
| Ta | 2 | 2 | 2 | 2 | 8 | 9 | 4 | 2 | 2 | 2 | 10 | 2 | 2 | 2 | 2 | 6 | 2 |
| W | 7 | 9 | 3 | 3 | 4 | 11 | 3 | 6 | 3 | 3 | 10 | 5 | 9 | 3 | 13 | 18 | 4 |
| Pb | 4 | 38 | 28 | 6 | 29 | 29 | 31 | 14 | 170 | 76 | 33 | 25 | 96 | 11 | 34 | 28 | 27 |
| Bi | 3 | 3 | 5 | 3 | 7 | 7 | 3 | 3 | 3 | 10 | 11 | 3 | 3 | 3 | 15 | 3 | 3 |
| Th | 15 | 22 | 22 | 22 | 19 | 28 | 40 | 30 | 37 | 39 | 11 | 13 | 38 | 6 | 22 | 34 | 11 |
| U | 6 | 10 | 7 | 16 | 6 | 13 | 18 | 11 | 39 | 11 | 31 | 16 | 11 | 12 | 2 | 5 | 2 |
| TOC | 0,17 | 0,20 | 0,24 | 0,05 | 0,16 | 0,82 | 0,46 | 0,96 | 7,03 | 0,14 | 3,84 | 1,55 | 0,29 | 0,29 | 0,25 | 0,25 | 0,11 |
| S | 0,13 | 0,00 | 0,00 | 0,00 | 0,00 | 0,00 | 1,85 | 0,05 | 5,49 | 7,28 | 5,06 | 2,76 | 6,83 | 2,29 | 0,01 | 0,01 | 0,00 |
| loss by HCl [%] | 30,4 | 23,3 | 20,6 | 19,6 | 17,4 | 14,2 | 34,9 | 11,8 | 23,1 | 45,3 | 32,1 |  | 46 | 48,1 | 14,9 | 19,7 | 17 |
| $\delta^{18}O$ (silic.) | 7,66 | 7,61 | 6,28 | 7,49 | 7,95 | 6,40 |  | 7,50 |  |  | 7,06 | 8,00 |  | 9,57 | 7,49 | 8,63 | 8,50 |
| $\delta^{18}O$ (silic.) | 8,07 | 7,81 | 6,85 | 7,41 | 8,14 | 6,21 |  | 7,59 |  |  | 6,69 | 8,31 |  | 9,65 | 7,93 | 8,50 | 8,62 |
| $\delta^{18}O$ (silic.) | 8,33 | 8,37 | 7,37 | 7,60 | 7,88 | 6,35 |  | 7,43 |  |  | 6,86 | 7,80 |  | 9,58 | 7,85 | 8,62 | 8,33 |
| mean $\delta^{18}O$ | 8,02 | 7,93 | 6,83 | 7,50 | 7,99 | 6,32 |  | 7,51 |  |  | 6,87 | 8,03 |  | 9,60 | 7,76 | 8,58 | 8,48 |
| std.dev. | 0,275 | 0,32 | 0,445 | 0,077 | 0,112 | 0,078 |  | 0,065 |  |  | 0,148 | 0,209 |  | 0,033 | 0,192 | 0,061 | 0,121 |
| S1 |  |  |  |  |  |  |  |  | 0,23 |  | 0,27 | 0,16 | 0,15 | 0,21 |  |  |  |
| S2 |  |  |  |  |  |  |  |  | 0,03 |  | 0,03 | 0,02 | 0,02 | 0,17 |  |  |  |
| S3 |  |  |  |  |  |  |  |  | 0,53 |  | 0,48 | 0,3 | 0,31 | 0,28 |  |  |  |
| HI |  |  |  |  |  |  |  |  | 0 |  | 1 | 1 | 4 | 31 |  |  |  |
| OI |  |  |  |  |  |  |  |  | 6 |  | 8 | 19 | 56 | 51 |  |  |  |
| $\delta^{13}Corg$ | -19,24 | -23,06 | -22,35 | -23,65 | -23,03 | -24,36 | -18,63 | -24,47 | -26,65 | -23,44 | -27,19 | -23,22 | -23,28 | -24,58 | -23,19 | -23,20 | -23,65 |
| $\delta^{13}Corg$ | -19,23 | -23,13 | -22,56 | -23,61 | -23,05 | -24,39 | -18,86 | -24,52 | -26,69 | -23,75 | -27,39 | -23,10 | -23,23 | -24,44 | -23,20 | -23,33 | -23,78 |

| Lab.-Nr. | 992656 | 992655 | 992627 | 992628 | 992629 | 992630 | 992631 | 992632 | 992633 | 992634 | 992635 | 992636 | 992637 | 992638 |
|---|---|---|---|---|---|---|---|---|---|---|---|---|---|---|
| Drill Nr. | core | core | 96 | 105 | 114 | 125 | 129 | 139 | 149 | 159 | 169 | 179 | 187 | 201 |
| Depth | 42 | 42,25 | 48,99-49,00 | 57,88-57,92 | 65,98-66,00 | 79,05-76,06 | 80,01-80,02 | 89,98-90,00 | 99,96-99,98 | 110,00-110,02 | 119,98-120,00 | 130,00-130,02 | 137,98-138,00 | 150,30-150,35 |
| Group | Dwyka | Dwyka | Dwyka | Dwyka | Dwyka | Dwyka | Dwyka | Dwyka | Dwyka | Dwyka | Dwyka | Dwyka | Dwyka | Dwyka |
| Formation | Dwyka | Dwyka | Dwyka | Dwyka | Dwyka | Dwyka | Dwyka | Dwyka | Dwyka | Dwyka | Dwyka | Dwyka | Dwyka | Dwyka |
| $SiO_2$ | 45,88 | 26,41 | 66,55 | 65,24 | 65,95 | 64,95 | 65,76 | 66,64 | 66,23 | 65,65 | 66,11 | 66,02 | 66,01 | 51,05 |
| $TiO_2$ | 0,65 | 0,25 | 0,68 | 0,68 | 0,67 | 0,68 | 0,65 | 0,67 | 0,62 | 0,66 | 0,62 | 0,63 | 0,63 | 0,96 |
| $Al_2O_3$ | 18,02 | 10,78 | 13,67 | 13,68 | 14,18 | 13,26 | 13,47 | 13,28 | 13,52 | 13,6 | 13,7 | 13,73 | 13,66 | 17,32 |
| $Fe_2O_3$ | 11,63 | 11,98 | 5,74 | 5,5 | 5,04 | 6,13 | 5,99 | 5,83 | 5,71 | 6,04 | 5,71 | 5,97 | 5,71 | 10,71 |
| MnO | 2,61 | 10,37 | 0,08 | 0,09 | 0,09 | 0,08 | 0,08 | 0,07 | 0,07 | 0,07 | 0,07 | 0,07 | 0,07 | 0,12 |
| MgO | 1,88 | 1,95 | 2,02 | 2,59 | 2,58 | 2,9 | 2,74 | 2,63 | 2,61 | 2,86 | 2,66 | 2,85 | 2,61 | 4,81 |
| CaO | 1,09 | 9,62 | 1,65 | 1,89 | 1,83 | 2,06 | 1,83 | 1,84 | 1,88 | 1,8 | 1,88 | 1,93 | 1,91 | 1,85 |
| $Na_2O$ | 0,22 | 0,02 | 1,87 | 2,24 | 2,61 | 2,45 | 2,91 | 3,01 | 3,15 | 3,4 | 3,4 | 3,38 | 3,46 | 3,95 |
| $K_2O$ | 3,5 | 1,51 | 3,28 | 3,18 | 3,22 | 3,02 | 2,72 | 2,6 | 2,73 | 2,71 | 2,7 | 2,73 | 2,78 | 3,58 |
| $P_2O_5$ | 0,291 | 4,574 | 0,171 | 0,178 | 0,174 | 0,152 | 0,149 | 0,154 | 0,14 | 0,135 | 0,127 | 0,13 | 0,131 | 0,228 |
| $SO_3$ | 1,873 | 1,79 | 0,012 | 0,012 | 0,012 | 0,012 | 0,012 | 0,012 | 0,012 | 0,012 | 0,012 | 0,012 | 0,012 | 0,047 |
| LOI | 7,68 | 18,98 | 3,94 | 4,56 | 3,30 | 3,43 | 2,32 | 2,74 | 3,88 | 2,57 | 2,41 | 1,85 | 2,79 | 4,93 |
| Sum | 95,32 | 98,23 | 99,66 | 99,84 | 99,66 | 99,12 | 98,63 | 99,48 | 100,55 | 99,51 | 99,40 | 99,30 | 99,77 | 99,56 |
| Sc | 23 | 9 | 14 | 7 | 15 | 19 | 8 | 15 | 12 | 6 | 15 | 17 | 18 | 27 |
| V | 334 | 128 | 88 | 87 | 92 | 99 | 83 | 96 | 81 | 102 | 98 | 96 | 86 | 157 |
| Cr | 68 | 5 | 72 | 77 | 62 | 107 | 97 | 106 | 116 | 110 | 111 | 122 | 112 | 190 |
| Co | 59 | 36 | 25 | 22 | 26 | 25 | 24 | 25 | 24 | 26 | 23 | 31 | 27 | 43 |
| Ni | 166 | 176 | 38 | 39 | 48 | 50 | 48 | 45 | 49 | 57 | 59 | 61 | 62 | 111 |
| Cu | 190 | 286 | 33 | 31 | 28 | 41 | 38 | 42 | 34 | 48 | 37 | 53 | 43 | 58 |
| Zn | 348 | 496 | 73 | 81 | 87 | 66 | 75 | 74 | 65 | 76 | 70 | 75 | 63 | 130 |
| Ga | 26 | 19 | 17 | 24 | 17 | 19 | 16 | 16 | 19 | 20 | 22 | 18 | 17 | 31 |
| As | 190 | 22 | 4 | 4 | 5 | 769 | 233 | 10 | 4 | 46 | 47 | 17 | 10 | 8 |
| Rb | 206 | 91 | 144 | 130 | 131 | 120 | 107 | 97 | 89 | 90 | 93 | 92 | 93 | 124 |
| Sr | 51 | 184 | 117 | 133 | 163 | 143 | 144 | 155 | 189 | 174 | 189 | 191 | 188 | 119 |
| Y | 43 | 213 | 35 | 31 | 37 | 31 | 27 | 29 | 29 | 27 | 25 | 25 | 28 | 36 |
| Zr | 330 | 93 | 249 | 232 | 217 | 207 | 199 | 205 | 193 | 178 | 196 | 336 | 189 | 164 |
| Nb | 10 | 2 | 7 | 7 | 9 | 4 | 9 | 8 | 9 | 7 | 2 | 6 | 11 | 13 |
| Mo | 37 | 2 | 2 | 3 | 3 | 2 | 2 | 4 | 2 | 2 | 2 | 2 | 5 | 3 |
| Sn | 28 | 7 | 14 | 7 | 7 | 14 | 11 | 7 | 7 | 7 | 31 | 7 | 7 | 15 |
| Ba | 507 | 286 | 731 | 816 | 879 | 825 | 770 | 847 | 1011 | 850 | 809 | 765 | 748 | 846 |
| La | 54 | 51 | 44 | 72 | 36 | 39 | 31 | 61 | 56 | 37 | 45 | 29 | 45 | 50 |
| Ce | 106 | 177 | 105 | 84 | 54 | 119 | 106 | 80 | 61 | 81 | 79 | 53 | 65 | 134 |
| Pr | 12 | 12 | 8 | 7 | 6 | 12 | 7 | 3 | 4 | 8 | 9 | 6 | 10 | 7 |
| Nd | 43 | 143 | 47 | 34 | 32 | 12 | 38 | 34 | 35 | 39 | 46 | 18 | 27 | 48 |
| Sm | 5 | 11 | 5 | 6 | 4 | 12 | 5 | 4 | 4 | 3 | 4 | 4 | 3 | 7 |
| Hf | 7 | 2 | 5 | 5 | 5 | 12 | 5 | 4 | 3 | 4 | 4 | 7 | 4 | 4 |
| Ta | 10 | 7 | 2 | 2 | 2 | 12 | 6 | 2 | 2 | 5 | 3 | 2 | 9 | 4 |
| W | 12 | 8 | 4 | 3 | 3 | 12 | 10 | 3 | 3 | 3 | 14 | 15 | 4 | 3 |
| Pb | 67 | 26 | 15 | 22 | 25 | 12 | 27 | 20 | 24 | 32 | 31 | 27 | 20 | 31 |
| Bi | 13 | 3 | 3 | 3 | 7 | 12 | 9 | 11 | 13 | 8 | 11 | 3 | 14 | 8 |
| Th | 19 | 18 | 6 | 19 | 9 | 12 | 28 | 11 | 2 | 9 | 2 | 8 | 2 | 33 |
| U | 10 | 6 | 2 | 3 | 2 | 12 | 5 | 2 | 4 | 3 | 2 | 3 | 7 | 7 |
| TOC | 2,68 | 0,41 | 0,12 | 0,13 | 0,13 | 12 | 0,07 | 0,06 | 0,05 | 0,05 | 0,05 | 0,09 | 0,06 | 0,12 |
| S | 1,63 | 3,74 | 0,00 | 0,17 | 0,01 | 12 | 0,00 | 0,00 | 0,00 | 0,00 | 0,00 | 0,01 | 0,00 | 0,12 |
| loss by HCl [%] | 29,2 | 65,6 | 14,8 | 19,8 | 16,1 | 12 | 17,6 | 16,9 |  | 17,9 | 15,3 | 17,3 | 16,9 | 25,5 |
| $\delta^{18}O$ (silic.) | 8,02 | 9,81 | 8,62 | 8,72 | 8,84 | 12 | 9,63 | 9,29 | 9,84 | 9,45 | 9,25 | 9,18 | 8,70 | 9,30 |
| $\delta^{18}O$ (silic.) | 5,35 | 10,89 | 8,87 | 8,67 | 9,17 | 12 | 9,78 | 9,63 | 9,75 | 9,54 | 9,25 | 9,53 | 8,56 | 9,26 |
| $\delta^{18}O$ (silic.) |  |  | 8,46 | 8,61 | 8,86 | 12 | 9,62 | 9,62 | 10,03 | 9,41 | 9,19 | 9,30 | 8,49 | 9,18 |
| mean $\delta^{18}O$ | 6,69 | 10,35 | 8,65 | 8,67 | 8,96 | 12 | 9,68 | 9,52 | 9,88 | 9,47 | 9,23 | 9,34 | 8,58 | 9,24 |
| std.dev. | 1,335 | 0,54 | 0,17 | 0,048 | 0,151 | 12 | 0,072 | 0,16 | 0,114 | 0,054 | 0,029 | 0,144 | 0,087 | 0,051 |
| S1 | 0,18 | 0,15 |  |  |  |  |  |  |  |  |  |  |  |  |
| S2 | 0,03 | 0,03 |  |  |  |  |  |  |  |  |  |  |  |  |
| S3 | 0,33 | 0,29 |  |  |  |  |  |  |  |  |  |  |  |  |
| HI | 1 | 3 |  |  |  |  |  |  |  |  |  |  |  |  |
| OI | 9 | 24 |  |  |  |  |  |  |  |  |  |  |  |  |
| $\delta^{13}$Corg | -23,68 | -23,44 | -23,65 | -23,70 | -22,95 | -23,08 | -23,06 | -23,24 | -24,00 | -23,56 | -23,37 | -22,99 | -23,78 | -23,51 |
| $\delta^{13}$Corg | -23,73 | -23,34 | -23,66 | -23,65 | -23,13 | -23,27 | -23,18 | -23,15 | -23,75 | -24,04 | -23,51 | -23,60 | -23,89 | -23,79 |

| Lab. Nr. | 992574 | 992575 | 992576 | 992577 | 992578 | 992579 | 992580 | 992581 | 992582 | 992583 | 992584 | 992585 | 992586 | 992587 | 992588 | 992589 | 992590 |
|---|---|---|---|---|---|---|---|---|---|---|---|---|---|---|---|---|---|
| Drill Nr. | 56 | 62 | 69 | 78 | 80 | 82 | 86 | 89 | 94 | 98 | 100 | 106 | 114 | 118 | 122 | 125 | 133 |
| Depth (m) | 141 | 159 | 180 | 205 | 208,5 | 213 | 225 | 231 | 246 | 258 | 264 | 282 | 306 | 318 | 327 | 332 | 352 |
| Group | Ecca | Ecca | Ecca | Ecca | Ecca | Ecca | Ecca | Ecca | Ecca | Ecca | Ecca | Ecca | Ecca | Ecca | Ecca | Ecca | Ecca |
| Formation | Mosolotsane | Mosolotsane | Mosolotsane | Mosolotsane | Mosolotsane | Mosolotsane | Mosolotsane | Tlhabala | Tlhabala | Tlhabala | Tlhabala | Tlhabala | Tlhabala | Tlhabala | Tlapana | Tlapana | Tlapana |
| $SiO_2$ | 75,74 | 85,95 | 89,03 | 64,04 | 59,76 | 87,45 | 92,16 | 34,85 | 66,21 | 64,11 | 60,07 | 34,49 | 64,56 | 66,06 | 55,71 | 5,55 | 48,95 |
| $TiO_2$ | 0,46 | 0,16 | 0,26 | 0,67 | 0,69 | 0,23 | 0,09 | 0,33 | 0,59 | 0,74 | 0,52 | 0,3 | 0,65 | 0,66 | 0,93 | 0,16 | 1,13 |
| $Al_2O_3$ | 10,67 | 6,11 | 5,04 | 15,95 | 17,52 | 3,46 | 1,57 | 7,37 | 14,16 | 15,84 | 12,21 | 6,66 | 16,6 | 15,81 | 18,82 | 1,93 | 19,9 |
| $Fe_2O_3$ | 3,52 | 1,16 | 1,44 | 5,85 | 7,11 | 0,83 | 0,57 | 2,29 | 4,51 | 5,48 | 3,42 | 2,73 | 4,54 | 4,19 | 6,84 | 28,28 | 5,85 |
| MnO | 0,03 | 0,03 | 0,02 | 0,03 | 0,04 | 0,04 | 0,01 | 0,28 | 0,02 | 0,02 | 0,1 | 0,44 | 0,02 | 0,03 | 0,02 | 0 | 0,03 |
| MgO | 1,23 | 0,45 | 0,29 | 2,22 | 2,65 | 0,36 | 0,37 | 1,31 | 2,44 | 2,35 | 2,21 | 1,21 | 1,72 | 1,54 | 0,7 | 0,04 | 0,53 |
| CaO | 0,8 | 1,02 | 0,13 | 0,51 | 0,7 | 2,76 | 2,31 | 27,38 | 0,94 | 0,51 | 7,37 | 28,11 | 0,93 | 0,96 | 0,23 | 0,11 | 0,15 |
| $Na_2O$ | 0,78 | 0,59 | 0,76 | 1,01 | 0,79 | 0,37 | 0,2 | 0,76 | 1,63 | 1,5 | 1,46 | 0,68 | 1,44 | 1,32 | 0,76 | 0,02 | 0,7 |
| $K_2O$ | 3,25 | 2,15 | 1,72 | 4,79 | 5,18 | 1,06 | 0,38 | 1,86 | 3,36 | 4,58 | 2,64 | 1,44 | 2,65 | 2,6 | 2,3 | 0,21 | 2,45 |
| $P_2O_5$ | 0,039 | 0,009 | 0,011 | 0,128 | 0,071 | 0,056 | 0,008 | 0,083 | 0,126 | 0,048 | 0,082 | 0,057 | 0,017 | 0,024 | 0,061 | 0,033 | 0,072 |
| $SO_3$ | 0,012 | 0,012 | 0,012 | 0,012 | 0,012 | 0,012 | 0,012 | 0,012 | 0,012 | 0,012 | 0,012 | 0,012 | 0,259 | 0,073 | 1,101 | 6,438 | 3,02 |
| L.O.I. | 3,87 | 2,54 | 1,89 | 4,78 | 5,87 | 2,19 | 1,58 | 23,98 | 5,17 | 4,57 | 9,83 | 22,44 | 6,92 | 6,78 | 12,25 | 54,39 | 17,49 |
| Sum | 100,40 | 100,18 | 100,60 | 99,99 | 100,39 | 98,82 | 99,26 | 100,51 | 99,17 | 99,76 | 99,92 | 98,57 | 100,31 | 100,05 | 99,72 | 97,16 | 100,27 |
| Sc | 7 | 8 | 4 | 10 | 18 | 2 | 4 | 10 | 3 | 23 | 4 | 2 | 17 | 10 | 14 | 10 | 17 |
| V | 55 | 6 | 28 | 344 | 81 | 43 | 3 | 33 | 56 | 703 | 59 | 51 | 66 | 65 | 103 | 286 | 134 |
| Cr | 38 | 15 | 15 | 103 | 75 | 7 | 5 | 16 | 40 | 67 | 31 | 14 | 41 | 41 | 98 | 121 | 139 |
| Co | 14 | 11 | 8 | 25 | 25 | 16 | 7 | 14 | 19 | 26 | 15 | 17 | 18 | 22 | 34 | 22 | 22 |
| Ni | 23 | 15 | 22 | 36 | 48 | 13 | 10 | 23 | 39 | 44 | 22 | 22 | 42 | 34 | 83 | 73 | 63 |
| Cu | 19 | 5 | 3 | 27 | 21 | 8 | 6 | 13 | 27 | 27 | 14 | 9 | 18 | 22 | 47 | 66 | 40 |
| Zn | 48 | 12 | 11 | 84 | 84 | 6 | 3 | 73 | 70 | 80 | 56 | 29 | 82 | 71 | 133 | 6 | 221 |
| Ga | 13 | 5 | 4 | 26 | 29 | 7 | 5 | 9 | 24 | 24 | 12 | 9 | 21 | 22 | 28 | 22 | 36 |
| As | 6 | 4 | 4 | 11 | 33 | 4 | 4 | 9 | 4 | 11 | 4 | 4 | 17 | 4 | 8 | 204 | 20 |
| Rb | 137 | 66 | 55 | 210 | 241 | 43 | 13 | 86 | 163 | 243 | 135 | 88 | 141 | 134 | 118 | 11 | 123 |
| Sr | 74 | 53 | 51 | 91 | 101 | 57 | 21 | 375 | 179 | 122 | 244 | 448 | 168 | 140 | 71 | 105 | 175 |
| Y | 21 | 13 | 17 | 46 | 26 | 15 | 7 | 65 | 26 | 29 | 33 | 33 | 24 | 31 | 27 | 20 | 31 |
| Zr | 200 | 125 | 362 | 273 | 185 | 146 | 80 | 140 | 202 | 265 | 185 | 105 | 199 | 189 | 261 | 1860 | 326 |
| Nb | 7 | 2 | 2 | 14 | 14 | 3 | 2 | 9 | 13 | 14 | 12 | 5 | 18 | 13 | 19 | 38 | 21 |
| Mo | 2 | 2 | 2 | 2 | 2 | 2 | 2 | 2 | 2 | 2 | 2 | 2 | 4 | 2 | 2 | 15 | 14 |
| Sn | 7 | 14 | 7 | 7 | 16 | 7 | 7 | 22 | 7 | 15 | 7 | 7 | 7 | 7 | 20 | 7 | 12 |
| Ba | 474 | 356 | 311 | 490 | 458 | 204 | 125 | 1939 | 508 | 441 | 412 | 254 | 325 | 332 | 410 | 13522 | 487 |
| La | 33 | 12 | 42 | 19 | 41 | 5 | 19 | 70 | 28 | 57 | 32 | 35 | 5 | 58 | 70 | 5 | 57 |
| Ce | 54 | 13 | 64 | 50 | 60 | 24 | 51 | 66 | 58 | 74 | 40 | 29 | 45 | 82 | 76 | 35 | 86 |
| Pr | 5 | 3 | 7 | 9 | 5 | 5 | 8 | 14 | 9 | 9 | 3 | 7 | 8 | 9 | 6 | 8 | 7 |
| Nd | 38 | 16 | 23 | 33 | 26 | 16 | 14 | 54 | 37 | 36 | 22 | 21 | 26 | 12 | 36 | 36 | 18 |
| Sm | 5 | 3 | 3 | 3 | 4 | 3 | 3 | 4 | 4 | 5 | 4 | 4 | 4 | 4 | 5 | 4 | 4 |
| Hf | 6 | 4 | 7 | 5 | 5 | 4 | 2 | 3 | 5 | 6 | 4 | 2 | 6 | 5 | 6 | 30 | 7 |
| Ta | 2 | 2 | 8 | 2 | 2 | 13 | 2 | 2 | 8 | 3 | 2 | 2 | 2 | 4 | 9 | 2 | 2 |
| W | 7 | 9 | 11 | 3 | 13 | 19 | 3 | 11 | 21 | 12 | 3 | 11 | 22 | 13 | 15 | 3 | 12 |
| Pb | 20 | 12 | 10 | 22 | 28 | 8 | 6 | 34 | 22 | 9 | 20 | 14 | 17 | 22 | 28 | 18 | 36 |
| Bi | 6 | 9 | 18 | 5 | 3 | 4 | 5 | 6 | 3 | 3 | 7 | 4 | 7 | 3 | 3 | 3 | 10 |
| Th | 31 | 12 | 23 | 2 | 5 | 8 | 13 | 15 | 20 | 25 | 14 | 2 | 24 | 18 | 19 | 15 | 21 |
| U | 2 | 2 | 6 | 5 | 2 | 2 | 2 | 2 | 6 | 8 | 2 | 2 | 4 | 2 | 7 | 2 | 5 |
| TOC | 0,029 | 0,027 | 0,03 | 0,107 | 0,029 | 0,022 | 0,026 | 0,057 | 0,077 | 0,448 | 0,077 | 0,054 | 0,084 | 0,182 | 3,83 | 18,993 | 9,113 |
| S | 0,029 | 0 | 0 | 0,027 | 0,021 | 0,001 | 0 | 0,078 | 0,012 | 0,056 | 0,011 | 0,012 | 1,411 | 1,155 | 3,88 | 14,419 | 3,569 |
| loss by HCl treat [%] | 6,1 | 5,3 | 3,9 | 8,7 | 9,7 | 7,1 | 5,8 | 57,5 | 8,9 | 17,6 | 18,8 | 58,7 | 32,6 | 10,9 | 10,3 | 38,4 | 10,7 |
| Tmax | | | | 0 | | | | | | 0 | | | | | 425 | 421 | 426 |
| S1 | | | | 0,11 | | | | | | 0,11 | | | | | 0,34 | 0,7 | 0,44 |
| S2 | | | | 0 | | | | | | 0 | | | | | 1,37 | 7,24 | 7,1 |
| S3 | | | | 0,18 | | | | | | 0,22 | | | | | 0,68 | 6,69 | 1,47 |
| HI | | | | 0 | | | | | | 0,22 | | | | | 32 | 23 | 70 |
| OI | | | | 150 | | | | | | 0,22 | | | | | 16 | 22 | 14 |
| $\delta^{13}$Corg | | | | -27,77 | | | | -26,2 | -24,3 | 0,22 | -23,71 | -24,19 | -23,51 | -23,65 | -23,33 | -22,7 | -23,19 |
| $\delta^{13}$Corg | | | | -27,46 | | | | -26,54 | -24,05 | 0,22 | -23,67 | -24,27 | -23,77 | -23,55 | -23,24 | -22,92 | -23,26 |
| mean $\delta^{13}$Corg | | | | -27,62 | | | | -26,37 | -24,18 | 0,22 | -23,69 | -24,23 | -23,64 | -23,6 | -23,28 | -22,81 | -23,23 |

| 992591 | 992592 | 992593 | 992594 | 992595 | 992596 | 992597 | 992598 | 992599 | 992600 | 992601 | 992602 | 992603 | 992604 | 992605 | 992606 | 992607 | 992608 | 992609 |
|---|---|---|---|---|---|---|---|---|---|---|---|---|---|---|---|---|---|---|
| 138 | 141 | 143 | 148 | 151 | 153 | 156 | 157 | 160 | 162 | 164 | 170 | 174 | 175 | 177 | 179 | 181 | 184 | 186 |
| 362,5 | 369 | 373,5 | 387 | 396 | 402 | 411 | 414 | 417 | 423 | 429 | 447 | 456 | 459 | 463,5 | 468 | 474 | 479 | 483 |
| Ecca | Ecca | Ecca | Ecca | Ecca | Ecca | Ecca | Ecca | Ecca | Ecca | Ecca | Ecca | Ecca | Ecca | Ecca | Ecca | Ecca | Ecca | Ecca |
| Tlapana | Mea | Mea | Mea | Mea | Mea | Tswane | Tswane | Tswane | Tswane | Tswane | Tswane | Tswane | Tswane | Tswane | Tswane | Tswane | Tswane | Tswane |
| 42,99 | 82,83 | 5,94 | 58,17 | 82,39 | 34,13 | 38,46 | 47,17 | 34,52 | 18,24 | 46,46 | 4,06 | 34,77 | 12,48 | 91,1 | 43,08 | 55,95 | 68,55 | 63,67 |
| 1,55 | 0,68 | 0,33 | 0,27 | 0,51 | 1,06 | 1,17 | 1,13 | 0,75 | 0,43 | 0,89 | 0,13 | 1,15 | 0,44 | 0,05 | 0,95 | 1 | 0,59 | 0,47 |
| 26,06 | 8,37 | 4,13 | 3,95 | 9,23 | 21,85 | 21,07 | 18,62 | 12,2 | 10,62 | 17,69 | 2,49 | 16,68 | 9,47 | 4,15 | 10,87 | 23,26 | 19,25 | 18,61 |
| 6,37 | 1,73 | 13,66 | 14,23 | 1,33 | 4,16 | 7,13 | 2,49 | 1,82 | 0,47 | 2,78 | 17,54 | 0,4 | 3,31 | 1,03 | 1,65 | 0,81 | 1,46 | 4,34 |
| 0,05 | 0,02 | 0,01 | 0,02 | 0,01 | 0,01 | 0,15 | 0 | 0,01 | 0 | 0,04 | 0 | 0 | 0,04 | 0 | 0,01 | 0 | 0,01 | 0,04 |
| 0,67 | 0,2 | 0,04 | 0,04 | 0,05 | 0,44 | 2,99 | 0,31 | 0,2 | 0,02 | 0,16 | 0,02 | 0,14 | 0,18 | 0,06 | 0,1 | 0,15 | 0,2 | 0,66 |
| 0,17 | 0,34 | 0,1 | 0,06 | 0,08 | 0,15 | 4,83 | 0,15 | 0,53 | 0,45 | 0,14 | 0,36 | 0,19 | 0,58 | 0,59 | 1,9 | 0,09 | 0,18 | 0,94 |
| 0,49 | 0,8 | 0,02 | 0,3 | 0,47 | 0,22 | 0,13 | 0,02 | 0,02 | 0,02 | 0,02 | 0,02 | 0,02 | 0,02 | 0,02 | 0,02 | 0,02 | 0,04 | 0,13 |
| 3,11 | 2,14 | 0,28 | 1,85 | 3,29 | 2,59 | 3,1 | 1,11 | 0,72 | 0,09 | 0,57 | 0,13 | 0,47 | 0,2 | 0,76 | 0,58 | 1,87 | 3,79 | 3,07 |
| 0,106 | 0,028 | 0,01 | 0,014 | 0,024 | 0,038 | 0,269 | 0,034 | 0,053 | 0,047 | 0,045 | 0,037 | 0,125 | 0,218 | 0,008 | 0,022 | 0,037 | 0,028 | 0,024 |
| 2,952 | 0,123 | 1,384 | 10,927 | 0,271 | 0,042 | 5,855 | 0,058 | 0,022 | 0,012 | 0,03 | 1,435 | 0,012 | 0,012 | 0,548 | 0,012 | 0,087 | 0,17 | 0,012 |
| 16,94 | 2,87 | - | 11,57 | 2,83 | 34,11 | 14,13 | 29,98 | 48,23 | - | 31,38 | - | 48,12 | - | 2,51 | 42,31 | 15,77 | 6,25 | 7,58 |
| 101,46 | 100,13 | 25,90 | 101,40 | 100,49 | 98,80 | 99,28 | 101,07 | 99,08 | 30,40 | 100,21 | 26,22 | 102,08 | 26,95 | 100,83 | 101,50 | 99,04 | 100,52 | 99,55 |
| 32 | 6 | 4 | 2 | 10 | 13 | 13 | 4 | 19 | 12 | 12 | 11 | 15 | 9 | 3 | 7 | 15 | 6 | 7 |
| 177 | 33 | 346 | 4 | 34 | 311 | 178 | 90 | 68 | 64 | 44 | 18 | 73 | 33 | 6 | 82 | 120 | 83 | 81 |
| 146 | 42 | 242 | 23 | 25 | 184 | 92 | 52 | 46 | 42 | 36 | 23 | 68 | 43 | 5 | 88 | 134 | 145 | 56 |
| 33 | 13 | 62 | 21 | 9 | 28 | 28 | 10 | 11 | 9 | 14 | 95 | 3 | 13 | 7 | 13 | 43 | 16 | 16 |
| 52 | 32 | 70 | 21 | 24 | 56 | 49 | 24 | 22 | 22 | 28 | 290 | 25 | 19 | 18 | 41 | 71 | 39 | 40 |
| 60 | 13 | 12 | 18 | 13 | 18 | 40 | 5 | 3 | 3 | 11 | 5 | 3 | 3 | 8 | 3 | 18 | 33 | 31 |
| 139 | 20 | 552 | 179 | 64 | 109 | 139 | 80 | 3 | 9 | 4 | 10 | 9 | 5 | 3 | 46 | 124 | 233 | 51 |
| 47 | 13 | 21 | 9 | 12 | 42 | 27 | 27 | 14 | 7 | 28 | 25 | 21 | 6 | 6 | 27 | 31 | 29 | 23 |
| 26 | 4 | 139 | 12 | 5 | 9 | 19 | 4 | 4 | 4 | 4 | 39 | 4 | 4 | 4 | 4 | 5 | 4 | 4 |
| 173 | 73 | 20 | 62 | 103 | 149 | 134 | 74 | 63 | 7 | 43 | 10 | 31 | 9 | 22 | 37 | 82 | 71 | 69 |
| 256 | 84 | 39 | 70 | 113 | 92 | 263 | 70 | 70 | 94 | 58 | 18 | 194 | 530 | 35 | 62 | 65 | 73 | 54 |
| 44 | 10 | 14 | 10 | 9 | 20 | 30 | 46 | 32 | 32 | 34 | 66 | 50 | 30 | 6 | 27 | 33 | 35 | 18 |
| 352 | 167 | 196 | 92 | 190 | 259 | 393 | 191 | 163 | 80 | 152 | 195 | 225 | 101 | 57 | 284 | 262 | 319 | 110 |
| 29 | 11 | 3 | 4 | 11 | 18 | 21 | 21 | 9 | 7 | 12 | 2 | 16 | 6 | 2 | 15 | 18 | 7 | 5 |
| 2 | 2 | 9 | 2 | 2 | 20 | 2 | 2 | 2 | 2 | 2 | 7 | 2 | 2 | 2 | 2 | 2 | 2 | 2 |
| 7 | 7 | 7 | 7 | 14 | 7 | 7 | 7 | 7 | 7 | 7 | 7 | 7 | 7 | 7 | 7 | 7 | 7 | 7 |
| 560 | 419 | 1692 | 363 | 648 | 415 | 734 | 228 | 182 | 136 | 206 | 55 | 349 | 438 | 155 | 144 | 387 | 1352 | 908 |
| 92 | 12 | 19 | 5 | 18 | 25 | 92 | 77 | 60 | 68 | 40 | 5 | 38 | 77 | 20 | 50 | 56 | 38 | 13 |
| 142 | 6 | 26 | 28 | 33 | 51 | 150 | 111 | 80 | 79 | 68 | 39 | 50 | 109 | 42 | 55 | 95 | 70 | 64 |
| 9 | 5 | 3 | 3 | 4 | 11 | 15 | 15 | 9 | 15 | 9 | 5 | 5 | 14 | 7 | 10 | 8 | 9 | 6 |
| 56 | 14 | 8 | 15 | 14 | 40 | 52 | 52 | 40 | 33 | 30 | 11 | 28 | 36 | 27 | 26 | 51 | 23 | 30 |
| 7 | 3 | 3 | 5 | 4 | 5 | 7 | 6 | 5 | 4 | 6 | 3 | 3 | 5 | 3 | 4 | 5 | 5 | 3 |
| 7 | 4 | 5 | 2 | 4 | 5 | 7 | 5 | 5 | 3 | 3 | 4 | 6 | 2 | 2 | 7 | 6 | 8 | 3 |
| 3 | 5 | 6 | 2 | 2 | 6 | 7 | 2 | 2 | 2 | 4 | 2 | 2 | 2 | 2 | 2 | 2 | 5 | 4 |
| 11 | 13 | 9 | 3 | 15 | 11 | 8 | 10 | 11 | 5 | 16 | 3 | 9 | 3 | 4 | 3 | 14 | 14 | 17 |
| 41 | 5 | 13 | 7 | 16 | 35 | 27 | 67 | 5 | 30 | 18 | 20 | 21 | 9 | 16 | 29 | 33 | 33 | 19 |
| 13 | 3 | 3 | 3 | 12 | 3 | 3 | 3 | 3 | 3 | 3 | 3 | 3 | 3 | 5 | 3 | 5 | 8 | 3 |
| 46 | 16 | 22 | 17 | 2 | 15 | 28 | 27 | 40 | 21 | 28 | 28 | 24 | 14 | 4 | 44 | 32 | 20 | 18 |
| 10 | 3 | 8 | 3 | 2 | 12 | 20 | 6 | 4 | 2 | 3 | 5 | 3 | 4 | 2 | 10 | 10 | 2 | 7 |
| 5,874 | 0,154 | 46,785 | 0,095 | 0,074 | 18,788 | 3,573 | 16,068 | 34,559 | 48,847 | 19,444 | 41,227 | 21,161 | 49,773 | 0,063 | 26,345 | 7,164 | 0,091 | 0,055 |
| 4,327 | 0,55 | 10,747 | 4,124 | 0,37 | 3,684 | 5,208 | 1,89 | 1,992 | 1,064 | 0,277 | 9,556 | 0,167 | 0,047 | 0,526 | 1,3 | 0,188 | 0,248 | 0,032 |
| 9,4 | 3,5 | 14 | 29 | 4,3 | 8,8 | 19 | 12,9 | 7,2 | 4,6 | 6,5 | 22,6 | 38,9 | 10,6 | 3,2 | 6,8 | 10,2 | 6,7 | 12,1 |
| 427 |  | 423 |  |  | 424 | 419 | 423 | 421 | 427 | 429 | 427 | 431 | 428 |  | 431 | 426 |  |  |
| 0,34 |  | 2,33 |  |  | 1,21 | 0,31 | 0,6 | 1,46 | 0,94 | 0,7 | 0,9 | 0,66 | 0,5 |  | 0,85 | 0,51 |  |  |
| 4,64 |  | 52,76 |  |  | 27,89 | 1,12 | 8,31 | 35,51 | 13,8 | 22,13 | 48,65 | 3,94 | 7,43 |  | 25,68 | 6,9 |  |  |
| 0,82 |  | 6,02 |  |  | 2,53 | 0,74 | 1,66 | 2,82 | 3,18 | 2,14 | 7,01 | 2,18 | 4,11 |  | 3,44 | 0,91 |  |  |
| 72 |  | 97 |  |  | 135 | 25 | 45 | 95 | 27 | 106 | 91 | 11 | 13 |  | 91 | 86 |  |  |
| 13 |  | 11 |  |  | 12 | 17 | 9 | 8 | 6 | 10 | 13 | 6 | 7 |  | 12 | 11 |  |  |
| -22,5 | -22,98 | -23,32 | -22,38 | -23,3 | -22,61 | -21,46 | -22,49 | -22,85 | -21,19 | -25,63 | -26,04 | -23,08 | -21,36 | -23,32 | -23,82 | -22,43 | -23,94 | -24,45 |
| -22,6 | -23 | -23,44 | -22,26 | -23,34 | -22,55 | -21,54 | -22,67 | -23,29 | -21,18 | -25,63 | -25,96 | -23,24 | -21,37 | -23,4 | -23,99 | -22,4 | -23,53 | -23,9 |
| -22,55 | -22,99 | -23,38 | -22,32 | -23,32 | -22,58 | -21,5 | -22,58 | -23,07 | -21,19 | -25,63 | -26 | -23,16 | -21,36 | -23,36 | -23,91 | -22,41 | -23,74 | -24,18 |

| Lab.-Nr. | 991914 | 991915 | 991916 | 991917 | 991918 | 991919 | 991920 | 991921 | 991922 | 991923 | 991924 | 991925 | 991926 | 991927 | 991928 | 991929 | 991930 |
|---|---|---|---|---|---|---|---|---|---|---|---|---|---|---|---|---|---|
| Group | Passa dois | Passa dois | Passa dois | Passa dois | Passa dois | Passa dois | Passa dois | Passa dois | Passa dois | Passa dois | Passa dois | Passa dois | Passa dois | Passa dois | Passa dois | Passa dois | Passa dois |
| Formation | Serra Alta | Serra Alta | Serra Alta | Serra Alta | Serra Alta | Irati | Irati | Irati | Irati | Irati | Irati | Irati | Irati | Irati | Irati | Irati | Irati |
| $SiO_2$ | 41,2 | 64,17 | 69,45 | 69,65 | 80,33 | 21,54 | 66,64 | 9,81 | 62,28 | 60,4 | 10,55 | 46,31 | 60,01 | 56,48 | 24,29 | 10,71 | 4,84 |
| $TiO_2$ | 0,32 | 0,59 | 0,58 | 0,57 | 0,22 | 0,04 | 0,33 | 0,03 | 0,34 | 0,34 | 0,02 | 3,82 | 0,25 | 0,27 | 0,02 | 0,05 | 0,03 |
| $Al_2O_3$ | 7,19 | 13,56 | 13,15 | 12,86 | 4,97 | 0,93 | 6,56 | 0,53 | 7,06 | 7,79 | 0,8 | 14,36 | 4,78 | 5,1 | 0,47 | 0,87 | 0,42 |
| $Fe_2O_3$ | 9,74 | 5,26 | 5,41 | 5,16 | 7,16 | 1,69 | 6,46 | 2,59 | 7,29 | 4,72 | 2 | 14,21 | 4,97 | 3,02 | 0,47 | 0,42 | 0,13 |
| MnO | 0,79 | 0,08 | 0,02 | 0,02 | 0,02 | 0,64 | 0,13 | 0,58 | 0,02 | 0,02 | 0,4 | 0,11 | 0,07 | 0,1 | 0,24 | 0,07 | 0,07 |
| MgO | 6,96 | 2,43 | 2,01 | 2,12 | 1,84 | 15,54 | 10,94 | 17,32 | 7,17 | 12,77 | 19,28 | 5,53 | 19,02 | 23,13 | 19,35 | 19,18 | 19,58 |
| CaO | 11,1 | 1,73 | 0,5 | 0,81 | 0,44 | 30,77 | 1,19 | 27,16 | 1,35 | 1,47 | 26,26 | 5,6 | 1,48 | 1,53 | 27,24 | 26,02 | 29,43 |
| $Na_2O$ | 2 | 2,71 | 1,59 | 1,99 | 0,5 | 0,02 | 0,95 | 0,11 | 0,96 | 1,26 | 0,14 | 2,72 | 0,38 | 0,32 | 0,02 | 0,12 | 0,07 |
| $K_2O$ | 1,41 | 3,34 | 3,34 | 3,02 | 0,55 | 0,04 | 1,24 | 0,03 | 1,62 | 1,16 | 0,02 | 1,08 | 0,4 | 0,46 | 0,01 | 0,17 | 0,09 |
| $P_2O_5$ | 0,158 | 0,223 | 0,155 | 0,34 | 0,258 | 0,051 | 0,262 | 0,069 | 0,158 | 0,151 | 0,063 | 0,435 | 0,067 | 0,07 | 0,064 | 0,043 | 0,033 |
| $SO_3$ | 0,012 | 0,012 | 0,012 | 0,012 | 0,012 | 0,012 | 0,012 | 0,124 | 3,992 | 1,699 | 0,094 | 0,889 | 0,671 | 0,462 | 0,073 | 0,137 | 0,072 |
| Sum | 80,88 | 94,105 | 96,217 | 96,552 | 96,3 | 71,273 | 94,714 | 58,353 | 92,24 | 91,78 | 59,627 | 95,064 | 92,098 | 90,942 | 72,247 | 57,79 | 54,765 |
| V | 249 | 93 | 79 | 79 | 66 | 34 | 72 | 14 | 89 | 71 | 14 | 586 | 57 | 74 | 28 | 18 | 5 |
| Cr | 13 | 42 | 35 | 38 | 16 | 5 | 16 | 5 | 26 | 23 | 5 | 49 | 21 | 114 | 5 | 5 | 5 |
| Co | 18 | 15 | 22 | 19 | 41 | 9 | 22 | 12 | 40 | 22 | 9 | 67 | 30 | 12 | 2 | 9 | 6 |
| Ni | 90 | 69 | 133 | 35 | 55 | 21 | 32 | 32 | 87 | 29 | 25 | 72 | 32 | 65 | 16 | 20 | 10 |
| Cu | 28 | 43 | 46 | 35 | 41 | 67 | 25 | 17 | 47 | 57 | 17 | 70 | 58 | 46 | 44 | 99 | 92 |
| Zn | 43 | 81 | 85 | 80 | 43 | 16 | 47 | 3 | 51 | 37 | 3 | 151 | 35 | 39 | 3 | 3 | 3 |
| Ga | 4 | 19 | 20 | 17 | 9 | 2 | 13 | 2 | 15 | 13 | 3 | 28 | 7 | 7 | 2 | 2 | 6 |
| As | 11 | 5 | 11 | 15 | 14 | 12 | 22 | 4 | 36 | 23 | 4 | 9 | 18 | 11 | 4 | 4 | 4 |
| Rb | 70 | 192 | 184 | 158 | 29 | 2 | 55 | 2 | 66 | 44 | 2 | 18 | 19 | 24 | 2 | 6 | 2 |
| Sr | 879 | 455 | 146 | 164 | 66 | 441 | 138 | 719 | 519 | 875 | 624 | 830 | 837 | 875 | 916 | 559 | 690 |
| Y | 28 | 29 | 21 | 29 | 26 | 12 | 30 | 10 | 26 | 19 | 14 | 38 | 16 | 25 | 16 | 13 | 11 |
| Zr | 109 | 144 | 125 | 128 | 106 | 20 | 135 | 25 | 107 | 115 | 18 | 257 | 100 | 106 | 28 | 32 | 25 |
| Nb | 2 | 5 | 10 | 11 | 2 | 2 | 2 | 2 | 4 | 5 | 2 | 18 | 2 | 7 | 2 | 2 | 2 |
| Mo | 2 | 2 | 6 | 2 | 4 | 2 | 4 | 243 | 5 | 2 | 2 | 6 | 3 | 3 | 2 | 2 | 2 |
| Sn | 19 | 23 | 30 | 26 | 7 | 7 | 7 | 24 | 13 | 7 | 7 | 7 | 7 | 7 | 7 | 7 | 7 |
| Ba | 364 | 567 | 418 | 425 | 251 | 254 | 384 | 95 | 487 | 502 | 115 | 660 | 260 | 315 | 97 | 86 | 110 |
| La | 10 | 38 | 30 | 39 | 27 | 29 | 58 | 5 | 36 | 14 | 5 | 20 | 6 | 39 | 23 | 23 | 42 |
| Ce | 73 | 74 | 51 | 75 | 68 | 33 | 76 | 6 | 37 | 47 | 18 | 66 | 21 | 24 | 6 | 17 | 6 |
| Pr | 3 | 7 | 3 | 8 | 3 | 3 | 3 | 6 | 7 | 3 | 3 | 5 | 3 | 3 | 3 | 5 | 3 |
| Nd | 19 | 50 | 37 | 32 | 33 | 17 | 32 | 3 | 34 | 37 | 13 | 25 | 12 | 25 | 5 | 23 | 3 |
| Sm | 4 | 5 | 4 | 6 | 4 | 4 | 5 | 3 | 4 | 4 | 3 | 7 | 3 | 3 | 3 | 3 | 3 |
| Hf | 2 | 3 | 4 | 3 | 3 | 2 | 3 | 2 | 2 | 2 | 2 | 5 | 2 | 2 | 2 | 2 | 2 |
| Ta | 3 | 4 | 4 | 2 | 5 | 6 | 2 | 2 | 5 | 2 | 4 | 2 | 2 | 4 | 5 | 15 | 10 |
| W | 9 | 9 | 19 | 3 | 13 | 10 | 9 | 3 | 9 | 6 | 5 | 3 | 12 | 3 | 9 | 16 | 14 |
| Pb | 12 | 8 | 9 | 15 | 3 | 3 | 15 | 13 | 23 | 25 | 3 | 9 | 15 | 8 | 3 | 3 | 3 |
| Bi | 3 | 3 | 3 | 3 | 3 | 3 | 3 | 4 | 3 | 3 | 3 | 3 | 3 | 3 | 3 | 3 | 3 |
| Th | 2 | 11 | 12 | 16 | 9 | 2 | 30 | 7 | 6 | 2 | 12 | 9 | 2 | 5 | 6 | 2 | 12 |
| U | 6 | 2 | 3 | 3 | 2 | 2 | 11 | 4 | 8 | 11 | 2 | 2 | 5 | 5 | 2 | 5 | 2 |
| TOC | 0,08 | 0,21 | 0,15 | 0,12 | 0,03 | 0,01 | 0,36 | 0,89 | 3,35 | 2,03 | 1,14 | 0,06 | 0,81 | 1,20 | 0,22 | 0,59 | 0,23 |
| S | 0,00 | 0,00 | 0,00 | 0,00 | 0,00 | 0,00 | 0,03 | 0,05 | 4,07 | 1,85 | 0,05 | 0,70 | 0,50 | 0,47 | 0,02 | 0,03 | 0,01 |
| loss by HCl [%] | 48,03 | 11,8 | 9,14 | 9,44 | 13,21 | 72,8 | 20,12 | 87,89 | 10,54 | 16,94 | 84,67 | 26,38 | 29,14 | 33,17 | 70,09 | 87,09 | 93,28 |
| $\delta^{18}O$ (silic.) | 19,65 | 19,14 | 17,52 | 18,68 | 18,97 | 19,05 | 19,21 | 22,157 | 19,039 | 18 | 21,563 | 12,772 | 18,993 | 17,94 | 20,296 | 22,22 | 18,131 |
| $\delta^{18}O$ (silic.) | 19,629 | 19,28 | 17,54 | 18,49 | 19,29 | 19,31 | 19,58 | 22,058 | 19,074 | 18,18 | 21,67 | 13,003 | 18,95 | 19,37 | 20,388 | 22,4 | 18,408 |
| mean $\delta^{18}O$ | 19,64 | 19,21 | 17,53 | 18,59 | 19,13 | 19,18 | 19,40 | 22,11 | 19,06 | 18,09 | 21,62 | 12,89 | 18,97 | 18,66 | 20,34 | 22,31 | 18,27 |
| std.dev. | 0,015 | 0,099 | 0,014 | 0,134 | 0,226 | 0,184 | 0,262 | 0,070 | 0,025 | 0,127 | 0,076 | 0,163 | 0,030 | 1,011 | 0,065 | 0,127 | 0,196 |
| $T_{max}$ | | | | | | | 380 | 419 | 392 | 401 | 418 | | 397 | 357 | 318 | 406 | 421 |
| S1 | | | | | | | 0,14 | 7,73 | 1,04 | 0,18 | 16,85 | | 0,19 | 0,16 | 0,24 | 6,39 | 4,64 |
| S2 | | | | | | | 0,01 | 17,3 | 1,1 | 0,02 | 35,8 | | 0,01 | 0,03 | 0,01 | 9,68 | 6,58 |
| S3 | | | | | | | 0,04 | 0,82 | 0,65 | 0,42 | 0,87 | | 0,21 | 0,19 | 0,09 | 0,8 | 0,77 |
| HI | | | | | | | 0 | 235 | 29 | 1 | 483 | | 1 | 2 | 1 | 211 | 192 |
| OI | | | | | | | 7 | 11 | 17 | 17 | 12 | | 18 | 11 | 12 | 17 | 23 |
| $\delta^{13}Corg$ | -23,53 | -23,37 | -21,86 | -22,47 | | | | -20,76 | -20,29 | -21,31 | -21,12 | | -19,4 | -20,12 | | -22,44 | -22,5 |
| $\delta^{13}Corg$ | -23,39 | -23,38 | -21,86 | -22,44 | | | | -20,76 | -20,33 | -21,28 | -21,12 | | -19,42 | -20,14 | | -22,37 | -22,53 |
| mean $\delta^{13}Corg$ | -23,46 | -23,38 | -21,86 | -22,46 | | | | -20,76 | -20,31 | -21,3 | -21,12 | | -19,41 | -20,13 | | -22,41 | -22,52 |

| **991931** | **991932** | **991933** | **991934** | **991935** | **991936** | **991937** | **991938** | **991939** | **991940** | **991941** | **991900** | **991942** | **991943** | **991944** | **991945** | **991946** |
|---|---|---|---|---|---|---|---|---|---|---|---|---|---|---|---|---|
| Passa dois | Passa dois | Passa dois | Passa dois | Passa dois | Passa dois | Passa dois | Guata | Guata | Guata | Guata | Guata | Guata | Guata | Itararé | Itararé | Itararé |
| Irati | Irati | Irati | Irati | Irati | Irati | Irati | Tatui | Tatui | Tatui | Tatui | Tatui | Tatui | Tatui | Rio do sul | Rio do sul | Rio do sul |
| 17,05 | 27,94 | 62,39 | 95,99 | 25,04 | 3,4 | 90,39 | 65,94 | 70,39 | 69,35 | 69,85 | 69,36 | 82,25 | 82,04 | 88,18 | 79,69 | 77,87 |
| 0,1 | 0,25 | 0,27 | 0,01 | 0,07 | 0,02 | 0,01 | 0,69 | 0,53 | 0,72 | 0,85 | 0,7 | 0,34 | 0,45 | 0,17 | 0,52 | 0,62 |
| 2,18 | 5,45 | 5,89 | 0,2 | 1,43 | 0,34 | 0,13 | 15,43 | 12,3 | 13,24 | 13,56 | 14,25 | 9,13 | 8,9 | 5,83 | 9,44 | 9,93 |
| 0,88 | 2,3 | 2,25 | 0,16 | 0,55 | 0,38 | 0,24 | 2,91 | 3,87 | 4,81 | 3,91 | 3,17 | 1,2 | 2,69 | 0,57 | 1,82 | 2,35 |
| 0,1 | 0,1 | 0,04 | 0,01 | 0,41 | 0,94 | 0,07 | 0,01 | 0,03 | 0,05 | 0,05 | 0,02 | 0,11 | 0,03 | 0 | 0,01 | 0,02 |
| 16,86 | 12,59 | 17,14 | 0,28 | 17,53 | 2,71 | 0,04 | 3,17 | 1,75 | 2,13 | 1,68 | 1,9 | 0,36 | 0,24 | 0,15 | 0,46 | 0,74 |
| 23,35 | 17,45 | 0,5 | 0,12 | 20,7 | 49,8 | 3,51 | 0,54 | 0,43 | 0,64 | 0,7 | 0,47 | 0,13 | 0,03 | 0,32 | 0,48 | 0,48 |
| 0,3 | 1,05 | 0,26 | 0,02 | 0,04 | 0,02 | 0,02 | 0,7 | 0,83 | 1,48 | 1,74 | 2,23 | 0,23 | 0,02 | 0,95 | 1,7 | 1,94 |
| 0,65 | 1,22 | 0,56 | 0,02 | 0,1 | 0,04 | 0,01 | 3,4 | 2,4 | 2,85 | 3,15 | 3,86 | 2,18 | 1,39 | 1,59 | 2,11 | 2,38 |
| 0,08 | 0,606 | 0,045 | 0,008 | 0,059 | 0,028 | 0,008 | 0,034 | 0,327 | 0,071 | 0,093 | 0,087 | 0,021 | 0,022 | 0,009 | 0,118 | 0,118 |
| 0,395 | 1,186 | 0,012 | 0,012 | 0,012 | 0,017 | 0,233 | 0,099 | 1,124 | 0,201 | 0,397 | 0,062 | 0,012 | 0,012 | 0,012 | 0,012 | 0,012 |
| 61,945 | 70,142 | 89,357 | 96,83 | 65,941 | 57,695 | 94,661 | 92,923 | 93,981 | 95,542 | 95,98 | 96,109 | 95,963 | 95,824 | 97,781 | 96,36 | 96,46 |
| 39 | 125 | 48 | 14 | 22 | 3 | 3 | 95 | 68 | 52 | 56 | 64 | 35 | 25 | 16 | 31 | 40 |
| 14 | 21 | 19 | 5 | 77 | 5 | 5 | 45 | 42 | 30 | 35 | 31 | 11 | 20 | 7 | 17 | 44 |
| 7 | 17 | 26 | 2 | 14 | 2 | 3 | 13 | 19 | 25 | 23 | 20 | 33 | 10 | 7 | 9 | 12 |
| 27 | 30 | 26 | 4 | 41 | 15 | 10 | 41 | 43 | 40 | 37 | 36 | 18 | 26 | 10 | 21 | 20 |
| 99 | 73 | 59 | 49 | 90 | 58 | 59 | 74 | 58 | 44 | 49 | 50 | 65 | 55 | 65 | 40 | 44 |
| 9 | 101 | 28 | 3 | 6 | 6 | 3 | 50 | 119 | 27 | 35 | 66 | 31 | 10 | 3 | 30 | 20 |
| 2 | 11 | 12 | 6 | 2 | 3 | 2 | 20 | 15 | 12 | 18 | 18 | 8 | 12 | 2 | 11 | 8 |
| 4 | 11 | 4 | 4 | 4 | 4 | 4 | 5 | 6 | 5 | 4 | 21 | 5 | 5 | 4 | 9 | 4 |
| 23 | 50 | 37 | 2 | 5 | 2 | 2 | 194 | 134 | 131 | 145 | 129 | 68 | 55 | 45 | 71 | 76 |
| 557 | 582 | 24 | 8 | 124 | 1949 | 200 | 158 | 133 | 163 | 186 | 118 | 58 | 26 | 84 | 100 | 92 |
| 26 | 45 | 42 | 2 | 18 | 6 | 4 | 15 | 48 | 37 | 47 | 27 | 78 | 56 | 10 | 49 | 16 |
| 49 | 87 | 76 | 2 | 25 | 56 | 3 | 145 | 157 | 290 | 308 | 227 | 251 | 386 | 138 | 286 | 292 |
| 3 | 5 | 2 | 2 | 2 | 2 | 2 | 9 | 8 | 15 | 19 | 9 | 4 | 7 | 2 | 6 | 10 |
| 2 | 30 | 2 | 4 | 2 | 3 | 2 | 2 | 3 | 2 | 2 | 2 | 2 | 2 | 2 | 2 | 3 |
| 14 | 15 | 7 | 7 | 7 | 16 | 7 | 7 | 7 | 10 | 18 | 17 | 7 | 7 | 7 | 14 | 12 |
| 175 | 269 | 110 | 39 | 70 | 4843 | 208 | 363 | 324 | 742 | 461 | 750 | 701 | 374 | 395 | 584 | 537 |
| 15 | 83 | 11 | 7 | 13 | 5 | 5 | 18 | 37 | 70 | 23 | 16 | 27 | 26 | 13 | 58 | 36 |
| 23 | 117 | 23 | 26 | 28 | 19 | 26 | 41 | 83 | 128 | 103 | 100 | 156 | 45 | 6 | 73 | 72 |
| 3 | 12 | 3 | 3 | 3 | 3 | 3 | 5 | 5 | 11 | 5 | 8 | 6 | 6 | 3 | 8 | 6 |
| 13 | 52 | 20 | 3 | 9 | 3 | 10 | 29 | 42 | 52 | 39 | 50 | 90 | 50 | 8 | 43 | 23 |
| 3 | 6 | 3 | 3 | 3 | 3 | 3 | 3 | 5 | 7 | 5 | 6 | 9 | 5 | 3 | 7 | 5 |
| 2 | 2 | 3 | 2 | 2 | 2 | 2 | 5 | 5 | 6 | 7 | 7 | 6 | 9 | 5 | 7 | 6 |
| 11 | 5 | 7 | 2 | 5 | 10 | 4 | 4 | 2 | 5 | 14 | 10 | 8 | 5 | 12 | 2 | 2 |
| 3 | 11 | 6 | 3 | 11 | 11 | 5 | 16 | 12 | 19 | 18 | 16 | 14 | 14 | 26 | 6 | 10 |
| 4 | 25 | 8 | 3 | 3 | 16 | 3 | 9 | 10 | 5 | 6 | 271 | 3 | 3 | 6 | 3 | 4 |
| 3 | 3 | 3 | 3 | 3 | 3 | 3 | 3 | 3 | 3 | 3 | 3 | 3 | 3 | 3 | 3 | 3 |
| 2 | 2 | 17 | 10 | 2 | 2 | 22 | 16 | 10 | 2 | 21 | 25 | 14 | 2 | 10 | 7 | 20 |
| 2 | 7 | 4 | 3 | 2 | 2 | 3 | 4 | 2 | 3 | 2 | 6 | 4 | 2 | 7 | 2 | 2 |
| 0,89 | 1,88 | 0,86 | 0,16 | 0,29 | 0,00 | 0,02 | 0,26 | 0,56 | 0,06 | 0,05 | 0,19 | 0,06 | 0,04 | 0,07 | 0,03 | 0,01 |
| 0,11 | 0,54 | 0,02 | 0,03 | 0,01 | 0,00 | 0,00 | 0,09 | 0,98 | 0,30 | 0,45 | 0,14 | 0,01 | 0,00 | 0,00 | 0,01 | 0,00 |
| 77,96 | 62,53 | 28,7 | 2,35 | 72,65 | 95,36 | 10,17 | 11,21 | 11,25 | 8,69 | 10,73 | 7,16 | 5,93 | 6,11 | 2,8 | 4,13 | 5,91 |
| 18,51 | 17,19 | 19,78 | 23,04 | 24,75 | | 25,66 | 16,92 | 17,4 | 14,21 | 14,32 | 14,59 | 13,6 | 18,59 | 12,04 | 12,98 | |
| 18,22 | 17,19 | 19,708 | 23,36 | 25,39 | | 25,5 | 17,3 | 17,33 | 14,43 | 14,53 | 14,84 | 13,2 | 18,23 | 12,36 | 13,43 | |
| 18,37 | 17,19 | 19,74 | 23,20 | 25,07 | | 25,58 | 17,11 | 17,37 | 14,32 | 14,43 | 14,72 | 13,40 | 18,41 | 12,20 | 13,21 | |
| 0,205 | 0,000 | 0,051 | 0,226 | 0,453 | | 0,113 | 0,269 | 0,049 | 0,156 | 0,148 | 0,177 | 0,283 | 0,255 | 0,226 | 0,318 | |
| 399 | 397 | 419 | | 423 | | | | 409 | | | | | | | | |
| 7,67 | 9,75 | 0,54 | | 0,49 | | | | 0,14 | | | | | | | | |
| 5,66 | 9,09 | 2,94 | | 2,64 | | | | 0,72 | | | | | | | | |
| 0,55 | 0,67 | 0,58 | | 0,4 | | | | 0,1 | | | | | | | | |
| 141 | 182 | 243 | | 254 | | | | 114 | | | | | | | | |
| 14 | 13 | 48 | | 38 | | | | 16 | | | | | | | | |
| -23,28 | -24,98 | -21,11 | | -21,8 | | | -23,4 | -26,24 | -25,94 | -24,69 | -24,97 | -25,97 | | -24,63 | | |
| -23,32 | -25,03 | -21,07 | | -21,87 | | | -23,49 | -27,01 | -25,5 | -24,68 | -25,14 | -26,08 | | -24,71 | | |
| -23,3 | -25,01 | -21,09 | | -21,84 | | | -23,45 | -26,63 | -25,72 | -24,69 | -25,06 | -26,03 | | -24,67 | | |

| Sample | Pc Basis | ZAUN 2 trace | ZAUN 2 chips | ZAUN 2 plates | Pw 14 | Pw 13 | Pw 12 | Pw 11 | Pw 10 | Pw 9 | Pw 8 | Pw mitte | Pw 7 | Pw 6 | Pw 5 | Pw 4 |
|---|---|---|---|---|---|---|---|---|---|---|---|---|---|---|---|---|
| Lab. Nr. | 994742 | 994809 | 994733 | 994732 | 994731 | 994730 | 994729 | 994728 | 994727 | 994726 | 994725 | 994724 | 994723 | 994722 | 994721 | 994720 |
| Position | 423 | 422,5 | 422 | 421,5 | 421 | 418,5 | 415 | 412 | 409,5 | 407 | 405 | 403,5 | 402 | 400 | 397 | 394 |
| Group | Ecca | Ecca | Ecca | Ecca | Ecca | Ecca | Ecca | Ecca | Ecca | Ecca | Ecca | Ecca | Ecca | Ecca | Ecca | Ecca |
| Fm. | Pc | Pw | Pw | Pw | Pw | Pw | Pw | Pw | Pw | Pw | Pw | Pw | Pw | Pw | Pw | Pw |
| $SiO_2$ | 70,18 | 68,97 | 70,42 | 69,03 | 67,36 | 71,93 | 75,39 | 74,62 | 69,56 | 71,57 | 63,16 | 67,27 | 74,14 | 66,39 | 68,79 | 66,55 |
| $TiO_2$ | 0,53 | 0,65 | 0,64 | 0,74 | 0,65 | 0,73 | 0,76 | 0,8 | 0,84 | 0,59 | 0,65 | 0,7 | 0,61 | 0,68 | 0,69 | 0,78 |
| $Al_2O_3$ | 14,63 | 16,72 | 13,42 | 16,62 | 15,99 | 14,55 | 12,87 | 12,73 | 15,63 | 15,81 | 18,13 | 17,62 | 13,95 | 12,48 | 14,48 | 13,14 |
| $Fe_2O_3$ | 3,36 | 0,32 | 0,58 | 0,62 | 0,85 | 0,9 | 0,33 | 0,38 | 0,48 | 0,59 | 4,47 | 0,96 | 0,39 | 0,89 | 0,73 | 1,84 |
| MnO | 0,03 | 0,03 | 0 | 0,01 | 0 | 0,01 | 0 | 0 | 0 | 0,01 | 0,06 | 0,01 | 0,01 | 0,01 | 0 | 0 |
| MgO | 1,39 | 0,43 | 0,61 | 0,65 | 1,02 | 0,55 | 0,41 | 0,42 | 0,55 | 0,5 | 1,57 | 0,72 | 0,39 | 1,22 | 0,51 | 0,58 |
| CaO | 0,76 | 0,81 | 0,35 | 0,28 | 0,61 | 0,29 | 0,27 | 0,27 | 0,3 | 0,38 | 0,8 | 0,95 | 0,54 | 0,22 | 0,33 | 0,21 |
| $Na_2O$ | 2,05 | 2,47 | 0,44 | 0,89 | 1,94 | 1,19 | 1,28 | 1,32 | 1,4 | 2,48 | 2,31 | 2,98 | 2,1 | 4,27 | 2,21 | 0,82 |
| $K_2O$ | 2,74 | 4,17 | 3,55 | 4,22 | 3,89 | 3,68 | 3,24 | 3,34 | 4,23 | 3,44 | 3,3 | 3,25 | 2,81 | 2,52 | 2,76 | 3,17 |
| $P_2O_5$ | 0,127 | 0,088 | 0,072 | 0,079 | 0,085 | 0,041 | 0,045 | 0,052 | 0,099 | 0,055 | 0,134 | 0,176 | 0,11 | 0,107 | 0,12 | 0,134 |
| $SO_3$ | 0,012 | 0,012 | 0,012 | 0,012 | 0,012 | 0,012 | 0,012 | 0,012 | 0,012 | 0,014 | 0,012 | 0,012 | 0,013 | 0,158 | 0,1 | 0,295 |
| L.O.I. | 4,75 | 5,82 | 9,23 | 7,32 | 8,65 | 6,44 | 5,72 | 6,98 | 6,32 | 4,25 | 5,00 | 5,16 | 4,87 | 9,78 | 10,32 | 12,53 |
| Sum | 100,56 | 100,49 | 99,32 | 100,47 | 101,06 | 100,32 | 100,33 | 100,92 | 99,42 | 99,69 | 99,60 | 99,81 | 99,93 | 98,73 | 101,04 | 100,05 |
| Sc | 21 | 9 | 25 | 27 | 11 | 37 | 21 | 17 | 21 | 21 | 13 | 21 | 22 | 18 | 11 | 23 |
| V | 111 | 134 | 141 | 180 | 160 | 178 | 145 | 119 | 167 | 127 | 147 | 159 | 125 | 146 | 131 | 148 |
| Cr | 30 | 31 | 36 | 40 | 34 | 52 | 37 | 31 | 47 | 36 | 32 | 41 | 26 | 39 | 37 | 44 |
| Co | 6 | 2 | 2 | 2 | 2 | 4 | 2 | 2 | 2 | 2 | 7 | 2 | 2 | 2 | 2 | 2 |
| Ni | 15 | 4 | 7 | 4 | 4 | 12 | 4 | 4 | 13 | 4 | 44 | 4 | 4 | 79 | 20 | 26 |
| Cu | 26 | 3 | 3 | 3 | 3 | 8 | 3 | 9 | 6 | 3 | 26 | 3 | 3 | 3 | 6 | 16 |
| Zn | 97 | 30 | 9 | 6 | 17 | 6 | 3 | 6 | 9 | 4 | 120 | 9 | 3 | 4 | 3 | 3 |
| Ga | 22 | 20 | 24 | 31 | 24 | 25 | 17 | 23 | 26 | 26 | 27 | 28 | 20 | 23 | 29 | 24 |
| As | 20 | 13 | 16 | 14 | 15 | 14 | 12 | 14 | 16 | 12 | 93 | 17 | 30 | 24 | 16 | 24 |
| Rb | 133 | 219 | 171 | 223 | 199 | 197 | 178 | 183 | 261 | 201 | 201 | 181 | 171 | 151 | 166 | 193 |
| Sr | 204 | 256 | 116 | 172 | 131 | 82 | 90 | 94 | 137 | 152 | 157 | 174 | 132 | 148 | 128 | 98 |
| Y | 34 | 33 | 37 | 32 | 34 | 32 | 29 | 28 | 32 | 14 | 34 | 30 | 20 | 30 | 25 | 23 |
| Zr | 142 | 158 | 153 | 159 | 144 | 159 | 145 | 162 | 159 | 116 | 142 | 146 | 123 | 177 | 157 | 156 |
| Nb | 12 | 12 | 15 | 13 | 13 | 14 | 17 | 15 | 17 | 11 | 12 | 13 | 9 | 16 | 13 | 13 |
| Mo | 2 | 2 | 2 | 2 | 2 | 2 | 2 | 2 | 2 | 2 | 2 | 2 | 2 | 4 | 2 | 2 |
| Sn | 7 | 7 | 7 | 7 | 7 | 15 | 7 | 7 | 7 | 7 | 7 | 7 | 7 | 7 | 7 | 7 |
| Ba | 675 | 517 | 497 | 584 | 702 | 579 | 474 | 507 | 540 | 515 | 420 | 430 | 465 | 756 | 470 | 663 |
| La | 29 | 42 | 42 | 58 | 38 | 41 | 42 | 42 | 46 | 11 | 19 | 21 | 19 | 32 | 22 | 35 |
| Ce | 30 | 65 | 74 | 97 | 67 | 83 | 88 | 89 | 80 | 6 | 69 | 55 | 21 | 111 | 116 | 63 |
| Pr | 7 | 9 | 6 | 14 | 13 | 11 | 9 | 11 | 9 | 3 | 3 | 11 | 3 | 13 | 14 | 3 |
| Nd | 41 | 27 | 30 | 46 | 24 | 46 | 29 | 34 | 44 | 10 | 28 | 32 | 3 | 33 | 38 | 30 |
| Sm | 5 | 5 | 7 | 5 | 4 | 8 | 7 | 5 | 4 | 3 | 5 | 5 | 4 | 6 | 7 | 5 |
| Hf | 6 | 5 | 6 | 3 | 2 | 5 | 5 | 5 | 5 | 3 | 4 | 6 | 2 | 5 | 3 | 4 |
| Ta | 2 | 2 | 2 | 2 | 2 | 2 | 2 | 2 | 2 | 2 | 2 | 2 | 2 | 2 | 2 | 2 |
| W | 3 | 3 | 3 | 3 | 3 | 3 | 3 | 3 | 3 | 3 | 3 | 3 | 3 | 3 | 3 | 3 |
| Pb | 13 | 31 | 31 | 31 | 35 | 34 | 21 | 26 | 41 | 13 | 21 | 30 | 28 | 56 | 52 | 47 |
| Bi | 3 | 3 | 3 | 3 | 3 | 3 | 6 | 5 | 3 | 3 | 3 | 4 | 3 | 3 | 3 | 3 |
| Th | 12 | 20 | 24 | 19 | 34 | 23 | 26 | 14 | 25 | 14 | 14 | 28 | 33 | 33 | 29 | 32 |
| U | 10 | 2 | 4 | 2 | 7 | 9 | 3 | 2 | 2 | 2 | 2 | 3 | 8 | 4 | 8 | 3 |
| TOC | 0,54 | 1,00 | 4,58 | 1,98 | 1,66 | 1,58 | 1,74 | 1,54 | 2,64 | 0,24 | 0,46 | 0,72 | 1,12 | 2,29 | 3,65 | 4,75 |
| TC | 0,54 | 1,22 | 5,03 | 2,14 | 1,90 | 1,88 | 1,88 | 1,66 | 2,91 | 0,28 | 0,56 | 0,84 | 1,30 | 2,64 | 4,07 | 5,37 |
| S | 0 |  | 0,109 | 0,05 | 0,067 | 0,04 | 0,014 | 0,013 | 0,056 | 0,112 | 0,029 | 0,249 | 0,134 | 1,009 | 0,648 | 1,163 |

| Pw <3.5 | Pw 3 | Pw 2 | Pw 1b | Pw 1a | Pp7 TJK | UHB Pp 97 | Pp6 TJK | Pp5 TJK | Pp4 TJK | Pp3 TJK | UHB Pp 80 | Pp2 TJK | Pp1 TJK | UHB Pp 65 | UHB Pp 55 | UHB Pp 45 |
|---|---|---|---|---|---|---|---|---|---|---|---|---|---|---|---|---|
| 994719 | 994718 | 994717 | 994716 | 994715 | 994714 | 994741 | 994713 | 994712 | 994711 | 994710 | 994740 | 994709 | 994708 | 994739 | 994738 | 994737 |
| 392 | 388 | 385,5 | 384 | 383 | 381 | 379 | 377 | 372 | 367 | 365 | 362 | 357 | 352 | 347 | 337 | 326 |
| Ecca | Ecca | Ecca | Ecca | Ecca | Ecca | Ecca | Ecca | Ecca | Ecca | Ecca | Ecca | Ecca | Ecca | Ecca | Ecca | Ecca |
| Pw | Pw | Pw | Pw | Pw | Pp | Pp | Pp | Pp | Pp | Pp | Pp | Pp | Pp | Pp | Pp | Pp |
| 67,88 | 62,87 | 63,2 | 68,4 | 66,14 | 67,81 | 64,8 | 71,23 | 63,86 | 63,44 | 66,37 | 63,71 | 62,24 | 60,96 | 65,16 | 65,01 | 67,54 |
| 0,81 | 0,25 | 0,56 | 0,61 | 0,6 | 0,52 | 0,56 | 0,46 | 0,64 | 0,64 | 0,54 | 0,61 | 0,64 | 0,64 | 0,56 | 0,68 | 0,54 |
| 14,1 | 11,24 | 13,78 | 18,4 | 17,52 | 16,3 | 17,27 | 14,08 | 18,63 | 18,49 | 15,96 | 18,3 | 19,11 | 19,29 | 17,25 | 17,33 | 15,38 |
| 0,43 | 1,4 | 0,75 | 0,68 | 5,42 | 4,96 | 5,22 | 4,36 | 4,72 | 5,05 | 5,27 | 5,12 | 5,58 | 6,16 | 5,28 | 5,05 | 5,3 |
| 0 | 0,07 | 0,05 | 0 | 0,06 | 0,03 | 0,04 | 0,01 | 0,03 | 0,03 | 0,04 | 0,04 | 0,04 | 0,05 | 0,03 | 0,03 | 0,04 |
| 1,04 | 5,79 | 4,53 | 0,66 | 1,54 | 1,58 | 2,03 | 1,21 | 1,66 | 1,84 | 1,77 | 1,94 | 1,92 | 2,06 | 1,79 | 1,88 | 1,79 |
| 0,07 | 5,29 | 2,83 | 0,44 | 0,47 | 0,27 | 0,54 | 0,18 | 0,35 | 0,32 | 0,32 | 0,26 | 0,34 | 0,31 | 0,27 | 0,29 | 0,25 |
| 1,29 | 2,64 | 2,99 | 2,03 | 1,66 | 1,73 | 2,24 | 1,36 | 1,4 | 1,35 | 1,68 | 1,6 | 1,32 | 1,14 | 1,5 | 1,64 | 1,06 |
| 3,55 | 0,83 | 4,37 | 3,73 | 2,84 | 3,03 | 3,2 | 2,58 | 3,66 | 3,63 | 2,98 | 3,54 | 3,89 | 3,68 | 3,36 | 3,05 | 2,85 |
| 0,077 | 0,209 | 0,288 | 0,206 | 0,154 | 0,081 | 0,182 | 0,076 | 0,084 | 0,086 | 0,074 | 0,106 | 0,08 | 0,079 | 0,087 | 0,091 | 0,074 |
| 0,06 | 0,131 | 0,018 | 0,012 | 0,012 | 0,012 | 0,012 | 0,012 | 0,012 | 0,012 | 0,012 | 0,012 | 0,012 | 0,012 | 0,012 | 0,012 | 0,012 |
| 10,57 | 9,77 | 7,21 | 5,66 | 4,11 | 3,97 | 4,66 | 5,53 | 4,56 | 5,88 | 5,84 | 5,12 | 4,89 | 5,67 | 4,72 | 5,71 | 6,04 |
| 99,88 | 100,49 | 100,58 | 100,83 | 100,53 | 100,29 | 100,75 | 101,09 | 99,61 | 100,77 | 100,86 | 100,36 | 100,06 | 100,05 | 100,02 | 100,77 | 100,88 |
| 21 | 24 | 29 | 20 | 23 | 23 | 31 | 15 | 14 | 27 | 23 | 26 | 28 | 29 | 24 | 10 | 23 |
| 147 | 81 | 116 | 165 | 141 | 133 | 146 | 134 | 163 | 145 | 125 | 160 | 157 | 148 | 149 | 143 | 125 |
| 43 | 15 | 37 | 39 | 44 | 37 | 41 | 32 | 56 | 58 | 36 | 56 | 56 | 53 | 43 | 46 | 42 |
| 2 | 2 | 2 | 2 | 19 | 24 | 12 | 10 | 13 | 33 | 17 | 15 | 12 | 20 | 11 | 23 | 8 |
| 5 | 19 | 16 | 4 | 52 | 39 | 23 | 13 | 35 | 58 | 24 | 42 | 31 | 39 | 38 | 42 | 46 |
| 17 | 26 | 13 | 3 | 35 | 58 | 35 | 31 | 31 | 45 | 37 | 33 | 67 | 47 | 40 | 44 | 41 |
| 4 | 28 | 24 | 9 | 75 | 118 | 103 | 100 | 178 | 152 | 132 | 97 | 163 | 171 | 115 | 136 | 86 |
| 28 | 27 | 18 | 24 | 24 | 16 | 24 | 21 | 22 | 27 | 20 | 29 | 30 | 28 | 27 | 25 | 16 |
| 27 | 11 | 22 | 12 | 14 | 42 | 30 | 13 | 34 | 32 | 19 | 27 | 36 | 26 | 26 | 26 | 26 |
| 234 | 75 | 182 | 218 | 171 | 202 | 196 | 169 | 230 | 237 | 192 | 228 | 246 | 229 | 221 | 197 | 174 |
| 75 | 217 | 235 | 96 | 212 | 87 | 90 | 69 | 79 | 72 | 75 | 100 | 79 | 76 | 95 | 89 | 58 |
| 25 | 15 | 13 | 25 | 28 | 28 | 33 | 33 | 33 | 34 | 27 | 29 | 34 | 33 | 28 | 37 | 24 |
| 152 | 61 | 114 | 141 | 139 | 136 | 156 | 136 | 179 | 176 | 132 | 165 | 168 | 163 | 162 | 184 | 139 |
| 12 | 4 | 8 | 11 | 10 | 10 | 10 | 8 | 14 | 12 | 11 | 12 | 12 | 13 | 11 | 14 | 11 |
| 2 | 2 | 2 | 2 | 2 | 2 | 2 | 2 | 2 | 2 | 2 | 2 | 2 | 2 | 5 | 2 | 2 |
| 7 | 7 | 7 | 7 | 7 | 7 | 7 | 7 | 7 | 7 | 7 | 7 | 27 | 17 | 12 | 7 | 7 |
| 432 | 280 | 608 | 1819 | 474 | 488 | 530 | 520 | 520 | 587 | 592 | 546 | 704 | 612 | 518 | 555 | 689 |
| 41 | 29 | 30 | 37 | 15 | 13 | 42 | 17 | 40 | 41 | 38 | 35 | 27 | 21 | 27 | 33 | 25 |
| 66 | 27 | 43 | 84 | 88 | 38 | 60 | 79 | 73 | 92 | 68 | 83 | 79 | 78 | 83 | 83 | 45 |
| 3 | 3 | 5 | 11 | 11 | 4 | 5 | 16 | 10 | 5 | 3 | 9 | 12 | 4 | 5 | 8 | 3 |
| 35 | 4 | 11 | 38 | 37 | 25 | 38 | 35 | 24 | 37 | 19 | 40 | 32 | 24 | 22 | 37 | 23 |
| 4 | 5 | 4 | 5 | 6 | 6 | 7 | 7 | 7 | 6 | 4 | 8 | 5 | 4 | 7 | 7 | 5 |
| 4 | 2 | 4 | 5 | 4 | 5 | 3 | 4 | 3 | 5 | 3 | 4 | 4 | 5 | 3 | 5 | 3 |
| 2 | 2 | 2 | 2 | 4 | 2 | 2 | 2 | 2 | 2 | 2 | 2 | 2 | 2 | 2 | 2 | 2 |
| 3 | 3 | 3 | 3 | 7 | 3 | 3 | 3 | 3 | 3 | 3 | 3 | 3 | 3 | 3 | 3 | 3 |
| 55 | 20 | 35 | 26 | 53 | 23 | 27 | 14 | 14 | 29 | 20 | 8 | 26 | 16 | 22 | 20 | 13 |
| 3 | 3 | 4 | 3 | 3 | 8 | 3 | 3 | 3 | 3 | 3 | 3 | 3 | 3 | 3 | 3 | 3 |
| 17 | 10 | 22 | 20 | 26 | 23 | 38 | 19 | 22 | 15 | 26 | 28 | 14 | 26 | 14 | 32 | 14 |
| 6 | 3 | 2 | 2 | 6 | 5 | 7 | 10 | 4 | 8 | 7 | 4 | 2 | 6 | 10 | 7 | 2 |
| 3,57 | 0,60 | 0,18 | 0,07 | 0,11 | 0,04 | 0,04 | 0,05 | 0,04 | 0,04 | 0,04 | 0,02 | 0,04 | 0,05 | 0,03 | 0,04 | 0,03 |
| 4,07 | 0,71 | 0,20 | 0,04 | 0,01 | 0,04 | 0,02 | 0,05 | 0,05 | 0,05 | 0,07 | 0,03 | 0,04 | 0,06 | 0,03 | 0,04 | 0,03 |
| 0,4537 | 0,555 | 0,275 | 0,002 | 0,004 | 0 | 0,006 | 0 | 0 | 0 | 0 | 0 | 0 | 0 | 0 | 0,001 | 0,001 |

| UHB Pp 30 | UHB Pp 20 | UHB Pp 10 | OG-Mt52 | OG18 | OG-Mt40 | OG17 | OG-Mt31,7 | OG-Mt26,7 | OG-Mt21,7 | OG16 | OG15a | OG14 | OG11 | OG9 Tuff | OG8 | OG5 |
|---|---|---|---|---|---|---|---|---|---|---|---|---|---|---|---|---|
| 994736 | 994735 | 994734 | 994343 | 993248 | 994342 | 993247 | 994341 | 994340 | 994339 | 993246 | 993245 | 993244 | 993243 | 993242 | 993241 | 993240 |
| 312 | 302 | 292 | 192 | 185,8 | 180 | 174,8 | 171,7 | 166,7 | 161,7 | 157,5 | 154,3 | 153,3 | 150,2 | 149,1 | 146,5 | 145,3 |
| Ecca | Ecca | Ecca | Ecca | Ecca | Ecca | Ecca | Ecca | Ecca | Ecca | Ecca | Ecca | Ecca | Ecca | Ecca | Ecca | Dwyka |
| Pp | Pp | Pp | Pp | Pp | Pp | Pp | Pp | Pp | Pp | Pp | Pp | Pp | Pp | Pp | Pp | Dwyka4 |
| 65,98 | 68,93 | 64,75 | 63,29 | 60,55 | 57,22 | 62,09 | 62,06 | 60,15 | 62,89 | 62,28 | 63,25 | 63,16 | 59,37 | 52 | 62,1 | 62,57 |
| 0,52 | 0,44 | 0,5 | 0,74 | 0,76 | 0,74 | 0,73 | 0,81 | 0,84 | 0,85 | 0,82 | 0,87 | 0,87 | 0,76 | 0,37 | 0,91 | 0,71 |
| 15,87 | 14,36 | 16,34 | 17,67 | 17,44 | 17,19 | 17,85 | 18,56 | 18,4 | 19,17 | 18,68 | 21,07 | 17,95 | 20,16 | 29,36 | 20,94 | 20,02 |
| 6,3 | 6,7 | 6,72 | 7,71 | 9,73 | 13,25 | 7,53 | 8,1 | 8,5 | 5,82 | 6,38 | 3,67 | 6,92 | 7,48 | 2,98 | 4,38 | 5,19 |
| 0,06 | 0,04 | 0,06 | 0,3 | 0,26 | 0,96 | 0,23 | 0,41 | 0,4 | 0,07 | 0,05 | 0,01 | 0,07 | 0,14 | 0,11 | 0,05 | 0,05 |
| 1,9 | 1,78 | 1,76 | 1,89 | 1,86 | 1,97 | 1,58 | 1,51 | 1,67 | 1,73 | 1,58 | 0,77 | 1,74 | 1,78 | 1,38 | 1,36 | 1,64 |
| 0,3 | 0,27 | 0,35 | 0,68 | 0,81 | 1,81 | 0,75 | 0,56 | 1,13 | 0,8 | 0,67 | 0,36 | 0,6 | 0,54 | 0,37 | 0,33 | 0,42 |
| 1,18 | 1,07 | 1,03 | 1,87 | 1,71 | 1,59 | 1,47 | 1,29 | 1,09 | 1,4 | 1,18 | 0,91 | 1,1 | 1,18 | 0,87 | 0,35 | 1,19 |
| 2,78 | 2,25 | 2,72 | 2,67 | 2,54 | 2,03 | 3 | 3,35 | 3,18 | 3,54 | 3,35 | 4,29 | 3,39 | 4,02 | 6,46 | 4,16 | 4,13 |
| 0,086 | 0,057 | 0,052 | 0,217 | 0,345 | 0,832 | 0,278 | 0,202 | 0,396 | 0,166 | 0,176 | 0,099 | 0,208 | 0,145 | 0,13 | 0,059 | 0,117 |
| 0,012 | 0,012 | 0,012 | 0,012 | 0,012 | 0,012 | 0,012 | 0,012 | 0,012 | 0,012 | 0,012 | 0,012 | 0,012 | 0,012 | 0,012 | 0,012 | 0,012 |
| 5,33 | 4,47 | 6,14 | 2,35 | 4,87 | 3,45 | 4,99 | 3,22 | 5,12 | 3,97 | 4,87 | 5,59 | 5,08 | 4,72 | 6,01 | 5,78 | 3,77 |
| 100,32 | 100,38 | 100,43 | 99,40 | 100,89 | 101,05 | 100,51 | 100,08 | 100,89 | 100,42 | 100,05 | 100,90 | 101,10 | 100,31 | 100,05 | 100,43 | 99,82 |
| 30 | 19 | 10 | 22 | 10 | 19 | 15 | 17 | 12 | 27 | 9 | 18 | 18 | 13 | 18 | 17 | 23 |
| 125 | 114 | 139 | 113 | 123 | 130 | 110 | 128 | 126 | 127 | 129 | 165 | 118 | 124 | 59 | 147 | 115 |
| 38 | 28 | 42 | 62 | 50 | 51 | 61 | 60 | 58 | 59 | 57 | 88 | 71 | 58 | 5 | 68 | 61 |
| 23 | 9 | 18 | 28 | 22 | 36 | 20 | 24 | 37 | 37 | 30 | 13 | 24 | 24 | 18 | 7 | 13 |
| 91 | 28 | 45 | 37 | 41 | 181 | 40 | 82 | 76 | 88 | 40 | 13 | 42 | 45 | 23 | 21 | 42 |
| 35 | 40 | 39 | 23 | 57 | 55 | 52 | 26 | 36 | 28 | 54 | 48 | 76 | 83 | 42 | 40 | 67 |
| 112 | 92 | 110 | 123 | 114 | 147 | 99 | 123 | 147 | 97 | 106 | 51 | 78 | 127 | 87 | 86 | 155 |
| 22 | 16 | 22 | 24 | 26 | 21 | 28 | 30 | 26 | 30 | 27 | 31 | 29 | 30 | 30 | 31 | 28 |
| 26 | 28 | 32 | 9 | 4 | 19 | 16 | 25 | 22 | 8 | 18 | 7 | 5 | 32 | 12 | 10 | 5 |
| 176 | 143 | 183 | 139 | 131 | 96 | 163 | 172 | 153 | 185 | 176 | 211 | 176 | 228 | 230 | 225 | 208 |
| 56 | 59 | 68 | 145 | 145 | 152 | 111 | 128 | 110 | 124 | 91 | 192 | 111 | 105 | 59 | 197 | 84 |
| 21 | 23 | 23 | 21 | 32 | 50 | 37 | 39 | 52 | 38 | 36 | 39 | 34 | 40 | 27 | 36 | 28 |
| 134 | 125 | 159 | 167 | 165 | 190 | 166 | 192 | 192 | 188 | 182 | 181 | 104 | 194 | 185 | 196 | 137 |
| 12 | 9 | 8 | 10 | 12 | 16 | 15 | 16 | 17 | 16 | 15 | 19 | 12 | 10 | 4 | 16 | 9 |
| 2 | 2 | 2 | 2 | 2 | 3 | 3 | 2 | 2 | 2 | 5 | 8 | 2 | 2 | 3 | 11 | 4 |
| 7 | 7 | 7 | 7 | 38 | 21 | 17 | 7 | 7 | 22 | 17 | 7 | 7 | 7 | 7 | 7 | 7 |
| 660 | 603 | 1265 | 540 | 538 | 525 | 619 | 692 | 637 | 631 | 620 | 796 | 620 | 777 | 909 | 760 | 713 |
| 35 | 23 | 24 | 35 | 23 | 30 | 16 | 37 | 44 | 34 | 79 | 67 | 89 | 62 | 120 | 84 | 10 |
| 63 | 86 | 48 | 82 | 99 | 63 | 98 | 84 | 105 | 79 | 85 | 133 | 127 | 98 | 177 | 107 | 36 |
| 6 | 9 | 7 | 7 | 12 | 7 | 6 | 5 | 10 | 8 | 4 | 14 | 10 | 11 | 19 | 11 | 8 |
| 26 | 14 | 12 | 53 | 34 | 36 | 32 | 38 | 67 | 47 | 32 | 42 | 52 | 43 | 83 | 55 | 28 |
| 5 | 5 | 4 | 6 | 6 | 5 | 6 | 7 | 5 | 6 | 6 | 7 | 8 | 5 | 7 | 6 | 4 |
| 3 | 5 | 5 | 5 | 4 | 7 | 4 | 6 | 5 | 4 | 5 | 4 | 4 | 5 | 6 | 5 | 3 |
| 2 | 2 | 2 | 2 | 2 | 12 | 2 | 2 | 2 | 2 | 2 | 2 | 7 | 7 | 8 | 3 | 2 |
| 3 | 3 | 3 | 3 | 12 | 12 | 8 | 3 | 59 | 113 | 18 | 14 | 12 | 12 | 12 | 17 | 9 |
| 10 | 3 | 15 | 22 | 25 | 38 | 23 | 17 | 17 | 20 | 13 | 33 | 21 | 20 | 40 | 30 | 27 |
| 3 | 3 | 3 | 3 | 7 | 3 | 3 | 3 | 3 | 3 | 7 | 3 | 3 | 5 | 4 | 10 | 11 |
| 24 | 20 | 31 | 38 | 10 | 16 | 3 | 27 | 17 | 18 | 28 | 17 | 36 | 38 | 41 | 20 | 12 |
| 5 | 12 | 2 | 3 | 5 | 2 | 2 | 3 | 2 | 11 | 7 | 7 | 3 | 14 | 4 | 8 | 3 |
| 0,04 | 0,05 | 0,05 | 0,25 | 0,27 | 0,39 | 0,16 | 0,12 | 0,94 | 1,71 | 0,64 | 0,08 | 0,13 | 0,12 | 0,08 | 0,07 | 0,09 |
| 0,04 | 0,06 | 0,06 | 0,21 | 0,26 | 0,20 | 0,12 | 0,09 | 0,93 | 1,26 | 0,67 | 0,03 | 0,07 | 0,05 | 0,04 | 0,04 | 0,04 |
| 0 | 0 | 0 | | | | | | | | | | | | | | |

| OG2 | H35<GCD | H30<GCD | H25<GCD | H21<GCD | H20<GCD | H15<GCD | H10<GCD | H5<GCD | H1<GCD | H0=GCD | H5/2-5 | H5/2-4 | H5/2-3 | S32 | S31 | S30 |
|---|---|---|---|---|---|---|---|---|---|---|---|---|---|---|---|---|
| 993239 | 994338 | 994337 | 994336 | 994335 | 994334 | 994333 | 994332 | 994331 | 994330 | 994329 | 994328 | 994327 | 994326 | 993238 | 993237 | 993236 |
| 142,8 | 135 | 130 | 125 | 121 | 120 | 115 | 110 | 105 | 101 | 100 | 87,5 | 75 | 70 | 64,5 | 62,5 | 60,5 |
| Dwyka | Dwyka | Dwyka | Dwyka | Dwyka | Dwyka | Dwyka | Dwyka | Dwyka | Dwyka | Dwyka | Dwyka | Dwyka | Dwyka | Dwyka | Dwyka | Dwyka |
| Dwyka4 | Dwyka4 | Dwyka4 | Dwyka4 | Dwyka4 | Dwyka4 | Dwyka4 | Dwyka4 | Dwyka4 | Dwyka4 | Dwyka4 | Dwyka 3 | Dwyka 3 | Dwyka 3 | Dwyka 3 | Dwyka 3 | Dwyka 3 |
| 60,83 | 59,67 | 61,69 | 59,92 | 55,09 | 58,52 | 64,08 | 62,33 | 62,3 | 63,95 | 70,02 | 63,45 | 61,14 | 62,25 | 66,4 | 60,8 | 62,59 |
| 0,83 | 0,87 | 0,91 | 0,81 | 0,54 | 0,93 | 0,7 | 0,85 | 0,76 | 0,59 | 0,65 | 0,82 | 0,77 | 0,3 | 0,61 | 0,69 | 0,65 |
| 20,51 | 18,22 | 18,28 | 20,87 | 16,45 | 21,22 | 16,03 | 18,72 | 18,97 | 12,58 | 13,19 | 18,94 | 18,55 | 10,94 | 15,43 | 17,18 | 17,34 |
| 5,2 | 10,02 | 7,89 | 6,58 | 16,68 | 6,36 | 6,96 | 5,84 | 6,23 | 10,12 | 5,9 | 5,07 | 7,07 | 13,97 | 5,35 | 6,64 | 5,54 |
| 0,16 | 0,07 | 0,07 | 0,07 | 0,11 | 0,07 | 0,14 | 0,12 | 0,11 | 0,27 | 0,11 | 0,04 | 0,09 | 0,86 | 0,03 | 0,06 | 0,03 |
| 1,88 | 2,64 | 2,26 | 2,02 | 4,18 | 2,42 | 2,59 | 2,29 | 2,24 | 3,01 | 2,1 | 2,27 | 2,67 | 3,59 | 1,92 | 2,38 | 2,28 |
| 0,33 | 0,53 | 0,58 | 0,44 | 0,28 | 0,46 | 1,17 | 0,76 | 0,47 | 3,34 | 1,63 | 0,37 | 0,65 | 2,18 | 0,43 | 0,74 | 0,47 |
| 1,21 | 1,49 | 1,84 | 1,23 | 0,78 | 1,36 | 2,19 | 1,83 | 1,31 | 2,31 | 2,57 | 1,14 | 1,71 | 0,51 | 1,13 | 1,21 | 1,26 |
| 4,12 | 3,32 | 3,39 | 4,27 | 1,53 | 4,35 | 1,96 | 3,27 | 3,71 | 0,33 | 1,2 | 3,82 | 3,43 | 0,53 | 3,02 | 3,37 | 3,49 |
| 0,063 | 0,204 | 0,208 | 0,187 | 0,051 | 0,129 | 0,131 | 0,149 | 0,108 | 0,168 | 0,103 | 0,097 | 0,12 | 1,342 | 0,112 | 0,179 | 0,154 |
| 0,012 | 0,012 | 0,012 | 0,012 | 0,012 | 0,012 | 0,012 | 0,012 | 0,012 | 0,012 | 0,012 | 0,012 | 0,012 | 0,012 | 0,053 | 0,855 | 0,333 |
| 5,88 | 3,68 | 3,31 | 4,11 | 4,88 | 5,65 | 4,64 | 4,98 | 4,74 | 4,34 | 3,21 | 4,45 | 4,55 | 4,11 | 6,31 | 6,56 | 5,98 |
| 101,03 | 100,73 | 100,44 | 100,52 | 100,58 | 101,49 | 100,60 | 101,15 | 100,96 | 101,02 | 100,70 | 100,48 | 100,76 | 100,59 | 100,80 | 100,66 | 100,12 |
| 13 | 24 | 10 | 27 | 11 | 23 | 15 | 18 | 13 | 16 | 9 | 12 | 17 | 22 | 16 | 17 | 6 |
| 112 | 138 | 127 | 164 | 103 | 145 | 103 | 125 | 116 | 112 | 95 | 124 | 131 | 91 | 154 | 144 | 139 |
| 50 | 100 | 107 | 78 | 9 | 90 | 80 | 86 | 59 | 70 | 79 | 79 | 74 | 40 | 70 | 55 | 64 |
| 21 | 20 | 24 | 29 | 33 | 34 | 18 | 22 | 25 | 30 | 8 | 11 | 21 | 19 | 17 | 37 | 29 |
| 56 | 40 | 91 | 112 | 97 | 84 | 58 | 32 | 55 | 41 | 63 | 25 | 149 | 291 | 38 | 80 | 54 |
| 75 | 64 | 29 | 73 | 204 | 44 | 27 | 22 | 38 | 20 | 11 | 21 | 43 | 141 | 52 | 68 | 34 |
| 132 | 155 | 127 | 149 | 218 | 200 | 155 | 133 | 104 | 128 | 98 | 83 | 127 | 157 | 122 | 257 | 216 |
| 32 | 24 | 30 | 26 | 19 | 35 | 23 | 23 | 26 | 23 | 20 | 30 | 23 | 14 | 23 | 25 | 26 |
| 36 | 5 | 4 | 25 | 14 | 7 | 4 | 11 | 14 | 6 | 4 | 8 | 5 | 9 | 16 | 13 | 5 |
| 202 | 183 | 178 | 209 | 77 | 208 | 99 | 163 | 183 | 25 | 63 | 176 | 162 | 29 | 150 | 170 | 180 |
| 95 | 113 | 117 | 80 | 78 | 93 | 143 | 90 | 75 | 207 | 124 | 53 | 91 | 123 | 72 | 93 | 85 |
| 41 | 53 | 37 | 35 | 31 | 43 | 32 | 30 | 36 | 51 | 23 | 34 | 27 | 62 | 32 | 43 | 38 |
| 179 | 140 | 134 | 160 | 84 | 174 | 182 | 166 | 165 | 120 | 161 | 155 | 158 | 99 | 146 | 172 | 189 |
| 19 | 17 | 16 | 15 | 15 | 17 | 11 | 13 | 17 | 9 | 13 | 15 | 11 | 6 | 11 | 14 | 14 |
| 9 | 2 | 2 | 2 | 2 | 2 | 2 | 2 | 2 | 2 | 2 | 2 | 2 | 2 | 2 | 5 | 6 |
| 10 | 17 | 24 | 20 | 7 | 13 | 7 | 7 | 13 | 18 | 7 | 14 | 26 | 16 | 7 | 10 | 8 |
| 775 | 489 | 605 | 739 | 317 | 748 | 391 | 569 | 658 | 210 | 351 | 677 | 627 | 210 | 618 | 622 | 684 |
| 58 | 56 | 47 | 34 | 6 | 10 | 42 | 28 | 54 | 44 | 5 | 37 | 29 | 5 | 43 | 41 | 5 |
| 105 | 130 | 85 | 69 | 50 | 94 | 91 | 66 | 58 | 82 | 91 | 91 | 111 | 22 | 76 | 73 | 124 |
| 10 | 13 | 7 | 11 | 3 | 8 | 10 | 3 | 5 | 7 | 3 | 10 | 7 | 3 | 7 | 6 | 12 |
| 37 | 55 | 54 | 27 | 21 | 35 | 70 | 20 | 30 | 21 | 16 | 36 | 50 | 36 | 38 | 29 | 37 |
| 5 | 8 | 7 | 5 | 5 | 6 | 7 | 3 | 6 | 6 | 6 | 7 | 6 | 5 | 7 | 5 | 7 |
| 5 | 3 | 5 | 6 | 2 | 8 | 5 | 6 | 4 | 3 | 2 | 6 | 6 | 2 | 4 | 4 | 4 |
| 14 | 2 | 2 | 2 | 4 | 14 | 2 | 2 | 3 | 2 | 5 | 5 | 2 | 2 | 7 | 2 | 2 |
| 16 | 3 | 55 | 3 | 31 | 15 | 4 | 81 | 89 | 80 | 3 | 8 | 7 | 8 | 18 | 39 | 28 |
| 28 | 26 | 20 | 14 | 59 | 16 | 27 | 3 | 3 | 23 | 21 | 10 | 19 | 7 | 14 | 35 | 23 |
| 11 | 3 | 4 | 3 | 3 | 3 | 3 | 3 | 3 | 3 | 3 | 3 | 3 | 3 | 6 | 6 | 3 |
| 22 | 31 | 26 | 21 | 17 | 10 | 23 | 41 | 35 | 9 | 21 | 34 | 30 | 28 | 21 | 12 | 20 |
| 10 | 8 | 4 | 2 | 8 | 3 | 5 | 2 | 7 | 4 | 6 | 3 | 4 | 13 | 3 | 5 | 5 |
| 0,07 | 0,11 | 0,12 | 0,09 | 0,06 | 0,10 | 0,25 | 0,16 | 0,10 | 0,72 | 0,35 | 0,08 | 0,14 | 1,47 | 0,09 | 1,59 | 0,10 |
| 0,05 | 0,06 | 0,06 | 0,05 | 0,08 | 0,06 | 0,04 | 0,06 | 0,05 | 0,14 | 0,05 | 0,04 | 0,64 | 0,10 |  | 1,48 |  |

| H5/2-2 | S29 | S28 | S27 | S26 | S25 | H5/2-1shales | S24 | S23 | S22 | S21 | S20 | S19 | S18 | S17 | S16 | S15 |
|---|---|---|---|---|---|---|---|---|---|---|---|---|---|---|---|---|
| 994325 | 993235 | 993234 | 993233 | 993232 | 993231 | 994323 | 993230 | 993229 | 993228 | 993227 | 993226 | 993225 | 993224 | 993223 | 993222 | 993221 |
| 58 | 58,5 | 56,25 | 54,25 | 52,25 | 50,25 | 48 | 47 | 45,75 | 43,25 | 40,75 | 37,75 | 36,5 | 34,5 | 32,5 | 30,25 | 28 |
| Dwyka | Dwyka | Dwyka | Dwyka | Dwyka | Dwyka | Dwyka | Dwyka | Dwyka | Dwyka | Dwyka | Dwyka | Dwyka | Dwyka | Dwyka | Dwyka | Dwyka |
| Dwyka 3 | Dwyka 3 | Dwyka 3 | Dwyka 3 | Dwyka 3 | Dwyka 3 | Dwyka 3 | Dwyka 3 | Dwyka 3 | Dwyka 3 | Dwyka 3 | Dwyka 2 | Dwyka 2 | Dwyka 2 | Dwyka 2 | Dwyka 2 | Dwyka 2 |
| 49,12 | 62,37 | 63,76 | 62,67 | 62,17 | 63,52 | 64,67 | 61,86 | 60,1 | 59,73 | 59,06 | 63,11 | 63,04 | 52,77 | 61,67 | 52,98 | 62,15 |
| 0,27 | 0,7 | 0,7 | 0,69 | 0,74 | 0,71 | 0,67 | 0,72 | 0,68 | 0,76 | 0,78 | 0,76 | 0,68 | 0,62 | 0,72 | 0,64 | 0,73 |
| 9,02 | 17,79 | 16,98 | 17,62 | 18,29 | 18,16 | 16,78 | 18 | 17,65 | 19,09 | 19,36 | 17,83 | 17,68 | 15,19 | 17,89 | 16,02 | 17,35 |
| 5,17 | 6,25 | 6,22 | 6,71 | 6,3 | 5,19 | 4,81 | 6,63 | 6,36 | 7,33 | 6,95 | 5,91 | 5,69 | 7,47 | 5,99 | 8,34 | 6,61 |
| 0,07 | 0,03 | 0,02 | 0,05 | 0,01 | 0,02 | 0,1 | 1,9 | 0,07 | 0,06 | 0,17 | 0,14 | 0,08 | 0,91 | 0,33 | 1,71 | 0,05 |
| 1,85 | 2,15 | 1,69 | 1,81 | 1,37 | 1,82 | 2,58 | 0,09 | 2,53 | 3,26 | 2,35 | 2,3 | 2,55 | 3,27 | 2,1 | 2,81 | 2,82 |
| 17,12 | 0,5 | 0,51 | 0,37 | 0,19 | 0,5 | 0,58 | 0,14 | 0,65 | 0,49 | 0,56 | 0,49 | 0,46 | 4,38 | 0,43 | 3,2 | 0,49 |
| 0,6 | 1,18 | 0,97 | 0,91 | 0,93 | 1,06 | 1,02 | 1,14 | 1,45 | 1,68 | 1,32 | 1,68 | 1,24 | 0,81 | 0,86 | 0,76 | 1,49 |
| 1,28 | 3,57 | 3,51 | 3,63 | 3,9 | 3,84 | 3,47 | 3,76 | 3,56 | 3,65 | 4,15 | 3,67 | 3,76 | 3,36 | 4,05 | 3,55 | 3,57 |
| 12,015 | 0,088 | 0,092 | 0,108 | 0,132 | 0,107 | 0,119 | 0,104 | 0,122 | 0,107 | 0,114 | 0,104 | 0,092 | 0,119 | 0,109 | 0,177 | 0,108 |
| 0,012 | 0,012 | 0,012 | 0,012 | 0,012 | 0,012 | 0,012 | 0,012 | 0,355 | 0,012 | 0,012 | 0,012 | 0,012 | 0,907 | 0,012 | 0,022 | 0,101 |
| 3,73 | 6,18 | 6,32 | 6,24 | 6,88 | 5,74 | 6,25 | 6,21 | 6,88 | 3,75 | 5,43 | 3,72 | 5,52 | 11,08 | 6,32 | 10,04 | 4,99 |
| 100,26 | 100,82 | 100,78 | 100,82 | 100,92 | 100,68 | 101,06 | 100,57 | 100,41 | 99,92 | 100,26 | 99,73 | 100,80 | 100,89 | 100,48 | 100,25 | 100,46 |
| 13 | 16 | 12 | 18 | 20 | 16 | 18 | 32 | 9 | 21 | 22 | 22 | 22 | 13 | 15 | 21 | 14 |
| 84 | 121 | 141 | 124 | 178 | 160 | 148 | 147 | 144 | 159 | 137 | 116 | 125 | 144 | 172 | 165 | 145 |
| 32 | 84 | 64 | 55 | 77 | 69 | 72 | 60 | 64 | 78 | 70 | 76 | 54 | 43 | 59 | 45 | 71 |
| 8 | 24 | 22 | 32 | 17 | 16 | 29 | 31 | 43 | 34 | 31 | 38 | 32 | 36 | 30 | 43 | 30 |
| 45 | 45 | 48 | 41 | 24 | 29 | 37 | 54 | 74 | 40 | 55 | 32 | 34 | 37 | 36 | 75 | 44 |
| 19 | 44 | 59 | 55 | 46 | 35 | 7 | 40 | 40 | 42 | 62 | 32 | 46 | 46 | 48 | 69 | 40 |
| 99 | 127 | 89 | 134 | 125 | 137 | 203 | 185 | 176 | 119 | 151 | 103 | 127 | 133 | 127 | 263 | 106 |
| 6 | 23 | 28 | 21 | 30 | 23 | 19 | 23 | 21 | 27 | 33 | 22 | 27 | 20 | 26 | 22 | 29 |
| 4 | 10 | 23 | 32 | 53 | 20 | 7 | 16 | 15 | 4 | 14 | 6 | 6 | 27 | 14 | 30 | 8 |
| 65 | 180 | 182 | 184 | 197 | 194 | 171 | 182 | 174 | 169 | 206 | 178 | 190 | 172 | 203 | 179 | 167 |
| 572 | 78 | 81 | 68 | 59 | 75 | 59 | 50 | 112 | 68 | 83 | 78 | 82 | 264 | 90 | 168 | 76 |
| 198 | 41 | 34 | 37 | 36 | 39 | 37 | 33 | 36 | 35 | 33 | 31 | 35 | 39 | 43 | 47 | 28 |
| 463 | 183 | 178 | 179 | 195 | 191 | 167 | 162 | 151 | 161 | 158 | 168 | 164 | 160 | 169 | 173 | 159 |
| 3 | 13 | 12 | 9 | 16 | 11 | 15 | 16 | 12 | 15 | 14 | 13 | 15 | 13 | 13 | 10 | 12 |
| 2 | 3 | 8 | 4 | 5 | 3 | 2 | 2 | 2 | 5 | 5 | 6 | 2 | 6 | 3 | 2 | 2 |
| 11 | 23 | 7 | 7 | 7 | 33 | 7 | 7 | 12 | 7 | 7 | 7 | 15 | 7 | 8 | 7 | 7 |
| 378 | 652 | 656 | 708 | 733 | 741 | 672 | 648 | 676 | 683 | 826 | 732 | 732 | 655 | 742 | 714 | 691 |
| 65 | 23 | 34 | 52 | 44 | 31 | 50 | 33 | 47 | 31 | 55 | 42 | 19 | 39 | 26 | 52 | 53 |
| 160 | 86 | 78 | 93 | 90 | 89 | 96 | 146 | 100 | 92 | 100 | 59 | 71 | 53 | 75 | 122 | 79 |
| 7 | 9 | 9 | 9 | 8 | 9 | 9 | 10 | 8 | 10 | 5 | 8 | 12 | 11 | 13 | 8 | 8 |
| 86 | 56 | 52 | 35 | 47 | 42 | 31 | 51 | 49 | 41 | 35 | 37 | 41 | 27 | 46 | 62 | 25 |
| 10 | 5 | 4 | 5 | 6 | 7 | 5 | 7 | 6 | 4 | 5 | 5 | 5 | 5 | 5 | 6 | 7 |
| 9 | 5 | 4 | 5 | 5 | 4 | 4 | 5 | 3 | 4 | 3 | 4 | 4 | 3 | 5 | 3 | 5 |
| 2 | 2 | 2 | 2 | 2 | 2 | 2 | 4 | 2 | 2 | 2 | 2 | 7 | 2 | 2 | 5 | 2 |
| 10 | 31 | 29 | 27 | 19 | 14 | 58 | 20 | 35 | 24 | 23 | 77 | 40 | 30 | 30 | 27 | 34 |
| 11 | 22 | 32 | 27 | 21 | 19 | 17 | 18 | 17 | 25 | 29 | 25 | 29 | 26 | 28 | 24 | 14 |
| 3 | 3 | 6 | 4 | 3 | 3 | 3 | 3 | 3 | 5 | 13 | 9 | 11 | 5 | 13 | 5 | 10 |
| 3 | 32 | 10 | 16 | 33 | 16 | 20 | 24 | 16 | 2 | 2 | 29 | 13 | 25 | 26 | 20 | 31 |
| 9 | 5 | 2 | 2 | 2 | 3 | 8 | 2 | 7 | 2 | 2 | 2 | 4 | 10 | 2 | 8 | 2 |
| 0,67 | 0,51 | 0,11 | 0,93 | 0,04 | 1,11 | 0,03 | 0,14 | 1,10 | 0,12 | 0,60 | 0,10 | 0,94 | 0,09 | 0,96 | 0,10 | 0,94 |
| 0,22 | 0,53 |  | 0,92 |  | 1,13 |  |  | 1,09 |  | 0,65 |  | 0,68 |  | 0,95 |  | 0,80 |

| S14 | S13 | S12 | S11 | S10 | S9 | S8 | S7 | S6 | S5 | S4 | S3 | S2 | S1 |
|---|---|---|---|---|---|---|---|---|---|---|---|---|---|
| 993220 | 993219 | 993218 | 993217 | 993216 | 993215 | 993214 | 993213 | 993212 | 993211 | 993210 | 993209 | 993208 | 993207 |
| 25,75 | 23,5 | 21,75 | 19,75 | 17,25 | 15,25 | 13,25 | 11,25 | 9,25 | 7 | 4,75 | 2,5 | 2 | 0,3 |
| Dwyka | Dwyka | Dwyka | Dwyka | Dwyka | Dwyka | Dwyka | Dwyka | Dwyka | Dwyka | Dwyka | Dwyka | Dwyka | Dwyka |
| Dwyka 2 | Dwyka 2 | Dwyka 2 | Dwyka 2 | Dwyka 2 | Dwyka 2 | Dwyka 2 | Dwyka 2 | Dwyka 2 | Dwyka 2 | Dwyka 2 | Dwyka 2 | Dwyka 2 | Dwyka 1 |
| 60,27 | 63,07 | 63,56 | 61,43 | 64,33 | 62,34 | 57,57 | 53,9 | 60,81 | 59,42 | 59,65 | 71,77 | 64,1 | 58,09 |
| 0,77 | 0,73 | 0,76 | 0,79 | 0,74 | 0,8 | 0,78 | 0,78 | 0,81 | 0,81 | 0,83 | 0,65 | 0,78 | 0,81 |
| 17,55 | 16,98 | 16,9 | 17,24 | 15,94 | 17,32 | 17,06 | 17,58 | 17,77 | 18,53 | 18,06 | 12,07 | 15,6 | 18,56 |
| 7,12 | 6,08 | 6,12 | 6,77 | 7,05 | 6,38 | 8,74 | 7,27 | 7,08 | 7,51 | 7,39 | 5,56 | 7,4 | 8,12 |
| 0,05 | 0,06 | 0,05 | 0,07 | 0,05 | 0,05 | 0,04 | 0,81 | 0,05 | 0,04 | 0,19 | 0,03 | 0,05 | 0,05 |
| 2,99 | 2,53 | 2,53 | 2,82 | 2,8 | 2,3 | 1,9 | 2,84 | 2,77 | 2,36 | 2,65 | 2,01 | 2,86 | 3,31 |
| 0,64 | 0,66 | 0,45 | 0,61 | 0,47 | 0,44 | 0,22 | 2,43 | 0,45 | 0,46 | 0,46 | 0,37 | 0,58 | 0,67 |
| 1,66 | 1,63 | 1,61 | 1,75 | 1,88 | 1,39 | 1,19 | 1,24 | 1,79 | 1,33 | 1,33 | 2,09 | 1,94 | 1,43 |
| 3,53 | 3,54 | 3,5 | 3,37 | 2,88 | 3,62 | 3,88 | 3,85 | 3,54 | 4,17 | 4,13 | 2,06 | 2,91 | 3,97 |
| 0,129 | 0,108 | 0,118 | 0,133 | 0,112 | 0,102 | 0,123 | 0,126 | 0,138 | 0,111 | 0,113 | 0,149 | 0,148 | 0,152 |
| 0,245 | 0,229 | 0,012 | 0,018 | 0,012 | 0,012 | 0,929 | 0,829 | 0,012 | 0,012 | 0,012 | 0,012 | 0,012 | 0,012 |
| 5,81 | 4,32 | 4,77 | 5,82 | 4,17 | 5,93 | 8,74 | 9,66 | 4,78 | 5,21 | 6,25 | 3,75 | 4,54 | 5,81 |
| 100,76 | 99,94 | 100,38 | 100,82 | 100,43 | 100,68 | 101,17 | 101,32 | 100,00 | 99,96 | 101,07 | 100,52 | 100,92 | 100,98 |
| 25 | 16 | 16 | 15 | 19 | 8 | 16 | 9 | 14 | 12 | 17 | 8 | 13 | 22 |
| 154 | 131 | 132 | 169 | 130 | 158 | 198 | 198 | 173 | 186 | 169 | 79 | 116 | 133 |
| 76 | 63 | 67 | 79 | 81 | 76 | 131 | 76 | 94 | 90 | 86 | 48 | 77 | 95 |
| 36 | 44 | 31 | 41 | 36 | 31 | 25 | 46 | 42 | 30 | 41 | 36 | 35 | 38 |
| 50 | 48 | 39 | 68 | 39 | 46 | 22 | 62 | 49 | 57 | 55 | 40 | 59 | 54 |
| 74 | 59 | 55 | 65 | 47 | 84 | 61 | 85 | 67 | 67 | 78 | 28 | 93 | 83 |
| 100 | 142 | 95 | 136 | 92 | 125 | 93 | 179 | 122 | 145 | 146 | 80 | 119 | 165 |
| 28 | 27 | 26 | 19 | 22 | 27 | 24 | 25 | 27 | 24 | 29 | 16 | 21 | 36 |
| 17 | 24 | 8 | 12 | 7 | 21 | 55 | 32 | 15 | 20 | 18 | 4 | 4 | 4 |
| 165 | 170 | 169 | 160 | 133 | 180 | 193 | 186 | 163 | 204 | 196 | 89 | 126 | 185 |
| 91 | 89 | 75 | 73 | 65 | 77 | 84 | 137 | 73 | 82 | 83 | 62 | 64 | 64 |
| 34 | 38 | 31 | 34 | 28 | 24 | 29 | 38 | 25 | 24 | 29 | 26 | 42 | 29 |
| 168 | 198 | 188 | 176 | 173 | 177 | 170 | 193 | 182 | 159 | 180 | 129 | 170 | 175 |
| 15 | 13 | 13 | 12 | 15 | 14 | 11 | 14 | 13 | 12 | 15 | 11 | 14 | 8 |
| 2 | 2 | 2 | 9 | 5 | 4 | 13 | 2 | 3 | 2 | 3 | 5 | 4 | 2 |
| 48 | 7 | 7 | 24 | 7 | 7 | 7 | 7 | 7 | 19 | 12 | 8 | 7 | 7 |
| 646 | 628 | 643 | 591 | 505 | 653 | 702 | 710 | 650 | 783 | 781 | 444 | 547 | 691 |
| 50 | 44 | 26 | 45 | 19 | 30 | 10 | 74 | 59 | 41 | 41 | 34 | 45 | 24 |
| 60 | 91 | 86 | 80 | 12 | 43 | 83 | 91 | 104 | 93 | 80 | 98 | 90 | 97 |
| 3 | 13 | 8 | 8 | 5 | 5 | 7 | 8 | 10 | 7 | 11 | 12 | 3 | 10 |
| 46 | 63 | 52 | 27 | 33 | 23 | 33 | 37 | 25 | 42 | 43 | 37 | 36 | 48 |
| 3 | 6 | 5 | 5 | 4 | 4 | 5 | 5 | 4 | 5 | 5 | 4 | 6 | 6 |
| 4 | 4 | 4 | 5 | 4 | 5 | 4 | 5 | 4 | 4 | 5 | 4 | 4 | 4 |
| 9 | 2 | 2 | 2 | 2 | 7 | 2 | 4 | 2 | 2 | 3 | 2 | 2 | 2 |
| 32 | 74 | 36 | 36 | 48 | 35 | 37 | 47 | 58 | 14 | 45 | 110 | 53 | 38 |
| 16 | 28 | 33 | 25 | 13 | 13 | 54 | 42 | 13 | 16 | 17 | 17 | 31 | 29 |
| 3 | 7 | 8 | 5 | 3 | 3 | 3 | 5 | 3 | 8 | 3 | 3 | 11 | 3 |
| 26 | 24 | 15 | 3 | 5 | 31 | 34 | 15 | 11 | 24 | 16 | 13 | 11 | 19 |
| 2 | 6 | 2 | 2 | 2 | 7 | 4 | 2 | 2 | 10 | 2 | 2 | 2 | 6 |
| 0,14 | 0,80 | 0,13 | 0,70 | 0,09 | 0,65 | 0,52 | 0,10 | 0,10 | 0,60 | 0,08 | 0,12 | 0,14 | 0,28 |
|  | 0,83 |  | 0,79 |  | 0,67 |  |  |  | 0,64 |  | 0,19 |  | 0,29 |

| Sample | sny16 | sny15 | sny14 | sny13 | sny12 | sny11 | sny10 | sny9 | sny8 | sny7 | sny6 | sny5 | sny4 | sny3 | sny2 | sny1 |
|---|---|---|---|---|---|---|---|---|---|---|---|---|---|---|---|---|
| Lab.-Nr. | 994359 | 994358 | 994357 | 994356 | 994355 | 994354 | 994353 | 995352 | 994351 | 994350 | 994349 | 994348 | 994347 | 994346 | 994345 | 994344 |
| Formation | Mukorob shale | Mukorob shale | Mukorob shale | Mukorob shale | Mukorob shale | Mukorob shale | Mukorob shale | Mukorob shale | Dwyka | Dwyka | Dwyka | Dwyka | Dwyka | Dwyka | Dwyka | Dwyka |
| rel. position | 144 | 130 | 121 | 109 | 95,5 | 89 | 84 | 79 | 66 | 60 | 50 | 40 | 30 | 15,5 | 10 | 2,8 |
| $SiO_2$ | 64,87 | 66,7 | 68,9 | 61 | 62,97 | 68,76 | 68,13 | 64,49 | 64,53 | 63,67 | 63,48 | 71,74 | 63,15 | 68,02 | 73,24 | 72,02 |
| $TiO_2$ | 0,77 | 0,64 | 0,65 | 0,88 | 0,79 | 0,72 | 0,76 | 0,71 | 0,77 | 0,75 | 0,72 | 0,63 | 0,74 | 0,78 | 0,62 | 0,65 |
| $Al_2O_3$ | 17,95 | 16,79 | 15,55 | 19,09 | 20,12 | 15,05 | 15,54 | 16,59 | 17,01 | 17,51 | 17,25 | 12,57 | 17,49 | 15,55 | 12,3 | 12,85 |
| $Fe_2O_3$ | 5,31 | 6,1 | 5,8 | 6,02 | 2,5 | 5,08 | 4,88 | 6,31 | 5,92 | 5,51 | 6,07 | 4,04 | 6,23 | 5,09 | 3,71 | 4,43 |
| MnO | 0,1 | 0,04 | 0,04 | 0,04 | 0,01 | 0,03 | 0,03 | 0,02 | 0,03 | 0,04 | 0,04 | 0,08 | 0,02 | 0,04 | 0,07 | 0,03 |
| MgO | 1,39 | 1,68 | 1,56 | 1,74 | 0,72 | 1,51 | 1,67 | 1,54 | 1,83 | 2,02 | 2,07 | 1,37 | 1,7 | 1,75 | 1,25 | 1,55 |
| CaO | 0,51 | 0,47 | 0,46 | 0,54 | 0,35 | 0,56 | 0,63 | 0,72 | 0,71 | 0,63 | 0,84 | 1,53 | 0,53 | 0,58 | 1,35 | 0,69 |
| $Na_2O$ | 1,28 | 1,63 | 1,22 | 1,27 | 1,1 | 2,22 | 3,05 | 1,46 | 2,26 | 1,49 | 1,43 | 2,33 | 1,21 | 1,76 | 1,83 | 2,1 |
| $K_2O$ | 2,84 | 2,48 | 2,54 | 3,17 | 3,45 | 2,18 | 1,99 | 2,91 | 2,81 | 3,24 | 3,21 | 2,12 | 3,53 | 3,15 | 2,37 | 2,47 |
| $P_2O_5$ | 0,113 | 0,086 | 0,078 | 0,088 | 0,035 | 0,083 | 0,107 | 0,145 | 0,148 | 0,089 | 0,291 | 0,1 | 0,088 | 0,104 | 0,103 | 0,139 |
| $SO_3$ | 0,012 | 0,012 | 0,012 | 0,012 | 0,012 | 0,012 | 0,012 | 0,012 | 0,012 | 0,012 | 0,012 | 0,012 | 0,012 | 0,012 | 0,012 | 0,012 |
| L.O.I. | 5,15 | 4,22 | 4,31 | 7,47 | 8,61 | 4,51 | 4,01 | 5,98 | 3,98 | 4,77 | 5,03 | 4,23 | 4,97 | 3,21 | 3,51 | 3,68 |
| Sum | 100,30 | 100,85 | 101,12 | 101,32 | 100,67 | 100,72 | 100,81 | 100,89 | 100,01 | 99,73 | 100,44 | 100,75 | 99,67 | 100,05 | 100,37 | 100,62 |
| Sc | 8 | 7 | 8 | 13 | 21 | 13 | 24 | 10 | 15 | 22 | 16 | 16 | 17 | 11 | 17 | 13 |
| V | 97 | 82 | 85 | 146 | 138 | 83 | 108 | 116 | 113 | 102 | 112 | 72 | 132 | 110 | 76 | 86 |
| Cr | 49 | 42 | 51 | 58 | 59 | 72 | 78 | 65 | 78 | 65 | 64 | 64 | 66 | 71 | 51 | 63 |
| Co | 21 | 26 | 25 | 29 | 4 | 36 | 46 | 26 | 37 | 38 | 35 | 92 | 17 | 52 | 59 | 144 |
| Ni | 39 | 50 | 53 | 41 | 10 | 62 | 45 | 34 | 88 | 40 | 42 | 23 | 54 | 48 | 22 | 32 |
| Cu | 22 | 23 | 18 | 32 | 3 | 8 | 13 | 29 | 28 | 5 | 19 | 10 | 26 | 16 | 4 | 9 |
| Zn | 114 | 112 | 99 | 129 | 36 | 93 | 76 | 124 | 106 | 90 | 95 | 54 | 109 | 72 | 51 | 67 |
| Ga | 25 | 25 | 19 | 28 | 25 | 14 | 16 | 24 | 22 | 26 | 24 | 14 | 23 | 19 | 15 | 15 |
| As | 14 | 6 | 19 | 9 | 7 | 8 | 13 | 17 | 52 | 5 | 7 | 4 | 16 | 5 | 7 | 7 |
| Rb | 167 | 133 | 146 | 172 | 184 | 112 | 106 | 156 | 141 | 166 | 165 | 94 | 186 | 129 | 97 | 106 |
| Sr | 126 | 112 | 95 | 125 | 108 | 114 | 119 | 99 | 107 | 95 | 103 | 141 | 132 | 98 | 105 | 94 |
| Y | 33 | 35 | 31 | 43 | 28 | 20 | 27 | 35 | 34 | 31 | 54 | 30 | 27 | 35 | 33 | 31 |
| Zr | 204 | 161 | 161 | 185 | 157 | 148 | 142 | 185 | 197 | 164 | 165 | 208 | 151 | 232 | 237 | 218 |
| Nb | 15 | 14 | 12 | 13 | 15 | 15 | 14 | 14 | 13 | 18 | 15 | 13 | 11 | 13 | 13 | 11 |
| Mo | 2 | 2 | 2 | 2 | 2 | 2 | 2 | 2 | 2 | 2 | 2 | 2 | 2 | 2 | 2 | 2 |
| Sn | 7 | 7 | 32 | 18 | 7 | 7 | 7 | 15 | 7 | 7 | 7 | 7 | 7 | 7 | 7 | 7 |
| Ba | 613 | 462 | 584 | 545 | 558 | 352 | 429 | 393 | 545 | 455 | 432 | 390 | 447 | 535 | 462 | 403 |
| La | 24 | 28 | 43 | 46 | 39 | 5 | 32 | 26 | 42 | 54 | 25 | 8 | 41 | 35 | 23 | 33 |
| Ce | 99 | 56 | 94 | 106 | 111 | 47 | 75 | 100 | 93 | 61 | 78 | 33 | 73 | 66 | 46 | 78 |
| Pr | 4 | 3 | 6 | 9 | 14 | 7 | 8 | 6 | 3 | 5 | 10 | 10 | 8 | 3 | 6 | 5 |
| Nd | 45 | 25 | 32 | 47 | 48 | 16 | 54 | 38 | 26 | 29 | 55 | 35 | 49 | 34 | 33 | 27 |
| Sm | 5 | 6 | 7 | 5 | 6 | 3 | 4 | 7 | 6 | 4 | 7 | 5 | 5 | 5 | 5 | 5 |
| Hf | 5 | 6 | 6 | 6 | 4 | 4 | 5 | 6 | 8 | 6 | 6 | 6 | 4 | 7 | 7 | 6 |
| Ta | 2 | 2 | 8 | 2 | 2 | 2 | 2 | 2 | 12 | 2 | 2 | 2 | 2 | 2 | 2 | 8 |
| W | 53 | 39 | 46 | 32 | 45 | 206 | 135 | 90 | 96 | 161 | 88 | 672 | 25 | 228 | 391 | 1125 |
| Pb | 23 | 23 | 22 | 20 | 6 | 7 | 11 | 11 | 9 | 6 | 14 | 8 | 20 | 11 | 9 | 17 |
| Bi | 3 | 3 | 3 | 3 | 3 | 3 | 3 | 3 | 3 | 3 | 3 | 3 | 3 | 3 | 3 | 3 |
| Th | 45 | 13 | 23 | 26 | 31 | 24 | 28 | 18 | 22 | 26 | 38 | 12 | 41 | 30 | 11 | 13 |
| U | 11 | 4 | 8 | 10 | 5 | 4 | 8 | 4 | 6 | 4 | 7 | 3 | 9 | 2 | 3 | 8 |

**XRD analyses of samples from the MPU core by D. Bühmann**

| Depth | Pyrite | Apatite | Spessartinite | siderite | Ankerite | Calcite | Gypsum | Albite | Microcline | Quartz | Anatase | Goethite | Kaolinite | Chlorite | Illite | Smectite |
|---|---|---|---|---|---|---|---|---|---|---|---|---|---|---|---|---|
| **1,02** | 0 | 0 | 0 | 0 | 0 | 0 | 0 | 0 | 0 | 72 | 0 | 0 | 8 | 0 | 21 | 0 |
| **2,02** | 0 | 0 | 0 | 0 | 0 | 0 | 0 | 0 | 0 | 66 | 0 | 0 | 6 | 0 | 25 | 3 |
| **2,62** | 0 | 0 | 0 | 1 | 0 | 0 | 0 | 0 | 0 | 70 | 0 | 2 | 5 | 0 | 19 | 5 |
| **2,67** | 0 | 0 | 0 | 0 | 0 | 0 | 0 | 0 | 0 | 61 | 0 | 0 | 5 | 0 | 24 | 10 |
| **3** | 0 | 5 | 0 | 0 | 0 | 0 | 0 | 0 | 0 | 62 | 0 | 3 | 5 | 0 | 19 | 5 |
| **3,86** | 0 | 0 | 0 | 0 | 0 | 0 | 0 | 0 | 0 | 69 | 3 | 5 | 8 | 0 | 10 | 5 |
| **4,4** | 0 | 0 | 0 | 0 | 0 | 0 | 0 | 0 | 2 | 57 | 0 | 0 | 0 | 0 | 32 | 9 |
| **4,7** | 0 | 57 | 0 | 0 | 0 | 0 | 0 | 0 | 0 | 22 | 0 | 0 | 0 | 0 | 4 | 18 |
| **5,04** | 0 | 0 | 0 | 0 | 0 | 0 | 0 | 0 | 0 | 60 | 0 | 2 | 0 | 0 | 23 | 15 |
| **5,7** | 0 | 0 | 0 | 0 | 0 | 0 | 0 | 0 | 0 | 58 | 0 | 2 | 0 | 0 | 20 | 18 |
| **6** | 0 | 0 | 0 | 0 | 0 | 0 | 0 | 0 | 0 | 68 | 0 | 2 | 6 | 0 | 22 | 4 |
| **6,44** | 0 | 0 | 0 | 0 | 0 | 0 | 0 | 0 | 0 | 66 | 0 | 2 | 6 | 0 | 22 | 4 |
| **7,06** | 0 | 0 | 0 | 0 | 0 | 0 | 0 | 0 | 0 | 58 | 0 | 7 | 7 | 0 | 28 | 0 |
| **7,25** | 0 | 0 | 0 | 0 | 0 | 0 | 0 | 0 | 0 | 63 | 0 | 6 | 10 | 0 | 21 | 0 |
| **7,35** | 0 | 0 | 0 | 0 | 0 | 0 | 0 | 0 | 0 | 68 | 0 | 2 | 6 | 0 | 23 | 0 |
| **7,8** | 0 | 0 | 0 | 0 | 0 | 0 | 0 | 0 | 0 | 69 | 0 | 4 | 8 | 0 | 20 | 0 |
| **8,04** | 0 | 0 | 0 | 0 | 0 | 0 | 0 | 0 | 0 | 62 | 0 | 4 | 6 | 0 | 21 | 8 |
| **8,96** | 0 | 0 | 0 | 0 | 0 | 0 | 0 | 0 | 0 | 60 | 0 | 2 | 6 | 0 | 23 | 9 |
| **10,03** | 0 | 0 | 0 | 0 | 0 | 0 | 0 | 0 | 0 | 61 | 0 | 0 | 2 | 0 | 20 | 16 |
| **10,97** | 0 | 0 | 0 | 0 | 0 | 0 | 0 | 0 | 0 | 56 | 0 | 4 | 0 | 0 | 21 | 19 |
| **12** | 0 | 0 | 0 | 0 | 0 | 0 | 0 | 0 | 2 | 56 | 0 | 2 | 2 | 0 | 23 | 15 |
| **12,51** | 0 | 0 | 0 | 0 | 0 | 0 | 0 | 0 | 0 | 66 | 0 | 0 | 5 | 0 | 27 | 2 |
| **12,55** | 0 | 0 | 0 | 0 | 0 | 0 | 0 | 0 | 0 | 64 | 0 | 0 | 7 | 0 | 27 | 0 |
| **13,04** | 0 | 0 | 0 | 0 | 0 | 0 | 0 | 0 | 0 | 56 | 0 | 11 | 0 | 0 | 33 | 0 |
| **13,53** | 0 | 0 | 0 | 0 | 0 | 0 | 0 | 0 | 0 | 58 | 0 | 6 | 6 | 0 | 20 | 10 |
| **14,09** | 0 | 0 | 0 | 0 | 0 | 0 | 0 | 0 | 0 | 69 | 0 | 0 | 7 | 0 | 24 | 0 |
| **14,1** | 0 | 0 | 0 | 0 | 0 | 0 | 0 | 0 | 0 | 70 | 0 | 0 | 7 | 0 | 22 | 2 |
| **15,01** | 0 | 0 | 0 | 0 | 0 | 0 | 0 | 0 | 0 | 69 | 0 | 0 | 4 | 0 | 21 | 6 |
| **15,53** | 0 | 0 | 0 | 0 | 0 | 0 | 0 | 0 | 0 | 69 | 0 | 0 | 4 | 0 | 18 | 8 |
| **16,06** | 0 | 0 | 20 | 0 | 0 | 0 | 0 | 0 | 0 | 68 | 0 | 0 | 0 | 3 | 3 | 5 |
| **16,45** | 0 | 0 | 0 | 0 | 0 | 0 | 0 | 0 | 0 | 66 | 0 | 0 | 3 | 0 | 25 | 7 |
| **16,85** | 0 | 0 | 0 | 0 | 0 | 0 | 0 | 0 | 0 | 79 | 0 | 0 | 3 | 0 | 17 | 0 |
| **16,9** | 0 | 0 | 0 | 0 | 0 | 0 | 0 | 0 | 0 | 84 | 0 | 5 | 5 | 0 | 7 | 0 |
| **17,1** | 0 | 0 | 0 | 0 | 0 | 0 | 0 | 0 | 0 | 75 | 0 | 0 | 0 | 22 | 3 | 0 |
| **17,33** | 0 | 0 | 0 | 0 | 0 | 0 | 0 | 0 | 0 | 76 | 0 | 0 | 6 | 0 | 13 | 5 |
| **17,5** | 0 | 0 | 0 | 0 | 0 | 0 | 0 | 0 | 0 | 61 | 0 | 0 | 2 | 0 | 27 | 11 |
| **18** | 0 | 0 | 0 | 0 | 0 | 0 | 0 | 0 | 0 | 53 | 0 | 0 | 2 | 0 | 38 | 7 |
| **18,28** | 0 | 0 | 0 | 0 | 0 | 0 | 0 | 0 | 0 | 57 | 0 | 0 | 5 | 0 | 38 | 0 |
| **19,01** | 0 | 0 | 0 | 0 | 0 | 0 | 0 | 0 | 0 | 48 | 0 | 0 | 0 | 0 | 38 | 14 |
| **20,09** | 0 | 0 | 25 | 0 | 0 | 0 | 0 | 0 | 0 | 64 | 0 | 0 | 4 | 0 | 0 | 7 |
| **20,6** | 0 | 0 | 0 | 0 | 0 | 0 | 0 | 0 | 0 | 55 | 0 | 0 | 5 | 0 | 22 | 18 |
| **20,62** | 0 | 0 | 0 | 0 | 0 | 0 | 0 | 0 | 0 | 44 | 0 | 0 | 5 | 0 | 29 | 23 |
| **20,99** | 0 | 0 | 0 | 0 | 0 | 0 | 0 | 0 | 0 | 44 | 0 | 0 | 4 | 0 | 35 | 18 |
| **21,93** | 0 | 0 | 0 | 0 | 0 | 0 | 0 | 0 | 0 | 54 | 0 | 6 | 3 | 0 | 21 | 16 |
| **22,08** | 0 | 0 | 0 | 0 | 0 | 0 | 0 | 0 | 0 | 46 | 0 | 7 | 4 | 0 | 27 | 16 |
| **22,1** | 0 | 0 | 0 | 0 | 0 | 0 | 0 | 0 | 0 | 45 | 0 | 0 | 4 | 0 | 34 | 17 |
| **22,21** | 0 | 0 | 0 | 0 | 0 | 0 | 0 | 0 | 0 | 44 | 0 | 4 | 4 | 0 | 31 | 17 |
| **22,25** | 0 | 0 | 0 | 0 | 0 | 0 | 0 | 0 | 0 | 45 | 0 | 0 | 4 | 0 | 35 | 16 |
| **23** | 0 | 0 | 0 | 0 | 0 | 0 | 0 | 0 | 0 | 46 | 0 | 0 | 0 | 25 | 29 | 0 |
| **24** | 0 | 4 | 0 | 0 | 0 | 0 | 0 | 0 | 0 | 43 | 0 | 0 | 0 | 24 | 29 | 0 |
| **24,75** | 4 | 14 | 0 | 17 | 0 | 0 | 0 | 0 | 0 | 4 | 0 | 0 | 0 | 62 | 0 | 0 |
| **24,83** | 0 | 10 | 0 | 0 | 0 | 0 | 0 | 0 | 0 | 43 | 0 | 0 | 0 | 35 | 12 | 0 |

| | | | | | | | | | | | | | | | | |
|---|---|---|---|---|---|---|---|---|---|---|---|---|---|---|---|---|
| **24,9** | 2 | 25 | 0 | 5 | 0 | 0 | 0 | 0 | 0 | 6 | 0 | 0 | 0 | 62 | 0 | 0 |
| **26** | 0 | 0 | 0 | 0 | 0 | 2 | 0 | 0 | 0 | 41 | 0 | 0 | 0 | 24 | 33 | 0 |
| **27** | 0 | 0 | 0 | 0 | 0 | 0 | 0 | 0 | 0 | 37 | 0 | 0 | 0 | 31 | 33 | 0 |
| **27,08** | 8 | 14 | 0 | 18 | 0 | 0 | 0 | 0 | 0 | 10 | 0 | 0 | 0 | 49 | 0 | 0 |
| **27,1** | 0 | 0 | 0 | 0 | 0 | 0 | 0 | 0 | 0 | 29 | 0 | 0 | 0 | 37 | 34 | 0 |
| **27,33** | 0 | 0 | 0 | 0 | 0 | 0 | 0 | 0 | 0 | 63 | 0 | 0 | 0 | 15 | 23 | 0 |
| **28** | 0 | 0 | 0 | 0 | 0 | 0 | 0 | 0 | 0 | 50 | 0 | 0 | 0 | 24 | 26 | 0 |
| **28,95** | 0 | 0 | 0 | 0 | 0 | 0 | 0 | 2 | 0 | 40 | 0 | 0 | 0 | 26 | 31 | 0 |
| **29,05** | 9 | 9 | 0 | 0 | 0 | 14 | 5 | 0 | 0 | 20 | 0 | 0 | 0 | 7 | 20 | 0 |
| **29,06** | 8 | 0 | 0 | 0 | 0 | 0 | 0 | 4 | 0 | 8 | 0 | 0 | 0 | 16 | 36 | 0 |
| **29,28** | 4 | 0 | 0 | 0 | 0 | 0 | 2 | 0 | 0 | 27 | 0 | 0 | 0 | 23 | 45 | 0 |
| **29,96** | 0 | 0 | 0 | 0 | 0 | 0 | 0 | 0 | 0 | 42 | 0 | 0 | 0 | 19 | 40 | 0 |
| **30,41** | 5 | 10 | 0 | 0 | 15 | 0 | 0 | 0 | 0 | 27 | 0 | 0 | 0 | 27 | 17 | 0 |
| **30,47** | 0 | 22 | 0 | 0 | 11 | 0 | 0 | 0 | 0 | 22 | 0 | 0 | 0 | 33 | 11 | 0 |
| **30,48** | 0 | 0 | 0 | 0 | 0 | 0 | 0 | 0 | 0 | 43 | 0 | 0 | 0 | 22 | 35 | 0 |
| **30,54** | 0 | 0 | 0 | 0 | 0 | 0 | 0 | 0 | 0 | 49 | 0 | 0 | 0 | 18 | 33 | 0 |
| **30,62** | 33 | 8 | 0 | 8 | 0 | 5 | 0 | 0 | 0 | 32 | 0 | 0 | 0 | 11 | 3 | 0 |
| **30,72** | 5 | 0 | 0 | 0 | 0 | 0 | 3 | 0 | 0 | 40 | 0 | 0 | 0 | 15 | 38 | 0 |
| **30,8** | 0 | 0 | 0 | 15 | 13 | 0 | 0 | 0 | 0 | 31 | 0 | 0 | 0 | 23 | 18 | 0 |
| **30,83** | 0 | 0 | 0 | 0 | 0 | 0 | 0 | 4 | 2 | 51 | 0 | 0 | 0 | 20 | 18 | 0 |
| **30,84** | 0 | 0 | 0 | 0 | 0 | 0 | 0 | 5 | 2 | 54 | 0 | 0 | 0 | 23 | 16 | 0 |
| **30,86** | 0 | 0 | 0 | 0 | 0 | 0 | 0 | 7 | 2 | 66 | 0 | 0 | 0 | 20 | 5 | 0 |
| **30,88** | 0 | 0 | 0 | 0 | 0 | 0 | 0 | 5 | 4 | 45 | 0 | 0 | 0 | 30 | 16 | 0 |
| **30,9** | 0 | 0 | 0 | 0 | 0 | 0 | 0 | 4 | 0 | 53 | 0 | 0 | 0 | 35 | 9 | 0 |
| **30,93** | 12 | 40 | 0 | 0 | 0 | 0 | 0 | 0 | 0 | 23 | 0 | 0 | 0 | 22 | 3 | 0 |
| **30,96** | 0 | 10 | 0 | 0 | 14 | 7 | 0 | 0 | 0 | 34 | 0 | 0 | 0 | 31 | 5 | 0 |
| **30,98** | 0 | 0 | 0 | 0 | 0 | 0 | 0 | 3 | 6 | 44 | 0 | 0 | 0 | 29 | 17 | 0 |
| **31** | 0 | 0 | 0 | 0 | 0 | 0 | 0 | 3 | 5 | 39 | 0 | 0 | 0 | 32 | 21 | 0 |
| **31,01** | 0 | 0 | 0 | 0 | 0 | 0 | 0 | 2 | 2 | 41 | 0 | 0 | 0 | 33 | 22 | 0 |
| **31,02** | 3 | 0 | 0 | 0 | 0 | 0 | 0 | 1 | 0 | 66 | 0 | 0 | 0 | 13 | 17 | 0 |
| **31,5** | 0 | 0 | 0 | 0 | 0 | 0 | 0 | 4 | 3 | 43 | 0 | 0 | 0 | 32 | 18 | 0 |
| **32** | 0 | 0 | 0 | 0 | 0 | 0 | 0 | 5 | 6 | 68 | 0 | 0 | 0 | 13 | 8 | 0 |
| **33,02** | 0 | 0 | 0 | 0 | 0 | 0 | 0 | 5 | 3 | 43 | 0 | 0 | 0 | 24 | 24 | 0 |
| **34** | 0 | 0 | 0 | 0 | 0 | 15 | 0 | 12 | 4 | 50 | 0 | 0 | 0 | 12 | 8 | 0 |
| **35,06** | 0 | 0 | 0 | 0 | 0 | 0 | 0 | 11 | 8 | 60 | 0 | 0 | 0 | 11 | 10 | 0 |
| **36** | 0 | 0 | 0 | 0 | 0 | 0 | 0 | 6 | 6 | 51 | 0 | 0 | 0 | 23 | 15 | 0 |
| **36,92** | 0 | 0 | 0 | 0 | 0 | 4 | 0 | 7 | 4 | 75 | 0 | 0 | -0 | 6 | 3 | 0 |
| **37** | 0 | 0 | 0 | 0 | 0 | 0 | 0 | 8 | 6 | 62 | 0 | 0 | 0 | 16 | 8 | 0 |
| **38** | 0 | 0 | 0 | 0 | 0 | 22 | 0 | 8 | 7 | 46 | 0 | 0 | 0 | 7 | 9 | 0 |
| **39** | 0 | 0 | 0 | 0 | 0 | 30 | 0 | 8 | 2 | 28 | 0 | 0 | 0 | 24 | 8 | 0 |
| **40** | 0 | 0 | 0 | 0 | 0 | 5 | 0 | 7 | 7 | 58 | 0 | 0 | 0 | 15 | 8 | 0 |
| **40,97** | 0 | 0 | 0 | 0 | 0 | 0 | 0 | 8 | 5 | 67 | 0 | 0 | 0 | 14 | 8 | 0 |
| **42** | 0 | 0 | 0 | 0 | 0 | 0 | 0 | 10 | 5 | 60 | 0 | 0 | 0 | 16 | 9 | 0 |
| **43** | 0 | 0 | 0 | 0 | 0 | 17 | 0 | 10 | 3 | 51 | 0 | 0 | 0 | 12 | 7 | 0 |
| **44** | 0 | 0 | 0 | 0 | 0 | 0 | 0 | 13 | 6 | 55 | 0 | 0 | 0 | 18 | 8 | 0 |
| **45** | 0 | 0 | 0 | 0 | 0 | 0 | 0 | 12 | 7 | 58 | 0 | 0 | 0 | 15 | 8 | 0 |
| **45,61** | 0 | 0 | 0 | 0 | 0 | 47 | 0 | 7 | 5 | 30 | 0 | 0 | 0 | 6 | 6 | 0 |
| **45,97** | 0 | 0 | 0 | 0 | 0 | 0 | 0 | 13 | 7 | 52 | 0 | 0 | 0 | 21 | 7 | 0 |
| **47,02** | 0 | 0 | 0 | 0 | 0 | 0 | 0 | 16 | 13 | 46 | 0 | 0 | 0 | 16 | 8 | 0 |
| **48,01** | 0 | 0 | 0 | 0 | 0 | 0 | 0 | 13 | 10 | 52 | 0 | 0 | 0 | 17 | 8 | 0 |
| **49** | 0 | 0 | 0 | 0 | 0 | 0 | 0 | 13 | 6 | 52 | 0 | 0 | 0 | 22 | 7 | 0 |
| **50,03** | 0 | 0 | 0 | 0 | 0 | 5 | 0 | 11 | 11 | 53 | 0 | 0 | 0 | 14 | 5 | 0 |
| **51,96** | 0 | 0 | 0 | 0 | 0 | 3 | 0 | 15 | 7 | 47 | 0 | 0 | 0 | 20 | 7 | 0 |
| **54** | 0 | 0 | 0 | 0 | 0 | 7 | 0 | 16 | 11 | 44 | 0 | 0 | 0 | 15 | 7 | 0 |
| **55,96** | 0 | 0 | 0 | 0 | 0 | 7 | 0 | 15 | 15 | 41 | 0 | 0 | 0 | 16 | 7 | 0 |
| **57,92** | 0 | 0 | 0 | 0 | 0 | 8 | 0 | 21 | 8 | 40 | 0 | 0 | 0 | 17 | 6 | 0 |
| **60** | 0 | 0 | 0 | 0 | 0 | 4 | 0 | 22 | 8 | 43 | 0 | 0 | 0 | 17 | 6 | 0 |
| **60,37** | 0 | 0 | 0 | 0 | 0 | 0 | 0 | 15 | 5 | 37 | 0 | 0 | 0 | 30 | 14 | 0 |
| **61,93** | 0 | 0 | 0 | 0 | 0 | 0 | 0 | 20 | 10 | 42 | 0 | 0 | 0 | 20 | 8 | 0 |

| | | | | | | | | | | | | | | | | |
|---|---|---|---|---|---|---|---|---|---|---|---|---|---|---|---|---|
| **64** | 0 | 0 | 0 | 0 | 0 | 2 | 0 | 17 | 7 | 48 | 0 | 0 | 0 | 19 | 6 | 0 |
| **66** | 0 | 0 | 0 | 0 | 0 | 0 | 0 | 19 | 9 | 51 | 0 | 0 | 0 | 15 | 6 | 0 |
| **68,03** | 0 | 0 | 0 | 0 | 0 | 6 | 0 | 15 | 6 | 50 | 0 | 0 | 0 | 15 | 8 | 0 |
| **70,06** | 0 | 0 | 0 | 0 | 0 | 0 | 0 | 13 | 15 | 52 | 0 | 0 | 0 | 15 | 4 | 0 |
| **72** | 0 | 0 | 0 | 0 | 0 | 0 | 0 | 19 | 4 | 51 | 0 | 0 | 0 | 19 | 7 | 0 |
| **74** | 0 | 0 | 0 | 0 | 0 | 15 | 0 | 18 | 7 | 35 | 0 | 0 | 0 | 19 | 6 | 0 |
| **76,06** | 0 | 0 | 0 | 0 | 0 | 17 | 0 | 16 | 5 | 38 | 0 | 0 | 0 | 17 | 6 | 0 |
| **78,01** | 0 | 0 | 0 | 0 | 0 | 0 | 0 | 15 | 5 | 61 | 0 | 0 | 0 | 15 | 5 | 0 |
| **80,02** | 0 | 0 | 0 | 0 | 0 | 0 | 0 | 20 | 6 | 44 | 0 | 0 | 0 | 26 | 5 | 0 |
| **82,02** | 0 | 0 | 0 | 0 | 0 | 0 | 0 | 19 | 6 | 47 | 0 | 0 | 0 | 23 | 6 | 0 |
| **84** | 0 | 0 | 0 | 0 | 0 | 0 | 0 | 25 | 2 | 36 | 0 | 0 | 0 | 34 | 4 | 0 |
| **85,99** | 0 | 0 | 0 | 0 | 0 | 2 | 0 | 26 | 6 | 42 | 0 | 0 | 0 | 20 | 4 | 0 |
| **88,07** | 0 | 0 | 0 | 0 | 0 | 0 | 0 | 23 | 4 | 48 | 0 | 0 | 0 | 21 | 4 | 0 |
| **90** | 0 | 0 | 0 | 0 | 0 | 2 | 0 | 24 | 8 | 43 | 0 | 0 | 0 | 20 | 4 | 0 |
| **91,97** | -0 | 0 | 0 | 0 | 0 | 5 | 0 | 25 | 6 | 44 | 0 | 0 | 0 | 17 | 3 | 0 |
| **94** | 0 | 0 | 0 | 0 | 0 | 0 | 0 | 21 | 4 | 52 | 0 | 0 | 0 | 19 | 4 | 0 |
| **95,98** | 0 | 0 | 0 | 0 | 0 | 2 | 0 | 31 | 6 | 39 | 0 | 0 | 0 | 19 | 4 | 0 |
| **98,02** | 0 | 0 | 0 | 0 | 0 | 4 | 0 | 24 | 11 | 41 | 0 | 0 | 0 | 15 | 6 | 0 |
| **99,98** | 0 | 0 | 0 | 0 | 0 | 2 | 0 | 23 | 5 | 49 | 0 | 0 | 0 | 18 | 3 | 0 |
| **101,96** | 0 | 0 | 0 | 0 | 0 | 0 | 0 | 24 | 4 | 50 | 0 | 0 | 0 | 19 | 4 | 0 |
| **104,02** | 0 | 0 | 0 | 0 | 0 | 0 | 0 | 24 | 5 | 47 | 0 | 0 | 0 | 20 | 4 | 0 |
| **106,02** | 0 | 0 | 0 | 0 | 0 | 0 | 0 | 24 | 7 | 47 | 0 | 0 | 0 | 18 | 4 | 0 |
| **108,01** | 0 | 0 | 0 | 0 | 0 | 0 | 0 | 27 | 10 | 47 | 0 | 0 | 0 | 15 | 2 | 0 |
| **110,02** | 0 | 0 | 0 | 0 | 0 | 0 | 0 | 30 | 7 | 43 | 0 | 0 | 0 | 18 | 3 | 0 |
| **112,02** | 0 | 0 | 0 | 0 | 0 | 0 | 0 | 21 | 28 | 32 | 0 | 0 | 0 | 16 | 2 | 0 |
| **114,02** | 0 | 0 | 0 | 0 | 0 | 0 | 0 | 24 | 6 | 48 | 0 | 0 | 0 | 19 | 3 | 0 |
| **116,04** | 0 | 0 | 0 | 0 | 0 | 4 | 0 | 21 | 6 | 51 | 0 | 0 | 0 | 16 | 2 | 0 |
| **118,02** | 0 | 0 | 0 | 0 | 0 | 0 | 0 | 26 | 11 | 42 | 0 | 0 | 0 | 18 | 2 | 0 |
| **120** | 0 | 0 | 0 | 0 | 0 | 0 | 0 | 31 | 6 | 43 | 0 | 0 | 0 | 17 | 2 | 0 |
| **122,04** | 0 | 0 | 0 | 0 | 0 | 0 | 0 | 26 | 4 | 48 | 0 | 0 | 0 | 20 | 2 | 0 |
| **124,03** | 0 | 0 | 0 | 0 | 0 | 0 | 0 | 25 | 7 | 36 | 0 | 0 | 0 | 28 | 3 | 0 |
| **126,02** | 0 | 0 | 0 | 0 | 0 | 0 | 0 | 28 | 2 | 50 | 0 | 0 | 0 | 18 | 2 | 0 |
| **128,02** | 0 | 0 | 0 | 0 | 0 | 0 | 0 | 26 | 3 | 51 | 0 | 0 | 0 | 18 | 3 | 0 |
| **130,02** | 0 | 0 | 0 | 0 | 0 | 0 | 0 | 33 | 7 | 42 | 0 | 0 | 0 | 15 | 2 | 0 |
| **132** | 0 | 0 | 0 | 0 | 0 | 0 | 0 | 22 | 16 | 44 | 0 | 0 | 0 | 16 | 2 | 0 |
| **134** | 0 | 0 | 0 | 0 | 0 | 0 | 0 | 26 | 7 | 51 | 0 | 0 | 0 | 14 | 2 | 0 |
| **136** | 0 | 0 | 0 | 0 | 0 | 0 | 0 | 29 | 9 | 41 | 0 | 0 | 0 | 18 | 3 | 0 |
| **138** | 0 | 0 | 0 | 0 | 0 | 0 | 0 | 29 | 9 | 40 | 0 | 0 | 0 | 18 | 3 | 0 |
| **139,91** | 0 | 0 | 0 | 0 | 0 | 0 | 0 | 31 | 6 | 45 | 0 | 0 | 0 | 16 | 2 | 0 |
| **139,93** | 0 | 0 | 0 | 0 | 0 | 0 | 0 | 4 | 2 | 59 | 0 | 0 | 0 | 9 | 26 | 0 |
| **142,02** | 0 | 0 | 0 | 0 | 0 | 0 | 0 | 27 | 8 | 43 | 0 | 0 | 0 | 19 | 3 | 0 |
| **144** | 0 | 0 | 0 | 0 | 0 | 0 | 0 | 27 | 9 | 39 | 0 | 0 | 0 | 23 | 2 | 0 |
| **146** | 0 | 0 | 0 | 0 | 0 | 0 | 0 | 33 | 7 | 37 | 0 | 0 | 0 | 22 | 2 | 0 |
| **148** | 0 | 0 | 0 | 0 | 0 | 0 | 0 | 30 | 7 | 44 | 0 | 0 | 0 | 17 | 1 | 0 |
| **149,02** | 0 | 0 | 0 | 0 | 0 | 0 | 0 | 24 | 6 | 46 | 0 | 0 | 0 | 22 | 2 | 0 |
| **149,5** | 0 | 0 | 0 | 0 | 0 | 0 | 0 | 26 | 7 | 49 | 0 | 0 | 0 | 18 | 0 | 0 |
| **150** | 0 | 0 | 0 | 0 | 0 | 0 | 0 | 24 | 16 | 44 | 0 | 0 | 0 | 13 | 2 | 0 |
| **150,35** | 0 | 0 | 0 | 0 | 0 | 0 | 0 | 32 | 11 | 14 | 0 | 0 | 0 | 41 | 2 | 0 |
| **150,48** | 0 | 0 | 0 | 0 | 0 | 0 | 0 | 35 | 10 | 34 | 0 | 0 | 0 | 19 | 2 | 0 |
| **150,57** | 0 | 0 | 0 | 0 | 0 | 0 | 0 | 38 | 9 | 35 | 0 | 0 | 0 | 19 | 0 | 0 |
| **150,66** | 0 | 0 | 0 | 0 | 0 | 0 | 0 | 33 | 10 | 41 | 0 | 0 | 0 | 16 | 0 | 0 |
| **150,92** | 0 | 0 | 0 | 0 | 0 | 0 | 0 | 24 | 13 | 46 | 0 | 0 | 0 | 17 | 0 | 0 |
| **150,98** | 0 | 0 | 0 | 0 | 0 | 0 | 0 | 30 | 7 | 49 | 0 | 0 | 0 | 14 | 0 | 0 |
| **151,13** | 0 | 0 | 0 | 0 | 0 | 8 | 0 | 25 | 8 | 49 | 0 | 0 | 0 | 8 | 1 | 0 |
| **151,22** | 0 | 0 | 0 | 0 | 0 | 7 | 0 | 25 | 6 | 48 | 0 | 0 | 0 | 13 | 1 | 0 |
| **151,37** | 0 | 0 | 0 | 0 | 0 | 18 | 0 | 11 | 9 | 39 | 0 | 0 | 0 | 15 | 8 | 0 |
| **151,55** | 0 | 0 | 0 | 0 | 0 | 0 | 0 | 18 | 2 | 15 | 0 | 0 | 0 | 58 | 7 | 0 |

**XRD analyses of samples from the OGT core by D. Bühmann**

| Depth | Calcite | Dolomite | Siderite | Pyrite | Barit | Szomolnokite | Clinopyroxene | Plagioclase | Kfs | Hematite | Qtz | Kaolinite | Chlorite | Dioctr. Mica | Trioctr. Mica | Il/Sm Interstr. | Smectite + Corrensite | Dioctr. Smectite | Trioctr. Smectite | Analcime | Stilbite | Epistilbite | Scolecite or Thomsonite | Laumonite-Leonhardite | Heulandite | Levyne | coal |
|---|---|---|---|---|---|---|---|---|---|---|---|---|---|---|---|---|---|---|---|---|---|---|---|---|---|---|---|
| **0** | 15 | 0 | 0 | 0 | 0 | 0 | 9 | 41 | 0 | 0 | 4 | 0 | 0 | 0 | 0 | 0 | 0 | 0 | 30 | 0 | 0 | 0 | 0 | 0 | 0 | 0 | 0 |
| **3** | 1 | 0 | 0 | 0 | 0 | 0 | 6 | 50 | 0 | 0 | 2 | 0 | 0 | 0 | 0 | 0 | 0 | 0 | 42 | 0 | 0 | 0 | 0 | 0 | 0 | 0 | 0 |
| **6** | 17 | 0 | 0 | 0 | 0 | 0 | 10 | 37 | 0 | 0 | 0 | 0 | 0 | 0 | 0 | 0 | 0 | 0 | 37 | 0 | 0 | 0 | 0 | 0 | 0 | 0 | 0 |
| **9** | 0 | 0 | 0 | 0 | 0 | 0 | 8 | 75 | 0 | 0 | 0 | 0 | 0 | 0 | 0 | 0 | 0 | 0 | 17 | 0 | 0 | 0 | 0 | 0 | 0 | 0 | 0 |
| **12** | 0 | 0 | 0 | 0 | 0 | 0 | 18 | 36 | 0 | 0 | 0 | 0 | 0 | 0 | 0 | 0 | 0 | 0 | 9 | 0 | 0 | 0 | 0 | 0 | 37 | 0 | 0 |
| **15** | 5 | 0 | 0 | 0 | 0 | 0 | 25 | 42 | 0 | 4 | 0 | 0 | 0 | 0 | 0 | 0 | 0 | 0 | 17 | 0 | 0 | 3 | 4 | 0 | 0 | 0 | 0 |
| **18** | 0 | 0 | 0 | 0 | 0 | 0 | 22 | 37 | 0 | 5 | 0 | 0 | 0 | 0 | 0 | 0 | 0 | 0 | 14 | 0 | 0 | 7 | 11 | 0 | 0 | 4 | 0 |
| **21** | 0 | 0 | 0 | 0 | 0 | 0 | 20 | 24 | 0 | 3 | 0 | 0 | 0 | 0 | 0 | 0 | 0 | 0 | 16 | 0 | 0 | 28 | 9 | 0 | 0 | 0 | 0 |
| **24** | 0 | 0 | 0 | 0 | 0 | 0 | 25 | 42 | 0 | 5 | 0 | 0 | 0 | 0 | 0 | 0 | 0 | 0 | 12 | 0 | 6 | 0 | 11 | 0 | 0 | 0 | 0 |
| **27** | 0 | 0 | 0 | 0 | 0 | 0 | 26 | 44 | 0 | 0 | 0 | 0 | 0 | 0 | 0 | 0 | 0 | 0 | 30 | 0 | 0 | 0 | 0 | 0 | 0 | 0 | 0 |
| **30** | 0 | 0 | 0 | 0 | 0 | 0 | 22 | 49 | 0 | 0 | 0 | 0 | 0 | 0 | 0 | 0 | 0 | 0 | 24 | 0 | 0 | 5 | 0 | 0 | 0 | 0 | 0 |
| **33** | 0 | 0 | 0 | 0 | 0 | 0 | 27 | 55 | 0 | 0 | 0 | 0 | 0 | 0 | 0 | 0 | 0 | 0 | 18 | 0 | 0 | 0 | 0 | 0 | 0 | 0 | 0 |
| **36** | 0 | 0 | 0 | 0 | 0 | 0 | 20 | 37 | 0 | 4 | 0 | 0 | 0 | 0 | 0 | 0 | 0 | 0 | 17 | 0 | 0 | 11 | 11 | 0 | 0 | 0 | 0 |
| **39** | 0 | 0 | 0 | 0 | 0 | 0 | 19 | 65 | 0 | 0 | 0 | 0 | 0 | 0 | 0 | 0 | 0 | 0 | 16 | 0 | 0 | 0 | 0 | 0 | 0 | 0 | 0 |
| **42** | 4 | 0 | 0 | 0 | 0 | 0 | 27 | 34 | 0 | 0 | 0 | 0 | 0 | 0 | 0 | 0 | 0 | 0 | 23 | 0 | 0 | 7 | 5 | 0 | 0 | 0 | 0 |
| **45** | 0 | 0 | 0 | 0 | 0 | 0 | 20 | 40 | 0 | 0 | 0 | 0 | 0 | 0 | 0 | 0 | 0 | 0 | 11 | 0 | 0 | 20 | 8 | 0 | 0 | 0 | 0 |
| **45,2** | 0 | 0 | 0 | 0 | 0 | 0 | 20 | 32 | 0 | 3 | 0 | 0 | 0 | 0 | 0 | 0 | 0 | 0 | 19 | 0 | 0 | 11 | 15 | 0 | 0 | 0 | 0 |
| **48** | 0 | 0 | 0 | 0 | 0 | 0 | 26 | 57 | 0 | 0 | 0 | 0 | 0 | 0 | 0 | 0 | 0 | 0 | 9 | 0 | 0 | 5 | 0 | 3 | 0 | 0 | 0 |
| **51** | 0 | 0 | 0 | 0 | 0 | 0 | 20 | 51 | 0 | 0 | 0 | 0 | 0 | 0 | 0 | 0 | 0 | 0 | 14 | 15 | 0 | 0 | 0 | 0 | 0 | 0 | 0 |
| **54** | 0 | 0 | 0 | 0 | 0 | 0 | 38 | 48 | 0 | 0 | 1 | 0 | 0 | 0 | 0 | 0 | 0 | 0 | 13 | 0 | 0 | 0 | 0 | 0 | 0 | 0 | 0 |
| **57** | 0 | 0 | 0 | 0 | 0 | 0 | 24 | 59 | 0 | 0 | 2 | 0 | 0 | 0 | 0 | 0 | 0 | 0 | 15 | 0 | 0 | 0 | 0 | 0 | 0 | 0 | 0 |
| **60** | 0 | 0 | 0 | 0 | 0 | 0 | 23 | 60 | 0 | 0 | 2 | 0 | 0 | 0 | 0 | 0 | 0 | 0 | 16 | 0 | 0 | 0 | 0 | 0 | 0 | 0 | 0 |
| **63** | 0 | 0 | 0 | 0 | 0 | 0 | 12 | 78 | 0 | 0 | 1 | 0 | 0 | 0 | 0 | 0 | 0 | 0 | 9 | 0 | 0 | 0 | 0 | 0 | 0 | 0 | 0 |
| **66** | 0 | 0 | 0 | 0 | 0 | 0 | 25 | 36 | 0 | 0 | 0 | 0 | 0 | 0 | 0 | 0 | 0 | 0 | 20 | 17 | 0 | 1 | 0 | 0 | 0 | 0 | 0 |
| **66** | 0 | 0 | 0 | 0 | 0 | 0 | 24 | 54 | 0 | 0 | 0 | 0 | 0 | 0 | 0 | 0 | 0 | 0 | 7 | 11 | 0 | 0 | 0 | 3 | 0 | 0 | 0 |
| **69** | 0 | 0 | 0 | 0 | 0 | 0 | 18 | 56 | 0 | 0 | 0 | 0 | 0 | 0 | 0 | 0 | 0 | 0 | 19 | 0 | 0 | 0 | 5 | 2 | 0 | 0 | 0 |
| **72** | 20 | 0 | 0 | 0 | 0 | 0 | 6 | 38 | 0 | 0 | 0 | 0 | 0 | 0 | 0 | 0 | 0 | 0 | 14 | 21 | 0 | 0 | 0 | 1 | 0 | 0 | 0 |
| **75** | 0 | 0 | 0 | 0 | 0 | 0 | 16 | 67 | 0 | 0 | 0 | 0 | 0 | 0 | 0 | 0 | 0 | 0 | 17 | 0 | 0 | 0 | 0 | 0 | 0 | 0 | 0 |
| **78** | 0 | 0 | 0 | 0 | 0 | 0 | 23 | 43 | 0 | 0 | 0 | 0 | 0 | 0 | 0 | 0 | 0 | 0 | 20 | 14 | 0 | 0 | 0 | 0 | 0 | 0 | 0 |
| **81** | 0 | 0 | 0 | 0 | 0 | 0 | 24 | 52 | 0 | 7 | 0 | 0 | 0 | 0 | 0 | 0 | 9 | 0 | 0 | 0 | 0 | 0 | 7 | 0 | 0 | 0 | 0 |
| **84** | 0 | 0 | 0 | 0 | 0 | 0 | 15 | 62 | 0 | 4 | 0 | 0 | 0 | 0 | 0 | 0 | 0 | 0 | 12 | 0 | 0 | 0 | 3 | 4 | 0 | 0 | 0 |
| **87** | 0 | 0 | 0 | 0 | 0 | 0 | 14 | 63 | 0 | 0 | 0 | 0 | 0 | 0 | 0 | 0 | 0 | 0 | 17 | 5 | 0 | 0 | 0 | 0 | 0 | 0 | 0 |
| **90** | 0 | 0 | 0 | 0 | 0 | 0 | 20 | 41 | 0 | 4 | 0 | 0 | 0 | 0 | 0 | 0 | 0 | 0 | 13 | 0 | 0 | 7 | 15 | 0 | 0 | 0 | 0 |
| **93** | 2 | 0 | 0 | 0 | 0 | 0 | 11 | 63 | 0 | 3 | 0 | 0 | 0 | 0 | 0 | 0 | 0 | 0 | 5 | 10 | 0 | 0 | 5 | 1 | 0 | 0 | 0 |
| **96** | 0 | 0 | 0 | 0 | 0 | 0 | 35 | 32 | 0 | 0 | 0 | 0 | 0 | 0 | 0 | 0 | 0 | 0 | 24 | 0 | 0 | 0 | 9 | 0 | 0 | 0 | 0 |
| **96,6** | 1 | 0 | 0 | 0 | 0 | 0 | 8 | 65 | 0 | 3 | 0 | 0 | 0 | 0 | 0 | 0 | 0 | 0 | 6 | 0 | 0 | 0 | 1 | 15 | 0 | 0 | 0 |
| **99** | 0 | 0 | 0 | 0 | 0 | 0 | 26 | 45 | 0 | 0 | 0 | 0 | 0 | 0 | 0 | 0 | 0 | 0 | 14 | 0 | 0 | 0 | 14 | 0 | 0 | 0 | 0 |
| **101** | 0 | 0 | 0 | 0 | 0 | 0 | 0 | 0 | 0 | 8 | 0 | 0 | 0 | 0 | 0 | 0 | 92 | 0 | 0 | 0 | 0 | 0 | 0 | 0 | 0 | 0 | 0 |
| **101** | 4 | 0 | 0 | 0 | 0 | 0 | 0 | 0 | 0 | 0 | 0 | 0 | 0 | 0 | 0 | 0 | 96 | 0 | 0 | 0 | 0 | 0 | 0 | 0 | 0 | 0 | 0 |
| **102** | 0 | 0 | 0 | 0 | 0 | 0 | 15 | 62 | 0 | 0 | 0 | 0 | 0 | 0 | 0 | 0 | 0 | 0 | 13 | 10 | 0 | 0 | 0 | 0 | 0 | 0 | 0 |
| **105** | 0 | 0 | 0 | 0 | 0 | 0 | 26 | 64 | 0 | 2 | 0 | 0 | 6 | 0 | 0 | 0 | 0 | 0 | 2 | 0 | 0 | 0 | 0 | 0 | 0 | 0 | 0 |
| **108** | 0 | 0 | 0 | 0 | 0 | 0 | 23 | 53 | 0 | 3 | 0 | 0 | 4 | 0 | 0 | 0 | 0 | 0 | 11 | 0 | 0 | 0 | 6 | 0 | 0 | 0 | 0 |
| **108** | 0 | 0 | 0 | 0 | 0 | 0 | 17 | 62 | 0 | 3 | 0 | 0 | 11 | 0 | 0 | 0 | 0 | 0 | 8 | 0 | 0 | 0 | 0 | 0 | 0 | 0 | 0 |
| **111** | 2 | 0 | 0 | 0 | 0 | 0 | 22 | 59 | 0 | 3 | 0 | 0 | 4 | 0 | 0 | 0 | 0 | 0 | 5 | 0 | 0 | 0 | 6 | 0 | 0 | 0 | 0 |
| **112** | 13 | 0 | 0 | 0 | 0 | 0 | 2 | 34 | 0 | 0 | 0 | 0 | 8 | 0 | 0 | 0 | 11 | 0 | 0 | 3 | 0 | 0 | 0 | 30 | 0 | 0 | 0 |
| **114** | 2 | 0 | 0 | 0 | 0 | 0 | 3 | 64 | 0 | 0 | 0 | 0 | 15 | 0 | 0 | 0 | 13 | 0 | 0 | 0 | 0 | 0 | 3 | 0 | 0 | 0 | 0 |
| **117** | 7 | 0 | 0 | 0 | 0 | 0 | 5 | 70 | 0 | 3 | 0 | 0 | 3 | 0 | 0 | 0 | 13 | 0 | 0 | 0 | 0 | 0 | 0 | 0 | 0 | 0 | 0 |
| **118** | 45 | 0 | 0 | 0 | 0 | 0 | 0 | 45 | 0 | 0 | 0 | 0 | 4 | 0 | 0 | 0 | 0 | 0 | 7 | 0 | 0 | 0 | 0 | 0 | 0 | 0 | 0 |
| **119** | 0 | 0 | 0 | 0 | 0 | 0 | 0 | 11 | 11 | 0 | 72 | 0 | 0 | 0 | 0 | 6 | 0 | 0 | 0 | 0 | 0 | 0 | 0 | 0 | 0 | 0 | 0 |
| **120** | 0 | 0 | 0 | 0 | 0 | 0 | 0 | 4 | 7 | 0 | 85 | 0 | 0 | 0 | 0 | 4 | 0 | 0 | 0 | 0 | 0 | 0 | 0 | 0 | 0 | 0 | 0 |
| **123** | 0 | 0 | 0 | 0 | 0 | 0 | 0 | 3 | 4 | 0 | 90 | 0 | 0 | 0 | 0 | 3 | 0 | 0 | 0 | 0 | 0 | 0 | 0 | 0 | 0 | 0 | 0 |
| **126** | 0 | 0 | 0 | 0 | 0 | 0 | 0 | 2 | 8 | 0 | 90 | 0 | 0 | 0 | 0 | 0 | 0 | 0 | 0 | 0 | 0 | 0 | 0 | 0 | 0 | 0 | 0 |
| **129** | 0 | 0 | 0 | 0 | 0 | 0 | 0 | 3 | 6 | 0 | 91 | 0 | 0 | 0 | 0 | 0 | 0 | 0 | 0 | 0 | 0 | 0 | 0 | 0 | 0 | 0 | 0 |
| **132** | 0 | 0 | 0 | 0 | 0 | 0 | 0 | 5 | 5 | 0 | 89 | 0 | 0 | 0 | 0 | 0 | 0 | 0 | 0 | 0 | 0 | 0 | 0 | 0 | 0 | 0 | 0 |
| **135** | 0 | 0 | 0 | 0 | 0 | 0 | 0 | 2 | 5 | 0 | 93 | 0 | 0 | 0 | 0 | 0 | 0 | 0 | 0 | 0 | 0 | 0 | 0 | 0 | 0 | 0 | 0 |
| **138** | 0 | 0 | 0 | 0 | 0 | 0 | 0 | 4 | 4 | 6 | 55 | 0 | 0 | 14 | 0 | 17 | 0 | 0 | 0 | 0 | 0 | 0 | 0 | 0 | 0 | 0 | 0 |
| **141** | 0 | 0 | 0 | 0 | 0 | 0 | 0 | 8 | 11 | 0 | 61 | 0 | 0 | 7 | 0 | 12 | 0 | 0 | 0 | 0 | 0 | 0 | 0 | 0 | 0 | 0 | 0 |
| **144** | 0 | 0 | 0 | 0 | 0 | 0 | 0 | 2 | 8 | 0 | 87 | 0 | 0 | 0 | 0 | 3 | 0 | 0 | 0 | 0 | 0 | 0 | 0 | 0 | 0 | 0 | 0 |
| **147** | 0 | 0 | 0 | 0 | 0 | 0 | 0 | 6 | 0 | 0 | 73 | 0 | 0 | 8 | 0 | 13 | 0 | 0 | 0 | 0 | 0 | 0 | 0 | 0 | 0 | 0 | 0 |
| **150** | 0 | 0 | 0 | 0 | 0 | 0 | 0 | 6 | 4 | 0 | 53 | 0 | 0 | 12 | 0 | 25 | 0 | 0 | 0 | 0 | 0 | 0 | 0 | 0 | 0 | 0 | 0 |
| **153** | 0 | 0 | 0 | 0 | 0 | 0 | 0 | 11 | 0 | 0 | 60 | 0 | 0 | 11 | 0 | 18 | 0 | 0 | 0 | 0 | 0 | 0 | 0 | 0 | 0 | 0 | 0 |
| **156** | 0 | 0 | 0 | 0 | 0 | 0 | 0 | 2 | 5 | 0 | 93 | 0 | 0 | 0 | 0 | 0 | 0 | 0 | 0 | 0 | 0 | 0 | 0 | 0 | 0 | 0 | 0 |
| **159** | 0 | 0 | 0 | 0 | 0 | 0 | 0 | 3 | 0 | 11 | 24 | 0 | 0 | 16 | 0 | 46 | 0 | 0 | 0 | 0 | 0 | 0 | 0 | 0 | 0 | 0 | 0 |
| **162** | 0 | 0 | 0 | 0 | 0 | 0 | 0 | 5 | 4 | 0 | 85 | 0 | 0 | 0 | 0 | 6 | 0 | 0 | 0 | 0 | 0 | 0 | 0 | 0 | 0 | 0 | 0 |

| | | | | | | | | | | | | | | | | | | | | | | | | | | | |
|---|---|---|---|---|---|---|---|---|---|---|---|---|---|---|---|---|---|---|---|---|---|---|---|---|---|---|---|
| **165** | 0 | 0 | 0 | 0 | 0 | 0 | 0 | 6 | 4 | 0 | 88 | 0 | 0 | 3 | 0 | 0 | 0 | 0 | 0 | 0 | 0 | 0 | 0 | 0 | 0 | 0 | 0 |
| **168** | 0 | 0 | 0 | 0 | 0 | 0 | 0 | 7 | 7 | 0 | 72 | 0 | 0 | 4 | 0 | 10 | 0 | 0 | 0 | 0 | 0 | 0 | 0 | 0 | 0 | 0 | 0 |
| **171** | 0 | 0 | 0 | 0 | 0 | 0 | 0 | 6 | 6 | 0 | 86 | 0 | 0 | 0 | 0 | 3 | 0 | 0 | 0 | 0 | 0 | 0 | 0 | 0 | 0 | 0 | 0 |
| **174** | 0 | 0 | 0 | 0 | 0 | 0 | 0 | 5 | 0 | 0 | 90 | 0 | 0 | 2 | 0 | 2 | 0 | 0 | 0 | 0 | 0 | 0 | 0 | 0 | 0 | 0 | 0 |
| **177** | 0 | 0 | 0 | 0 | 0 | 0 | 0 | 4 | 3 | 0 | 88 | 0 | 0 | 0 | 0 | 5 | 0 | 0 | 0 | 0 | 0 | 0 | 0 | 0 | 0 | 0 | 0 |
| **180** | 0 | 0 | 0 | 0 | 0 | 0 | 0 | 4 | 3 | 0 | 93 | -0 | 0 | 0 | 0 | 0 | 0 | 0 | 0 | 0 | 0 | 0 | 0 | 0 | 0 | 0 | 0 |
| **183** | 0 | 0 | 0 | 0 | 0 | 0 | 0 | 4 | 4 | 0 | 92 | 0 | 0 | 0 | 0 | 0 | 0 | 0 | 0 | 0 | 0 | 0 | 0 | 0 | 0 | 0 | 0 |
| **186** | 0 | 0 | 0 | 0 | 0 | 0 | 0 | 12 | 9 | 0 | 61 | 0 | 0 | 5 | 0 | 12 | 0 | 0 | 0 | 0 | 0 | 0 | 0 | 0 | 0 | 0 | 0 |
| **189** | 0 | 0 | 0 | 0 | 0 | 0 | 0 | 8 | 0 | 5 | 60 | 0 | 0 | 9 | 0 | 17 | 0 | 0 | 0 | 0 | 0 | 0 | 0 | 0 | 0 | 0 | 0 |
| **192** | 0 | 0 | 0 | 0 | 0 | 0 | 0 | 8 | 4 | 0 | 88 | 0 | 0 | 0 | 0 | 0 | 0 | 0 | 0 | 0 | 0 | 0 | 0 | 0 | 0 | 0 | 0 |
| **195** | 0 | 0 | 0 | 0 | 0 | 0 | 0 | 11 | 0 | 6 | 54 | 0 | 0 | 13 | 0 | 16 | 0 | 0 | 0 | 0 | 0 | 0 | 0 | 0 | 0 | 0 | 0 |
| **198** | 0 | 0 | 0 | 0 | 0 | 0 | 0 | 6 | 3 | 0 | 84 | 0 | 0 | 2 | 0 | 5 | 0 | 0 | 0 | 0 | 0 | 0 | 0 | 0 | 0 | 0 | 0 |
| **201** | 0 | 0 | 0 | 0 | | 0 | 0 | 4 | 2 | 0 | 92 | 0 | 0 | 3 | 0 | 0 | 0 | 0 | 0 | 0 | 0 | 0 | 0 | 0 | 0 | 0 | 0 |
| **204** | 0 | 0 | 0 | 0 | 0 | 0 | 0 | 6 | 4 | 0 | 90 | 0 | 0 | 0 | 0 | 0 | 0 | 0 | 0 | 0 | 0 | 0 | 0 | 0 | 0 | 0 | 0 |
| **205** | 0 | 0 | 0 | 0 | 0 | 0 | 0 | 8 | 0 | 0 | 50 | 0 | 0 | 13 | 0 | 29 | 0 | 0 | 0 | 0 | 0 | 0 | 0 | 0 | 0 | 0 | 0 |
| **207** | 0 | 0 | 0 | 0 | 0 | 0 | 0 | 12 | 5 | 0 | 69 | 0 | 0 | 4 | 0 | 10 | 0 | 0 | 0 | 0 | 0 | 0 | 0 | 0 | 0 | 0 | 0 |
| **208,5** | 0 | 0 | 0 | 0 | 0 | 0 | 0 | 7 | 0 | 0 | 33 | -0 | 0 | 15 | 0 | 46 | 0 | 0 | 0 | 0 | 0 | 0 | 0 | 0 | 0 | 0 | 0 |
| **210** | 0 | 0 | 0 | 0 | 0 | 0 | 0 | 9 | 0 | 8 | 58 | 0 | 0 | 0 | 0 | 26 | 0 | 0 | 0 | 0 | 0 | 0 | 0 | 0 | 0 | 0 | 0 |
| **213** | 6 | 0 | 0 | 0 | 0 | 0 | 0 | 2 | 2 | 0 | 84 | 0 | 0 | 0 | 0 | 6 | 0 | 0 | 0 | 0 | 0 | 0 | 0 | 0 | 0 | 0 | 0 |
| **216** | 0 | 0 | 0 | 0 | 0 | 0 | 0 | 18 | 9 | 0 | 55 | 0 | 0 | 0 | 0 | 17 | 0 | 0 | 0 | 0 | 0 | 0 | 0 | 0 | 0 | 0 | 0 |
| **219** | 2 | 0 | 0 | 0 | 0 | 0 | 0 | 8 | 5 | 0 | 81 | 0 | 0 | 0 | 0 | 4 | 0 | 0 | 0 | 0 | 0 | 0 | 0 | 0 | 0 | 0 | 0 |
| **222** | 0 | 0 | 0 | 0 | 0 | 0 | 0 | 3 | 1 | 0 | 96 | 0 | 0 | 0 | 0 | 0 | 0 | 0 | 0 | 0 | 0 | 0 | 0 | 0 | 0 | 0 | 0 |
| **225** | 5 | 0 | 0 | 0 | 0 | 0 | 0 | 2 | 2 | 0 | 92 | 0 | 0 | 0 | 0 | 0 | 0 | 0 | 0 | 0 | 0 | 0 | 0 | 0 | 0 | 0 | 0 |
| **228** | 0 | 0 | 0 | 0 | 0 | 0 | 0 | 11 | 5 | 7 | 76 | 0 | 0 | 0 | 0 | 0 | 0 | 0 | 0 | 0 | 0 | 0 | 0 | 0 | 0 | 0 | 0 |
| **229** | 0 | 0 | 0 | 0 | 0 | 0 | 0 | 13 | 0 | 0 | 41 | 0 | 0 | 15 | 0 | 32 | 0 | 0 | 0 | 0 | 0 | 0 | 0 | 0 | 0 | 0 | 0 |
| **231** | 66 | 0 | 0 | 0 | 0 | 0 | 0 | 3 | 0 | 0 | 19 | 0 | 0 | 3 | 0 | 8 | 0 | 0 | 0 | 0 | 0 | 0 | 0 | 0 | 0 | 0 | 0 |
| **234** | 15 | 0 | 0 | 0 | 0 | 0 | 0 | 15 | 0 | 0 | 38 | 0 | 0 | 7 | 0 | 11 | 0 | 14 | 0 | 0 | 0 | 0 | 0 | 0 | 0 | 0 | 0 |
| **237** | 0 | 6 | 0 | 0 | 0 | 0 | 0 | 13 | 0 | 0 | 46 | 0 | 0 | 8 | 0 | 0 | 0 | 26 | 0 | 0 | 0 | 0 | 0 | 0 | 0 | 0 | 0 |
| **240** | 0 | 0 | 0 | 0 | 0 | 0 | 0 | 10 | 0 | 0 | 46 | 0 | 0 | 9 | 0 | 12 | 0 | 23 | 0 | 0 | 0 | 0 | 0 | 0 | 0 | 0 | 0 |
| **243** | 0 | 0 | 0 | 0 | 0 | 0 | 0 | 8 | 0 | 0 | 57 | 0 | 0 | 8 | 0 | 8 | 0 | 20 | 0 | 0 | 0 | 0 | 0 | 0 | 0 | 0 | 0 |
| **246** | 0 | 0 | 0 | 0 | 0 | 0 | 0 | 14 | 0 | 0 | 48 | 0 | 0 | 8 | 0 | 10 | 0 | 20 | 0 | 0 | 0 | 0 | 0 | 0 | 0 | 0 | 0 |
| **249** | 0 | 0 | 0 | 0 | 0 | 0 | 0 | 8 | 0 | 0 | 52 | 0 | 0 | 8 | 0 | 20 | 0 | 12 | 0 | 0 | 0 | 0 | 0 | 0 | 0 | 0 | 0 |
| **252** | 5 | 0 | 0 | 0 | 0 | 0 | 0 | 12 | 0 | 5 | 45 | 0 | 0 | 8 | 0 | 19 | 0 | 7 | 0 | 0 | 0 | 0 | 0 | 0 | 0 | 0 | 0 |
| **255** | 0 | 0 | 0 | 0 | 0 | 0 | 0 | 17 | 0 | 0 | 46 | 0 | 0 | 15 | 0 | 22 | 0 | 0 | 0 | 0 | 0 | 0 | 0 | 0 | 0 | 0 | 0 |
| **258** | 0 | 0 | 0 | 0 | 0 | 0 | 0 | 10 | 0 | 0 | 51 | 0 | 0 | 16 | 0 | 23 | 0 | 0 | 0 | 0 | 0 | 0 | 0 | 0 | 0 | 0 | 0 |
| **261** | 5 | 0 | 0 | 0 | 0 | 0 | 0 | 13 | 0 | 0 | 49 | 0 | 0 | 7 | 0 | 8 | 0 | 18 | 0 | 0 | 0 | 0 | 0 | 0 | 0 | 0 | 0 |
| **264** | 22 | 0 | 0 | 0 | 0 | 0 | 0 | 9 | 0 | 0 | 41 | 0 | 0 | 5 | 0 | 7 | 0 | 16 | 0 | 0 | 0 | 0 | 0 | 0 | 0 | 0 | 0 |
| **267** | 9 | 0 | 0 | 0 | 0 | 0 | 0 | 11 | 0 | 0 | 41 | 0 | 0 | 8 | 0 | 8 | 0 | 23 | 0 | 0 | 0 | 0 | 0 | 0 | 0 | 0 | 0 |
| **270** | 12 | 0 | 0 | 0 | 0 | 0 | 0 | 10 | 0 | 0 | 41 | 0 | 0 | 10 | 0 | 10 | 0 | 18 | 0 | 0 | 0 | 0 | 0 | 0 | 0 | 0 | 0 |
| **273** | 13 | 0 | 0 | 0 | 0 | 0 | 0 | 8 | 0 | 0 | 42 | 0 | 0 | 8 | 0 | 12 | 0 | 18 | 0 | 0 | 0 | 0 | 0 | 0 | 0 | 0 | 0 |
| **276** | 11 | 0 | 0 | 0 | 0 | 0 | 0 | 10 | 0 | 0 | 41 | 0 | 0 | 7 | 0 | 8 | 0 | 23 | 0 | 0 | 0 | 0 | 0 | 0 | 0 | 0 | 0 |
| **279** | 0 | 0 | 0 | 0 | 0 | 0 | 0 | 11 | 0 | 0 | 56 | 0 | 0 | 7 | 0 | 8 | 0 | 17 | 0 | 0 | 0 | 0 | 0 | 0 | 0 | 0 | 0 |
| **282** | 65 | 0 | 0 | 0 | 0 | 0 | 0 | 7 | 0 | 0 | 20 | 0 | 0 | 0 | 0 | 9 | 0 | 0 | 0 | 0 | 0 | 0 | 0 | 0 | 0 | 0 | 0 |
| **285** | 0 | 0 | 0 | 0 | 0 | 0 | 0 | 11 | 0 | 0 | 50 | 0 | 0 | 6 | 0 | 13 | 0 | 20 | 0 | 0 | 0 | 0 | 0 | 0 | 0 | 0 | 0 |
| **288** | 0 | 0 | 0 | 0 | 0 | 0 | 0 | 7 | 0 | 5 | 51 | 0 | 0 | 5 | 0 | 13 | 0 | 17 | 0 | 0 | 0 | 0 | 0 | 0 | 0 | 0 | 0 |
| **291** | 30 | 0 | 0 | 0 | 0 | 0 | 0 | 10 | 0 | 6 | 33 | 0 | 0 | 0 | 0 | 7 | 0 | 15 | 0 | 0 | 0 | 0 | 0 | 0 | 0 | 0 | 0 |
| **294** | 0 | 0 | 0 | 0 | 0 | 0 | 0 | 0 | 0 | 13 | 43 | 0 | 0 | 4 | 0 | 18 | 0 | 22 | 0 | 0 | 0 | 0 | 0 | 0 | 0 | 0 | 0 |
| **297** | 0 | 0 | 0 | 0 | 0 | 0 | 0 | 11 | 0 | 14 | 45 | 0 | 0 | 0 | 0 | 18 | 0 | 12 | 0 | 0 | 0 | 0 | 0 | 0 | 0 | 0 | 0 |
| **300** | 0 | 0 | 0 | 0 | 0 | 0 | 0 | 10 | 0 | 6 | 47 | 0 | 0 | 5 | 0 | 16 | 0 | 16 | 0 | 0 | 0 | 0 | 0 | 0 | 0 | 0 | 0 |
| **303** | 0 | 0 | 0 | 0 | 0 | 0 | 0 | 8 | 0 | 6 | 61 | 14 | 0 | 0 | 0 | 11 | 0 | 0 | 0 | 0 | 0 | 0 | 0 | 0 | 0 | 0 | 0 |
| **306** | 0 | 0 | 0 | 0 | 0 | 0 | 0 | 8 | 0 | 10 | 40 | 12 | 0 | 0 | 0 | 12 | 0 | 18 | 0 | 0 | 0 | 0 | 0 | 0 | 0 | 0 | 0 |
| **309** | 0 | 0 | 0 | 0 | 0 | 0 | 0 | 9 | 0 | 6 | 48 | 5 | 0 | 4 | 0 | 14 | 0 | 13 | 0 | 0 | 0 | 0 | 0 | 0 | 0 | 0 | 0 |
| **312** | 0 | 0 | 0 | 0 | 0 | 0 | 0 | 7 | 0 | 16 | 55 | 0 | 0 | 0 | 0 | 22 | 0 | 0 | 0 | 0 | 0 | 0 | 0 | 0 | 0 | 0 | 0 |
| **315** | 0 | 0 | 0 | 0 | 0 | 0 | 0 | 6 | 0 | 0 | 54 | 11 | 0 | 5 | 0 | 23 | 0 | 0 | 0 | 0 | 0 | 0 | 0 | 0 | 0 | 0 | 0 |
| **318** | 0 | 0 | 0 | 0 | 0 | 0 | 0 | 9 | 0 | 5 | 51 | 15 | 0 | 6 | 0 | 0 | 0 | 13 | 0 | 0 | 0 | 0 | 0 | 0 | 0 | 0 | 0 |
| **321** | 0 | 0 | 0 | 0 | 0 | 0 | 0 | 6 | 0 | 10 | 50 | 5 | 0 | 5 | 0 | 25 | 0 | 0 | 0 | 0 | 0 | 0 | 0 | 0 | 0 | 0 | 0 |
| **323** | 0 | 0 | 0 | 0 | 0 | 0 | 0 | 4 | 7 | 7 | 69 | 7 | 0 | 4 | 0 | 3 | 0 | 0 | 0 | 0 | 0 | 0 | 0 | 0 | 0 | 0 | 0 |
| **324** | 0 | 0 | 0 | 0 | 0 | 0 | 0 | 8 | 0 | 8 | 59 | 20 | 0 | 6 | 0 | 0 | 0 | 0 | 0 | 0 | 0 | 0 | 0 | 0 | 0 | 0 | 0 |
| **327** | 0 | 0 | 0 | 0 | 0 | 0 | 0 | 3 | 3 | 8 | 39 | 34 | 0 | 13 | 0 | 0 | 0 | 0 | 0 | 0 | 0 | 0 | 0 | 0 | 0 | 0 | 0 |
| **328,5** | 5 | 5 | 0 | 0 | 0 | 0 | 0 | 6 | 6 | 2 | 63 | 12 | 0 | 2 | 0 | 0 | 0 | 0 | 0 | 0 | 0 | 0 | 0 | 0 | 0 | 0 | 0 |
| **330** | 0 | 0 | 0 | 0 | 0 | 0 | 0 | 8 | 4 | 1 | 34 | 41 | 0 | 12 | 0 | 0 | 0 | 0 | 0 | 0 | 0 | 0 | 0 | 0 | 0 | 0 | 0 |
| **332** | 0 | 0 | 0 | 70 | 23 | 0 | 0 | 0 | 0 | 0 | 2 | 5 | 0 | 0 | 0 | 0 | 0 | 0 | 0 | 0 | 0 | 0 | 0 | 0 | 0 | 0 | 0 |
| **333** | 0 | 0 | 7 | 4 | 0 | 0 | 0 | 4 | 4 | 0 | 44 | 29 | 0 | 8 | 0 | 0 | 0 | 0 | 0 | 0 | 0 | 0 | 0 | 0 | 0 | 0 | 0 |
| **336** | 0 | 0 | 10 | 0 | 0 | 0 | 0 | 3 | 3 | 3 | 38 | 35 | 0 | 9 | 0 | 0 | 0 | 0 | 0 | 0 | 0 | 0 | 0 | 0 | 0 | 0 | 0 |
| **339** | 0 | 0 | 7 | 0 | 0 | 0 | 0 | 4 | 1 | 4 | 48 | 29 | 0 | 8 | 0 | 0 | 0 | 0 | 0 | 0 | 0 | 0 | 0 | 0 | 0 | 0 | 0 |
| **342** | 0 | 0 | 0 | 0 | 0 | 0 | 0 | 3 | 2 | 10 | 9 | 63 | 0 | 13 | 0 | 0 | 0 | 0 | 0 | 0 | 0 | 0 | 0 | 0 | 0 | 0 | 0 |
| **345** | 0 | 0 | 0 | 0 | 0 | 0 | 0 | 4 | 13 | 0 | 63 | 16 | 0 | 3 | 0 | 0 | 0 | 0 | 0 | 0 | 0 | 0 | 0 | 0 | 0 | 0 | 0 |
| **348** | 0 | 0 | 0 | 0 | 0 | 0 | 0 | 3 | 7 | 0 | 77 | 11 | 0 | 2 | 0 | 0 | 0 | 0 | 0 | 0 | 0 | 0 | 0 | 0 | 0 | 0 | 0 |
| **351** | 0 | 0 | 0 | 8 | 0 | 0 | 0 | 5 | 4 | 0 | 35 | 31 | 0 | 17 | 0 | 0 | 0 | 0 | 0 | 0 | 0 | 0 | 0 | 0 | 0 | 0 | 0 |
| **352** | 0 | 0 | 0 | 13 | 0 | 0 | 0 | 4 | 2 | 0 | 33 | 36 | 0 | 12 | 0 | 0 | 0 | 0 | 0 | 0 | 0 | 0 | 0 | 0 | 0 | 0 | 0 |
| **354** | 0 | 0 | 0 | 5 | 0 | 0 | 0 | 3 | 4 | 0 | 35 | 37 | 0 | 16 | 0 | 0 | 0 | 0 | 0 | 0 | 0 | 0 | 0 | 0 | 0 | 0 | 0 |
| **357** | 0 | 0 | 0 | 4 | 0 | 0 | 0 | 3 | 3 | 0 | 58 | 21 | 0 | 10 | 0 | 0 | 0 | 0 | 0 | 0 | 0 | 0 | 0 | 0 | 0 | 0 | 0 |
| **360** | 0 | 0 | 0 | 7 | 0 | 0 | 0 | 3 | 2 | 0 | 39 | 35 | 0 | 15 | 0 | 0 | 0 | 0 | 0 | 0 | 0 | 0 | 0 | 0 | 0 | 0 | 0 |
| **361** | 0 | 0 | 0 | 5 | 0 | 0 | 0 | 1 | 1 | 0 | 31 | 51 | 0 | 10 | 0 | 0 | 0 | 0 | 0 | 0 | 0 | 0 | 0 | 0 | 0 | 0 | 0 |
| **362,5** | 0 | 0 | 0 | 8 | 0 | 0 | 0 | 2 | 2 | 0 | 3 | 63 | 0 | 22 | 0 | 0 | 0 | 0 | 0 | 0 | 0 | 0 | 0 | 0 | 0 | 0 | 0 |
| **363** | 0 | 0 | 0 | 13 | 0 | 0 | 0 | 2 | 1 | 0 | 15 | 52 | 0 | 18 | 0 | 0 | 0 | 0 | 0 | 0 | 0 | 0 | 0 | 0 | 0 | 0 | 0 |
| **366** | 0 | 0 | 0 | 9 | 0 | 0 | 0 | 2 | 1 | 0 | 27 | 48 | 0 | 14 | 0 | 0 | 0 | 0 | 0 | 0 | 0 | 0 | 0 | 0 | 0 | 0 | 0 |

| | | | | | | | | | | | | | | | | | | | | | | | | | | | |
|---|---|---|---|---|---|---|---|---|---|---|---|---|---|---|---|---|---|---|---|---|---|---|---|---|---|---|---|
| **369** | 0 | 0 | 0 | 3 | 0 | 0 | 0 | 5 | 5 | 0 | 71 | 12 | 0 | 4 | 0 | 0 | 0 | 0 | 0 | 0 | 0 | 0 | 0 | 0 | 0 | 0 | 0 |
| **372** | 0 | 0 | 0 | 4 | 0 | 0 | 0 | 2 | 4 | 0 | 61 | 24 | 0 | 4 | 0 | 0 | 0 | 0 | 0 | 0 | 0 | 0 | 0 | 0 | 0 | 0 | 0 |
| **373,5** | 0 | 0 | 0 | 68 | 0 | 13 | 0 | 0 | 0 | 0 | 2 | 17 | 0 | 0 | 0 | 0 | 0 | 0 | 0 | 0 | 0 | 0 | 0 | 0 | 0 | 0 | 0 |
| **375** | 0 | 0 | 0 | 5 | 0 | 0 | 0 | 2 | 3 | 0 | 61 | 25 | 0 | 5 | 0 | 0 | 0 | 0 | 0 | 0 | 0 | 0 | 0 | 0 | 0 | 0 | 0 |
| **378** | 0 | 0 | 0 | 3 | 0 | 0 | 0 | 3 | 4 | 0 | 75 | 14 | 0 | 0 | 0 | 0 | 0 | 0 | 0 | 0 | 0 | 0 | 0 | 0 | 0 | 0 | 0 |
| **381** | 0 | 0 | 0 | 0 | 0 | 0 | 0 | 3 | 8 | 0 | 83 | 6 | 0 | 0 | 0 | 0 | 0 | 0 | 0 | 0 | 0 | 0 | 0 | 0 | 0 | 0 | 0 |
| **384** | 0 | 0 | 0 | 3 | 0 | 0 | 0 | 3 | 8 | 0 | 77 | 8 | 0 | 1 | 0 | 0 | 0 | 0 | 0 | 0 | 0 | 0 | 0 | 0 | 0 | 0 | 0 |
| **387** | 0 | 0 | 0 | 31 | 0 | 23 | 0 | 2 | 5 | 0 | 38 | 0 | 0 | 0 | 0 | 0 | 0 | 0 | 0 | 0 | 0 | 0 | 0 | 0 | 0 | 0 | 0 |
| **390** | 0 | 0 | 0 | 0 | 0 | 0 | 0 | 2 | 4 | 0 | 86 | 8 | 0 | 0 | 0 | 0 | 0 | 0 | 0 | 0 | 0 | 0 | 0 | 0 | 0 | 0 | 0 |
| **393** | 0 | 0 | 0 | 0 | 0 | 0 | 0 | 2 | 6 | 0 | 89 | 4 | 0 | 0 | 0 | 0 | 0 | 0 | 0 | 0 | 0 | 0 | 0 | 0 | 0 | 0 | 0 |
| **396** | 0 | 0 | 0 | 0 | 0 | 0 | 0 | 2 | 11 | 0 | 70 | 17 | 0 | 0 | 0 | 0 | 0 | 0 | 0 | 0 | 0 | 0 | 0 | 0 | 0 | 0 | 0 |
| **399** | 0 | 0 | 0 | 0 | 0 | 0 | 0 | 2 | 9 | 0 | 83 | 6 | 0 | 0 | 0 | 0 | 0 | 0 | 0 | 0 | 0 | 0 | 0 | 0 | 0 | 0 | 0 |
| **402** | 0 | 0 | 0 | 14 | 0 | 0 | 0 | 2 | 1 | 0 | 1 | 75 | 0 | 7 | 0 | 0 | 0 | 0 | 0 | 0 | 0 | 0 | 0 | 0 | 0 | 0 | 0 |
| **405** | 0 | 0 | 0 | 0 | 0 | 0 | 0 | 3 | 11 | 0 | 80 | 6 | 0 | 0 | 0 | 0 | 0 | 0 | 0 | 0 | 0 | 0 | 0 | 0 | 0 | 0 | 0 |
| **408** | 0 | 0 | 0 | 0 | 0 | 0 | 0 | 2 | 10 | 0 | 86 | 2 | 0 | 0 | 0 | 0 | 0 | 0 | 0 | 0 | 0 | 0 | 0 | 0 | 0 | 0 | 0 |
| **411** | 0 | 14 | 0 | 12 | 0 | 0 | 0 | 0 | 9 | 0 | 8 | 49 | 0 | 8 | 0 | 0 | 0 | 0 | 0 | 0 | 0 | 0 | 0 | 0 | 0 | 0 | 0 |
| **414** | 0 | 0 | 0 | 7 | 0 | 0 | 0 | 0 | 0 | 0 | 54 | 39 | 0 | 0 | 0 | 0 | 0 | 0 | 0 | 0 | 0 | 0 | 0 | 0 | 0 | 0 | 0 |
| **415,5** | 0 | 0 | 0 | 0 | 0 | 0 | 0 | 0 | 0 | 0 | 51 | 49 | 0 | 0 | 0 | 0 | 0 | 0 | 0 | 0 | 0 | 0 | 0 | 0 | 0 | 0 | 0 |
| **416** | 0 | 0 | 0 | 0 | 0 | 0 | 0 | 0 | 0 | 0 | 65 | 35 | 0 | 0 | 0 | 0 | 0 | 0 | 0 | 0 | 0 | 0 | 0 | 0 | 0 | 0 | 0 |
| **417** | 0 | 0 | 0 | 9 | 0 | 0 | 0 | 0 | 0 | 0 | 45 | 46 | 0 | 0 | 0 | 0 | 0 | 0 | 0 | 0 | 0 | 0 | 0 | 0 | 0 | 0 | 0 |
| **420** | 0 | 0 | 0 | 8 | 0 | 0 | 0 | 0 | 0 | 0 | 41 | 50 | 0 | 0 | 0 | 0 | 0 | 0 | 0 | 0 | 0 | 0 | 0 | 0 | 0 | 0 | 0 |
| **423** | 2 | 0 | 0 | 0 | 0 | 0 | 0 | 0 | 0 | 0 | 16 | 82 | 0 | 0 | 0 | 0 | 0 | 0 | 0 | 0 | 0 | 0 | 0 | 0 | 0 | 0 | 0 |
| **426** | 0 | 0 | 0 | 0 | 0 | 0 | 0 | 0 | 0 | 0 | 75 | 25 | 0 | 0 | 0 | 0 | 0 | 0 | 0 | 0 | 0 | 0 | 0 | 0 | 0 | 0 | 0 |
| **429** | 0 | 0 | 8 | 0 | 0 | 0 | 0 | 0 | 0 | 0 | 50 | 40 | 0 | 3 | 0 | 0 | 0 | 0 | 0 | 0 | 0 | 0 | 0 | 0 | 0 | 0 | 0 |
| **432** | 0 | 0 | 0 | 0 | 0 | 0 | 0 | 0 | 15 | 0 | 63 | 20 | 0 | 2 | 0 | 0 | 0 | 0 | 0 | 0 | 0 | 0 | 0 | 0 | 0 | 0 | 0 |
| **435** | 0 | 0 | 0 | 0 | 0 | 0 | 0 | 0 | 17 | 0 | 68 | 15 | 0 | 0 | 0 | 0 | 0 | 0 | 0 | 0 | 0 | 0 | 0 | 0 | 0 | 0 | 0 |
| **438** | 0 | 0 | 0 | 0 | 0 | 0 | 0 | 0 | 13 | 0 | 75 | 13 | 0 | 0 | 0 | 0 | 0 | 0 | 0 | 0 | 0 | 0 | 0 | 0 | 0 | 0 | 0 |
| **441** | 0 | 0 | 4 | 0 | 0 | 0 | 0 | 0 | 8 | 0 | 49 | 33 | 0 | 6 | 0 | 0 | 0 | 0 | 0 | 0 | 0 | 0 | 0 | 0 | 0 | 0 | 0 |
| **444** | 0 | 0 | 0 | 0 | 0 | 0 | 0 | 0 | 13 | 0 | 76 | 11 | 0 | 0 | 0 | 0 | 0 | 0 | 0 | 0 | 0 | 0 | 0 | 0 | 0 | 0 | 0 |
| **447** | 0 | 0 | 0 | 56 | 0 | 27 | 0 | 0 | 0 | 0 | 4 | 13 | 0 | 0 | 0 | 0 | 0 | 0 | 0 | 0 | 0 | 0 | 0 | 0 | 0 | 0 | 0 |
| **450** | 0 | 0 | 0 | 0 | 0 | 0 | 0 | 0 | 2 | 0 | 21 | 69 | 0 | 8 | 0 | 0 | 0 | 0 | 0 | 0 | 0 | 0 | 0 | 0 | 0 | 0 | 0 |
| **453** | 0 | 0 | 0 | 0 | 0 | 0 | 0 | 0 | 0 | 0 | 23 | 68 | 0 | 9 | 0 | 0 | 0 | 0 | 0 | 0 | 0 | 0 | 0 | 0 | 0 | 0 | 0 |
| **456** | 0 | 0 | 0 | 0 | 0 | 0 | 0 | 0 | 0 | 0 | 41 | 59 | 0 | 0 | 0 | 0 | 0 | 0 | 0 | 0 | 0 | 0 | 0 | 0 | 0 | 0 | 0 |
| **459** | 0 | 0 | 14 | 0 | 0 | 0 | 0 | 0 | 0 | 0 | 3 | 83 | 0 | 0 | 0 | 0 | 0 | 0 | 0 | 0 | 0 | 0 | 0 | 0 | 0 | 0 | 0 |
| **462** | 4 | 0 | 0 | 0 | 0 | 0 | 0 | 0 | 0 | 0 | 22 | 74 | 0 | 0 | 0 | 0 | 0 | 0 | 0 | 0 | 0 | 0 | 0 | 0 | 0 | 0 | 0 |
| **463,5** | 2 | 0 | 0 | 0 | 0 | 0 | 0 | 0 | 3 | 0 | 82 | 12 | 0 | 0 | 0 | 0 | 0 | 0 | 0 | 0 | 0 | 0 | 0 | 0 | 0 | 0 | 0 |
| **465** | 0 | 0 | 0 | 0 | 0 | 0 | 0 | 0 | 0 | 0 | 39 | 61 | 0 | 0 | 0 | 0 | 0 | 0 | 0 | 0 | 0 | 0 | 0 | 0 | 0 | 0 | 0 |
| **468** | 6 | 0 | 0 | 4 | 0 | 0 | 0 | 0 | 0 | 0 | 56 | 34 | 0 | 0 | 0 | 0 | 0 | 0 | 0 | 0 | 0 | 0 | 0 | 0 | 0 | 0 | 0 |
| **471** | 0 | 0 | 0 | 0 | 0 | 0 | 0 | 0 | 4 | 0 | 47 | 49 | 0 | 0 | 0 | 0 | 0 | 0 | 0 | 0 | 0 | 0 | 0 | 0 | 0 | 0 | 0 |
| **474** | 0 | 0 | 0 | 0 | 0 | 0 | 0 | 0 | 6 | 0 | 39 | 51 | 0 | 4 | 0 | 0 | 0 | 0 | 0 | 0 | 0 | 0 | 0 | 0 | 0 | 0 | 0 |
| **477** | 0 | 0 | 0 | 0 | 0 | 0 | 0 | 0 | 2 | 0 | 62 | 33 | 0 | 2 | 0 | 0 | 0 | 0 | 0 | 0 | 0 | 0 | 0 | 0 | 0 | 0 | 0 |
| **478** | 0 | 0 | 0 | 0 | 0 | 0 | 0 | 0 | 6 | 0 | 64 | 29 | 0 | 2 | 0 | 0 | 0 | 0 | 0 | 0 | 0 | 0 | 0 | 0 | 0 | 0 | 0 |
| **479** | 0 | 0 | 0 | 0 | 0 | 0 | 0 | 0 | 10 | 0 | 51 | 36 | 0 | 4 | 0 | 0 | 0 | 0 | 0 | 0 | 0 | 0 | 0 | 0 | 0 | 0 | 0 |
| **480** | 0 | 0 | 3 | 0 | 0 | 0 | 0 | 0 | 9 | 0 | 48 | 35 | 0 | 6 | 0 | 0 | 0 | 0 | 0 | 0 | 0 | 0 | 0 | 0 | 0 | 0 | 0 |
| **483** | 0 | 0 | 6 | 0 | 0 | 0 | 0 | 0 | 6 | 0 | 41 | 43 | 0 | 4 | 0 | 0 | 0 | 0 | 0 | 0 | 0 | 0 | 0 | 0 | 0 | 0 | 0 |
| **486** | 0 | 0 | 4 | 0 | 0 | 0 | 0 | 0 | 6 | 0 | 63 | 20 | 0 | 6 | 0 | 0 | 0 | 0 | 0 | 0 | 0 | 0 | 0 | 0 | 0 | 0 | 0 |
| **489** | 3 | 0 | 0 | 0 | 0 | 0 | 0 | 10 | 0 | 0 | 30 | 0 | 20 | 0 | 37 | 0 | 0 | 0 | 0 | 0 | 0 | 0 | 0 | 0 | 0 | 0 | 0 |
| **492** | 0 | 0 | 0 | 0 | 0 | 0 | 0 | 20 | 7 | 0 | 48 | 0 | 12 | 0 | 13 | 0 | 0 | 0 | 0 | 0 | 0 | 0 | 0 | 0 | 0 | 0 | 0 |
| **495** | 0 | 0 | 0 | 0 | 0 | 0 | 0 | 21 | 7 | 0 | 45 | 0 | 16 | 0 | 11 | 0 | 0 | 0 | 0 | 0 | 0 | 0 | 0 | 0 | 0 | 0 | 0 |
| **498** | 0 | 0 | 0 | 0 | 0 | 0 | 0 | 22 | 10 | 0 | 44 | 1 | 8 | 0 | 15 | 0 | 0 | 0 | 0 | 0 | 0 | 0 | 0 | 0 | 0 | 0 | 0 |

**peak area of n-alkanes and isoprenoids from GC-FID**

| Sample | C10 | C11 | C12 | C13 | C14 | C15 | C16 | C17 | pristane | C18 | phytane | C19 | C20 | C21 | C22 | C23 |
|---|---|---|---|---|---|---|---|---|---|---|---|---|---|---|---|---|
| **991915** | 0 | 0 | 0 | 0 | 3102 | 5672 | 8622 | 22216 | 15830 | 35998 | 24864 | 36709 | 29337 | 20699 | 23735 | 34826 |
| **991920** | 2887 | 10746 | 15903 | 18947 | 10671 | 7309 | 7428 | 19453 | 15182 | 32375 | 22674 | 35134 | 24925 | 14016 | 8384 | 8075 |
| **991921** | 10111 | 41654 | 79576 | 134566 | 180414 | 260344 | 217290 | 283924 | 1381079 | 175964 | 793592 | 220465 | 164392 | 151358 | 138479 | 141653 |
| **991923** | 62365 | 190881 | 181327 | 187016 | 164788 | 180555 | 123125 | 154592 | 422578 | 76340 | 231762 | 93725 | 63070 | 55599 | 50346 | 50884 |
| **991924** | 10896 | 29799 | 37702 | 63476 | 85175 | 126173 | 95542 | 158330 | 571773 | 69100 | 347044 | 89007 | 62439 | 55305 | 52417 | 55650 |
| **991925** | 11569 | 6107 | 15808 | 21489 | 11801 | 15907 | 17217 | 30568 | 33438 | 38411 | 31084 | 45620 | 35412 | 22337 | 14459 | 14274 |
| **991926** | 21634 | 191390 | 231390 | 196803 | 101312 | 59752 | 32212 | 32534 | 20559 | 23306 | 14827 | 22649 | 15411 | 10487 | 6096 | 4721 |
| **991927** | 0 | 0 | 89911 | 185113 | 173458 | 135332 | 82604 | 79877 | 70217 | 69032 | 53808 | 65765 | 41439 | 22634 | 11504 | 8695 |
| **991929** | 0 | 0 | 6399 | 27559 | 61788 | 92640 | 87254 | 124035 | 462102 | 96616 | 461866 | 112467 | 98346 | 80306 | 81578 | 84431 |
| **991930** | 0 |  | 4223 | 4812 | 11675 | 16897 | 26845 | 61749 | 275398 | 64201 | 308513 | 71776 | 99259 | 62884 | 65668 | 82438 |
| **991931** | 0 | 0 | 0 | 70348 | 224171 | 150668 | 235851 | 260443 | 1461718 | 254387 | 1243284 | 277779 | 326886 | 206157 | 196198 | 230614 |
| **991933** | 6288 | 25320 | 32838 | 47665 | 70064 | 121222 | 124490 | 590864 | 901911 | 170653 | 837650 | 222821 | 107316 | 164823 | 61696 | 95023 |
| **991938** | 0 | 0 | 5462 | 10199 | 13433 | 41574 | 68936 | 110685 | 39372 | 144928 | 90144 | 125167 | 152658 | 100496 | 123125 | 85891 |
| **991939** | 5698 | 18221 | 36233 | 77234 | 113792 | 193739 | 188660 | 183145 | 55403 | 183307 | 211884 | 160703 | 198389 | 150749 | 156879 | 123858 |

| Sample | St. | C24 | C25 | C26 | C27 | C28 | C29 | C30 | C31 | C32 | C33 | C34 | C35 | C36 | C37 | C38 |
|---|---|---|---|---|---|---|---|---|---|---|---|---|---|---|---|---|
| **991915** | 164238 | 44949 | 63249 | 53574 | 59184 | 46166 | 45118 | 26329 | 18259 | 12780 | 11794 | 10375 | 9628 | 6636 | 5873 | 4410 |
| **991920** | 169811 | 7616 | 7917 | 6888 | 6959 | 5403 | 5927 | 4093 | 5517 | 3292 | 2731 | 2402 | 2371 | 0 | 0 | 0 |
| **991921** | 356684 | 148452 | 211586 | 146169 | 184997 | 100141 | 134943 | 0 | 0 | 0 | 0 | 0 | 0 | 0 | 0 | 0 |
| **991923** | 46592 | 50030 | 59333 | 45044 | 56591 | 30893 | 32477 | 0 | 0 | 0 | 0 | 0 | 0 | 0 | 0 | 0 |
| **991924** | 177393 | 55919 | 71379 | 57207 | 86336 | 39350 | 52761 | 0 | 0 | 0 | 0 | 0 | 0 | 0 | 0 | 0 |
| **991925** | 366859 | 14572 | 14799 | 13131 | 14017 | 10444 | 10417 | 7814 | 7112 | 5323 | 0 | 0 | 0 | 0 | 0 | 0 |
| **991926** | 231635 | 3726 | 4205 | 3388 | 3263 | 2740 | 2671 | 2131 | 2113 | 1499 | 0 | 0 | 0 | 0 | 0 | 0 |
| **991927** | 406542 | 7958 | 8531 | 6460 | 8603 | 4952 | 6421 | 3976 | 5812 | 3687 | 2968 | 0 | 0 | 0 | 0 | 0 |
| **991929** | 160405 | 85746 | 152405 | 79621 | 79162 | 57939 | 43951 | 44856 | 30283 | 0 | 0 | 0 | 0 | 0 | 0 | 0 |
| **991930** | 138173 | 79708 | 134736 | 97533 | 92861 | 81826 | 50323 | 55806 | 0 | 0 | 0 | 0 | 0 | 0 | 0 | 0 |
| **991931** |  | 207531 | 442566 | 257368 | 288654 | 160501 | 100426 | 156165 | 0 | 0 | 0 | 0 | 0 | 0 | 0 | 0 |
| **991933** | 1285816 | 41581 | 70384 | 35225 | 91126 | 0 | 0 | 0 | 0 | 0 | 0 | 0 | 0 | 0 | 0 | 0 |
| **991938** |  | 139952 | 148043 | 275171 | 314754 | 466818 | 351665 | 519439 | 0 | 0 | 0 | 0 | 0 | 0 | 0 | 0 |
| **991939** | 146443 | 139596 | 115772 | 145353 | 143087 | 203730 | 122983 | 175558 | 80984 | 81718 | 36471 | 28358 | 22383 | 0 | 0 | 0 |

**peak area of n-alkanes and isoprenoids from GC-FID**

| | C10 | C11 | C12 | C13 | C14 | i-C16 | C15 | C16 | nor-pristane | C17 | pristane | C18 | phytane | C19 | C20 |
|---|---|---|---|---|---|---|---|---|---|---|---|---|---|---|---|
| **992651** | 25829 | 76844 | 130810 | 174302 | 227001 | 148900 | 252746 | 292587 | 78855 | 317040 | 509056 | 345529 | 85735 | 406963 | 480257 |
| **992652** | 26525 | 68652 | 116917 | 119556 | 105493 | 286884 | 119906 | 129960 | 113990 | 166757 | 931985 | 200685 | 83259 | 268432 | 285423 |
| **992646** | 32227 | 147128 | 275925 | 218924 | 142975 | 66560 | 147342 | 182432 | 36220 | 158513 | 179615 | 149897 | 51196 | 144805 | 153852 |
| **992647** | 49212 | 135009 | 174910 | 149604 | 127835 | 34820 | 117141 | 123800 | 17097 | 102665 | 72656 | 93759 | 32041 | 87261 | 85603 |
| **992648** | | 20876 | 110056 | 143302 | 121655 | 39373 | 141699 | 187745 | 26251 | 174158 | 94202 | 168669 | 61893 | 166320 | 153447 |
| **992649** | | 26006 | 117011 | 165384 | 170047 | 112141 | 199179 | 235792 | 54041 | 264892 | 315612 | 305435 | 52574 | 357655 | 423300 |
| **992650** | 47358 | 123289 | 147595 | 112739 | 112093 | 26756 | 114640 | 157607 | 20194 | 123717 | 61033 | 101573 | 53400 | 80077 | 72694 |
| **992645** | 28483 | 78780 | 148371 | 182712 | 196972 | 153184 | 227532 | 261415 | 77076 | 292608 | 415008 | 327710 | 63597 | 403012 | 427990 |
| **992644** | 18121 | 71715 | 143312 | 154865 | 150167 | 137970 | 168204 | 182633 | 72746 | 202117 | 390440 | 212524 | 51449 | 243829 | 230543 |
| **992642** | 9819 | 39645 | 85334 | 90546 | 76403 | 148560 | 94089 | 125498 | 105002 | 146219 | 846612 | 175701 | 98516 | 229322 | 255670 |
| **992643** | 5365 | 66153 | 186075 | 141376 | 55847 | 7571 | 66724 | 148445 | 12282 | 99529 | 26717 | 68515 | 45455 | 40822 | 31627 |
| **992641** | 19056 | 97085 | 184062 | 182553 | 158870 | 67254 | 190195 | 293520 | 50831 | 266271 | 198561 | 218280 | 79997 | 192685 | 187744 |
| **992639** | 58837 | 114729 | 184136 | 186986 | 194133 | 218857 | 206737 | 247976 | 123147 | 266979 | 1028437 | 320858 | 104929 | 409263 | 501167 |
| **992640** | 115616 | 224958 | 309698 | 364739 | 399427 | 235169 | 407680 | 403236 | 119978 | 395829 | 859820 | 399247 | 86075 | 411864 | 408108 |
| **992653** | | 8741 | 98923 | 186538 | 12090 | | 13172 | 18527 | | 20863 | 17667 | 19963 | 18427 | 21490 | 19433 |
| **992654** | 65074 | 116370 | 169075 | 195201 | 187051 | 156972 | 178655 | 182438 | | 193221 | 684230 | 214347 | 69381 | 236228 | 245821 |

| | C21 | C22 | C23 | C24 | C25 | C26 | C27 | C28 | C29 | C30 |
|---|---|---|---|---|---|---|---|---|---|---|
| **992651** | 583611 | 669809 | 839917 | 656762 | 843651 | 236541 | 259260 | 111343 | 110580 | 50690 |
| **992652** | 337774 | 412249 | 525710 | 436000 | 533051 | 211923 | 229839 | 86950 | 98608 | 33080 |
| **992646** | 160858 | 155335 | 282393 | 124145 | 232583 | 52442 | 59889 | 23137 | 22611 | 11569 |
| **992647** | 98367 | 95089 | 113361 | 97633 | 118102 | 53210 | 59546 | 23356 | 26752 | 11969 |
| **992648** | 169912 | 155151 | 186799 | 143090 | 199503 | 102380 | 127382 | 50935 | 51841 | 21708 |
| **992649** | 495904 | 512159 | 940132 | 438194 | 718308 | 184796 | 239493 | 85115 | 90441 | 39208 |
| **992650** | 68692 | 56563 | 61352 | 49109 | 46129 | 27003 | 24153 | 11848 | 14763 | 7955 |
| **992645** | 509927 | 562485 | 874842 | 571857 | 1052528 | 272244 | 368851 | 118341 | 144890 | 51641 |
| **992644** | 260518 | 276601 | 321478 | 285785 | 365353 | 160439 | 189771 | 75175 | 76772 | 31763 |
| **992642** | 312034 | 345451 | 457164 | 370996 | 358143 | 218612 | 229081 | 118586 | 141963 | 44449 |
| **992643** | 28362 | 18270 | 23710 | 15572 | 15454 | 10631 | 8042 | 4054 | 6038 | 3797 |
| **992641** | 208417 | 197350 | 234745 | 187614 | 218098 | 124469 | 131940 | 49006 | 40574 | 14602 |
| **992639** | 616697 | 663454 | 841168 | 684392 | 601260 | 391523 | 396412 | 240213 | 248221 | 127371 |
| **992640** | 428210 | 393378 | 431124 | 329370 | 272011 | 158109 | 161556 | 83221 | 93908 | 52277 |
| **992653** | 25541 | 25345 | 27420 | 24788 | 30191 | 20479 | 18586 | 14964 | 15829 | 13152 |
| **992654** | 274375 | 262923 | 298915 | 237853 | 203247 | 120622 | 132675 | 67286 | 72329 | 37383 |